**UNIVERSIDADE DE LISBOA**

**INSTITUTO SUPERIOR TÉCNICO**

# Aerobic granular sludge bioprocesses for textile wastewater treatment

**Rita Dias Guardão Moreira da Franca**

**Supervisor: Doctor Nídia Dana Mariano Lourenço**

**Co-Supervisors:**

**Doctor Helena Maria Rodrigues Vasconcelos Pinheiro**

**Doctor Marinus Cornelis Maria (Mark) van Loosdrecht**

**Thesis approved in public session to obtain the PhD Degree in Biotechnology and Biosciences**

**Jury final classification: Pass with Distinction and Honour**

**2019**

TÉCNICO LISBOA

# UNIVERSIDADE DE LISBOA

# INSTITUTO SUPERIOR TÉCNICO

# Aerobic granular sludge bioprocesses for textile wastewater treatment

**Rita Dias Guardão Moreira da Franca**

**Supervisor: Doctor Nídia Dana Mariano Lourenço**

**Co-Supervisors:**

**Doctor Helena Maria Rodrigues Vasconcelos Pinheiro**

**Doctor Marinus Cornelis Maria (Mark) van Loosdrecht**

**Thesis approved in public session to obtain the PhD Degree in**

**Biotechnology and Biosciences**

**Jury final classification: Pass with Distinction and Honour**

**Jury**

**Chairperson: Doctor Duarte Miguel de França Teixeira dos Prazeres, Instituto Superior Técnico, Universidade de Lisboa**

**Members of the Committee:**

**Doctor Maria d'Ascenção Carvalho Fernandes de Miranda Reis, Faculdade de Ciências e Tecnologia, Universidade Nova de Lisboa**

**Doctor Maria Madalena dos Santos Alves, Escola de Engenharia, Universidade do Minho**

**Doctor Maria Manuela Regalo da Fonseca, Instituto Superior Técnico, Universidade de Lisboa**

**Doctor Nídia Dana Mariano Lourenço, NOVA.ID.FCT, Faculdade de Ciências e Tecnologia, Universidade Nova de Lisboa**

**Doctor Ana Cristina Anjinho Madeira Viegas, Instituto Superior Técnico, Universidade de Lisboa**

**Funding Institution**

**Fundação para a Ciência e a Tecnologia**

**2019**

# Resumo

As águas residuais têxteis (TWWs) são uma relevante fonte de poluição à escala mundial, contendo elevadas cargas orgânicas, corantes recalcitrantes (*ca*. 80% dos corantes têxteis são corantes azo) e, mais recentemente, nanopartículas fabricadas, nomeadamente nanopartículas de prata (AgNP). A presente tese teve como objetivo contribuir para o desenvolvimento de um bioprocesso eficiente de tratamento de TWWs utilizando a tecnologia de lamas granulares aeróbias (AGS) em reatores descontínuos sequenciais (SBRs). Demonstrou-se a aplicabilidade de AGS ao tratamento de TWWs contendo um corante azo (Acid Red 14; AR14) em SBRs anaeróbio-aeróbios não tubulares. Atingiram-se rendimentos de remoção de cor e carga orgânica de 80% em ciclos de 6 h após 3-14 dias de adaptação da biomassa, sendo mais de metade da carga orgânica removida em condições anaeróbicas. Após a biodescoloração por redução completa do corante azo ao longo da fase anaeróbia (1,5 h), a bioconversão de uma das aminas aromáticas resultantes (ácido 4-amino-naftaleno-1-sulfónico; 4A1NS) durante a fase aeróbica (3,5 h) foi observada aquando da operação com um valor elevado de idade de lamas. A frequente perda de biomassa do SBR perturbou significativamente a eficiência da descoloração. No entanto, o sistema AGS-SBR provou ser robusto ao lidar com choques de aumento de concentração de corante e de carga orgânica, mantendo elevados rendimentos de remoção destes poluentes. Além disso, as AGS resistiram a um período de armazenamento de 6,5 meses, recuperando-se o elevado desempenho de tratamento (exceto relativamente à remoção de 4A1NS) bem como a excelente sedimentabilidade da biomassa, ao fim de 2 semanas após a reativação das AGS em SBRs. O regime hidrodinâmico foi otimizado, com ênfase na granulação aeróbia e descoloração. A granulação foi alcançada com sucesso após 50 dias, independentemente do regime hidrodinâmico utilizado, mas a remoção completa da cor através da biorredução do corante azo revelou estar dependente da existência de uma fase anaeróbia agitada no ciclo operacional. O desempenho ótimo do sistema relativamente ao tratamento e à estabilidade das AGS foi obtido usando uma alimentação em regime de fluxo tipo-pistão de 1,5 h seguida de uma fase anaeróbia agitada de 1 h e de uma fase aeróbia de 3,5 h, nomeadamente face a choques de concentração de poluentes e variabilidade do substrato na TWW. O potencial de biodegradação aeróbia de aminas aromáticas foi demonstrado em diferentes regimes hidrodinâmicos, sendo a conversão irreversível da amina 4A1NS consistentemente observada no SBR anaeróbio-aeróbio alimentado em regime de fluxo tipo-pistão por mais de 300 dias, nomeadamente após um período de armazenamento de biomassa de 18 dias. A análise por espectrometria de massa revelou pelo menos 19 moléculas possivelmente associadas à biodegradação do corante AR14, algumas das quais potencialmente resultantes da auto-oxidação espontânea da amina aromática instável (ácido 1-naftol-2-amino-4-sulfónico) formando produtos diméricos estáveis. A biodegradação aeróbia da amina 4A1NS ocorreu potencialmente via desaminação e hidroxilação do anel aromático. Aquando da suplementação da TWW com nitrato,

observou-se uma diferente via de biodegradação do AR14, provavelmente envolvendo a rápida desaminação da amina 4A1NS em condições anaeróbias. As reduções de nitrato e de AR14 ocorreram simultaneamente durante a fase anaeróbia, não ficando a eficiência de descoloração comprometida pela presença de nitrato. As AgNP (adicionadas em concentrações de 10 ou 20 mg $L^{-1}$ na TWW simulada) adsorveram à biomassa, mas não afetaram negativamente a granulação (decorrida ao longo de 35 dias) nem a eficiência do tratamento (em termos de remoção de carga orgânica e biodegradação do corante azo), nomeadamente durante a reativação das AGS após 18-40 dias de paragem operacional. Além disso, as AgNP promoveram uma melhor sedimentação das AGS a longo prazo. Finalmente, uma estirpe bacteriana potencialmente promissora para a biodegradação de corantes azo foi isolada de um SBR anaeróbio-aeróbio alimentado com a TWW sintética suplementada com AR14. Especificamente, a capacidade de *Oerskovia* sp. para descolorar o corante e biodegradar parcialmente uma amina aromática recalcitrante foi reportada pela primeira vez. Em geral, estes resultados contribuíram para o desenvolvimento da aplicação da tecnologia de AGS ao tratamento de TWW coradas.

**Palavras-chave:** águas residuais têxteis; biodegradação de corantes azo; lamas granulares aeróbias; nanopartículas de prata; reatores descontínuos sequenciais.

# Abstract

Textile wastewater (TWW) represent a major source of pollution worldwide, carrying high organic loads, recalcitrant dyes (*ca*. 80% of textile dyes being azo dyes) and, more recently, engineered nanoparticles, namely silver nanoparticles (AgNP). The present thesis aimed to contribute for the development of an effective TWW treatment bioprocess using the novel, cost-effective aerobic granular sludge (AGS) anaerobic-aerobic sequencing batch reactor (SBR) technology. The applicability of AGS in the treatment of an azo dye-containing synthetic TWW in non-tubular, anaerobic-aerobic SBRs was demonstrated for the dye Acid Red 14 (AR14). Color and organic load removal yields of 80% were reached in 6-h cycles after 3-14 days of biomass adaptation, with more than half of the organic load being removed anaerobically. After biodecolorization through complete azo dye reduction along the 1.5-h anaerobic phase, further bioconversion of one of the resulting aromatic amines (4-amino-naphthalene-1-sulfonic acid; 4A1NS) during the 3.5-h aerobic phase was observed under high operational sludge age values. Frequent biomass wastage from the SBR negatively affected the decolorization performance. Yet, AGS SBR proved to be a robust system able to deal with organic and dye shock loads, maintaining high removal yields. Moreover, AGS resisted a 6.5-month storage period, efficiently reactivating its former treatment performance (except for 4A1NS removal) within 2 weeks and restoring good settleability. The SBR hydrodynamic regimen was optimized, with emphasis on granulation and decolorization. Aerobic granulation was successfully reached after 50 days irrespective of the applied hydrodynamic regimen, but complete color removal through azo dye bioreduction depended on the inclusion of a mixed anaerobic phase in the operational cycle. Optimal treatment performance and AGS long-term stability were obtained with a 1.5-h plug-flow feed followed by 1-h anaerobic stirred phase and 3.5-h aerobic phase, including when dealing with shock loads and substrate variability in the TWW. The potential for aerobic biodegradation of aromatic amines was demonstrated in different hydrodynamic regimens, irreversible 4A1NS conversion being consistently observed in the plug-flow fed, anaerobic-aerobic SBR regimen for more than 300 days, namely after an 18-day biomass storage period. Mass spectrometry analysis revealed at least 19 molecules possibly associated with AR14 biodegradation, some of which potentially resulting from spontaneous autoxidation of the instable aromatic amine 1-naphthol-2-amino-4-sulfonic acid forming dimeric, stable products. Biotransformation of 4A1NS was proposed to follow deamination and hydroxylation of the aromatic ring. A different AR14 biodegradation pathway was observed upon supplementation of the feed with nitrate, probably involving the rapid deamination of 4A1NS under anaerobic conditions. Nitrate and AR14 reduction occurred simultaneously during the anaerobic phase, the decolorization efficiency not being compromised by the presence of nitrate. AgNP (at 10 or 20 mg $L^{-1}$ in the simulated TWW) adsorbed to the biomass but did not negatively affect granulation (completed after 35 days) or the treatment performance (both in terms of organic load and azo dye

biodegradation), namely during AGS reactivation after 18-40 days of idle storage. In fact, AgNP slightly enhanced AGS settling properties in the long-term operation. Finally, a promising bacterial strain for azo dye biodegradation applications was isolated from an anaerobic-aerobic SBR treating an AR14-supplemented synthetic TWW. Specifically, *Oerskovia* sp. decolorization capacity and further partial biodegradation of a recalcitrant sulfonated aromatic amine was for the first time reported. Overall, this thesis provided relevant evidence in support of the application of AGS in dye-laden TWW treatment.

**Keywords:** Aerobic granular sludge; azo dye biodegradation; sequencing batch reactors; silver nanoparticles; textile wastewater treatment.

# Acknowledgements

I would like to acknowledge the financial support from Fundação para a Ciência e a Tecnologia (FCT, Portugal) through a doctoral grant (SFRH/BD/95415/2013). The work here presented was financed by FCT (projects PTDC/EBB-EBI/120624/2010 and PTDC/AAG-TEC/4501/2014 – national funds, PIDDAC Program), iBB (project UID/BIO/04565/2013) and Programa Operacional Regional de Lisboa 2020 (projects N. 007317 and RNEM-022125). This work was also supported by UCIBIO and iNOVA4Health, which are co-funded by FCT/MCES, through national funds (UID/Multi/04378/2013, UID/BIO/04565/2013) and by FEDER under the PT2020 Partnership Agreement (POCI-01-0145-FEDER-007728, POCI-01-0145-FEDER-007728 and LISBOA-01-0145-FEDER-007344).

I acknowledge Professor Joaquim Sampaio Cabral for receiving me in the Institute for Bioengineering and Biosciences (iBB) group, allowing me to conduct my PhD core experimental work, as well as Professor Isabel Sá Correia for accepting me in the PhD Program of Biotechnology and Biosciences, at Instituto Superior Técnico (IST).

Most of all, I would like to thank my supervisor Doctor Nídia Lourenço, principal investigator of the main research projects that provided a solid ground for the development of my PhD work. Thank you for guiding me through this challenge, as well as for the trust and opportunities to share my PhD results from Portugal to Australia. Your optimism and enthusiasm are contagious and encouraged me to keep this PhD rolling.

A special thanks to my co-supervisor Professor Helena Pinheiro for the essential scientific guidance, professionalism and kindness. Thank you for the availability, dedication and encouragement in crucial moments of this PhD. Your keen eye for detail is priceless. Also, I would like to thank my co-supervisor Professor Mark van Loosdrecht for the expert advice provided in key meetings as well as for contributing to Chapter II with invaluable insights regarding future perspectives for the AGS technology. Your innovative research in wastewater treatment bioprocesses is truly inspiring.

I am grateful to Doctor Ana Mata for sharing her experience and teaching me all the practical details regarding the operation and monitoring of AGS bioreactors. I also thank Manuela Moreira for all the instructions regarding laboratory techniques and procedures.

The experimental results that are here described were obtained with the help of very dedicated master students and research fellows. I would like to thank Joana Ortigueira, João Bento, João Silva, Kateřina Rádlová, Marta Rodrigues, Miguel Coelho, Pedro Silva, Regina Rosa and Sofia Sousa for the extra motivation and tireless help in the operation and monitoring of the bioreactors. Thank you all for your engagement and commitment in this special “bioreactor co-parenting”.

I would like to thank Anabela Vieira, Catarina Carvalho and Doctor Gilda Carvalho, who conducted the FISH analyses presented in this thesis. In addition, I am also grateful to Anabela who played a major role in the study presented in Chapter IX, namely in the bacterial isolation and decolorization screening assays. Thank you, Anabela, for the dedicated guidance and joyful collaboration through the work we developed with pure cultures at iBET (Chapter IX). In the context of the same study, I thank Professor Teresa Crespo for allowing me to temporarily join the Microbiology of Man-Made Environments Laboratory, and Doctor Adrian Oehmen for producing the modelling data presented in Chapter IX. Moreover, I would like to further acknowledge Doctor Gilda Carvalho and Doctor Adrian Oehmen for the guidelines and advices shared during crucial meetings.

A special thanks to Doctor Conceição Oliveira and Ana Dias, who conducted the mass spectrometry analyses presented in Chapter VIII. Thank you, Doctor Conceição Oliveira, for accepting to supervise me under the scope of the Advanced Experimental Techniques course, for the guidance through the technique and kind availability to clarify me during data interpretation. I would like to thank Doctor Teresa Pinheiro for conducting the elemental distribution analyses presented in Chapter VI, as well as for the availability to discuss the results. Also, I greatly appreciate the help of Srdjana Kolakovic with the solid-phase extraction system, employed during the study presented in Chapter VIII.

I also acknowledge Royal HaskoningDHV and SIMTEJO for kindly providing the AGS and CAS (Frielas and Chelas wastewater treatment plants, Portugal) used as inocula for the bioreactors operated in this work.

I would like to extend my gratitude to Isabel Marques for all the assistance with paperwork-related issues, as well as to Dona Rosa for her dedication in taking good care of the laboratory material in the washing room. Also, a special thanks to Sara Rosa and colleagues in the neighbouring laboratory for the good work environment and prompt help.

In addition to all the above mentioned students and research fellows, I would like to extend my gratitude to everyone else from the “environmental lab family” for creating such a great work environment, namely Bárbara Abreu, Carolina Almeida, Celso Gonçalves, Daniel Saraiva, Joana Duarte, João Magalhães, Laura Mager, Lília Alexandre, Renata Ferreira, Rita Silva, Rui Fragoso and Tomáš Pánek. Cheers to the joyful moments we shared together, thank you for your friendship and for the dedicated and delicious vegan birthday cakes.

Finally, I would like to mention all the love and support from my family, Pedro Biscaia and close friends, who played an essential role in helping me to reach my goals. Above all, I am grateful to my mother for the constant love, endless care and for teaching me to always look at the bright side.

Thank you all,

Rita Franca

# List of abbreviations

| | |
|---|---|
| 1N2A4S | 1-naphthol-2-amino-4-sulfonic acid |
| 4A1NS | 4-amino-naphthalene-1-sulfonic acid |
| AG | aerobic granules |
| AgNP | silver nanoparticles |
| AGS | aerobic granular sludge |
| AHL | N-acylhomo-serine lactones |
| AI-2 | autoinducer-2 |
| AOB | ammonia-oxidizing bacteria |
| AOP | advanced oxidation processes |
| AR14 | acid red 14 |
| ATU | allylthiourea |
| BOD | biochemical oxygen demand |
| c-di-GMP | cyclic-dimeric-guanosine monophosphate |
| Ca/P | calcium-to-phosphorus ratio |
| CAS | conventional activated sludge |
| Cy3 | cyanine 3 |
| Cy5 | cyanine 5 |
| COD | chemical oxygen demand |
| DO | dissolved oxygen |
| ENP | engineered nanoparticles |
| EPS | extracellular polymeric substances |
| ESI | electrospray ionization |
| F/M | food-to-microorganism ratio |
| FISH | fluorescence *in situ* hybridization |
| FITC | fluorescein isothiocyanate |
| GAO | glycogen-accumulating organisms |
| GC | gas chromatography |
| H/D | height-to-diameter ratio |

| | |
|---|---|
| HPLC | high-performance liquid chromatography |
| HRMS/MS | high resolution tandem mass spectrometry |
| HRT | hydraulic retention time |
| IPS | intracellular polymeric substances |
| LB-EPS | loosely bound-extracellular polymeric substances |
| LC | liquid chromatography |
| LLE | liquid-liquid extraction |
| *m/z* | mass-to-charge ratio |
| MS | mass spectrometry |
| $MS^2$ | sequential mass spectrometry |
| MS/MS | tandem mass spectrometry |
| N/COD | nitrogen-to-chemical oxygen demand ratio |
| $NH_4$-N | ammonia-nitrogen |
| NMR | nuclear magnetic resonance |
| NOB | nitrite-oxidizing bacteria |
| OD | optical density |
| OLR | organic loading rate |
| ORP | oxidation-reduction potential |
| OUR | oxygen uptake rate |
| OTU | operational taxonomic unit |
| P/COD | phosphorus-to-chemical oxygen demand ratio |
| PAO | polyphosphate-accumulating organisms |
| PBS | phosphate-buffered saline |
| PHA | polyhydroxyalkanoates |
| PN | extracellular proteins |
| PS | extracellular polysaccharides |
| PVP | polyvinylpyrrolidone |
| ROS | reactive oxygen species |
| RT | retention time |
| SBBGR | sequencing batch biofilter granular reactor |

| | |
|---|---|
| SBR | sequencing batch reactor |
| SPE | solid-phase extraction |
| SRT | sludge retention time |
| SVI | sludge volume index |
| TB-EPS | tightly bound-extracellular polymeric substances |
| TDS | total dissolved solids |
| TIC | total ion chromatogram |
| $TiO_2$-NP | titanium dioxide nanoparticles |
| TSS | total suspended solids |
| TWW | textile wastewater |
| UASB | upflow anaerobic sludge blanket |
| UV | ultraviolet |
| VSS | volatile suspended solids |
| VFA | volatile fatty acids |
| WWTP | wastewater treatment plant |
| YE | yeast extract |
| ZnO-NP | zinc oxide nanoparticles |

# Table of contents

Resumo ..... i
Abstract ..... iii
Acknowledgements ..... v
List of abbreviations ..... vii
Table of contents ..... xi
I. Introduction ..... 3
I.1. Context and relevance of the thesis subject ..... 3
I.2. Objectives of the thesis ..... 3
I.3. Outline of the thesis ..... 3
II. Literature review ..... 9
II.1. Stability of aerobic granular sludge (AGS) during long-term bioreactor operation ..... 11
II.1.1. Context and objective ..... 11
II.1.2. Introduction ..... 11
II.1.2.1. Conventional activated sludge ..... 11
II.1.2.2. AGS ..... 12
II.1.2.3. Aerobic granulation process ..... 14
II.1.2.4. AGS technology application ..... 16
II.1.2.5. AGS process limitations ..... 17
II.1.3. Operational conditions and the stability of aerobic granules (AG) ..... 19
II.1.3.1. Organic loading rate ..... 19
II.1.3.2. Biomass loading rate ..... 23
II.1.3.3. Substrate type ..... 23
II.1.3.4. Carbon-to-nitrogen ratio ..... 25
II.1.3.5. Aeration rate ..... 25
II.1.3.6. Toxic substances ..... 26
II.1.3.7. Intermittent feast-famine and aerobic and non-aerated conditions ..... 27
II.1.3.8. Temperature ..... 29
II.1.4. Stability-related properties of AG ..... 29
II.1.4.1. Granule size and filamentous organisms ..... 29
II.1.4.2. Maximal growth rate of the microbial population ..... 33
II.1.4.3. Microbial growth in the granule core ..... 35
II.1.4.4. Extracellular polymeric substances composition ..... 35
II.1.4.5. Quorum-sensing ..... 37
II.1.4.6. Mineral complexes and precipitates ..... 38
II.1.5. Practical solutions to improve long-term stability of AG ..... 39
II.1.5.1. Selective sludge discharge ..... 39

II.1.5.2. Feeding regimen ..... 41
II.1.5.3. Aeration rate adjustment ..... 44
II.1.5.4. Alternative strategies ..... 44
II.1.6. Concluding remarks and perspectives ..... 45
II.2. AGS application to textile wastewater (TWW) treatment ..... 47
II.2.1. Context and objective ..... 47
II.2.2. Introduction ..... 49
II.2.2.1. Textile industry demand, pollution and water consumption ..... 49
II.2.2.2. Textile industry wastewater ..... 50
II.2.2.2.1. Emission volumes ..... 50
II.2.2.2.2. Composition ..... 50
II.2.2.2.3. Discharge limits and environmental impact ..... 52
II.2.2.3. Textile dyes – Characteristics, presence in TWW and environmental impact ..... 53
II.2.2.4. Azo dyes ..... 54
II.2.2.4.1. Characteristics ..... 54
II.2.2.4.2. Aromatic amines and environmental hazard ..... 55
II.2.2.4.3. Treatment solutions ..... 55
II.2.2.4.3.1. Physicochemical processes ..... 56
II.2.2.4.3.2. Biological processes ..... 56
II.2.2.4.3.3. Combined processes ..... 58
II.2.2.4.4. Azo dye decolorization by bacteria ..... 59
II.2.2.4.4.1. Proposed mechanisms ..... 59
II.2.2.4.4.2. Efficiency factors ..... 61
II.2.2.5. Azo dye-laden TWW treatment in bacterial systems ..... 62
II.2.2.5.1. Anaerobic-aerobic treatment systems for azo dye biodegradation ..... 62
II.2.2.5.2. Aerobic biodegradation of aromatic amines ..... 63
II.2.2.5.2.1. General aspects ..... 63
II.2.2.5.2.2. Proposed mechanism for aromatic amines biodegradation ..... 64
II.2.2.5.2.3. Autoxidation of aromatic amines ..... 64
II.2.2.5.2.4. Fate of sulfonated aromatic amines in anaerobic-aerobic bioreactors ..... 65
II.2.2.6. Engineered nanoparticles (ENP) in the textile industry ..... 72
II.2.2.6.1. Characteristics and application ..... 72
II.2.2.6.2. Environmental and health concerns ..... 72
II.2.2.6.3. Fate in wastewater treatment plants (WWTPs) ..... 73
II.2.2.7. Silver nanoparticles (AgNP) ..... 74
II.2.2.7.1. Characteristics and consumption ..... 74
II.2.2.7.2. Antimicrobial mechanisms ..... 75

II.2.2.7.3. Release into the environment ..... 76
II.2.2.7.4. Fate in WWTPs ..... 77
II.2.2.7.5. Effect in WWTPs ..... 80
II.2.3. TWW treatment in AGS sequencing batch reactor (SBR) systems ..... 83
II.2.3.1. Removal of textile dyes by AGS ..... 83
II.2.3.2. Removal of ENP by AGS ..... 97
II.2.4. Concluding remarks and perspectives ..... 102
III. Effect of an azo dye on the performance of an AGS SBR treating a simulated TWW ..... 105
III.1. Abstract ..... 107
III.2. Introduction ..... 107
III.3. Materials and methods ..... 108
III.3.1. Chemicals ..... 108
III.3.1.1. Carbon source and dye stock solutions ..... 108
III.3.1.2. Synthetic wastewater composition ..... 109
III.3.2. SBR setup and operation ..... 109
III.3.3. Analytical methods ..... 110
III.3.3.1. Physicochemical parameters ..... 110
III.3.3.2. Microbial community characterization ..... 111
III.3.3.2.1. Fluorescence *in situ* hybridization (FISH) analysis and quantitative FISH ..... 111
III.3.3.2.2. Microbial community analysis ..... 112
III.3.3.2.2.1. Library preparation and DNA sequencing ..... 112
III.3.3.2.2.2. Bioinformatic processing ..... 114
III.4. Results ..... 114
III.4.1. AGS morphology and properties ..... 114
III.4.1.1. Granule size and settling properties ..... 114
III.4.1.2. AGS morphology ..... 116
III.4.2. Microbial community dynamics ..... 116
III.4.2.1. FISH analysis ..... 116
III.4.2.2. Microbial community analysis ..... 118
III.4.3. AGS SBR treatment performance ..... 121
III.4.3.1. Biomass inventory ..... 121
III.4.3.2. Anaerobic and overall chemical oxygen demand (COD) removal ..... 122
III.4.3.3. Azo dye biodegradation ..... 123
III.4.3.4. Oxidation-reduction potential profile ..... 126
III.5. Discussion ..... 127
III.5.1. Effect of the azo dye on AGS long-term stability ..... 127
III.5.2. AGS SBR treatment performance ..... 130

III.5.2.1. COD removal ..... 130
III.5.2.2. Azo dye biodegradation ..... 131
III.6. Conclusions ..... 134
IV. Comparing AGS reactivation and operation performance in two SBR hydrodynamic regimens treating a synthetic TWW ..... 137
IV.1. Abstract ..... 139
IV.2. Introduction ..... 139
IV.3. Materials and methods ..... 140
IV.3.1. Feed components ..... 140
IV.3.2. SBR setup and operation ..... 140
IV.3.3. Analytical methods ..... 141
IV.4. Results and discussion ..... 141
IV.4.1. AGS morphology and properties ..... 141
IV.4.2. AGS SBR treatment performance ..... 143
IV.4.2.1. Biomass inventory and sludge age ..... 143
IV.4.2.2. COD removal performance ..... 144
IV.4.2.3. Azo dye biodegradation performance ..... 145
IV.4.3. Microbial community dynamics ..... 146
IV.5. Conclusions ..... 151
V. Effect of SBR feeding strategy and feed composition on the stability of AGS in the treatment of a simulated TWW ..... 153
V.1. Abstract ..... 155
V.2. Introduction ..... 155
V.3. Materials and methods ..... 156
V.3.1. Chemicals ..... 156
V.3.2. SBR setup and operation ..... 156
V.3.3. Analytical methods ..... 157
V.4. Results and discussion ..... 158
V.4.1. Biomass inventory and AGS properties ..... 158
V.4.2. Color and carbon load removal performance ..... 160
V.4.3. Azo dye biodegradation and metabolite formation ..... 163
V.4.4. Microbial community dynamics ..... 164
V.5. Conclusions ..... 168
VI. Comparing hydrodynamic regimens in TWW treatment with AGS: granulation, stability and reactivation ..... 171
VI.1. Abstract ..... 173
VI.2. Introduction ..... 174
VI.3. Materials and methods ..... 176

VI.3.1. Chemicals ..... 176
VI.3.2. SBR setup and operation ..... 176
VI.3.3. Analytical methods ..... 178
VI.4. Results ..... 179
VI.4.1. AGS morphology and properties ..... 179
VI.4.1.1. Granule size and settling properties ..... 179
VI.4.1.2. AGS morphology ..... 182
VI.4.1.3. Elemental distribution in AG ..... 184
VI.4.2. AGS SBR treatment performance ..... 188
VI.4.2.1. Biomass inventory ..... 188
VI.4.2.2. Anaerobic and overall COD removal ..... 191
VI.4.2.3. Azo dye biodegradation ..... 194
VI.4.2.3.1. Color removal ..... 194
VI.4.2.3.2. Fate of aromatic amines ..... 196
VI.4.2.3.3. Nitrate *versus* azo dye reduction ..... 203
VI.4.3. Microbial community dynamics ..... 205
VI.4.3.1. FISH analysis ..... 205
VI.4.3.2. Microbial community analysis ..... 207
VI.5. Discussion ..... 209
VI.5.1. AGS morphology and properties ..... 209
VI.5.1.1. Granulation and AG size ..... 209
VI.5.1.2. AGS stability ..... 211
VI.5.1.3. AGS reactivation ..... 212
VI.5.1.4. Dye-shock load and nitrate supplementation ..... 213
VI.5.2. AGS SBR treatment performance ..... 214
VI.5.2.1. Organic load removal ..... 214
VI.5.2.2. Azo dye biodegradation ..... 216
VI.5.2.2.1. Color removal ..... 216
VI.5.2.2.2. Nitrate *versus* azo dye reduction ..... 217
VI.5.2.2.3. Fate of aromatic amines ..... 218
VI.6. Conclusions ..... 221
VII. Impact of AgNP on long-term operation of an AGS SBR for TWW treatment ..... 225
VII.1. Abstract ..... 227
VII.2. Introduction ..... 228
VII.3. Materials and methods ..... 229
VII.3.1. Chemicals ..... 229
VII.3.2. SBR setup and operation ..... 229

VII.3.3. Analytical methods ..... 230
VII.4. Results ..... 231
VII.4.1. AGS morphology and properties ..... 231
VII.4.1.1. Granule size and settling properties ..... 231
VII.4.1.2. AGS morphology ..... 234
VII.4.2. AGS SBR treatment performance ..... 235
VII.4.2.1. Biomass inventory ..... 235
VII.4.2.2. Anaerobic and overall COD removal ..... 239
VII.4.2.3. Azo dye biodegradation ..... 242
VII.4.2.3.1. Color removal ..... 242
VII.4.2.3.2. Fate of aromatic amines ..... 244
VII.4.3. Microbial community dynamics ..... 248
VII.4.3.1. FISH analysis ..... 248
VII.4.3.2. Microbial community analysis ..... 249
VII.5. Discussion ..... 251
VII.5.1. AGS morphology and properties ..... 251
VII.5.2. AGS SBR treatment performance ..... 255
VII.5.2.1. Anaerobic and overall COD removal ..... 255
VII.5.2.2. Azo dye biodegradation ..... 256
VII.5.3. Microbial community dynamics ..... 257
VII.6. Conclusions ..... 259
VIII. Biodegradation products of a sulfonated azo dye in AGS SBRs treating a simulated TWW ..... 263
VIII.1. Abstract ..... 265
VIII.2. Introduction ..... 265
VIII.2.1. Context and aim of this work ..... 265
VIII.2.2. Liquid chromatography-mass spectrometry (LC-MS) application to TWW samples ..... 266
VIII.3. Materials and methods ..... 270
VIII.3.1. SBR setup and operation ..... 270
VIII.3.2. Sample selection ..... 270
VIII.3.3. Sample pre-treatment ..... 271
VIII.3.4. Liquid chromatography-sequential mass spectrometry (LC-$MS^2$) ..... 272
VIII.3.5. Liquid chromatography-tandem high resolution mass spectrometry (LC-HRMS/MS) ..... 272
VIII.4. Results and discussion ..... 273
VIII.4.1. LC-MS analysis ..... 273
VIII.4.2. LC-HRMS/MS analysis ..... 276
VIII.5. Conclusions ..... 282

IX. *Oerskovia paurometabola* isolated from a laboratory mixed culture treating a simulated TWW efficiently decolorizes azo dye Acid Red 14 with further aerobic aromatic amine conversion ..... 285
IX.1. Abstract ..... 287
IX.2. Introduction ..... 287
IX.3. Materials and methods ..... 289
IX.3.1. Chemicals and synthetic TWW ..... 289
IX.3.2. Isolation and identification of bacterial strains with decolorization capacity ..... 289
IX.3.3. Screening of azo dye decolorizing bacteria ..... 290
IX.3.4. Growth assays of a selected bacterial isolate ..... 290
IX.3.5. Decolorization assays with a selected bacterial isolate ..... 290
IX.3.6. Abiotic assay with a selected bacterial isolate ..... 291
IX.3.7. Modelling of Acid Red 14 (AR14) decolorization by a selected bacterial isolate ..... 291
IX.4. Results and discussion ..... 292
IX.4.1. Decolorization capacity screening of bacterial isolates ..... 292
IX.4.2. Aerobic and anaerobic growth profiles of *Oerskovia paurometabola* ..... 295
IX.4.3. Azo dye biodegradation by *Oerskovia paurometabola* ..... 296
IX.4.3.1. Decolorization performance ..... 296
IX.4.3.2. Azo dye metabolite fate ..... 297
IX.4.4. Modelling of AR14 decolorization by *Oerskovia paurometabola* ..... 300
IX.5. Conclusions ..... 301
X. Conclusions and Perspectives ..... 303
X.1. Conclusions ..... 305
X.2. Final remarks and perspectives ..... 308
References ..... 313
Appendices ..... 339
Appendix A – Supporting Information for Chapter III ..... 341
Appendix B – Supporting Information for Chapter IV ..... 345
Appendix C – Supporting Information for Chapter V ..... 348
Appendix D – Supporting Information for Chapter VI ..... 350
Appendix E – Supporting Information for Chapter VII ..... 360
Appendix F – Supporting Information for Chapter VIII ..... 367
F.VIII.1. Sample pre-treatment optimization ..... 367
F.VIII.2. LC conditions optimization ..... 373
F.VIII.3. LC-MS analysis of AR14 commercial product ..... 376
F.VIII.4. Correlation between metabolites detected by LC-MS and HPLC ..... 377
F.VIII.5. Summary of results obtained in LC-$MS^2$ analysis ..... 379
F.VIII.6. Fragmentation patterns according to LC-HRMS/MS analysis ..... 379
F.VIII.7. LC-HRMS/MS results: ion chromatograms, MS and MS/MS spectra ..... 385

Appendix G – Scientific publications and communications ..... 391
List of publications ..... 391
List of oral communications ..... 392
List of poster communications ..... 392

# I. Introduction

## I.1. Context and relevance of the thesis subject

Textile industry wastewaters represent a major source of pollution worldwide, carrying high organic loads, recalcitrant dyes and, more recently, engineered nanoparticles (ENP), namely silver nanoparticles (AgNP), which are increasingly used by the textile industry for their antimicrobial properties, despite their effect and fate in wastewater treatment systems being unknown. In addition to compromising aquatic life by reducing sunlight penetration in water, azo dyes (*ca*. 80% of the textile dyes used) can generate potentially toxic and carcinogenic breakdown products, *e.g.*, aromatic amines. Based on the bacteria capacity to remove the color by anaerobically reducing azo dyes, and to potentially aerobically oxidize the resulting aromatic amines, anaerobic-aerobic sequencing batch reactors (SBRs) have been proposed as an economic and environmentally friendly alternative to physicochemical dye removal processes.

Recent studies proposed the treatment of textile wastewater (TWW) using the sustainable and cost-effective aerobic granular sludge (AGS) SBR technology, regarded as the upcoming new standard for biological treatment of domestic and industrial wastewaters. Operation of SBRs with AGS, composed of aerobic granules (AG; dense, compact, self-immobilized microbial aggregates), allows better sludge-water separation, and thereby higher biomass concentration and sludge retention time (SRT) values than conventional activated sludge (CAS). The AG structure allows the co-existence of different microenvironments (anaerobic/anoxic/aerobic) and diverse microbial populations, as well as a higher resistance towards high organic loads and toxic compounds. These factors strongly motivate the application of AGS technology to TWW treatment, although few studies have addressed this opportunity so far. In addition, despite the relevant advances regarding the process of AGS formation from CAS (aerobic granulation), sustaining AG structural stability during long-term operation is a current technological challenge.

## I.2. Objectives of the thesis

The present thesis aimed to contribute for the development of an effective TWW treatment bioprocess using the novel AGS technology. Four specific objectives were established, focusing on the main environmental problems raised by TWW: 1) assess the applicability of AGS in the treatment of dye-containing TWW in an anaerobic-aerobic SBR; 2) optimize the SBR hydrodynamic regimen, with emphasis on granulation and decolorization; 3) assess the potential aerobic biodegradation of aromatic amines and 4) evaluate the fate of AgNP in the AGS system, including their effects on aerobic granulation and treatment performance.

## I.3. Outline of the thesis

This thesis contains ten chapters.

Chapter I is intended to present the general context and relevance of the scientific research developed, as well as to specify the main objectives and to give an overview of the thesis structure. In the context of the thesis, Chapter II presents an up-to-date review of the literature focusing on two main subjects: 1) AGS stability, aiming to contribute to the identification of crucial factors for promoting long-term stability of AG and to a better understanding of the underlying mechanisms; 2) AGS application to TWW treatment, providing a review of the available studies foccused on this specific application, particularly regarding the removal of organic load, textile dyes and aromatic amines, as well as nanoparticles from wastewater. Chapters III to IX present the experimental work, its results and the respective discussion. Finally, Chapter X brings together the main conclusions of this work and draws perspectives for future work. After the references list, the scientific output resulting from this doctoral work are listed at the end of the appendices section.

Regarding the seven chapters dedicated to the experimental work, Figure I.1 gives a detailed representation of the different tested scenarios regarding the application of AGS for the treatment of a simulated TWW. Specifically, 5 experimental runs were conducted using non-tubular 1.5-L SBRs (2.5 of height-to-diameter ratio, H/D) operated with 6-h cycles. The SBRs were generally fed with a synthetic TWW containing a starch-based carbon source corresponding to a sizing agent commercially used in the cotton textile industry, a model azo dye (Acid Red 14, AR14), pH buffering phosphates and nutrients. AGS SBR performance was monitored through several analyses and biomass samples were stored for subsequent microbial population analysis.

The aim of the first experiment (Chapter III) was to analyze the effect of an azo dye on the performance of an anaerobic-aerobic AGS SBR system in the treatment of a synthetic TWW. Two SBRs were inoculated with AGS from a domestic wastewater treatment plant (WWTP), SBR1 being used as a dye-free control, and run for 102 days. Both reactors had a 18-min static feeding, a 1.5-h mixed anaerobic phase, and a 3.5-h aerobic phase, followed by 5 min of settling, 1 min of drain and an idle period. The SRT value was controled on a specific period and the capacity of the system to deal with shocks of high dye concentration and organic load was tested at the end of the operation.

The biomass from the dye-fed SBR operated in the first experiment was stored for 6.5 months and used to inoculate two new SBRs to conduct a second experiment aiming to study the effect of the hydrodynamic regimen on AGS reactivation performance (Chapter IV). While SBR1 was operated under the same conditions as the previous dye-fed SBR, SBR2 had a 2-h plug-flow feeding period and no anaerobic mixed phase.

After 80 days of operation the AGS from each SBR was stored for 2.5 months and used to re-inoculate the respective SBR, a mixed anaerobic phase being introduced in SBR2 after the plug-flow feeding stage in order to optimize the decolorization performance (Chapter V). This experimental run lasted 315 days to assess the effect of the hydrodynamic regimen on AGS stability and SBR performance,

namely when dealing with dye and organic shock loads, as well as variations in the carbon source type.

These two hydrodynamic regimens were further compared in a fourth study (Chapter VI), regarding AGS stability and treatment performance during aerobic granulation, long-term operation and reactivation after an idle period. These factors were analyzed in two experimental runs, initiated with the inoculation of two SBRs with CAS from a domestic WWTP. The experimental run I (404 days, including a 40-day idle period) focused on the optimization of the cycle conditions, and the experimental run II (434 days, including an 18-day idle period) focused on the synthetic TWW composition, specifically on the effect of azo dye shock loads, supplementation with AgNP and nitrate.

A fifth study (Chapter VII) was conducted in parallel to the fourth specifically to assess the impact of AgNP on TWW treatment performance in anaerobic-aerobic AGS SBRs during long-term operation, including aerobic granulation and AGS reactivation after idle periods. The experimental run II tested twice the AgNP concentration applied during the experimental run I, an AgNP-free SBR being used as a control. In addition, after an AgNP clean-up period, the effect of nitrate in the azo dye biodegradation performance was also analyzed at the end of the experimental run II.

Aiming to further investigate the fate of the azo dye breakdown products during the aerobic phase, specific treatment cycles from the fourth study were further examined by mass spectrometry, the results being presented in a separate chapter (Chapter VIII).

Finally, a promising bacterial strain for azo dye biodegradation applications was isolated from an anaerobic-aerobic SBR treating the synthetic TWW and further characterized, the results being presented in Chapter IX.

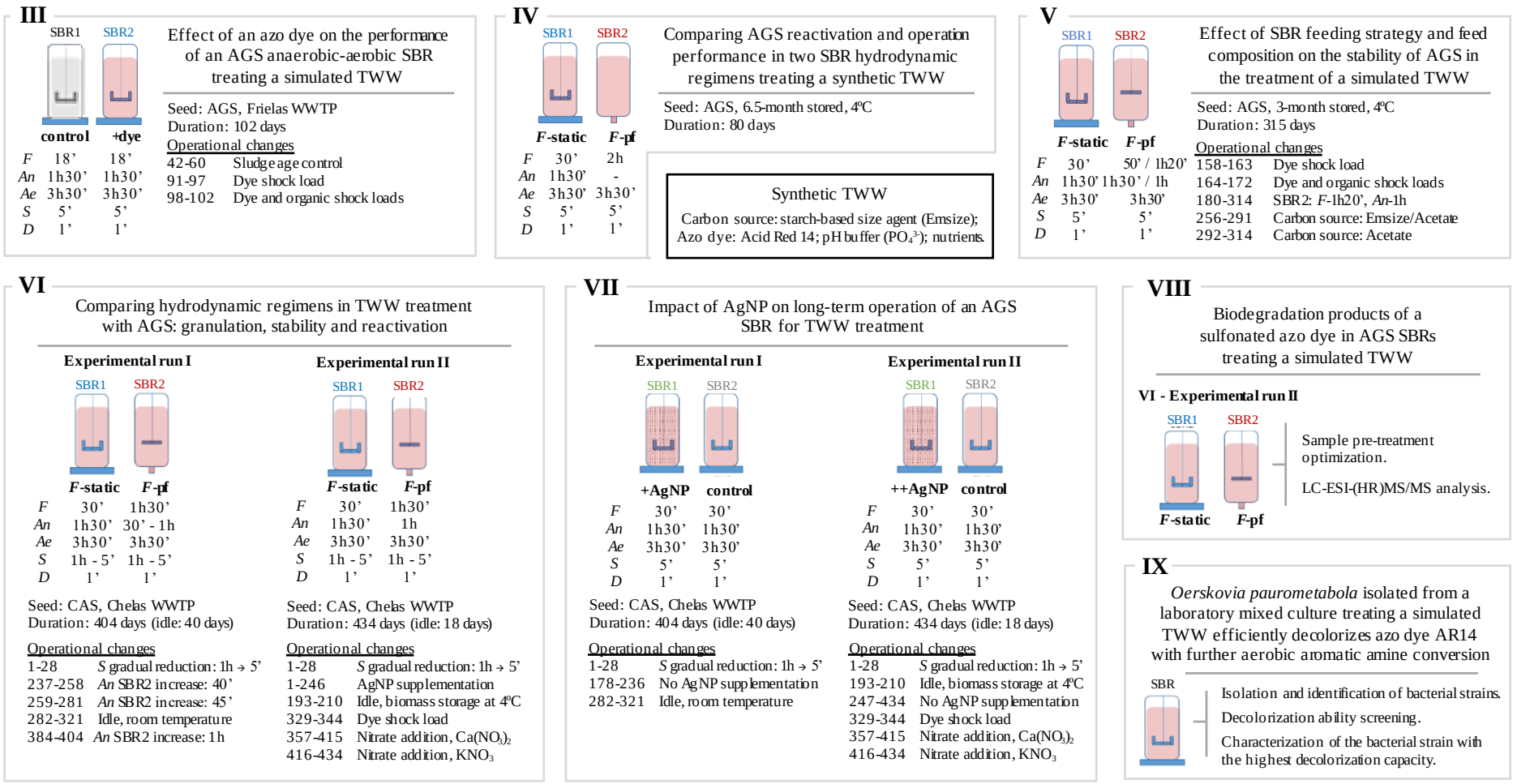


**Figure I.1 -** Schematic representation of the experimental work decribed in Chapters III-IX, with indication of the general composition of the synthetic textile wastewater (TWW) used, the sequencing batch reactors (SBRs) cycle time periods (F – Feeding phase, An – Stirred anaerobic phase; Ae – Aerobic phase; S – Settling phase; D – Drain phase) and operational conditions. AgNP: silver nanoparticles; AGS: aerobic granular sludge; AR14: Acid Red 14; CAS: conventional activated sludge; LC-ESI-(HR)MS/MS: liquid chromatography coupled with electrospray ionization (high resolution) tandem mass spectrometry; pf: plug-flow; WWTP: wastewater treatment plant.

# II. Literature review

The information included in this chapter was partially published in:

Franca, R.D.G., Pinheiro, H.M., van Loosdrecht, M.C.M., Lourenço, N.D., 2018. Stability of aerobic granules during long-term bioreactor operation. *Biotechnology Advances* 36, 228-246. DOI: 10.1016/j.biotechadv.2017.11.005.

## II.1. Stability of aerobic granular sludge (AGS) during long-term bioreactor operation

### II.1.1. Context and objective

AGS technology has been extensively studied over the past 20 years and is regarded as the upcoming new standard for biological treatment of domestic and industrial wastewaters. AG are dense, compact, self-immobilized microbial aggregates that allow better sludge-water separation and thereby higher biomass concentrations in the bioreactor than CAS aggregates. This brings potential practical advantages in terms of investment cost, energy consumption and footprint. Following the successful scale-up of the AGS technology for municipal wastewater treatment, future directions include application of this innovative process to a wider range of wastewaters, specifically from industrial sources. However, this type of effluent would normally impose a variable feed composition and high loading rates on the bioreactor, which, to some extent, have been shown to affect the stability of AG (Long *et al*., 2015). Furthermore, recent efforts have been made to operate AGS in continuous-flow reactors, widely used in WWTPs, but stability of AG has been shown to be impaired under this continuous-flow regimen (Juang *et al.*, 2010; Liu *et al.*, 2012). Overall, despite the relevant advances regarding the process of AG formation, instability of AG during long-term operation is still seen as a major barrier for a broad practical application of this technology.

This chapter presents an up-to-date review of the literature focusing on AG stability, aiming to contribute to the identification of key factors for promoting long-term stability of AG and to a better understanding of the underlying mechanisms. In this sense, biological and physicochemical characteristics of AG specifically related to their physical integrity are explored, and the operational conditions determinant to granule long-term stability are highlighted. Specifically, operational conditions leading to AG disintegration are described, including high organic loads, particulate substrates in the influent, toxic feed components, aerobic feeding and too short famine periods. These operational and influent wastewater composition conditions were shown to influence the microenvironment of AG, consequently affecting their stability. Granule stability is generally favored by the presence of a dense core, with microbial growth throughout the AG depth being a crucial intrinsic factor determining its structural integrity. Accordingly, possible practical solutions to improve granule long-term stability are described, namely through the promotion of minimal substrate concentration gradients and control of microbial growth rates within AG, including anaerobic, plug-flow feeding and specific sludge removal strategies.

### II.1.2. Introduction

#### II.1.2.1. Conventional activated sludge

Biological treatment of municipal and industrial wastewaters is considered the most environment-friendly and cost-effective way for removing organic compounds and nutrients, such as nitrogen and

phosphorus, from wastewater, as opposed to physicochemical methods (Lemaire *et al.*, 2008). In 2014, activated sludge-based technologies celebrated their 100$^{th}$ anniversary, still being the most widely used processes for the treatment of wastewaters.

The efficiency of CAS processes depends on the balance between two main types of bacteria: the floc-forming bacteria, which bond together mainly through the action of excreted extracellular polymeric substances (EPS), and the filamentous bacteria, which have been proposed as an attachment support for the former type of bacteria (Zhu *et al.*, 2015). Excess filamentous bacterial growth is usually detrimental to CAS systems as it commonly leads to operational disorders such as foaming in aeration tanks and sludge bulking in secondary settling tanks. In fact, a crucial step in the CAS treatment process is the secondary clarification, where the biomass is separated from the treated wastewater and concentrated to be recycled to the bioreactor, while ensuring a low concentration of suspended solids in the effluent.

During the last century, the CAS technology offered the possibility of protecting the water environment while providing an alternative water resource through reuse and recycling. However, due to the operational problems often encountered in CAS treatment systems, namely sludge bulking, new separation techniques for activated sludge have been developed, either by improving sludge settling properties or introducing alternative physical separation processes (*e.g.*, membrane bioreactors). On the other hand, research on biological wastewater treatment must nowadays be directed towards energy, water and resources recovery, as well as footprint reduction. In this sense, a significant part of this research has been focused on the development of compact systems, characterized by a greater capacity to reach high biomass concentrations. This has been achieved by growing biofilms adhered to solid supports (*e.g.*, in moving bed biofilm systems and fluidized bed or airlift reactors) or by enhancing the settling ability of the suspended biomass through cultivation in conditions inducing the formation of dense aggregates, best exemplified by the anaerobic granule bioreactors such as upflow anaerobic sludge blanket (UASB) reactors (Mosquera-Corral *et al.*, 2005).

### II.1.2.2. AGS

Recently, a new form of activated sludge has been cultured in aerated reactors: the AGS (Beun *et al.*, 1999; Morgenroth *et al.*, 1997). While in CAS systems microorganisms form small, irregular aggregates or flocs with sizes around 50-300 µm (Lemaire *et al.*, 2008), under specific operational conditions, larger, near-spherical aggregates with a compact and dense structure can be formed, constituting the so-called AG (Figure II.1). At the First Aerobic Granule Workshop, 2004 (Munich, Germany), AG were defined as “aggregates of microbial origin, which do not coagulate under reduced hydrodynamic shear, and which subsequently settle significantly faster than activated sludge flocs” (de Kreuk *et al.*, 2007). In fact, their large size and compact, dense structure provide AG with a high specific gravity, resulting in an outstanding settling ability, as indicated by sludge volume index (SVI)

measurements. Specifically, since it is an indicator of the extent of thickening after settling, the difference between the SVI values registered after 5 and 30 min of settling has been used to differentiate AGS from CAS. Additionally, a minimum aggregate size for AG was set at 0.2 mm, as a reference.

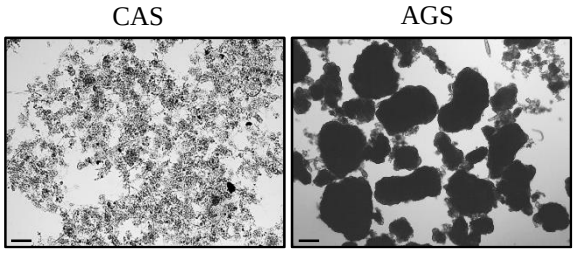


**Figure II.1 -** Microscopic images (magnification 40) of conventional activated sludge (CAS) and aerobic granular sludge (AGS). Scale bar = 0.2 mm.

Because AG are self-immobilized, dense aggregates mainly composed of bacteria and EPS, they can be considered as a special case of biofilm growth without carrier material (Beun *et al.*, 1999). The three-dimensional structure of AG creates dissolved oxygen (DO) and substrate concentration gradients along the radial direction, leading to stratification in layers of different types of microorganisms and metabolisms (L. Liu *et al.*, 2010). Accordingly, AG are generally regarded as a layered microbial structure (Figure II.2), made up of an aerobic outer layer, containing a mixture of heterotrophic and autotrophic organisms, and an anoxic or anaerobic core, where denitrifying and anaerobic organisms are present (Winkler *et al.*, 2013). These microenvironments thus enable the presence of different bacterial populations performing specific roles in the biodegradation of water pollutants, such as polyphosphate-accumulating organisms (PAO), and glycogen-accumulating organisms (GAO), as well as nitrifying and denitrifying bacteria (de Kreuk *et al.*, 2005a). As an advantage over conventional biofilm technology, where the surface area needed for mass transfer is limited by the reactor configuration or the support morphology, therefore determining conversion process rates, when biofilms are grown in granular shape a higher surface area per volume of biomass can be obtained (de Kreuk and van Loosdrecht, 2004).

Aerobic granular biomass offers many advantages over CAS systems (Adav *et al.*, 2008b). The good settleability of AGS allows higher biomass concentrations in the bioreactor and better sludge-water separation, thus favoring a compact reactor design, which can be operated batchwise without the need for a secondary settler. In addition, the high biomass retention capacity enhances the volumetric conversion capacity, thus enabling the system to handle high organic loading rates (OLRs; Maszenan *et al.*, 2011). Moreover, the wider range of possible operational SRT values allows the development of a more diverse microbial community in the system (Lourenço *et al.*, 2015), including slow-growing microorganisms, leading to lower sludge production rates than in CAS (Liu and Tay, 2007a).

At the microscopic level, the strong, compact and layered physical structure characteristic of AG is important to provide tolerance to high toxicity levels, as well as the capacity to withstand wide load variations and high-strength wastewaters, usually associated to the treatment of industrial effluents (Beun *et al.*, 2000; Liu and Tay, 2004). Due to microbial population stratification, and the simultaneous existence of anaerobic, aerobic and anoxic conditions within AG, removal of organic matter, nitrogen and phosphorus can be achieved in a single unit with high efficiencies (Figure II.2; Bassin *et al.*, 2012a; de Kreuk *et al.*, 2005a). In addition to the no longer necessary secondary settler, this feature potentially means that the need for multiple tanks and recirculation piping and pumps is avoided, thus significantly reducing the footprint, and the investment and operational costs of the WWTP (de Bruin *et al.*, 2004).

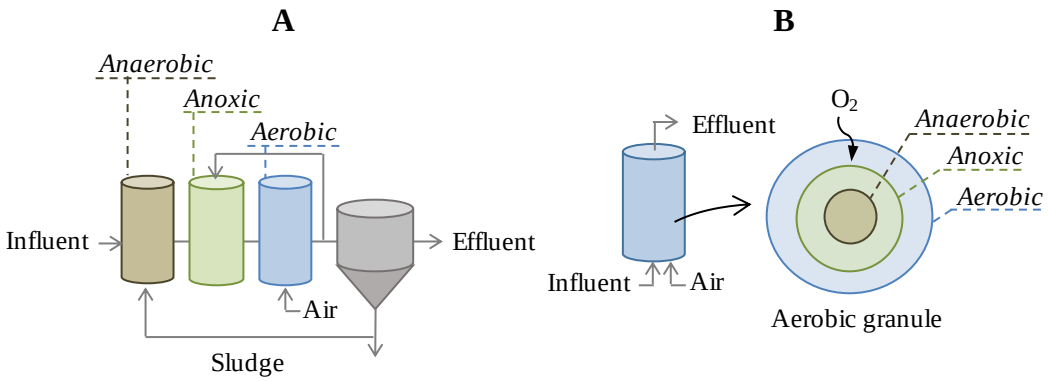


**Figure II.2** - Simplified schematic representation of the main operational units in the process of removing organic load, nitrogen and phosphorus from wastewater using A) conventional activated sludge or B) aerobic granular sludge (detail of the layered structure of an aerobic granule).

### II.1.2.3. Aerobic granulation process

Formation of AG, *i.e.*, aerobic granulation, is a complex physicochemical and biological process. Microbial self-immobilization is induced by environmental stress conditions, involving physical shear, physicochemical or biochemical interactions and microbial attraction mechanisms (Liu and Tay, 2002). Granulation using CAS as seed sludge was suggested to start from single colony outgrowth or aggregation of smaller colonies to form dense clusters, followed by outgrowth and further aggregation, with collisions between granules producing stable, dense granules of larger sizes. Considering that a variety of microbial species is able to form granules, granulation most likely depends on reactor operating conditions rather than on the presence of specific microbial groups (Beun *et al.*, 1999). Tay *et al.* (2001a) suggested that increased cell hydrophobicity, and consequently, enhanced cell-to-cell interaction, contribute for keeping the aggregated bacteria tightly together, although further research is still required to support this view.

Numerous studies have focused on understanding the molecular factors behind the formation of AG as well as on optimizing the reactor operating conditions promoting aerobic granulation. So far, AGS formation has been mainly achieved in SBRs (Show *et al.*, 2012). The operation of SBRs is based on a

fill-and-draw principle, consisting of five successive stages: fill, react, settle, draw, and idle. The characteristics of SBR operation, such as the batchwise regimen, the controllable regulation of sludge discharge and the uniform hydraulic shear forces, create an ideal environment for aerobic granulation (Figure II.3). Conversely, formation of AGS in continuous-flow reactors has been proven as difficult to achieve (Juang *et al.*, 2010).

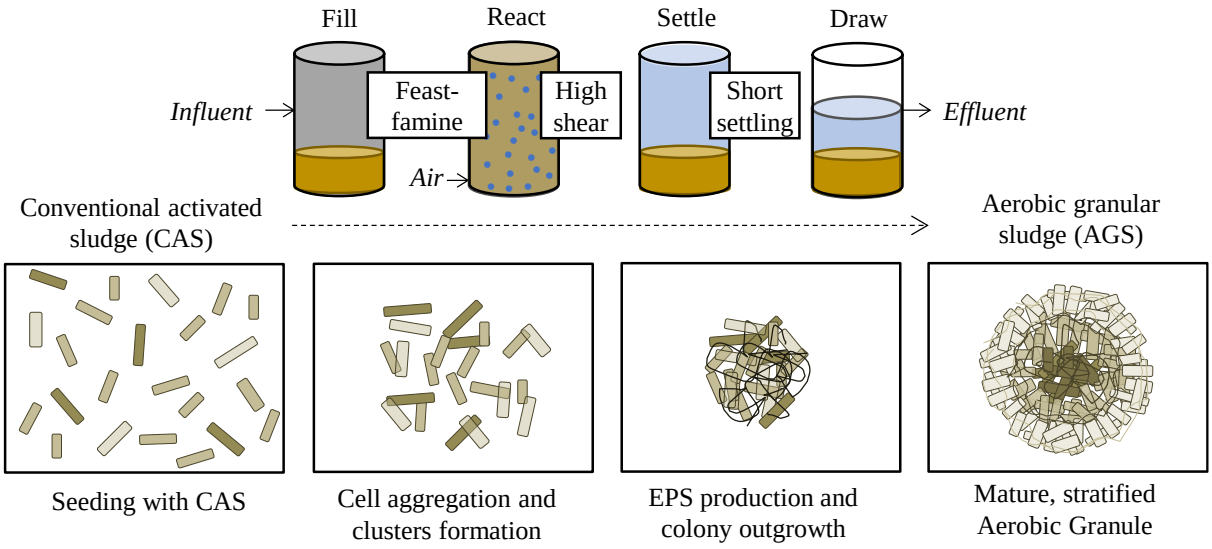


**Figure II.3 -** Schematic representation of sequencing batch reactor operational stages (operational conditions contributing for the formation of aerobic granular sludge are highlighted) and of the mechanisms involved in the aerobic granulation process.

Among the operational factors reported to influence the granulation process in SBRs are the selection pressure obtained through changing the allowed settling time (Beun *et al.*, 2000), the imposed hydraulic shear stress or superficial air velocities (Liu and Tay, 2002), periodic starvation times (Liu and Tay, 2008), hydraulic retention times (HRTs; Muda *et al.*, 2011), substrate composition and OLR (Gao *et al.*, 2011), DO levels (Sturm and Irvine, 2008), concentration of divalent ions (Adav *et al.*, 2008a; Show *et al.*, 2012), pH and temperature fluctuations (de Kreuk *et al.*, 2005b), and the type of seed sludge (Verawaty *et al.*, 2013).

Settling time control has been highlighted among these factors as an effective and strong selection pressure strategy to trigger initial granulation (Liu and Tay, 2004). Based on the higher settling rate of AGS in comparison with CAS, imposing a minimal settling velocity by gradually shortening the settling period in SBRs (*e.g.*, from 30 min to 3 min) has been used as a strategy to select fast-settling over slow-settling aggregates, since the latter are washed out from the system (Beun *et al.*, 2000). Moreover, periodical aerobic starvation was also described as an effective trigger for aerobic granulation (Tay *et al.*, 2001a), possibly by inducing EPS secretion, with a suggested positive effect on cell surface hydrophobicity (Liu and Tay, 2008; Wang *et al.*, 2006).

Regarding the role of hydraulic shear stress, Beun *et al.* (1999) found that a sufficiently high level of hydrodynamic shear force during aeration, together with oxygen stress (*i.e.*, a high DO concentration),

were favorable for aerobic granulation when using aerobic feeding of wastewater containing easily degradable chemical oxygen demand (COD). In addition to its role in shaping AG through promoting inter-particle collisions, a high shear force regimen has been proposed to induce EPS production, which is essential for AG formation (Liu and Tay, 2002; Tay *et al.*, 2001b). Results from a study aiming to differentiate the roles of shear force and DO on the formation of aerobically-fed AGS, indicated that DO played a more significant role than shear force, since AG could not be formed at DO levels below 5 mg $L^{-1}$, even under high shear force (Sturm and Irvine, 2008). Similarly, Mosquera-Corral *et al.* (2005) could not achieve stable granulation when oxygen saturation was reduced to 40%. On the other hand, de Kreuk and van Loosdrecht (2004) reported that the formation of dense AG was also possible at low DO concentrations, when conditions that select for slow-growing microorganisms were applied. In fact, a recent study (Pronk *et al.*, 2015a) showed that the anaerobic uptake of easily biodegradable substrates, prior to the aerobic reaction phase, and/or substrate conversion by relatively slow-growing bacteria during the aerobic period, are essential conditions to achieve stable granulation when using easily biodegradable COD. In this case, the selection of relatively slow-growing bacteria (de Kreuk *et al.*, 2005a) plays an equally or even more important role for attaining efficient granulation, when compared with the settling time-based selection strategy.

### II.1.2.4. AGS technology application

Research and development of AGS started around 1993 at the Delft University of Technology (TU Delft), with stable granulation being first reported in 1997 (Morgenroth *et al.*, 1997), and subsequent demonstration for the treatment of municipal wastewater (de Kreuk and van Loosdrecht, 2006). Since then, Royal HaskoningDHV, in collaboration with the Dutch waterboards and TU Delft, has engineered the process to suit commercial applications and developed the AGS technology commercially branded as Nereda® Technology (Inocêncio *et al.*, 2013). Since 2003, several pilot plants have been in operation for both industrial and municipal wastewater treatment and the first industrial full-scale Nereda® prototype was implemented in 2005 in The Netherlands. In parallel, the scale-up of the AGS technology for municipal applications resulted in two Nereda® demonstration plants (South Africa and Portugal), as well as in the design and construction of the full-scale Epe WWTP (The Netherlands) in 2010-2011. Compared to CAS systems, AGS-operated plants have demonstrated significant improvements with regard to footprint, process stability, effluent quality and energy savings (Inocêncio *et al.*, 2013). A recent report on the Garmerwolde full-scale AGS plant (The Netherlands) treating domestic wastewater since 2013 indicated that, following a 5-month start-up period, effluent requirements were met and the energy usage was 58-63% lower than the average CAS treatment plant in The Netherlands (Pronk *et al.*, 2015b). For these reasons, AGS technology is already considered the most important process breakthrough offspring of activated sludge. In fact, as highlighted during the IWA World Water Congress & Exhibition 2014, AGS technology is set to become the new standard for aerobic treatment of municipal and industrial wastewater.

### II.1.2.5. AGS process limitations

Despite the significant advances in the development of the AGS process, there are still challenging issues and relevant limitations to the broader application of this innovative technology, namely to the treatment of industrial wastewaters (Zhang *et al.*, 2016b). Long start-up periods and instability of the AG are regularly described as the main critical issues. The first issue has been extensively investigated over the last 20 years through the examination of the various factors influencing aerobic granulation, which has greatly improved the start-up time. However, the second issue remains unresolved, being considered a major constraint for practical application of the AGS technology, since it questions the possibility of a reliable and stable full-scale operation (Lee *et al.*, 2010; Show *et al.*, 2012; Zhang *et al.*, 2016b).

The stability concept for AGS is regarded as a null variation in the activity and size distribution of granules, as well as no occurrence of granule break-up and washout from reactors, in long-term operation. A large number of studies reported AG disintegration and washout in long-term operation, leading to high suspended solids concentrations in the treated effluent, treatment performance deterioration and, eventually, to the overall failure of the bioreactor system (Lee *et al.*, 2010; Wan *et al.*, 2013; Table II.1). So far, the mechanisms behind the loss of AGS stability have not been fully understood. Therefore, one of the current challenges to the success of AGS is to find the right conditions to maintain the structural stability of AG during long-term operation. Studies have shown that, similarly to granule formation, the stability of AGS is closely related to the bioreactor operating parameters (Show *et al.*, 2012). However, not all the operating conditions leading to the formation of AG are appropriate for their stability. For instance, although AG can be cultivated at different OLRs, they can gradually lose stability during long-term reactor operation at high OLR (Zheng *et al.*, 2006). In addition, Liu and Tay (2008) showed that although a short starvation time could speed up the formation of granules, this condition had a negative impact on the stability of AG. Furthermore, a recent study confirmed that the crucial conditions for aerobic granulation and AG stability maintenance might be different, and should be modulated to achieve fast granulation and long-term stability, respectively (Liu and Tay, 2015).

**Table II.1** - Operational conditions and respective effects at the aerobic granular level in studies reporting instability of aerobic granules. Ae: aerobic phase; An: anaerobic phase; COD: chemical oxygen demand; COD/N: COD-to-nitrogen ratio; $d_{AG}$: aerobic granule diameter; diss: dissolved; DO: dissolved oxygen; FQ: fluoroquinolones; H/D: height-to-diameter ratio; n.i.: not indicated; OLR: organic loading rate; SAV: superficial airflow velocity; SBAR: sequencing batch airlift reactor; SBR: sequencing batch reactor; Set: settling phase; SRT: sludge retention time; VFR: volumetric flow rate; WW: wastewater; ↑: increased; ↓: decreased.

| **WW, Substrate** | **OLR** (kgCOD $m^3$ $d^{-1}$) | **Reactor H/D** | **Reactor operation** (phase times in min) | **VFR** ($m^3$ $h^{-1}$) **SAV** (cm $s^{-1}$) **DO** (mg $L^{-1}$) | **SRT** (d) | **$d_{AG}$** (mm) | **Effects on AG stability** | **Reference** |
|---|---|---|---|---|---|---|---|---|
| Acetate | 4 | SBR 11.8 | ~ 150 d<br>4-h cycle; Fill 5; Ae 215-228; Set 2-5 | SAV: 1.2 | n.i. | Average 1.3 | - AG instability mainly due to the low DO during feast period, resulting from high biomass concentration. | Liu and Tay, 2007b |
| Acetate, COD/N: 8.3 | 1.6 | SBAR 13.9 | 230 d<br>3-h cycle; Fill 3; Ae 169; Set 3 | VFR: 24<br>SAV: 2.5<br>DO: 40-100% | 8-35 | Average 1.6<br>Filamentous outgrowth | - At low DO (40%), AG became small, with filamentous outgrowth and low density; AG disintegrated; impossible to obtain stable AG. | Mosquera-Corral *et al.*, 2005 |
| Acetate and propionate | 0.6 | SBR 4.1 | ~75 d<br>5-h cycle; Fill 5; An (mix) 90; Ae 120; Anoxic (mix) 60; Set 3-20 | VFR: 1.7<br>SAV: 0.6<br>DO: 5 | n.i. | Up to 1.4 | - Unstable AG when $d_{AG}$ > 1 mm.<br>- Disaggregation of large AG due to low substrate concentration and mass transfer limitation. | Zhang *et al.*, 2011 |
| Acetate, propionate, and sucrose | 1.7 | SBR 7.2 | 330 d<br>3-h cycle; Fill 60; Ae 114; Set 3 | SAV: 0.8-1.6<br>DO: 6-8 | 20 and 11 | Average 2.4 | - Long-term operation led to the accumulation of inorganic particles in AG (P-salts precipitation), causing instability of mature AG. | Isanta *et al.*, 2012 |
| Sucrose | 6 | SBR 15.7 | 85 d<br>4-h cycle; Fill (top) 10; Ae 220; Set 5-8 | SAV: 2.0<br>DO: 5 | 10-15 | Up to 16<br>Filamentous outgrowth | - When filamentous AG reached 16 mm, AG disintegrated and were washed out; reactor failure. | Zheng *et al.*, 2006 |
| Acetate<br>FQ shocks | n.i. | SBR 16.9 | 340 d<br>3/8-h cycle; Fill (bottom): 60; Ae: 112/452; Set: 3 | VFR: 0.2<br>SAV: 2.4 | n.i. | n.i. | - Exposure to FQ caused AG size ↓ and promoted AG disintegration. | Amorim *et al.*, 2014 |
| Real (dairy industry), Particulate matter | 4.5-5.9 (diss: 2.4-2.9) | SBR 5.4 | ~ 140 d<br>8-h cycle; Fill (bottom) 60; An 0-60; Ae 335-405; Set 4-15 | VFR: 0.6<br>SAV: 1.1 | n.i. | Up to 5 | - Filamentous outgrowth in absence of famine period.<br>- AG size ↑ and AG disintegrated. | Schwarzenbeck *et al.*, 2005 |
| Real (abattoir), Particulate matter, COD/N: 6.2 | 2.7 (diss: 1.9) | SBR n.i. | > 4 months<br>8-h cycle; Fill 18; An/Anoxic (mix) 60; Ae 315; Anoxic (mix) 80; Set 2 | DO: 3-3.5 | 15-20 | > 0.6 | - Complex WW probably promoted disintegration of large AG due to clogging of pores and channels.<br>- Low pH leading to dissolution of mineral complexes associated to the EPS might have caused structural damages in AG. | Lemaire *et al.*, 2008 |
| Real (palm oil mill) | 3-6 | SBR 6.7 | 170 d<br>6-h cycle; Fill 10; Ae 340; Set 0.5 | VFR: 0.3 | n.i. | Up to 4 | - AG disintegrated upon reaching the max. $d_{AG}$. | Gobi *et al.*, 2011 |
| Real (seafood industry) | 2-13 | SBR 5.6 | 330 d<br>3-h cycle; Fill (top) 3; Ae 171; Set 1-3 | DO: 4-8 | 2-13 | Up to 8.5 | - Change in OLR from 3 to 13 kg COD $m^3$ $d^{-1}$ caused AG disintegration. | Val del Río *et al.*, 2013 |

## II.1.3. Operational conditions and the stability of aerobic granules (AG)

Bioreactor operating parameters, such as OLR, feast-famine conditions, shear stress, DO level, substrate type, nitrogen and carbon (as COD) contents and toxic substances present in wastewater are known to influence not only the macroscopic characteristics of AG, namely their size, shape and settleability, but also the internal bacteria distribution and their metabolic activity. Therefore, a relevant effect at the level of AG stability is expected from changes in these operational factors (Table II.2). This section reviews studies reporting on these factors and their effects. The physical properties of AGS, as well as other indicator parameters of the bioreactor system, have been used to assess and quantify the stability of AG, *e.g*., the presence of suspended solids in the treated effluent, treatment performance deterioration, SVI, settling velocity, and integrity coefficient values of AGS, cell surface hydrophobicity and AG morphological analysis.

### II.1.3.1. Organic loading rate

Domestic wastewater is a low-strength wastewater, and its organic content can be drastically reduced during the rainy season, resulting in OLR values lower than 0.6 kg COD $m^{-3}$ $d^{-1}$. Peyong *et al*. (2012), who studied the changes in microbial morphology and structure of AG under low OLRs (0.13-1.2 kg COD $m^{-3}$ $d^{-1}$), described the resulting acetate-fed granules as fluffy, loose structures containing filamentous organisms (Table II.2). Furthermore, the stability of mature AG (2.2 mm average size) fed with a real domestic wastewater at an OLR of 0.54 kg COD $m^{-3}$ $d^{-1}$, deteriorated over a 2-month operational period, *i.e.*, the large granules gradually disintegrated into small debris that were subsequently washed out from the reactor (Peyong *et al*., 2012). However, upon subsequent application of an OLR of 0.6 kg COD $m^{-3}$ $d^{-1}$, the integrity of AG could be maintained. In addition, Zhang *et al*. (2011) reported that AG operated with a low OLR (0.58 kg COD $m^{-3}$ $d^{-1}$) and low aeration rates presented a loose, porous and hollow structure and became unstable when their diameter increased above 1 mm (Table II.1). In parallel with the deterioration of the settling capacity, the EPS content in AG decreased, thus reducing the overall strength of the granular structure. Subsequent disintegration of the larger granules suggested that small sized AG are more favorable for the long-term treatment of wastewaters under low substrate loading rate.

While most activated sludge systems operate at relatively low OLRs (0.5-2.0 kg COD $m^{-3}$ $d^{-1}$), operation at high OLRs is desirable in biological wastewater treatment systems in order to enable the treatment of high-strength wastewaters, namely industrial effluents, in compact bioreactors. In this sense, and given the advantageous characteristics of AG in dealing with high and variable loading rates, several studies focused on operating AGS SBRs in the high OLR range (2.5-22.5 kg COD $m^{-3}$ $d^{-1}$; Liu and Tay, 2004). Beun *et al*. (1999) were among the first authors reporting that high OLRs led to the outgrowth of filamentous microorganisms, resulting in unstable operation of AGS SBRs. This association was later confirmed by several studies. Namely, Zheng *et al*. (2006) showed that compact

AG (1 mm in size) cultivated at an OLR of 6.0 kg COD $m^{-3}$ $d^{-1}$ gradually evolved into large-sized filamentous granules, with low cell surface hydrophobicity (Table II.1). As the filament-dominated granules grew larger (up to 10 mm) the sludge settling rate increased sharply. However, a further increase in size (up to 16 mm) led to the disintegration of the large filamentous AG, deterioration of the sludge settling capacity and washout of AGS, with the consequent failure of the reactor. The fast growth of filamentous microorganisms was suggested to be induced by the decrease in the food-to-microorganism ratio (F/M) as biomass accumulated in the SBR. In a study using real dairy wastewater, AG structural deficiencies due to filamentous outgrowth were also reported at the same OLR (Schwarzenbeck *et al*., 2005; Table II.1). Recently, a study focused on developing a fast granulation strategy concluded that although a high OLR was favorable for fast granulation, it also led to fluffy granules in about 2 weeks (Liu and Tay, 2015). The OLR had to be lowered from 12 to 6 kg COD $m^{-3}$ $d^{-1}$ to maintain granule stability throughout a 6-month operational period.

In order to assess the capacity of AG to handle increasing OLRs, acetate- or glucose-fed AG, previously formed at 6 kg COD $m^{-3}$ $d^{-1}$, were sequentially subjected to 9, 12 and 15 kg COD $m^{-3}$ $d^{-1}$ values (Moy *et al*., 2002). Although granule size increased with both substrates, the two types of granules presented different stability levels under high OLRs. Glucose-fed granules, characterized by a smooth, irregular microstructure, could withstand the highest OLR, because their settling ability and strength improved with the increase in OLR. On the other hand, acetate-fed granules, which had a dense, compact and regular microstructure, disintegrated within a week after the OLR level of 9 kg COD $m^{-3}$ $d^{-1}$ was applied, and AG fragments were washed out (Table II.2). These results show that the ability of the granules to handle high OLR values significantly depends on the granule microstructure morphology, which in turn is influenced by the type of substrate.

The effect of a sudden increase in the OLR (from 3 to 6 kg COD $m^{-3}$ $d^{-1}$) was also studied using real wastewaters (Table II.1), namely a palm oil mill effluent, leading to AG growth and subsequent disintegration upon reaching a maximum size (Gobi *et al*., 2011). In another system, after AG were cultivated using a seafood industry effluent at high OLR (2-5 kg COD $m^{-3}$ $d^{-1}$), attaining 2.4 mm in size with smooth surface and compact structure, sudden fluctuating loads (3-13 kg COD $m^{-3}$ $d^{-1}$) were applied to assess AG stability (Val del Río *et al*., 2013). As a result, AG drastically increased in size (up to 11 mm), and further broke up into small debris, which were subsequently washed out (Table II.1). Nevertheless, new granules with good settling properties were rapidly formed when a lower OLR level was restored, and good treatment performance was maintained (90% of COD removal) even at the highest OLR.

On the other hand, a recent study showed that mature, acetate-fed AG could maintain their stability for 65 days in a continuous-flow reactor under gradually increasing OLRs (5-15 kg COD $m^{-3}$ $d^{-1}$), evolving to increased particle sizes (up to 1.8 mm) and lower SVI values (Long *et al*., 2015).

However, when further subjected to 18 kg COD $m^{-3}$ $d^{-1}$, AG larger than 1.4 mm disintegrated due to the formation of black, oxygen- and substrate-depleted cores with dead cells (Table II.2). This condition finally led to high levels of flocculent sludge in the effluent and to the deterioration of organic load removal performances. No filamentous bacteria overgrowth was observed in this continuous-flow reactor, where an alternating feed regimen to two interconnected compartments created solute concentration gradients along the reaction volume mimicking the time-gradients observed in an SBR configuration.

Overall, AG instability at high OLR has been attributed to three main aspects: overgrowth of filamentous microorganisms (Liu and Liu, 2006), intracellular protein hydrolysis and degradation at the anaerobic granule core (Zheng *et al*., 2006), and, according to some indications, loss of the capacity of microorganisms for auto-aggregation due to a reduction in the quantity of extracellularly secreted protein (Adav *et al*., 2010). These factors are further explored in section II.1.4.

**Table II.2 -** Studies testing the effect of specific operational conditions on the stability of aerobic granules (AG). COD: chemical oxygen demand; COD/N: COD-to-nitrogen ratio; conc.: concentration; DO: dissolved oxygen; EPS: extracellular polymeric substances; OLR: organic loading rate; PN: extracellular proteins; PS: extracellular polysaccharides; SAV: superficial airflow velocity; SBR: sequencing batch reactor; SOUR: specific oxygen uptake rate; SRT: sludge retention time; TB-EPS: tightly bound-EPS; WW: wastewater; 4-ClA: 4-chloroaniline; ↑: increase; ↓: decrease.

| Operational condition | Effect on AG stability | Reference |
|---|---|---|
| OLR | Compact acetate-fed AG disintegrated at high OLR due to nutrients mass transfer limitation. | Moy *et al*., 2002 |
| OLR | - Low OLR: filaments became dominant in AG.<br>- High OLR: disappearance of filaments, dominance of rod-shaped bacteria.<br>- High OLR can be an effective means of helping to control fungal growth, recover bacterial dominance and restore the stability of AG. | Li *et al*., 2010a |
| OLR | - Integrity of AG maintained with OLR as low as 0.6 kg COD $m^{-3}$ $d^{-1}$.<br>- Particulate COD from real WW induced filamentous and protozoa growth. | Peyong *et al*., 2012 |
| OLR | - Over a specific OLR: AG instability due to AG size ↑ and consequent mass transfer limitations, anaerobic cores being formed by massive cell death. | Long *et al*., 2015 |
| OLR<br>Settling time<br>Starvation period<br>Shear force | - Higher OLR: formation of larger AG.<br>- Short settling time: fastest granulation, higher EPS, higher storage stability.<br>- Extended starvation period, high shear force: longer granulation, smaller size and higher integrity/physical strength. | Gao *et al*., 2011 |
| Cycle time (1.5, 4, 8h) | - 1.5-h cycles: big AG, poor stability due to mass transfer limitation.<br>- 4-h cycles: most compact AG.<br>- 8-h cycles: smaller AG, with highest COD removal and SOUR because of lower mass transfer resistance. | Liu and Tay, 2007b |
| Cycle time (1.5, 4, 8h)<br>Starvation period | - Reasonable starvation time necessary to maintain the long-term stability.<br>- Shorter cycle/starvation times: speed up granulation but unstable AG with filamentous organisms were formed.<br>- Longer cycle/starvation times: long-term stable AG.<br>- Optimal starvation time depends on substrate type and initial conc. | Liu and Tay, 2008 |
| Nutrient starvation | Short-term C-, N-, P- and K- starvations decreased AG structural stability, due to reduced EPS content and microbial activity inhibition. | Wang *et al*. 2006 |
| Anaerobic period | - Aerobic SBR had large-sized AG with filamentous organisms.<br>- Short anaerobic phase positively affected AG density and stability.<br>- Higher TB-EPS in long anaerobic phase did not guarantee stability. | Moghaddam and Moghaddam, 2015 |

**Table II.2** (continued) - Studies testing the effect of specific operational conditions on the stability of aerobic granules (AG). COD: chemical oxygen demand; COD/N: COD-to-nitrogen ratio; conc.: concentration; DO: dissolved oxygen; EPS: extracellular polymeric substances; OLR: organic loading rate; PN: extracellular proteins; PS: extracellular polysaccharides; SAV: superficial airflow velocity; SBR: sequencing batch reactor; SOUR: specific oxygen uptake rate; SRT: sludge retention time; TB-EPS: tightly bound-EPS; WW: wastewater; 4-ClA: 4-chloroaniline; ↑: increase; ↓: decrease.

| Operational condition | Effect on AG stability | Reference |
|---|---|---|
| Anoxic/anaerobic-aerobic | - Filamentous growth on AG surface in anaerobic-aerobic operation due to easily biodegradable COD present at the end of the anaerobic phase.<br>- To obtain stable AG in long-term SBR operation, it is necessary to maximize substrate use during non-aerated/anaerobic/anoxic phase. | Filali *et al*., 2012 |
| Anoxic-aerobic *vs* aerobic-anoxic | - Anoxic-aerobic generates AG with higher stability, greater sizes (1.8-3.5 mm) and almost complete denitrification. | Erşan and Erguder, 2013 |
| Aeration in famine period | - Stable AG at reduced aeration rate in famine period for > 3 months.<br>- Lower shear stress requirement in famine period for AG stability due to lower microbial growth rate.<br>- Aeration rate ↓ in famine period could maintain the good AG settleability. | Liu and Tay, 2006 |
| Shear stress (SAV) | - < 1 cm $s^{-1}$: AG disintegrated.<br>- SAV ↓ caused DO to ↓, affecting feast-famine conditions.<br>- Substrate removal kinetics and DO are more significant to AG formation than shear force. | Sturm and Irvine, 2008 |
| COD/N | - COD/N ↓ affected nitrification and led to AG disintegration.<br>- Reduction in net tyrosine production in EPS, microbial community shift with reduction in filamentous bacteria, leading to collapse of AG. | Luo *et al*., 2014 |
| Ammonia conc. | - Lowest $NH_4$ conc.: filamentous overgrowth and AG disintegration.<br>- Highest $NH_4$ conc.: AG did not form due to free ammonia inhibition.<br>- Step-wise $NH_4$ ↑ created stable AG by gradually selecting slow-growing nitrifying bacteria, which suppressed filamentous growth. | Wang *et al*., 2007b |
| Ammonium salts | - Unstable AG after 3 d cultivation with low ammonium and phosphates.<br>- AG stability in continuous-flow reactors with high ammonium salts conc.<br>- Stable AG had enriched denitrifier community and high phosphate conc. | Juang *et al*., 2010 |
| Particulate substrate | - Particulate or colloidal substrate: filamentous and irregular AG structure, with consequent reduced stability.<br>- Starch adsorbed and consumed at AG surface (low starch hydrolysis rates): available substrate during aeration period (extended feast period) led to high substrate gradients over AG and less uniform AG development. | de Kreuk *et al*., 2010 |
| 4-ClA shock loads | - High 4-ClA shock can cause the disintegration of AG.<br>- PN ↓ in EPS has a negative impact on AG stability. | Zhu *et al*., 2013a |
| Temperature | - Start-up at 8ºC caused AG instability.<br>- Start-up at 20ºC and lowering to 15ºC and 8ºC did not affect AG stability.<br>- Presence of COD during the aerobic phase (fast-growing bacteria) is considered to be the major reason for AG instability. | de Kreuk *et al*., 2005b |
| Sludge removal | - Removing fresh AG effectively maintained stable AG (1-2 mm).<br>- Removing aged AG led to disintegration of AG (4-5 mm).<br>- Removing completely mixed sludge resulted in AG with good settleability but too large (4-5 mm). | Li *et al*., 2006 |
| Sludge removal | - Long SRT of AG leads to deterioration of AG stability.<br>- Selective sludge discharge (proportional discharge of aging AG and retention of enough new-born flocs) favored AG stability. | Zhu *et al*., 2013b |
| Direct current | - More compact and dense AG in the electro-augmentation SBR, possibly due to stimulated EPS production and higher cations accumulation in AG.<br>- Novel method for enhancing nitrification and structural stability of AG. | Huang *et al*., 2014 |

### II.1.3.2. Biomass loading rate

Dissimilar AG stability levels reported in different studies using the same OLR may be attributed to operation at distinct biomass concentrations. In fact, the biomass loading rate, or the F/M, which depends on both the OLR and suspended solids, has been associated with AGS quality. Li *et al.* (2011), who investigated the effect of F/M on AG formation, size, and stability, observed a direct, linear relationship between F/M and granule diameter. Specifically, while a high F/M value (1.1 g COD $gVSS^{-1}$ $d^{-1}$) promoted faster granulation and larger granules (mean diameter 4.5 mm), a low F/M value (0.3 g COD $gVSS^{-1}$ $d^{-1}$) led to slower AG formation and smaller granules (mean diameter 1.5 mm). Although initially high F/M values were shown to accelerate the start-up of the granulation process by enhancing microbial growth, the authors suggested that the F/M should be subsequently reduced (to 0.3 g COD $gVSS^{-1}$ $d^{-1}$) in order to sustain stable granules in long-term treatment operation. Accordingly, a study focusing on the stability of AGS treating industrial wastewater revealed the deterioration of AG physical properties following an increase in the F/M values from 0.3-0.6 to 1-2.5 g COD $gVSS^{-1}$ $d^{-1}$ (Val del Río *et al.*, 2013). In addition, while comparing AGS formation under different OLRs, which resulted in distinct initial F/M values (ranging from 0.3 to 6 g COD $gVSS^{-1}$ $d^{-1}$), stable granules were observed after 60 days of operation as the F/M gradually stabilized at 0.5 g COD $gVSS^{-1}$ $d^{-1}$, irrespective of the employed OLR value (Li *et al.*, 2008).

On the other hand, another study indicated that a low F/M, resulting from an increase in biomass concentration, promoted the fast growth of filamentous organisms, leading to large (mean size 5.5 mm), unstable AG, which disintegrated after 200 days of operation (Zhu *et al.*, 2008). Additionally, Liu and Liu (2006) suggested that the decrease in F/M (from 0.6 to levels below 0.1 g COD $gVSS^{-1}$ $d^{-1}$), as a result of biomass concentration increase during the granulation process, was the cause of the filamentous growth observed in an AGS SBR operated under high biomass concentrations. Overall, relatively low F/M values can help maintain small, dense and stable AG in systems operated in the absence of a long anaerobic feeding, but there seems to be a threshold under which the enhancement of filamentous growth can compromise AG stability. For systems with anaerobic feeding no explicit information on the effect of the F/M value is available.

### II.1.3.3. Substrate type

The distinct AG stability behavior reported by different studies using the same OLR indicates that the type of substrate and other wastewater composition factors play a role in AG stability (Table II.1). In fact, the type of carbon source highly influences the morphology and structure of AG (Franca *et al.*, 2017). For example, glucose-fed AG have been shown to be characterized by a loose morphology and fluffy surface due to a dominance of filamentous bacteria, whereas acetate-fed AG were reported to present a compact microstructure dominated by rod-like bacteria tightly packed together (Moy *et al.*, 2002; Tay *et al.*, 2001a). This indicates that energy-rich substrates (*e.g.*, glucose, sucrose) might

induce the proliferation of filamentous bacteria. As discussed by Moy *et al*. (2002), relatively complex organic substrates such as carbohydrates, which are degraded through multistep processes, produce AG with layered and complex microstructures and a greater diversity of microorganisms, whereas simple carbon substrates (*e.g.*, acetate, formate) select for simple, uniform microstructures.

Real wastewaters, either from domestic or industrial origin, contain diverse carbon sources along with a variety of other organic and inorganic compounds. This complex composition and the different substrate degradation rates are likely to have an effect on AG stability since they will affect the microbial community within AG and the type of EPS produced (Lemaire *et al*., 2008; Schwarzenbeck *et al*., 2005; Table II.1).

Another aspect of real wastewaters is that, in addition to the substrates present in dissolved form, a significant fraction of the pollutants is present in the form of colloids and particulate matter, which are not readily biodegradable. In fact, higher instability and poorer physical properties of AG have been reported for real wastewaters, when compared to studies using synthetic effluents (Y.Q. Liu *et al*., 2010). Specifically, when comparing AG fed with acetate or with domestic sewage, the latter were found to be lower in strength and less stable, due to their irregular and less dense structure (Nor-Anuar *et al*., 2012). Similarly, in a study using real dairy industry wastewater (Schwarzenbeck *et al*., 2005), filamentous granules were formed at much lower OLR values than those reported by Moy *et al*. (2002), who used a synthetic wastewater. These differences were attributed to the presence of slowly degradable substrates in the real wastewaters (colloids and particulate matter). Accordingly, Peyong *et al*. (2012) suggested that particulate COD present in this type of influent was responsible for the filamentous growth observed on AG, since after the external addition of soluble COD AG became filament-free, evolving to a more compact and denser structure (Table II.2).

A study specifically focused on the influence of suspended solids and colloidal substrates on AG morphology showed that, after being adsorbed onto the AG surface, slowly biodegradable substrates were hydrolyzed and the products consumed by bacteria on the surface, instead of accumulating inside the granules as reported for soluble substrates (de Kreuk *et al*., 2010). As in the report of Schwarzenbeck *et al*. (2005), this insoluble substrate situation resulted in filamentous outgrowth and an irregular structure in AG, along with the excessive presence of protozoa and metazoans at the surface of AG (Table II.1). A study focusing on the fate of mature AG treating wastewater from an abattoir (including particulate and colloidal matter, oil and grease), attributed the disintegration of large mature granules grown to a size range of 1.5-2.0 mm to a rapid clogging of the granule pores and channels, which were supposed to play a key role in the transport of substrates and metabolites within AG (Lemaire *et al*., 2008; Table II.1). In addition, the large abundance of ciliates on the AG surface, feeding on organic particulate matter, was suggested to have an impact on the overall diffusion rates of oxygen and substrates in AG.

Recently, Pronk *et al*. (2015a) discussed the effect of different carbon sources and their feeding regimen on AG stability in SBR. The authors concluded that the feeding regimen plays a major role in determining the AG stability, as different feeding conditions for the same type of substrate led to different AG integrity results. These findings allowed the design of practical solutions to improve AG stability, as further discussed in section II.1.5.2.

### II.1.3.4. Carbon-to-nitrogen ratio

In light of the often variable COD-to-nitrogen ratio (COD/N) in industrial wastewaters, Luo *et al*. (2014) investigated the impact of this ratio on AG disintegration. Decreasing the COD/N value from 4 to 1 caused a large shift in the microbial community and a reduction in EPS content, leading to the reduction of the nitrification rate and of AG physical strength, size and settleability, indicating a collapse of AG structure. This study highlighted the importance of tyrosine production for EPS in maintaining AG stability. Regarding the decrease in nitrification efficiency, although a greater abundance of ammonia-oxidizing bacteria (AOB), namely *Nitrosomonas*, was observed at lower COD/N values, the presence of nitrite-oxidizing bacteria (NOB), *Nitrospira* and *Nitrobacter*, decreased when the COD/N was reduced to 1. This was attributed to growth inhibition by free ammonia and to a reduction in the SRT value, a consequence of biomass washout due to settleability deterioration under decreasing COD/N. More recently, Kocaturk and Erguder (2016) indicated that while high COD/N values (7.5-30) favored fast-growing heterotrophs forming white, fluffy flocs and large granules, the low COD/N range (2-5) led to stable, small and dense granules enriched in slow-growing nitrifiers. In the same study the optimum COD/N, in terms of high COD and nitrogen removal rates and granule stability, was found to be 7.5.

### II.1.3.5. Aeration rate

The aeration rate exerts its influence on AG formation and stability both through the supply of oxygen and hydrodynamic shear stress (Tay *et al*., 2001b). Several studies regarding AGS settleability and stability suggested that oxygen deficiency, *i.e.*, a low DO concentration, favored filamentous growth and led to the breakage of AG (Liu and Liu, 2006). Namely, de Kreuk and van Loosdrecht (2004) reported that decreasing the mixed liquor DO saturation level to 40% led to granule instability, filamentous growth and biomass washout.

Liu and Tay (2007a) repeatedly observed that above a certain biomass concentration limit (around 8.0 g $l^{-1}$) the morphology of larger AG changed from clear and regular to irregular shapes with a netlike structure, subsequently disintegrating and leading to a sharp increase in SVI and biomass washout (Table II.1). The consequent decrease in biomass concentration in the reactor allowed the formation of new, regular granules. Due to the higher biomass concentration, an increased supply of oxygen was required when a high substrate concentration was present, as indicated by the low DO levels reached

in the mixed liquor. This condition was proposed to be responsible for the AG instability in the bubble column SBR employed, which was operated with a constant superficial air velocity of 1.2 cm $s^{-1}$. Accordingly, Sturm and Irvine (2008) reported that when air velocity lower than 1 cm $s^{-1}$ was applied AG disintegrated into flocs (Table II.2). Nevertheless, AGS grown in an airlift reactor at the same superficial air velocity of the bubble column SBR presented good stability along a period of 151 days (Liu and Tay, 2007b). This difference was attributed to distinct biomass distribution patterns in the reactors. Contrarily to the homogeneous distribution in the airlift, the higher biomass concentration in the lower part of the bubble column could have enhanced the competition for substrate and DO, leading to the disintegration of AG at low aeration rates.

In addition, Mosquera-Corral *et al*. (2005) specifically analyzed the long-term implications of reducing the aeration rate in an AGS system. Following stable operation for 150 days at an oxygen saturation of 70%, this value was decreased to 40%. As a result, filamentous organisms developed at the surface of AG which subsequently disintegrated leading to biomass washout (Table II.1). The same AG behavior was described in a study where the DO concentration was reduced from 100% saturation to 40% and further to 20% (de Kreuk and van Loosdrecht, 2004). According to these results, high mixed liquor DO concentrations would be required in order to avoid oxygen supply limitation in AG and maintain AG stability. Nevertheless, the oxygen supply should be optimized in order to minimize energy consumption in full-scale AGS systems and ensure efficient N-removal. No general minimum aeration rate or DO concentration values for AGS operation have been suggested because oxygen requirements in the presence of high substrate concentrations depend on specific factors, such as biomass concentration, AG size, substrate type and loading and the microbial community within AG.

### II.1.3.6. Toxic substances

Owing to its intrinsic characteristics, AGS has been described as a promising technology for the treatment of wastewaters containing toxic compounds and several studies reported AGS formation in such conditions (Maszenan *et al*., 2011). Recently, a study focused on the effect of aniline on AGS stability (Dai *et al*., 2015) showed that, although the AG properties (strength, growth rate, SVI) slightly deteriorated upon aniline supplementation, this effect was subsequently removed due to the adaptation of AG, evolving to a denser structure, and to the emergence of microorganisms with aniline biodegradation ability within the microbial community. In addition, Ramos *et al*. (2016) demonstrated the long-term stability of AGS (200-day operational period) that completely biodegraded a mixture of *p*-nitrophenol, *o*-cresol and phenol in a continuous airlift reactor.

On the other hand, structural instability of AG has been shown to become more evident in the presence of toxic, non-degradable substances. Amorim *et al*. (2014) operated an AGS SBR for 340 days for treating a synthetic wastewater containing fluoroquinolones. The latter were shown to adsorb onto the

AG and no biodegradation occurred. Although the COD removal yields, as well as the AOB and NOB populations, were not affected, denitrifying activity and PAO were inhibited. In terms of granule stability, the exposure of mature AGS to these compounds affected AG morphology, noted by a decrease in AG size and a change to a more compact structure, and further promoted disintegration of AG and biomass washout (Table II.1). The development of a compact structure is regarded as a defensive strategy against the inhibitory effects of toxic compounds (Tay *et al*., 2005). Accordingly, the withdrawal of the fluoroquinolones from the inlet stream of the SBR resulted in an increase in granule size. Zhu *et al*. (2013a) showed that the structural stability of AG was susceptible to high 4-chloroaniline shock loads, which caused the complete disintegration of the granular structure within a week. AG that initially had a smooth surface and dense structure evolved into flocs with a rough surface and loose structure, with a significant decrease in the average granule size. This was correlated with variations in the microbial community, *i.e.*, the disappearance of functional bacteria associated with EPS production and the appearance of bacteria involved in proteolysis. Accordingly, the protein content of the AGS EPS significantly decreased (Table II.2).

It has been reported that a high concentration of free ammonia has a negative effect on the hydrophobicity of cells in granules, on specific oxygen uptake rate (OUR) and on EPS production, thus influencing the stability of granules (Peyong *et al*., 2012; Table II.2). Specifically, AG instability was associated with a weakening of the granular structure due to a decrease in EPS production, which in turn was ascribed to the high toxicity of free ammonia present at around 17.9 mg-N $l^{-1}$ (Huang *et al*., 2014).

### II.1.3.7. Intermittent feast-famine and aerobic and non-aerated conditions

Intermittent feeding has been shown to stimulate the growth of dense and smooth AG (Beun *et al*., 2000). This result was associated to the creation of periodic, distinct feast and famine conditions during each SBR cycle, due to the sequential abundance and shortage of soluble organic matter, respectively, in the mixed liquor. Specifically, Gao *et al*. (2011) reported that longer starvation periods, which resulted in longer endogenous respiration phases at slow microbial growth rates, produced small, compact AG with high integrity and physical strength (Table II.2). Accordingly, other studies reported that bacterial cells increased their surface hydrophobicity when subjected to long aerobic starvation periods (Y. Liu *et al*., 2005; Liu and Tay, 2002). Conversely, granules were observed to become increasingly filamentous when feast periods prevailed over famine periods (Muda *et al*., 2011). In addition, Schwarzenbeck *et al*. (2005) indicated that the maximal OLR value above which AGS stability was compromised depended on the occurrence of distinct feast and famine conditions for avoiding filamentous outgrowth, which occurred in the absence of a sufficiently long starvation period. Therefore, to promote a long and distinct famine period, the SBR volumetric exchange ratio was reduced (Schwarzenbeck *et al*., 2005). However, this operational change would

decrease the efficiency of the use of a minimal settling velocity as a tool for selecting fast-settling granules *vs* slow-settling flocs (Beun *et al*., 2000), since a lower fraction of flocs would be removed.

Liu and Tay (2008) studied the influence of different starvation times on the formation and stability of AG in an SBR (Table II.2). Although a shorter cycle time (1.5 h), with a consequently shorter starvation period, speeded up the granulation process, granules became unstable after a 4-month operational period, as the originally compact AG became larger, with filamentous bacteria on the surface and poor settleability. This change in properties finally resulted in the collapse of the reactor on operational day 160. On the other hand, AG formed in SBRs with longer cycle times, and consequently longer starvation periods, showed good stability during long-term operation.

In contrast, compact AG grown in an aerobic SBR were reported to gradually change into unstable, filamentous, large-sized AG (2-5 mm) due to the excessively long starvation period caused by the prolonged aeration time (Moghaddam and Moghaddam, 2015). Furthermore, the introduction of an anaerobic reaction period, preceding the aerobic phase (equal time periods), created AG with loose structures and poor settleability. In this case, filamentous outgrowth was attributed to the too short starvation period, a consequence of the presence of residual COD at the end of the aerobic phase (Table II.2). Therefore, feast and famine conditions had to be optimized in order to produce stable granules. A rescheduling of the anaerobic/aerobic reaction times created a starvation period accounting for 68% of the cycle time, which positively affected the compactness and stability of AG. Accordingly, López-Palau *et al.* (2012) stated that a feast:famine cycle time ratio of 1:2 ensured the compactness of the produced AG.

Erşan and Erguder (2013) studied the effects of anoxic-aerobic and aerobic-anoxic cycle sequences on AG formation and stability (Table II.2). The former conditions enabled the development of compact, dense, large AG (1.8-3.5 mm) with high stability, which was attributed to almost complete denitrification during the anoxic periods. Contrarily, the aerobic-anoxic sequence led to small, loose AG that further disintegrated after 2 months of operation, reportedly due to the limited residual carbon source availability in the anoxic phase. Similarly, Filali *et al*. (2012) compared the stability of mature AG operated under anoxic-aerobic and anaerobic-aerobic cycle regimens (Table II.2). The latter led to the growth of filamentous heterotrophic bacteria on the AG surface, which was attributed to a significant fraction of easily biodegradable organic substrate remaining at the end of the anaerobic phase, subsequently degraded in the aerobic period. Conversely, under anoxic-aerobic conditions the fed COD was fully removed during the anoxic phase resulting in stable AG. Additionally, long-term AG stability could also be obtained under anaerobic-aerobic-anoxic SBR operation, because most of the organic substrate was used during the anaerobic-anoxic periods, resulting in a famine aerobic phase, which is known to enhance microbial auto-aggregation (Zhang *et al*., 2011). These studies demonstrate the need for maximizing substrate removal during non-aerated phases preceding the

aerobic stage to ensure stability of AG. Therefore, an adequate combination of anoxic, anaerobic and aerobic phases should be selected according to the ratio between COD, nitrogen and phosphorus contents in the influent. In fact, although a starvation period seems to be crucial to maintain long-term stability of AG, the optimal starvation time highly depends on the substrate type and initial concentration.

#### II.1.3.8. Temperature

Because the morphology of AG is strongly related to the type and growth rate of the microorganisms involved, temperature variations could also affect AG stability. In this sense, de Kreuk *et al*. (2005b) investigated the effect of temperature changes on the conversion processes and the stability of AG in bioreactors operated under the anaerobic-aerobic cycle regimen (Table II.2). Start-up at 8ºC resulted in irregular-sized AG that aggregated during settling, causing severe biomass washout and unstable operation. This behavior was attributed to the presence of residual, soluble COD at the start of the aerobic phase, a condition promoting filamentous growth. On the other hand, start-up at 20ºC followed by a decrease of the temperature to 15ºC and 8ºC did not affect AG long-term stability. Therefore, it was concluded that the start-up of a new system should take place in summer, when temperature is high and metabolic processes are fast, resulting in complete consumption of readily biodegradable COD during the anaerobic phase.

### II.1.4. Stability-related properties of AG

The reviewed studies reporting instability of AG under specific operational conditions (section II.1.3) provide insights into associated changes in the physical and chemical characteristics of AG, as well as at the level of the microbial community (Table II.2). The key factors leading to granule disintegration, at the level of the AG microenvironment, are discussed in this section. Specifically, the mechanisms proposed to explain the dependence of AG stability on biomass concentration, AG particle size, biomass growth rate, substrate mass transfer and concentration distribution in the granule, and microbial community interactions, are here reviewed (Table II.3).

#### II.1.4.1. Granule size and filamentous organisms

During granulation, AG growth results in increasing settling velocity and density (Toh *et al*., 2003). However, this tendency has a size limit. As AG increase in size, substrate removal typically becomes mass transfer-limited and organisms compete for substrates and space within the aggregate. In fact, active bacteria are mainly detected on the surface of AG, whereas the core is mainly composed of EPS. The dimension and the complex internal structure of AG (*e.g.*, density, size and distribution of pores) have a significant impact on the substrate mass transfer processes, and severely affects stability of AG (L. Liu *et al*., 2010). Therefore, the effects of several key operating parameters (*e.g.*, DO concentration, shear force, allowed settling time, feast-famine regimen and OLR) on granule size were

comprehensively investigated with different carbon substrates (acetate, glucose and phenol; Liu and Tay, 2004). Under selected operational conditions AG tend to grow to a maximum size, above which problems associated with diffusion limitation become insurmountable (Moy *et al*., 2002; Peyong *et al*., 2012; Pijuan *et al*., 2009; Val del Río *et al*., 2013; Zheng *et al*., 2006).

Adding to this, several other authors reported that once filamentous growth dominated the surface of AG, deterioration of AG structure and settleability occurred, leading to subsequent biomass washout and eventual failure of the AGS system (Liu and Liu, 2006; Schwarzenbeck *et al*., 2005; Tay *et al*., 2001a). Filamentous microorganisms, including fungi, have a competitive advantage over non-filamentous, aggregate-forming species in AG because they are able to take up more nutrients from media with low levels of substrate, owing to their high surface area-to-volume ratio and preferential growth in a single direction (Liu and Liu, 2006). For these reasons, filamentous organisms show higher maximum growth rate values at lower substrate concentrations than aggregate-forming organisms. Under these circumstances, the excessive growth of filamentous bacteria on the AG surface enhances gradients of substrate concentration inside AG. In fact, during operation at low OLR or with an influent rich in slowly biodegradable substrates, filamentous organisms have been shown to outcompete other bacteria, giving rise to large, unstable AG (de Kreuk *et al*., 2010; Li *et al*., 2010a; Peyong *et al*., 2012; Zhang *et al*., 2011). Accordingly, filamentous growth and AG physical strength deterioration have also been reported under operation at low DO concentrations (Mosquera-Corral *et al*., 2005). In fact, measurements of DO concentration distribution in AG showed that oxygen was rapidly consumed in the outer layers of AG (L. Liu *et al*., 2010), and that DO limitation in the inner layers occurred for AG with sizes over 0.5 mm (Li and Liu, 2005). This size limit highly depended on AG density and biomass specific activity.

Granule size plays a significant role in the limitation of substrate mass transport also because of variations in the porosity of these structures, which was shown to diminish with the increase in size and age (Toh *et al*., 2003). Accordingly, nutrient accessibility and outflow of unfavorable products become size-dependent events, inflicting great impact on microbial viability, and on the microenvironment and microstructure of the microbial organization. Therefore, as the AG diameter increases, AG undergo physical changes that could cause problems to the reactor operation. While thick biofilms have been shown to contain cell-free channel structures that are thought to facilitate the transport of substrates into and waste products out of deep biofilm regions, these channels may eventually be plugged by the secondary colonization microorganisms. In addition, Zheng and Yu (2007) attributed the decreased porosity of large AG to plugging of the pores by EPS, leading to a decrease in the biological activity due to deficient nutrient or metabolite transport. Moreover, the particulate and colloidal matter commonly present in real wastewater might also contribute to the clogging of AG pores and channels (Lemaire *et al*., 2008).

Both filamentous outgrowth and pore clogging in large AG compromise the effective diffusion of nutrients and DO down to the deeper layers of AG. The consequent starvation conditions and the anaerobic environment created in the core of AG lead to decreased microbial activity, endogenous respiration and cell lysis (Figure II.4). Moreover, to sustain their survival certain starved bacterial cells consume EPS located at the AG core as an energy source, and EPS is considered a crucial scaffold for microbial structural self-assembly (Adav *et al*., 2008b; Lee *et al*., 2010). Metabolic products such as inhibitors, hydrolytic exoenzymes and toxic substances can accumulate in the inner region of AG, thus further inflicting detrimental effects on the EPS matrix and biomass growth. These phenomena may eventually lead to the formation of hollow cavities in the core region of the AG, decreasing the strength and cohesion of the AG structure, which thus becomes more susceptible to break-up under operational shear conditions (Toh *et al*., 2003; Figure II.4).

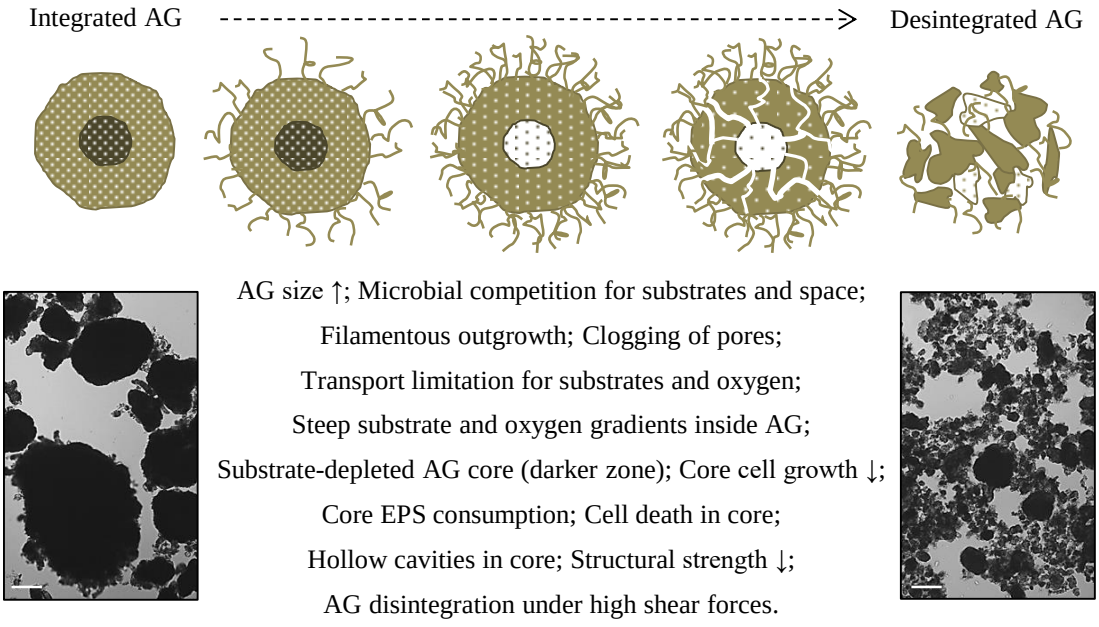


**Figure II.4** - Schematic representation of the successive events within the aerobic granule (AG) involved in the process of AG disintegration. EPS: extracellular polymeric substances. ↑: increase; ↓: decrease. Scale bar = 0.2 mm.

While assessing the effect of AG size on microbial viability distribution in AG (Table II.3), the presence of anaerobic zones with dead microbial cells has been reported at a depth of 0.8-0.9 mm from the surface, whereas AG smaller than 0.6 mm consisted entirely of live biomass (Tay *et al*., 2002; Toh *et al*., 2003). Accordingly, a study on the relation between size and mass transfer difficulty indicated that diffusion would be a limiting factor for substrate removal in AG larger than 0.7 mm (Y.Q. Liu *et al*., 2005). On the other hand, the generally more compact structure of small AG could imply that large molecules would not penetrate their pores (L. Liu *et al*., 2010).

In this context, specific AG size ranges have been suggested to maximize microbial viability in AG and further optimize the performance and economic efficiency of AGS systems. Specifically, Zhang *et al*. (2011) indicated that a size smaller than 1 mm was favorable for the settling performance and long-

term operation stability of AG treating low-strength wastewater. The same was suggested by Toh *et al*. (2003). However, as discussed by the latter authors, for a large-scale reactor operating under high OLR, to maintain such a small AG size would require very high shear forces, which would markedly increase energy consumption. Consequently, 1-3 mm was indicated as the optimal granule size range for large-scale SBR operation (Toh *et al*., 2003; Wang *et al*., 2007b). Nevertheless, the optimal AG size will depend on various physical and operational conditions of the reactor, as well as the wastewater composition.

**Table II.3 -** Studies focused on stability-related changes in aerobic granule (AG) properties ("stability factors"). AHL: N-acylhomo-serine lactones; AI-2: autoinducer-2; c-di-GMP: cyclic-dimeric-guanosine monophosphate; COD: chemical oxygen demand ratio; DO: dissolved oxygen; EPS: extracellular polymeric substances; GAO: glycogen-accumulating organisms; LB-EPS: loosely bound-EPS; N/COD: nitrogen-to-COD; PAO: polyphosphate-accumulating organisms; PHA: polyhydroxyalkanoates; PN: extracellular proteins; PS: extracellular polysaccharides; TB-EPS: tightly bound-EPS.

| Stability factor | Effect on AG stability | Reference |
|---|---|---|
| Size | - Solution to improve stability: manage biomass washout in order to maintain a quantity of AG above a particular size. | Verawaty *et al*., 2013 |
| Size<br>Mass transfer | - Diffusion resistance increased with the increase of the size of AG. | Liu and Liu, 2006 |
| AG size | - Size > 4 mm: low AG strength.<br>- Optimal suggested AG size-range for large-scale SBR operation to avoid mass transport limitation: 1-3 mm. | Toh *et al*., 2003 |
| Slow-growing (nitrifying) bacteria | - AG with low growth rates (due to enrichment in nitrifiers) showed strong structure and high stability.<br>- Selection of slow-growing nitrifying bacteria through N/COD increase suggested as strategy for improving AG stability. | Liu *et al*., 2004 |
| Slow-growing bacteria (PAO, GAO) | - Selection of PAO and GAO led to stable AG, even at low DO.<br>- Prolonged anaerobic feeding period to select for slow-growing organisms: PAO and GAO convert easily degradable substrates into slowly degradable COD, *i.e.*, microbial storage polymers (*e.g*,. PHA). | de Kreuk and van Loosdrecht, 2004 |
| Denitrification | - Significant denitrification in core of AG.<br>- Denitrification during aerobic phase depends on AG size.<br>- Nitrate contributes to the densification of AG under aerobic conditions. | Wan and Sperandio, 2009 |
| Strength<br>Denitrification | Granules were maintained and high denitrification rate was achieved under mechanical stir condition. | Zhong *et al*., 2014 |
| EPS | - COD increase caused changes in EPS composition (higher PS/PN) leading to lower cell surface hydrophobicity. | Zhang *et al*., 2007 |
| EPS | - OLR increase caused lower settling.<br>- Best settleability: highest TB-EPS content and highest PN/PS in EPS.<br>- Poor settleability: highest LB-EPS content. | Chen *et al*., 2010 |
| PS | - PS contributes for AG formation and stability.<br>- PS production seems to be stimulated by hydrodynamic shear force. | Tay *et al*., 2001c |
| c-di-GMP<br>EPS | - Addition of $Mn^{2+}$: c-di-GMP and EPS decreased causing AG disintegration. | Wan *et al*., 2013 |
| AI-2, AHL | - ATP-dependent quorum sensing (AI-2 and AHL) and EPS were essential for sustaining the structure stability and integrity of AG. | Jiang and Liu, 2013 |
| PN<br>AI-2, AHL | - AG disintegration due to hydrolysis of PN by Proteinase K and inhibition of signaling AI-2 and AHL. | Xiong and Liu, 2013 |
| $MgCO_3$ precipitates | - Magnesium salts improved AG strength.<br>- $MgCO_3$-precipitated AG could be used in continuous-flow reactor. | Lee and Chen, 2015 |

### II.1.4.2. Maximal growth rate of the microbial population

As described in section II.1.3.7, stable granulation has been associated with the creation of periodical, distinct feast and famine conditions during the SBR operational cycle, induced by sequential abundance and shortage of soluble organic matter (Beun *et al*., 2000). The intrinsic reason behind this observation is related to the microbial growth rate of the microorganisms constituting the AG. Specifically, higher stability is reportedly due to the selection for bacteria with lower maximal growth rates as selected under feast-famine regimens. These organisms compete by rapidly storing substrate in the feast phase combined with a relatively slow growth process in the famine phase. In fact, slow-growing organisms have long been shown to positively influence the density and stability of biofilms (van Loosdrecht *et al*., 1997). Conversely, low AG stability has been associated with selecting for bacteria with high microbial growth rates, *e.g.*, overgrowth of filamentous organisms when easily degradable substrate is present under aerobic conditions. In addition, a low biomass growth rate has been suggested to decrease both the demand for higher oxygen concentrations and the shear stress requirements for the formation and stability of AG. In this sense, selection of slow-growing bacteria was proposed both for enhancing AG stability and to decrease energy consumption for aeration (de Kreuk and van Loosdrecht, 2004; Liu *et al*., 2004). Heterotrophic organisms exhibit lower growth rates when growing on slowly biodegradable COD, such as microbial storage polymers, *e.g.*, glycogen and polyhydroxyalkanoates (PHA), when compared to growth on easily biodegradable substrates, such as acetate or glucose. Therefore, de Kreuk and van Loosdrecht (2004) suggested that organisms performing this substrate conversion, such as PAO and GAO, should be selected for in AGS reactor operation (Table II.3).

Specifically, under anaerobic conditions PAO store external carbon sources (volatile fatty acids, VFA) as intracellular polymers (PHA), which are subsequently used as carbon and energy source for biomass growth as well as for enhanced phosphorus uptake. The latter occurs under aerobic (oxygen as electron acceptor) or anoxic (nitrite or nitrate as electron acceptor) conditions, in PAO or denitrifying PAO, respectively (de Kreuk *et al*., 2005a; Figure II.5). Therefore, under these alternating conditions PAO and autotrophic organisms win the competition for space and substrates in AG, as proliferation of other heterotrophic bacteria is suppressed by the lack of soluble carbon source under aerobic conditions. In fact, PAO have been cultivated in AGS SBRs by alternating anaerobic, oxic and anoxic conditions, as reported in a study aiming to simultaneously remove COD, phosphate and nitrogen (de Kreuk *et al*., 2005a). As a consequence of the slow-growing microbial population established in the conditions of this study, a lower COD requirement for nutrient removal and a lower sludge production were observed (de Kreuk *et al*., 2005a).

As an alternative approach, Liu *et al*. (2004) selected slow-growing nitrifying bacteria in AGS, through controlling the nitrogen-to-COD ratio (N/COD) in the SBR influent, for improving the

stability of AG (Figure II.5). Namely, as the N/COD value was increased, the microbial population became enriched in nitrifiers, resulting in mature, small AG exhibiting high stability in terms of specific gravity, SVI and cell hydrophobicity. Moreover, as a result of the competition between different organisms for space, oxygen and substrates, fast-growing heterotrophic bacteria became less dominant in AG under the applied conditions (Table II.3). Conversely, Wan and Sperandio (2009) showed that in the absence of nitrification, oxygen was mainly used by heterotrophic bacteria for removing organic substrates, and filamentous AG structures were developed. As a microbial selection pressure favoring the growth of nitrifying bacteria, Wang *et al.* (2007b) increased the ammonia-nitrogen ($NH_4$-N) concentration in the bioreactor influent. This study showed that a high $NH_4$-N concentration prevented granulation due to inhibition by free ammonia, whereas a low ammonia concentration generated filamentous-dominated AG, which disintegrated after 131 days of operation. On the other hand, through a stepwise increase in ammonia concentration slow-growing nitrifying bacteria were gradually selected and filamentous growth was suppressed, while free ammonia inhibition was avoided. As a result, AG exhibited a compact structure and the system was steadily operated along 283 days.

Furthermore, Zhang *et al.* (2011) showed that by coupling the alternating anaerobic/oxic/anoxic operation with high N/COD and phosphorus-to-COD ratio (P/COD) and low OLR values, slow-growing organisms (nitrifiers, denitrifiers and PAO) competed more effectively with fast-growing heterotrophs. This microbial selection resulted in a lower overall growth rate when compared to AG formed under fully aerobic conditions. Consequently, the shear force selection pressure became less critical and a dynamic equilibrium could be reached between the slow growth of AG and the low hydrodynamic shear force required to form smooth and dense AG under low aeration rate values.

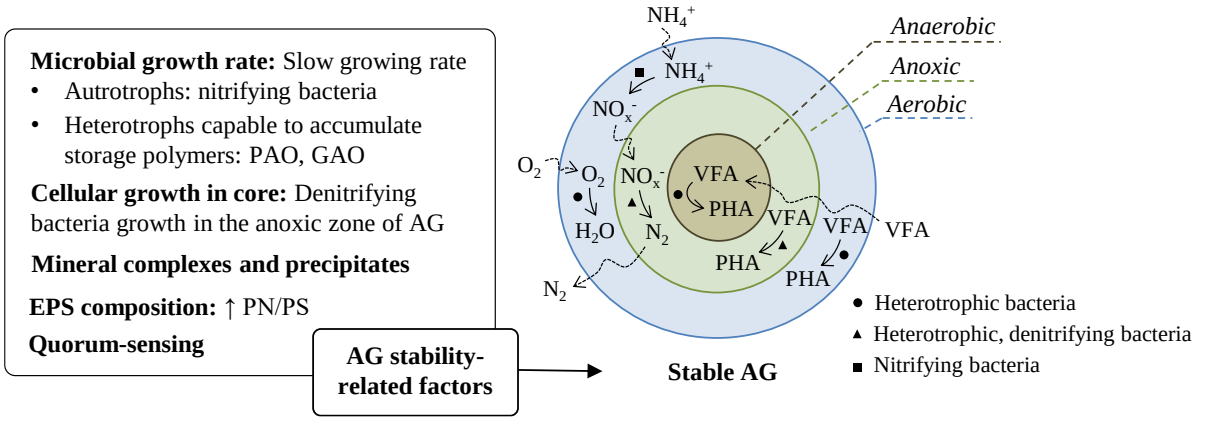


**Figure II.5 -** List of intrinsic factors related to the stability of aerobic granules (AG) and schematic representation of the reactions conducted by different bacteria within an AG. The aerobic/anoxic/aerobic layers occur under external aeration through the mixed liquor, but heterotrophic conversion of volatile fatty acids (VFA) to storage polymers (*e.g.*, polyhydroxyalkanoates, PHA) occurs essentially during non-aerated periods, *e.g.*, plug-flow or mixed feeding, during which the entire granule is in anaerobic conditions. GAO: glycogen-accumulating organisms; PAO: polyphosphate-accumulating organisms; PN/PS: extracellular proteins-to-extracellular polysaccharides ratio; ↑: increase.

### II.1.4.3. Microbial growth in the granule core

The occurrence of mass transport limitation in large AG became evident from studies reporting that live cells were located in the peripheral zone of the AG, whereas dead biomass was spread across the inner region (L. Liu *et al*., 2010; Toh *et al*., 2003). Under these circumstances, the low cell density at the AG core strongly contributes to the deterioration of the granular structure under high shear forces (Figure II.4). In fact, a recent study reported that with the increase in OLR and particle size, dead cells were observed in the AG cores, eventually leading to the collapse of the system (Long *et al*., 2015). Conversely, when AG are small enough in size to avoid substrate mass transfer resistance problems, active growth in the AG core further strengthens the aggregate, potentially preventing its disintegration. It has been shown that aggregate strength (or cohesion) and surface detachment (erosion) control AG breakage, *i.e.*, AG breakage is likely to occur if the stress applied to the surface overcomes the bonding strength in the core (Nor-Anuar *et al*., 2012; Wan *et al*., 2011).

Therefore, densification of the AG core by promoting cellular growth was suggested to be essential to increase the strength of the whole granule (Franca *et al*., 2015). In fact, denitrification in the core of AG has been shown to be beneficial for AG stability. For example, AG with denitrifying activity exhibited strong resistance to shear forces imposed by mechanical stirring and maintained their stability during 50 days under these conditions (Zhong *et al*., 2014; Table II.3).

Simultaneous nitrification and denitrification can occur in AG because of the existence of aerobic zones in the outer layers and anoxic, substrate-rich layers in the inner regions. Specifically, nitrification takes place in the aerobic outer layers of AG as ammonia is converted to nitrate, which subsequently diffuses to the oxygen-deprived interior of the AG, where it is used as electron acceptor for cell maintenance and growth on stored carbon substrates, via denitrification (Figure II.5). In these systems, the lower the DO concentration in the bulk liquid, the lower the oxygen penetration depth in AG and, thus, the higher the fraction of biomass subjected to an anoxic environment (Beun *et al*., 2001). Therefore, denitrification depends on the extent of DO penetration which also decreases with increasing AG size, the latter being influenced by operational hydrodynamic conditions (Wan and Sperandio, 2009; Zhong *et al*. 2014; Table II.3). In fact, changes in AG size have been shown to affect the efficiency of simultaneous nitrification and denitrification processes due to the variation of the anoxic volume inside the granules (de Kreuk and van Loosdrecht, 2004).

### II.1.4.4. Extracellular polymeric substances composition

EPS are organic macromolecules or polymers such as polysaccharides, proteins, nucleic acids and lipids, secreted by bacterial cells under specific environmental conditions (Adav *et al*., 2008b; Sheng *et al*., 2010). AG have been described as mixed microbial populations imbedded in a three-dimensional matrix of EPS, with specific inter-crossed linkages with extracellular polysaccharides

(PS) and proteins (PN), involving hydrophobic and ionic interactions. This cross-linked network provides a stable support for bacteria, keeping them in close proximity and thus allowing cell-to-cell communication in microbial aggregates and offering protection from unfavorable environments (Sheng *et al*., 2010; Zhu *et al*., 2013a). Specifically, the sharp increase in the PN content during granulation, and its dominance over PS, have suggested that PN plays the most important role in initial microbial aggregation (Gao *et al*., 2011; Tay *et al*., 2001c). Besides its crucial role during the granulation process, evidence shows that EPS is essential for maintaining the structural stability of AG (Liu and Tay, 2004; Xiong and Liu, 2013; Zhu *et al*., 2012). As described in section II.1.4.3, diffusional limitations in AG can induce cell decay and lysis after the EPS in the core is consumed, eventually leading to a hollow and fragile granular structure (Y.Q. Liu *et al*., 2005; Figure II.4).

Most research papers support that PN plays the major role in maintaining the bacterial aggregate core structure, and therefore in long-term AG stability (Adav *et al*., 2008b; Erşan and Erguder, 2013; Zhang *et al*., 2007; Zhu *et al*., 2012). Specifically, the analysis of EPS inside mature AG and AG disintegrated due to a 4-chloroaniline shock load, associated AG breakage to a decrease in PN content (Zhu *et al*., 2013a). Accordingly, Zhang *et al*. (2007) analyzed the EPS composition during both the granulation process and the AG deterioration period. As PN secretion increased during the granulation process, cell surfaces became more hydrophobic and less negatively charged, properties suggested to favor cell-to-cell interaction. Conversely, disintegration of AG at high OLR was hypothesized to occur due to a decrease in PN and an increase in PS concentrations, which was reflected in lower cell surface hydrophobicity (Table II.3). This may explain in essence why the deterioration of AG occurred at the high COD loading regimen, from a standpoint of microbial cell surface properties. Recently, a study reporting on the culturing of AG with a PN-to-PS ratio (PN/PS) higher than 20 showed that the PN-rich granules could sustain their structural stability in a continuous-flow reactor for 216 days, with OLR values up to 39 kg COD $m^3$ $d^{-1}$ (Chen *et al*., 2016). On the other hand, some authors reported that PS contribute more to the structural stability of AG than PN (Tay *et al*., 2001c). These contradictory results can be explained by the use of non-standardized analytical procedures, limiting the possibilities of comparison between the reported EPS results in terms of content and composition. In addition, the colorimetric methods generally used to assess the PS and PN content in wastewater present intrinsic limitations, the results being influenced by variation in sample composition and by the presence of a wide variety of interfering substances, thus potentially leading to under- or over-estimations (Le *et al*., 2016; Le and Stuckey, 2016).

Furthermore, Chen *et al*. (2010) indicated that the distribution of EPS fractions, identified as loosely bound-EPS (LB-EPS) and tightly bound-EPS (TB-EPS), plays a decisive role in the structural stability of AG. The deterioration of AGS settleability upon OLR increase was attributed to a sharp increase in LB-EPS content (Chen *et al*., 2010; Moghaddam and Moghaddam, 2015). Conversely, a higher TB-EPS content was observed in AG with good settleability, further suggesting that the latter plays an

important role in maintaining the matrix structure of AG (Table II.3). In addition, AG with the best settleability showed the highest PN/PS values in both LB-EPS and TB-EPS. Moreover, this study showed that AG stability is favored by high PN/PS at the AG surface and low PN/PS in the inner structure, denoting the important role of PS in the AG inner structure. Accordingly, Moghaddam and Moghaddam (2015) suggested that, upon nutrient scarcity in the core of AG due to substrate mass transfer limitation, the PS from TB-EPS can be easily metabolized as carbon and energy source by starved microorganisms enabling their survival.

Despite recent advances in EPS characterization, a review on the type of exopolysaccharides produced by AGS (Seviour *et al*., 2012) highlighted that developing suitable methods to isolate and characterize structural exopolysaccharides is crucial for understanding the mechanisms by which granule stability is maintained.

### II.1.4.5. Quorum-sensing

Recently, new information regarding the granular structure integrity and stability at the levels of energy metabolism and cell-to-cell communication has been published. Reports show that EPS production in AG correlates with the accumulation of compounds that are potentially involved in cell-cell communication in many bacterial species via quorum sensing, and a number of quorum sensing-regulated genes potentially involved in EPS synthesis have been identified (Table II.3).

Similar to biofilms, AG structural integrity highly depends on cell-cell interaction. The secondary messenger cyclic-dimeric-guanosine monophosphate (c-di-GMP), which is widely used by bacteria to regulate the synthesis of PS during the transition from a motile lifestyle to a sessile state, was proposed to be an intracellular regulator for biofilm stability (Whiteley and Lee, 2015). In this sense, Wan *et al*. (2013) studied the correlation between AG stability and the concentration of intracellular c-di-GMP. Disintegration of AG after addition of manganese ions was attributed to a decline in the polysaccharide content of EPS, which is correlated with a decrease in c-di-GMP concentration (Table II.3). In addition, the protein content was also reduced and specific microbial PS producers were lost. Accordingly, the authors proposed the following mechanism for granule disintegration: the manganese ions diffuse into the cells and activate the synthesis of phosphodiesterases, responsible for degrading c-di-GMP to two GMP molecules; the decrease in c-di-GMP level slows down PS synthesis, thus weakening the EPS matrix in the AG core, leading to AG disintegration; granular fragments are washed out, and the remaining biomass aggregates in flocs with low EPS content. Results from this study suggest that c-di-GMP is a key chemical factor epistatic to quorum sensing to determine granular stability. In this sense, though further research is still required to support this, stimulation of c-di-GMP synthesis could represent a potential way to accelerate granule formation and enhance long-term stability of AG (Wan *et al*., 2014).

In a different approach, a typical chemical uncoupler able to inhibit ATP generation without affecting substrate consumption (as confirmed by stable COD removal yields), was used to investigate possible roles of ATP and cell communication in maintaining AG stability (Jiang and Liu, 2013). Inhibition of ATP synthesis resulted in reduced production of two quorum sensing signaling molecules required for the formation of biofilms, specifically autoinducer-2 (AI-2) and N-acylhomo-serine lactones (AHL), their synthesis being ATP-dependent. Concomitantly, EPS secretion decreased and mature AG broke up (Table II.3). The results suggest that, to some extent, reduced AI-2 and AHL levels would be responsible for the observed AG disintegration. On the other hand, inhibition of ATP synthesis directly resulted in less energy being available for EPS production. Overall, this study presented some indications that ATP-dependent quorum sensing and EPS synthesis might be required for sustaining AG structural stability. However, a direct correlation between reduced ATP production and EPS synthesis is a more probable mechanism for AG disintegration than those reported.

### II.1.4.6. Mineral complexes and precipitates

Previous research indicates that divalent and trivalent cations, such as $Ca^{2+}$, $Mg^{2+}$, $Fe^{2+}$ and $Fe^{3+}$, have positive effects on AG stability (Figure II.5). AG with calcium carbonate accumulated in their core had higher structural strength than AG without this accumulation (Ren *et al*., 2008). Similarly, mature AG with high magnesium content or iron aggregation showed higher EPS production yields and better settling properties (Huang *et al*., 2014). Thus, the enhanced AG stability upon accumulation of divalent and trivalent cations seems to be closely linked to EPS. In fact, the presence of more cations and EPS probably enables a stronger cross-linked network, further enhancing the structural integrity of AG. Accordingly, the dissolution of mineral complexes associated with the EPS matrix was suggested to be the main reason for the structural damage of AG at pH 6.5 (Lemaire *et al*., 2008). Specifically, pH variations led to the decline of smooth and compact AG structures, and most of the smaller AG completely disintegrated. Owing to the AG intrinsic characteristics, the presence of sharp pH gradients inside large granules was expected to protect them from total disintegration, as opposed to small granules, which have a lower pH buffer capacity.

Isanta *et al*. (2012) showed that mature AG prevailed in a 100-L SBR during 5 months but their long-term stability was impaired by progressive precipitation and accumulation of inorganic P-salts (probably apatite) in their core. The authors suggested that this situation can be further accelerated at high pH values. Contrariwise, in another study mature AG were internally supplemented with precipitated $MgCO_3$ to enhance their long-term structural stability, being further tested in continuous-flow reactors for 220 days at different OLRs, HRT and temperature values (Lee and Chen, 2015). The carbonate salt precipitate markedly improved AG strength without causing significant changes in morphology, microbial community or biological activity (Table II.3). In addition, a local alkaline environment at the AG core was proposed to delay dissolution of the $MgCO_3$ precipitate, hence

preventing early collapse of the granular structure under shear. Moreover, another study aiming to operate continuous-flow reactors with AG reported that granules cultivated under a low supply of ammonium and phosphate lost structural stability within 3 days (Juang *et al*., 2010). Conversely, AG cultivation under high levels of ammonium salts produced stable AG during long-term operation (216 days). This enhanced stability was attributed to large amounts of calcium and iron precipitates in the alkaline AG core, phosphates and hydroxides being the main species composing the precipitates. In addition, the authors proposed that both denitrification and high concentrations of phosphates in the AG core contributed to buffer against wastewater pH changes, thus enhancing long-term AG stability.

### II.1.5. Practical solutions to improve long-term stability of AG

As detailed in the previous sections of this review, different operational conditions lead to different characteristics of AG, which in turn affect their long-term stability. Building on this knowledge, ongoing research has been increasingly focused on developing practical strategies to improve the stability of AG (Figure II.6). The following sections highlight some of the proposed methods.

#### II.1.5.1. Selective sludge discharge

The increased concentration of suspended solids in the treated effluent, as a consequence of the break-up of AG, is highly undesirable. Furthermore, this situation leads to a decrease in SRT, which along with variations in AG size significantly affect the presence of specific populations, such as nitrifying and denitrifying bacteria, compromising the treatment efficiency. Accordingly, it has been shown that the specific SRT of nitrifiers located in the outer layers of AG is actually shorter than the mean SRT in the reactor (Winkler *et al*., 2012), further highlighting the susceptibility of nitrification to AG disintegration. To overcome this problem, Val del Río *et al*. (2013) suggested the use of a selective biomass purge when AG reached a given size, prior to the point of disintegration.

In contrast, AGS operation under long SRT values was pointed out as a major cause of process deterioration (Zhu *et al*., 2013b). In order to improve the long-term stability of AG, Zhu *et al*. (2013b) optimized the control of SRT through a selective sludge discharge technique that achieved the discharge of aging granular sludge and the retention of enough new-born flocs (Table II.2). Specifically, the $SRT_{Flocs}$ and the $SRT_{Granules}$ were simultaneously controlled, respectively, by adjusting the sludge settling time, with flocculent sludge being discharge from the top of the reactor, and by discharging a given volume of aged granular sludge from the bottom of the reactor (Figure II.6) (estimated values were 5.3 days for $SRT_{Total}$, 9.9 days for $SRT_{Granules}$, and 2.7 days for $SRT_{Flocs}$). This strategy enabled the retention of flocs and new-born AG, enriching the AGS in AG with optimal size (2.3 mm) and a favorable structure for denitrification (*i.e.*, containing anaerobic, anoxic and aerobic microenvironments).

Moreover, in a study suggesting the accumulation of P-salts in the core of AG as a possible cause for granule disintegration (Isanta *et al*., 2012), a similar strategy was proposed to selectively remove granules with an inorganic core. A regular sludge purge based on the inorganic content was proposed to help avoid the instability of AG. Specifically, AG with higher mineral content were selectively withdrawn from the bottom of the reactor, since those showed higher settling velocity. However, this strategy should be carefully evaluated, since it could lead to GAO proliferation over the PAO population, therefore decreasing P-removal efficiency (Winkler *et al*., 2011). In fact, Winkler *et al*. (2011) efficiently selected PAO, which have been associated with high AG stability (de Kreuk and van Loosdrecht, 2004), over GAO by discharging biomass exclusively from the top of the sludge bed (Figure II.6). However, this strategy to selectively enrich AGS with PAO would not be feasible in low H/D reactors as it should require a column-shaped configuration, where an efficient segregation can occur through the different settling velocities of granules. Recently, however, the combination of an increased settling time with the purge of selected fractions of the sludge bed was successfully used to increase the abundance of PAO in a reactor with a H/D of 1.8 (Henriet *et al*., 2016).

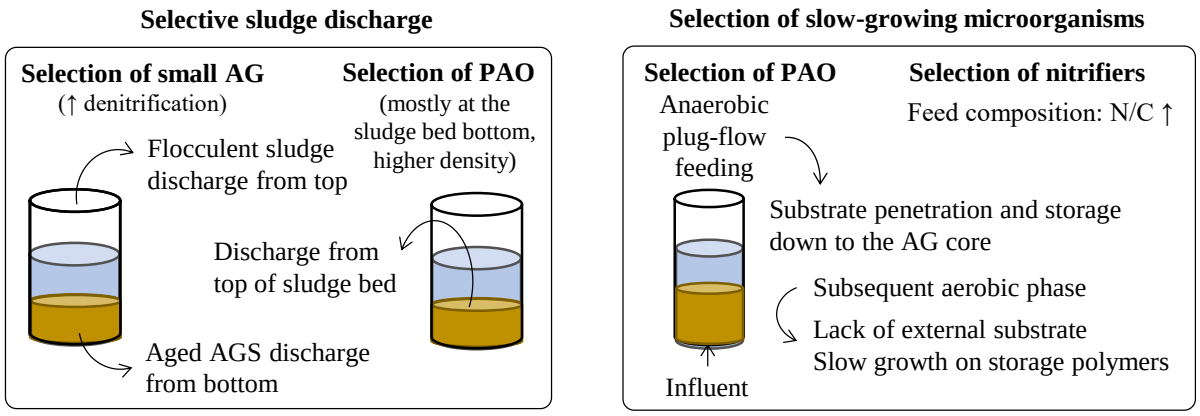


**Figure II.6** - Schematic representation of some operational strategies developed to enhance aerobic granule (AG) stability. AGS: aerobic granular sludge; N/C: nitrogen-to-carbon ratio; PAO: polyphosphate-accumulating organisms; ↑: increase.

Substrate diffusion limitation has been generally regarded as one of the main causes for the breaking up of large mature granules. Hence, control of AG size in the smaller ranges seems to be essential for the long-term stability of AG. Controlling AG size has been attempted by selectively wasting particular AG size fractions, and the effect of this on AGS stability was evaluated (Li *et al*., 2006). Specifically, removing new granules effectively limited AG sizes within the 1-2 mm range and improved their structure, whereas removing aged granules selected for large AG (3-4 mm) with loose structures that further disintegrated (Table II.2). In addition, removing mixed sludge unselectively resulted in granules with good settleability but with a morphology that has been associated with instability.

Verawaty *et al*. (2013) investigated the influence of granule size on mature AG breakage propensity and its influence on long-term granule size distribution (Table II.3). The results revealed a steady-state

distribution of AG sizes spread around a critical size (0.6-0.8 mm), determined by the relative rates of granule growth and breakage, which in turn were influenced by the operational conditions. Namely, for granules larger than the critical size, the rates of attrition/erosion by particle collision and of breakage due to structural weakness exceeded the granule growth rate, leading to reduction in AG size. The opposite occurred for AG smaller than the critical size. At the critical size, overall growth and size reduction processes were balanced and AG size stabilized. Therefore, this study confirmed that larger granules have a stronger tendency to break-up than smaller granules, due to substrate limitations leading to a weakened inner core. On the other hand, these same authors had previously shown that fragments resulting from larger AG breakage act as a viable seed material for new AG. Hence, maintaining a certain fraction of granules with sizes above a particular range was recommended for granule formation during start-up and for process stability in AGS systems. Overall, the authors highlighted that biomass washout should be carefully managed in order to optimize AG formation and long-term stability.

Recently, Zhang *et al*. (2015) achieved AG stability during 220 days in an SBR treating a low strength wastewater by limiting the diameter of AG (under 800 μm) through the use of a combination of strategies, namely different sludge discharge modes. Specifically, during granulation sludge was mainly discharged from the top of the SBR. After granulation was completed, the larger, mature granules were subsequently discharged from the lower part of the SBR, allowing the newly formed, small granules to accumulate. In parallel, alternating anaerobic/aerobic/anoxic conditions were employed in the SBR, which further contributed to ensure the long-term stability of AG through the selection of slow-growing AOB, NOB, PAO and GAO. In fact, as detailed in section II.1.5.2, the use of an anaerobic feed mode acted as a selective pressure by restraining the proliferation of other heterotrophic bacteria and filamentous microorganisms (Zhang *et al*., 2015).

### II.1.5.2. Feeding regimen

The combination of substrate diffusion and microbial consumption rates determines the substrate gradient inside a biofilm, which has been shown to determine its stability. In systems without substrate gradients, regular and compact structures are expected to develop, whereas systems with substrate gradients stimulate filamentous outgrowth (de Kreuk *et al*., 2010). In this sense, specific operational strategies are needed in order to run stable AGS reactors at low oxygen concentrations, aiming at the decrease in energy consumption for aeration and the increase in N-removal efficiency (Mosquera-Corral *et al*., 2005). As previously discussed (section II.1.4.2), the growth rate of microorganisms inside AG plays a major role in AG stability. Specifically, studies showed that selection for slow-growing bacteria could help suppress filamentous growth and improve the stability of AG under low DO concentrations (Liu *et al*., 2004; Wang *et al*., 2007b). For the selection of slow-growers, two major strategies were proposed: increasing the N/COD in the feed to favor the growth of nitrifying

bacteria (Liu *et al.*, 2004) or alternating anaerobic feast and aerobic famine conditions to select for PAO or GAO (Figure II.6), which anaerobically convert easily biodegradable substrates to slowly biodegradable storage polymers (de Kreuk and van Loosdrecht, 2004).

In this sense, de Kreuk and van Loosdrecht (2004) proposed a prolonged, anaerobic low-flow feeding period preceding the aerobic reaction period for the selection of PAO in AGS SBR. The low influent superficial velocity (0.5 m $h^{-1}$) created a plug-flow hydrodynamic regimen rising through the settled bed, with high substrate concentration, thus allowing the substrate to penetrate the entire granule depth and be converted to storage polymers by PAO. Throughout the subsequent aerobic phase, these microorganisms grew at a low rate on their internally stored carbon source. On the other hand, fast-growing heterotrophic microorganisms suffered carbon starvation during this phase (famine period), being outcompeted for substrate and AG space. Contrarily to aerobic pulse-feeding, which led to AGS instability (Beun *et al*., 2000), this anaerobic plug-flow feeding regimen resulted in stable AG. In addition to improving AG stability, the combination of PAO with nitrifying and denitrifying bacteria further improved the treatment efficiency as 100% COD removal, 99% P removal and 90% total-N removal were obtained at 20% DO saturation.

Moreover, studies focusing on AG stability problems raised by the presence of slowly degradable substrates in real wastewaters (colloids, polymeric and particulate substrates), suggested to run the wastewater through an anaerobic hydrolysis step prior to feeding it to the SBR, so as to avoid filamentous outgrowth on the surface of AG (Schwarzenbeck *et al*., 2005). Accordingly, de Kreuk *et al*. (2010) indicated that these substrates need to be hydrolyzed extracellularly to soluble components before they can be used by bacteria in a wastewater treatment reactor. Therefore, longer anaerobic feeding periods in the SBR cycle may allow the hydrolysis and fermentation of slowly degradable substrates, to be subsequently uptaken by the AGS.

Recently, Pronk *et al*. (2015a) further discussed the effect of different carbon sources and of the feeding regimen on AG stability. The authors concluded that the feeding regimen, either plug-flow anaerobic feeding, fast aerobic feeding or slow aerobic feeding, plays a major role in determining AG stability (Table II.4). In summary, during the plug-flow feeding of easily biodegradable, soluble substrates (*e.g.*, acetate), the latter diffuse down to the core of AG and can be converted into storage polymers by PAO and GAO (de Kreuk and van Loosdrecht, 2004). During the subsequent aerobic phase, oxidation of these polymers allows slow microbial growth both in the outer and inner layers of the AG using, respectively, oxygen and other electron acceptors (*e.g.*, nitrate or nitrite when nitrification occurs in the AG outer layers), thus ensuring a stable AG structure. A similar result occurs in case of substrates that are not used by PAO or GAO (*e.g.*, alcohols), but are uptaken by other heterotrophs and allow growth throughout the entire AG depth (Pronk *et al*., 2015a). As for particulate substrates (*e.g.*, starch, proteins) which first need to be hydrolyzed, the stability of AG depends on

their anaerobic hydrolysis rate. Specifically, if complete anaerobic hydrolysis is achieved and the resulting products are converted into storage polymers throughout the granule, stable granulation will occur (de Kreuk *et al*., 2010). On the other hand, if hydrolysis is only partially achieved during the anaerobic plug-flow feeding period, substrate hydrolysis and microbial growth on the hydrolysis products on the AG outer layers during the subsequent aerobic phase may lead to steep substrate concentration gradients across the granule. This situation induces filamentous outgrowth and the occurrence of substrate-depleted AG cores, leading to AG instability (Mosquera-Corral *et al*., 2003).

**Table II.4 -** Effect of different feeding regimens and carbon sources on aerobic granule (AG) stability. $\mu_{max}$: maximal growth rate on the substrate; n.d.: not determined.

| Substrate | | Anaerobic feeding | Aerobic mixed feeding (pulse) | Aerobic mixed feeding (slow) |
|---|---|---|---|---|
| Easily biodegradable soluble | High $\mu_{max}$ | Stable AG | Stable AG | Unstable AG |
| | Low $\mu_{max}$ | Stable AG | Unstable AG | Unstable AG |
| Polymeric | | Stable AG | n.d. | n.d. |

The aerobic, slow feeding of easily biodegradable substrates leads to their rapid oxidation in the outer layers of AG, promoting the proliferation of filamentous microorganisms and severe substrate limitation at the granule core, thus impairing the formation of stable AG (Martins *et al*., 2003). Similarly, the aerobic, fast feeding of the same type of substrates also allows the soluble COD to be mainly oxidized at the AG surface layers, with the same overall consequences (intensified by low DO concentration and shear stress; Beun *et al*., 2002). Nevertheless, in the case of substrates that are aerobically converted by relatively slow-growing bacteria (*e.g.*, ammonium and methanol), the fast aerobic feeding regimen may allow the development of stable granules (Mosquera-Corral *et al*., 2003). Overall, Pronk *et al*. (2015a) concluded that the anaerobic, plug-flow feeding strategy is the most adequate for obtaining stable granules using different types of substrates.

As an alternative to slow anaerobic feeding, fast anaerobic feeding followed by an anaerobic mixing stage was also shown to be successful in the development of stable AG (Rocktäschel *et al*., 2013). As a possible advantage over the plug-flow feeding strategy, the anaerobically-fed mixed system allowed the substrate to be evenly distributed throughout the reactor working volume, instead of creating a substrate gradient along the reactor axis. With plug-flow feeding, the efficiency of substrate distribution depended on the reactor geometry, *i.e.*, reactors with a low H/D tended to develop heterogeneous flow patterns through the granular bed. These channeling effects led to short contact times between the substrate and the biomass and thus to incomplete anaerobic carbon uptake. Consequently, most of the fed COD was still present in soluble form when the aerated reaction phase started, resulting in unstable AG. Only by altering the anaerobic feeding strategy from plug-flow to mixed, could the development of stable AG be reestablished in the reactor with a low H/D. Therefore, it was concluded that achieving efficient anaerobic COD uptake is less dependent on reactor geometry if a mixed, instead of a plug-flow, regimen is applied in the feeding step. Moreover, although lower biomass concentrations were achieved with the anaerobic, mixed feeding strategy, growth of AG was

more stable and resulted in an optimal balance between heterotrophic and autotrophic microorganisms. Thus, feeding under anaerobic, mixed conditions was suggested to be a good alternative for use in full-scale SBR, since conditions approaching plug-flow are difficult to achieve at this scale. Recently, a study on the effect of SBR feeding strategy on the AGS stability in the treatment of a simulated TWW combined both strategies by using an anaerobic plug-flow fed, anaerobic-aerobic SBR (Franca *et al*., 2017). This new hydrodynamic regimen allowed faster AGS recovery from imposed disturbances in the feed composition, when compared with a control anaerobic-aerobic SBR.

### II.1.5.3. Aeration rate adjustment

The differences in AG cell physiology and metabolic kinetics between the feast and famine periods of the SBR operational cycle lead to different oxygen supply and shear stress requirements to ensure the stability of AG. Specifically, owing to the low DO consumption rate by microorganisms during the famine period and the consequent lower shear stress requirement to promote granular cohesion, Liu and Tay (2006) explored the possibility of decreasing the aeration rate during the famine period in order to reduce the overall aeration requirements and associated energy demand (Table II.2). Results demonstrated that a reduced aeration rate (at a superficial velocity of 0.55 cm $s^{-1}$) during famine conditions could maintain stable AG for more than 3 months. Therefore, lowering the aeration rate during the starvation period could be used as a strategy to effectively reduce the total energy input of the AGS system without compromising the stability of AG. Nevertheless, adequate quantification of the oxygen and shear stress requirements in feast and famine periods for the stability of AG still needs further research.

### II.1.5.4. Alternative strategies

Electric fields have been demonstrated to influence the metabolism, physiology, shape and movement of microorganisms. In this context, Huang *et al*. (2014) investigated the effect of the application of a low, direct current electric field on the nitrification performance and structural stability of AG treating ammonia-containing wastewater with low values of the COD-to-$NH_4$-N ratio (in the range of 1.2-6). By applying a 5 V direct current to the SBR, this study provided a novel method for enhancing nitrification, microbial tolerance to free ammonia toxicity and the structural stability of AG (Table II.2). Specifically, the improvement of granule stability was suggested to be due to the stimulation of EPS excretion and a higher accumulation of divalent and trivalent cations in AG, both resulting from the electro-augmentation of the AGS system. In addition, specific microbial classes, such as *Nitrospira*, were enriched in these AG, further enhancing nitrification efficiency and resistance to free ammonia toxicity during long-term operation.

Since conventional continuous-flow reactors cannot easily provide a hydrodynamic regimen inducing sufficient biomass washout, long aerobic starvation periods or high fluid shear, AG generally lose their

stability when cultivated in such reactors (Juang *et al*., 2010). Nevertheless, following the improved structural stability of AG obtained with internal magnesium carbonate precipitation, Lee and Chen (2015) proposed the use of direct chemical precipitation to enhance granule stability in continuous-flow reactors, enabling AGS wastewater treatment at low cost and with less complex processing (Table II.3).

Recently, a novel funnel-shaped internal feature for an SBR was proposed to enhance AGS stability by optimizing granule size distribution (Zhou *et al*., 2016). Specifically, a funnel-shaped steel-wire screen with a mesh size of 2.5 mm was installed inside the column reactor to selectively apply a higher shear rate on larger granules, thus restricting AG overgrowth.

### II.1.6. Concluding remarks and perspectives

AGS technology is regarded as one of the most promising biological wastewater treatment technologies in the 21$^{st}$ century. AG are formed by the self-aggregation of microorganisms performing different and specialized roles in the biodegradation of organic pollutants and biological nutrient removal from wastewaters. This biotechnological innovation presents an attractive, energy-efficient, cost-effective and low-footprint alternative to the conventional flocculent activated sludge process for both municipal and industrial wastewater treatment. Over the last two decades, the AGS technology has developed, matured, and undergone scale-up from laboratory, pilot and prototype systems into full-scale applications. Nevertheless, despite the advances in achieving aerobic granulation and in the characterization of AG, fundamental aspects are still to be improved, such as the problem of AG stability, a key factor for long-term, steady operation of AGS bioreactors.

Granule structure and physical size are critical for the performance of an AGS system and are dependent on the imposed operational conditions and feed wastewater composition. In fact, the type of substrates, the mode of influent addition (aerobic/anaerobic), the loading rate, the applied hydraulic shear forces, the allowed settling time, the volumetric exchange ratio, and the operational HRT and SRT values, all influence the microenvironment of AG, consequently affecting their stability. The most consensual mechanisms involved in loss of AG integrity include the outgrowth of filamentous organisms, cell lysis and EPS hydrolysis at the substrate-depleted core, heterotrophic microorganisms growing at high rates, changes in the spatial distribution of microbial populations, variations in EPS composition and the toxicity of heavy metal ions. These mechanisms, and their association, ultimately lead to the decrease in AG density, with their consequent break-up into small particles with low settleability which are readily washed out from the bioreactor. For instance, AG instability due to high OLRs generally results from rapid heterotrophic growth on the AG outer surface and oxygen limitation at the inner layers. In turn, establishing an optimal OLR value will depend on the substrate type.

In this context, research has focused on understanding the microstructural characteristics that provide AG with good integrity and, with this knowledge, further developing operational strategies to achieve long-term stability of AG. Among all aspects associated with granulation, selecting a microbial population with a low maximal growth rate is arguably the main factor for stabilizing AG. In fact, keeping stable AG in mixed aerobic reactors is apparently only possible with a minimum N/COD value in the feed wastewater, to promote the dominance of slow-growing nitrifiers. Aerobic feeding or excessively long feeding periods generally lead to fast microbial growth or substrate storage only in the outer shell of AG, respectively. The AG core thus becomes substrate-depleted, in both the soluble and storage forms, leading to biomass and EPS decay, the formation of hollows, and the weakening of the AG structure. In this sense, an anaerobic, plug-flow feeding strategy has been developed for selecting bacteria (*e.g.*, PAO, GAO) capable of anaerobically storing the soluble carbon source in the form of slowly-biodegradable internally stored polymers, which results in a low growth-rate under the subsequent aerobic mixed conditions of the aerated reaction phase. Provided that readily biodegradable substrates are essentially removed from the mixed liquor before the aerobic phase, this strategy strengthens the structure of AG by ensuring the supply of substrate throughout the entire granule volume (in AG up to 2 mm in size). Recently, an alternative, anaerobic mixed feeding regimen has been proposed for reactors with a low H/D, though further research is required to achieve optimal mixing conditions (*e.g.*, type of impellers, reactor geometry). In addition, for achieving stable AG using the latter strategy, the substrate feeding rate should not be lower than its maximal removal rate. A different strategy to achieve AG stability relies on the selective removal of AGS fractions, *e.g.*, to increase PAO abundance or to select for AG with the proper size. In fact, despite the selective removal of flocs being more important during the initial granulation process at reactor start-up, thereafter selective sludge discharge should also not be neglected.

With AGS reaching full commercial scale, further development and research should focus even more on the basic principles of granular development and stability. Until now, the emphasis has been on municipal wastewater applications where PAO/GAO bacteria can be easily selected. However, for industrial wastewater treatment, different types of organisms need to be selected since a very different COD composition is expected. Potentially the anaerobic feeding is a general approach, although there is a range of substrates in industrial wastewater that might not be anaerobically metabolized by bacteria. Although it is clear that the structural EPS is key in developing AG, suitable methods for isolating, quantifying and characterizing structural EPS are still absent. This hampers the in-depth understanding of the mechanisms of granule formation and stability. Moreover, it is as yet unclear which microbial group is actually responsible for the EPS generation. Modern genomic tools should be capable of elucidating the responsible microbial community. The correlation between quorum sensing molecules and maintenance of stable AG structures needs more consistent studies. If true causal relations are known, these signal molecules might be actively regulated to steer granule

formation and stability directly. An exciting development might be the use of AGS as a source of structural gel-forming polymers (Lin *et al*., 2015). Most of these polymers have no direct chemical alternatives and can be a way to integrate wastewater treatment in a future more circular economy. In light of this future direction, better characterization of EPS and control over its production are urgently needed.

## II.2. AGS application to textile wastewater (TWW) treatment

### II.2.1. Context and objective

The AGS technology has been scaled-up and implemented for industrial and municipal wastewater treatment under the trade name Nereda® since 2006 and 2009, respectively, leading to the construction of the first full-scale domestic AGS WWTP in 2010 (Epe WWTP, The Netherlands; Giesen *et al*., 2013). The Nereda® technology consists in a sequencing fed-batch process with a simultaneous plug-flow feeding and effluent discharge step, an aeration stage and a settling stage (Pronk *et al*., 2015b), allowing the simultaneous removal of COD, nitrogen and phosphate by AGS (de Kreuk *et al*., 2005a).

According to Royal HaskoningDHV, there are currently more than 50 Nereda® WWTPs in operation or under construction, most of which treating domestic or domestic mixed with industrial wastewaters. For instance, the Epe WWTP treats municipal wastewater with a high contribution of industrial wastewater (35%) from slaughterhouses (Giesen *et al*., 2013), while Yancang WWTP (China) is fed with 30% domestic and 70% industrial wastewater from printing and dyeing, chemical, textile and beverage industries (Li *et al*., 2014). Specifically, in addition to 45 municipal plants, Nereda® WWTPs also include 6 industrial plants, mainly operated for treating wastewaters from the food industry. Two operational Nereda® WWTPs treat wastewater from oils and fats producing facilities, two other are dedicated to dairy industries (one of which under design) and one to a meat industry, treating wastewater from a pig slaughterhouse. In addition, a new plant is under construction for application in the treatment of pulp and paper industry wastewater in Lanaken, Belgium.

Following the successful establishment of this innovative process as a sustainable and cost-effective treatment for municipal wastewater (Pronk *et al*., 2015b), future directions include the application of the AGS technology to a wider range of wastewaters, namely from different industrial sources. In addition, in order to allow the wide-spread implementation of AGS based systems, some knowledge gaps deserve specific attention, such as the AGS stability issue (Nancharaiah and Reddy, 2018) extensively covered in the first part of this chapter, section II.1 (Franca *et al*., 2018).

Many AGS studies, mostly carried out at lab-scale using simulated wastewater, have generated invaluable knowledge on the possible application of AGS SBR systems in the treatment of various industrial wastewaters such as textile, dairy, abattoir, livestock, winery, brewery, palm oil mill, rubber, petrochemical and landfill leachate (Nancharaiah and Reddy, 2018). Overall, AGS has been shown to

potentially enable bioremediation of xenobiotic aromatic compounds including phenol, toluene, pyridine and textile dyes (Adav *et al*., 2008a), as well as removal of micropollutants such as pharmaceuticals and personal care products, and metal ions (Nancharaiah and Reddy, 2018). Moreover, studies using real industrial effluents demonstrated the capacity of AGS to treat not only readily biodegradable wastewaters, such as those of dairy, malting and brewery origin, but also toxic or recalcitrant wastewaters from the textile industry (Nancharaiah and Reddy, 2018).

In fact, in addition to the demonstrated AGS enhanced tolerance to high organic loads and toxic recalcitrant compounds and resistance to shock loadings, the coexistence of aerobic and anoxic-anaerobic zones within the AG (Winkler *et al*., 2013) constitutes a further potential advantage for treating TWW, since both anaerobic and aerobic conditions are required to achieve complete biodegradation of the main type of textile dyes used, azo dyes (Muda *et al*., 2010). Furthermore, the operational SRT flexibility of AGS systems (de Kreuk and van Loosdrecht, 2004) can promote the presence of a more diverse microbial community within the SBR, namely slow-growing populations, whose activity may be advantageous for the biodegradation of toxic and recalcitrant compounds (Clara *et al*., 2005; Langford *et al*., 2005; Lourenço *et al.*, 2015).

Aiming to explore the potential treatment of effluents from the textile industry using the AGS technology, this subchapter presents an up-to-date review of the existing literature on AGS application to TWW treatment, with a focus on the removal of two main TWW pollutants, azo dyes and AgNP. To contextualize, the composition and main environmental problems raised by textile industry wastewaters are initially described. Particular attention is given to the main type of textile dyes used, the azo dyes, their environmental impact and existing solutions for their removal from wastewater being addressed. In the context of the proposed biological treatment processes, studies focused in azo dye biodegradation in anaerobic-aerobic SBR systems are reviewed, namely highlighting the few, recent ones employing the novel AGS technology. In addition to the azo dyes, a separate section is dedicated to an emergent pollutant, AgNP, which have been increasingly used by the textile industry and represent a novel concern regarding the environmental impact of the textile sector. Specifically, data regarding the presence of these ENP in TWW is presented and studies focused on AgNP fate and effects during wastewater treatment, namely in AGS SBR systems, are reviewed in order to provide a state-of-the-art preamble for the investigation at hand.

## II.2.2. Introduction

### II.2.2.1. Textile industry demand, pollution and water consumption

The textile industry can be divided in four main sectors: yarn formation, fabric formation, finishing and fabrication. These cover a broad range of activities from the transformation of natural (*e.g.*, cotton, flax, wool, hemp, jute) or synthetic (*e.g.*, viscose, polyester, nylon, glass, carbon) fibers into yarns and fabrics, to the production of a wide variety of products from hi-tech synthetic yarns to home furnishings and clothing (European Commission, 2017). Owing to the increasing demand for textile products by a growing population, the textile industry and its pollutant wastewaters have been increasing proportionally, making it one of the main sources of water pollution problems worldwide, along with tanneries and pulp and paper industry (Nimkar, 2018). The prediction of a further increase in the world population from over 7.5 billion today to 11 billion by the turn of the century, along with the rise in the standard of living in developing countries, raises serious environmental issues. On average, a person consumes 7 kg of clothing per year, corresponding to a current worldwide annual consumption of over 49 billion kg of textile products (Nimkar, 2018). Following the population growth trend, this demand for textiles is expected to further increase, the textile production and associated pollution presumably rising alongside it.

The textile industry comprises the dry and wet fabric industry, which generate solid and liquid wastes, respectively. The wet processing operations (including desizing, scouring, bleaching, mercerizing, dyeing, printing and finishing stages; comprehensively described by Holkar *et al*., 2016) are responsible for intensive water and chemicals consumption (namely dyes and auxiliary chemicals, *e.g,*. salts and organic compounds) as well as consequent wastewater discharge containing a variety of water pollutants. Overall, TWWs are extremely variable and complex, being characterized by high organic loads and salinity, as well as low biodegradability, especially due to recalcitrant dyes. As a result, the textile industry is rated as one of the most chemically intensive industries on Earth and, possibly, the main industrial consumer and polluter of potable water worldwide (Holkar *et al*., 2016).

Global industrial water requirements are estimated to increase to 1,500 billion $m^3$ by 2030 (800 billion $m^3$ being registered in 2009; Vajnhandl and Valh, 2014). As previously mentioned, the textile industry is one of the most water-consuming industrial sectors, the wet textile process generally consuming more than 100 L per kg of fabric processed (Vajnhandl and Valh, 2014). Accordingly, average sized textiles plants have been reported to consume about 200 L of water per kg of fabric processed, in some cases leading to up to 3,000 $m^3$ of water consumed per day (Ghaly *et al*., 2014; Sarayu and Sandhya, 2012). Specifically in Europe, textile companies consume 50-240 $m^3$ of water per ton of finished product (EWA, 2005), corresponding to up to 500,000 $m^3$ of water per year, on average (Vajnhandl and Valh, 2014). Similarly, the textile industry in India was estimated to consume around 200 $m^3$ of water per ton of fabricated textiles (Dasgupta *et al*., 2015).

### II.2.2.2. Textile industry wastewater

#### II.2.2.2.1. Emission volumes

Following the high water consumption levels, the textile industry generates large amounts of wastewater with a complex mixture of chemicals and extremely variable characteristics. The wastewater generated by textile industry includes cleaning wastewater, process wastewater, noncontact cooling systems wastewater, and storm water (Verma *et al*., 2012). Textile processes like scouring, dyeing, printing and finishing generate the majority of TWW, as they require multiple rinsing sequences, 60-90% of the total water consumption being used for these purposes (Vajnhandl and Valh, 2014). The dyeing and finishing process steps, which involve dyeing of the man-made or natural fibers and their processing into final commercial products, are responsible for around 17-20% of the total TWW produced (Holkar *et al*., 2016). According to previous studies, textile industries typically generate 200-350 $m^3$ of wastewater per ton of finished product resulting in an average pollution of 100 kg COD per ton of fabric (Verma *et al*., 2012). In Europe, 108 million tons of TWW are yearly produced, from which 36 million tons of chemicals and auxiliaries have to be removed (Vajnhandl and Valh, 2014). Typically, all the wastewater streams produced along the various textile processing stages are mixed, collected through the wastewater network and pH-neutralized, thus generating an extremely complex, final TWW that is subsequently sent to the municipal WWTP (Vajnhandl and Valh, 2014).

In accordance with the more significant presence of textile industry in developing countries (Nimkar, 2018), these are the main contributors to the generation of TWW (Verma *et al*., 2012). The textile industry wastewater produced in developing countries of South Asia in 2001 accounted for 35% of all industrial wastewater generated in South Asia (Verma *et al*., 2012). Specifically in India, the largest manufacturer of textiles in this region, wastewater generation from the textile industry has been estimated to be within 200-350 $m^3$ per ton of finished product (Dasgupta *et al*., 2015), corresponding to around 55 million $m^3$ of wastewater per day, of which approximately 70,000 $m^3$ were directly dumped into local rivers and streams without prior treatment (Verma *et al*., 2012). More specifically, Sarayu and Sandhya (2012) reviewed data regarding the quantity of wastewater generated by textile industries in India, from facilities processing different types of fibers.

#### II.2.2.2.2. Composition

The composition of the TWW depends on the type of fiber, dyes and assisting chemicals employed, as well as final product characteristics (Dasgupta *et al*., 2015). Worldwide, approximately 8,000 different chemicals (such as dyes, salts, organic and inorganic acids, alkalis, hydrogen peroxide, starch, surfactants, soaps, heavy metals, resins, solvents, waxes, oils), corresponding to around 5 million ton of dyes, pigments and finishing chemicals, are currently used at various textile manufacturing stages

(Nimkar, 2018). Most of these end up being discharged in the wastewater of the textile plant. For instance, sizing agents, applied to yarn before fabric production to ensure fast and secure weaving processes, are subsequently removed from the woven fabrics in a wet process (desizing), the desizing wastewater representing up to 50% of the organic load in the wastewater discharged from the textile finishing industry (Sarayu and Sandhya, 2012). Each process operation is associated with the release of specific chemicals, as described in several previous reviews (Verma *et al.*, 2012; Holkar *et al.*, 2016; Figure II.7). Furthermore, specialty chemicals have been recently developed to impart functional properties to the final textile fabric, such as softening, wrinkle-free effect, oil and water repellency, flame retardancy and anti-microbial characteristics. Approximately 90% of these finishing chemicals remain on the substrate, the remaining 10% being washed off during processing and subsequent consumer use (Nimkar, 2018).

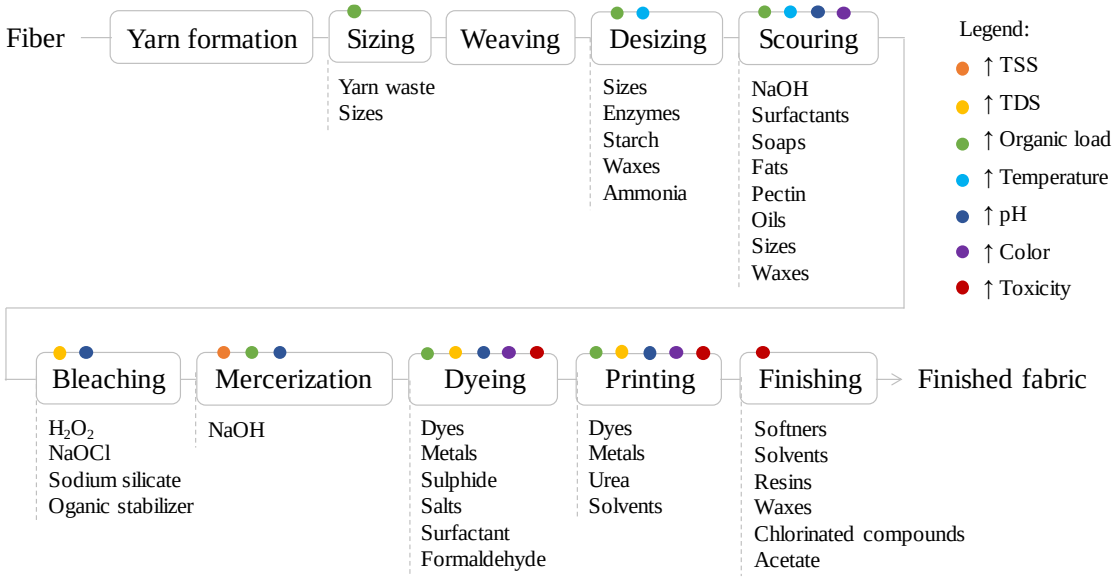


**Figure II.7** - Typical pollutants released in each textile production operational process, and identification of the major contributors for the presence of high total suspended solids (TSS), total dissolved solids (TDS), organic load, temperature, pH, color and toxicity in textile wastewater (adapted from dos Santos *et al.*, 2007); ↑: increased.

As a consequence of discharging a significant amount of the chemicals employed along the textile processing, TWWs are generally high in color, biochemical oxygen demand (BOD), COD, total suspended solids (TSS), total dissolved solids (TDS), pH extremes, temperature, turbidity, salinity and toxic chemicals, some of which can breakdown into further harmful metabolites. This potentially results in contamination of natural water bodies from indiscriminate wastewater discharges, due to inadequate management and control in implementing wastewater discharge laws in many textile producing countries (Nimkar, 2018).

Furthermore, the seasonality of the textile industry and diversity of final textile products manufactured lead to a significant variability in the TWW characteristics, namely in terms of pH (2-14), conductivity (0.1-120 mS $cm^{-1}$), TSS (50-24,000 mg $L^{-1}$), TDS (50-6,000 mg $L^{-1}$), turbidity (0-200 NTU), COD (50-18,000 mg $O_2$ $L^{-1}$), $BOD_5$ (100-6,000 mg $L^{-1}$) and light absorbance (up to 200) due to strong color

(Vajnhandl and Valh, 2014; Verma *et al*., 2012). Moreover, the BOD-to-COD ratio of TWW has been reported to average 0.25 (Ghaly *et al*., 2014), generally being within the 0.2-0.5 range (Solís *et al.*, 2012), which denotes the presence of a large proportion of non-biodegradable, oxidable substances. Dasgupta *et al.* (2015) and dos Santos *et al*. (2007) presented typical physicochemical parameter levels characterizing wastewater streams derived from the different textile processing stages, while Sarayu and Sandhya (2012) compared the final wastewater from different types of textile industries in terms of pH, TSS, COD, BOD, oil, phenol, chloride, sulfate and sodium.

### II.2.2.2.3. Discharge limits and environmental impact

Regarding India, one of the largest textile producers in the world, Dasgupta *et al.* (2015) indicated discharge limit standards into public sewers in terms of pH (5.5-9.0), TSS (100 mg $L^{-1}$), TDS (2,100 mg $L^{-1}$), COD (250-500 mg $L^{-1}$), $BOD_5$ (30 mg $L^{-1}$), color (colorless), chlorides (600-1,000 mg $L^{-1}$) and sulfate (50-300 mg $L^{-1}$). Table II.5 presents representative ranges for these TWW parameters in India and Portugal, along with regulatory limits established for the discharge of TWW into surface waters and sewers in different European countries. Comparing the discharge limits with the typical range of values for the most relevant physicochemical properties of TWW (Table II.5), it is clear that wastewater treatment facilities within the textile mill sector are fundamental to achieve compliance with the legal restrictions imposed in order to avoid severe environmental damage.

**Table II.5 -** Typical physicochemical properties of textile wastewaters and respective standard discharge limits into public sewers and surface waters in different countries. The values regarding Italy and Spain refer to the Legislative Decree No. 152 (2006) and Industrial Liquid Dumping Law to Integrated Systems of Sanitation (2015), respectively (adapted from Bento, 2016 and Coelho, 2018). COD: chemical oxygen demand; $BOD_5$: biochemical oxygen demand; TSS: total suspended solids. n.v.: not visible.

| Parameter | Typical ranges | | Standard discharge limits | | | | | |
|---|---|---|---|---|---|---|---|---|
| | Untreated textile wastewater | | Public sewers | | | | Surface waters | |
| | India [a] | Portugal [b] | India [c] | Spain [d] | Portugal [b] | Italy [d] | Portugal [b] | Italy [d] |
| COD (mg $O_2$ $L^{-1}$) | 150 - 12,000 | 102 - 11,000 | 250 - 500 | 1,750 | 1,000 | 500 | 150 | 160 |
| $BOD_5$ (mg $L^{-1}$) | 80 - 6,000 | 9 - 2,580 | 30 | 1,000 | 500 | 250 | 40 | 40 |
| TSS (mg $L^{-1}$) | 15 - 8,000 | <3 - 2,500 | 100 | 1,000 | 1,000 | 200 | 60 | 80 |
| pH | 6 - 10 | 4.7 - 11.8 | 5.5 - 9.0 | 6 - 10 | 5.5 - 9.5 | - | 6-9 | 5.5 - 9.0 |
| T (ºC) | 35 - 45 | 16 - 41 | - | 40 | 30 | 30 | - | 30 |
| Color | 50 - 2.500 Pt-Co* | - | n.v. | - | - | n.v.[1] | n.v.[2] | n.v.[2] |

[1] sample dilution 1:40; [2] sample dilution 1:20; [a] Ghaly *et al*., 2014; [b] Citeve, 2012; [c] Dasgupta *et al.*, 2015; [d] ZDHC, 2015.
* The platinum-cobalt (Pt-Co) scale is used to evaluate color levels in wastewater.

In fact, direct discharge of untreated TWWs into surface waters can affect fauna, flora and microbial communities. Specifically, the high organic and nutrient loads typically associated with these effluents can promote the overgrowth of aquatic flora and consequent depletion of DO, thus negatively affecting the fauna. Ultimately, this situation can lead to eutrophication of the water body (Sarayu and Sandhya, 2012). Furthermore, the presence of color and suspended solids can inhibit the photosynthetic processes by decreasing sunlight penetration in water, thus eliminating or reducing the

primary producers in the food chain and disturbing the ecological balance (Pandey *et al*., 2007). In addition, some inorganic chemicals found in TWWs, namely hydrochloric acid, sodium hypochlorite and sodium hydroxide, as well as heavy metals (such as chromium, arsenic, copper and zinc), can be acutely toxic to aquatic life (Ghaly *et al*., 2013).

The following sections will further address two main polluters in TWW: textile dyes, specifically azo dyes, and ENP, specifically AgNP, focusing on their environmental impact and potential for biological removal from TWW, namely through the use of AGS SBRs.

### II.2.2.3. Textile dyes – Characteristics, presence in TWW and environmental impact

Among the various complex constituents present in TWWs, dyes are considered one of the strongest sources of contamination. Dyes are classified according to their application (reactive, acid, direct, basic, mordant, disperse, vat, sulfur, pigment, anionic, ingrain, and solvent dyes; Rangabhashiyam *et al*., 2013) and their chemical structure. The latter comprises chromophores (such as azo, carbonyl, nitro, methine, ethenyl, imino and quinoid groups, responsible for providing the color; Raman and Kanmani, 2016) and auxochromes (electron withdrawing or donating substituents, such as amino, carboxyl, sulfonyl and hydroxyl groups that intensify the color and improve solubility and dye adherence to the fiber; Verma *et al*., 2012). Owing to their chemical structure, dyes can absorb light with wavelength in the visible region (350-700 nm), which is why light penetration in water bodies is diminished in the presence of these compounds (Sarayu and Sandhya, 2012).

There are more than 100,000 commercially available dyes and the world annual dyestuff production is estimated to round 900,000 tons (Rawat *et al*., 2016), nearly two-thirds of which are consumed by the textile industry (Rangabhashiyam *et al*., 2013). Specifically, the textile industry in India consumes around 80% of the total dyestuff production, in response to the high global demand for colored polyester and cotton fabrics (Holkar *et al*., 2016). Hence, reactive and disperse dyes represent approximately half of the world demand for dyes. According to previous estimations, more than 10-15% of the processed dyestuffs are predictably released into the environment during their synthesis and the textile dyeing stages (Sarayu and Sandhya, 2012; Verma *et al*., 2012). More recently, up to 50% of the annual dye production has been estimated to reach the environment (Rawat *et al*., 2016). Worldwide, 280,000 tons of textile dyes have been reported to be yearly discharged in textile industrial effluents, due to inefficient dye fixation processes onto the fibers (Singh *et al*., 2015; Solís *et al.*, 2012). The degree of dye losses into the wastewater depends on different factors, namely the dyestuff type and the application method (Table II.6). Specifically, reactive dyes (representing approximately 30% of the total dye market; Pearce *et al*., 2003) have the lowest level of dye-fiber fixation efficacy (10-50%; O'Neill *et al*., 1999; Raman and Kanmani, 2016).

Due to the significant loss of unfixed dyes, color is the first pollution indicator in textile wastewater, because it can be visually detected at dye concentrations as low as 1 mg $L^{-1}$ (Sarayu and Sandhya,

2012), even lower levels of 0.005 mg $L^{-1}$ for certain dyes being specifically reported as visible in clear river water (Pearce *et al.*, 2003). Despite the extremely variable color content in effluents from the textile industry, typical dye concentrations in TWW have been reported within the 10-250 mg $L^{-1}$ range (O'Neill *et al.*, 1999; Pandey *et al*., 2007). Synthetic dyes are designed to have high durability, which gives them high stability in water and a recalcitrant nature, resistant to biodegradation. Therefore, conventional biological wastewater treatment processes fail in efficiently removing textile dyes from wastewaters, potentially leading to their long-term persistence in natural water bodies (Dasgupta *et al*., 2015; dos Santos *et al*., 2007). As a first impact, water coloration raises social alarm due to the aesthetic impact and decrease in water transparency. As previously mentioned, colored wastewater discharges compromise aquatic life by hindering light penetration in water, reducing photosynthetic activity and, consequently, the DO concentration (Collivignarelli *et al*., 2019). Furthermore, other hazardous effects on the flora and fauna can occur, owing to the toxicity, mutagenicity and carcinogenicity of some dyes and their breakdown products, especially in the case of azo dyes (Hisaindee *et al*., 2013).

**Table II.6 -** Chemical dye types for the main classes of synthetic dyestuffs used in the textile industry, with indication of respective estimated degree of loss to the textile wastewater in the dyeing process of typical fibers (adapted from O'Neill *et al.*, 1999). n.d.: not defined.

| Class | Chemical types | Fiber | Loss (%) |
|---|---|---|---|
| Acid | Azo, azine, nitro, nitroso, triphenylmethane, xanthene | Polyamide | 5-20 |
| Basic | Azo, anthraquinone, azine, acridine, cyanine, diazocarbocyanine diazohemicyanine, diphenylmethane, hemicyanine, oxazine, triarylmethane, xanthene | Acrylic | 0-5 |
| Direct | Azo, oxazine, phthalocyanine, stilbene | Cellulose | 5-30 |
| Disperse | Azo, anthraquinone, benzodifuranone, nitro, styryl | Polyester | 0-10 |
| Mordant | Azo, anthraquinone | Wool | n.d. |
| Reactive | Azo, anthraquinone, basic, formazan, oxazine, phthalocyanine | Cellulose | 10-50 |
| Sulfur | Indeterminate or poorly understood structures | Cellulose | 10-40 |
| Vat | Anthraquinone, indigoids | Cellulose | 5-20 |

### II.2.2.4. Azo dyes

#### II.2.2.4.1. Characteristics

Structurally, azo dyes are complex aromatic compounds characterized by the presence of one or more azo groups (–N=N–), linked to phenyl and naphthyl groups, which are usually substituted with some combinations of functional groups including amino ($-NH_2$), carboxyl (−COOH), chloro (−Cl), hydroxyl (−OH), methyl ($-CH_3$), nitro ($-NO_2$) and sulfonic acid ($-SO_3H$) groups (Saratale *et al*., 2011). This allows a significant structural diversity, accounting for more than 3000 different varieties of azo colorants (including dyes and pigments), spread through the main classes of synthetic dyestuffs (Pinheiro *et al*., 2004; Table II.6). Owing to the ease and cost effectiveness of their synthesis, and their stability, color fastness and variety, azo dyes account for more than 70% by weight of all dyestuffs

used worldwide, being used in textile, food, paper, printing, leather, cosmetic and pharmaceutical industries (Rawat *et al*., 2016). In fact, azo dyes are the largest and the most versatile class of synthetic colorants applied in textile processing (approximately 80% by weight) and, consequently, the most commonly released into the environment (Saratale *et al*., 2011; Singh *et al*., 2015).

#### II.2.2.4.2. Aromatic amines and environmental hazard

The resistance of the azo dyes to conventional aerobic bioprocesses in WWTPs results in severe contamination of the rivers and ground water in areas with high concentration of dyeing industries (Stolz, 2001). In addition to the previously described negative impact caused by the discharge of colored effluents into natural water bodies, azo dyes further threaten the flora, fauna and humans, due to the toxicity and potential carcinogenicity and mutagenicity of some of them and their breakdown products (Solís *et al*., 2012). In fact, under certain environmental conditions, namely under low DO concentrations, the natural remediation potential of ecosystems may lead to partial degradation of these compounds through reductive cleavage of the azo bond, originating metabolites that can be more toxic than the original dye, specifically aromatic amines (Pinheiro *et al*., 2004; Rawat *et al*., 2016). In this sense, the use of azo dyes that could breakdown to potentially carcinogenic aromatic amines has been restricted in Europe (Pinheiro *et al*., 2004; Directive 2002/61/EC; Regulation (EC) 1907/2006). Even so, careful evaluation of treated TWW (geno)toxicity still remains recommendable (van der Zee and Villaverde, 2005).

In this context, azo dye-laden wastewater treatment strategies should be designed to achieve complete degradation of the azo dye, including the breakdown of any intermediate metabolites (van der Zee and Villaverde, 2005).

#### II.2.2.4.3. Treatment solutions

Regarding the treatment of dye-laden TWW, while water-insoluble dyes (such as some disperse, vat and sulfur dyes) are often removed in the primary treatment of conventional WWTPs, most of the water-soluble dyes are neither efficiently adsorbed nor biodegraded by the biomass in the secondary treatment, resulting in the discharge of colored effluents (O'Neill *et al*., 1999; Saratale *et al*., 2011). In this sense, the combined effect of conventional sewage treatment and dilution are generally not sufficient to meet the color consent limits. In addition, municipal wastewater treatment tariffs have been increasing. Therefore, textile industries have been compelled to search for innovative wastewater decolorizing technologies and develop dedicated on-site facilities to treat their own wastewater before discharge (Collivignarelli *et al*., 2019; Pearce *et al*., 2003).

In general, color removal occurs either by breaking down the dye molecule (at least partially) or by transferring it onto the sludge fractions. The latter can potentially contaminate the soil or the air, if disposed of into landfills or incinerated (Nimkar, 2018). Incidently, it has been estimated that 90% of

the dyes and chemicals that are on the fabrics will end up in landfills and leach out to the water bodies (Nimkar, 2018). Owing to the increasingly stricter environmental regulations, it is likely that dye degradation technologies will prevail (Pearce *et al*., 2003). Moreover, in the context of resource recovery, wastewater treatment technologies should focus on removing toxicity, mineralizing aromatic compounds and producing reusable water, as well as recovering valuable compounds, rather than simply removing the color by producing toxic sludge (Holkar *et al*., 2016).

### II.2.2.4.3.1. Physicochemical processes

Many review articles (Collivignarelli *et al*., 2019; Dasgupta *et al*., 2015; Holkar *et al*., 2016; Solís *et al*., 2012) have focused on different methods to treat colored TWW, namely oxidation methods (cavitation, Fenton processes, photocatalytic oxidation, chemical oxidation such as ozonation and peroxidation), physical methods (adsorption, coagulation/flocculation and membrane filtration) and biological methods (using fungi, algae, bacteria, and microbial fuel cells). Regarding physicochemical methods, coagulation/flocculation methods have been used for many years for the main treatment or pre-treatment of TWW, both in developed and developing countries (Verma *et al*., 2012). However, the cost of treating the typically large volumes of contaminated sludge produced by these methods, and the increasing restrictions concerning their disposal, limit the application of coagulation/flocculation processes to treat TWW. While some advanced oxidation processes (AOP) have also been more recently employed, full-scale application of promising biological processes and electrochemical processes require further development (Collivignarelli *et al*., 2019).

Conventional and advanced treatment methods differ in terms of efficiency, cost and environmental impact. In general, the implementation of the physicochemical methods for color removal (extensively reviewed by several authors; Dasgupta *et al*., 2015; dos Santos *et al*., 2007; Fatima *et al*., 2017; Pearce *et al*., 2003; Raman and Kanmani, 2016; Saratale *et al*., 2011; Solís *et al*., 2012; Verma *et al*., 2012) has inherent drawbacks (Table II.7), such as high cost due to intense energy demand and excessive chemicals use, transfer of contaminants without transformation, generation of high volumes of concentrated, polluting sludges requiring safe disposal, inefficient removal of recalcitrant azo dyes and their metabolites, as well as formation of hazardous by-products (Forgacs *et al*., 2004; Saratale *et al*., 2011).

### II.2.2.4.3.2. Biological processes

Regarding biological methods for azo dye removal, different microorganisms have been studied for bioremediation of TWW, including aerobic and anaerobic bacteria, yeast, filamentous fungi and algae, as comprehensively reviewed by Solís *et al.* (2012). In addition, the azo dye decolorization capacity of land plants has been shown in phytoremediation studies (Khandare and Govindwar, 2015), and enzymatic processes for TWW treatment have also been explored (Singh *et al*., 2015).

Biodecolorization can occur either via biosorption on microbial cells and/or via biodegradation, involving enzymatic activity (Solís *et al*., 2012). In fact, although azo dyes are generally considered as xenobiotic compounds and recalcitrant to biodegradation (namely during treatment with CAS), several microorganisms are able to transform azo dyes into non-colored breakdown products (partial biodegradation) or even to completely mineralize these metabolites (total biodegradation), under certain environmental conditions (Stolz, 2001; van der Zee and Villaverde, 2005).

**Table II.7 -** Drawbacks of physicochemical methods regarding their application to treat colored textile wastewaters (dos Santos *et al*., 2007; Holkar *et al*., 2016; Raman and Kanmani, 2016; Saratale *et al*., 2011; Solís *et al*., 2012; Verma *et al*., 2012). TWW: textile wastewater.

| Treatment method | Limitations |
|---|---|
| Adsorption | - General high cost of the adsorbent (activated carbon is the most used adsorbent);<br>- Difficult adsorbent regeneration;<br>- Transfer of contaminants from one phase to another without transformation;<br>- Low efficiency towards dyes other than disperse dyes;<br>- Sludge generation;<br>- High cost of handling/disposal of the spent adsorbent;<br>- Excessive maintenance costs;<br>- Need for a pre-treatment to reduce the total suspended solids content. |
| Coagulation/flocculation | - Low decolorization efficiency of some dyes (acid, direct, reactive and vat dyes);<br>- Excessive use of chemicals;<br>- Large generation of sludge requiring treatment before disposal. |
| Membrane filtration (*e.g.*, ultrafiltration, nanofiltration, reverse osmosis) | - High initial investment cost;<br>- Frequent membrane fouling;<br>- Requirement of different pre-treatments depending on the wastewater;<br>- Generation of concentrated streams requiring treatment before disposal. |
| Advanced Oxidation Processes (*e.g.*, Fenton processes, ozonation, peroxidation, photocatalysis) | - High cost (high energy demand; short half-life of ozone, in case of ozonation);<br>- Generation of toxic byproducts;<br>- Effectiveness dependent on the TWW (*e.g.*, pH, dye type and concentration);<br>- Complex procedures;<br>- High sludge production (in case of Fenton processes). |

Several biological methods have been designed to promote anaerobic and/or aerobic dye degradation by pure microbial populations, mixed microbial communities, or isolated enzymes. The use of algae and systems based on yeasts or filamentous fungi for the removal of azo dyes from TWW have been recently reviewed (Holkar *et al*., 2016; Sen *et al*., 2016). Moreover, Singh *et al*. (2015) extensively reviewed different azo dye decolorization and degradation systems using enzymes isolated from bacteria, fungi and yeasts, specifically reductases and oxidases (such as azoreductase, laccase, peroxidase, tyrosinase and polyphenol oxidase). The oxidative degradation of azo dyes is catalyzed by peroxidases and phenoloxidases, such as manganese peroxidase, lignin peroxidase, laccase, tyrosinase, N-demethylase, dye-decolorizing peroxidases, and cellobiose dehydrogenase. These oxidases are found in filamentous fungi, bacteria and yeasts (Solís *et al.*, 2012). Yet, in the context of TWW treatment, the use of whole cells rather than isolated enzymes is more realistic, owing to the costs associated with enzyme purification and the fact that degradation is best carried out by a number of

enzymes working sequentially, which would be difficult to achieve using individually extracted enzymes (Pearce *et al*., 2003). Overall, bacteria represent the vast majority of researched microorganisms for the decolorization of azo dyes (Forgacs *et al.*, 2004; Holkar *et al*, 2016; Pearce *et al*., 2003; Saratale *et al*., 2011), namely owing to their fast growth and capacity to efficiently adapt to a wide range of environmental conditions (Solís *et al*., 2012). The bacterial capacity to decolorize azo dyes is further explored in section II.2.2.4.4.

### II.2.2.4.3.3. Combined processes

To date, there is no single economically and technically effective method to solve the TWW-related environmental issue (Collivignarelli *et al*., 2019). In fact, a universal end-of-pipe solution is impractical because of the complex and highly variable composition of TWW (Pearce *et al*., 2003). Thus, Collivignarelli *et al*. (2019) suggested that to achieve efficient TWW treatment, each case should be individually assessed. Furthermore, optimal solutions providing the best overall economic and environmental performance might reside in the combination of different types of processes to enable an effective wastewater treatment at an affordable cost for the textile industries (Collivignarelli *et al*., 2019; Holkar *et al*., 2016; Pearce *et al*., 2003; Verma *et al*., 2012). Furthermore, a review of different studies where oxidation methods were combined with biological methods for the degradation of dyes in TWW (Holkar *et al*., 2016), concluded that the efficiency potential of the biological method has to be maximally exploited in order to decrease the cost of treatment. In fact, the total cost of a biological WWTP has been estimated to be 70-80% lower than that of a chemical WWTP (Holkar *et al*., 2016).

In general, biological methods have been considered an attractive alternative for the treatment of large volumes of dye-laden TWW due to their cost effectiveness and environmentally friendly nature (Pandey *et al*., 2007; Solís *et al*., 2012; Singh *et al*., 2015; van der Zee and Villaverde, 2005). In contrast with physicochemical methods, biological treatment methods generally involve simpler processes, lower operation costs, higher versatility, reduced water consumption and waste sludge generation, and can potentially convert (in some cases, fully mineralize) azo dyes into non-hazardous end-products (Dasgupta *et al*., 2015; Holkar *et al*., 2016; van der Zee and Villaverde 2005). Yet, TWW parameters after biological treatment commonly fail to comply with discharge standards. In this sense, it has been suggested that, prior to the biological method, recalcitrant organic compounds such as dyes should be partly oxidized chemically with AOP to reduce the inhibitory effect of toxic compounds on bacteria and increase the biodegradability of the wastewater (Holkar *et al*., 2016; Solís *et al*., 2012). Conversely, AOP have also been tested as post-treatments, after application of a biological method, being restricted to the final degradation of the non-biodegradable, recalcitrant compounds, thus minimizing the AOP-associated chemicals and energy consumption (Solís *et al*., 2012). This combined biological and AOP treatment takes advantage of both the cost-efficiency of the

biological process and the AOP efficiency for complete aromatic amine degradation (Jonstrup *et al*., 2011).

### II.2.2.4.4. Azo dye decolorization by bacteria

Azo dye decolorization studies have used pure bacterial cultures, co-cultures and mixed bacterial cultures (Holkar *et al*., 2016; Pearce *et al*., 2003; Saratale *et al*., 2011). Single microbial strains are able to decolorize azo dyes, but the degradation products (specifically, aromatic amines) are frequently more toxic and recalcitrant than the parent dye (Solís *et al.*, 2012). In fact, although the use of pure culture systems ensures reproducible data and facilitates the understanding of biodegradation mechanisms (Saratale *et al*., 2011), they are not suitable for practical TWW treatment applications. On the other hand, mixed bacterial cultures generally achieve a higher degree of biodegradation and mineralization of dyes, owing to the complementarity/synergism of metabolic activities within a microbial community (Holkar *et al*., 2016; Pearce *et al*., 2003).

#### II.2.2.4.4.1. Proposed mechanisms

Reductive cleavage of the highly electrophilic azo bond in the dye molecule, leading to the formation of colorless aromatic amines, allows decolorization and corresponds to the initial step of bacterial degradation of azo dyes. This azo dye decolorizing step has been reported to occur under anaerobic (methanogenic), anoxic and aerobic conditions, being undertaken by different groups of bacteria (Pandey *et al*., 2007). Few bacterial strains, isolated from TWW or dye contaminated soils, have been reported to aerobically use simple azo dyes as growth substrates, presumably also starting with azo bond cleavage by specific azo reductases (Stolz, 2001). In this case, long periods of culture are usually required for microbial adaptation to specific dyes, their decolorization capacity being limited to a narrow dye substrate range (Pandey *et al*., 2007), which is impractical for real TWW treatment applications. In fact, azo dyes are not readily metabolized under aerobic conditions, resulting in the persistence of color during conventional aerobic biological treatment in WWTPs. In contrast to the few reports of aerobic decolorization of azo dyes, a wide range of bacteria are able to reduce azo compounds under anaerobic conditions (van der Zee and Villaverde, 2005).

Under anaerobic conditions, the azo dye decolorization mechanism is considered to be unspecific regarding both the microorganisms and the azo dyes (Stolz, 2001), which represents a clear practical advantage in light of the diversity of azo dyes present in TWWs. Specifically, the transfer of four-electrons to the azo bond results in its cleavage and produces colorless aromatic amines. These electrons are originally generated from the biological oxidation of an organic substrate. Therefore, the anaerobic decolorization process depends on the presence of an organic substrate as the primary source of the reducing equivalents, the azo dye being the terminal electron acceptor (dos Santos *et al*., 2007).

Overall, the azo bond reduction process may occur intracellularly or extracellularly and may involve enzymes, redox mediators (*e.g.*, quinones) and biogenic reductants (*e.g.*, sulfide and ferrous ion). There is no clear evidence of specific anaerobic azo reductases or non-specific enzymes that directly catalyze the reduction of a wide range of electron-withdrawing contaminants, such as azo dyes (Pandey *et al*., 2007). Moreover, intracellular azo dye reduction cannot be responsible for the conversion of all types of azo dyes, as most azo dyes have high molecular weight and contain highly polar sulfonated groups, resulting in limited cell membrane permeation (Stolz, 2001). Furthermore, no correlation was found between the decolorization rate of azo dyes and their molecular weight (Pandey *et al*., 2007). Therefore, the anaerobic azo dye reduction is generally considered to be a non-specific, extracellular, co-metabolic reaction in which reducing equivalents from either biological or chemical sources are transferred to the dye (van der Zee and Villaverde, 2005).

A previous hypothesis of extracellular azo dye reduction by reduced flavins formed by cytoplasmic flavin-dependent azoreductases has been discarded owing to the almost impermeable nature of bacterial membranes towards flavin-containing cofactors (Pearce *et al*., 2003). Therefore, the link between the intracellular electron transport systems and extracellular azo dyes was hypothesized to be established at the cell membrane level (outer membrane in the case of Gram-negative bacteria). Specifically, Brigé *et al.* (2008) demonstrated that the extracellular azo dye reduction requires a multicomponent electron transfer pathway, comprising cytoplasmic membrane, periplasmic and outer membrane components. In this sense, the electron transport components can directly contact with either the azo dye substrate or a redox mediator at the cell surface (Pearce *et al*., 2003). In the latter case, the involvement of electron transport systems in the cell membrane of aerobic or facultative anaerobic bacteria has been suggested, through the transfer of electrons from the respiratory chain to redox mediators at the cell membrane level, which in turn reduce the extracellular azo dyes (Pandey *et al*., 2007).

Most authors agree that the decolorization of high molecular weight, sulfonate-containing azo dyes involves a redox mediator that is enzymatically reduced (or chemically, by bulk reductants in the extracellular space) and that, in turn, chemically reduces the azo dye (dos Santos *et al*., 2007; Stolz, 2001). This allows a very unspecific reduction process, mainly controlled by the redox potentials of the azo dye and the redox mediator (Stolz, 2001). In fact, azo dye decolorization can eventually occur from purely chemical reactions with reduced biogenic inorganic compounds that are formed as end-products of anaerobic bacterial metabolic reactions (*e.g.*, sulfide and ferrous ion) and that directly or indirectly (via further reduction of another redox mediator) reduce the azo dye (Pandey *et al*., 2007).

In summary, direct or indirect enzymatically-mediated azo dye reduction can potentially occur intracellularly for the few azo dyes that are able to cross the cell membrane. In contrast, high molecular weight and/or sulfonated azo dyes (representing their vast majority) can be directly or

indirectly reduced by bacterial enzymes in the extracellular space (Figure II.8). In this case, the direct reaction implies that the enzyme is either located at the membrane level, where contact between the enzyme and the azo dye could potentially occur, or synthesized and secreted without accumulation in the cell interior (this has been hypothesized for a cytoplasmic dehydrogenase enzyme; Singh *et al*., 2015). On the other hand, the indirect transfer of enzymatically-produced reducing equivalents to the extracellular azo dye involves redox mediators, which may be organic or inorganic compounds metabolically produced by bacteria or externally added to the medium (Pearce *et al.*, 2003). During this indirect azo dye reduction process, although the final reduction of azo dyes is a dominantly chemical redox reaction, the redox mediators depend on bacterial reducing enzymes to supply electrons (Pearce *et al*., 2003).

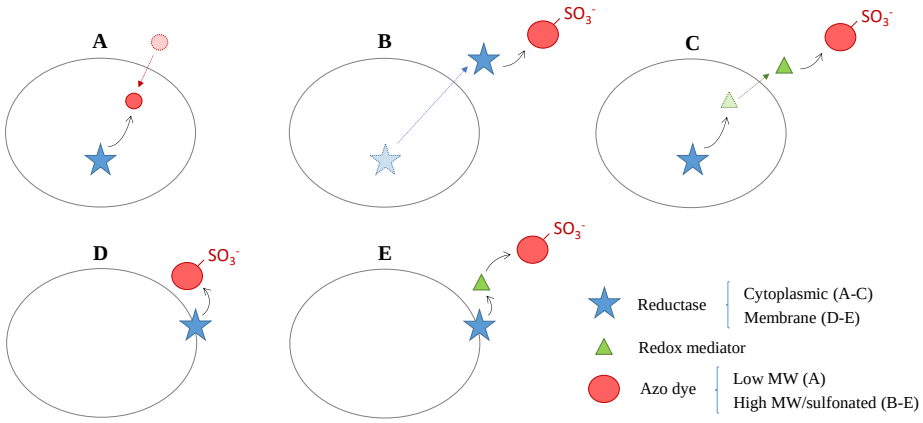


**Figure II.8 -** Summary of alternative, enzymatically-mediated azo dye reduction mechanisms: A) direct, intracellular; B and D) direct, extracellular; C and E) indirect; extracellular. The large, grey circumference represents a microbial cell. MW: molecular weight.

### II.2.2.4.4.2. Efficiency factors

Since the azo dye decolorization process is essentially a redox reaction, it is highly inhibited by the presence of oxygen, which is a preferable electron acceptor owing to its higher redox potential (dos Santos *et al*., 2007; Solís *et al*., 2012). Similarly, the presence of nitrate has also been reported to inhibit decolorization by competing with the azo dye for the reducing equivalents (Lourenço *et al*., 2000, van der Zee e Villaverde 2005). In addition to the DO level, the decolorization efficiency depends on the azo dye concentration and chemical structure, the type and concentration of carbon and nitrogen sources, the presence and redox potential of redox mediators, salinity level, temperature and pH (typically optimal at 35-45ºC and pH 6-10; Saratale *et al*., 2011), as well as the presence of toxic compounds in the TWW (Holkar *et al*., 2016; Solís *et al*., 2012).

The decolorization efficiency may be negatively affected by high dye concentrations, either due to exceeding the biologically-mediated azo dye reduction capacity or by exerting toxicity on the biomass, either directly or as a consequence of the higher concentration of produced aromatic amines. In fact, it has been reported that although the initial decolorization rate increases, the net color removal efficiency decreases in the presence of higher dye concentrations (van der Zee and Villaverde, 2005).

Regarding dye chemical structure, decolorization of monoazo dyes is faster than in case of compounds with a higher number of azo bonds. Moreover, the presence of hydroxyl or amino groups facilitates the azo reduction, as opposed to the presence of methyl, methoxy, sulpho or nitro groups (Saratale *et al*., 2011). Furthermore, the presence of electron-withdrawing substituents, such as sulfonate, in the *para*- or *ortho*-positions relative to the azo bond has been associated with higher decolorization rates (Solís *et al*., 2012). The same effect is observed in the presence of a higher concentration of the substrate acting as primary carbon and energy source for bacteria, which is also the primary donor of reducing equivalents for the azo dye reduction process (Solís *et al*., 2012). In fact, although the stoichiometric substrate quantity needed for azo dye reduction is low (*i.e.*, 32 mg COD per mmol of monoazo dye, corresponding to four reducing equivalents per azo linkage), a higher primary substrate concentration kinetically benefits the azo dye reduction process (van der Zee and Villaverde, 2005). Finally, the color removal rate depends on the establishment of low redox potential values, accordingly increasing when the redox potential of the system decreases (Pearce *et al*., 2003).

### II.2.2.5. Azo dye-laden TWW treatment in bacterial systems

#### II.2.2.5.1. Anaerobic-aerobic treatment systems for azo dye biodegradation

Several bacterial mixed culture systems have been investigated for the treatment of TWW, comprising aerobic, anaerobic and combined anaerobic-aerobic systems (Sarayu and Sandhya, 2012; van der Zee and Villaverde, 2005). Conventional aerobic wastewater treatment methods are considered ineffective for the treatment of colored TWW, since bacteria are generally unable to biodegrade azo dyes under aerobic conditions (Saratale *et al*., 2011). In some cases, the occurrence of partial color removal in CAS systems is due to the physical adsorption of certain dyes (usually about 40-80%) onto the sludge (Stolz, 2001).

On the other hand, anaerobic systems provide the optimal environment for azo dye decolorization through the reductive cleavage of the azo bond (dos Santos *et al*., 2007), as previously explained. In addition, anaerobic bioreactors, such as UASB reactors, are generally well suited for the treatment of industrial wastewaters, being capable of removing high organic loads while producing low sludge and generating energy in the form of biogas used to heat the wastewater in order to speed up the treatment process (Henze *et al*., 2002). For instance, Somasiri *et al.* (2008) reported over 90% of COD and color removal in a UASB reactor treating real TWW treatment.

However, in addition to the intrinsic limitations of the anaerobic granular technology (such as long start-up periods, the need for a relatively high operation temperature and inefficient nutrient removal), the aromatic amines resulting from azo dye reduction are resistant to further anaerobic mineralization (except for few, simple aromatic amines; Kalyuzhnyi *et al.*, 2000; Razo-Flores *et al*., 1997; Pandey *et al*., 2007). On the other hand, several authors reported that aromatic amines are susceptible to aerobic

biodegradation, ultimately resulting in azo dye mineralization (Pinheiro *et al*., 2004). Therefore, owing to the potential further degradation of these azo dye breakdown products under aerobic conditions, promising systems for the complete biodegradation of azo dyes are based on a combination of anaerobic and aerobic processes (van der Zee and Villaverde, 2005). According to this approach, bacterial azo dye biodegradation generally proceeds in two stages: 1) the anaerobic phase, responsible for color removal through reductive cleavage of the azo bond, resulting in the formation of generally colorless, but potentially hazardous, aromatic amines; 2) the aerobic phase involving further degradation of aromatic amines (van der Zee and Villaverde, 2005). Furthermore, the combination of anaerobic and aerobic conditions can allow the effective removal of nutrients (nitrogen and phosphorus). In addition to the removal of high organic loads during the anaerobic process, the residual BOD can be further eliminated under aerobic conditions (Delée *et al*., 1998).

Different anaerobic-aerobic reactor system approaches for treating azo dye-laden TWWs have been extensively reviewed (van der Zee and Villaverde, 2005; Sarayu and Sandhya, 2012). The anaerobic-aerobic treatments can occur sequentially (continuously in separate vessels, or in the same reactor by physical or temporal separation of anaerobic and aerobic phases), or simultaneously (based on the principle of limited oxygen diffusion in microbial biofilms, which contain anaerobic zones within aerobic bulk phases; Stolz, 2001). Irrespective of the system configuration employed, of color removal yields (70-100%) were achieved under anaerobic conditions provided an electron donor (*e.g.*, biodegradable carbon source) was present and competing electron acceptors (*e.g.*, oxygen, nitrate, nitrite) were limited to low concentrations (van der Zee and Villaverde, 2005). Integrated anaerobic-aerobic bioreactors, where aerobic and anaerobic conditions are combined in a single reactor can generally enhance the overall degradation efficiency, are cost effective and have reduced footprints. In this context, sequential anaerobic-aerobic systems such as anaerobic-aerobic SBRs have been mostly employed in the study of TWW biological treatment, offering a compact layout, operational flexibility and simplicity (Lourenço *et al*., 2001).

### II.2.2.5.2. Aerobic biodegradation of aromatic amines

#### II.2.2.5.2.1. General aspects

Generally, successful reports on aerobic degradation of aromatic amines involved culture enrichment in specialized aerobes, with a very narrow substrate range (Pinheiro *et al*., 2004). In practice, several studies showed that activated sludge systems are not always able to aerobically degrade aromatic amines resulting from previous anaerobic azo dye reduction (van der Zee and Villaverde, 2005). In fact, the biodegradation potential of aromatic amines can range from highly degradable to non-biodegradable, depending on the position, type and number of substituents in the aromatic ring (Lourenço *et al*., 2003). Moreover, the difficulty in achieving complete azo dye biodegradation is commonly associated with the generation of recalcitrant sulfonated aromatic amines, owing to the

hydrophilic nature of the sulfonate group (Lourenço *et al*., 2009; Tan *et al*., 2005). Few pure cultures and microbial consortia capable of degrading specific sulfonated naphthylamines have been isolated (Barsing *et al*., 2011; Hong *et al*., 2007; Juárez-Ramírez *et al*., 2012; Pandey *et al*., 2007). In fact, biodegradation of this type of compounds has mostly been demonstrated for relatively simple sulfonated aminobenzene and aminonaphthalene compounds (Haug *et al*., 1991; Tan *et al*., 2000), often requiring extensive biomass acclimation (Tan *et al*., 2005). Accordingly, unadapted microbial populations in activated sludge were shown to fail in completely degrading sulfonated naphthalenes (Nortemann *et al*., 1986). This difficulty in mineralizing azo dye reduction products under aerobic conditions has generally been attributed to the lack of an adequate aerobic microbial population capable of metabolizing such compounds (Tan *et al*., 1999a). Therefore, the cultivation of microbial consortia capable of efficiently degrading a mixture of aromatic amines has been suggested for bioaugmentation of aerobic treatment units (Pandey *et al*., 2007). These specialized microbial communities can be selected if persistently exposed to the aromatic substrates to induce metabolic adaptation (Tan *et al*., 2005).

#### II.2.2.5.2.2. Proposed mechanism for aromatic amines biodegradation

Regarding the biodegradation mechanisms, aerobic metabolization of aromatic amines is generally suggested to occur via a hydroxylation pathway involving a ring-opening mechanism in the presence of oxygen (Pereira *et al*., 2015; Stolz and Knackmuss, 1993). Specifically, under aerobic conditions, hydroxylases can replace different substituents of the aromatic ring (such as the amino group) with hydroxyl groups, followed by cleavage of the aromatic structure through incorporation of two oxygen atoms, catalyzed by oxygenases (Pearce *et al*., 2003). According to Solís *et al*. (2012), the most common oxidases involved in azo dye degradation are bacterial laccases, which have non-specific oxidation capacity and use readily available oxygen as an electron acceptor. Nortemann *et al*. (1994) suggested that the breakdown of substituted naphthalene sulfonates requires an uptake system and naphthylsulfonate dioxygenase with low substrate specificity. In addition to dioxygenase activity, complete aromatic amine mineralization typically involves ubiquitous metabolites (such as catechol, protocatechuate and gentisate) responsible for establishing the link with central metabolic pathways, eventually leading to full oxidation of the aromatic substrate (Çinar and Demiröz, 2010).

#### II.2.2.5.2.3. Autoxidation of aromatic amines

As suggested by Nortemann *et al.* (1994), biodegradation of hydroxynaphthalene aromatic amines requires the microbial capacity to counteract autoxidation of hydroxynaphthalenes. In fact, upon exposure to aerobic conditions, a large fraction of azo dye metabolites (especially aromatic amines *ortho*-substituted with hydroxyl groups), are susceptible to autoxidation, as oxygen reacts with the aromatic products via free radical mechanisms, oxidizing hydroxyl and amino groups to quinines and quinine imines (Barsing *et al*., 2011; Kudlich *et al*., 1999). These compounds can undergo

dimerization or polymerization, generally yielding thermodynamically stable, soluble, colored oligomers (or, less commonly, insoluble polymers) resistant to further biodegradation and potentially toxic and mutagenic (Field *et al.*, 1995; Kudlich *et al.*, 1999; Solís *et al.*, 2012). These chemical, spontaneous reactions make it difficult to predict the fate of aromatic amines during anaerobic-aerobic treatment of azo dyes (van der Zee and Villaverde, 2005). Moreover, the competition between biodegradation and autoxidation (especially regarding *o*-aminohydroxynaphthalenes) should be further assessed, as well as the possibilities for biological mineralization of autoxidation products (Stolz, 2001). Given this scenario, complete biomineralization of azo dyes is still the focus of much research in the context of the environmental impact of textile industry wastewater.

### II.2.2.5.2.4. Fate of sulfonated aromatic amines in anaerobic-aerobic bioreactors

According to a recent review (Raman and Kanmani, 2016), most studies indicate complete removal of azo dyes from TWW to be achieved simply based on successful decolorization results, which is not an accurate conclusion. In contrast with the notable success in the anaerobic decolorization stage, information regarding the fate of the breakdown aromatic amines during the aerobic stage, when available, revealed that most of these amines were not aerobically degraded, being considered a health hazard (Pinheiro *et al.*, 2004; van der Zee and Villaverde, 2005). In fact, the few studies monitoring the removal of total organic carbon, as well as dye intermediates or end-products formed, generally conclude that only partial mineralization of the textile dye is achieved (Raman and Kanmani, 2016). By definition, organic matter mineralization is the transformation of organic carbon and nutrients into inorganic forms or into smaller, simpler organic compounds if mineralization is not complete (Bridgham and Ye, 2013). As previously mentioned, incomplete azo dye mineralization is commonly associated with the production of sulfonated aromatic amines, which are among the most common products of bacterial decolorization of azo dyes (Pandey *et al.*, 2007). Moreover, when their removal was reported, the process (adsorption, biological or chemical transformations) was not clear, the aerobic fate of (sulfonated) aromatic amines thus deserving more investigation (van der Zee and Villaverde, 2005).

This section presents an overview of studies in which azo dye-laden TWW treatment was carried out by mixed bacterial cultures in bioreactor systems, including an anaerobic treatment stage for the reductive cleavage of azo dyes, followed by an aerobic stage for degradation of potentially toxic, colorless breakdown aromatic amines. This review specifically focuses on studies addressing the formation and fate of sulfonated aromatic amines. Accordingly, Table II.8 specifies the operational conditions used in the different bioreactor systems, as well as the main treatment performance indicators in terms of COD, color and aromatic amines removal, while Table II.9 further specifies the conclusions derived by the authors regarding the fate of aromatic amines. Among the reviewed studies on the biodegradation of sulfonated azo dyes in anaerobic-aerobic bacterial systems (Table II.9),

different aromatic amine fates were reported: mineralization (Balapure *et al*., 2015; Işik and Sponza, 2004a; Libra *et al*., 2004; Sponza and Işik, 2002), nearly complete biodegradation (FitzGerald and Bishop, 1995; Forss and Welander, 2011; Sponza and Işik, 2005b), further/partial degradation (Jonstrup *et al*., 2011; Paździor *et al*., 2009) or, more specifically, degradation to non-aromatic, polar compounds (Khehra *et al*., 2006; O'Neill *et al*., 2000), incomplete (Shaw *et al*., 2002) or no mineralization (Libra *et al*., 2004; Lourenço *et al*., 2003; Lourenço *et al*., 2009).

The reported cases of partial or complete aerobic removal of the azo dye-derived aromatic amines (Table II.9) were mostly based on indirect observations, such as: decreases in ultraviolet (UV) absorbance (Dafale *et al*., 2008; Jonstrup *et al*., 2011; Shaw *et al*., 2002; You and Teng, 2009), toxicity (Balapure *et al*., 2015; Işik and Sponza, 2004b) and total aromatic amines levels measured by diazotization-based colorimetric methods (the standard usually corresponding to one of the expected metabolites; Spagni *et al*., 2010; Sponza and Işik, 2005b); the decrease in overall high-performance liquid chromatography (HPLC) peak areas (including unidentified peaks) and shift of peaks to lower retention times (RTs) during the aerobic phase, indicating the formation of less aromatic and more polar compounds (Koupaie *et al*., 2011); the disappearance of signals at low field zone in $^{1}$H NMR (proton nuclear magnetic resonance) analysis indicating the loss of aromaticity (Balapure *et al*., 2015; Khehra *et al*., 2006); the decrease in FTIR (Fourier-transform infrared spectroscopy) peaks associated with aromatic structures (Balapure *et al*., 2015); the detection of lower molecular weight aliphatic compounds in gas chromatography coupled with mass spectrometry (GC-MS; Balapure *et al*., 2015). Moreover, quantification of the expected azo dye intermediates through chromatographic techniques is limited to the availability of the respective standard. Among the reviewed studies (Table II.8), authentic standards have been used for 4-amino-naphthalene-1-sulfonic acid (4A1NS; Koupaie *et al*., 2011; Koupaie *et al*., 2013), benzidine (Işik and Sponza, 2004b; Sponza and Işik, 2005b; Işik and Sponza, 2004a), orthanilic acid (Paździor *et al*., 2009), p-aminobenzene-2-hydroxyethylsulfonic acid and 1,2-ketimino-7-amino-8-hydroxynaphthalene-3,6-disulfonic acid (Libra *et al*., 2004). Except for the latter, all of these metabolites were suggested to be mineralized in the aerobic phase, based on HPLC, liquid chromatography coupled with mass spectrometry (LC-MS) and GC-MS analyses. On the other hand, some aromatic amines cannot be quantified due to the unavailability of an authentic standard. Moreover, the fate of unidentified metabolites generated along the treatment can be qualitatively assessed based on their chromatographic peak area variation (O'Neill *et al*., 2000; Sponza and Işik. 2005b).

A sound comparison between studies testing the biodegradation of the same azo dye is difficult because of the differences in operational conditions. Although using different reactor system configurations, inocula and substrates, three studies focused on Reactive Black 5 (Table II.9) reported that the aromatic amines resulting from the reductive cleavage of the azo dye were mineralized (Sponza and Işik, 2002) or significantly removed during the aerobic stage, with an overall 62-73%

removal yield (Dafale *et al*., 2008; You and Teng, 2009). However, while these conclusions were based on UV-visible spectral results, another study using a more accurate method for analyzing the individual fate of azo dye metabolites (LC-MS; Libra *et al*., 2004), concluded that only one of the aromatic amines was mineralized, the other being recalcitrant under aerobic conditions. Regarding the treatment of Reactive Violet 5 (Table II.8), biodegradation of the resulting aromatic amines was reported by Çinar *et al*. (2008), the aerobic removal yields being 92% for the benzene-based amine and 64% for the naphthalene-base amine, according to HPLC analysis. On the other hand, other studies specifically focused on the fate of these aromatic amines showed that despite the also observed decrease in the respective HPLC peak area, effective biodegradation of the benzene-based amine did not occur, as it was partially converted into an unknown metabolite (Lourenço *et al*., 2003; Lourenço *et al*., 2009). Moreover, the naphthalene-base amine remained practically unchanged in the latter studies, being considered recalcitrant under the employed conditions.

Contradictory conclusions regarding the biodegradation potential of the same azo dye in anaerobic-aerobic treatment systems may not only be attributable to differences in the operational conditions, but also to incomplete metabolite analysis or inaccurate data interpretation. For instance, owing to the low recovery of expected azo dye metabolites at the end of the anaerobic treatment, as detected by LC-MS or GC-MS, authors concluded that biodegradation of the intermediates occurred under anaerobic conditions (FitzGerald and Bishop, 1995; Işik and Sponza, 2004b; Sponza and Işik, 2005b), which is unlikely. On the other hand, You and Teng (2009) stated that the azo dye metabolites formed in the anaerobic phase were further mineralized in the aerobic phase, based on a 62%-reduction in UV absorbance. Also based on UV-visible spectral analysis, Sponza and Işik (2002) finally concluded that the azo dye intermediates were aerobically mineralized, despite previously hypothesizing the occurrence of aromatic amine autoxidation and polymerization due to the slight increase in the color levels. Conversely, other studies using LC-MS or GC-MS reported mineralization of aromatic amines as the formation of higher molecular weight compounds was not observed, with no trace of aromatic amines polymerization or dimerization (Balapure *et al*., 2015; Forss and Welander, 2011).

Overall, some studies suggested partial or even complete mineralization of the aromatic amines, while others reported that mineralization was not achieved because the formation of new intermediates was observed (Table II.9). Moreover, the new metabolites, such as polymerization or dimerization products resulting from autoxidation of aromatic amines, may arise during the aerobic stage without being properly detected by HPLC, depending on the conditions of analysis. Overall, despite most of the reviewed studies further supporting the potential for biodegradation of sulfonated aromatic amines, clear evidence for complete azo dye mineralization was rarely provided, requiring further investigation and more conclusive data.

**Table II.8 -** Sequential anaerobic-aerobic reactor systems treating azo dye-laden textile wastewater.

| Bioreactor system [a] | Seed sludge [b] | HRT (h) [c] | | | SRT (d) [d] | Textile wastewater | | | Removal performance (%) | | | Method for AA analysis [i] | Reference |
|---|---|---|---|---|---|---|---|---|---|---|---|---|---|
| | | An | Ae | Total | | Type [e] | Substrate [f] (COD, mg $O_2$ $L^{-1}$) | Azo dyes [g] (mg $L^{-1}$) | COD | Color | AA [h] | | |
| **Anaerobic** fixed film fluidized bed reactor + **Aerobic** reactor | An-1<br>Ae-1 | 31 | 3.1 | 43 | n.i. | S | Trout chow, BE, YE, peptone (170) | AO10, AR14 or AR18 (10) | 85 | 65-90 | >99 (An) | LC-MS | FitzGerald and Bishop, 1995 |
| **Anaerobic** SBR + **Aerobic** MB-SBBR | An-2<br>Ae-1 | 66<br>*21 | 66<br>*22.5 | 132<br>*48 | n.i. | S | Glucose, lactose (2950-3725) | AR18 (100-1000) | 80 | 98 | >84 (4A1NS)<br>50-60 (Total) | HPLC | Koupaie *et al.*, 2011 |
| Integrated **anaerobic-aerobic** fixed bed SBBR | An+Ae | *14 | *8 | 168<br>*24 | n.i. | S | Glucose, lactose (1030-1045) | AR18 (100) | >92 | >95 | >96 (4A1NS)<br>>51 (Total) | HPLC | Koupaie *et al.*, 2013 |
| **(Anoxic)** fixed film column reactor + **Aerobic** CSTR | BC | 12 | n.i. | n.i. | n.i. | S | Glucose (1630) | AR88 (100) | 95 | 98 | n.q. | UV-vis, TLC<br>$^1$H NMR | Khehra *et al.*, 2006 |
| **Anaerobic** UASB reactor + **Aerobic** CSTR | An-3<br>Ae-2 | 15 | 55 | 70 | 18 (Ae) | S | Glucose (2000) | DBk38 (3200) | 84 | 86 | 52 (TAA) | DCM1<br>GC-MS | Sponza and Işik, 2005a |
| **Anaerobic** UASB reactor + **Aerobic** CSTR | An-3<br>Ae-3 | 86 | 432 | 518 | 86 (An) | S | Glucose (4100) | DBk38 (3200) | 92 | 94 | 86 (TAA)<br>45 (Benzidine) | HPLC-DAD<br>GC-MS, DCM1 | Işik and Sponza, 2004b |
| **Anaerobic** UASB reactor + **Aerobic** CSTR | An-3<br>Ae-2 | 19 | 67 | 86 | 12-16 (Ae) | S | Glucose (3000) | DR28 (4000) | 88 | 99 | 91 (TAA) | DCM1 | Işik and Sponza, 2003 |
| **Anaerobic** UASB reactor + **Aerobic** CSTR | An-3<br>Ae-3 | 1728 | 432 | 2160 | n.i. | S | Glucose (5377) | DR28 (3200) | 91 | 96 | 97 (TAA)<br>91 (Benzidine) | HPLC-DAD<br>GC-MS, DCM1 | Sponza and Işik, 2005b |
| 3 biofilter reactors:<br>2 **Anaerobic** + 1 **Aerobic** | FR | 232 | 116 | 348 | n.i. | S | n.i. | Mixture A (400; 200 each) | n.i. | 86-90 | n.q. | LC-MS | Forss and Welander, 2011 |
| **Anaerobic** UASB reactor + **Aerobic** CSTR | An-3<br>Ae-2 | 100 | 360 | 460 | 25 (Ae) | S | Starch, CMC, acetate, glucose (4214±241) | Mixture B (250; 50 each) | 97 | 91 | 70-85 (TAA) | DCM1 | Işik and Sponza, 2008 |
| **Anaerobic** UASB reactor + **Aerobic** CSTR | An-3<br>Ae-2 | 30 | 108 | 138 | n.i. | R | Cotton textile mill WW + glucose (600-2000) | Mixture B (100-500) | 40-85 | 39-81 | 37-87 (TAA) | HPLC<br>DCM1 | Işik and Sponza, 2004a |
| **Microaerophilic** fixed film reactor (DO ~ 0.07 mg $L^{-1}$) | BC acclim. to RB160 | n.i. | n.i. | 24 | n.i. | S | Starch, glucose (7200) | Mixture C (300; 50 each) | 98 | 100 | n.q. | FTIR<br>$^1$H NMR<br>GC-MS | Balapure *et al.*, 2015 |
| **Anoxic** reactor + **Aerobic** reactor | BC acclim. to RBk5 | n.i. | n.i. | 24 | n.i. | S | Glucose (2000) | RBk5 (100) | >90 | >90 | 73 (Total) | UV-vis | Dafale *et al.*, 2008 |
| **Anaerobic** UASB reactor + **Aerobic** CSTR | An-3<br>Ae-2 | 30 | 108 | 138 | 11 (Ae) | S | Glucose (3000) | RBk5 (100) | 96 | 95 | n.q. | UV-vis | Sponza and Işik, 2002 |
| **Anaerobic** SBR + **Aerobic** MBR | TS | 48<br>*21.5 | 24 | 72 | n.i. | S | Milk powder, sucrose, acetate (300) | RBk5 (6) | 98 | 83 | 62 (Total) | UV-vis | You and Teng, 2009 |
| **Anaerobic** RDR + **Aerobic** RDR | n.i. | 15* | 7.5* | n.i. | n.i. | S | YE, acetate (580 mg $L^{-1}$ as DOC) | RBk5 (530) | 80-90 | 65 | n.q. | LC-MS | Libra *et al.*, 2004 |
| **Anaerobic** biofilter + **Anoxic** reactor + **Aerobic** MBR | An-1<br>Ae-1 | n.i. | n.i. | 24-94 | 80-100 | S | Glucose (800) | RO16 (5-38) | 79 | 90 | n.q. | DCM2 | Spagni *et al.*, 2010 |
| **Anaerobic**-**Aerobic** SBR or **Anaerobic** + **Aerobic** SBRs | MS | 48<br>*19.3 | 96<br>*3 | 144<br>*24 | n.i. | R + S | Cotton dyeing WW, acetate, peptone (570) | RR120 (n.i.) | 93-98<br>95-98 | 93-98<br>92-97 | n.q. | HPLC | Paździor *et al.*, 2009 |
| **Anaerobic** UASB reactor + **Aerobic** reactor | An-4<br>Ae-4 | 24 | 19 | n.i. | n.i. | S | Modified starch, acetate (3343) | RR141 (450) | 85 | 75 | n.q. | HPLC | O'Neill *et al.*, 2000 |
| **Anaerobic-aerobic** SBR | An-5 | *18.5 | *0.5 | 62<br>*24 | n.i. | S | Polyvinyl alcohols (3916) | RR5 (533) | 66 | 94 | n.q. | UV-vis | Shaw *et al.*, 2002 |
| **Anaerobic-aerobic** SBR | Ae-4 | *9-13 | *8-12 | 26-53<br>*24 | n.i. | S | Modified starch (750-1500) | RV5 ($C_i$, 90) | 80 | 90 | n.q. | HPLC | Lourenço *et al.*, 2003 |
| **Anaerobic-aerobic** SBR + **Aerobic** SBR | Ae-4 | *9 | *12 | 52.8<br>*24 | 15 | S | Modified starch (1000) | RV5 ($C_i$, 100) | 38 | 90 | n.q. | HPLC | Lourenço *et al.*, 2009 |
| **Anaerobic-aerobic** SBR | Ae-5 | *12 | *12 | *24 | 10 | S | Glucose (1000) | RV5 (100) | >75 | 89 | 92 (BBA)<br>64 (NBA) | HPLC [&] | Çinar *et al.*, 2008 |
| **Anaerobic** biofilm reactor + **Aerobic** reactor | An-1<br>Ae-1 or Ae-6 | 24-72 | n.i. | n.i. | n.i. | S | Glucose (1000) | Remazol Red RR (100) [#] | 82-95 | 98 | 30 (Total) | UV-vis<br>HPLC | Jonstrup *et al.*, 2011 |

[a] CSTR: continuous stirred-tank reactor; DO: dissolved oxygen; MB: moving bed; MBR: membrane bioreactor; RDR: rotating disc reactor; SBBR: sequencing batch biofilm reactor; SBR: sequencing batch reactor; UASB: upflow anaerobic sludge blanket.

[b] acclim.: acclimatized; Ae: seed sludge in the aerobic reactor; Ae-1: activated sludge from a municipal wastewater treatment plant (WWTP); Ae-2: activated sludge from a dye industry; Ae-3: activated sludge from a lab scale CSTR treating molasses; Ae-4: activated sludge from a WWTP treating mixed municipal/industrial wastewater; Ae-5: Activated sludge from a textile WWTP; Ae-6: Aerobic reactor: activated sludge from a nitroaromatics industry or a textile industry; Ae: seed sludge in the anaerobic reactor; An-1: sludge from an anaerobic digester treating municipal WWTP; An-2: granulated anaerobic sludge from a UASB reactor treating dairy factory; An-3: partially granulated sludge from a methanogenic reactor of an yeast baker factory; An-4: granules from a paper-pulp processing plant; An-5: Anaerobic granules from a UASB reactor treating wastewater from a potato processing factory; An+Ae: Mixture of anaerobic granular sludge from a full-scale UASB reactor and activated sludge from a municipal WWTP; BC: Bacterial consortium isolated from waste disposal sites of textile processing industries; FR: Forest residues (soft wood shavings); MS: Surplus activated sludge and fermented sludge from a methane fermentation stage of a municipal WWTP; n.i.: not indicated; RB160: Reactive Blue 160; RBk5: Reactive Black 5; TS: Sludge from industrial WWTP treating highly colored textile wastewater.

[c] Ae: Aerobic stage; An: Anaerobic stage; n.i.: not indicated; HRT: Hydraulic retention time; *: duration, in hours, of the anaerobic reaction phase, aerobic reaction phase or total cycle indicated in the respective An, Ae and Total columns (only indicated for SBRs and SBBRs).

[d] Ae: Aerobic stage; An: Anaerobic stage; n.i.: not indicated: duration; SRT: Sludge retention time.

[e] S: simulated textile wastewater; R: real textile wastewater.

[f] BE: beef extract; CMC: carboxymethyl cellulose; DOC: dissolved organic carbon; n.i.: not indicated; WW: wastewater; YE: yeast extract.

[g] AO: Acid Orange; AR: Acid Red; $C_i$: Initial dye concentration in the reactor; DBk: Direct Black; DBr: Direct Brown; DR: Direct Red; DY: Direct Yellow; RBk: Reactive Black; RO: Reactive Orange; RR: Reactive Red; RV: Reactive Violet; [#]: Other reactive azo dyes (Remazol Blue RR and Remazol Yellow RR) were used in batch tests; Mixture A: Mixture of RBk5 and RR2; Mixture B: Mixture of RBk5, DR28, DBk38, DBr2 and DY12; Mixture C: Mix of RR2, RR198, RR120, RB160, RB13 and RB172.

[h] 4A1NS: 4-amino-naphthalene-1-sulfonic acid; AA: aromatic amines; An: Anaerobic stage; BBA: benzene-based amine; NBA: naphthalene-based amine; n.q.: not quantified; TAA: Total aromatic amines; Total: Total azo dye metabolites.

[i] DAD: Diode-Array Detection; DCM1: Diazotization-based colorimetric method 1 [colorimetric analysis of total aromatic amines after reaction with 4-dimethylamino benzaldehyde-HCl; quantification of total aromatic amines (TAA) using benzidine as standard]; DCM2: Diazotization-based colorimetric method 2 [diazotization-coupling reaction with or N-(1-naphthyl)ethylenediamine; quantification of TAA using sulfanilic acid (chemical structure similar to one of the expected AA) as standard]; FTIR: Fourier-transform infrared spectroscopy; GC: Gas chromatography; $^{1}$H NMR: Proton nuclear magnetic resonance; HPLC: High-performance liquid chromatography; LC: Liquid chromatography; MS: Mass spectrometry; TLC: Thin layer chromatography; UV-vis: Ultraviolet-visible spectrophotometry; [&]: Relative quantification by attributing the maximum aromatic amine concentration (100%) to the highest peak.

**Table II.9 -** Comments on the fate of aromatic amines (AA) in sequential anaerobic-aerobic reactor systems treating azo dye-laden textile wastewater (operational details in Table II.8).

| Azo dyes [a] | AA removal (%) [b] | Method [c] | Authors comments regarding AA fate [d] | Reference |
|---|---|---|---|---|
| AO10<br>AR14<br>AR18 | >99 (An) | LC-MS | . AA quantitative analysis using standards for the respective metabolites or compounds having the same chemical formula but similar structure.<br>. Low metabolites recovery (<1%) at the end of An. Adsorption to biomass and low recovery efficiencies have been ruled out.<br>. Further studies must be conducted to confirm the hypothesized (>99%) anaerobic biodegradation of the intermediates. | FitzGerald and Bishop, 1995 |
| AR18 | >84 (4A1NS)<br>>50 (Total) | HPLC | . Except for 4A1NS, the other intermediates were not quantified due to unavailability of authentic standards.<br>. Overall HPLC peak area analysis revealed that >50% of total dye metabolites detected at the end of the An were removed during the Ae.<br>. The HPLC peak area decreased and shifted to lower RT during the Ae, indicating the formation of less aromatic and more polar compounds. | Koupaie *et al*., 2011 and 2013 |
| AR88 | n.q. | UV-vis, TLC<br>$^{1}$H NMR | . $^{1}$H NMR analysis indicated complete loss of aromaticity from the azo dye after sequential anoxic-aerobic treatment.<br>. TLC and $^{1}$H NMR revealed that the aromatic intermediates produced under anoxic conditions were degraded to non-aromatic metabolites in the Ae. | Khehra *et al*., 2006 |
| DBk38 | 52 (TAA) | DCM1<br>GC-MS | . Two of the four azo dye breakdown products (benzidine, aniline) were recovered (95%) in the An, but not all were further mineralized in the Ae.<br>. Low levels of AA and absence of breakdown products in GC-MS spectra indicated that most of the AA were metabolized.<br>. Comparison between UV-vis scans of benzidine with the reactors' influent and effluent indicated the complete mineralization of TAA. | Sponza and Işik, 2005a |
| | 86 (TAA)<br>45 (Benzidine) | HPLC-DAD<br>GC-MS<br>DCM1 | . Only two of the four expected dye metabolites were detected (namely benzidine), the authors suggesting that part of AA were removed in the An.<br>. The area of the two HPLC peaks significantly decreased during the Ae, but GC-MS showed that the azo dye was not completely mineralized.<br>. Toxicity of the Ae effluent were significantly lower than the An effluent, suggesting complete aerobic mineralization of carcinogenic amines.<br>. The authors concluded that dyes could be mineralized in the system, despite some residual presence of benzidine in the final effluent. | Işik and Sponza, 2004b |
| DR28 | 97 (TAA)<br>91 (Benzidine) | HPLC-DAD<br>GC-MS<br>DCM1 | . Only 25% (as TAA) of the expected dye metabolites were recovered at the end of the An, the authors suggesting that 75% were removed in the An.<br>. The TAA recovered at the end of the An could be removed in the Ae (91%). Only benzidine was identified by HPLC and GC-MS analysis.<br>. The decrease in the area of two HPLC peaks indicated partial aerobic degradation of benzidine (confirmed by GC-MS) and an unknown metabolite.<br>. The authors concluded that the system allowed nearly complete biodegradation of the benzidine-based azo dye, leading to detoxification. | Sponza and Işik, 2005b |
| Mixture A | n.q. | LC-MS | . Two metabolites were degraded to below the DL in the Ae, with no trace of AA polymerization or dimerization, their mineralization being suggested.<br>. The structure of the two detected metabolites could not be identified, owing to the lack of standardized MS-libraries for LC. | Forss and Welander, 2011 |
| Mixture B | 37-87 (TAA) | DCM<br>HPLC | . The authors concluded that the azo dyes were reductively decolorized in the An and mineralized in the Ae.<br>. Benzidine, produced from the azo bond cleavage in the An, was effectively removed in the Ae, as confirmed by HPLC with authentic standard. | Işik and Sponza, 2004a |
| Mixture C | n.q. | FTIR<br>$^{1}$H NMR<br>GC-MS | . Loss of aromaticity or fission of benzene rings from the dyes during the Ae was indicated by FTIR and by the absence of peaks in the UV region.<br>. GC-MS showed that lower molecular weight aliphatic compounds were formed, which indicated complete cleavage of AA into aliphatic compounds.<br>. The disappearance of all signals at low field zone in $^{1}$H NMR analysis indicated the complete mineralization of dyes.<br>. Higher MW compounds were not detected, indicating the complete mineralization of the WW, further supported by the decrease in toxicity. | Balapure *et al.*, 2015 |
| RBk5 | 73 (Total) | UV-vis | . The UV-vis spectral changes represent the disappearance of the azo dye and concomitant formation of metabolites during the anoxic reaction.<br>. The decrease in the UV major absorbance peak indicated that the AA formed in the anoxic reactor were significantly removed (73%) in the Ae. | Dafale *et al.*, 2008 |
| | n.q. | UV-vis | . The slight increase in the color during the Ae suggested the occurrence of oxidation or polymerization of intermediate compounds formed in the An.<br>. The authors concluded that the released intermediates were mineralized in the Ae. | Sponza and Işik, 2002 |
| | 62 (Total) | UV-vis | . UV-vis results showed that the AA intermediate metabolites formed in the An were further mineralized in the Ae (62% of degradation). | You and Teng, 2009 |
| | n.q. | LC-MS | . Partial mineralization of the fully hydrolyzed azo dye was achieved.<br>. Specifically, one of AA was mineralized (*p*-ABHES), but the other metabolite (TAHNDS) was not removed in the aerobic stage. | Libra *et al.*, 2004 |
| RO16 | n.q. | DCM2 | . At least the sulfonated AA formed under anaerobic conditions were recalcitrant to biodegradation. | Spagni *et al*., 2010 |
| RR120 | n.q. | HPLC | . Two HPLC peaks were formed in the An, one of which corresponded to orthanilic acid.<br>. Orthanilic acid (confirmed by standard) was further biodegraded under aerobic conditions, while the second peak was recalcitrant to biodegradation.<br>. The orthanilic acid was further degraded in the Ae of the two-stage anaerobic/aerobic system, but not in the integrated anaerobic-aerobic SBR. | Paździor *et al*., 2009 |
| RR141 | n.q. | HPLC | . The HPLC-detected compounds (none corresponding to the expected AA) were aerobically removed or converted to highly polar compounds.<br>. Toxicity of the effluent was eliminated after the Ae.<br>. This study qualitatively showed that AA-derivatives formed during the An were degraded into more polar, non-aromatic by-products during the Ae. | O'Neill *et a*l., 2000 |
| RR5 | n.q. | UV-vis | . The intensity of peaks in the UV region was slightly reduced during the Ae, the authors concluding that AA were not completely mineralized. | Shaw *et al*., 2002 |
| RV5 | n.q. | HPLC | . The two AA resulting from the anaerobic azo bond reduction were detected by HPLC analysis, but not mineralized during the subsequent Ae.<br>. Despite interconversions between the BBA and an unknown metabolite, no effective biodegradation was observed along the operation (>810 days).<br>. Prolonging the Ae resulted in partial conversion of the BBA into the unknown metabolite, but the NBA remained practically unchanged. | Lourenço *et al.*, 2003 and 2009 |
| Remazol Red RR [#] | 30 (Total) | UV-vis<br>HPLC | . Partial degradation of AA during the Ae was suggested by the 30% reduction in the UV peak absorbance level.<br>. Four HPLC peaks (not identified) were detected at the end of the An, three of which were absent at the end of the Ae.<br>. Batch tests using sludge acclimatised to nitroaromatics or azo dyes revealed that only partial degradation of AA from Remazol Red RR and from Remazol Blue RR was achieved, while autoxidation of Remazol Yellow RR metabolites occurred during the Ae, forming a recalcitrant product. | Jonstrup *et al*., 2011 |

[a] AO: Acid Orange; AR: Acid Red; DBk: Direct Black; DR: Direct Red; RBk: Reactive Black; RO: Reactive Orange; RR: Reactive Red; RV: Reactive Violet; [#]: Other reactive azo dyes (Remazol Blue RR and Remazol Yellow RR) were used in batch tests; Mixture A: Mixture of RBk5 and RR2; Mixture B: Mixture of RBk5, DR28, DBk38, DBr2 and DY12; Mixture C: Mix of RR2, RR198, RR120, RB160, RB13 and RB172.

[b] 4A1NS: 4-amino-naphthalene-1-sulfonic acid; AA: aromatic amines; An: Anaerobic stage; Total: Total azo dye metabolites; n.q.: not quantified; TAA: Total aromatic amines.

[c] DAD: Diode-Array Detection; DCM1: Diazotization-based colorimetric method 1 (colorimetric analysis of total aromatic amines after reaction with 4-dimethylamino benzaldehyde-HCl; quantification of total aromatic amines (TAA) using benzidine as standard); DCM2: Diazotization-based colorimetric method 2 (diazotization-coupling reaction with or N-(1-naphthyl)ethylenediamine; quantification of TAA using sulfanilic acid (chemical structure similar to one of the expected AA) as standard); FTIR: Fourier-transform infrared spectroscopy; GC: Gas chromatography; $^{1}$H NMR: Proton nuclear magnetic resonance; HPLC: High-performance liquid chromatography; LC: Liquid chromatography; MS: Mass spectrometry; TLC: Thin layer chromatography; UV-vis: Ultraviolet-visible spectrophotometry; [&]: Relative quantification by attributing the maximum aromatic amine concentration (100%) to the highest peak.

[d] 4A1NS: 4-amino-naphthalene-1-sulfonic acid; AA: Aromatic amines; Ae: Aerobic stage; An: Anaerobic stage; BBA: benzene-based amine; DL: detection limit; FTIR: Fourier-transform infrared spectroscopy; GC: Gas chromatography; $^{1}$H NMR: Proton nuclear magnetic resonance; HPLC: High-performance liquid chromatography; LC: Liquid chromatography; MS: Mass spectrometry; MW: molecular weight; NBA: naphthalene-based amine; *p*-ABHES: *p*-aminobenzene-2-hydroxyethylsulfonic acid; RT: retention times; TAA: Total aromatic amines; TAHNDS: 1,2-ketimino-7-amino-8-hydroxynaphthalene-3,6-disulfonic acid; TLC: Thin layer chromatography; UV-vis: Ultraviolet-visible spectrophotometry; WW: wastewater.

### II.2.2.6. Engineered nanoparticles (ENP) in the textile industry

#### II.2.2.6.1. Characteristics and application

By definition, nanoparticles are natural or man-made (engineered) materials with three external dimensions at the nanoscale, *i.e.*, size range from ~1-100 nm (ISO TS27687). Owing to their high surface area to volume ratios, they present physicochemical characteristics different from those of the correspondent macro or micro sized materials, namely high reactivity and conductivity (Huangfu *et al*., 2019).

ENP have been increasingly used in consumer products (sporting goods, stain resistant clothing, sunscreens, toothpaste, food additives, tires and others), the ENP production in 2011-2020 being predicted to round 58,000 tons (Rezić, 2011). In addition, as the worldwide number of ENP-containing products is constantly increasing and new, widespread applications in different industrial fields (textile, cosmetic, pharmaceutical, electronic, agriculture and environmental sectors) are being developed every year, the ENP concentration in the environment is consequently expected to dramatically rise in the near future (Brar *et. al*., 2010).

Application of ENP in woven and non-woven textiles (*e.g.*, rainwear, protective clothing, sportswear and automobile interior fabrics) represents one of the fastest developing process branches. The textile industry has recognized the excellent characteristics that ENP confer to textile materials, such as antimicrobial and protective properties, enhanced stain and water resistance, as well as increased ability to absorb dyes and change wettability (Rezić, 2011). A list of the different ENP applied on textile materials has been provided by Rezić (2011), including metals (*e.g*., Ag, Au, Cu, Fe, Ni, Zn), metal oxides (*e.g*., $Al_2O_3$, $Fe_3O_4$, $SiO_2$, $TiO_2$, ZnO) and other compounds (*e.g*., SiC, $TiB_2$, $YbF_3$, ZrC).

#### II.2.2.6.2. Environmental and health concerns

The widespread and growing application of ENP in commercial products, namely in textile goods, has recently raised awareness regarding the implication of the likely high ENP concentration in the environment (air, water and soil) and its impact on human health (Brar *et al*., 2010). In fact, the release of ENP into the environment may occur during their synthesis, their incorporation into products, during the use of these goods and, finally, upon their recycling or disposal. Rezić (2011) presented the different stages of ENP release from textile materials throughout their entire life cycle (Figure II.9). Accordingly, exposure of the human body to ENP contained in textile materials can primarily occur through skin absorption, inhalation and ingestion, being potentially toxic and harmful to human health (Rezić, 2011). In fact, although the health and environmental effects of common metals are well-known, the physicochemical behavior and hazards of nanoparticles are yet to be fully understood, as comprehensive risk assessment studies and in-depth evaluation regarding their toxicity, carcinogenicity and mutagenic effects are still lacking.

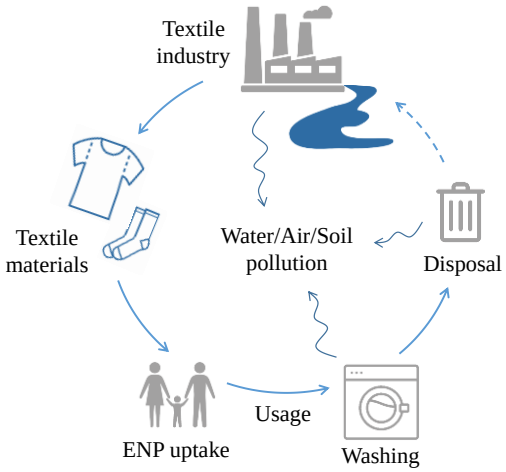


**Figure II.9** - Release of engineered nanoparticles (ENP) from textile materials into the environment throughout their life cycle.

According to Rezić (2011), the most important sources of textile ENP released to the environment are considered to be textile industry wastewaters and waters from large hospital or hotel laundries. Due to the potential long-term contamination of the aquatic and soil ecosystems with ENP if these escape from WWTPs, an understanding of the presence, behavior, fate and impact of ENP in wastewater and wastewater sludge along their treatment systems is urgently needed (Brar *et al*., 2010). In addition to the impact that wastewater treatment has on nanomaterials, regarding the potential for ENP removal, also the effect that nanomaterials have on wastewater treatment performance has been pointed out as a relevant issue, requiring further investigation.

### II.2.2.6.3. Fate in wastewater treatment plants (WWTPs)

ENP have been classified as emerging contaminants, posing challenges to conventional waste treatment systems (Demirel, 2016). The fate of ENP in a typical WWTP has been hypothesized by Brar *et al*. (2010), who predicted possible removal processes of ENP along the various unit operations. Overall, while bar screening and other mechanical treatment methods are not expected to effectively remove ENP, the primary and secondary treatments present the highest potential for ENP removal, mostly through adsorption, agglomeration and/or aggregation and settling. The efficiency of these removal mechanisms likely depends on the physiochemical properties of the ENP, and their residence times in the different WWTP compartments, as well as on characteristics of the wastewater (namely, pH and suspended solids content) and its sludge. For instance, settling of ENP could be enhanced by entrapment in the larger sludge flocs (Brar *et al*., 2010).

In light of the proposed ENP pathway in a WWTP (Brar *et al*., 2010), ENP mostly end up in the sewage sludge during primary and secondary treatments. Accordingly, through the use of probabilistic flow models, Sun *et al.* (2014) predicted environmental concentrations of widely used ENP accumulating mainly in WWTP sludge (*e.g.*, 170 mg $TiO_2$, 24 mg ZnO and 0.02 mg $Ag^0$ per kg of sludge in the European Union). The partition of ENP to WWTP sludge represents a potential threat to

agricultural ecosystems where the digested, dewatered, ENP-contaminated sludge is directly applied as fertilizer (biosolids). In fact, *ca.* 50% of the total biosolids generated in Europe and USA is used in agriculture and soil conditioning (Sun *et al.*, 2014). In this context, nanoecotoxicology has emerged as a new field of science to study the fate and physicochemical modifications of ENP in the environment, namely to address the possible transfer of ENP from biosolids into food chains (Castillo-Michel *et al*., 2017). This also raises concerns regarding the potential leachability of ENP into groundwater and sub-surface waters (Brar *et al*., 2010). Keller *et al*., (2013) estimated that 63-91% of over 260,000-309,000 metric tons of global ENP production in 2010 ended up in landfills, with release into soils (8-28 %), water bodies (0.4-7 %), and the atmosphere (0.1-1.5 %). In this sense, the fate of ENP during sludge stabilization, incineration, and landfill disposal should be further investigated.

In summary, WWTP represent intermediate pathways for ENP release to water and soil. Depending on the ENP pathway along the WWTP, the subsequent fate of these contaminants can either be associated with the sewage sludge, potentially affecting soil ecosystems upon land application and incineration, or with the discharged water, eventually compromising life in aquatic ecosystems (Brar *et al*., 2010). Overall, sewage sludge, wastewater, and waste incineration of ENP-containing products were shown to be the major ENP entry flows into the environment (Gottschalk and Nowack, 2011).

### II.2.2.7. Silver nanoparticles (AgNP)

#### II.2.2.7.1. Characteristics and consumption

AgNP have been the most commonly used nanomaterial in consumer products (from antibacterial socks and nasal/throat sprays to beauty creams, toothpastes and vacuum cleaners), being one of the fastest-growing product categories in these industrial sectors (Sheng and Liu., 2017; Zhang *et al*., 2016a). Specifically, AgNP, clusters of zero-valent silver ($Ag^0$) with at least one dimension within the 1-100 nm range, provide antimicrobial and antibacterial characteristics to textiles, which is especially advantageous for medical, healthcare, hygiene and sports applications (Zhang *et al*., 2016a). In 2000, the global production of textiles exhibiting antimicrobial properties was estimated to round 100,000 tons, with a European annual growth higher than 15% (Voelker *et al*., 2015). Several antimicrobial agents have been used by the textile industry in antimicrobial finishing processes, such as metal salts and peroxyacids, in order to minimize microbial growth on textiles and its associated negative effects (namely, unpleasant odor, stains, decolorization and contamination). However, AgNP, as well as other ENP ($TiO_2$ and CuO), have presented superior antimicrobial action in terms of efficiency and durability, being successfully applied in t-shirts, socks, underwear, sports clothing and many other commercial textile products (Radetić, 2013). Globally, the amount of AgNP applied in textiles has been estimated as 36 tons (Windler *et al*., 2013).

### II.2.2.7.2. Antimicrobial mechanisms

The strong antimicrobial activity of AgNP is non-specific, covering a broad range of microorganisms even at concentrations below 1 mg AgNP $L^{-1}$ (Zhang *et al*., 2016a). The toxicity of nanoparticles varies with their physicochemical properties, namely surface characteristics (area, porosity, charge, surface modification and coating), size, shape, composition, chemical structure, and reactivity, being also dependent on several environmental conditions, such as pH, ionic strength and light (Rezić, 2011), among other factors further discussed in section II.2.2.7.5.

Depending on the degree of $Ag^+$ release from AgNP, the toxicity of AgNP can be derived from the toxicity mechanisms of silver ions ($Ag^+$; ion-related toxicity) and/or silver particles (AgNP; particle-related toxicity), their respective contribution for the overall toxicity being still under debate (Sheng and Liu, 2017). Yet, the release of $Ag^+$ from AgNP is generally regarded as the main toxicity effector (Zhang *et al*., 2016a), and occurs in aqueous solution under oxic conditions, through a dissolution reaction where DO acts as an oxidant to produce a soluble silver oxide (Huangfu *et al*., 2019). In fact, many investigations have attributed the toxicity of AgNP primarily to the release of $Ag^+$, even when it accounts for less than 10% of total silver (Fabrega *et al*., 2009, Peretyazhko *et al*., 2014; Zhang *et al.*, 2018a).

Owing to its high affinity for sulfur and phosphorus compounds, the ion-related toxicity generally involves $Ag^+$ binding to proteins, peptides and/or DNA, leading to enzyme deactivation, membrane permeability disruption and accumulation of intracellular radicals, resulting in microbial growth inhibition, cell death and lysis. Specifically, when present inside the microbial cell, $Ag^+$ can react with the $H_2O_2$ produced in the mitochondria or interact with DO to generate reactive oxygen species (ROS, such as superoxide radicals) that can damage the cell membrane, enzymes and DNA (Huangfu *et al*., 2019; Zhang *et al*., 2018a). In addition, $Ag^+$ may also interact with respiratory chain enzymes, such as NADH dehydrogenase, and cause the uncoupling of respiration from ATP synthesis. $Ag^+$ could also result in proton leakage and collapse of the proton motive force by binding with transport proteins. Furthermore, $Ag^+$ can inhibit the assimilation of phosphate and lead to the excretion of intracellular phosphate. Finally, it has also been hypothesized that $Ag^+$ can increase DNA mutation frequencies during polymerase chain reactions (Huangfu *et al.*, 2019).

Regarding the particle-related toxicity mechanism, AgNP have been shown to enter the cell, where, similarly to $Ag^+$, $Ag^0$ at the surface of AgNP potentially interacts with proteins and DNA molecules, consequently disrupting key metabolic processes. The cell internalization process of AgNP can occur through penetration and endocytosis. Owing to intrinsic AgNP surface characteristics (*e.g*., roughness, hydrophobicity and cationic charge), nonspecific binding can lead to direct penetration of the cell membrane, resulting in direct physical damage (Huangfu *et al*., 2019). In contrast, endocytosis of AgNP results from specific receptor-ligand interactions (Nel *et al*., 2009).

In this context, the toxicity of AgNP results from the combined effects of three interconnected toxicity pathways involving 1) the release and uptake of $Ag^+$ with consequent cellular enzyme deactivation, 2) the generation of ROS (oxidative stress-related toxicity mechanism) on the surface of the AgNP or by the action of $Ag^+$, 3) cell membrane damage and permeability disruption inflicted directly by AgNP or indirectly by $Ag^+$ (Sheng and Liu, 2017). Further investigations are required to fully understand the toxic mechanisms of AgNP (Zhang *et al*., 2018a).

### II.2.2.7.3. Release into the environment

Although there is still no evidence that humans are adversely affected by AgNP, the daily exposure to AgNP-containing products with the growing presence of AgNP in the environment raises strong concerns for environmental and human health risks regarding their bioaccumulation and possible toxic effects in natural ecosystems and along the food chain. In fact, the presence of AgNP in the environment has been registered, with concentrations of 0.01-0.03 μg $L^{-1}$ in water, 0.0017-0.0014 μg $m^{-3}$ in air, and 0.02-0.43 μg $kg^{-1}$ in soil (Rezić, 2011). Specifically, an increased amount of AgNP is expected to be released into domestic and industrial waste streams due to its extensive application in consumer products (Sheng *et al*., 2018). Regarding textile products, AgNP may be discharged into the environment during synthesis, manufacturing and incorporation of AgNP into textiles, usage and washing of AgNP-containing textiles, as well as upon their recycling or disposal (Demirel, 2016). Specifically, more than 50% of AgNP could be released from certain products (such as clothes) upon their first wash (Zhang *et al*., 2018a). As a result, AgNP have been detected in the influent of municipal WWTPs (Hoque *et al*., 2012). Zhang *et al*. (2016a) reviewed several studies reporting measured or predicted silver concentrations in sewage streams and concluded that AgNP concentrations the influent of full-scale WWTPs are generally in the μg $L^{-1}$ order of magnitude Specifically, up to 2 μg $L^{-1}$ and 15 μg $L^{-1}$ were reported for AgNP and total silver, respectively, in municipal WWTPs (Zhang *et al*., 2016a). However, in case of full-scale WWTPs receiving industrial wastewaters with high silver loadings, higher values of total silver concentration (up to 193 μg $L^{-1}$) were detected in the influent (Zhang *et al*., 2016a).

In general, results suggest that the majority of AgNP in consumer products will reach WWTPs, which represent important barriers to prevent nanoparticles from directly entering the environment (Blaser *et al*., 2008). Some studies have elucidated the possible mechanisms through which AgNP can be removed in WWTPs, namely via aggregation, settling, precipitation and adsorption (Brar *et al*., 2010; Huangfu *et al*., 2019). Nevertheless, the retention of AgNP in activated sludge has raised concerns regarding eventual negative impacts on the WWTP treatment efficiency, owing to the AgNP antimicrobial properties (Zhang *et al*., 2016a). In this sense, results from studies focused on the fate and effect of AgNP in conventional WWTPs are further described in the next sections.

### II.2.2.7.4. Fate in WWTPs

Metallic silver is well-known for its thermodynamic instability. The various possible AgNP transformation pathways under the complex conditions present in real water environments make it difficult to assess their fate in WWTPs, and consequent environmental risk. As previously mentioned, the transformations that ENP generally undergo in aqueous environments include oxidation, dissolution, adsorption, aggregation and sedimentation. Specifically, Zhang *et al*. (2018a) reviewed four major chemical environmental AgNP transformations (oxidative dissolution, photoreduction, sulfidation and chlorination) that impact the fate and toxicity of AgNP under aqueous conditions. Recently, Huangfu *et al.* (2019) reviewed the possible interactions between ENP and microbial cells. Accordingly, Figure II.10 schematically summarizes the different chemical, physical and biological processes involved in the interaction between AgNP and microbial cells in a biological wastewater treatment system, as subsequently explained on the basis of the literature assessing AgNP fate in WWTPs.

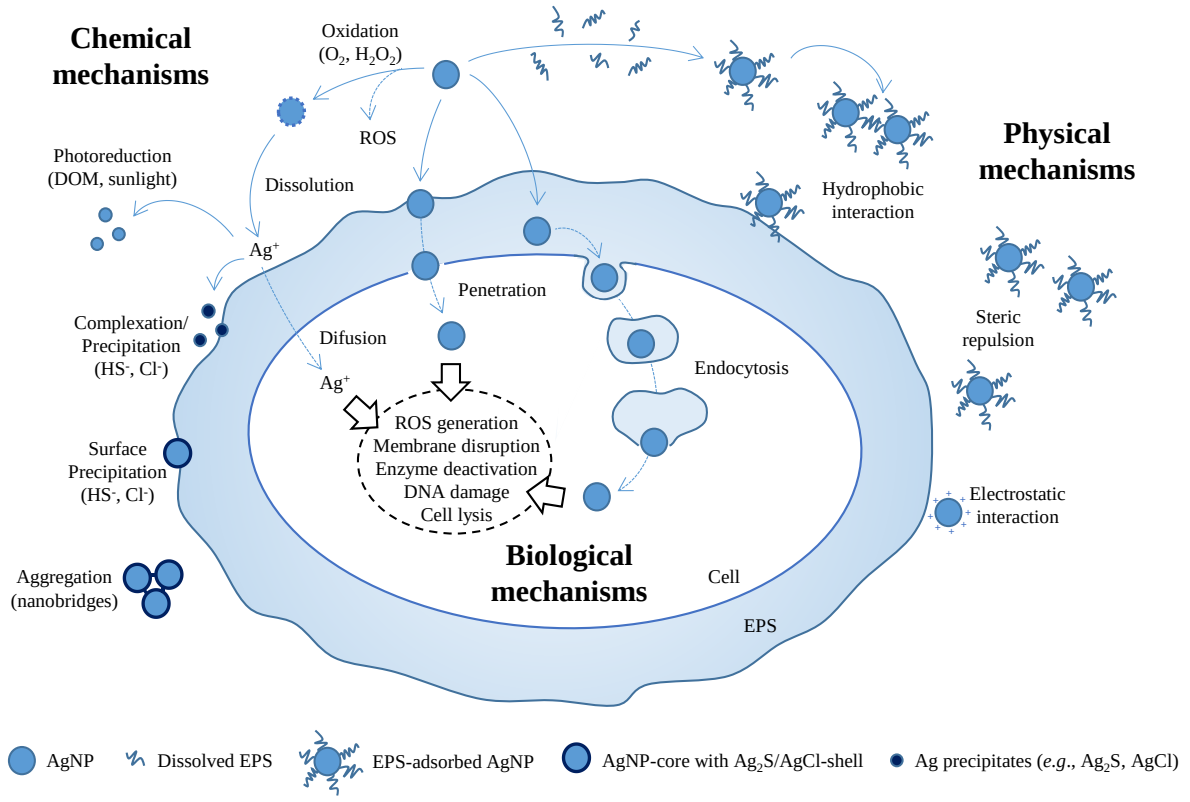


**Figure II.10** - Chemical, physical and biological mechanisms involved in the interaction between silver nanoparticles (AgNP) and microbial cells. DOM: Dissolved organic matter; EPS: extracellular polymeric substances; ROS: reactive oxygen species.

As previously stated, the bactericidal activity of AgNP is in great part attributable to the release of $Ag^+$ through oxidative dissolution under oxygen-rich aqueous conditions, depending on the DO and pH (oxidative dissolution is hindered under anoxic or alkaline conditions). In oxic water solutions, the oxidation of AgNP surfaces by $O_2$ or $H_2O_2$ to generate $Ag_2O$ is a slow and rate-determining step for the subsequent, relatively quick dissolution of $Ag_2O$. Moreover, as the formed $Ag_2O$ can adhere to the

AgNP surface forming a $Ag_2O$ shell surrounding a AgNP core, it can protect AgNP from further oxidation and decrease the surface available for dissolution. Furthermore, as $Ag^+$ release is lower for smaller AgNP surface areas, larger AgNP particle sizes and concentrations (homoaggregation trend) tend to lose fewer $Ag^+$ (Zhang *et al*., 2018a). On the other hand, dissolved $Ag^+$ can be reduced by dissolved organic matter (such as phenol, quinone, ketone and hydroxyl groups) to form AgNP under (simulated) sunlight irradiation, through photoreduction (Yu *et al*., 2016). Therefore, oxidative dissolution of AgNP and photoreduction of $Ag^+$ will occur simultaneously, reaching a dynamic equilibrium (Peretyazhko *et al*., 2014).

The natural presence of sulfur in aqueous environments allows the direct or indirect sulfidation of AgNP, owing to the high affinity of AgNP and $Ag^+$ towards sulfur. Specifically, the high sulfide concentrations present in anaerobic environments typically allow the direct transformation of AgNP into $Ag_2S$ nanoparticles (direct sulfidation). On the other hand, under low sulfide concentrations, $Ag^+$ previously formed from AgNP oxidative dissolution can rapidly precipitate with sulfide (indirect sulfidation), the formation of $Ag^+$ being the rate-determining step. Owing to the fact that $Ag_2S$ nanoparticles are thermodynamically more stable than AgNP and that $Ag_2S$ can block the surface of AgNP, sulfidation decreases the overall concentration of free $Ag^+$, diminishing the associated toxicity level (Zhang *et al*., 2018a). Moreover, $Ag_2S$ precipitated on the AgNP surface has been shown to form $Ag_2S$ nanobridges, linking neighboring AgNP, thus contributing to AgNP aggregation (Levard *et al*., 2012).

Although AgNP are mainly reprecipitated as $Ag_2S$, indirect chlorination of AgNP can occur in seawater or chloride-rich water as $Ag^+$ resulting from AgNP oxidative dissolution precipitates in the form of AgCl. Although sulfidation and chlorination can generally mitigate the toxicity of AgNP by decreasing the availability of $Ag^+$ species and their release from AgNP, the transformation products ($Ag_2S$ and AgCl) are still bioavailable and toxic to some organisms (Zhang *et al*., 2018a). In fact, in complex water environments AgNP are likely to yield stable transformation products such as $Ag_2S$ and AgCl, which possess high stability, resulting in long-term persistence in the environment (Zhang *et al*., 2018a). Similarly, the reaction of $Ag^+$ with phosphate or simple, common organic molecules relevant in aqueous environmental media (*e.g.*, glucose or soluble microbial products) has been found to have a decelerating effect on AgNP dissolution (Loza *et al*., 2014).

The above mentioned environmental transformations of AgNP progress simultaneously in complex aquatic environments. Yet, the oxidative dissolution of AgNP represents a primary step for most of the other chemical processes (except for direct sulfidation), the DO playing a vital role in AgNP transformations. These chemical transformation products resulting from environmental transformations of AgNP should be considered when deriving a complete assessment of the AgNP environmental risk.

Effective AgNP toxicity in the biological unit of a WWTP is dependent on the AgNP transformations occurring during transport through sewage networks and inside the bioreactor (Zhang *et al*., 2016a). Kaegi *et al.* (2013) analyzed the fate and transformation of AgNP (with different sizes and coatings) in a sewer channel and laboratory batch experiments using raw wastewater and activated sludge. The authors concluded that AgNP are transported in sewer systems without substantial losses to the sewer biofilm, the extent of AgNP sulfidation strongly depending on the AgNP size and on sulfide availability (Kaegi *et al*., 2013). Moreover, the vast majority of the AgNP were retained in the activated sludge flocs by heteroaggregation, irrespective of AgNP size (10-100 nm) and coating (citrate or polyvinylpyrrolidone, PVP). In this sense, the authors suggested that measures to reduce TSS in the effluent should be implemented in order to avoid the associated AgNP escape from the WWTP (Kaegi *et al.*, 2013).

Geyik and Çeçen (2016) demonstrated that EPS can biosorb both $Ag^+$ and AgNP, which were effectively removed by entrapment within the EPS matrix. In fact, the retention of AgNP in activated sludge has been associated to EPS, which can act as a permeability barrier to hinder ENP intracellular penetration, thus attenuating toxicity (Huangfu *et al*., 2019). Yet, some ENP can eventually spread into bacterial cells and come into contact with intracellular polymeric substances (IPS), such as glycogen, PHA, and polyphosphate. In this sense, the interaction mechanisms between specific ENP and EPS or IPS during physical, chemical and biological transformation processes related to ENP in WWTPs were recently reviewed (Huangfu *et al*., 2019), contributing for a better understanding of the extracellular and intracellular fates of ENP.

Research has suggested that most ENP are effectively removed from wastewater by being embedded within the EPS-rich, porous structure of biofilms through hydrophobic interactions (Huangfu *et al*., 2019). The level of interaction varies with the ENP coating and the biofilm surface porosity. Specifically, the hydrophobic behavior of PVP-coated AgNP led to stronger retention in EPS than the hydrophilic citrate-coated AgNP (Xiao and Wiesner, 2013). The biofilm surface porosity depends on the EPS properties, which in turn vary with the sludge type (Gu *et al*., 2014) and the ionic strength of the medium (Huangfu *et al*., 2019). In addition, retention of AgNP in EPS through precipitation of $Ag^+$ onto EPS has also been suggested as a mechanism for ENP removal from wastewater. In fact, organosulfur compounds from EPS can play a role in the formation of sulfides, which can react with silver thiolates to produce $Ag_2O$ (Huangfu *et al*., 2019). In addition, thiols can strongly interact with AgNP and influence the rates of sulfidation (Levard *et al*., 2012). Finally, complexation has also been proposed, as several EPS functional groups (e.g., carboxyl, hydroxyl, ether, amine and sulfhydryl groups) can act as binding sites for ENP and dissolved metal ions. Similarly, in case of endocytosis of AgNP (biological mechanism), the latter have been shown to bind to IPS, such as sulfur-containing proteins and phosphorus-containing substances (*e.g.*, DNA) and release $Ag^+$, which can lead to the

deactivation of cellular enzymes and DNA and generation of ROS, as previously described in section II.2.2.7.2 (Morones *et al*., 2005).

### II.2.2.7.5. Effect in WWTPs

Due to their strong antimicrobial properties, the presence of AgNP in WWTP has raised strong concerns and great controversy regarding their potential adverse effects on wastewater ecosystems and biological wastewater treatment performance, potentially deteriorating contaminant removal effectiveness. In general, the ecotoxicity and extent of the negative effects of AgNP on wastewater treatment efficiency depend on several factors related to AgNP and to the treatment system (Sheng and Liu, 2017; Sheng *et al*., 2018; Zhang *et al*., 2016a):

- AgNP properties, including size, shape and surface coating: larger, spherical and PVP-coated AgNP tend to have weaker bactericidal action. Generally, small AgNP can cause the severest damage on cell membranes through direct contact because of their large surface area to volume ratio and consequent high chemical activity. However, larger AgNP with a lower reactivity on the surface can persist and gradually release $Ag^+$ for prolonged periods in the environment, inducing potential long-term ecological hazards (Huangfu *et al*., 2019).

- Reaction conditions: anaerobic conditions inhibit $Ag^+$ release from the surfaces of AgNP and enable the steady conversion of AgNP to $Ag_2S$ (lower solubility and toxicity), thereby minimizing the toxicity effects of AgNP on wastewater microorganisms. As a result, AgNP generally do not affect the performance of anaerobic bioreactors (Zhang *et al*., 2016a).

- Presence of potential ligands in the WWTP: binding of AgNP or released $Ag^+$ to dissolved organic carbon and inorganic ions (namely sulfide and chloride) lower their bactericidal effects. Particularly, sulfidation has been shown to play an important role on the fate of AgNP, significantly reducing their toxicity in wastewater treatment systems by converting AgNP to $Ag_2S$ through reaction with sulfide (Levard *et al*., 2012, Kaegi *et al*., 2013).

- Type of culture: mixed cultures are more resistant to the adverse effects of AgNP than pure cultures due to microbial functional redundancy that maintains the process stability of a wastewater treatment system. Specifically, deterioration of a mixed culture bioreactor performance by AgNP can be minimal because different microbial groups carry out the same biological processes or functions, but are differently affected by AgNP (Zhang *et al*., 2016a). In fact, the application of high AgNP concentrations (mg $L^{-1}$ levels or higher) can cause major shifts in the bacteria community structure without significantly affecting the reactor performance (mainly COD degradation and nitrification).

- AgNP dose and time of exposure: higher concentrations of AgNP often result in more significant adverse effects. On the other hand, the dissolution of $Ag^+$ from AgNP in sub-lethal concentrations has been proposed to contribute to the tolerance, resistance and stimulatory response of microorganisms to

AgNP (Zhang *et al*., 2016a). Evidences for this stimulus-driven effect of AgNP have been shown both in pure culture and complex biological wastewater treatment systems (Sheng and Liu, 2017). Therefore, it was concluded that microbial functional redundancy and adaptability towards AgNP considerably alleviate its adverse effects on wastewater treatment performance, namely in full-scale WWTP (Zhang *et al*., 2016a).

- Physical structure of sludge: bacteria located on the surface of sludge flocs are more exposed to AgNP and at greater risk than the bacteria inside the flocs, which are better protected. Accordingly, microorganisms in attached-growth bioreactors (biofilm/granular sludge) are less susceptible to AgNP exposure than in suspended-growth bioreactors (flocculent sludge; Gu *et al*., 2014; Sheng and Liu, 2011). Specifically, AgNP has been shown to alter the microbial community and the floc properties of an activated sludge sample from either a full-scale or a lab-scale suspended-growth bioreactor at relatively low silver levels (below 1 mg $L^{-1}$). On the other hand, the better resistance of biofilms to AgNP is generally attributed to the protective effect of the EPS matrix. Furthermore, high biofilm bacterial tolerance is often observed when AgNP (up to 200 mg $L^{-1}$) are added to mature biofilms, but AgNP can inhibit biofilm formation if sufficiently high concentrations are applied (Sheng and Liu, 2017).

- Bacterial species: susceptibility of microorganisms to AgNP has been considered species-specific, as different wastewater microbial species/groups are differently affected by AgNP (Zhang *et al*., 2016a). In general, heterotrophic bacteria responsible for organic matter removal are more resistant to AgNP when compared to autotrophic bacteria, namely nitrifying bacteria (Choi *et al*., 2008). Specifically, it has been reported that AOB are more susceptible to inhibition by AgNP than NOB and organics oxidation heterotrophs (Sheng and Liu, 2017; Sheng *et al*., 2018). Consequently, AgNP usually have stronger adverse effects on nitrification than on COD removal in wastewater treatment systems (Liang *et al*., 2010; Zhang *et al*., 2016a). Furthermore, AgNP have been shown to differently affect the phylum *Chloroflexi*, which is filamentous and possesses important functions in activated sludge, and nitrifying bacteria such as *Nitrosomonas* spp. and *Nitrosococcus* spp. (Zhang *et al*., 2016a).

- Treatment system/reactor configuration: transport of AgNP before the biological treatment process contributes to reducing the AgNP adverse effects by significantly decreasing their concentration and changing their chemical structure. Specifically, the sewer collection network is estimated to transform 10-95% of AgNP into silver complexes and precipitates (*e.g*., $Ag_2S$) with lower ecotoxicity (Kaegi *et al*., 2013; Zhang *et al*., 2016a). In addition, preliminary and primary treatment processes in full-scale WWTPs have been shown to partially transfer AgNP to sludge (*e.g*., through heteroaggregation, adsorption, settling/sedimentation), prior to the biological treatment units (King *et al*., 2015). For instance, approximately 35% and over 97% of the influent AgNP were removed during the mechanical processes of nine full-scale WWTPs and the primary treatment in a pilot-scale WWTP, respectively

(Impellitteri *et al*., 2013; Li *et al*., 2013). In contrast, only a small portion of AgNP (approximately 10%) was removed in the sewer channel and primary clarification in a lab-scale wastewater treatment study (Hou *et al*., 2012; Kaegi *et al*., 2013). In this sense, direct addition of AgNP to lab-scale bioreactors without a sewage collection system and/or a preliminary/primary treatment process has stronger adverse effects on microorganisms and may deteriorate the reactor performance at sufficiently high concentrations (mg $L^{-1}$ levels or higher; Zhang *et al*., 2016a). Zhang *et al*. (2016a) reviewed several studies regarding the potential effects of AgNP on the performance and microbial communities of SBRs. In general, AgNP at mg $L^{-1}$ levels do not significantly affect wastewater microbes or long-term reactor performance of an SBR. Despite the apparently low susceptibility of SBRs to AgNP, the effect of AgNP in a continuous-flow reactor performance can be different from that exerted in an SBR, owing to the distinct physiochemical environments present (Zhang *et al*., 2016a).

Due to the many factors determining the ecotoxicity and detrimental effect of AgNP in wastewater treatment performance, studies have reported different consequences in biological treatment systems exposed to AgNP. For instance, Jeong *et al*. (2014) reported a decrease in the microbial community diversity and wastewater treatment efficiency after 50 days of AgNP supplementation. Similarly, addition of AgNP (1-5 mg $L^{-1}$) caused phosphorus removal deterioration and microbial community changes, subsequently stabilizing with persistent exposure to AgNP (Yuan *et al*., 2015). Moreover, 1 mg $L^{-1}$ AgNP was reported to inhibit nitrification by 47% after more than 1 month of bioreactor operation (Liang *et al*., 2010). On the other hand, long-term (3 months) addition of 1 mg $L^{-1}$ of spherical, PVP-coated AgNP in activated sludge bioreactors fed with a synthetic municipal wastewater was suggested to contribute to a higher microbial diversity and biomass concentration, without significantly affecting pollutant removal (COD and ammonium removal maintained above 90% and 99%, respectively; Sheng *et al*., 2018). In fact, recent studies focusing on long-term effects of AgNP in WWTP, indicated that although an acute inhibition by AgNP is often initially observed, the system subsequently recovers (Sheng *et al*., 2018). Accordingly, in the presence of minimal $Ag^{+}$ dissolution from AgNP, the microbial community diversity and function have been maintained in activated sludge after long-term wastewater treatment (Sheng and Liu, 2017). Similarly, continuous, long-term AgNP loading at low concentrations (0.1 mg $L^{-1}$ or lower) had minimal impact on activated sludge wastewater treatment process, as the microbial community structure and abundance, as well as the effluent water quality were not affected, despite the significant increase in the copy number of a silver resistance gene (Zhang *et al*., 2014).

Overall, in light of the full-scale treatment system configuration, microbial functional redundancy, and microbial adaptability, Zhang *et al.* (2016a) argue that AgNP at environmentally realistic concentrations (μg $L^{-1}$ or lower) do not cause significant risks to wastewater microorganisms and have minimal adverse effects of on the performance of a full-scale municipal WWTP. Yet, long-term

monitoring of the AgNP toxicity in full-scale WWTP should be further investigated, as well as the long-term impacts of AgNP transformation products formed in sewage ecosystems.

### II.2.3. TWW treatment in AGS sequencing batch reactor (SBR) systems

#### II.2.3.1. Removal of textile dyes by AGS

Aiming to achieve complete mineralization of an azo dye, Kudlich *et al.* (1996) immobilized in alginate beads azo dye-reducing bacteria together with bacteria able to mineralize the reduction products. Following this unsuccessful attempt, the authors highlighted the need for a more rigid and mechanically stable material that would still allow the establishment of an oxygen gradient, similarly to biofilms. In this sense, Tan *et al.* (1999a) subsequently tested the use of anaerobic granular sludge as a self-immobilization system providing both anaerobic and aerobic microniches when operated under aerobic conditions. Yet, the aromatic amines formed upon azo dye reduction were not further transformed in the presence of oxygen. This was attributed to the absence of a suitable aerobic microbial population within the anaerobic granular sludge capable of metabolizing aromatic amines. Therefore, the authors indicated that addition of adapted aerobic biomass would be probably required to achieve azo dye mineralization (Tan *et al*., 1999b). In this context, AG might be the solution for this problem. As hypothesized by Manavi *et al.* (2007), the channels present within AG could be used for transport of dyes and organic substrates into the anaerobic core region of the granules, where (facultative) anaerobic bacteria would reduce azo dyes using the reducing equivalents resulting from the oxidation of the organic compounds. Subsequently, the AG channels would allow the resulting aromatic amines to migrate from the core to the aerobic outer layers of the AG, where they could be mineralized by aerobic bacterial populations (Manavi *et al.*, 2007).

Overall, in addition to the general advantages over the conventional flocculent sludge, AGS has characteristics that might potentially promote the complete biomineralization of azo dyes. Specifically, the coexistence of aerobic and anoxic-anaerobic zones within the granules (Winkler *et al*., 2013) and their enhanced resistance to high organic loads and toxic recalcitrant compounds (Franca *et al*., 2018) might be advantageous for treating TWW. Furthermore, their superior capacity to biodegrade toxic and recalcitrant pollutants derives from the wide range of possible operational SRT values in AGS systems (de Kreuk and van Loosdrecht, 2004). In fact, the operational SRT flexibility of AGS systems enables the presence of a more diverse microbial community within the SBR, namely slow-growing populations, whose activity may be advantageous for the degradation of recalcitrant compounds (Clara *et al*., 2005; Langford *et al*., 2005; Lourenço *et al*., 2015). In addition, results from previous studies using flocculent activated sludge for TWW treatment (Lourenço *et al*., 2000) suggest that systems with higher biomass retention capacity are probably advantageous for allowing the development of a more diverse microbial population capable of degrading a broader range of dyes. Accordingly, a study

reported the biodegradation of a sulfonated aromatic amine (4A1NS), described as highly recalcitrant, through the use of biofilm reactors, which allow a high biomass retention (Koupaie *et al*., 2013).

Although using the AGS technology for the treatment of high strength, dye-laden TWW offers great promise for the above mentioned reasons, only few reports have been published on the use of AGS SBRs for this specific application, most of which using synthetic TWW (Kodam and Kolekar, 2014; Nancharaiah and Reddy, 2018). Furthermore, although biodegradation and biosorption are generally reported as the dye removal processes in biological systems, the mechanisms and metabolic pathways occurring in AGS systems are still poorly addressed in the literature and deserve more investigation (Rollemberg *et al*., 2018).

The first published study on this subject (Muda *et al*., 2010) used CAS and anaerobic granules as inoculum to form AGS in an intermittent anaerobic-aerobic SBR (6-h cycles with a total of 1.4-h anaerobic and 4.4-h aerobic reaction stages), fed with synthetic wastewater containing a mixture of textile dyes (Table II.10). The imposed operational conditions allowed the development of stable, mature AG with excellent settleability, composed of non-filamentous bacteria tightly linked and wrapped in EPS. In terms of treatment performance, while high COD and ammonia removal yields were reached (mainly during the aerobic reaction phases), the AGS SBR system was unable to remove more than 62% of color (45% removed during the anaerobic stages), presumably occurring through azo bond reduction. The relatively low and inconsistent decolorization yields were attributed to insufficient microbial adaptation time to the recalcitrant dyes (20 days of operation), to possible aerobic formation of colored autoxidation products from unstable aromatic amines and/or to color removal through adsorption of dyes to the biomass. In fact, as the formation of aromatic amines was not assessed, the decolorization process was uncertain, especially regarding the partial color removal observed under aerobic conditions (ca. 17%), which was suggested by the authors to derive from azo bond reduction within the anaerobic core of the AG. Moreover, despite not providing clear evidence, the authors attributed the high OUR registered during the last aerobic stage to the mineralization of the (unassessed) aromatic amines. Finally, owing to the high ammonia removal yield observed during the aerobic phases (94%), it should also be considered that the nitrate generated from the nitrification process may have contributed to the low anaerobic decolorization yields reported, through being a preferred electron acceptor over the azo dyes.

Similarly, a subsequent study using different cycle conditions (8-h cycle with 3.8-h anaerobic and 3.8-h aerobic stages; Table II.10) only reached 55% of color removal (Muda *et al*., 2012). Aiming to optimize the treatment performance, these authors also analyzed the effect of the HRT on the intermittent anaerobic-aerobic AGS SBR system (Muda *et al*., 2011). In this sense, a HRT of 24 h with a long anaerobic phase (24-h cycles with a total of 18-h anaerobic and 6-h aerobic stages; Table II.10) was selected for allowing the highest dye and COD removal yields (94% and 87%, respectively), as well as the best AGS properties. These results indicated that the aerobic granular

structure provided protection towards the presumably high concentrations of dyestuff degradation products (Muda *et al*., 2011).

The same research group tested a similar intermittent anaerobic-aerobic SBR (24-h cycles with a total of 11.8-h anaerobic and 11.8-h aerobic phases) in the development and treatment performance evaluation of AGS towards a sterilized, real TWW (Ibrahim *et al*., 2010; Table II.10). Stable, large AG with good sedimentation properties were formed using an inoculum composed of sterilized sludge from a textile WWTP and a feed-acclimatized bacterial consortium (composed of *Bacillus*, *Brevibacillus* and *Lysinibacillus* strains; supplemented to the SBR at every cycle). Furthermore, this AGS was successfully able to treat real TWW, as 90% of color and 80% of COD removal yields were achieved after 9 days of operation with a HRT of 24 h, which is in accordance with the results of Muda *et al.* (2011). The same inoculum was used in a subsequently published study (Kee *et al*., 2014) to form AGS in an anaerobic-aerobic SBR operated in 6-h cycles (2.8-h anaerobic and 2.8-h aerobic phases; Table II.10). Once successful granulation was achieved in this study (Kee *et al*., 2014), the system's performance in treating a sterilized, real TWW was tested. Similarly to the previous studies, best results (61% and 46% of color and COD removal, respectively) were achieved when the HRT was increased to 24 h, using 24-h cycles with an 18-h anaerobic phase followed by a 6-h aerobic phase. Further increasing the HRT to 48 h led to a reduction in the color removal yield, possibly due to autoxidation of aromatic amine metabolites.

As an alternative aerobic, granular-based system, a different research group has proposed a sequencing batch biofilter granular reactor (SBBGR), comprising a sludge bed where biomass grew in the form of granules and biofilms (Table II.10), as a promising on-site pre-treatment for colored TWW before discharging into the municipal sewer system (Lotito *et al.*, 2012b). Specifically, during the treatment of real wastewater from a dyeing and finishing factory at high OLR (up to 2.6 kg $O_2$ $m^{-3}$ $d^{-1}$) in 6-to-8-h cycles (20-h HRT), the system was able to meet the COD limit for discharge into the local sewer system (500 mg $O_2$ $L^{-1}$). In contrast with the COD removal performance, the color removal yields were highly unstable (0-60%) due to the wide dye variability in the raw wastewater composition. Yet, although the treatment levels were insufficient for direct discharge into superficial water bodies, the treated wastewater was apparently allowed into the municipal sewer system (*i.e.*, color not visible after a 40-fold dilution). Although the decolorization process (biodegradation and/or adsorption) was not investigated, the authors suggested that the high operating SRT could promote the development of species able to degrade dyes, and the presence of anoxic niches in the sludge could allow the reduction of dyes. Yet, the capacity of the system to effectively degrade azo dyes and to detoxify wastewater should be assessed in the future. The SBBGR sludge, described as a mixture of biofilm and (aerobic) granules packed in a filling material, was characterized in another study, revealing good settling and dewatering properties (Lotito *et al*., 2012a).

This system was further studied (Lotito *et al*., 2014) regarding the treatment of a mixed municipal-TWW, corresponding to the influent of a biological reactor in a WWTP. The good COD, nitrogen, TSS and surfactants removal yields, as well as the partial color removal yields (Table II.10) achieved by the SBBGR system alone, complied with the local limits for direct discharge (*i.e.*, color not visible after a 20-fold dilution). Comparing with a conventional WWTP (secondary and tertiary treatments, including biological treatment, coagulation-flocculation and ozonation), the SBBGR system produced an effluent of comparable quality using a simpler treatment scheme, with lower HRT (11 h *vs* 30 h) and sludge production, which further supported the application of this aerobic, granular-based system as a main treatment unit at WWTPs treating mixed municipal-TWW (Lotito *et al*., 2014). Furthermore, microbial community analysis indicated that *Betaproteobacteria* represented more than 40% of the biomass, *Actinobacteria* and *Alphaproteobacteria* being other relevant groups in the SBBGR. In addition, the presence of nitrifying and denitrifying bacteria was confirmed, corresponding to approximately 3% and 6% of active bacteria in the bioreactor, respectively (Lotito *et al*., 2014).

In addition to some of the previous reports (Ibrahim *et al*., 2010, Kee *et al*., 2014, Lotito *et al*., 2012b, Lotito *et al*., 2014), a more recent study also assessed the performance of AGS in the treatment of real TWW containing a mixture of textile dyes (Manavi *et al*., 2017). Specifically, after successfully achieving granulation in an anaerobic-aerobic SBR (6-h cycles; Table II.10) fed with a synthetic wastewater, the mature AGS were used for treating a diluted real dyeing wastewater, by gradually decreasing the dilution factor and increasing the HRT and anaerobic-to-aerobic phases duration ratio. Overall, the AG successfully adapted to the real dyeing wastewater, achieving 73% of color removal (mostly in the anaerobic phase) and 68% of COD removal (mostly in the aerobic phase) in 24-h cycles (comprising an 18-h anaerobic stage followed by a 3-h aerobic period). In addition, some color formation during the aerobic phase was hypothetically attributed to the autoxidation of the dye reduction metabolites. On the other hand, color removal during the aerobic phase was registered when AG with sizes above 0.3 mm represented more than half of the biomass. In this context, the authors considered the possible partial contribution of dye biosorption to the surface of AG, but also suggested the occurrence of azo dye reduction inside AG during the aerobic phase, which was further supported by the presence of cavities within the tightly linked bacterial structure, potentially serving as channels for movement of dyes and metabolic products within AG. Owing to the high variability in TWW, and the limitation of the color removal yield to 73% reported in this study, the authors suggested that in addition to further optimization of the SBR operational conditions, implementation of a subsequent physicochemical treatment might be necessary for decolorizing textile dyes of types other than azo dyes, which are presumably recalcitrant under these operational conditions. Regarding AG stability, exposure of AGS to the increasing concentration of the real dyeing wastewater, concomitantly with the extension of the anaerobic-to-aerobic duration phase ratio and HRT, enhanced EPS production but reduced the granular mass fraction in the sludge, which indicated the occurrence of AG disintegration

along SBR operation. In this sense, the authors highlighted that further assessment of the AG instability during long-term operation with real dyeing wastewater is needed before this technology can be considered for this application.

The use of real TWW (Ibrahim *et al*., 2010, Kee *et al*., 2014, Lotito *et al*., 2012b, Lotito *et al*., 2014; Manavi *et al*., 2017) or synthetic TWW containing a mixture of several textile dyes (Muda *et al*., 2010, 2011 and 2012) better mimics the complexity of real environmental conditions, which is essential to evaluate the potential for AGS application to TWW treatment. However, optimization of AGS SBR systems specifically towards an efficient decolorization performance and analysis of the underlying mechanisms requires the use of simpler feed wastewater compositions. In this sense, the subsequently reviewed AGS studies focused on decolorization by employing simulated TWW containing only one textile dye.

By using bacterial isolates from soil and sludge contaminated with textile dye industrial wastewater, Kolekar *et al.* (2012) developed AGS in an aerobic SBR, the azo dye removal and degradation performance of which was subsequently tested under static, anoxic conditions (batch tests; Table II.10). The AG were able to completely decolorize up to 5 g $L^{-1}$ of Reactive Blue 59 (within 8-12 h) through azo bond reduction, as confirmed by the disappearance of the azo dye peak in HPLC chromatograms and emergence of new, unidentified peaks at higher RTs. The azo dye biotransformation products presented no genotoxicity, as opposed to the parental dye. In addition, induction of azo reductase and cytochrome p450 levels in the dye decolorizing AGS suggested their involvement in biodecolorization. The COD removal yield decreased with increasing initial dye concentrations, 56% being reached when 5 g $L^{-1}$ of Reactive Blue 59 were applied. Finally, although exposure to this high azo dye concentration was associated to significant changes in the microbial community (except for the unaffected *Acidobacteria* phylum), the azo dye decolorizing AGS were characterized by a diverse microbial community belonging to *Alpha-*, *Beta-*, and *Gamma-proteobacteria* (Kolekar *et al.*, 2012).

Similarly to Kolekar *et al*. (2012), a recent study developed AGS in an aerobic SBR (6-h cycles) using dye-free synthetic wastewater and subsequently monitored the mature AGS performance regarding the decolorization of an azo dye (Reactive Yellow 15) under different conditions (Sarvajith *et al*., 2018; Table II.10). When exposed to the dye-laden synthetic TWW, AGS was able to effectively decolorize the azo dye under anaerobic and microaerophilic conditions (78 and 85% removal yield, respectively). Moreover, the carbon and nutrients removal performance was not affected by the azo dye load (poor phosphorus removal was registered irrespective of the presence of dye). In fact, stable and efficient azo dye, TOC, ammonia and total nitrogen removal yields (80-100%) were achieved over 80 days in 24-h cycles under microaerophilic conditions (DO maintained within 0.1-0.5 mg $L^{-1}$ during the first 12 h, subsequently stabilizing within 1.5-2.0 mg $L^{-1}$). Furthermore, this work confirmed that azo dye biodecolorization and ammonia removal via the nitrite pathway occurred simultaneously under

microaerophilic conditions, which is advantageous over the conventional nitrification-denitrification process in terms of oxygen and COD requirements (Sarvajith *et al*., 2018). In this sense, the authors suggested that AGS operation under microaerophilic conditions is promising for treating dye-laden TWW either onsite in textile industries or after dilution with domestic sewage.

Specifically regarding color removal, Sarvajith *et al.* (2018) showed that Reactive Yellow 15 adsorbed to the AG when a carbon source was absent, but this was revealed to be a reversible and unstable process. On the other hand, the azo dye was sustainably decolorized in the presence of lactate and at DO values lower than 0.5 mg $L^{-1}$. Although the microaerophilic conditions might allow both reductive and oxidative reactions, thus potentially leading to complete azo dye biodegradation, HPLC analysis was unsuccessful in identifying biotransformation intermediates (Sarvajith *et al*., 2018). Moreover, the presented general absorbance decrease in the UV-visible spectra (300-800 nm) and lack of information regarding the absorbance profile in the wavelength range below 300 nm, provided insufficient evidence to conclude about the biodecolorization mechanism, thus requiring further analysis. Nevertheless, the authors proposed a metabolic pathway depicting lactate, azo dye and $NH_4$-N removal processes in an AGS system, where lactate acted as source of reducing equivalents for both azo dye and nitrite reduction.

Finally, this study showed that AGS recovered good settling properties after initial granule break-up due to changes in operational conditions (*i.e*., switch in the carbon source from acetate to lactate, as well as exposure to the azo dye and low DO), which also induced a shift in the AGS bacterial community (Sarvajith *et al*., 2018). Specifically, while acetate-fermenting bacteria were eliminated, the bacterial community became enriched in specific microorganisms previously associated with azo dye decolorization (*e.g*., laccase producing *Streptomyces* sp., *Vagococcus* sp., *Enterococcus* sp., *Bacillus* sp., *Brevibacillus* sp., and *Staphylococcus* sp., as well as *Rhodococcus* sp. and *Stenotrophomonas* sp.). Likewise, comammox microorganisms, namely *Nitrospirae*, were detected in the Reactive Yellow 15-decolorizing AGS.

Treatment of a synthetic TWW containing a different model azo dye (Acid Red 18) using AGS was studied by Moghaddam and Moghaddam (2016), after successfully achieving granulation in an anaerobic-aerobic SBR (6-h cycles, comprising 1.3 h of stirred anaerobic phase, followed by 4.3 h of aeration) in the absence of the azo dye (Table II.10). The mature AGS removed more than 85% of COD and around 54% of color. Similarly to Manavi *et al*. (2017), despite the fact that most of the decolorization occurred during the anaerobic phase, presumably through azo bond reduction, significant color removal was further registered during the aerobic phase, its contribution (*ca*. 25%) to the overall color removal yield increasing when larger AG were observed (AG with diameters over 2.4 mm represented around 37% of the biomass), potentially providing larger anaerobic cores (Moghaddam and Moghaddam, 2016). Moreover, the contribution of dye adsorption onto AGS for decolorization was insignificant (less than 8%). In this sense, Moghaddam and Moghaddam (2016)

hypothesized that Acid Red 18 could reach the AG inner layers, where anaerobic microorganisms performed azo dye reduction during the aerobic phase (DO in the range of 5-6 mg $L^{-1}$; ORP around +150 mV), coupled with the use of TB-EPS as carbon and energy source. On the other hand, UV-visible spectra analysis (200-900 nm) revealed that the AGS was unable to further aerobically degrade the intermediates produced from Acid Red 18 reduction (namely the recalcitrant aromatic amine 4A1NS). While the developed granules presented a stable and compact structure in the treatment of synthetic wastewater containing 50 mg $L^{-1}$ of azo dye, AG disintegration occurred when the dye concentration was doubled and the system's color removal yield deteriorated to 30% (Moghaddam and Moghaddam, 2016). In addition to the AG instability, the decreased color removal efficiency was attributed to the presence of excess LB-EPS on the surface of AG resulting from the azo dye shock load, possibly leading to AG pore clogging and consequently to reduced dye penetration and decolorization in the AG inner zones.

Overall, despite the well described presence of anaerobic and anoxic regions within AG (Winkler *et al*., 2013), color removal by AGS under aerobic conditions has only been significantly observed in few studies, though in relatively low extents when compared to the removal yields registered under anaerobic conditions (Manavi *et al*., 2017; Moghaddam and Moghaddam, 2016; Muda *et al*., 2010). Moreover, none of these studies confirmed (*e.g*., by HPLC) that the observed aerobic decolorization effectively resulted from azo bond reduction occurring in the anaerobic core of AG during the aerobic phase, which would imply that azo dyes diffused into the AG center. In fact, color removal has mainly been reported during the anaerobic phase, indicating that the use of combined anaerobic-aerobic AGS processes is more appropriate for the treatment of dye-laden TWW. In this sense, most of the studies addressing this particular application also included an anaerobic phase during initial AGS formation, irrespective of the presence of dyes during this period (Table II.10). However, most of the studies investigating granulation and AGS system performance have been conducted in aerobic or anoxic-aerobic cycles (Franca *et al*., 2018). Therefore, there is comparably less information regarding the development and especially the long-term stability of AG under anaerobic-aerobic cycles, which requires further study (Manavi *et al*., 2017). This is especially relevant when mechanical stirring is used during the anaerobic phase. Most of the studies previously reviewed promoted anaerobic conditions either through liquid recirculation (Muda *et al*., 2010 and 2011), static conditions (Ibrahim *et al*., 2010; Kolekar *et al*., 2012) or nitrogen gas sparging (Manavi *et al*., 2017). As further reviewed, in addition to Moghaddam and Moghaddam (2016), a mechanically stirred anaerobic phase to promote azo dye reduction was only employed by another research group (Mata *et al*., 2015; Lourenço et al., 2015; Franca *et al*., 2015 and 2017), which operated SBRs with the lowest reported H/D (*i.e*., 2.5; non-tubular reactors), representing a potential advantage in terms of full-scale implementation.

Mata *et al.* (2015) were the first to report the use of a stirred anaerobic-aerobic, non-tubular SBR for the development and operation of AGS in the treatment of a synthetic TWW, which contained the azo

dye AR14 and a hydrolyzed hydroxypropyl starch derivative as carbon source (commercial sizing product, typically used in the cotton textile industry; Table II.10). The granulation period was similar to those of most of the literature studies employing tubular SBRs, but the produced AG were smaller (sizes up to 0.5 mm), possibly due to lower selective pressure (H/D=2.5) and higher shear stress (mechanical stirring). In addition, better granulation was achieved in the presence of AR14, in comparison to a dye-free control. High overall color and COD removal yields (up to 85% and 80%, respectively) were achieved under two 6-h sequencing batch cycle strategies, *i.e.*, with a single anaerobic-aerobic reaction phase (3.5-h anaerobic phase and 2-h aerobic phase) or under intermittent aeration (6 alternated phases with 30-min anaerobic and 20-min aerobic conditions; Table II.10). When compared to the former, the latter strategy led to faster settling AG, higher anaerobic COD removal yields, and equivalently high overall color removal yields, but lower initial decolorization rates. HPLC analysis proved that decolorization was a result of complete azo bond reduction, producing a stable aromatic amine (4A1NS) in stoichiometric amounts, which was not aerobically degraded, similarly to another study (Moghaddam and Moghaddam, 2016). Finally, Mata *et al.* (2015) suggested that prolonging the aerobic phase (and consequently the exposure to shear stress and the famine period) could possibly further improve granulation and COD removal performance.

In light of AGS application to treat real TWW, Manavi *et al.* (2017) raised the question of whether AG should be developed in wastewater containing no dyes, with the advantage of granulation not being adversely affected by them or other potentially toxic components, or whether it should occur in dye-containing wastewater, in which case the microbial community within AG would adapt sooner to the TWW components and potentially perform better in its treatment. Overall, formation of AGS has been successfully performed using uncolored synthetic wastewater (Chaudhari *et al*., 2017; Kolekar *et al*., 2012; Manavi *et al*., 2017; Moghaddam and Moghaddam, 2016), dye-laden textile synthetic wastewater (Mata *et al*., 2015; Muda *et al*., 2010 and 2012) and real TWW (Ibrahim *et al*., 2010; Kee *et al*., 2014), with varying granulation times (20-180 days, 30-87 days and 42-112 days, respectively). Furthermore, Franca *et al*. (2015) used mature AGS, previously developed with real wastewater in a municipal WWTP (Frielas WWTP, Portugal), as inoculum for treating a synthetic TWW in a lab-scale SBR.

Following the study of Mata *et al.* (2015), Franca *et al.* (2015) studied the effect of AR14 on the performance of an AGS SBR system operated with 6-h anaerobic-aerobic cycles (comprising a 1.5-h stirred anaerobic phase followed by a 3.5-h aerobic phase; Table II.10) in the treatment of the same simulated TWW as Mata *et al.* (2015). High shear stress caused by mechanical stirring resulted in initial disintegration of the large AG used as inoculum (with sizes up to 5 mm, harvested from a bioreactor treating domestic wastewater) giving rise to small, compact granules (sizes up to 1 mm) with excellent settling properties (Table II.10). Overall, the dye and its breakdown products negatively affected neither biomass growth in the reactors nor treatment performance, as COD removal yields

higher than 80% were attained in both the dye-free (control) and dye-fed reactors after 14 days of operation. Moreover, up to 77% of COD removal was registered during the anaerobic phase, being correlated with an increase in the abundance of *Defluviicoccus vanus*-related GAO, known to be able to take up saccharides anaerobically. The decrease in the anaerobic-to-aerobic phase time ratio, when compared to the previous work (Mata *et al*., 2015), allowed the complete bioconversion of the aromatic amine (4A1NS), identified as primary dye reduction product, along the aerobic reaction phase (when the SRT was above 25 days), without compromising the high color removal efficiency during the anaerobic phase. Yet, the stable dye reduction yields (above 90%, reached after 11 days of operation) suffered a 30% reduction during a 2-week period, when daily biomass harvesting was conducted to control the SRT at 15 days. These results highlighted the importance of SRT control flexibility in AGS systems for the development of a more diverse microbial population with the ability to remove color through azo bond reduction and to further mineralize the resulting aromatic amines. Finally, the capacity of the system to deal with shocks of high dye concentration and organic load in the feed was successfully demonstrated, as granule stability, high color and COD removal yields were sustained, in contrast with a previously mentioned study (Moghaddam and Moghaddam, 2016).

By comparing the anaerobic-aerobic AGS SBR system described by Franca *et al.* (2015) with an anaerobic-aerobic CAS SBR treating the same wastewater, Lourenço *et al*. (2015) reported that similar color removal yields (75-80%) were attained in the two systems but with higher anaerobic and overall COD removal yields in the AGS SBR. The superior AGS performance is possibly related with the protective effect provided by the granular structure, alleviating the apparent inhibitory effect of the azo dye towards the organic load removal by CAS. In addition, detoxification of the wastewater was only observed during the aerobic reaction phase in the AGS SBR system (after 70 days of operation), where at least one of the azo dye metabolites (4A1NS) was aerobically biotransformed (Franca *et al*., 2015), as opposed to the CAS SBR, where the same metabolite remained unconverted (Lourenço *et al*., 2015). These findings further highlighted the better performance of the AGS system comparatively to conventional anaerobic-aerobic SBR technology based on floc-forming bacteria. Overall, according to this comparative study, the three main practical factors supporting the application of the AGS technology for TWW treatment in replacement of flocculent biomass SBR are as follows (Lourenço *et al*., 2015): 1) the excellent settling properties of AGS allow shorter SBR cycles with similar color removal and higher COD removal yields; 2) the granular structure increases the tolerance to toxicity and to high organic loads; 3) the excellent biomass retention of AGS systems allows bioreactor operation at higher SRT values, possibly favoring the establishment of a more diverse microbial population with the potential ability to biodegrade recalcitrant aromatic compounds such as aromatic amines.

In terms of stability, Franca *et al*. (2015) also reported that granule break-up after long-term operation only occurred in a dye-free control SBR, and not in a dye-fed SBR operated alongside it. The authors

suggested that the azo dye may play a role in improving AG stability by acting as electron acceptor and thus promoting heterotrophic growth in the anaerobic core of AG. In fact, FISH analysis confirmed the compact structure of the dye-fed AG, microbial activity being apparently maintained in the granule core, as opposed to the dye-free control (Franca *et al.*, 2015). As highlighted by Manavi *et al.* (2017), stability of AG during long-term exposure to dye-containing wastewaters is an important issue that deserves further investigation, as well as the AG disintegration effect associated with the presence of high azo dye concentrations (Moghaddam and Moghaddam, 2016). In this context, Franca *et al.* (2017) compared two feeding strategies regarding the capacity of anaerobic-aerobic SBRs to deal with disturbances in the composition of a simulated TWW containing the azo dye AR14 (Table II.10). Both a statically fed, anaerobic-aerobic SBR and an anaerobic plug-flow fed, anaerobic-aerobic SBR (where the biomass contacted more thoroughly with the feed during the fill stage) could cope with shocks of high azo dye concentration and organic load, the overall COD and color removal yields being rapidly restored to 80%. Yet, the shock loads had a negative effect on AG integrity and aerobic bioconversion of the amine metabolite (4A1NS) was not observed along the 315-day run. Moreover, switching from a hydrolyzed starch-based to an acetate-based feed deteriorated AGS stability. In addition, although COD uptake was minimal in the plug-flow feeding stage, the fraction of COD removed anaerobically was generally higher in the plug-flow fed SBR. Overall, the latter recovered more rapidly from the imposed disturbances, revealing a higher capacity to deal with substrate-related variations. These results further highlighted the need for more research to ensure long-term AGS stability during the treatment of azo dye-laden TWW.

Differently from the aforementioned studies, Hailei *et al*. (2010) developed AG bioaugmented with a specific fungal strain (white rot fungus *Phanerochaete* sp. HSD) able to form micro-mycelium pellets and to degrade azo dyes using its manganese peroxidase system (Table II.10). Specifically, by seeding an aerobic SBR with micro-mycelium pellets and CAS, granulation was achieved faster than in an SBR seeded only with CAS, probably because the small pellets served as primary matrices acting as nuclei for initial AG formation (Hailei *et al.*, 2010). However, 92% of the analyzed mature AG did not have a micro-mycelium pellet as nucleus. In terms of treatment performance, the bioaugmented AG presented a higher tolerance and decolorization efficiency towards the azo dye (Eriochrome Black T)-laden synthetic TWW, when compared to CAS and conventional AG under the employed operational conditions (aerobic reaction). Since the contribution of adsorption was not relevant at the tested dye concentrations (Table II.10), the authors proposed that the bioaugmented AG probably removed the dye Eriochrome Black T through azo bond cleavage and further degradation of the generated aromatic amines by manganese peroxidase, the activity of which was detected in the SBR.

In addition to azo dyes, which are the most prevalent class of dyes used by the textile industry, AGS has also been studied regarding the decolorization of other types of dyes. For instance, Chaudhari *et al.* (2017) showed that AGS were able to effectively decolorize an anthraquinone dye (Reactive Blue

4) at concentrations up to 1 g $L^{-1}$ (Table II.10), mainly via initial reductive conversion. In addition to the significant decrease in COD, other analyses (HPLC, FTIR and GC-MS) confirmed the presence of non-toxic metabolites resulting from the biotransformation of the dye, which was initially found to be phytotoxic, cytotoxic and genotoxic (Chaudhari *et al.*, 2017). Specifically, results indicated that AGS effectively removed halogenated and amino groups from the dye, a Reactive Blue 4 biotransformation pathway by AGS being suggested (Chaudhari *et al.*, 2017). Regarding the microbial community in AGS, exposure to Reactive Blue 4 promoted the presence of several groups, among which *Proteobacteria* (*Alpha*-, *Beta*-and *Gamma*-), *Firmicutes* and *Bacteroidetes* were highlighted for being able to tolerate the dye and for potentially being involved in its degradation (Chaudhari *et al.*, 2017). These results supported the potential application of AGS for biotransformation and detoxification of the recalcitrant anthraquinone dye Reactive Blue 4.

In a previous study (Ma *et al*., 2011), AGS was successfully developed in an anoxic-aerobic SBR fed with a synthetic wastewater containing a cationic dye (Methylene Blue; Table II.10). The COD and dye removal yields achieved in the AGS SBR system were 93% and 56%, respectively, color removal occurring both during the anaerobic and aerobic phases, with very low contribution from dye adsorption onto AG (Ma *et al*., 2011). In this context, the authors suggested the use of AGS technology for the pre-treatment of industrial wastewater containing Methylene Blue.

Among the literature regarding the use of AGS for the treatment of TWW, some works were specifically focused on the removal of textile dyes through adsorption onto AG. Overall, researchers have explored the opportunity for using excess AGS produced during wastewater treatment as cheap sorbents for removing contaminants from wastewater (Nancharaiah and Reddy, 2018). As previously reviewed (Adav *et al*., 2008a), post-separation from the treated water, stability of biosorbents and regeneration after use are some of the drawbacks that limit the application of suspended adsorbents for the removal of dyestuffs from industrial wastewater. On the other hand, the high surface area, porosity and good settling properties of AG are attractive characteristics for removal of dyes and metals from wastewater through biosorption (Adav *et al*., 2008a). In fact, AG have been rated with a three-fold higher maximum adsorption density than sludge flocs, regarding the cationic dye Rhodamine B (Zheng *et al*., 2005). Accordingly, Gao *et al*. (2010a) concluded that inactive (non-living) AGS could be effectively used as a low-cost, alternative biosorbent for the removal of Acid Yellow 17 dye from wastewater. The same authors also studied the competitive biosorption of Yellow 2G and Reactive Brilliant Red K-2G onto inactive AG, indicating that amine, hydroxyl and carboxyl groups were the main functional groups involved in biosorption of these dyes (Gao *et al*., 2010b). More recently, other studies successfully demonstrated the use of inactive AGS in the adsorption of Sunset Yellow FCF (Zhang *et al*., 2016c), Methylene Blue (Wei *et al*., 2015), Methyl Orange and Crystal Violet (Huang *et al*., 2018). Furthermore, Wei *et al*. (2015) distinguished between the contributions of EPS and sludge in the adsorption of Methylene Blue onto AGS, corresponding to 9.4% and 80.7%, respectively, of the

overall effect. In addition to AGS biosorption, the same research group also analyzed the use of acid $TiO_2$ hydrosol as self-cleaning eluent for biosorbent recovery and photocatalytic dye degradation (Huang *et al*., 2018), the results supporting the combination of AGS biosorption and photocatalysis for dye-containing wastewater treatment.

Overall, the reported studies support the use of AGS in the treatment of dye-laden TWW, further research being necessary to achieve maximal and consistent biodecolorization and detoxification of these wastewaters before the scaling up of this specific application. Most of these studies were still done at laboratory scale and used synthetic wastewaters, reports on pilot-scale and full-scale implementation of anaerobic-aerobic AGS SBRs being still scarce. Li *et al*. (2014) reported that the full-scale AGS SBR at Yancang WWTP (China) treating a wastewater composed of 30% sewage and 70% industrial wastewater from printing, dyeing, chemical, textile and beverage industries exhibited excellent performance in terms of COD and $NH_4$-N removal, but color removal was not assessed. In addition, AG remained stable during long-term operation (Li *et al*., 2014), denoting the resistance of AGS to the toxic nature of these wastewaters. Furthermore, microbial community analysis of mature and stable AGS collected from a WWTP treating the same type of wastewaters (Haining, China) indicated that AGS was primarily composed of *Planctomycetes*, *Proteobacteria* and *Bacteroidetes* (Liu *et al*., 2017a). *Euryarchaeota* phylum was found to constitute the majority of the archaea in AG while, more specifically, *Methanosaeta* genus was dominant in flocs. The higher diversity of bacteria and archaea in AG (*vs* the higher diversity of fungi in flocs) suggested that bacteria and archaeal microorganisms uniquely associated to AG may play a key role in their structure formation and stability, being maintained in the system by the long SRT values employed (Liu *et al*., 2017a).

**Table II.10 -** Summary of operational conditions and main results of studies employing aerobic granular sludge in the treatment of dye-laden textile wastewater.

| System[a] | H/D; V (L)[b] | VER (%)[c] | OLR[d] | HRT (h)[e] | SRT (d)[f] | Seed[g] | WW type (COD)[h] | Substrate[i] | Dye (mg $L^{-1}$)[j] | Cycle[k] | Op.; Gr. (d)[l] | AG size (mm)[m] | $SVI_{30}$ (mL $g^{-1}$)[n] | Color (%)[o] | COD (%)[p] | $NH_4$-N (%)[q] | Aromatic amine formation and fate[r] | Reference |
|---|---|---|---|---|---|---|---|---|---|---|---|---|---|---|---|---|---|---|
| Int.An-Ae SBR | 12.5; 4.0 | 50 | 2.4 | n.i. | 1.4-8.3 | i | Dye-SWW (1270) | Glucose, ethanol, acetate | Mixture of dyes (50) | Total (6 h): F (5') + An1* (0.7 h) + Ae1 (2.2 h) + An2* (0.7 h) + Ae2 (2.2 h) + S (5') + D (5') | 66; n.i. | 2.3±1.0 max.: 4 | 69 | 62 | 94 | 95 | n.i. | Muda *et al.*, 2010 |
| An-Ae SBR | 20.0; 1.5 | 50 | 2.5 | 8 | n.i. | ii | Dye-SWW (1240) | | | Total (8 h): F (5') + An# (3.8 h) + Ae (3.8 h) + S (5') + D (5') | 72; 60 | 0.9 max.: 2.5 | 61 | 56 | 93 | 93 | n.i. | Muda *et al.*, 2012 |
| Int.An-Ae SBR | 13.0; 4.0 | 50 | 0.8 | 6-24 | 72.5±23.3 | iii | Dye-SWW (1270) | | | Total (24 h): F (15') + An1* (8.9 h) + Ae1 (2.9 h) + An2* (8.9 h, RC) + Ae2 (2.9 h) + S (5') + D (5') | 46 of 278; n.i. | 0.6 | 15.5±1.3 | 87 | 94 | n.i. | n.i. | Muda *et al.*, 2011 |
| Int.An-Ae SBR | 15.3; 1.5 | 50 | 0.1-1.5 | 24 | n.i. | iv | Sterilized RTWW (200-3000) | n.i. | n.i. (550-2000 ADMI) | Total (24 h): F (15') + An1# (5.9 h) + Ae1 (5.9 h) + An2# (5.9 h) + Ae2 (5.9 h) + S (5') + D (5') | 42; 42 | 3-10 | 90-130 | 90 | 80 | n.i. | n.i. | Ibrahim *et al.*, 2010 |
| An-Ae SBR | 15.0; 1.0 | 50 | 2 | 24 | n.i. | v | Sterilized RTWW (800-1000) | n.i. | n.i. (1400-1800 ADMI) | gr.: Total (6 h): F (5') + An (2.8 h) + Ae (2.8 h) + S (5') + D (5') / dec.: Total (24 h): F (n.i.) + An (18 h) + Ae (6 h) + S (n.i.) + D (n.i.) | 112; 112 | 3.3±0.9 | 35.1±5.5 | 61 | 46 | n.i. | n.i. | Kee *et al.*, 2014 |
| SBBGR | n.i.; 14 | n.i. | 0.4-3.4 | 17-53 | 160 | vi | RTWW (688±280) | n.i. | Direct, disperse and reactive dyes | Total (6-8 h): F (n.i., up-flow through sludge bed) + Ae (n.i.; WW continuously aerated and recycled) + D (15') | 200; n.i. | 0.5 | 60-80 | 0-60 | 55-78 | n.i. | n.i. | Lotito *et al.*, 2012b |
| SBBGR | n.i.; 9 | n.i. | 2 | 11 | >150 | vii | 30% RMWW + 70% RTWW (249±65) | n.i. | n.i. | Total (6 h): F (15', up-flow through sludge bed) + Ae (330'; WW continuously aerated and recycled) + D (15') | 200; 90 | n.i. | n.i. | 33.9±8.0 41.9±6.9 52.6±9.8 | 82.1±3.6 | 95.0±7.4 | n.i. | Lotito *et al.*, 2014 |
| An-Ae SBR | 17.1; 4.0 | 71 | 1 | 34.3 | n.i. | viii | gr.-SWW dec.- 7% SWW + 93% RTWW (Ci: 1200) | Acetate | Mixture of textile dyes (Ci: 180 SU) | gr.: Total (6 h): F (4') + An* (1 h) + Ae (4.8 h) + S (3-7') + D (3') / dec.: Total (24 h): F (n.d.) + An (18 h, $N_2$) + Ae (6 h) | 187; 94 | > 0.3 (80%) > 0.5 (50%) | 70 | 73 | 68 | n.i. | n.i. | Manavi *et al.*, 2017 |
| gr.: Ae SBR dec.: BSR | 27.3; 3.0 | 50 | n.i. | n.i. | n.i. | ix | gr.: SWW dec.: Dye-SWW (64000) | Peptone, Yeast extract | Reactive Blue 59 (5000) | gr.: Total (6 h): F (10', static anoxic) + Ae (5.6 h) + S (5') + D (10') / dec.: Batch reactor, static anoxic conditions | 60; 20 | 1-2 | 300 | Complete after 8-12 h | 55.5 | n.i. | Formation of unidentified metabolites | Kolekar *et al.*, 2012 |
| gr.: Ae SBR dec.: BMR | n.i.; gr.: 3 dec.:1 | 70 | n.i. | n.i. | n.i. | x | Dye-SWW (TOC:16 mg $L^{-1}$) | dec.: Lactate | Reactive Yellow 15 (5-50) | gr.: Total (6 h): F (60') + Ae (4.5 h) + S (5') + D (10') / dec.: Microaerophilic batch tests**: 24 h for 80 days | 80; 45 | 1.2±0.4 | $SVI_5$: 38.4 | 89-100 | 79-95 | 92-100 | n.i. | Sarvajith *et al.*, 2018 |
| An-Ae SBR | 4.0; 5.0 | 67 | 2.8 | 9 | n.i. | xi | gr.: SWW dec.: Dye-SWW (700) | Acetate | Acid Red 18 (Ci: 50-100) | Total (6 h): F (4') + An$^{\theta}$ (80') + Ae (4.3 h) + S (5') + D (1') | 75; 30 | 0.9-1.2 | 50 | 30-55 | >85 | n.i. | No metabolite transformation | Moghaddam, Moghaddam, 2016 |
| I: An-Ae SBR II: Int.An-Ae SBR | 2.5; 1.5 | 50 | 2 | 12 | 6-15 | xii | Dye-SWW (1000) | Emsize E1 | Acid Red 14 (40) | Total (6 h): F (15') + An$^{\theta}$ [3.5 h (I) or 6 x 0.5 h (II)] + Ae [2 h (I) or 6 x 20 h (II)] + S (3-4') + D (1') | 75; 30 | 0.5 | 67 | 80-85 | 80 | n.i. | Formation of 4A1NS and unknown metabolites; No 4A1NS conversion | Mata *et al.*, 2015 |
| An-Ae SBR | 2.5; 1.5 | 50 | 2-6 | 12 | >25 | xiii | Dye-SWW (1000-3000) | Emsize E1 | Acid Red 14 (40-120) | Total (6 h): F (18') + An$^{\theta}$ (1.5 h) + Ae (3.5 h) + S (5') + D (1') | 102; n.i. | 0.3-1.0 | 17 | >90 | 80 | n.i. | Formation of 4A1NS and unknown metabolites. Complete 4A1NS conversion after day 71 | Franca *et al.*, 2015 |
| An-Ae SBR with static (A) *vs* PF (B) feeding | 2.5; 1.5 | 50 | 2-6 | 12 | 2-9 (A) *vs* 6-18 (B) | xiv | Dye-SWW (1000-3000) | Emsize E1 and/or acetate | Acid Red 14 (40-120) | Total (6 h): F [30' (A) *vs* 50-80' (B)] + An$^{\theta}$ [1.5 h (A) *vs* 1.0-1.5 h (B)] + Ae (3.5 h) + S (5') + D (1') | 315; n.i. | <0.6 (E1) >1.0 (Acetate) | 54-310 (A) 51-179 (B) | 66-91 | 68-90 | n.i. | Formation of 4A1NS in and other unknown metabolites. No 4A1NS conversion | Franca *et al.*, 2017 |
| Ae SBR | 5.5; 4.0 | n.i. | n.i. | n.i. | n.i. | xv | Dye-SWW (n.i.) | Glucose | Eriochrome Black T (50-400) | Total: 6 h [or 12-24 h for dye conc. > 200 mg $L^{-1}$]: F (10') + Ae (4.5 h) + S (30') | n.i.; 15 | 1.0-4.7 | 72 | >96 | 94 | n.i. | n.i. | Hailei *et al.*, 2010 |
| gr.: Ae SBR dec.: BSSR | 27.3; 3.0 | 50 | n.i. | n.i. | n.i. | xvi | gr.: SWW dec.: Dye-SWW (n.i.) | Peptone, Yeast extract | Reactive Blue 4 (Ci: 50-1000) | gr.: Total (6 h): F (10', static anoxic) + Ae (5.6 h) + S (5') + D (10') / dec.: Batch reactor, static + shaking conditions | n.i.; 180 | 7-9 | n.i. | 48-72 (after 48 h) | 90 (after 72 h static) | n.i. | Maximal amines conc. after 48 h under static cond; 95%↓ under shaking | Chaudhari *et al.*, 2017 |
| Anoxic-aerobic SBR | 12.5; 4.0 | 50 | n.i. | 8 | n.i. | xvii | Dye-SWW (Ci: 500) | Glucose, acetate, etc | Methylene Blue (4-10) | Total: 4 h F (3') + Anoxic# (0.5 h) + Ae (3.3 h) + S (2') + D (5') | 173; 87 | 2-4 | 43 | 56 | 93 | n.i. | n.i. | Ma *et al.*, 2011 |

Footnotes are specified on the next page.

[a] Ae: Aerobic; An: Anaerobic; BMR: batch microaerophilic reactor; BSSR: batch static-shaking reactor; BSR: batch static reactor; dec.: decolorization experiment; gr.: granulation experiment; Int.: intermittent PF: plug-flow feeding through the sludge bed; SBBGR: sequencing batch biofilm granular reactor, composed by a microbial bed developed on plastic support material kept between two sieves (bottom of the reactor) and a liquid phase (top layer); SBR: sequencing batch reactor.

[b] dec.: decolorization experiment; gr.: granulation experiment; H/D: height-to-diameter ratio of the reactor; n.i.: not indicated; V: volume of the reactor.

[c] n.i.: not indicated; VER: volumetric exchange ratio.

[d] n.i.: not indicated; OLR: organic loading rate (expressed as kg $O_2$ $m^{-3}$ $d^{-1}$).

[e] HRT: hydraulic retention time; n.i.: not indicated.

[f] n.i.: not indicated; SRT: sludge retention time.

[g] i) mixture of conventional activated sludge (CAS) from a municipal wastewater treatment plant (WWTP), CAS from textile mill WWTP, and anaerobic granules from an upflow anaerobic sludge blanket reactor treating paper mill industrial wastewater; ii) aerobic granular sludge (AGS) developed according to Muda *et al.*, 2010; iii) Sterilized sludge from a textile WWTP and an acclimatised mixed bacterial culture (*Alcaligenes* sp., *Bacillus* sp., *Acinetobacter* sp. and *Stenotrophomonas* sp.) added in every cycle filling stage; iv) CAS from municipal WWTP; v) Isolates from soil/sludge contaminated with textile dye industrial wastewater; vi) CAS with synthetic wastewater containing acetate (for the granulation experiment) or AGS acclimatized to the dye in 72 h cycle for 19 days (decolorization experiment); vii) AGS from a municipal WWTP; viii) Stored AGS, previously acclimatized to Acid Red 14; ix) CAS and micro-mycelium pellets from a white rot fungus; x) Bacterial cultures from a dye-contaminated area; xi) CAS from a municipal WWTP, acclimatized to Methylene Blue.

[h] Ci: initial substrate concentration in the reactor; COD: chemical oxygen demand (expressed as mg $O_2$ $L^{-1}$); dec.: decolorization experiment; Dye-SWW: dye-laden synthetic wastewater; gr.: granulation experiment; n.i.: not indicated; RMWW: real municipal wastewater; RTWW: real textile wastewater; SWW: synthetic wastewater; TOC: total organic carbon; WW: wastewater. The COD values refer to the feed, except where Ci is indicated.

[i] Emsize E1: hydrolyzed hydroxypropyl starch; etc: starch, peptone, meat extract; dec.: decolorization experiment; n.i.: not indicated.

[j] ADMI: American Dye Manufacturing Units; Mixture of dyes: Sumifix Black EXA, Sumifix Navy Blue EXF and Synozol Red K-4B; Ci: initial dye concentration in the reactor; n.i.: not indicated; SU: space units. The dye concentration values refer to the feed, except where Ci is indicated.

[k] *: Mixed liquor recirculation; #: static conditions; θ: mechanical mixing; ': minutes; Ae: aerobic phase; An: anaerobic phase; D: drain phase; dec.: decolorization experiment; F: feeding phase; gr.: granulation experiment; $N_2$: sparging with nitrogen gas; n.i.: not indicated; S: settling phase. **: microaerophilic conditions imposed in loosely screw-capped bottles, incubated at 30ºC, 140 rpm in an orbital shaker; WW: wastewater.

[l] Gr.: granulation period; n.i.: not indicated; Op.: operational period.

[m] AG: aerobic granules; E1: Emsize E1 (hydrolyzed hydroxypropyl starch); max.: maximal size; n.i.: not indicated.

[n] n.i.: not indicated; $SVI_{30}$: sludge volume index after 30 minutes of settling; $SVI_5$: sludge volume index after 5 minutes of settling.

[o] Color removal yield.

[p] Chemical oxygen demand (COD) removal yield.

[q] $NH_4$-N: Ammonia-nitrogen removal yield; n.i.: not indicated.

[r] ↓: decrease; 4A1NS: 4-amino-naphthalene-1-sulfonic acid; conc.: concentration; n.i.: not indicated.

### II.2.3.2. Removal of ENP by AGS

Sheng *et al.* (2015) showed that exposure of biofilm samples from a full-scale rotating biological contactor treating municipal sewage to high AgNP concentrations (200 mg $L^{-1}$) reduced the biofilm community diversity but did not significantly alter the microbial community functions. Furthermore, LB-EPS was shown to play a key role in the reported high resistance of biofilms to AgNP toxicity (Sheng and Liu, 2011). In fact, sludge from attached-growth bioreactors, namely biofilm reactors, has been generally rated with higher resistance to AgNP than sludge from suspended-growth bioreactors, such as CAS bioreactors (Zhang *et al*., 2016a). Overall, this effect has been associated with two major aspects (Tang *et al*., 2018): 1) physical structure, *i.e.*, strong bacterial cohesion and EPS provide a dense physical barrier against exposure of the biofilm inner cells to ENP; and 2) community structure, *i.e.*, adaptation mechanisms such as proliferation of resistant individual strains, community resilience and functional redundancy are accentuated by microbial diversity and interaction within aggregates. In this context, AGS, described as a self-supported form of biofilm, is therefore regarded as a promising solution for the treatment of AgNP-laden wastewaters, namely those produced by the textile industry. Yet, although several studies have focused on the interactions of AgNP with flocculent activated sludge (Sheng and Liu, 2017; Sheng *et al.*, 2018; Zhang *et al*., 2016a), reports on the fate and effect of AgNP in AGS treatment systems are rare.

Gu *et al.* (2014) were the first to present results on the fate and effect of AgNP in AGS systems (Table II.11), comparing them with flocculent sludge systems. In general, results indicated that homoaggregation and sedimentation played an important role in removing AgNP from the liquid phase, the presence of biomass further increasing the AgNP removal through bioadsorption and co-sedimentation. Yet, at high concentrations, AgNP formed large aggregates and a smaller proportion of nanoparticles adsorbed to the sludge, homoaggregation being the main contributor for AgNP removal under these conditions. Specifically, flocculent sludge was more efficient in removing AgNP (30-58%) than AGS (3-9%), probably due to the former's larger specific surface area favoring adsorption. This study also showed a higher release of $Ag^+$ from AgNP (10 mg $L^{-1}$) in the presence of flocculent sludge when compared to AGS (12% *vs* 7% of total silver, respectively). This difference was attributed to the higher adsorption of AgNP onto flocculent sludge, leading to a better dispersion of small AgNP with higher effective surface area for $Ag^+$ dissolution. Conversely, the comparatively low adsorption of AgNP onto AGS probably led to a higher concentration of AgNP in the liquid, resulting in AgNP homoaggregation into larger particles, which tend to release less $Ag^+$ due to a lower surface area.

In terms of AgNP inhibitory effects, AGS was more resistant to AgNP toxicity than flocculent sludge, after both short- and long-term exposure (Gu *et al*., 2014). In fact, short-term (12 h) exposure to AgNP (1-100 mg $L^{-1}$) only inhibited the rate of ammonia oxidation (21-25%) in the case of flocculent sludge,

indicating that nitrifying bacteria were more protected in the AG, the latter's granular structure potentially hindering the diffusion of AgNP and $Ag^+$ into them. On the other hand, the probably low level of toxic stress associated with exposure to low concentrations of AgNP apparently stimulated denitrification in both sludges, since denitrifying organisms are generally located in sheltered, anoxic zones (Winkler *et al*., 2013). Moreover, while the flocculent sludge's OUR was negatively affected by low AgNP concentrations (1 mg $L^{-1}$), AGS only exhibited OUR inhibition at higher AgNP levels (50-100 mg $L^{-1}$). However, this OUR inhibition effect in AGS was not observed after long-term exposure (22 days) to the same AgNP concentration, possibly due to adaptation mechanisms.

In contrast to the insignificant microbial activity inhibition in AGS, long-term exposure of flocculent sludge to AgNP (5 and 50 mg $L^{-1}$) further inhibited the rate of ammonia oxidation and OUR, in addition to negatively affecting denitrification (Gu *et al*., 2014). As hypothesized by the authors, the granular structure provided protection for microbes against toxic compounds not only by retarding their contact with AgNP but also due to the possible binding of EPS to dissolved $Ag^+$. Nevertheless, observation of cells in AG under live/dead staining suggested that AgNP or the released $Ag^+$ can penetrate into the core layers of AG and cause toxicity to the innermost cells. Based on the observed independent generation of ROS and release of lactate dehydrogenase (indicator of membrane permeability and integrity), the toxicity caused by AgNP was attributed to the oxidative stress induced by small AgNP (<10 nm) and by the released $Ag^+$, as well as to cell membrane damage caused by both small and large (>10 nm) AgNP, probably through physical penetration or chemical reactions.

In a subsequent study, the same research group further analyzed the long-term (69 days) effect of exposing AGS to AgNP (Quan *et al*., 2015; Table II.11). Although high COD and $NH_4$-N removal yields (>98%) were maintained, the AGS microbial activity was negatively affected by the presence of AgNP from operational day 36 on, namely in terms of rate of ammonia oxidation (33%), respiration rate (18-46%) and denitrification rate (7%), in addition to a reduction in the activity of specific enzymes involved in nitrogen removal (ammonia mono-oxygenase and nitrate reductase). Similarly to that reported by Gu *et al*. (2014), the registered inhibition levels were independent of AgNP concentrations, probably due to the greater tendency of larger and more concentrated AgNP to aggregate, leading to reduced AgNP bioavailability or $Ag^+$ release from them (Quan *et al*., 2015).

In terms of sludge properties, SVI values gradually increased in the AGS SBR during the first month of exposure to AgNP, as compared with the AgNP-free control, the latter retaining higher biomass concentrations thereafter (Quan *et al*., 2015). On the other hand, long-term exposure to AgNP did not significantly affect the AG shape and size, only slightly larger dimensions (*ca.* 900 μm) and a looser structure than in the control AG being noted. Finally, the dominant microbial population remained stable despite slight changes in the microbial community structure, denoting the good shelter that the granular structure provides to bacteria more vulnerable to toxic environments.

In spite of the overall AGS tolerance to AgNP and absence of acute toxicity, the authors warned of a possible chronic, long-term toxicity effect resulting from the cumulative adsorption of AgNP onto AGS (Quan *et al*., 2015). In fact, large AgNP aggregates were found on the surface of AGS and trapped within the EPS matrix. Furthermore, AgNP were shown to accumulate in AGS along the exposure period, stimulating the preferential production of PN over PS in EPS as a response to the toxic stress, similarly to the AgNP long-term effect observed in anammox granules (Zhang *et al*., 2018c). In addition, although AgNP were primarily found in major amounts in EPS, the silver content remaining in the AGS fraction after EPS extraction became more relevant at the end of the operation. These observations suggested that the continued silver influx into EPS, which served as initial barrier against AgNP and $Ag^{+}$, can eventually result in silver binding to cell membranes or penetrating into cells. Accordingly, the cell integrity in AGS was damaged and oxidative stress increased at high AgNP dosage. In addition, dead cells were found distributed from the periphery to the core of AG, the dead-to-live cells ratio being significantly higher (21-31%) than that of the AgNP-free AGS control, confirming that long-term exposure to AgNP resulted in chronic toxicity to AGS and led to cell death.

More recently, Bento *et al.* (2017) characterized the interaction of AgNP with AGS (Table II.11) in an anaerobic-aerobic SBR treating a synthetic TWW containing the azo dye AR14 and 10 mg $L^{-1}$ of AgNP. Nuclear microscopy analysis showed that AgNP typically clustered in agglomerates (<10 μm) distributed throughout the biomass granules and external EPS, being preferentially associated with the latter. This observation is in accordance with the two previous studies (Gu *et al*., 2014; Quan *et al*., 2015), where the role of EPS in the capture and physical retention of AgNP was also highlighted, 500-nm clusters of silver being observed on the surface of AG (Gu *et al*., 2014). Furthermore, a different study reported the capacity of AGS to produce and retain palladium nanoparticles, Pd(0), through reductive precipitation of Pd(II) ions under fermentative conditions (Suja *et al.*, 2014). This observation introduces the hypothesis of $Ag^{+}$ reduction back to Ag(0) also occurring in the EPS of AGS.

In addition to the three reviewed studies focusing on the behavior and effect of AgNP in AGS systems (Bento *et al*., 2017; Gu *et al.*, 2014; Quan *et al*., 2015), only three reports were to date found in the literature regarding the interaction between AGS and other ENP (He *et al*., 2017a and 2017b; Li *et al*., 2015), specifically zinc oxide and titanium oxide nanoparticles (ZnO-NP and $TiO_2$-NP, respectively), which are also used by the textile industry (Rezić *et al*., 2011). For instance, He *et al*. (2017a) investigated the response of AGS to increasing concentrations of ZnO-NP along 180 days in an aerobic-oxic-anoxic SBR (Table II.11). In terms of AGS properties, while settleability was not affected by the presence of ZnO-NP, the EPS content and its PN/PS value significantly increased. Moreover, exposure to ZnO-NP triggered a shift in the microbial community structure (especially at the phylum and genus levels), which became predominantly composed of *Proteobacteria* and *Bacteroidetes*. Furthermore, while the relative abundance of GAO and AOB decreased, ZnO-NP

induced the accumulation of NOB, denitrifying bacteria, PAO and denitrifying PAO, the latter two being more resistant to ZnO-NP, even at high concentrations and under long-term exposure. This allowed an efficient biological phosphorus removal performance to be maintained along the experiment, in parallel with an enhanced COD removal. On the other hand, ZnO-NP led to the inhibition of both nitrification and denitrification, which is in accordance with the decreased relative abundance of AOB.

The same experimental system was further evaluated regarding the effect of ZnO-NP shock loadings on AGS (He *et al*., 2017b; Table II.11). Similarly to the reported ZnO-NP long-term effect (He *et al*., 2017a), shock loading of these ENP stimulated the secretion of EPS (especially PN) and COD uptake, having no effect the total phosphorus removal, but inhibiting nitrogen transformation (including nitrification and denitrification). Accordingly, this study also showed that ZnO-NP significantly increased the OUR and caused acute inhibition of the rate of ammonia oxidation, but also increased phosphorus release and uptake in AGS. Overall, both studies indicated that nitrification and denitrification were more vulnerable to ZnO-NP when compared to COD and phosphorus removal (He *et al*., 2017a and 2017b).

Similarly to ZnO-NP, $TiO_2$-NP also represent a relevant, emergent pollutant in wastewaters, namely in those generated by the textile industry (Rezić *et al*., 2011). In this sense, Li *et al*. (2015) studied the effect of $TiO_2$-NP on the formation of algal-bacterial AG (Table II.11). The presence of $TiO_2$-NP (10-50 mg $L^{-1}$) was shown to enhance the granulation process, stable and compact algal-bacterial granules being formed and maintained for 100 days. Conversely, in the $TiO_2$-NP-free SBR (control) the granulation rate was lower and AG gradually lost their structural stability after 90 days of operation (mainly due to algae overgrowth). In terms of treatment performance, the nitritration efficiency, as well as the organics and phosphorus removal yields were not affected by the presence of $TiO_2$-NP, which, in turn, significantly improved nitratation efficiency at concentrations above 30 mg $TiO_2$-NP $L^{-1}$. In this sense, the authors suggested that $TiO_2$-NP supplementation might be a strategy to prevent AG disintegration, enhancing the long-term stability of algal-bacterial granules, possibly through stimulation of EPS secretion and inhibition of filamentous overgrowth. Irrespective of the presence of $TiO_2$-NP, the AG microbial community was predominantly composed of *Actinobacteria*, *Bacteroidetes* (*Flavobacteria* and *Sphingobacteriia*), *Nitrospiraceae*, and *Proteobacteria* (*Alpha-*, *Beta-*, *Gamma-* and *Delta-proteobacteria*).

Overall, although some promising results have been published regarding AGS resistance towards ENP, the potential for AgNP chronic toxic effects has been highlighted. In this sense, longer operation times are required to further assess the long-term impacts of AgNP on the physical stability, biochemical properties and microbial community of AGS. Moreover, the AgNP fate, transformations and toxicity mechanisms also deserve more investigation.

**Table II.11 -** Summary of operational conditions of studies on the fate and/or effect of engineered nanoparticles in aerobic granular sludge systems.

| System [a] (Operation) | H/D; [b] V (L); VER (%) | Inoculum [c] | WW [c] | Substrate [d] (COD) | ENP; [e] size (nm) | ENP [e] (mg $L^{-1}$) | Cycle [f] | AG size [g] (mm) | $SVI_{30}$ [g] (mL $g^{-1}$) | EPS [g] | COD removal [g] (%) | Nitrogen removal [g] (%) | Phosphorus removal [g] (%) | ENP fate | Reference |
|---|---|---|---|---|---|---|---|---|---|---|---|---|---|---|---|
| Aerobic SBR (22 d) | 16; 1.5; 50 | SWW-acclim. AGS | SWW | Glucose (n.i.) | Ag; 20 | 1-100 | Total: 4 h F: 10‘ Ae: 3.5 h S: 20’; D: 3’ | 850±30; (n.i.) | 40 (n.i.) | n.i. | OUR: (→, <50 mg AgNP $L^{-1}$); (↓, >50 mg AgNP $L^{-1}$) | AOR (→) DNR (→) | n.i. | Removed mainly by homoaggregation + sedimentation; Adsorption to AGS (500-nm Ag clusters; 3-9% at 1-8 mg AgNP $L^{-1}$) + co-sedimentation. | Gu *et al*., 2014 |
| Aerobic SBR (69) | n.i.; 1.5; n.i. | SWW-acclim. AGS | SWW | Glucose (1000) | Ag; 20-70 | 5-50 | Total: 4 h F: 10’ Ae: 3.7 h S: 1’; D: 5’ | 853-999 (↑) | 20-40 (↑) | EPS (→) PN/PS (↑) | >98 (→) OUR (↓) | >98% (→) AOR (↓) DNR (↓) | n.i. | 80-98% of total Ag removed by aggregation or adsorption (to EPS and surface if AGS) after 4-h contact. | Quan *et al*., 2015 |
| Anaerobic-aerobic SBR (178) | 2.5; 1.5; 50 | CAS from a municipal WWTP | Dye-laden STWW | Emsize E1 (1000) | Ag; <100 | 10 | Total: 6 h F: 30’ An*: 1.5 h Ae: 3.5 h S: 5’; D: 1’ | n.i. | n.i. | n.i. | n.i. | n.i. | n.i. | AgNP clustered in agglomerates of small dimensions (<10 μm), preferentially associated with EPS. | Bento *et al*., 2017 |
| Anaerobic/ oxic/anoxic SBR (180) | 5; 3.6; 50 | SWW-acclim. AGS | SWW | Acetate (183) | ZnO; 50-200 | 5-20 | Total: 6 h F: 2’ An*: 2 h Ae: 1.5 h Anx*: 2.4 h S: 2’; D: 2’ | n.i. | $SVI_5$: 21.8-23.2 (→) | PN (↑) PS (↑) PN/PS (↑) | 90-99 (↑) | TN: >50% (↓36%) $NH_4$: >60% (↓25%) | 89-98% (↓) | n.i. | He *et al*., 2017a |
| Anaerobic/ oxic/anoxic SBR (n.i) | 5; 3.6; 50 | SWW-acclim. AGS | SWW | Acetate (150) | ZnO; 50-200 | 10-100 | Total: 6 h F: 2’ An*: 2 h Ae: 1.5 h Anx*: 2.4 h S: 2’; D: 2’ | 1.5±0.5 (n.i.) | $SVI_5$: 22.6±0.7 (n.i.) | PN (↑) PS (→) PN/PS (↑) | 88-97 (↑) | $NH_4$: 78-93 (↓) TN: 57-80 (↓) AOR (↓10-35%) | TPUR (↓ 17-38%) | n.i. | He *et al*., 2017b |
| Anaerobic-aerobic SBR (100) | 10; 1.4; 50 | CAS from a municipal WWTP | SWW | Glucose, acetate (600) | $TiO_2$; <25 | 10-50 | Total: 4 h F: 6’ An**: 30’ Ae: 195’ S: 4’; D: 5’ | 0.2-1.1 (↑) | 25-30 (↓) | PN (↑) PS (→) PN/PS (↑) | 96 (→) | $NH_4$: >98 (→) Nitratation (↑) | 46% (→) | n.i. | Li *et al*., 2015 |

[a] d: days; n.i.: not indicated; SBR: sequencing batch reactor.

[b] H/D: height-to-diameter ratio; n.i.: not indicated; V: volume; VER: volumetric exchange ratio.

[c] acclim.: acclimatized; AGS: aerobic granular sludge; CAS: conventional activated sludge; SWW: synthetic wastewater; STWW: synthetic textile wastewater; WW: wastewater; WWTP: wastewater treatment plant.

[d] COD: chemical oxygen demand (mg $O_2$ $L^{-1}$); Emsize E1: hydrolyzed hydroxypropyl starch; n.i.: not indicated;

[e] Ag: silver nanoparticles; ENP: engineered nanoparticles; ZnO: zinc oxide nanoparticles; $TiO_2$: titanium oxide nanoparticles.

[f] ‘: min; *:stirred; **: static; Ae: aerobic period; An: anaerobic period; Anx: anoxic phase; D: drain phase; F: feeding period; S: settling phase.

[g] Effect of the ENP on AGS properties and treatment performance indicated in brackets: (→) remained unaffected; (↑) increased; (↓) decreased; AG: aerobic granules; AOR: ammonia oxidizing rate; DNR: denitrification rate; EPS: extracellular polymeric substances; n.i.: not indicated; $NH_4$: ammonia; OUR: oxygen uptake rate; PN: proteins; PS: polysaccharides; $SVI_5$ and $SVI_{30}$: sludge volume index after 5 and 30 min of settling, respectively; TN: total nitrogen; TPUR: total phosphorus uptake rate.

## II.2.4. Concluding remarks and perspectives

As environmental protection becomes a global concern, textile industries are looking for novel technologies capable of diminishing their environmental impact. The environmental concern associated with the textile industry is mainly derived from the water pollution caused by the widespread discharge of untreated or poorly treated TWWs (Solís *et al*., 2012). This severely affects the ecosystems in receiving water bodies, not only because colored TWWs impair light penetration in water leading to lower oxygen levels (Pandey *et al*., 2007), but also due their toxic effects on plants, aquatic organisms and human health (Verma *et al*., 2012). According to Ghaly *et al.* (2014), countries of the Indian subcontinent, China and European Union represented approximately 70% of the world textile dyeing industries. Previous data regarding the textile industry in Germany indicated that 11% of the plants released their effluents directly into surface waters (Vajnhandl and Valh, 2014). In general, textile companies typically discharge their wastewater into municipal WWTPs without proper pre-treatment, because sophisticated wastewater treatment technologies are unaffordable for small to medium-sized textile companies (Vajnhandl and Valh, 2014). Given the fact that these constitute the majority of the textile plants (Vajnhandl and Valh, 2014), the development of affordable and efficient TWW treatment technology is imperative. The importance of this cost factor is further reinforced by the fact that the textile production, which started in the West, has gradually moved to lower cost manufacturing countries since the 1950's, mainly to developing countries in Asia, where inadequate legislation and compliance control has led to the pollution of natural water bodies (Nimkar, 2018). Consequently, pollution caused by textile processing has moved along with the continuous shifting of the textile industry (presently to countries such as Myanmar, Nicaragua, Kenya, Madagascar and Ethiopia; Nimkar, 2018).

The urgent demand for efficient, environmentally friendly and economically attractive TWW treatment solutions represents a current challenge, owing to the complexity and variability of this type of effluents (Raman and Kanmani, 2016; Verma *et al*., 2012). Although various physical, chemical and biological methods have been investigated and proposed for treating TWW, each one presents significant limitations. Up to this point, there is no single and economically attractive treatment method that can effectively decolorize and detoxify the TWW. In fact, the development of a single, global TWW treatment method is unlikely due to the complex, highly variable (seasonally, often daily) composition of TWWs, which also differ from company to company. Thus, in order to meet the regulatory standards, combinations of different treatment processes deserve to be further investigated (Vajnhandl and Valh, 2014), namely the combination of AOP with biological processes (Pandey *et al*., 2007). The choice of the treatment technologies will depend on the effluent composition, characteristics of the dye and other polluting constituents, cost, toxicity of the treatment by-products and subsequent uses of the treated water (Solís *et al*., 2012).

While approximately 10% of the employed textile dyes and specialty chemicals are discharged into the wastewater during manufacture, the remaining 90% that stay on the fabric will end up in landfills, where they can degrade over time and leach out to water bodies (Nimkar, 2018). In light of this major issue, the textile industry also faces the challenging demand to move towards a cleaner production, abandoning the use of hazardous chemicals and replacing them with more sustainable chemicals that degrade into safer metabolites at the end of product life (Nimkar, 2018). In fact, the use and discharge of harmful chemicals accross the textile supply chain in different countries from where global apparel brands source their products has been exposed in several Greenpeace reports (Nimkar, 2018). In order to tackle the problem, the Manufacturing Restricted Substances List has been established within the Zero Discharge of Hazardous Chemicals Program (Nimkar, 2018), to define usage limits for hazardous substances (including azo dyes) potentially employed in textile manufacturing and discharged into the environment. To address this challenge, the industry has invested on sustainable chemistry innovative solutions, involving the use of biodegradable auxiliary agents, colorants from bio-waste sources, as well as reduction or elimination of water usage and wastewater discharge through implementation of low/no-water textile processing technologies and water reuse strategies within the textile plant (Vajnhandl and Valh, 2014).

In this context, to tackle the environmental impact of the textile industry, future research into the problem of TWW should mainly focus on: 1) achieving dye mineralization in addition to decoloration, avoiding the persistence of potentially toxic dye intermediates; 2) designing novel dyes and auxiliary chemicals with enhanced biodegradability; 3) developing suitable processes to reduce water consumption, eliminate or minimize the discharge of toxic chemicals, and optimize water re-use to render companies more eco-friendly at competitive costs. Specifically regarding the optimization of TWW treatment efficiency, the use of complex microbial communities and the identification of azo dye metabolites are essential to conduct an ecologically relevant assessment of the potential for microbial degradation of azo dyes. This would allow the development of environmental policies on regulation of potentially toxic dyes and management of industrial wastewaters (Rawat *et al*., 2016). Similarly, the need for ENP risk assessment and regulation in real WWTPs (Wu *et al*., 2018b), namely through the development of a specific toxicology model (Sheng *et al*., 2018), have been highlighted. In fact, the increasing application of diverse ENP in different industrial fields will inevitably cause their release into industrial and municipal WWTPs. However, ENP fate (*e.g*., aggregation, adsorption, dissolution, precipitation, and sulfidation) and potential toxic effect in biological treatment systems has mainly been assessed in lab-scale tests, and there is still great controversy on the subject, thus requiring further investigation.

# III. Effect of an azo dye on the performance of an AGS SBR treating a simulated TWW

The information included in this chapter was partially published in:

Franca, R.D.G., Vieira, A., Mata, A.M.T., Carvalho, G.S., Pinheiro, H.M., Lourenço, N.D., 2015. Effect of an azo dye on the performance of an aerobic granular sludge sequencing batch reactor treating a simulated textile wastewater. *Water Research* 85, 327-336. DOI: 10.1016/j.watres.2015.08.043.

Franca, R.D.G., Mata, A.M.T., Pinheiro, H.M., Lourenço, N.D., 2014. Effect of sludge retention time on azo dye biodegradation in an aerobic granular sludge SBR. *IWA World Water Congress & Exhibition*, 21-26 September, Lisbon, Portugal.

## III.1. Abstract

This study analyzed the effect of an azo dye (AR14) on the performance of an AGS SBR system operated with 6-h anaerobic-aerobic cycles for the treatment of a synthetic TWW. In this sense, two SBRs inoculated with AGS from a domestic WWTP were run in parallel, being one supplied with the dye and the other used as a dye-free control. The AGS successfully adapted to the new hydrodynamic conditions forming smaller, denser granules in both reactors, with optimal SVI values of 19 and 17 mL $g^{-1}$ after 5-min and 30-min settling, respectively. As a result, high biomass concentration levels and sludge age values were registered, up to 13 gTSS $L^{-1}$ and 40 days, respectively, when deliberate biomass wastage was limited to the sampling needs. Stable dye removal yields above 90% were attained during the anaerobic reaction phase, confirmed by the formation of one of the aromatic amines arising from azo bond reduction. The control of the SRT to 15 days triggered a 30% reduction in the biodecolorization yield. However, the increase of the SRT values back to levels above 25 days reverted this effect and also promoted the complete bioconversion of the identified aromatic amine during the aerobic reaction phase. The dye and its breakdown products did not negatively affect the treatment performance, as organic load removal yields higher than 80% were attained in both reactors, up to 77% occurring in the anaerobic phase. These high anaerobic organic removal levels were correlated to an increase of *Defluviicoccus vanus*-related GAO in the biomass. Also, the capacity of the system to deal with shocks of high dye concentration and organic load was successfully demonstrated. Granule break-up after long-term operation only occurred in the dye-free control SBR, suggesting that the azo dye plays an important role in improving granule stability. Fluorescence *in situ* hybridization (FISH) analysis confirmed the compact structure of the dye-fed granules, microbial activity being apparently maintained in the granule core, as opposed to the dye-free control. These findings support the potential application of the AGS technology for TWW treatment.

## III.2. Introduction

With the increasing demand for textile products, the textile industry wastewater represents one of the main sources of water pollution problems worldwide, mainly due to high organic loads and recalcitrant dyes (dos Santos *et al*., 2007). Textile dyes are responsible for the presence of color in TWW, impairing light penetration and compromising ecosystems in the receiving water media. Bacterial decolorization of azo dyes, the main type of synthetic textile dyes used, is generally accomplished through anaerobic azo bond cleavage with colorless aromatic amine formation. However, these potentially toxic breakdown intermediates are generally not further degraded anaerobically.

In this context, anaerobic-aerobic SBRs with flocculent activated sludge have been proposed for complete biodegradation of azo dyes through azo bond reduction in the anaerobic phase, with concomitant color removal, followed by aromatic amine mineralization in the subsequent aerobic step

(van der Zee and Villaverde, 2005). Nevertheless, despite the notable success in the anaerobic decolorization stage (Lourenço *et al*. 2000; Albuquerque *et al.* 2005), information regarding the fate of the breakdown aromatic amines during the aerobic stage, when available, revealed that most of these amines were not degraded (van der Zee and Villaverde, 2005). This difficulty in mineralizing azo dye reduction products under aerobic conditions has generally been attributed to the lack of an adequate microbial population capable of metabolizing such compounds (Lourenço *et al.* 2009). Given this troubling scenario, there is an urgent need for effective, environmentally friendly and economically attractive technologies for TWW treatment.

Furthermore, intrinsic operational problems of flocculent activated sludge systems, such as poor settling properties, compromise the treatment efficiency and lead to large footprint requirements. The use of AGS has been recently suggested to overcome these problems. The AGS technology, with near spherical structures of self-aggregated microorganisms formed under specific SBR operational conditions (Beun *et al*., 2002), has been implemented in several domestic and industrial treatment plants, being often referred as the next generation of wastewater treatment (Giesen *et al*., 2013). In addition to the outstanding settling characteristics of AGS, the co-existence of aerobic and anoxic-anaerobic zones within the granules (Winkler *et al*., 2013) and their resistance to high organic loads and toxic compounds (Giesen *et al*., 2013) reinforce the promising application of the AGS technology for TWW treatment, though practical demonstration has scarcely been reported (Muda *et al.*, 2010). Moreover, the operational SRT flexibility of AGS systems enables the presence of a more diverse microbial community within the SBR, namely slow-growing populations, whose activity may be advantageous for the degradation of recalcitrant compounds (Clara *et al.*, 2005).

In this context, the aim of this work was to study the effect of an azo dye in the characteristics and performance of AGS in an anaerobic-aerobic SBR system treating synthetic TWW. The performance of two AGS SBRs run in parallel (one supplied with the dye and the other used as a dye-free control) was evaluated in terms of AGS stability, microbial community, azo dye and intermediate aromatic amine biodegradation and COD removal efficiency. The capacity of the system to deal with sudden, high dye concentrations and organic loads in the feed was also evaluated.

## III.3. Materials and methods

### III.3.1. Chemicals

#### III.3.1.1. Carbon source and dye stock solutions

A starch-based sizing agent used in the textile industry, Emsize E1 (Emsland-Stärke GmbH, Germany), was used as carbon source. The stock solution (100 g $L^{-1}$) was prepared by hydrolyzing a solution of Emsize E1 in distilled water, in alkaline conditions, based on a set of desizing conditions indicated by the manufacturer. Specifically, 40 g of sodium hydroxide and 100 g of Emsize E1 were

dissolved in distilled water and stirred during approximately 15 h at room temperature. The hydrolyzed solution was then neutralized to pH 7.0±0.05 with 37% HCl and diluted to 1 L with distilled water.

The azo dye stock solution was prepared by dissolving AR14 (Chromotrope FB, Sigma-Aldrich, 50% dye content) in distilled water to a final concentration of 3.0 g $L^{-1}$.

### III.3.1.2. Synthetic wastewater composition

The synthetic TWW used as feed solution was prepared by diluting the carbon source stock solution in distilled water to a COD content of 1000 mg $O_2$ $L^{-1}$ (1.15 g $L^{-1}$ Emsize E1), and supplementing it with pH buffering phosphates and nutrients to the following concentrations: 2310 mg $L^{-1}$ $Na_2HPO_4 \cdot 12H_2O$, 762 mg $L^{-1}$ $KH_2PO_4$, 143 mg $L^{-1}$ $NH_4Cl$, 22.5 mg $L^{-1}$ $MgSO_4 \cdot 7H_2O$, 27.5 mg $L^{-1}$ $CaCl_2$, 250 µg $L^{-1}$ $FeCl_3 \cdot 6H_2O$, 40 µg $L^{-1}$ $MnSO_4 \cdot 4H_2O$, 57 µg $L^{-1}$ $H_3BO_3$, 43 µg $L^{-1}$ $ZnSO_4 \cdot 7H_2O$, 35 µg $L^{-1}$ $(NH_4)_6Mo_7O_{24} \cdot 4H_2O$. All salts were analytical grade. In this feed solution the COD:N:P mass ratio was 100:3.7:37. The low N supply was used to avoid the occurrence of nitrification. For the carbon shock load assays the Emsize E1 and $NH_4Cl$ concentrations in the feed were the triple of those indicated above.

### III.3.2. SBR setup and operation

Two bubble-column SBRs with a working volume of 1.5 L (H/D of 2.5) were seeded with AGS harvested from the Nereda® demonstration plant at the Frielas domestic WWTP, Portugal, which is operated in a sequencing batch mode with an anaerobic filling stage followed by an aerobic reaction phase.

Mechanical mixing (70 rpm) was provided by magnetic stirrers and aeration (2 v.v.m.) was supplied by air compressors via a porous membrane diffuser at the bottom of each bioreactor. The synthetic wastewater was fed into both SBRs at the bottom with an exchange ratio of 50% (effluent withdrawal at mid-height), the volumetric OLR being 2.0 kg COD $m^{-3}$ $d^{-1}$. While one bioreactor was used as a dye-free control (SBR1), the other was fed with the azo dye stock solution (SBR2) to an initial dye concentration of 20 mg $L^{-1}$ at the onset of the reaction phase.

The SBRs were run in parallel for 102 days, comprising five experimental periods (I-V), characterized in Table III.1. Deliberate biomass wastage was limited to sampling, except during period II, when the SRT was controlled at 15 days through daily biomass purging from SBR mixed liquor. To test the capacity of the system to deal with high dye and organic loads, the initial dye concentration in SBR2 was increased to 60 mg $L^{-1}$ from day 91 on (period IV), and the volumetric OLR was increased to 6.0 kg COD $m^{-3}$ $d^{-1}$ from day 98 on (period V).

Reactors were operated at room temperature (23ºC, on average) in a sequencing batch mode with 6-h cycles, of which the first 1.5 h of reaction were anaerobic (with mechanical mixing), followed by 3.5 h of aeration. The static filling period was fixed at 18 min, the dye stock solution being added at the top of SBR2 during the last 1.5 min of this period. The settling and effluent withdrawal times were 5 min and 1 min, respectively. The mixed liquor pH value (uncontrolled) varied within the 6.5-6.7 range along each cycle.

**Table III.1** - Overview of the operational conditions imposed to the system during the five consecutive stages of the experimental run. Sludge retention time (SRT) was controlled at 15 days during period II through daily biomass purging. Three-fold increases in the feed dye (Acid Red 14, AR14) and chemical oxygen demand (COD) concentrations were applied during periods IV and V, respectively. Accordingly, the organic loading rate (OLR), excluding the dye contribution, is indicated for each period. * Valid only for the dye-fed sequencing batch reactor (SBR2).

| Period | I | II | III | IV * | V |
|---|---|---|---|---|---|
| Period description | Biomass accumulation | SRT control | Biomass accumulation | Dye shock load | Organic shock load |
| Operational days | 1-41 | 42-60 | 61-90 | 91-97 | 98-102 |
| SRT (days) | No control | 15 | No control | No control | No control |
| AR14 (mg $L^{-1}$) * | 20 | 20 | 20 | 60 | 60 |
| OLR (kg COD $m^{-3}$ $d^{-1}$) | 2 | 2 | 2 | 2 | 6 |

## III.3.3. Analytical methods

### III.3.3.1. Physicochemical parameters

TSS, volatile suspended solids (VSS) and COD were determined according to standard procedures (APHA, 1995). SVI was determined by measuring the volume occupied by the sludge settled from 1 L of mixed liquor after settling times of 5 and 30 min in an Imhoff cone ($SVI_5$ and $SVI_{30}$, respectively), and dividing it by the mixed liquor TSS value (APHA, 1995). Biomass morphological analysis was carried out using a transmission light microscope (BA200, Motic) fitted with a digital camera and respective software (Moticam 2, Motic). The proportion of large granules (sizes above 0.65 mm), small granules (sizes within the 0.25-0.65 mm range) and flocs (sizes under 0.25 mm) in the SBRs was estimated by sieving mixed liquor samples through 0.65-mm and 0.25-mm net sieves, and determining the biomass content in each collected fraction using the TSS analysis protocol.

The pH of centrifuged samples was determined on selected cycles, using a Metrohm 6.0262.100 glass electrode connected to a Metrohm 1.691.0010 potentiometer (pH meter 691, Metrohm, Switzerland). The oxidation-reduction potential (ORP) was continuously followed throughout operating cycles using a combination ORP electrode with platinum ring indicator equipped with ARGENTHAL™ reference systems (InLab® Redox-L, Mettler Toledo). Measured values were converted to the standard hydrogen electrode basis by adding +207 mV (for an average temperature of 25ºC), according to the manufacturer. The DO was monitored along selected cycles using a standard luminescent DO probe

(LDO101, Hach, USA) connected to a multi parameter meter (HQ40d, Hach, USA) fitted with a temperature probe immersed in the mixed liquor to a depth of approximately 3 cm.

The UV-visible absorbance spectra of clarified (centrifuged) samples was monitored along selected treatment cycles in a UV-visible spectrophotometer (Specord 200, Analytik Jena). Azo dye and breakdown metabolites were analyzed by reversed-phase HPLC (Merck-Hitachi LC-organizer, L-4250 UV-visible detector, L-6200A intelligent pump, Interface D-7000 and Autosampler L-7200) using a LiChroCART Purospher STAR RP-18e column (250 mm x 4 mm; Merck, Germany). The eluent consisted of phosphate buffer (25 mM, pH 5.5) and acetonitrile at a flow rate of 700 μL $min^{-1}$. The gradient conditions were as follows: 0-30 min, linear gradient from 0 to 50% acetonitrile; 30-35 min, linear gradient to 85% acetonitrile; 10 min isocratic 0% acetonitrile for column re-equilibration. Spectrophotometric detection was performed at 220 nm. AR14 and 4A1NS standards (Sigma-Aldrich) were used to quantify these compounds based on the areas of the respective HPLC peaks.

### III.3.3.2. Microbial community characterization

#### III.3.3.2.1. Fluorescence *in situ* hybridization (FISH) analysis and quantitative FISH

Biomass samples harvested from the SBRs were fixed in a 1:3 ratio with 4% paraformaldehyde solution for 1-3 h at 4ºC, subsequently washed with 1x phosphate-buffered saline (PBS) and stored in cold 1:1 PBS/ethanol at -20ºC. FISH analysis was performed according to Amann (1995). FISH was carried out on homogenized biomass samples and also on isolated granules for structure and microbial spatial distribution analysis. For quantification purposes, homogenized biomass samples were used.

FISH analysis was initially carried out on homogenized biomass samples using oligonucleotide probes expected to cover the core community typically detected in WWTPs (Saunders *et al*., 2015): Fluorescein isothiocyanate (FITC)-labeled EUBmix [mixture of EUB338 (Amann *et al.*, 1990), EUB338-II and EUB338-III (Daims *et al*., 1999)] for all *Bacteria*; Cyanine 3 (Cy3)-labeled ALF969 for *Alphaproteobacteria* (Oehmen *et al*, 2007); BET42a for *Betaproteobacteria*; GAM42a for *Gammaproteobacteria* (Manz *et al*., 1992); CF319a for most *Flavobacteria*, some *Bacteroidetes* and some *Sphingobacteriia* (Manz *et al*., 1996); HGC69a for *Actinobacteria* (Roller *et al*., 1994); LGCmix [mixture of LGC354A, LGC354B and LGC354C (Meier *et al*., 1999)] for *Firmicutes*; SuperDFmix [mixture of TFOmix – TFO_DF218 and TFO_DF618 (Wong *et al*., 2004), DFmix – DF988 and DF1020 (Meyer *et al*., 2006), and DF198 (Meyer *et al*., 2005)] for *Defluviicoccus vanus*-related GAO; Par651 for *Paracoccus* (Neef *et al*., 1996). Olympus BX51 epifluorescence microscope (Japan) equipped with a camera was used for observation of the hybridized samples and image acquisition. FITC and Cy3 were excited with an argon laser (488 nm), a helium neon laser (543 nm) and their emissions collected with 500-530 nm BP (bandpass) and 550-625 nm BP emission filters, respectively. Each sample and set of probes were carefully examined and a semi-quantitative

assessment of the relative abundance of each specific probe was determined by comparison with the number of cells targeted by EUBmix.

For granule analysis, fixed granules were preserved in tissue-freezing medium OCT™ (Tissue-Tek, Sakura Finetech) within plastic molds and stored at -20ºC. Granules were then sectioned in slices with a thickness of 20 μm using a Cryostat (Leica). FISH was carried out on sliced granules using the following oligonucleotide probes: Cyanine 5 (Cy5)-labeled EUBmix [EUB338 (Amann *et al.,* 1990), EUB338-II and EUB338-III (Daims *et al*., 1999)] for all *Bacteria*; Cy3-labeled NSO 1225 (Mobarry *et al*., 1996) for AOB; FITC-labeled PAOmix (PAO462, PAO651, and PAO846; Crocetti *et al.,* 2000) for most *Candidatus* Accumulibacter phosphatis, the most relevant PAO. A Zeiss LSM 510 Meta confocal laser scanning microscope (CLSM) was used for observation of the hybridized samples and image acquisition. FITC and the iodocarboamide dyes Cy3 and Cy5 were excited with an argon laser (488 nm), a helium neon laser (543 nm) and a red diode laser (637 nm) and their emissions collected with 500-530 nm BP, 550-625 nm BP and 660 nm LP (longpass) emission filters, respectively.

For quantification of PAO and GAO the specific FISH probes used were as follows: PAOmix for *Accumulibacter*; TET892, TET266, TET174 and TET654 (Nguyen *et al*., 2011) for *Tetrasphaera*-related PAO; GAOmix (GAOQ989 and GB_G2; Crocetti *et al*., 2002 and Kong *et al.*, 2002) for *Candidatus* Competibacter phosphatis; regarding the *Defluviicoccus vanus*-related GAO, TFOmix (TFO_DF218 and TFO_DF618; Wong *et al*., 2004) was used for cluster I, DFmix (DF988 and DF1020; Meyer *et al*., 2006) for cluster II, DF1013 and DF1004 (Nittami *et al*., 2009) for cluster III, and DF181A and DF181B (McIlroy and Seviour, 2009) for cluster IV. Image analysis of at least 20 randomly selected fields was performed by means of the Daime Software (Daims *et al*., 2006) using EUBmix as the general probe labeled with Cy5, and each of the specific probes labeled with Cy3. The abundance of PAO and GAO as percentage of all *Bacteria* (as biovolume) was calculated as the area covered by the specific probes divided by the area covered by EUBmix. The standard error of the mean was calculated as the standard deviation divided by the square root of the number of images.

#### III.3.3.2.2. Microbial community analysis

Biomass samples were harvested from SBR1 and SBR2 on selected operational days, centrifuged and stored at -80ºC, to subsequently quantify the abundance of different bacteria along the experimental run through high-throughput DNA sequencing, performed by the DNASense ApS (Aalborg, Denmark).

##### III.3.3.2.2.1. Library preparation and DNA sequencing

Regarding the library preparation, the procedure for bacterial 16S rRNA amplicon sequencing targeting the V1-3 variable regions was based on Caporaso *et al*. (2012), using primers adapted from the Human Gut Consortium (Ward *et al*., 2012). Specifically, 10 ng of extracted DNA were used as

template and the PCR reaction (25 μL) contained deoxynucleotides (dNTPs; 400 nM of each), $MgSO_4$ (1.5 mM), Platinum® Taq DNA polymerase HF (2mU), 1X Platinum® High Fidelity buffer (Thermo Fisher Scientific, USA), and barcoded library adaptors (400 nM) containing V1-3 specific primers: 27F AGAGTTTGATCCTGGCTCAG and 534R ATTACCGCGGCTGCTGG. The PCR settings were as follows: initial denaturation at 95ºC for 2 min, 30 amplification cycles of 95ºC for 20 s, 56ºC for 30 s, 72ºC for 60 s and final elongation at 72ºC for 5 min). All PCR reactions were run in duplicate and pooled afterwards. The amplicon libraries were purified using the Agencourt® AMpure XP bead protocol (Beckmann Coulter, USA) with the following specifications: the sample/bead solution ratio was 5/4, and the purified DNA was eluted in 33 μL nuclease-free water (Qiagen, Germany).

Concerning the fungal analysis, fungal ITS1 amplicon libraries were prepared as follows (Illumina, 2015): up to 10 ng of extracted DNA were used as template for PCR amplification, each PCR reaction (25 μL) containing dNTPs (0.1 mM of each), $MgSO_4$ (1.5 mM), Platinum® Taq DNA polymerase HF (0.5U/rxn), 1x Platinum® High Fidelity buffer (Thermo Fisher Scientific, USA) and tailed primermix (0.4 μM of each forward and reverse). The PCR settings were as follows: initial denaturation at 95ºC for 2 min, 35 amplification cycles of 95ºC for 20 s, 54ºC for 30 s, 72ºC for 60 s and a final elongation at 72ºC for 5 min). The forward and reverse tailed primers were designed according to Illumina (2015) and contained primer sequences targeting the fungal ITS1: 5'-CTTGGTCATTTAGAGGAAGTAA (ITS1f) and 5'-GCTGCGTTCTTCATCGATGC (ITS2; Ghannoum *et al*., 2010). The amplicon libraries were purified as described for the bacteria library, but using 25 μL of nuclease-free water instead of 33 μL. Sequencing libraries were prepare from the purified ITS1 amplicon libraries using a second PCR: each PCR reaction (25 μL) contained 1x PCRBIO HiFi buffer (PCRBiosystems, UK), PCRBIO HiFi Polymerase (1U/rxn) (PCRBiosystems, UK), nextera adaptor mix (0.4 μM of each forward and reverse) and up to 10 ng of amplicon library template. The PCR settings were as follows: initial denaturation at 95ºC for 2 min, 8 cycles of amplification (95ºC for 20 s, 55ºC for 30 s, 72ºC for 60 s) and a final elongation at 72ºC for 5 min. The sequencing libraries were purified as previously.

DNA concentration of the bacterial sequencing libraries and fungal amplicon and sequencing libraries was measured using Qubit dsDNA HS assay (Thermo Fisher Scientific, USA). Each sample (1 μL) was measured once. Gel electrophoresis was run on a subset of samples to validate library size and purity using a Tapestation 2200 with High Sensitivity D1000 ScreenTapes (Agilent, USA). The purified bacterial and fungal sequencing libraries were separately pooled in equimolar concentrations. Bacterial library pool was diluted to 6 nM and fungal library pool was diluted to 2 nM. These samples were paired-end sequenced (2x301 bp) on a MiSeq (Illumina) using a MiSeq Reagent kit v3, 600 cycles (Illumina) following the standard guidelines for preparing and loading samples on the MiSeq. To overcome low complexity issue, often observed with amplicon samples, >10% Phix control library was spiked in.

#### III.3.3.2.2.2. Bioinformatic processing

Regarding the bacterial 16S V1-3 rRNA bioinformatic processing, forward and reverse reads were trimmed for quality using Trimmomatic v. 0.32 (Bolger *et al*., 2014) with the settings SLIDINGWINDOW:5:3 and MINLEN:275. The trimmed forward and reverse reads were merged using FLASH v. 1.2.7 (Magoc and Salzberg, 2011) with the settings -m 25 -M 200. The merged reads were dereplicated and formatted for use in the UPARSE workflow (Edgar, 2013). The dereplicated reads were clustered, using the usearch v. 7.0.1090 -cluster_otus command with default settings. Operational taxonomic unit (OTU) abundances ware estimated using the usearch v. 7.0.1090 -usearch_global command with -id 0.97. Taxonomy was assigned using the RDP classifier (Wang *et al*., 2007a) as implemented in the parallel_assign_taxonomy_rdp.py script in QIIME (Caporaso *et al*., 2010), using the MiDAS database v.1.20 (McIlroy *et al*., 2015). The results were analyzed in R (R Core Team, 2015) through the Rstudio IDE using the ampvis package v.2.0.1 (Albertsen *et al*., 2015).

As for the fungal ITS1 bioinformatic processing, forward reads were trimmed using cutadapt v. 1.13 with cutadapt -g GCTGCGTTCTTCATCGATGC -a TTACTTCCTCTAAATGACCAAG -a CTGTCTCTTATACACATCT -n 3 -m 100 -l 200 -q 20. The trimmed data dereplicated using usearch v. 9.2 with usearch -fastx_uniques -sizeout. The dereplicated data was clustered at 98.5% identity threshold with usearch -cluster_otus 1.5 -minsize 2. Taxonomy was assigned to OTUs with usearch -sintax -db utax_ITS_ref_20160822.fasta -strand both -sintax_cutoff 0.8. The database used was the UNITE usearch/utax reference dataset v7.1 (2016-08-22, https://unite.ut.ee/). An OTU table was generated by mapping the trimmed reads to the OTUs with usearch -usearch_global -strand plus –id 0.985. The results were analyzed in R, as described above.

## III.4. Results

### III.4.1. AGS morphology and properties

#### III.4.1.1. Granule size and settling properties

The proportion of granules and flocs in the reactors was followed along the experimental period, through sieve analysis. The large, mature AG (sizes above 0.65 mm, up to 5 mm) present in the inoculum disintegrated over time in both reactors, most likely due to the shear imposed by mechanical stirring during the anaerobic phase. As a result, 77 days after inoculation with AGS containing 75% of large granules (and 25% of flocs), the biomass in both SBRs was composed of less than 10% of large, original-like granules, and around 30-45% of smaller granules (0.25-0.65 mm; Figure III.1). From this point on, the sludge composition in the two reactors significantly diverged. While in the dye-fed SBR2 the granules/flocs ratio slightly increased, even after the application of dye and organic substrate shock loads, total granule disintegration was registered in the dye-free control SBR1 (Figure III.1).

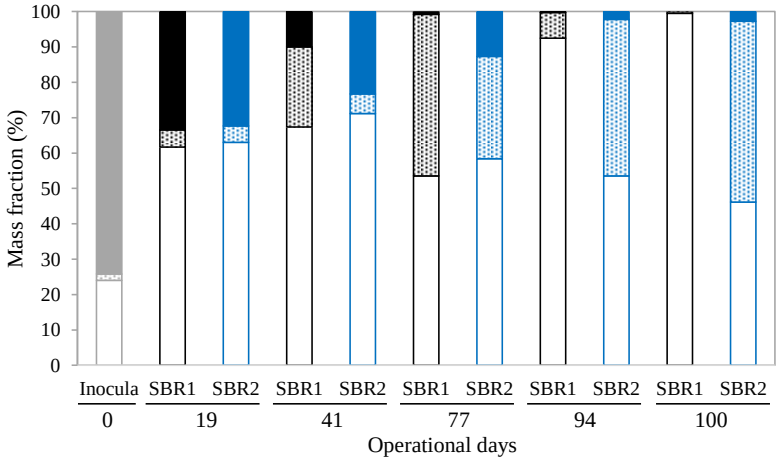


**Figure III.1** - Distribution of particle sizes along the experimental run. Comparison between the mass percentage of flocs (white bars; dimensions under 0.25 mm), small granules (dotted bars; sizes within the 0.25-0.65 mm range) and large granules (colored bars; sizes above 0.65 mm) in the dye-free control SBR1 (black) and in the dye-fed SBR2 (blue), along the operation. Changes in the operational conditions: sludge retention time control at 15 days from day 42 to 60 (period II), three-fold increase in the dye concentration from day 91 on (period IV) and three-fold increase in the organic load from day 98 on (period V).

Analysis of the biomass settling properties gave results consistent with the observed changes in the percentages of granules and flocs along the experimental period. Compared to the initial settling characteristics of the seed sludge, the marked increase in SVI values observed in both reactors two days after inoculation (Figure III.2) came as a consequence of the initial granule disintegration, as previously mentioned. Nevertheless, despite the smaller size of the granules subsequently developed in the reactors, the biomass evolved to exceptional settling properties, as the $SVI_5$ and $SVI_{30}$ values consistently decreased up to day 74 reaching 25 and 19 mL $gTSS^{-1}$ in SBR1, and 19 and 17 mL $gTSS^{-1}$ in SBR2, respectively. Subsequently, while low SVI values were registered in SBR2 up to the end of the experimental period, SBR1 presented increasing and progressively diverging values of $SVI_5$ and $SVI_{30}$ due to the decrease in the granule content of the sludge.

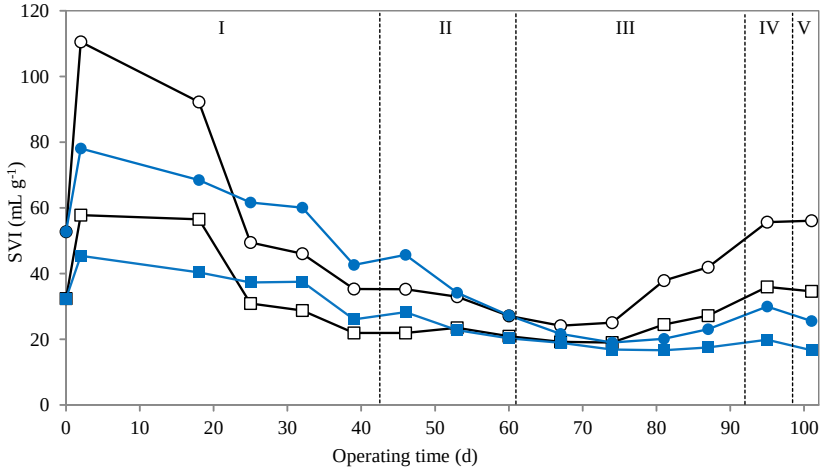


**Figure III.2** - Sludge volume index (SVI) profile along the experimental periods. SVI values measured after 5-min settling ($SVI_5$) for the dye-free control SBR1 (○) and the dye-fed SBR2 (●), and after 30-min settling ($SVI_{30}$) for SBR1 (□) and SBR2 (■). Period I (days 0 to 41) − no control of SRT (biomass wastage was limited to sampling needs); period II (days 42 to 60) − SRT control at 15 days through daily biomass purging; period III (days 60 to 90) − no control of SRT; period IV (days 91 to 97) − three-fold increase in the dye concentration in SBR2; period V (days 98 to 102) − three-fold increase in the organic load.

### III.4.1.2. AGS morphology

Biomass morphology analysis through light microscopy showed that the smaller granules developed in the reactors did not have well-defined, round or oval shapes (Figure III.3). They were instead dense and compact biomass clusters with irregular outlines. Moreover, the morphology of the remaining flocculent fraction in the sludge exhibited distinct nuclei, unlike the even pin-point flocs appearing in CAS. As shown in Figure III.3, there was a marked reduction in the flocculent fraction from day 39 to day 59, promoted by deliberate biomass removal for SRT control at 15 days during period II (days 42 to 60; Table III.1). From day 67 to day 74, biomass was no longer removed, leading to its accumulation and to the increase of SRT up to 40 days. In this period, the size of granules was quickly enlarged from a maximum of 0.3 up to 1.0 mm in both reactors. However, this granule size was subsequently maintained only in SBR2, granule disintegration and floc formation having occurred in SBR1.

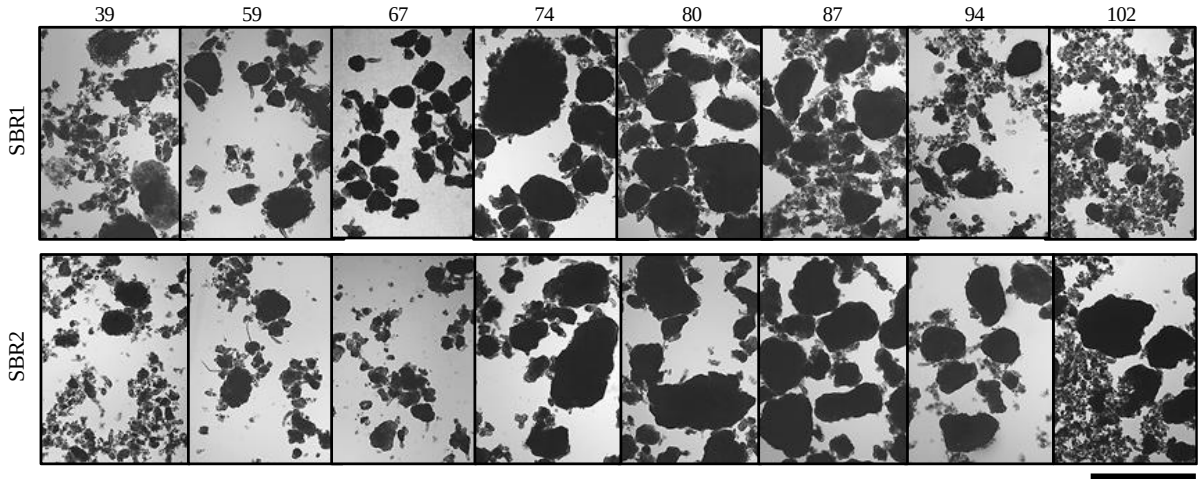


**Figure III.3** - Morphological development of granular sludge in the sequencing batch reactors (SBRs) along the experimental run. Microscopic images (magnification 40) from biomass samples harvested from the dye-free control SBR1 (upper row) and the dye-fed SBR2 (lower row) on the indicated operational days (on top). Changes in the operational conditions: sludge retention time control at 15 days from day 42 to 60 (period II), three-fold increase in the initial dye concentration from day 91 on (period IV) and three-fold increase in the organic load from day 98 on (period V). Scale bar = 1 mm.

## III.4.2. Microbial community dynamics

### III.4.2.1. FISH analysis

FISH analysis was performed on biomass samples harvested from SBR2 on days 0 (corresponding to the inoculum), 37, 58, 79 and 100 of the experimental run in order to assess the evolution in the bacterial distribution through six major groups upon changes in the operational conditions. As represented in Figure III.4, the inoculum contained a high abundance of *Betaproteobacteria*, which was outcompeted under the new operating conditions, namely by bacteria from the *Alphaproteobacteria* group, which thrived in SBR2 along the experimental run. The absence of SRT

control until day 42 allowed the growth of *Gammaproteobacteria* populations, representing the dominant group on day 37 (Figure III.4). The subsequent control of the SRT at 15 days through daily sludge wastage (from day 42 to 60) affected the microbial community, further reinforcing the dominance of *Alphaproteobacteria* and *Gammaproteobacteria*, followed by *Actinobacteria*, on day 58 (Figure III.4). This bacterial distribution was maintained until the end of the operation (days 79 and 100), despite the SRT control interruption from day 60 on and the three-fold increase in the dye and COD load applied on days 93 and 98, respectively (Figure III.4). In addition, a morphological change in the *Alphaproteobacteria* communities was registered from day 58 to days 79 and 100, as the rod-shaped bacterial community was replaced by cocci-form bacteria growing in tetrads (Carvalho, 2016). In fact, the application of two specific probes for *Alphaproteobacteria* communities allowed the identification of *Defluviicoccus vanus*-related GAO, representing the majority of the *Alphaproteobacteria* group on days 79 and 100 (Figure III.4).

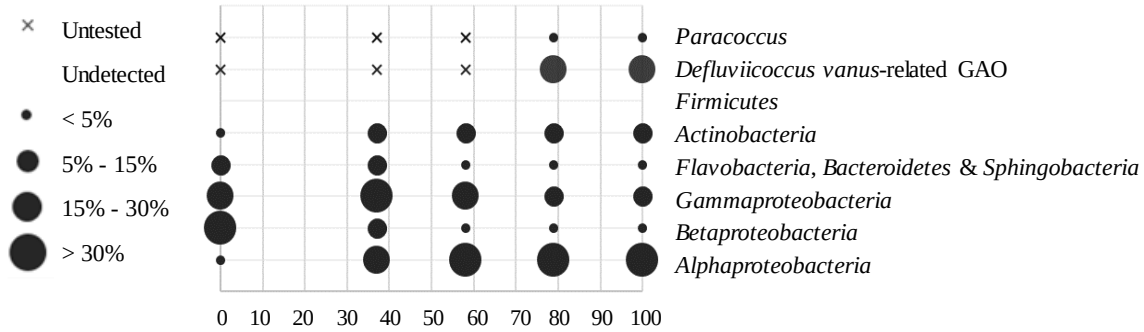


**Figure III.4** - Abundance of the selected *Bacteria* detected by FISH analysis in the mixed microbial culture samples harvested from the dye-fed sequencing batch reactor (SBR2) along the experimental run. Adapted from Carvalho (2016). GAO: glycogen-accumulating organisms.

FISH analysis was also conducted on cryosectioned granules collected from the bioreactors at selected treatment cycles along the experimental period, for identification of AOB and PAO amongst the *Bacteria* population. Figure III.5 shows FISH micrographs from a granule of the AGS used as inoculum, and from granules collected from SBR1 and SBR2 on operational day 86. A decrease in the AOB and PAO contents was observed in both reactors, relative to those in the inoculum. Moreover, FISH micrographs revealed wider channels and in higher numbers in SBR1 granules than in those of SBR2. In the latter, the observed FISH signal was more intense down to the core of the granules.

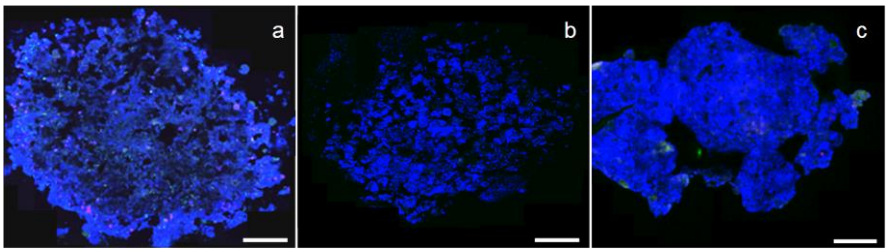


**Figure III.5** - FISH micrographs of cryosectioned granules. Granules taken from the inoculum (a), and after 86 days of operation from the dye-free control SBR1 (b) and the dye-fed SBR2 (c). Ammonia-oxidizing bacteria are in magenta, polyphosphate-accumulating organisms in cyan and other *Bacteria* in blue. Scale bar = 200 μm.

Quantitative FISH analysis was carried out to quantify the presence of PAO and GAO in the biomass throughout the study. The results, summarized in Table III.2, showed that the number of PAO (*Accumulibacter* and *Tetrasphaera*-related) was significantly reduced after the first 37 days of operation. On the other hand, the number of *Competibacter* GAO doubled in the same period, in both reactors. Subsequently, up to day 86, two other GAO clusters, belonging to the *Defluviicoccus vanus*-related group, significantly increased in numbers, in the two SBRs (supplementary Figure III.S1).

**Table III.2 -** Percentage of polyphosphate- and glycogen-accumulating organisms (PAO and GAO, respectively) in granules. Quantification of PAO and GAO in the initial inoculum (day 0) and in the dye-free control SBR1 and the dye-fed SBR2 at low (day 37) and high (day 86) organic load removal in the anaerobic phase. Quantification is given as percentage of total biovolume estimated with the EUBmix probe and the standard error of the mean (SEM) in presented parentheses. Other tested probes had abundances below 1% in all samples.

| | Bacteria (probe) | Inoculum | SBR1 | | SBR2 | |
|---|---|---|---|---|---|---|
| | | Day 0 | Day 37 | Day 86 | Day 37 | Day 86 |
| PAO | *Accumulibacter* (PAOmix) | 19.5% (3.6) | <1% | <1% | <1% | <1% |
| | *Tetrasphaera*-related PAO (TET892) | 34.1% (2.8) | 3.6% (0.7) | 4.9% (0.6) | 3.8% (0.8) | 7.1% (1.5) |
| GAO | *Competibacter* (GAOmix) | 14.4% (2.7) | 35.1% (2.2) | 26.0% (1.6) | 28.9% (1.9) | 22.1% (2.0) |
| | *Defluviicoccus* cluster I (TFOmix) | 2.8% (0.3) | <1% | 6.1% (1.5) | <1% | 7.8% (2.6) |
| | *Defluviicoccus* cluster II (DFmix) | 3.2% (0.7) | 1.5% (0.6) | 9.0% (1.8) | 2.0% (0.6) | 5.8% (1.2) |

### III.4.2.2. Microbial community analysis

In terms of phyla, *Actinobacteria*, *Bacteroidetes*, *Chlorobi*, *Chloroflexi*, *Firmicutes*, *Planctomycetes*, *Proteobacteria*, *Saccharibacteria* and *Verrucomicrobia* constituted more than 95% of the microbial community in all of the analyzed SBRs samples, including the inoculum (Figure III.S2, in Appendix A). Overall, the dominant phyla were *Bacteroidetes*, *Proteobacteria* and *Actinobacteria*.

After a 30-day adaptation period to the laboratory operational conditions, the main changes observed in the microbial community, relative to the inoculum, were a decrease in *Chloroflexi* and *Firmicutes*, and an increase in *Bacteroidetes* relative abundances (Figure III.S2, in Appendix A). Moreover, at the class level, while *Flavobacteria* and *Deltaproteobacteria* became relatively more abundant under the laboratory operational conditions, *Alphaproteobacteria* presence within the community was reduced along the first month of operation (Figure III.6). Further analysis of the microbial community dynamics regarding the 20 most abundant bacteria between all of the analyzed samples, indicated that the new operational conditions induced the development of a completely new microbial community. In fact, the 20 most abundant OTUs in the SBRs represent more than 50% of the microbial community in the bioreactors, but account for only 4% of the microbial community in the inoculum (Figure III.S3, in Appendix A).

The effect of the dye on the microbial community after 30 days of operation was apparent in the abundance of *Bacteroidetes* (mainly belonging to *Sphingobacteriia* class) and *Verrucomicrobia* (specifically, *Opitutae* class), which were present in 8% lower and 8% higher relative abundances, respectively, in the dye-free reactor, when comparing to SBR2 (Figure III.6 and Figure III.S2, in Appendix A). Except for *Opitutae*, the presence of dye not did limit the development of any other bacterial class. The distribution of *Proteobacteria* through *Alpha-*, *Delta-* and *Gammaproteobacteria* classes was more balanced in SBR2, the *Betaproteobacteria* class being in minority, irrespective of the presence of dye (Figure III.S2, in Appendix A). Furthermore, the presence of dye apparently promoted the development of groups of bacteria from the *Xanthomonadaceae* genus and from the *Saprospiraceae* family, while hindering the growth of bacteria from the *Opitutus* and *Amaricoccus* genera (Figure III.S3, in Appendix A). In fact, while SBR1 bacterial community was mainly dominated by groups belonging to *Desulfobulbus*, *Flavobacterium*, *Opitutus* and *Amaricoccus* genera, SBR2 exhibited a major presence of specific bacteria from the *Xanthomonadaceae* genus, *Saprospiraceae* family, *Desulfobulbus* genus, *Flavobacterium* genus and from the *Bacteroidetes* family on the experimental day 30 (Figure III.S3, in Appendix A).

Comparison between samples from days 30 and 51, suggested that the SRT control through a daily biomass purge did not cause major changes in SBR2 bacterial community, except for a slight increase in the *Saccharibacteria* phylum (Figure III.S2, in Appendix A) and a decrease in the *Gammaproteobacteria* relative abundance (Figure III.6). As for SBR1, the relative abundance of *Verrucomicrobia* and *Alphaproteobacteria* decreased to the same levels observed in SBR2, whereas *Bacteroidetes* (specifically, *Sphingobacterirra* class) increased to levels above those registered in SBR2 (Figure III.6). Moreover, *Deltaproteobacteria* became relatively more abundant in both SBRs (Figure III.6). More specifically, the main differences observed in period II (day 51) regarding the most abundant bacteria, were a decrease in the relative abundance of bacterial groups from the *Opitutus* genus and the *Sphingobacteriiaceae* family in SBR1, as well as a decrease in a bacterial group from the *Saprospiraceae* family in SBR2 (Figure III.S3, in Appendix A).

Conversely, the interruption of the sludge wastage on day 60 introduced some changes in the microbial community along period III. At the phylum level, *Chloroflexi* and *Planctomycetes* increased their presence in SBR1, in detriment of *Bacteroidetes* (Figure III.S2, in Appendix A). As for SBR2, the emergence of *Chlorobi* (specifically, *Chlorobia* class) in relevant amounts, as well as an increase in the *Planctomycetes* (*Planctomycetacia* class), *Firmicutes* (*Clostridia* class) and *Verrucomicrobia* (*Opitutae* class) relative abundances were compensated by a significant decrease in *Proteobacteria* relative abundance (Figure III.6 and Figure III.S2, in Appendix A). More specifically, among the 20 most abundant bacteria, members of the *Planctomyces*, *Sphingobacterium*, *Opitutus*, *Ferruginibacter* genera had their relative abundance increased in SBR2 on period III (days 72 and 86), relative to period II (day 51), in addition to specific bacteria from the *Subdoligranulum* genus (*Firmicutes*

phylum, *Clostridia* class) and from *Chlorobia* class (Figure III.S3, in Appendix A). Except for the last two, these bacteria were also present in SBR1.

Comparing the results from days 86 and 100, the organic load shock promoted a significant increase in *Planctomycetes* (specifically, *Planctomyces* genus) relative abundance, mainly in detriment of *Bacteroidetes* in both SBRs (Figure III.6 and Figure III.S2, in Appendix A). Moreover, the relative abundance of specific bacteria belonging to *Polaribacter*, *Tetrasphera* and *Kaistia* genera decreased, while *Opitutus* increased in SBR1 on day 100 (Figure III.S3, in Appendix A). A specific difference between SBR1 and SBR2 on day 100 was the presence of bacterial groups from the *Subdoligranulum* genus and the *Chlorobia* class in SBR2, as opposed to SBR1 (Figure III.S3, in Appendix A).

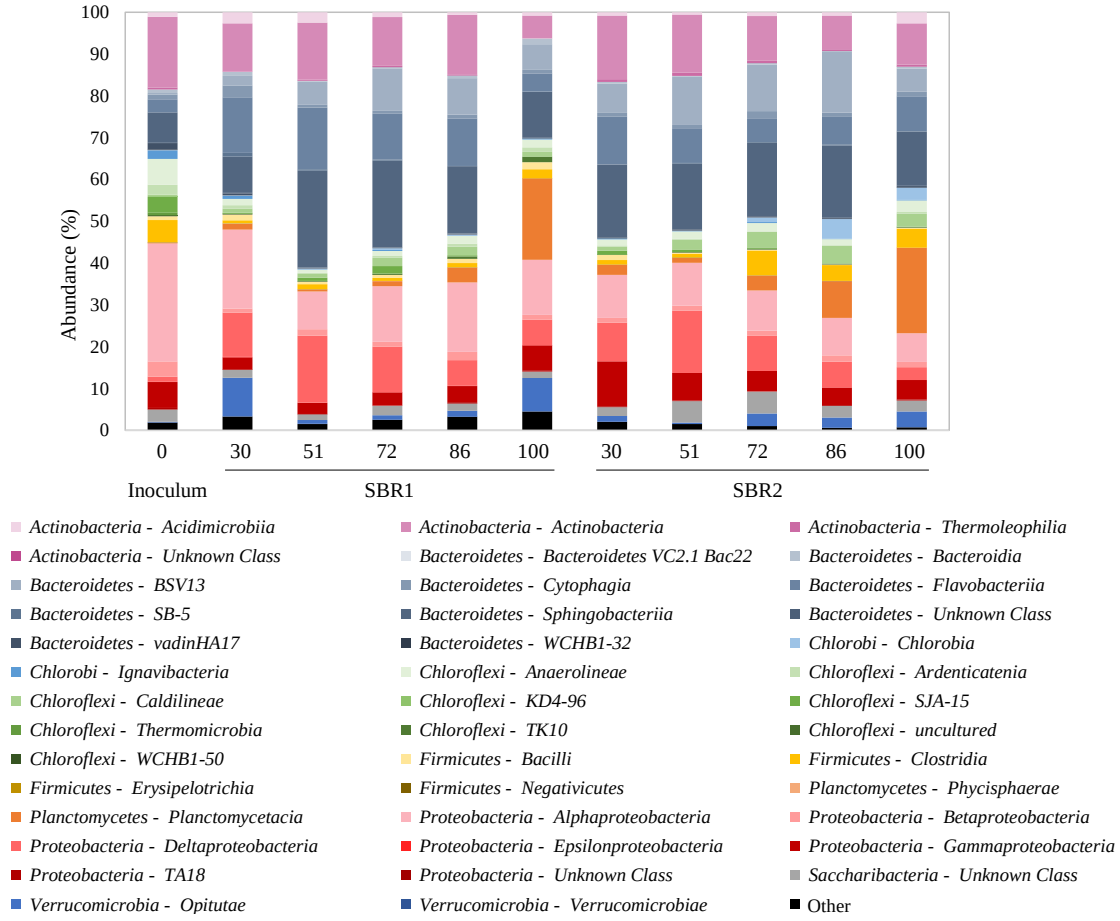


**Figure III.6 -** Composition of bacterial communities at the class level in the inoculum, as well as in the sequencing batch reactors SBR1 and SBR2 on the indicated operational days, obtained by 16S rRNA gene sequencing analysis. The most representative "Phylum - Class" are indicated below the chart.

Overall, in terms of bacterial community, the major phyla and classes were common between SBR1 and SBR2, their evolution along the experimental run varying in a generally similar way. In contrast, these bioreactors were characterized by completely different fungal communities. At the phylum level, while SBR2 was dominated by *Basidiomycota* (mostly, *Tremellomycetes* class), the fungal community in SBR1 was mainly of unknown phyla (Figure III.7 and Figure III.S4, in Appendix A). Moreover, the relative abundance of *Ascomycota* (namely, *Saccharomycetes* class) was similar between both SBRs

(less than 10%) and quite stable along the experimental run (Figure III.7). Despite the lack of information regarding the taxonomic classification of the most abundant OTUs detected in the analysis, the fungal community profile was clearly different between the two SBRs (Figure III.S5, in Appendix A). In fact, SBR2 was mainly dominated by two groups belonging to the *Trichosporon* genus, which, on the other hand, constituted less than 13% of SBR1 fungal community (Figure III.S5, in Appendix A). Although with different outcomes, both SBRs presented major changes in their fungal communities on days 86 and 100 of operation, characterized by the emergence of new, unclassified groups of fungi in relevant amounts (Figure III.S5, in Appendix A).

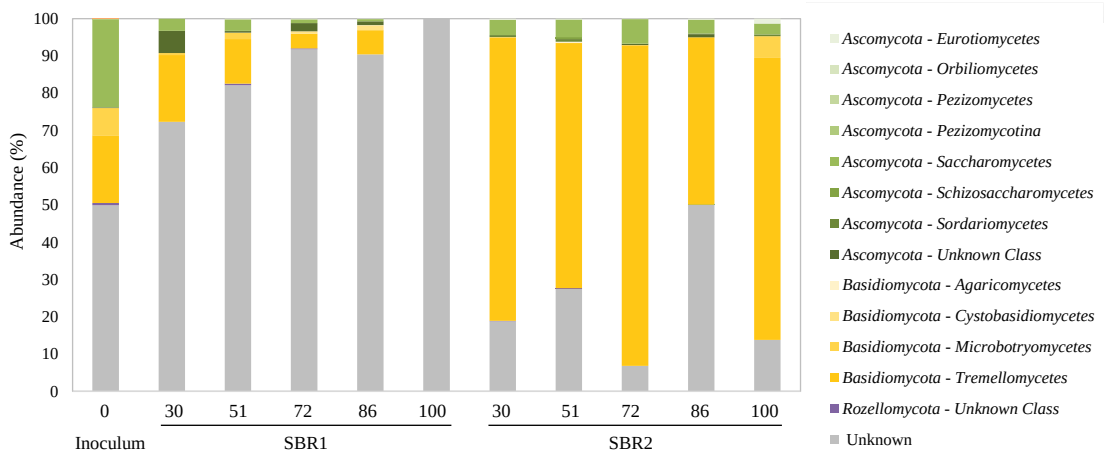


**Figure III.7** - Composition of fungal communities at the class level in the inoculum, as well as in the sequencing batch reactors SBR1 and SBR2 on the indicated operational days, obtained by rRNA gene and internal transcribed spacer (ITS) sequencing analysis. The most representative "Phylum - Class" are indicated on the right.

## III.4.3. AGS SBR treatment performance

### III.4.3.1. Biomass inventory

The biomass inventory in the SBRs was assessed by measuring TSS values in the mixed liquor and in the discharged effluent along the operational run (Figure III.8). The VSS-to-TSS ratio varied within the 81-94% range. As shown in Figure III.8, the biomass progressively accumulated in both reactors along the first 41 days of operation (period I; Table III.1), reaching a concentration of 13 gTSS $L^{-1}$, with low biomass levels in the discharged effluent, under 0.1 gTSS $L^{-1}$. At this point the settled sludge level was close to that of the effluent withdrawal pipe, with the consequent risk of excessive biomass discharge in the treated wastewater. Therefore, biomass purging was carried out from day 42 to day 60 (period II; Table III.1), so as to control the SRT value at 15 days. This resulted in the reduction of the mixed liquor biomass levels to around 10 and 8 gTSS $L^{-1}$ in SBR1 and SBR2, respectively, during period II. Conversely, once the biomass purging was interrupted after day 60 (period III; Table III.1), the biomass accumulated again in the reactors, recovering levels of 12-13 gTSS $L^{-1}$ on day 85, together with minimal biomass levels in the effluent, 0.04 gTSS $L^{-1}$. During period III, SRT values concomitantly increased, reaching a maximum of 40 days.

The three-fold increase in the fed COD load introduced on day 98 (period V; Table III.1) caused a rapid increase in biomass concentration in SBR2, up to 17 gTSS $L^{-1}$, without compromising the quality of the discharged effluent. On the other hand, high biomass washout levels were registered in SBR1 from day 92 on (up to 1 gTSS $L^{-1}$ in the settled effluent), with a consequent reduction in the mixed liquor TSS values to approximately 10 gTSS $L^{-1}$.

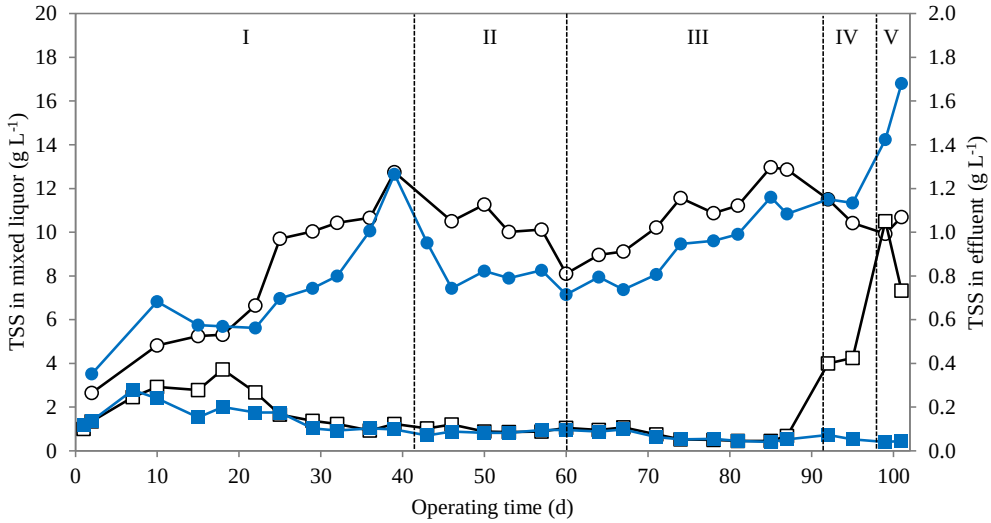


**Figure III.8** - Biomass concentration profile along the experimental periods. Total suspended solids (TSS) present in the mixed liquor of the dye-free control SBR1 (○) and in the dye-fed SBR2 (●), as well as in the effluent discharged from SBR1 (□) and from SBR2 (■). Period I (days 0 to 41) − no control of sludge retention time (SRT; biomass wastage was limited to sampling needs); period II (days 42 to 60) − SRT control at 15 days through daily biomass purging; period III (days 60 to 90) − no control of SRT; period IV (days 91 to 97) − three-fold increase in the dye concentration in SBR2; period V (days 98 to 102) − three-fold increase in the organic load.

### III.4.3.2. Anaerobic and overall chemical oxygen demand (COD) removal

The carbon load removal performance of the AGS SBR systems was evaluated through measurements of COD removal levels during several treatment cycles along the experimental period. The overall COD removal yield values, as well as the fraction of this overall yield that was removed anaerobically, are represented in Figure III.9. The initial, low COD removal levels were probably due to the change in the nature of the main carbon substrate, from domestic wastewater to the synthetic textile effluent with hydrolyzed hydroxypropyl starch as the carbon source. However, AGS efficiently adapted to the new carbon source, reaching stable COD removal yields within the 80-90% range after 14 days of operation, irrespective of the presence of dye. On average, 55% of the overall COD removal occurred during the 1.5-h anaerobic phase. However, from day 70 to day 88, the anaerobic COD removal gradually increased in both reactors reaching 77% of the overall COD removal. High COD removal yields were also sustained in both reactors at the final stage of the experiment, when the capacity of the AGS SBR systems to deal with disturbances was tested by imposing a three-fold increase in the initial dye concentration and in the carbon load to SBR2 and to both reactors, respectively.

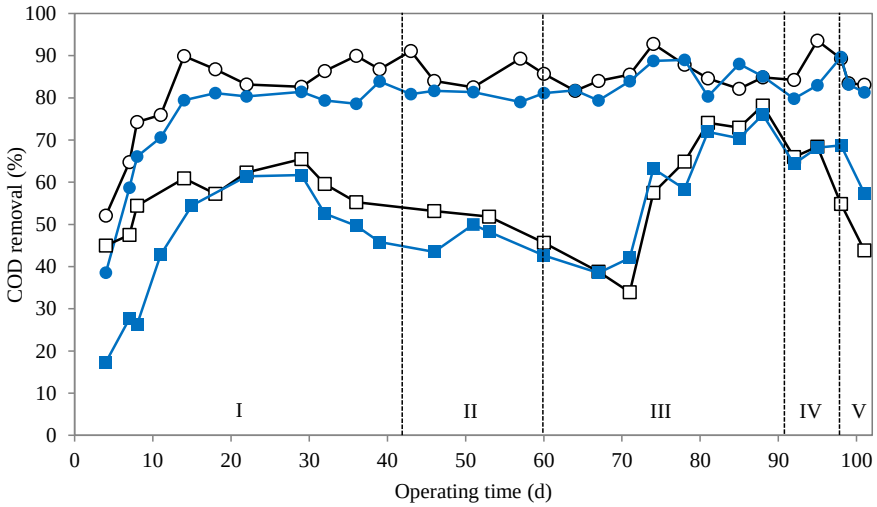


**Figure III.9** - Chemical oxygen demand (COD) removal performance along the experimental periods. Total COD removal yield in the dye-free control SBR1 (○) and the dye-fed SBR2 (●), and percentage of COD removed during the anaerobic phase in SBR1 (□) and SBR2 (■). Period I (days 0 to 41) − no control of sludge retention time (SRT; biomass wastage was limited to sampling needs); period II (days 42 to 60) − SRT control at 15 days through daily biomass purging; period III (days 60 to 90) − no control of SRT; period IV (days 91 to 97) − three-fold increase in the dye concentration in SBR2; period V (days 98 to 102) − three-fold increase in the organic load.

### III.4.3.3. Azo dye biodegradation

Azo dye removal yield and SRT profiles throughout SBR2 operational run are represented in Figure III.10. It should be noted that SRT values calculated for the initial days of SBR operation do not represent the microbial population diversity of the seed AGS, which resulted from high SRT at the WWTP. The biomass rapidly adapted to the synthetic textile effluent since AR14 removal levels higher than 85% were attained after 7 days of operation (Figure III.10, period I). Within the first 3 days following the start of the daily biomass purging for SRT control, the AR14 removal yield decreased from 92% to stable values around 65% (Figure III.10, period II). Conversely, after interruption of the SRT control on day 60, which allowed the biomass to accumulate and SRT values to increase up to 38 days until day 74, the AR14 removal performance gradually improved, restoring yields above 92% (Figure III.10, period III). From then on, despite the SRT decrease to stable values within the 25-30 days range due to higher sampling needs, the high decolorization performance was maintained, namely during the dye and COD shock loads (periods IV and V, respectively).

HPLC analysis confirmed that the azo dye was anaerobically reduced, generating two sulfonated aromatic amines (Figure III.11): 4A1NS and 1-naphthol-2-amino-4-sulfonic acid (1N2A4S). Through comparison with the RT of HPLC peaks of standards, the HPLC peaks corresponding to AR14 (RT: 26 min) and to 4A1NS (RT: 14 min) were identified and their areas converted to concentration units. Due to unavailability of the correspondent standard, it was not possible to quantify 1N2A4S. Also, the latter is expected to undergo autoxidation reactions in the presence of oxygen due to the hydroxyl group in *ortho*-position to the amino group (Kudlich *et al.*, 1999). On the other hand, it has been reported that 1N2A4S may act as redox mediator in the AR14 reducing reaction (Liu *et al.*, 2009).

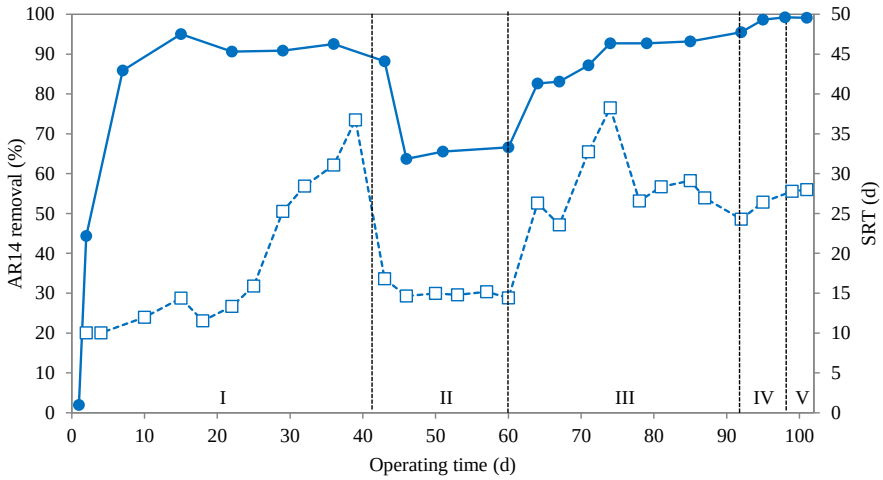


**Figure III.10** - Azo dye (AR14) removal yield (●) and sludge retention time (SRT; □) profiles in the dye-fed bioreactor (SBR2) along the experimental periods. Period I (days 0 to 41) − no control of SRT (biomass wastage was limited to sampling needs); period II (days 42 to 60) − SRT control at 15 days through daily biomass purging; period III (days 60 to 90) − no control of SRT; period IV (days 91 to 97) − three-fold increase in the dye concentration in SBR2; period V (days 98 to 102) − three-fold increase in the organic load.

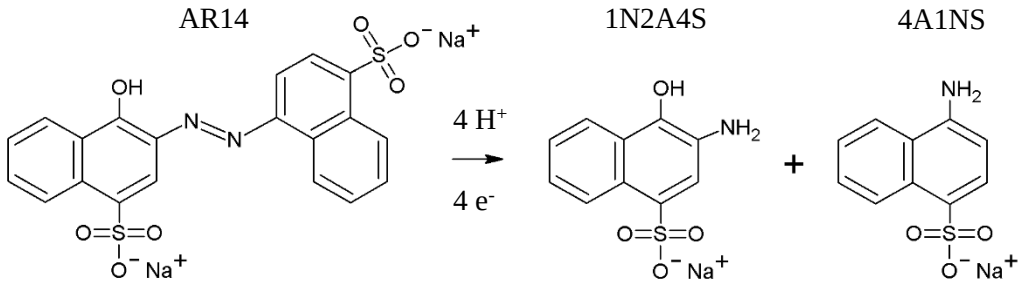


**Figure III.11** - Chemical structures of the azo dye Acid Red 14 (AR14) and of the two aromatic amines formed during the azo bond reduction reaction, 1-naphthol-2-amino-4-sulfonic acid (1N2A4S) and 4-amino-naphthalene-1-sulfonic acid (4A1NS).

Specific SBR2 cycles representative of operational periods I, II, III and IV (Table III.1) were selected to analyze the azo dye and breakdown metabolite profiles during the 5-h reaction phase (Figure III.12). The concentration of 4A1NS increased along the anaerobic phase of each operational period, while the concentration of AR14 decreased, as expected. During period II, and in agreement with the AR14 removal yield profile (Figure III.10), a lower amount of 4A1NS was formed during the anaerobic phase, as less AR14 reduction took place (Figure III.12, II).

Regarding the subsequent aerobic phase, relevant differences were observed in the 4A1NS concentration profile between the four operational periods. Specifically, while in period I and II the 4A1NS peak was absent immediately after 30 min of aeration, but subsequently re-appeared (Figure III.12, I and II), gradual disappearance of the 4A1NS peak along the 3.5-h aerated stage was consistently observed from day 71 on (Figure III.12, III), including when the fed dye concentration was three-fold higher (Figure III.12, IV). The 4A1NS concentration profiles I and II suggested a reversible chemical oxidation of the aromatic amine at the onset of aeration. In fact, the analysis of the time profile of several unknown metabolites, with peak areas significantly lower than that from

4A1NS, revealed that in some cycles one unknown metabolite (RT: 24 min) apparently established an equilibrium with 4A1NS (Figure III.12, I and II), suggested by the symmetrical time profiles of the two metabolites. In contrast, this symmetrical trend was not observed in periods III and IV. Conversely, what appeared to be the same unknown metabolite (RT around 24 min) followed a time profile similar to that of 4A1NS. HPLC chromatograms of samples harvested from SBR2 along a cycle's reaction phase on day 71 (Figure III.S6, in Appendix A) show the absence of 4A1NS peak at the end of the operation.

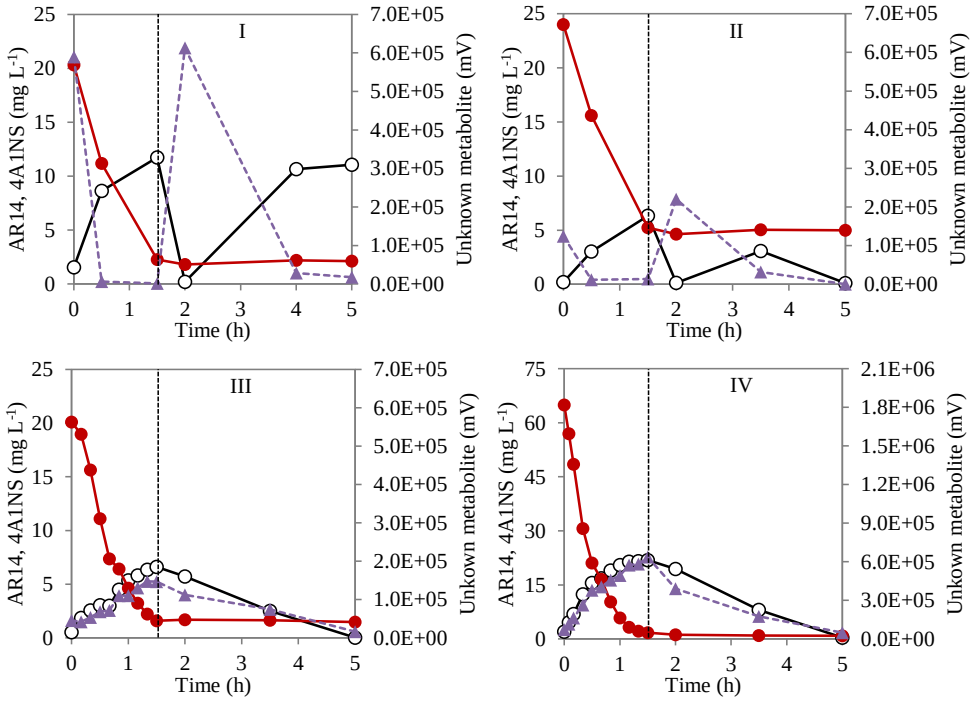


**Figure III.12** - Concentration-time profiles of the azo dye AR14 (●) and of its cleavage product 4-amino-naphthalene-1-sulfonic acid, 4AN1S (○), and area-time profiles of HPLC peaks corresponding to an unknown metabolite (▲) along the reaction phase in the dye-fed bioreactor, SBR2, representative of each operational period (I, II, III and IV corresponding to operational days 29, 59, 79 and 95, respectively). Vertical lines at 1.5 h represent the end of the anaerobic phase, upon the aeration onset. The experimental conditions of each period are described in Table III.1.

According to the HPLC analysis (detector at 220 nm), relevant differences were encountered along the experimental run regarding the UV-visible spectrum of samples harvested along the aerobic phase. Specifically, when comparing the UV-visible spectra corresponding to the start and end of the aerobic phase, no relevant differences were observed until day 18 of operation (Figure III.S7-a). Subsequently, from day 22 to 32, the absorbance peaks at 240 nm and 320 nm were slightly reduced along the aerobic phase, whereas the absorbance increased at around 200 nm (Figure III.S7-b). These differences became more intense from day 39 to 67 (Figure III.S7-c). After day 74, in addition to the relevant absorbance decrease at 240 nm and 320 nm, also the peak at 220 nm significantly reduced its intensity (Figure III.S7-d). This profile was maintained until the end of the operation, namely during the azo dye shock load period.

### III.4.3.4. Oxidation-reduction potential profile

ORP monitoring and DO concentration measurements were carried out on several cycles throughout the experiment. Similarly for both reactors, DO levels were below 0.2 mg $L^{-1}$ during the anaerobic phase, rising above 7 mg $L^{-1}$ during the aerated phase. In contrast, specific differences were consistently observed in ORP profiles from the two SBRs (Figure III.13a). While the ORP continuously decreased at a low rate along the anaerobic phase in SBR1, SBR2 presented a sharp initial ORP drop to approximately -50 mV, subsequently stabilizing around this value until the end of this phase. The difference in the ORP reducing rates was not caused by the presence of the azo dye *per se*, because the ORP sharp drop in SBR2 was not observed in the first operated cycles. In fact, this profile was only observed in SBR2 after the operational day 8, the ORP decay rate in the anaerobic phase gradually increasing along the first week of operation. Overall, from day 8 on, few variations were observed in the ORP profile during the anaerobic phase. The only relevant difference occurred during period II, as the ORP anaerobic plateau gradually increased from values around -90 mV (day 36) up to -30 mV (day 60).

Regarding the aerobic phase, the ORP immediately rose to positive values in both SBRs upon the onset of aeration (Figure III.13a). Contrarily to SBR1, where the ORP rapidly attained a maximal ORP steady stage around +300 mV, SBR2 presented a gradual, staged ORP increase, at successive lower rates as the ORP reached +100 mV, +140 mV, +220 mV and +250 mV after 2 min, 10 min, 1.5 h and 3 h of aeration (Figure III.13a). Moreover, throughout the experimental run, SBR2 presented three clearly different ORP profiles along the aerobic phase (Figure III.13b): until day 29 the ORP increasing rate gradually decreased (Profile 1); from day 29 until day 44, an ORP peak was formed after 1 h of aeration (Profile 2), gradually becoming less pronounced from day 44 to 60 (period II); from day 63 on, a 30-min ORP steady stage at around 150 mV was formed, after which the ORP increased again until gradually stabilizing (Profile 3); finally, an ORP peak similar to the one observed in Profile 2 suddenly re-appeared on day 91 when the dye concentration was three-times increased.

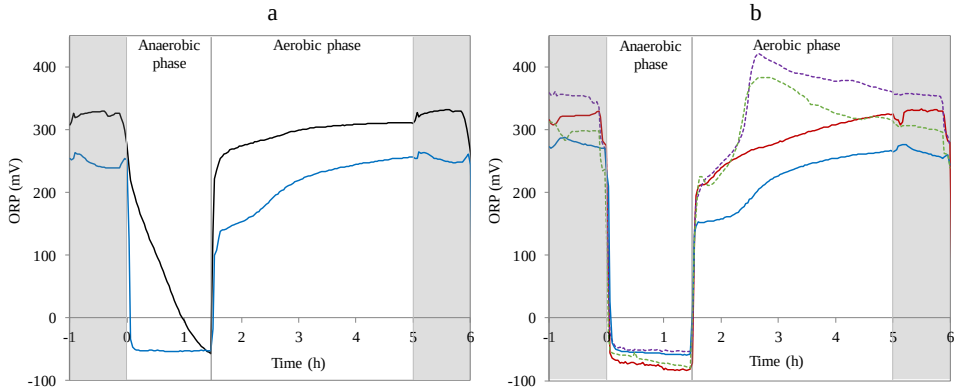


**Figure III.13** - Representative oxidation-reduction potential (ORP) profiles along the 5-h reaction phase (white area). a) ORP profiles from the dye-fed sequencing batch reactor SBR2 (blue line) and the control, dye-free bioreactor SBR1 (black line) registered on days 73 and 74, respectively. b) SBR2 ORP profiles from day 29 (red full line, Profile 1), day 44 (purple dashed line, Profile 2), day 79 (blue full line, Profile 3), day 94 (green dashed line).

## III.5. Discussion

### III.5.1. Effect of the azo dye on AGS long-term stability

After being introduced in the two SBRs, the large, mature granules in the inoculum were fragmented due to high shear stress caused by the mechanical mixing during the SBR cycle's anaerobic phase. Nevertheless, AGS was able to adapt to the new hydrodynamic conditions developing smaller granules with excellent settling properties, as evidenced by the low SVI values registered after around 60-70 days of operation, irrespective of the presence of dye (Figure III.2). Up to this point of the experimental run, the two SBRs presented very similar characteristics, both in terms of AGS physical properties and treatment performance. Nevertheless, just 2 weeks after the marked growth in granule size which followed the interruption of SRT control, very significant differences were registered between the two SBRs in terms of granule stability. While the biomass in the SBR supplemented with dye (SBR2) maintained its granular structure and low SVI values up to the end of the operational period, the dye-free reactor (SBR1) became unstable, entering a degranulation process that resulted in almost complete loss of the granular morphology (Figure III.3) and extensive formation of flocs (Figure III.1). As a result, $SVI_5$ and $SVI_{30}$ values rose in SBR1 from day 80 on, diverging from those of SBR2 and leading to high biomass washout levels from day 87 on (Figure III.8). In fact, one of the main technical problems encountered when operating AGS reactors is the loss of granule stability over long-term operation (Giesen *et al.*, 2013). Despite being associated with many cases of AGS instability, filamentous overgrowth was not observed in SBR1.

Since the only relevant operational difference between the two reactors was the absence or presence of dye, these results suggest that the latter prevented granule break-up, thus enhancing AGS long-term stability. This might be associated with the azo dye acting as an electron acceptor, which results in its decolorization (dos Santos *et al.*, 2007). Wan *et al.* (2008) reported that denitrification of nitrate in the inner part of the granule allows anoxic heterotrophic growth in this core zone, thus inducing the densification of these biological aggregates. Similarly to denitrifying bacteria, it is possible that azo dye-reducing bacteria would be preferably located at the center of the granules contributing to keep granule integrity. Lourenço *et al.* (2000) showed that nitrate can compete with azo dyes for the reducing equivalents formed during the non-aerated reaction phase of an SBR cycle fed with a simulated textile effluent. Conversely, in the present experiment the azo dye could readily be used in SBR2 as electron acceptor under non-aerated conditions since the formation of nitrate in the aerated phase was probably avoided. The latter effect results from the low level of ammonia supplied in the feed, which induced a low AOB content in the granules, as confirmed by FISH (Figure III.5). In fact, FISH analysis of cryosectioned granules revealed more abundant and wider channels in the granules of the dye-free SBR1 than in those of the dye-supplemented SBR2, after 86 days of operation (Figure III.5). In SBR2, granules had a denser structure and provided a more intense FISH signal down to their

core, suggesting higher activity in the inner part of these granules than in those of SBR1. This difference could be related to the higher level of granule disaggregation in SBR1 and to the overall smaller granule size at this later stage of the experiment.

Li and Liu (2005) estimated that when granule size is higher than 0.5 mm, oxygen diffusion into the granule inner layers may become a limiting factor for microbial growth. Accordingly, early granule overgrowth in both reactors might have resulted in anaerobic conditions at their core. Under these conditions, the supply of azo dye in SBR2 hypothetically enabled heterotrophic growth in these deeper layers of the granules. In contrast, under oxygen diffusional limitation bacteria in the inner layers of SBR1 granules could not readily consume the carbon source due to unavailability of a favorable electron acceptor. Consequently, bacteria at the core of these granules suffered decay, giving rise to a granular structure with lower density which was more susceptible to shear forces, ultimately leading to granule break-up. In fact, Beun *et al*. (2002) reported that when nitrate was not available at the core of the granules (beyond the depth of oxygen penetration) to be used as electron acceptor in the oxidation of acetate, lysis of cells occurred in that region, resulting in granule break-up.

The significantly distinct ORP profiles registered in SBR1 and SBR2 during the anaerobic phase (Figure III.13a) indicate that the presence of the azo dye induced specific differences in the bacterial metabolism. Jacob (1970) showed that after inoculation of a nutrient solution the rate and extent to which the ORP became more negative was dependent on the growth rate and on the physiological type of bacteria. Specifically, in cultures of aerobic bacteria the ORP decreasing rate was lower than in cultures of facultative anaerobes, where the lowest ORP value was rapidly reached. In this sense, the presence of the azo dye in SBR2 seems to have induced the development of a microbial population capable of rapidly using the azo dye as electron acceptor under anaerobic conditions, resulting in a higher activity of facultative anaerobes than in SBR1.

The microbial community analysis revealed that the new operational conditions induced the development of a completely new microbial community in the SBRs, the 20 most abundant OTUs in the SBRs (more than 50% of the microbial community), only accounting for 4% of the microbial community in the inoculum (Figure III.S3, in Appendix A). Meerbergen *et al*. (2017) observed a shift from diverse towards specialized microbial communities upon exposure to recalcitrant azo dyes. In fact, the presence of the azo dye AR14 profusely affected the fungal community (Figure III.7), promoting the dominance of fungi from the *Trichosporon* genus (*Tremellomycetes* class; Figure III.S5, in Appendix A). This genus has been associated with azo dye reducing yeasts (Meerbergen *et al*., 2017). In addition, fungi from the *Tremellomycetes* class were previously identified within the fungal community of AGS (Weber *et al*., 2009). In accordance to the present study, Weber *et al*. (2009) concluded that the fungal community composition in AG depended on the wastewater type and the phase of granule development. Regarding the bacterial community, the AGS in both SBRs was mainly

constituted by *Bacteroidetes*, *Proteobacteria* and *Actinobacteria*, the presence of *Chloroflexi* and *Firmicutes*, significantly decreasing along the first month of operation (Figure III.S2, in Appendix A). *Bacteroidetes*, *Proteobacteria*, *Firmicutes* and *Chloroflexi* have been commonly reported as the most abundant phyla in azo dye treatment systems (Cao *et al*., 2019; Forss *et al*., 2013; Rasool *et al*., 2016; Wang *et al*., 2018b; Zhu *et al*., 2018). *Bacteroidetes* are considered to specialize in degrading complex organic matter, namely polysaccharides and proteins, while *Proteobacteria*, *Firmicutes* and *Actinobacteria* phyla have been associated with biodegradation of aromatic hydrocarbons (Wang *et al*., 2018b). Specifically in the context of AGS, the most represented phylum is *Proteobacteria* (Winckler *et al.*, 2018), suggested to play a major role in formation AG through the production of EPS (Liu *et al.*, 2017b). Furthermore, the phyla *Actinobacteria*, *Bacteroidetes* and *Firmicutes* contain multiple genera that have been isolated from AG (Winckler *et al*., 2018).

Comparing to the inoculum, *Flavobacteria* and *Deltaproteobacteria* classes became relatively more abundant under the laboratory, anaerobic-aerobic conditions, as opposed to *Alphaproteobacteria* (Figure III.6). Overall, *Alpha-*, *Delta-* and *Gammaproteobacteria* classes were more balanced in SBR2 than in SBR1, the *Betaproteobacteria* class being a minority, irrespective of the presence of dye (Figure III.6). These classes were also observed in sequential bioreactors treating TWW (Yurtsever *et al*., 2017), *Alpha-*, *Beta-* and *Gammaproteobacteria* being present in an aerobic reactor, while *Deltaproteobacteria* predominating under anaerobic conditions. In addition, Kolekar *et al.* (2012) revealed that the diverse microbial community found in an azo dye-degrading AGS SBR belonged to *Alpha-*, *Beta-*, and *Gammaproteobacteria*, suggesting the involvement of these groups in azo dye biodegradation.

In addition to *Proteobacteria*, *Verrucomicrobiae* has also been reported to adapt to the granulation process, increasing their relative abundance (Wu *et al*., 2018a). This was only observed in the dye-free SBR (Figure III.S2, in Appendix A), thus suggesting a susceptibility of this group of bacteria towards the azo dye. In fact, after 1 month of operation, the dye-fed SBR had an 8% lower relative abundance of *Verrucomicrobia* (specifically, *Opitutae* class), and 8% higher relative abundance of *Bacteroidetes* (mainly belonging to *Sphingobacteriia* class) than SBR1 (Figure III.6 and Figure III.S2, in Appendix A). More specifically, the azo dye promoted the growth of bacteria from the *Xanthomonadaceae* genus and from the *Saprospiraceae* family, while hindering the growth of bacteria from the *Opitutus* and *Amaricoccus* genera (Figure III.S3, in Appendix A). Accordingly, *Xanthomonadaceae* bacteria were consistently present in the biological processes of a full-scale printing and dyeing wastewater treatment system, as reported by Yang *et al*. (2012). *Opitutus* is a group of obligate anaerobic bacteria, with denitrification capacity (Chin *et al*., 2001); *Amaricoccus* has been selected under feast-famine conditions and shown to store PHA (Oliveira *et al*., 2017), its growth being favored under long SRT operation (Wang *et al*., 2017). Moreover, *Desulfobulbus* and *Flavobacterium* were relevant groups in

both SBRs, irrespective of the presence of the dye (Figure III.S3, in Appendix A), the latter being commonly found in activated sludge from WWTPs (Wang *et al*., 2017).

During the last days of the experimental run, the relative abundance of bacteria belonging to *Polaribacter*, *Tetrasphera* and *Kaistia* genera decreased in SBR1, while the bacterial group belonging to *Opitutus* increased (Figure III.S3, in Appendix A). These specific changes in the microbial community may be related with the concomitantly granular instability registered in SBR1. In fact, at least the presence of PAO, namely *Tetrasphera*, have been reported as a key element for maintaining long-term stability of AG (de Kreuk and van Loosdrecht, 2004). In addition, on day 100, bacterial groups from the *Subdoligranulum* genus and the *Chlorobia* class were observed in SBR2 but not in SBR1 (Figure III.S3, in Appendix A), thus also being potentially associated with AG stability.

## III.5.2. AGS SBR treatment performance

### III.5.2.1. COD removal

Despite the slightly higher mixed liquor TSS values measured in SBR1 along the experimental run, the biomass accumulation rate was comparable in the two reactors up to day 90. This, together with the very low biomass washout levels in SBR2 (Figure III.8), indicates that the presence of the azo dye negatively affected neither the biomass settling properties nor the biomass growth in the reactor. Moreover, since no significant differences were noted between the COD removal performance in the two reactors, even when a three-fold increase in the fed dye concentration was applied to SBR2 (Figure III.9), it is presumed that neither the dye nor its potentially toxic breakdown metabolites negatively affected the carbon substrate uptake. This highlights the remarkable capacity of AGS to withstand shock loadings and the presence of potential toxicants in wastewaters (Giesen *et al*., 2013).

The maximal COD fraction removed in the anaerobic phase, 77%, was here significantly higher than the values observed in comparable SBR systems operated with flocculent activated sludge in 24-h cycles, fed with the same carbon source. Specifically, in cycles providing a total COD removal around 80%, Lourenço *et al*. (2000) indicated 30% removal in 9 h of anaerobic reaction and Albuquerque *et al*. (2005) reported 49-71% removal in 10.5-h anaerobic reaction phases. In the present study, the outstanding capacity of the AGS to remove COD under anaerobic conditions in much shorter cycles was demonstrated, a feature which is of much importance for performance optimization in wastewater treatment.

The significant increase in the anaerobic COD removal yield registered from day 70 to day 88 (Figure III.9) was probably a result of the increased biomass concentration, since specific COD removal values were maintained within a stable range. Nevertheless, this behavior was not observed in the early stages of the operational period, up to when the same TSS levels were attained around day 40. This points to differences at the metabolic or microbial population levels. In addition, the highest

anaerobic COD removal levels were registered during the period of faster growth of the mean size of AG in both SBRs (Figure III.3). Granule overgrowth was thus a probable consequence of the higher COD uptake rate under anaerobic conditions. Quantitative FISH analysis was carried out to assess the presence and relative abundance of PAO and GAO in the granular biomass at different stages throughout the study period (Table III.2). It was found that, despite the very high P/COD resulting from the use of phosphates as pH buffers in the synthetic TWW, the number of PAO was significantly reduced shortly after inoculation, probably due to competition from GAO at the operating pH, 6.6, on average (Oehmen *et al*., 2007). Indeed, the abundance of *Competibacter* GAO doubled after 37 days of operation in both reactors, despite the fact that these organisms are unable to take up saccharides (the main carbon products in the synthetic feed, resulting from Emsize hydrolysis). The fact that these GAO thrived in the present system suggests that saccharide fermentation was taking place by the action of other members of the consortium, which resulted in VFA that could then be consumed by the identified GAO. While the number of *Competibacter* did not further increase after the initial response to the new operating conditions, two other types of GAO, belonging to the *Defluviicoccus vanus*-related group, increased significantly in abundance from day 37 to day 86 of operation. This could explain the increase in anaerobic COD removal observed in the latter period, since *Defluviicoccus vanus*-related GAO are known to take up glucose anaerobically (Oehmen *et al*., 2007).

In addition, both SBRs presented major changes in their fungal communities on days 86 and 100 of operation, characterized by the emergence of new, unclassified groups of fungi in relevant amounts (Figure III.S5, in Appendix A). Finally, the organic shock load applied on day 98, together with a proportional increase in ammonium chloride concentration, induced a significant increase in *Planctomycetes* (specifically, *Planctomyces* genus) relative abundance, mainly in detriment of *Bacteroidetes* in both SBRs (Figure III.6 and Figure III.S2, in Appendix A). *Planctomycetes*, known to include anammox bacteria, have been described as important players in the removal of pollutants, namely in organic and nitrogen removal (Liu *et al.*, 2017c).

### III.5.2.2. Azo dye biodegradation

Decrease in the biodecolorization levels during period II could have been the result of the lower biomass concentration (8 gTSS $l^{-1}$; Figure III.8), a consequence of the daily biomass purging for SRT control. However, AR14 removal yields of 95% were obtained on day 15 with lower biomass concentration levels (6 gTSS $l^{-1}$; Figure III.8), indicating that the decrease of the SRT values affected the bacterial population with decolorization capacity, with a rapid negative impact in its performance. Similarly, in a study using flocculent activated sludge (Lourenço *et al.*, 2000), reduction of the SRT from 15 to 10 days lowered the color removal levels from 90% to 30-50%, the situation being reverted when the SRT was increased back to 15 days. In addition, Lourenço *et al*. (2001) proposed that color removal efficiency might be related to the capacity to lower the medium ORP in the anaerobic phase

through generation of reducing equivalents. In fact, according to Jacob (1970), the ORP steady stage registered throughout the anaerobic stage (as shown in Figure III.13a) is a buffering effect caused by redox dyes during their reduction process in culture solutions. Furthermore, Bromley-Challenor *et al.* (2000) showed that the highest rate of decolorization was attained when the ORP was at its most negative. Specifically, the establishment of low ORP values (*i.e.*, under -150 mV) under anaerobic conditions was required for efficient color removal of Remazol Brilliant Violet 5R dye (Lourenço *et al*., 2000). Although results from this study showed that AR14 reduction occurred at relatively high ORP values, *i.e*., around -50 mV (Figure III.13), it was also verified that lower ORP values contributed for higher decolorization. In fact, a slight increase in the ORP from around -90 mV to -30 mV was registered during the period when the color removal yield decreased from 80% to 60% (period II).

The microbial community analysis revealed that the biomass wastage during period II caused a decrease in the *Gammaproteobacteria* relative abundance in both SBRs (Figure III.6), as well in a specific bacterial group from the *Saprospiraceae* family (*Bacteroidetes* phylum) in SBR2 (Figure III.S3, in Appendix A), suggesting their involvement in the decolorization process. In fact, members of the *Bacteroidetes* and *Gammaproteobacteria* phyla have been shown to possess the capacity to reduce azo dyes (Forss *et al*., 2013; Kolekar *et al*., 2012). Accordingly, a study on the impact of the SRT on the TWW treatment performance in sequential anaerobic and aerobic membrane bioreactors (Yurtsever *et al*., 2017) showed that *Gammaproteobacteria* relative abundance slightly decreased when the SRT was decreased to 30 days. However, despite the SRT-dependent changes in the microbial community registered in both membrane bioreactors, shortening the SRT to 30 days did not have a significant impact on the dye removal efficiency in the anaerobic bioreactor (Yurtsever *et al*., 2017).

Regardless of the conversions apparently occurring between 4A1NS and an unknown metabolite during experimental periods I and II (Figure III.12, I and II), no effective biodegradation of 4A1NS took place during the aerobic phase. The highly recalcitrant character of this sulfonated aromatic amine was also observed in previous studies using flocculent activated sludge (Kudlich *et al*., 1999). Owing to the hydrophilic nature of the sulfonate group, difficulty in mineralizing sulfonated azo dye reduction products has been reported by many authors (Lourenço *et al*. 2009, 2000; Tan *et al*, 2005; van der Zee and Villaverde, 2005), being generally attributed to the lack of an adequate aerobic microbial population capable of metabolizing such compounds.

From day 71 on, upon high biomass accumulation and SRT increase to values above 25 days, a gradual decrease in the 4A1NS concentration to values close to zero was observed along the aerobic phase of SBR2 cycles, at a relatively constant rate (Figure III.12, III and IV), suggesting the complete bioconversion of 4A1NS, accompanied by a similar time profile of a detected unknown metabolite

(RT around 24 min). The reduction of the three UV absorption peaks (at 220, 240 and 320 nm) along the aerobic phase, solely registered after day 74 (Figure III.S7, in Appendix A), further supported the potential 4A1NS complete bioconversion during this period. In addition to the HPLC and UV-visible results, the variation in the SBR2 aerobic ORP profile along the experimental run most likely reflects a change in the azo dye metabolites fate. Specifically on day 79, a large ORP plateau at around 150 mV was observed upon the onset of aeration (Figure III.13b, Profile 3), suggesting that the reduced substances formed during the anaerobic phase in SBR2 were being oxidized, their depletion subsequently leading to a rise in ORP. In addition, yeast-based toxicity assays comparing SBR2 cycle samples from day 25 and 71 (SRT of 16 and 33, respectively) revealed that detoxification of aromatic amine containing-wastewater during the aerobic phase was only observed on day 71 (Lourenço *et al*., 2015).

Accordingly, studies assessing the effect of the SRT in the microbial degradation of synthetic organic pollutants in water (Clara *et al.*, 2005) revealed higher biodegradation performance when increasing the SRT, which was attributed to greater species diversity. In addition, a recent study reported more than 96% removal of 4A1NS in 24-h cycles using an anaerobic-aerobic fixed-bed sequencing batch biofilm reactor (Koupaie *et al.*, 2013). In this sense, systems with higher biomass retention capacity, such as AGS, could potentially improve the treatment efficiency of dye-laden TWW through allowing the development of a more diverse microbial population. Furthermore, comparison of the toxicity (based on an yeast-based assay) of samples collected from SBR2 on day 71 and from a flocculent SBR fed with the same dye-laden TWW, highlighted the better performance of SBR2, with respect to detoxification potential (Lourenço *et al*., 2015). This was hypothetically attributed to the typically higher SRT values at which the AGS SBRs are operated, comparing to flocculent SBRs, possibly favoring the establishment of a more diverse microbial population with the potential ability to biodegrade recalcitrant aromatic compounds such as aromatic amines.

Despite the variations in the SBR2 color removal performance along the experimental run, namely the recovery registered from period II to period III, no significant changes were detected in terms of major microbial groups in the FISH analysis (Figure III.4), which indicates the functional redundancy within the community regarding the azo dye reduction capacity. Moreover, the same bacterial distribution through the proteobacterial groups studied was observed irrespective of the differences registered in the 4A1NS profile from day 58 to 79 (Figure III.4, Figure III.12). These results suggested that the aerobic bioconversion of 4A1NS was performed by a specific community within one of the proteobacterial groups studied. In fact, the application of two specific probes for *Alphaproteobacteria* communities allowed the identification of *Defluviicoccus vanus*-related GAO on days 79 and 100, concomitantly with the 4A1NS further biotransformation. Although the respective probe was not applied in the biomass samples from days 37 and 58, the typical tetrad morphology of *Defluviicoccus vanus*-related GAO was not observed, indicating the absence of the latter. The fact that *Defluviicoccus*

*vanus*-related GAO represented the majority of the *Alphaproteobacteria* dominant group in the biomass samples harvested on days 79 and 100, further support the potential role of these bacteria in the 4A1NS transformation.

Further studying the microbial community through high throughput DNA sequencing revealed the emergence of bacteria from the *Chlorobia* class in relevant amounts during period III, as well as an increase in the relative abundance of members of the *Planctomyces*, *Sphingobacterium*, *Opitutus* (*Verrucomicrobia*) and *Ferruginibacter* genera, and *Clostridia* (*Firmicutes*) class, comparing to period II (Figure III.S3, in Appendix A). The concomitant 4A1NS transformation suggests the potential involvement of these bacteria in the aromatic amine aerobic conversion. A recent study, focused on the characterization of functional microbial communities involved in diazo dyes decolorization and mineralization stages (Zhu *et al*., 2018), highlighted several genera possibly involved in 4A1NS biodegradation (*Lactococcus*, *Desulfovibrio*, *Kerstersia*, *Anaerovorax*, *Proteiniclasticum*, *Anaerovirgula* and *Pusillimonas*). Specifically, *Desulfovibrio*, which was suggested to contribute to 4A1NS desulfonation and aromatic ring breakage, was present in relevant amounts in SBR2 along the experimental run (2-4% of relative abundance). Furthermore, the presence of a dynamic and diverse fungal community in SBR2, especially on day 86 (Figure III.S5, in Appendix A), contributed for a broader range of extracellular, oxidative enzymes. In this context, a specific fungal-bacterial consortium may be responsible for the AR14 biodegradation, namely in 4A1NS further biotransformation. According to a recent review on fungal bioremediation of pollutant aromatic amines, the fungi mostly applied for biotransformation of aromatic amines belong to the *Ascomycota* phylum (de Lima *et al.*, 2018), which represented at least up to 7% of the fungal community in SBR2.

## III.6. Conclusions

Overall, this study supports the potential for application of the AGS technology in dye-laden TWW treatment. The main conclusions derived from the obtained results are as follows:

- The presence of an azo dye did not affect biomass growth in the reactors, since comparable biomass concentration evolution profiles were registered in the dye-fed SBR and the control SBR.

- High shear stress caused by mechanical stirring resulted in disintegration of the large inoculated granules (sizes up to 5 mm) giving rise to small, compact granules (sizes up to 1 mm) which exhibited excellent settling properties ($SVI_5$ and $SVI_{30}$ of 19 and 17 mL $gTSS^{-1}$, respectively).

- Fast granule outgrowth led to later granule break-up, but only in the absence of dye, resulting in high SVI values and biomass washout levels. The dye-fed SBR however maintained a stable operation with the enlarged granule size. Presumably, even under oxygen diffusional limitation, the heterotrophic growth could proceed in the granule core due to the dye being able to act as electron acceptor under anaerobic conditions, thus improving granule stability. Conversely, in absence of the azo dye, granules

became less dense and more susceptible to shear forces, resulting in their break-up. This presumably reduced microbial activity in the core of dye-free granules was confirmed by FISH.

- Efficient azo dye bioreduction with aromatic amine formation was achieved with AGS during the 1.5-h anaerobic phase, corresponding to dye removal yields above 90%, with stable values being reached after 11 days of operation after inoculation.

- COD removal efficiency was affected neither by the presence of the azo dye nor by that of its breakdown metabolites. After a 14-day adaptation period, both SBRs achieved stable, high COD removal yields within the 80-90% range, with 55%, on average, occurring during the anaerobic phase. Maximal values (77%) of the fraction of COD removed anaerobically occurred when AGS reached maximal granule size, which was found to be correlated with an increase in the abundance of *Defluviicoccus vanus*-related GAO, known to be able to take up saccharides anaerobically.

- The dye-fed SBR proved to be a robust system able to deal with COD and dye shock loads maintaining granule stability and high color and COD removal yields.

- The SRT had a relevant effect on azo dye biodegradation in AGS systems. Dye removal performance significantly decreased when the SRT was lowered from 39 to 15 days, the effect being reverted upon reestablishment of SRT values above 25 days. Under the latter conditions, complete bioconversion of the aromatic amine 4A1NS could be achieved during the 3.5-h aerobic phase. This highlights the potential of SRT flexibility in AGS systems for the development of a more diverse microbial population with ability to remove color through azo dye reduction and to further mineralize the resulting aromatic amines.

# IV. Comparing AGS reactivation and operation performance in two SBR hydrodynamic regimens treating a synthetic TWW

The information included in this chapter was partially published in:

Franca, R.D.G., Carvalho, C.I.S., Carvalho, G., Pinheiro, H.M., Lourenço, N.D., 2017. Aerobic granular sludge reactivation under different hydrodynamic regimens: microbial ecology and bioreactor performance. *MICROBIOTEC'17*, 7-9 December, Porto, Portugal.

Franca, R.D.G., Pinheiro, H.M., Lourenço, N.D., 2016. Comparing AGS reactivation and operation performance in two SBR hydrodynamic regimes treating a synthetic textile wastewater. *IWA World Water Congress & Exhibition*, 9-14 October, Brisbane, Australia.

Franca, R.D.G., Pinheiro, H.M., Lourenço, N.D., 2014. Aerobic granular sludge reactivation performance in an anaerobic-aerobic sequencing batch reactor after long-term storage. *ChemPor 2014, 12th International Chemical and Biological Engineering Conference*, 10-12 September, Porto, Portugal.

## IV.1. Abstract

Aiming to optimize the treatment of a colored synthetic TWW in AGS SBRs, two hydrodynamic regimens were compared in terms of post-storage AGS reactivation performance, with a focus on azo dye biodegradation and organic load removal efficiencies. A 6.5-month stored AGS recovered its 80% organic load removal efficiency 9 days after inoculation in both a statically fed, stirred anaerobic-aerobic SBR1 and a plug-flow fed anaerobic-aerobic SBR2. In color removal yield, SBR1 reached 80%, whereas SBR2 presented levels under 30% apparently due to unfavorable mass transfer conditions in the plug-flow feeding stage. However, SBR2 developed better AGS settling properties and reached a higher biomass concentration. Yet, none of the SBRs were able to attain high, stable sludge age values after inoculation with stored biomass. Possibly due to this, aromatic amines resulting from primary azo dye reduction were apparently not aerobically bioconverted. This study provides new, relevant insights into the application of AGS for intermittent TWW treatment.

## IV.2. Introduction

The textile industry is one of the main water pollution sources in the world, releasing wastewaters with high organic loads and recalcitrant dyes, of which azo dyes are the main type used (O'Neill *et al*., 1999). Based on the demonstrated biological reductive cleavage of the azo bond and subsequent aerobic degradation of some of the resulting, potentially toxic, aromatic amines (van der Zee and Villaverde, 2005), staged anaerobic-aerobic SBRs using CAS have been proposed as an alternative to physicochemical dye removal processes (Lourenço *et al*., 2000).

Treatment of TWW with the groundbreaking AGS technology (de Kreuk and van Loosdrecht, 2004) has been recently suggested (Muda *et al*., 2010, Lourenço *et al*., 2015) in order to overcome the intrinsic limitations of CAS. In fact, besides the excellent settleability of AGS, allowing improvements in domestic WWTP footprint, process stability, effluent quality and energy demand (Inocêncio *et al*., 2013), AGS has potentially advantageous characteristics for the treatment of TWWs. Specifically, the possible co-existence of aerobic and anoxic-anaerobic microenvironments within AG, and their resistance to toxic compounds, as well as to prolonged storage periods (Lee *et al*., 2010), are important factors for the wet textile processing industry, characterized by discontinuous production processes and intermittent wastewater discharges.

This study aimed to analyze the reactivation of AGS after a 6.5-month storage period and its operation performance in the treatment of a synthetic TWW, focusing on azo dye biodegradation and organic load removal efficiencies. Two hydrodynamic regimens were compared: a mechanically stirred, anaerobic-aerobic SBR (Franca *et al*., 2015) *vs* a non-stirred aerobic SBR with prolongued anaerobic plug-flow feeding through the sludge bed. A recent study, comparing these two regimens in terms of AG formation in an SBR treating municipal wastewater, showed that the anaerobic stirred phase can

replace the more extensively reported anaerobic plug-flow feeding phase (Rocktäschel *et al*., 2013). Nevertheless, the authors found that the better performance of one configuration over the other depended on the specific operational conditions. Although good performance in the treatment of a synthetic TWW has been demonstrated in a stirred anaerobic-aerobic SBR (Franca *et al*., 2015), the shear stress from mechanical stirring has been shown to decrease the physical strength of AG (Nor-Anuar *et al.*, 2012). In contrast, the anaerobic plug-flow feed regimen has been associated with improved structural stability of AGS (de Kreuk and van Loosdrecht, 2004). In this context, this study compared the two hydrodynamic regimens in the treatment of a dye-laden synthetic TWW.

## IV.3. Materials and methods

### IV.3.1. Feed components

The carbon source (Emsize E1) stock solution and synthetic TWW used as feed solution were prepared as described in sections III.3.1.1 and III.3.1.2, respectively. The azo dye stock solution (5.0 g $L^{-1}$) was prepared by dissolving AR14 (Chromotrope FB, Sigma-Aldrich, 50% dye content) in distilled water.

### IV.3.2. SBR setup and operation

Two non-tubular, 1.5-L SBRs (H/D=2.5; Figure IV.1) were seeded with pre-developed AGS. Specifically, this seed had initially been harvested from a Nereda® SBR (Frielas WWTP, Portugal), was subsequently used for synthetic TWW treatment during 102 days (Franca *et al*., 2015) and was finally stored for 6.5 months (4ºC). The SBRs were operated for 80 days in 6-h cycles including a static fill (30-min in SBR1; 2-h plug-flow through the settled AGS bed in SBR2), a 1.5-h stirred anaerobic phase (only in SBR1), 3.5-h aeration, 5-min settling, 1-min drain and an idle period. Mechanical stirring in SBR1 was provided by an anchor-like impeller at 70 rpm, and aeration was supplied by air compressors via porous diffusers at the bottom of each bioreactor. The synthetic TWW was fed to the SBRs with a volumetric exchange ratio of 50% (effluent withdrawal at liquor mid-height), a HRT of 12 h and a volumetric OLR, as COD, of 2.0 kg $O_2$ $m^{-3}$ $d^{-1}$. The reactors were operated at room temperature.

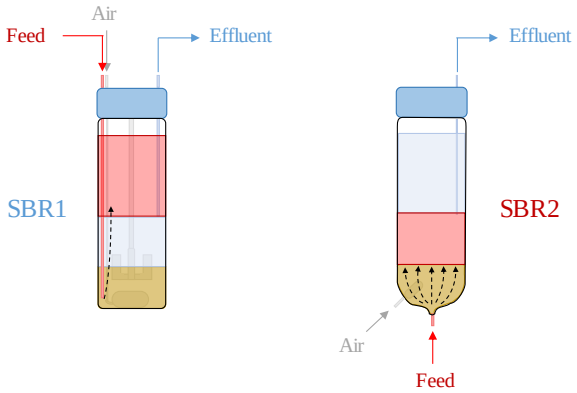


**Figure IV.1** - Schematic representation of the two non-tubular sequencing batch reactor (SBR) configurations used. Prior to an aerated reaction phase, SBR1 went through a static fill phase followed by a stirred anaerobic phase and SBR2 went through a prolongued anaerobic plug-flow fill through the settled sludge bed.

### IV.3.3. Analytical methods

TSS, SVI, biomass morphological analysis, COD, UV-visible absorbance spectra, dye degradation and metabolite formation were determined as described in section III.3.3.1. In addition, color removal was followed by reading the absorbance of clarified (centrifuged) samples at 515 nm (AR14 maximal absorbance wavelength in the visible region) in a UV-visible spectrophotometer (Specord 200, Analytik Jena) against distilled water. Dye concentration in terms of color-equivalents (dye-color) was determined from a calibration curve obtained through absorbance measurements of standard AR14 solutions.

Cell viability was assessed by fluorescent nucleic acid staining (LIVE/DEAD BacLight$^{TM}$ Bacterial Viability Kit L13152, Molecular Probes), visualized by fluorescence microscopy (microscope BA410 fitted with episcopic fluorescence attachment EF-UPR-III, TRITC (Rhodamine)/Dil/Cy3 and FITC/RSGFP/Fluo 3/DiO Acradine Orange (+RNA) filter sets, Motic). Microbial community analysis was assessed by FISH analysis on selected, homogenized biomass samples using oligonucleotide probes for the core community typically detected in WWTPs, as well as by high throughput DNA sequencing as described in sections III.3.3.2.1 and III.3.3.2.2, respectively.

## IV.4. Results and discussion

### IV.4.1. AGS morphology and properties

The cell viability analyses on AGS harvested after the 6.5-month storage period revealed a layer of viable cells which were apparently mostly gathered on the periphery of the AG (Figure IV.2-a). Along the first week of the operational run, microorganisms were able to rapidly proliferate within the AG (Figure IV.2-b). Nevertheless, on day 22 there were still some AG in SBR2 with a core mostly dominated by dead cells (Figure IV.2-c2), in contrast with SBR1, where this was not observed. This most likely is due to the smaller size of the SBR1 aggregates observed at this point of the operational run (Figure IV.2-c1).

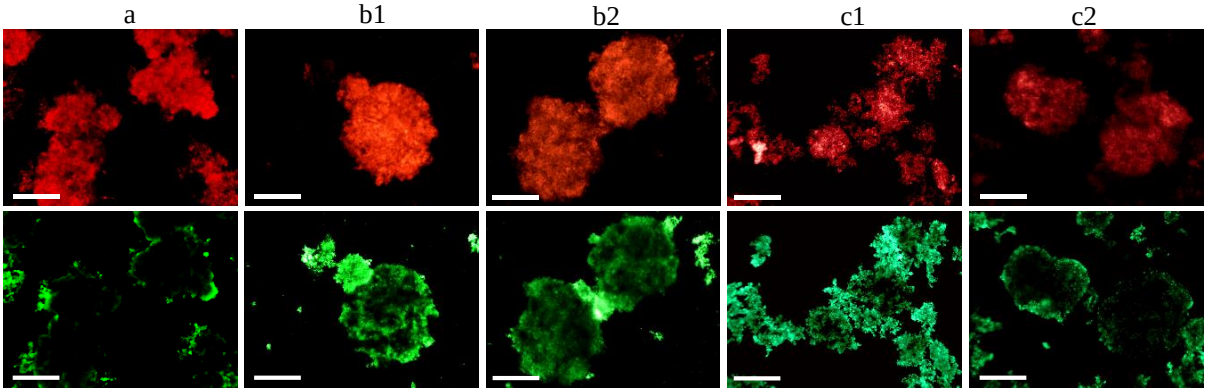


**Figure IV.2** - Fluorescent nucleic acid staining micrographs (magnification 100) of biomass samples after a 6.5-month storage at 4ºC and used as inoculum (a), and of biomass samples harvested from the sequencing batch reactors (SBRs) on operational days 8 (b) and 22 (c). Numbers 1 and 2 refer to SBR1 and SBR2, respectively. Red and green fluorescence represent dead and live cells, respectively. Scale bar = 200 µm.

Morphological analysis through light microscopy showed that AG maintained their morphology during the storage period (Figure IV.3-a,b). However, along the first 44 days of the operational run, maximum AG diameters decreased to below 600 µm, and the relative abundance of biomass flocs increased in both SBRs (Figure IV.3-c). At this point, AG in SBR1 presented a more round and regular shape than those in SBR2 (Figure IV.3-c), although AG were more abundant in the latter. Furthermore, from day 50 on, while SBR1 started to develop many new, small and round-shaped AG, apparently with a very low cell density, in SBR2 small AG presented irregular shapes and denser structures. In both SBRs, a significant amount of flocs and small biomass clusters were present throughout the experimental run. Moreover, the protozoa community was significantly affected by the storage period. Rotifers, which were abundant in the SBR prior to the biomass storage period, were only observed again in SBR1 and SBR2 from day 28 on. Nematodes, previously present the AGS SBR, were never observed during this experimental run.

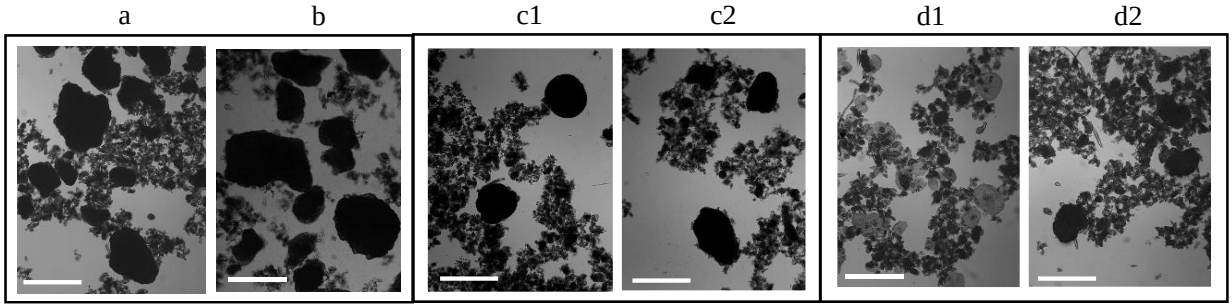


**Figure IV.3** - Morphological development of aerobic granular sludge examined by light microscopy along the experimental run. Micrographs (magnification 40) from biomass samples taken just before (a) and after (b) the 6.5-month storage at 4ºC, and from biomass samples harvested from the sequencing batch reactors (SBRs) on operational days 44 (c) and 79 (d). Numbers 1 and 2 refer to SBR1 and SBR2, respectively. Scale bar = 600 µm.

In accordance with the low viable cell density in the AG core after the long-term storage period (Figure IV.2) possibly causing the subsequent decrease in AG dimensions up to day 44 (Figure IV.3), SVI values gradually increased after inoculation of the SBRs with the stored AGS (Figure IV.4). From day 44 on, while SBR2 improved $SVI_5$ and $SVI_{30}$ values to 61 and 36 mL $gTSS^{-1}$, respectively, SBR1 maintained high values around 93 and 60 mL $gTSS^{-1}$, respectively, up to the end of the operational run.

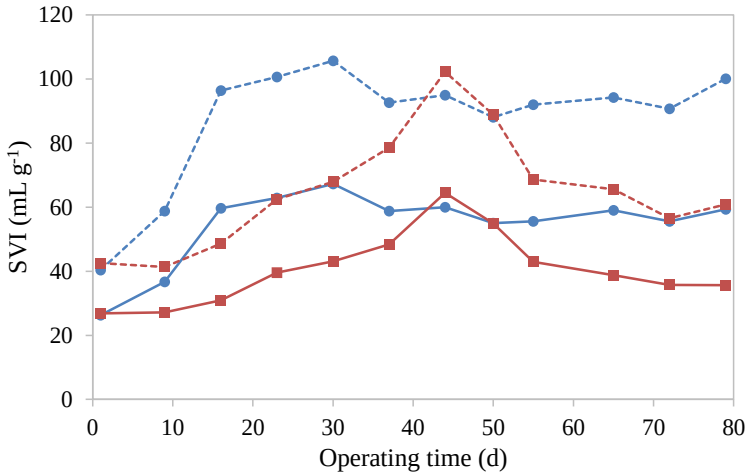


Figure IV.4 - Sludge volume index for settling periods of 5 min ($SVI_5$; dashed line) and 30 min ($SVI_{30}$; full line) in the sequencing batch reactors SBR1 (●) and SBR2 (■) along the experimental run.

## IV.4.2. AGS SBR treatment performance

### IV.4.2.1. Biomass inventory and sludge age

After inoculation with the stored AGS, biomass progressively accumulated in both reactors at comparable rates until day 16, from 2.5 gTSS $L^{-1}$ to 6.5 gTSS $L^{-1}$ (Figure IV.5-A), the SRT values gradually increasing to 38 days (Figure IV.5-B).

Subsequently, sporadic biomass washout episodes in SBR1 (up to 2 gTSS $L^{-1}$ in the treated effluent on day 19) caused the biomass concentration and the SRT to stabilize around 6.0 gTSS $L^{-1}$ and 9 days, respectively. In contrast, SBR2 could maintain higher levels of biomass concentration up to day 37, around 8.3 gTSS $L^{-1}$ (Figure IV.5-A). Afterwards, similarly to SBR1, biomass concentration decreased to 6.0 gTSS $L^{-1}$ due to a biomass washout episode on day 41 (1.4 gTSS $L^{-1}$ in the treated effluent). Nevertheless, contrarily to SBR1, biomass accumulation resumed, stabilizing around 10.2 gTSS $L^{-1}$ (Figure IV.5-A). Following the TSS profile in SBR2, SRT values decreased to 5 days on day 41, subsequently increasing to 45 days (Figure IV.5-B). Nevertheless, sludge age values dropped to 13 days at the end of the experiment, again due to increased biomass loss in the effluent.

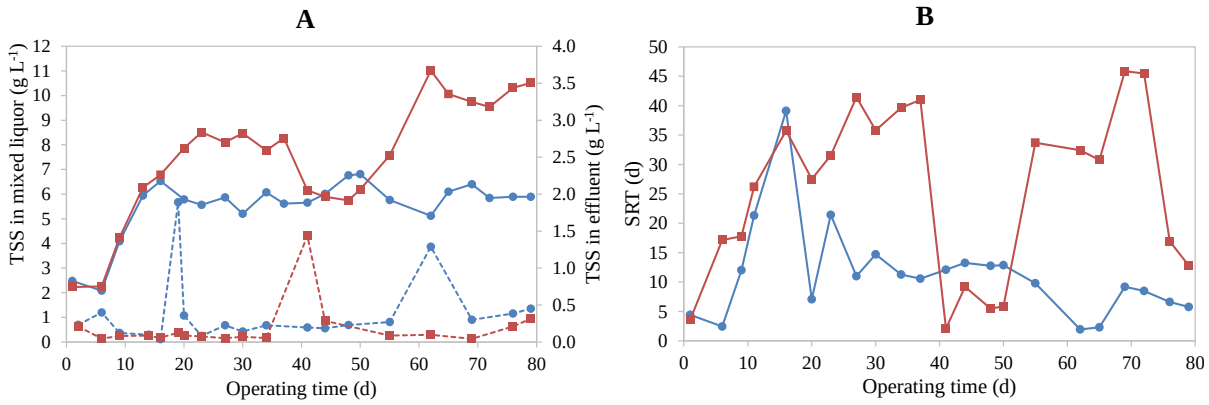


**Figure IV.5** - A) Profiles of total suspended solids (TSS) present in the mixed liquor (full line) and in the discharged effluent (dashed line) and B) profiles of sludge retention time (SRT) in the sequencing batch reactors SBR1 (●) and SBR2 (■), along the experimental run.

## IV.4.2.2. COD removal performance

In terms of organic load removal, both SBRs presented a good AGS reactivation performance, reaching 80% of COD removal yield on day 9 (Figure IV.6-A), most of it being removed aerobically (up to 75% in SBR1 and 100% in SBR2), namely during the first 30 min of aeration (Figure IV.6-B). SBR2 presented very low and erratic COD removal levels during the 2-h anaerobic plug-flow feed through the sludge bed (Figure IV.6-B), resulting in generally high biodegradable COD levels still remaining in the mixed liquor at the start of the aerobic phase. According to Pronk *et al.* (2015a), this situation usually leads to AG structural instability. In contrast, the fraction of COD removed during the stirred anaerobic phase of SBR1 could be maintained in the 30-40% range.

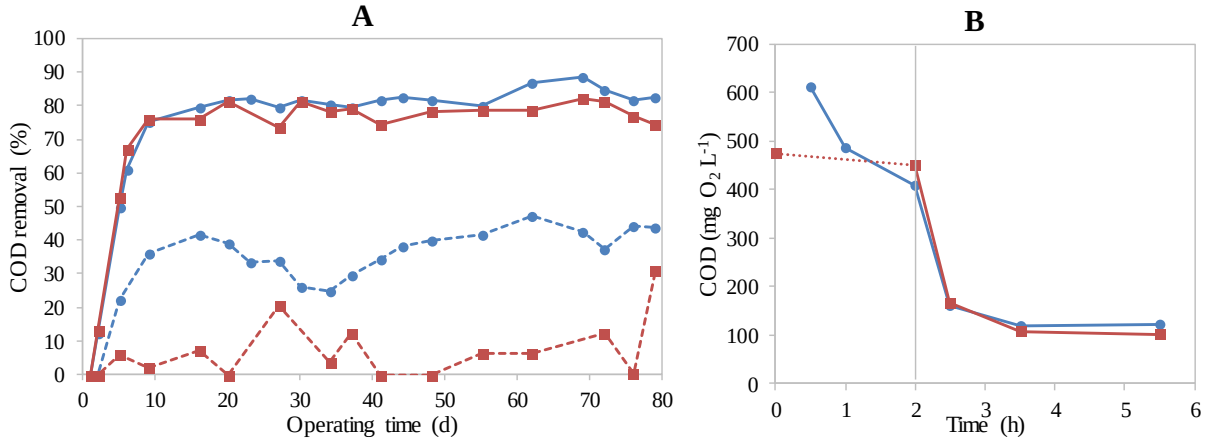


**Figure IV.6** - A) Organic load removal yield, as chemical oxygen demand (COD), in the sequencing batch reactors SBR1 (●) and SBR2 (■): total COD removal yield (full line) and percentage of COD removed during the anaerobic phase (dashed line). B) COD removal profiles along one representative treatment cycle (day 55) in SBR1 (●) and SBR2 (■); the dotted line represents the plug-flow filling stage in SBR2, the first COD value point being estimated from values measured in the feed solution (50% of total volume) and in the treated effluent left over from the previous cycle; the vertical line at 2 h marks the end of the anaerobic phase, upon the aeration onset.

### IV.4.2.3. Azo dye biodegradation performance

Regarding the decolorization performance after re-inoculation with the stored biomass, high color removal yields around 80% were rapidly recovered in SBR1, already on day 9 (Figure IV.7-A). In contrast, color removal in SBR2 remained within much lower values, 20-37%, from day 13 on (Figure IV.7-A). This was possibly due to the inefficient mass transfer conditions between the feed solution and the AGS bed, a consequence of the low H/D in the non-tubular SBR. In accordance with the proposed biodecolorization mechanism through reduction of the azo bond (dos Santos *et al.*, 2007), color levels decreased during the anaerobic phase, and remained constant throughout the subsequent aerobic phase, in both reactors (Figure IV.7-B). The higher initial color in the shown SBR2 cycle (Figure IV.7-B) reflected the accumulation of azo dye from the previous cycle, due to the low color removal yield.

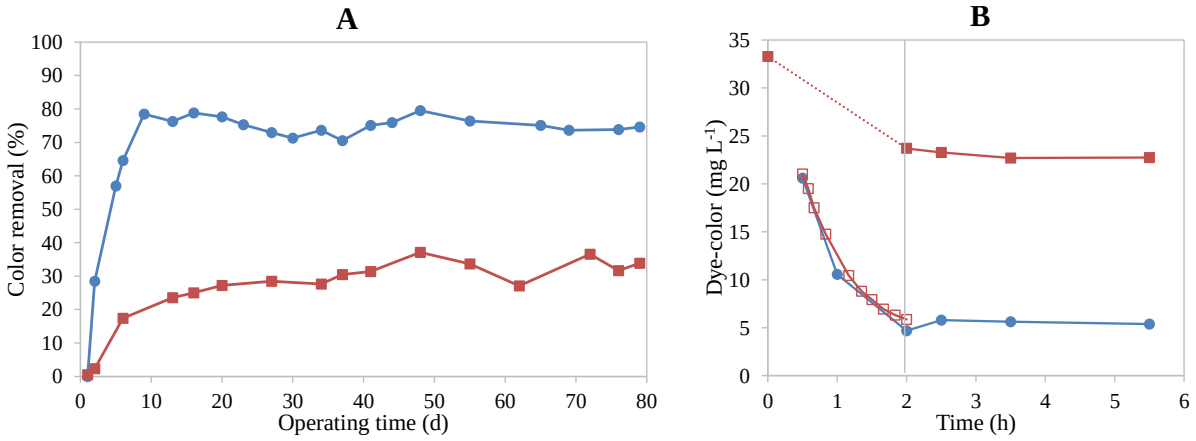


**Figure IV.7** - A) Color removal yields in the sequencing batch reactors SBR1 (●) and SBR2 (■) along the experimental run. B) Color removal profiles, as color-equivalents, along one representative treatment cycle (day 76) in SBR1 (●) and SBR2 (■); color removal profile in a batch experiment (□) subjecting a mixed liquor sample harvested from SBR2 at the end of the aerobic phase and diluted with fresh, dye-ladden synthetic textile wastewater to a 1.5-h anaerobic incubation run with magnetic stirring; the dotted line represents the plug-flow filling stage in SBR2, the first dye-color value point being estimated from a mass balance calculation with values measured in the feed solution (50% of total volume) and in the treated effluent left over from the previous cycle; the vertical line at 2 h marks the end of the anaerobic phase, upon the aeration onset..

In order to assess the ability of SBR2 biomass to decolorize AR14, a stirred anaerobic batch test was performed using a mixed liquor sample harvested from SBR2 at the end of the aerobic phase. The color removal followed the same rate profile registered in SBR1 (Figure 7-B), reaching 80% removal yield, confirming that the poor anaerobic treatment efficiency in the SBR2 configuration is probably due to inadequate mass transfer conditions.

Decolorization along the anaerobic phase of the treatment cycles resulted from the reduction of the azo bond of AR14, as confirmed by HPLC, generating two sulfonated aromatic amines: 4A1NS and 1N2A4S. Through comparison with the RT of standards, the peaks corresponding to AR14 (RT: 26 min) and 4A1NS (RT: 14 min) were identified and their areas converted to concentration units using a calibration curve. The 1N2A4S metabolite is expected to undergo autoxidation in the presence of

oxygen due to the hydroxyl group being in *ortho*-position in relation to the amino group (Kudlich *et al*., 1999). Thus, it could not be identified in the chromatograms due to its instability.

During the experimental run used to develop the AGS that was subsequently stored (Franca *et al*., 2015), 4A1NS was bioconverted in the aerobic reaction stage, being absent at the end of the treatment cycles (as described in section III.4.3.3). However, HPLC analysis of several treatment cycles along the present operational run revealed that the residual AR14 concentration remained unchanged over the aerobic phase, and that the aromatic amine 4A1NS concentration did not decrease (Figure IV.8). The slight increase in 4A1NS concentration in SBR1 (day 72) and SBR2 (day 23) can be attributed to the reversible conversion of this aromatic amine into an unknown intermediate, as previously observed (Franca *et al*., 2015). In fact, a consistent decrease in 4A1NS concentration along the aerobic phase was no longer observed after the storage of this AGS, not even during the cycles when the SBRs were operated at higher SRT levels. Accordingly, no relevant differences were encountered in this experimental run regarding the UV-visible spectrum of SBR1 and SBR2 samples harvested along the aerobic phase, except for a slight absorption reduction at 220 and 240 nm in SBR1 (Figure IV.S1, in Appendix B). These results suggest that the microbial population responsible for the aromatic amine transformation did not survive the long-term storage.

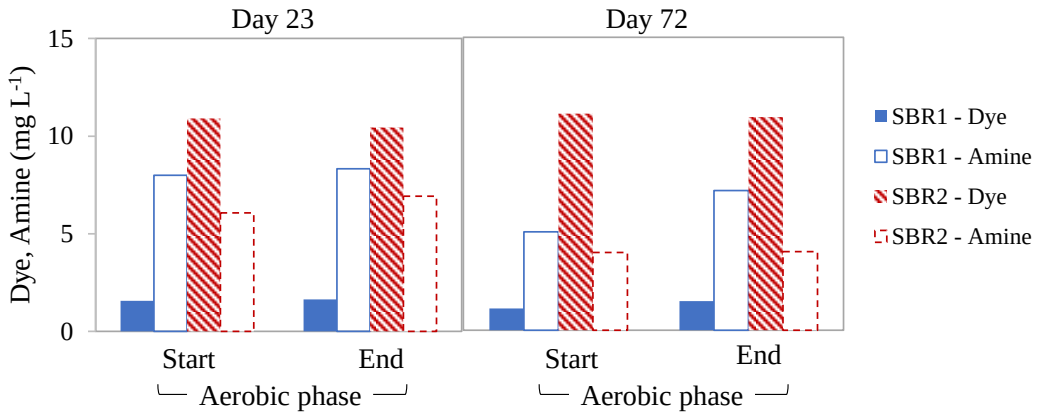


**Figure IV.8** - Concentrations of dye (Acid Red 14) and aromatic amine (4-amino-naphthalene-1-sulfonic acid) in the sequencing batch reactors SBR1 (filled bar and full outlined bar, respectively) and SBR2 (striped bar and dashed outlined bar, respectively), at the start and at the end of the aerobic phase in treatment cycles from days 23 and 72 of the experimental run.

## IV.4.3. Microbial community dynamics

The relative abundance of major bacterial groups was assessed by FISH in biomass samples from before and after the 6.5-month storage at 4ºC and from both reactors on day 70 of this experimental run (Figure IV.9). Regarding the effect of storage, it was observed that *Alphaproteobacteria* populations were susceptible to the storage conditions, namely the genus *Paracoccus*, that became less relatively abundant in the sludge, as well as *Defluviicoccus vanus*-related GAO, which were previously suggested to be potentially involved in 4A1NS bioconversion (section III.5.2.2). The loss

of 4A1NS aerobic biotransformation capacity after the biomass storage period further supports the previous hypothesis. In fact, in contrast to the previously dominant tetrad-morphology, only *Alphaproteobacteria* populations with rod-shape bacteria morphology survived the storage. On the other hand, *Gammaproteobacteria* withstood the long-term storage conditions, thus being dominant in the inoculum of this experimental run (Figure IV.9). The same was observed for *Actinobacteria*, possibly owing to the spore-forming capacity of some microorganisms belonging to this phylum.

Concerning the effect of the hydrodynamic regimen, while SBR1 promoted the dominance of *Gammaproteobacteria* and *Actinobacteria*, SBR2 developed a more evenly distributed microbial community along the operation, with very similar relative abundance levels among the five microbial groups assessed at the end of the operation (Figure IV.9). These different microbial community profiles might be explained by the different feeding regimens employed in the bioreactors. In fact, the 1.5-h plug-flow feeding imposed in SBR2 allowed for a spatially differentiated distribution of substrate concentration inside the bioreactor. Specifically, the microorganisms at the bottom of the SBR could contact with higher COD and nutrient concentrations than those located in the upper part of the settled sludge bed during the feeding phase. This gradient feeding pattern potentially resulted in a variety of microniches that simultaneously promoted the growth of microorganisms with different substrate affinities, thus creating the conditions for a more balanced growth of various bacterial groups. On the other hand, the microbial community was homogeneously exposed to the same COD and nutrients concentrations in SBR1, where the feed solution was thoroughly mixed with the residual treated effluent from the previous cycle during the short feeding phase. The uniform feed conditions applied in this reactor thus potentially favored the growth of specific microorganisms, better adapted to the specific conditions imposed, namely *Gammaproteobacteria* and *Actinobacteria*, the other groups being present at lower abundances within the community. Furthermore, a rod-shaped bacterial population within the *Gammaproteobacteria* group represented the majority of the SBR1 biomass sample on day 70, distinct from the cocci morphology observed in the corresponding SBR2 sample.

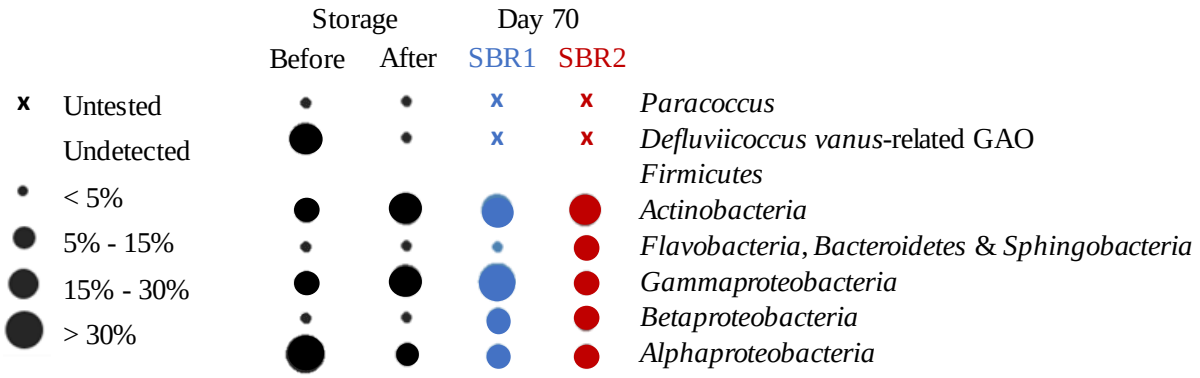


**Figure IV.9** - Abundance of the selected *Bacteria* detected by FISH analysis in the mixed microbial culture samples harvested before and after the 6.5-month biomass storage period, as well as from the sequencing batch reactors SBR1 (blue circles) and SBR2 (red circles) on experimental day 70. Adapted from Carvalho (2016).

Previous studies reported that the microbial community of AGS significantly and irreversibly shifted during prolonged storage conditions (He *et al*., 2017c). The comparison between the bacterial community in the inoculum before and after the 6.5-month storage period indicated that *Proteobacteria* (namely, *Alphaproteobacteria* class) and *Saccharibacteria* phyla were slightly susceptible to the storage conditions, since their relative abundance decreased by 7-9% over this period (Figure IV.S2, in Appendix B). Yet, *Proteobacteria* still accounted for 32% (*Alphaproteobacteria* corresponding to 27%) of the bacterial community after storage (Figure IV.10 and Figure IV.S2, in Appendix B). Similarly, *Proteobacteria* was reported to be one of the most abundant phyla in a study focused on the bacterial population dynamics in an AGS SBR during reactivation after extended idle conditions (58 days; He *et al*., 2017c). Within this phylum, *Alphaproteobacteria* has been shown to better resist to prolonged storage conditions than *Betaproteobacteria* (He *et al*., 2017c). On the other hand, *Actinobacteria* and *Bacteroidetes* (mainly composed of *Sphingobacteriia*) increased their relative abundance over the storage period (Figure IV.10 and Figure IV.S2, in Appendix B). In accordance with the present study, Wan *et al*., (2014) reported that a bacterial consortium composed of *Alphaproteobacteria, Flavobacteria, Betaproteobacteria, Gammaproteobacteria, Actinobacteria, Sphingobacteriia* and *Clostridia* (constituting more than 90% of AGS) was well preserved in AG, after one year of storage at 4ºC in liquid media. In addition, *Firmicutes*, which were virtually irrelevant in the biomass sample analyzed before storage, became visible within the community after the idle period (Figure IV.S2, in Appendix B), similarly to a previous study (He *et al*., 2017c). Two specific groups of bacteria belonging to the *Salana* and *Niabella* genera were dominant after the storage period (Figure IV.S3, in Appendix B), denoting an excellent capacity for resisting long starvation periods. The *Salana* genus (*Actinobacteria*) are Gram-positive, facultatively anaerobic bacteria (Wintzingerode *et al*., 2001), while the *Niabella* genus (*Bacteroidetes*) comprises Gram-negative, strictly aerobic, non-flagellated, non-spore-forming, rod-shaped bacteria (Weon *et al*., 2009).

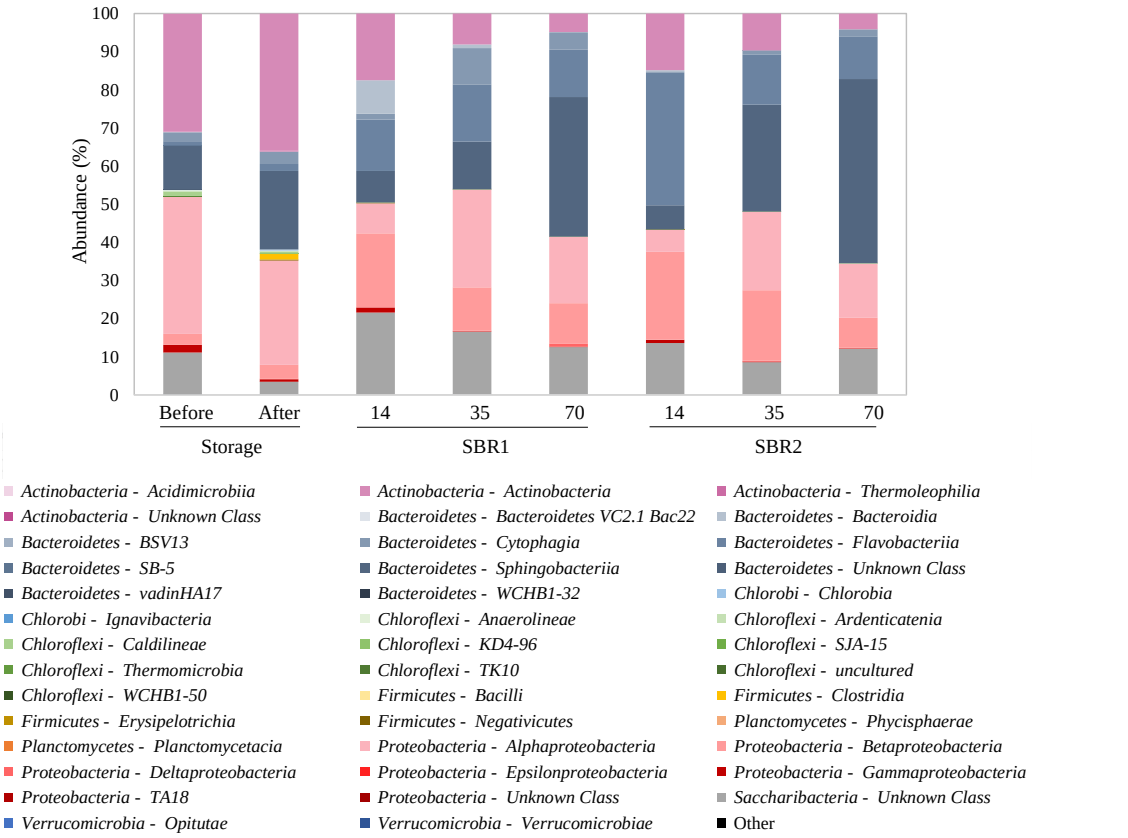


**Figure IV.10** - Composition of bacterial communities at the class level before and after the 6.5-month storage period, as well as in the sequencing batch reactors SBR1 and SBR2 on the indicated operational days, obtained by 16S rRNA gene sequencing analysis. The most representative "Phylum-Class" are represented below the chart.

As for the fungal community, the storage period led to a decrease in the relative abundance of *Basidiomycota* (both *Microbotryomycetes* and *Tremellomycetes* classes), and an increase in the relative abundance of *Ascomycota* populations (namely, *Eurotiomycetes*) and of other unknown fungi (Figure IV.11 and Figure IV.S4, in Appendix B). As visually explicit in Figure IV.S5 (in Appendix B), the diversity of the fungal community decreased substantially after storage, being mainly dominated by specific fungi from the *Trichosporon* and *Exophiala* genera, in addition to a taxonomically unclassified fungal group. Accordingly, the dominance of *Trichosporonaceae* members in different AGS samples regardless of the inoculum origin (Muñoz-Palazon *et al*., 2018) showed that these fungi easily adapted to AGS SBR operating conditions, potentially playing a crucial role in aerobic granulation through the formation of a fungal filament network as support for bacterial colonization. The corresponding phyla, *Tremellomycetes*, was highlighted as important for AGS ecology, namely for its formation and stabilization, possibly due to its good settling properties (Muñoz-Palazon *et al*., 2018).

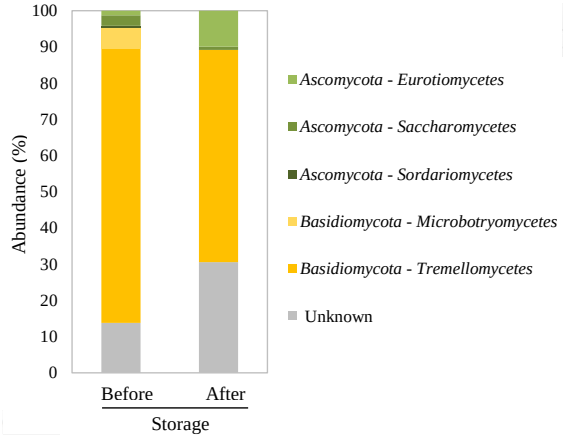


**Figure IV.11** - Composition of fungal communities at the class level before and after the 6.5-month storage period, obtained by rRNA gene and internal transcribed spacer (ITS) sequencing analysis. The most representative "Phylum-Class" are represented on the right.

Overall, the microbial community was comparable between the two SBRs, evolving similarly along the experimental run. Specifically, both reactors were dominated by *Bacteroidetes*, *Proteobacteria*, *Saccharibacteria* and *Actinobacteria* phyla, with *Chloroflexi* and *Firmicutes* becoming negligible at least 14 days after inoculation (Figure IV.S2, in Appendix B). At the class level, *Sphingobacteriia* drastically increased its relative abundance in both SBR throughout their operation, as opposed to *Thermoleophilia* and *Betaproteobacteria* (Figure IV.10). *Sphingobacteriia* has been described as a promising group of bacteria regarding dye degradation (Forss *et al*., 2013). More specifically, on day 14 of operation, *Bacteroidia* and *Flavobacteriia* had a higher relative abundance in SBR1 and SBR2, respectively; on day 35, SBR1 presented a relatively higher abundance of *Cytophagia* and *Saccharibacteria* than SBR2, where *Sphingobacteriia* and *Betaproteobacteria* were in higher relative abundance (Figure IV.10). Despite these differences, the microbial community in both SBRs was practically equivalent at the class level at the end of the operation, on day 70 (Figure IV.10).

Furthermore, the analysis of the 20 most abundant bacteria revealed a major decrease in the relative abundance of bacteria belonging to the *Salana* genus, as well as others from the *Hyphomicrobiacea* family, *Rhizomicrobium* and *Caulobacter* genera in both reactors 2 weeks after inoculation (Figure IV.S3, in Appendix B). On the other hand, the relative abundance of bacteria from *Cryseobacterium*, *Acidovorax*, *Massilia* and *Saccharibacteria* increased in the SBRs during the same period, the only relevant difference between the bioreactors on day 14 being the more significant presence of *Dysgonomonas* in SBR1 (Figure IV.S3, in Appendix B). *Cryseobacterium* (Figueroa *et al.*, 2015) and *Acidovorax* (Weissbrodt *et al*., 2013) have been identified in AGS and classified as ordinary heterotrophic organisms and denitrifying ordinary heterotrophic organisms, respectively, in the context of their function within the AGS microbial community (de Sousa Rollemberg *et al.*, 2018).

The relatively well balanced microbial distribution observed on day 14 in both reactors gradually evolved into a scenario where specific bacteria from the *Niabella* genus became predominant,

especially in SBR2 (Figure IV.S3, in Appendix B). Despite the generally similar composition of the microbial communities in both SBRs at the end of the experimental run (day 70), a marked difference was the relevant presence of two groups of bacteria from the *Comamonadaceae* family and from the *Amaricoccus* genus in SBR1, not observed in SBR2, as well as the presence of bacteria from the *Acidovorax* genus solely detected in the latter (Figure IV.S3, in Appendix B).

## IV.5. Conclusions

Having in mind the application of AGS to intermittent treatment of wastewater from the textile industry, stored AGS was re-inoculated into two SBRs operated under different hydrodynamic regimens, namely stirred anaerobic-aerobic (SBR1) and non-stirred, plug-flow feed, anaerobic-aerobic (SBR2), fed with a dye-laden synthetic TWW. After AGS storage, viable cells were still present mainly in the outer layer of AG. Despite the apparently intact morphology of the stored AG, the putative lower cell density in the AG core resulted in AG disintegration in both SBRs, and in SVI increase along the first month of the reactivation experiment. Yet, high COD removal yields were rapidly reached (80%, already from day 9 on). In terms of color removal yields, while SBR1 reached 80% (from day 9 on), SBR2 only reached 37%. This was found to apparently result from inadequate mass transfer between the feed solution and the AGS bed in the anaerobic stage of SBR2, as a consequence of the low H/D. On the other hand, the absence of stirring in SBR2 was apparently advantageous for AGS properties, the higher biomass settleability allowing higher biomass concentrations and SRT values to be attained in SBR2. Overall, the plug-flow regimen was advantageous for AGS properties and promoted a microbial community more evenly distributed across the quantified bacterial groups. Yet, even at elevated SRT values, the previously observed aromatic amine bioconversion capacity of AGS was not observed in any of the SBRs. In fact, loss of the capacity to aerobically bioconvert the aromatic amine resulting from dye degradation, observed after the biomass storage period, might be related to loss of *Defluviicoccus vanus*-related GAO, which were susceptible to the storage conditions. Overall, this study provided relevant data regarding the potential of AGS application for intermittent textile effluent treatment.

# V. Effect of SBR feeding strategy and feed composition on the stability of AGS in the treatment of a simulated TWW

The information included in this chapter was partially published in:

Franca, R.D.G., Ortigueira, J., Pinheiro, H.M., Lourenço, N.D., 2017. Effect of SBR feeding strategy and feed composition on the stability of aerobic granular sludge in the treatment of a simulated textile wastewater. *Water Science and Technology* 76.5, 1188-1195. DOI: 10.2166/wst.2017.300.

Franca, R.D.G., Ortigueira, J., Pinheiro, H.M., Lourenço, N.D., 2016. Effect of SBR feeding strategy and feed composition on the stability of aerobic granular sludge in the treatment of a simulated textile wastewater. *IWA World Water Congress & Exhibition*, 9-14 October, Brisbane, Australia.

## V.1. Abstract

Treatment of the highly polluting and variable textile industry wastewater using AGS SBRs has been recently suggested. Aiming to develop this technology application, two feeding strategies were compared regarding the capacity of anaerobic-aerobic SBRs to deal with disturbances in the composition of the simulated TWW feed. Both a statically fed, anaerobic-aerobic SBR and an anaerobic plug-flow fed, anaerobic-aerobic SBR could cope with shocks of high azo dye concentration and organic load, the overall COD and color removal yields being rapidly restored to 80%. Yet, subsequent azo dye metabolite bioconversion was not observed, along the 315-day run. Moreover, switching from a starch-based substrate to acetate in the feed composition deteriorated AGS stability. Overall, the plug-flow fed SBR recovered more rapidly from the imposed disturbances. Further research is needed towards guaranteeing long-term AGS stability during the treatment of TWW.

## V.2. Introduction

High organic loads, recalcitrant dyes and potentially toxic azo dye breakdown products have long been considered the top environmental issues associated to textile industry wastewater (O'Neill *et al*., 1999). The need for efficient and environmentally friendly dye removal processes led to the study of biological wastewater treatment, as an alternative to physical and/or chemical processes, which are expensive and create secondary pollution problems (dos Santos *et al*., 2007). The ability of bacteria to decolorize azo dyes (the dominant textile dye type) via anaerobic reduction, and to aerobically mineralize some of the resulting aromatic amines, motivated the application of anaerobic-aerobic SBRs to treat TWW (Sarayu and Sandhya, 2012). Nevertheless, despite the success reported for the anaerobic decolorization stage (Lourenço *et al.,* 2000), data on the fate of the aromatic amines during the aerobic stage, when available, revealed that most were not degraded (van der Zee and Villaverde, 2005). In this context, the novel AGS (Beun *et al*., 1999; Pronk *et al*., 2015b), known for its high settleability, its resistance to toxic compounds and its potential for the co-existence of aerobic/anoxic microenvironments within granules, has been recently applied in studies with simulated TWW (Muda *et al.*, 2010; Franca *et al*. 2015).

Despite the advances in AGS technology, long-term stability of AG, a key factor for stable operation of AGS SBRs, is still a challenge (Lee *et al*. 2010; Zhang *et al*., 2016b). A low microbial growth rate inside AG has been described as an important factor to keep AG stability (de Kreuk and van Loosdrecht, 2004). Regarding the SBR hydrodynamic and aeration regimens, anaerobic plug-flow feeding followed by aerobic reaction has been associated with improved structural stability of AGS in tubular SBRs, being attributed to the selection of heterotrophic microorganisms able to anaerobically convert easily biodegradable substrates to slowly biodegradable storage polymers, thus exhibiting lower growth rates in the aerobic phase (de Kreuk and van Loosdrecht, 2004; Pronk *et al*., 2015a). On

the other hand, when compared with the use of an anaerobic plug-flow feeding, a stirred anaerobic phase following a fast feeding period has been suggested to improve anaerobic substrate uptake prior to the aerobic stage in small H/D reactors (non-tubular), and consequently enhance AGS stability (Rocktäschel *et al.* 2013).

The reaction stage of both SBRs used in the present work (small H/D) included an anaerobic stirred phase followed by an aerobic stage, the difference between the reactors lying in the feeding strategy. Specifically, this study assessed the effect of two feeding regimens – an anaerobic plug-flow feeding through the sludge bed and a static anaerobic feeding – on the stability of AGS in non-tubular SBRs treating a synthetic TWW, namely when subjected to changes in feed composition, with a focus on azo dye biodegradation and COD removal.

## V.3. Materials and methods

### V.3.1. Chemicals

Sodium acetate (analytical grade, AppliChem GmbH, Germany) and/or a starch-based sizing agent used in the cotton textile industry, Emsize E1 (Emsland-Starke GmbH, Germany), were used as carbon source. The Emsize E1 and the azo dye AR14 stock solutions were prepared as described in section IV.3.1.

The synthetic TWW used as feed solution was prepared as described in section III.3.1.2, with the addition of the azo dye to a concentration of 40 mg AR14 $L^{-1}$. When acetate was used as carbon source instead of Emsize E1, sodium acetate was directly dissolved in the synthetic TWW as a part of its preparation.

### V.3.2. SBR setup and operation

AGS from previously operated lab-scale SBRs was used to inoculate two 1.5-L SBRs (H/D=2.5; Figure V.1) after a 2.5-month storage period. The new reactors were operated for 315 days, comprising six experimental periods (A-F), characterized in Table V.1. Filling was performed at the bottom of the reactors (Figure V.1): as a plug-flow regimen in SBR2, allowing the feed to distribute and rise through the sludge bed; or at a peripheral site at the bottom of SBR1, the feed rapidly channeling above the settled biomass with no relevant contact between them. Both SBRs were operated in 6-h cycles including a 30-min static anaerobic feeding in SBR1 and a 50-min static plug-flow feeding, through the sludge bed, in SBR2 (changed to 1.3-h in SBR2 from day 180 on), followed by a 1.5-h stirred anaerobic phase (changed to 1-h in SBR2 from day 180 on), 3.5-h aeration, 5-min settling, 1-min drain and idle. Mechanical mixing was provided by an anchor-like impeller at 70 rpm and by a 4-blade axial impeller at 280 rpm in SBR1 and SBR2, respectively, and aeration was supplied by air compressors via porous, bottom diffusers (Figure V.1).

The feed was supplied to the SBRs with a HRT of 12 h. Three-fold increases in dye and Emsize (the latter together with $NH_4Cl$) concentrations in the SBR feed, to 120 mg AR14 $L^{-1}$ and to an OLR of 6.0 kg COD $m^{-3}$ $d^{-1}$, were applied on days 158-164 (period B) and 165-172 (period C), respectively (Table V.1). Following a transition period, when the original operating conditions were restored (days 173-179, period A'), acetate was introduced in the feed, the carbon source being changed from 100% to 50% Emsize (days 256-291, period E), and finally to 100% acetate (days 292-314, period F). In fact, starches (such as Emsize E1) and acetic acid (acetate as conjugate base) are among the major pollutants found in TWW contributing for the high organic load characteristic of these effluents, arising from desizing, scouring, washing and dyeing processes (Delée *et al.*, 1998).

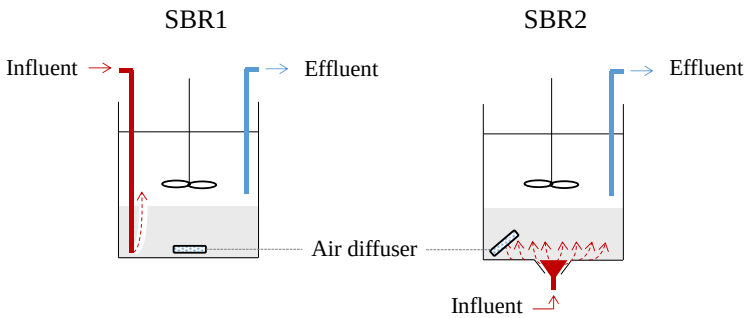


**Figure V.1** - Schematic representation of the sequencing batch reactors (SBRs) used in this study employing two different feeding strategies: SBR1 had an anaerobic static feeding, followed by a stirred anaerobic phase and an aerobic stage; SBR2 had an anaerobic plug-flow feeding stage through the sludge bed, followed by a stirred anaerobic phase and an aerobic stage. The dashed arrows represent the feed flow pattern in each SBR.

**Table V.1** - Summary of the operational conditions for the sequencing batch reactors SBR1 (static anaerobic feeding) and SBR2 (plug-flow feeding) along the experimental periods, regarding feed composition in both SBRs, and anaerobic phase duration in SBR2 (E1 – Emsize; Ac – Acetate; AR14 – Acid Red 14). The indicated food-to-microorganism ratio (F/M) was calculated for each period, taking into account the respective feed COD and average VSS measured in the reactors.

| Period | Days | Feed composition (SBR1 and SBR2) | | SBR2 Anaerobic phases | | F/M (gCOD $gVSS^{-1}$ $d^{-1}$) | |
|---|---|---|---|---|---|---|---|
| | | Substrate − COD (mg $O_2$ $L^{-1}$) | AR14 (mg $L^{-1}$) | Filling (min) | Stirring (min) | SBR1 | SBR2 |
| A | 0-157 | E1 − 1000 | 40 | 50 | 90 | 0.4 | 0.3 |
| B | 158-164 | E1 − 1000 | 120 | | | 0.5 | 0.4 |
| C | 165-172 | E1 − 3000 | 120 | | | 1.2 | 0.9 |
| A' | 173-179 | E1 − 1000 | 40 | | | 0.6 | 0.5 |
| D | 180-255 | E1 − 1000 | 40 | 80 | 60 | 0.4 | 0.5 |
| E | 256-291 | 50% E1+50% Ac − 1000 | 40 | | | 1.1 | 0.5 |
| F | 292-315 | Ac − 1000 | 40 | | | 1.8 | 1.0 |

## V.3.3. Analytical methods

TSS, VSS, SVI, morphological analysis, pH, COD, UV-visible absorbance spectra, dye degradation and metabolite formation were determined as described in section III.3.3.1. In addition, color removal

was followed as described in section IV.3.3. Staining of intracellular lipids was performed with Nile Blue according to Ostle and Holt (1982), visualized through fluorescence microscopy (BA410 microscope with episcopic fluorescence attachment EF-UPR-III and TRITC (Rhodamine)/Dil/Cy3 filter set, Motic). Microbial community analysis was assessed by FISH analysis on selected, homogenized biomass samples using oligonucleotide probes for the core community typically detected in WWTPs, as well as by high throughput DNA sequencing as described in sections III.3.3.2.1 (except for the use of SuperDFmix and Par651 probes) and III.3.3.2.2, respectively.

## V.4. Results and discussion

### V.4.1. Biomass inventory and AGS properties

Inoculation with a 2.5-month stored AGS led to different biomass profiles in the two SBRs, with distinct settling characteristics. SBR1 presented a peak in the $SVI_5$ and $SVI_{30}$ values on day 48 (177 and 98 mL $gTSS^{-1}$, respectively), subsequently stabilizing along period A at higher levels than those registered in SBR2 (Table V.2). Though SVI was more stable in the latter during period A, the shock loads applied in periods B-C caused a sharp increase in the SBR2 SVI values, high levels being maintained throughout the subsequent period D (Table V.2). As a result of this settleability shift, TSS levels decreased from 7 to 5 gTSS $L^{-1}$ in SBR2 after period C, in contrast with SBR1, which maintained an average value of 5 gTSS $L^{-1}$ throughout periods A-D (Table V.2). Accordingly, while the SRT levels in SBR1 were mostly stable until the end of period D (9 days, on average), in SBR2, the initial average sludge age of 18 days deteriorated to 6 days after the shock loads were applied (Table V.2). Subsequently, upon introduction of acetate as 50% and 100% of the carbon source load in the feed (periods E and F, respectively), biomass settleability was significantly reduced in both reactors (Table V.2), reaching maximal $SVI_5$ and $SVI_{30}$ values of 592 and 282 mL $gTSS^{-1}$ in SBR1, and 400 and 255 mL $gTSS^{-1}$ in SBR2, respectively, on day 299. This substrate switch led to an almost complete biomass washout, resulting in biomass concentrations around 1.5 gTSS $L^{-1}$ in both SBRs. Yet, after adaptation to the new carbon source, SBR2 resumed biomass accumulation along period F, with $SVI_5$ and $SVI_{30}$ levels gradually decreasing to final values of 225 and 123 mL $gTSS^{-1}$, respectively. Overall, the average and standard deviation values for the TSS and SVI in each experimental period (Table V.2) showed that for both SBR1 and SBR2, periods A, B and C presented similar results in terms of biomass properties. In contrast, significant differences were observed in periods D, E and F between the two reactors.

The morphology of the AGS before the 2.5-month storage period was comparable for SBR1 and SBR2, as shown in Figure V.2. Similarly, throughout this experimental run, both SBRs presented a mixture of AG, flocs and dispersed biomass, SBR2 retaining the highest fraction of AG in period A (Figure V.2). The increase in carbon load (period C) induced AG size growth (to diameters still below

600 μm). However, in accordance with the SVI results, the shock loads apparently had a negative effect in AG integrity, as later granules gradually became smaller and less abundant (period D, Figure V.2). In period E, fed with the mixed carbon source, AG morphology was significantly altered. Larger granules (diameters up to 600 μm), with a well-defined, round outline were formed (Figure V.2), their morphology suggesting low density, and high EPS content. The change to acetate as sole carbon source (period F) caused AG to further increase in size (to diameters above 1 mm). Moreover, the substrate change caused a marked decrease in the flocculent sludge fraction in both reactors, as well as in the abundance of protozoa, such as rotifers, which were no longer observed in periods E-F.

**Table V.2** - Summary of average and standard deviation values registered for the total suspended solids (TSS), sludge volume index after 5 and 30 min settling ($SVI_5$ and $SVI_{30}$, respectively) and sludge retention time (SRT) in each experimental period, for the two sequencing batch reactors (SBRs). The indicated SRT corresponds to the average of the SRT values calculated for each week (weekly SRT) along the respective period. This data is graphically represented in Figure V.S1, in Appendix C.

| Period | SBR1 | | | | SBR2 | | | |
|---|---|---|---|---|---|---|---|---|
| | TSS ($g\ L^{-1}$) | $SVI_5$ ($mL\ gTSS^{-1}$) | $SVI_{30}$ ($mL\ gTSS^{-1}$) | SRT (days) | TSS ($g\ L^{-1}$) | $SVI_5$ ($mL\ gTSS^{-1}$) | $SVI_{30}$ ($mL\ gTSS^{-1}$) | SRT (days) |
| A | 4.8 ± 1.0 | 119 ± 20 | 72 ± 10 | 9 ± 6 | 7.4 ± 1.4 | 85 ± 11 | 51 ± 7 | 18 ± 10 |
| B | 4.8 ± 0.0 | 111 ± 5 | 72 ± 1 | 7 ± 1 | 6.3 ± 0.9 | 110 ± 11 | 64 ± 7 | 13 ± 3 |
| C | 5.8 ± 0.2 | 99 ± 8 | 65 ± 6 | 7 ± 1 | 7.3 ± 0.2 | 91 ± 2 | 57 ± 1 | 6 ± 1 |
| D | 3.9 ± 0.0 | 103 ± 13 | 64 ± 9 | 9 ± 6 | 4.6 ± 0.0 | 138 ± 15 | 85 ± 9 | 6 ± 4 |
| E | 5.1 ± 0.7 | 357 ± 123 | 237 ± 81 | 2 ± 0 | 4.9 ± 0.5 | 180 ± 46 | 112 ± 29 | 6 ± 4 |
| F | 2.0 ± 0.9 | 502 ± 105 | 310 ± 53 | 2 ± 1 | 4.4 ± 1.1 | 284 ± 71 | 179 ± 51 | 9 ± 6 |

The F/M values in SBR1 and SBR2 (Table V.1) follow the same trend along periods A-D. In periods A and B the F/M values were within the range of 0.3-0.5 $gCOD\ gVSS^{-1}\ d^{-1}$. Higher values were achieved in period C (1.2 and 0.9 $gCOD\ gVSS^{-1}\ d^{-1}$ in SBR1 and SBR2, respectively), when a three-fold higher organic load was applied, subsequently decreasing upon reestablishment of the initial feed conditions (period D: 0.4 and 0.5 $gCOD\ gVSS^{-1}\ d^{-1}$ in SBR1 and SBR2, respectively). Accordingly, the biomass morphology evolved similarly in the two reactors along these periods (Figure V.2).

Upon introduction of acetate as carbon source (periods E and F), significant differences were observed in the biomass morphology in both reactors (Figure V.2). In fact, the F/M increased (Table V.1), more significantly in SBR1 (periods E and F: 1.1 and 1.8 $gCOD\ gVSS^{-1}\ d^{-1}$, respectively) than in SBR2 (periods E and F: 0.5 and 1.0 $gCOD\ gVSS^{-1}\ d^{-1}$, respectively). Similarly to the apparent lower density of the granules microscopically observed, these F/M values denote the deterioration in the sludge settleability, especially in SBR1.

The low average SRT levels observed (Table V.2) were mainly caused by erratic, intense biomass washout episodes in the SBRs. This likely indicated the dominance of heterotrophic fast-growing

organisms, which have been associated with AG instability (Pronk *et al*., 2015a). High microbial growth rates are a consequence of high residual COD levels at the start of the aeration phase (de Kreuk and van Loosdrecht, 2004). Filamentous bacteria are usually associated to these operational conditions, but none were observed during this study. This might result from the starvation stage at the end of the aerobic phase, since the feast-famine regimen has been shown to prevent filamentous outgrowth in AG (de Kreuk and van Loosdrecht, 2004). In addition, the shear stress caused by mechanical stirring might also have impaired the development of filamentous organisms.

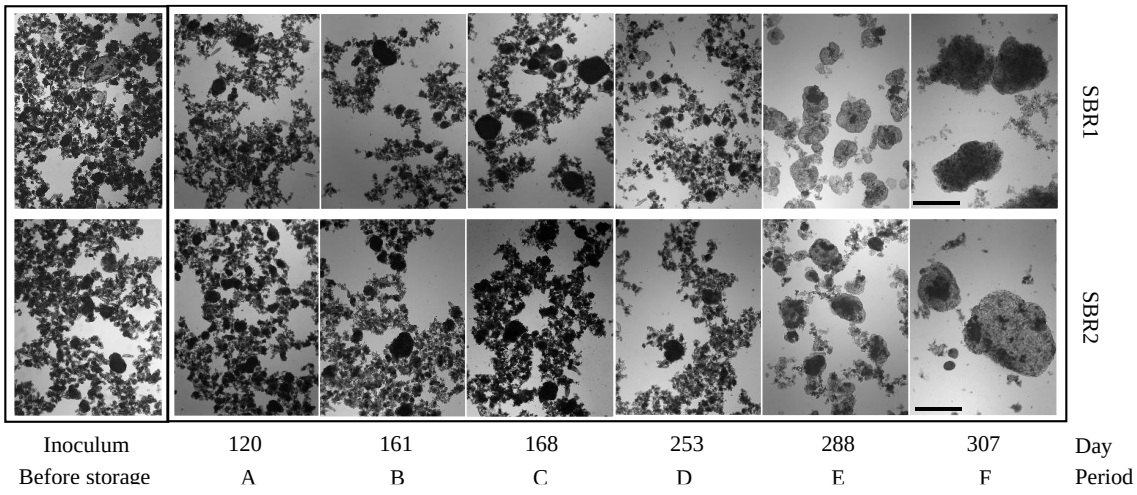


**Figure V.2** - Micrographs (magnification 40) from biomass samples harvested from the sequencing batch reactors SBR1 and SBR2 on the indicated periods (see Table V.1) and respective operational days. Scale bar = 600 µm.

## V.4.2. Color and carbon load removal performance

High color removal yields (around 80%) were attained under anaerobic conditions in both SBRs, with no further decolorization during the aerated phase. The overall COD removal was 80%, of which up to 70% and 80% were removed anaerobically in SBR1 and SBR2, respectively. The plug-flow feeding stage of SBR2 contributed minimally for this (Figure V.3-A). Upon the dye concentration shock, the decolorization rate increased (Figure V.3-B), denoting first-order kinetics, and was further improved to 90% removal yield when the shock step in OLR was applied (Figure V.3-C). In period C, overall COD removal decreased to 68%, SBR2 removing a higher fraction anaerobically (30% *vs* 5% in SBR1). In addition, the three-fold increase in feed COD (period C) caused a marked acidification of the medium during the anaerobic phase (Figure V.3-C), as compared with the typical pH profile (Figure V.3-A). This suggested a higher VFA production upon fermentation of the hydrolyzed starch-based substrate during the anaerobic period, and subsequent VFA consumption in the first 30 min of aeration. Upon re-establishment of the initial feed conditions, 80% COD removal was resumed in both reactors, but decolorization yields decreased to 74% and 66% in SBR1 and SBR2, respectively. Nevertheless, high color and COD removal efficiencies were resumed in SBR2 after adaptation to the shorter stirred anaerobic phase (Table V.1, Figure V.3-D), which aimed to reduce energy consumption in SBR2.

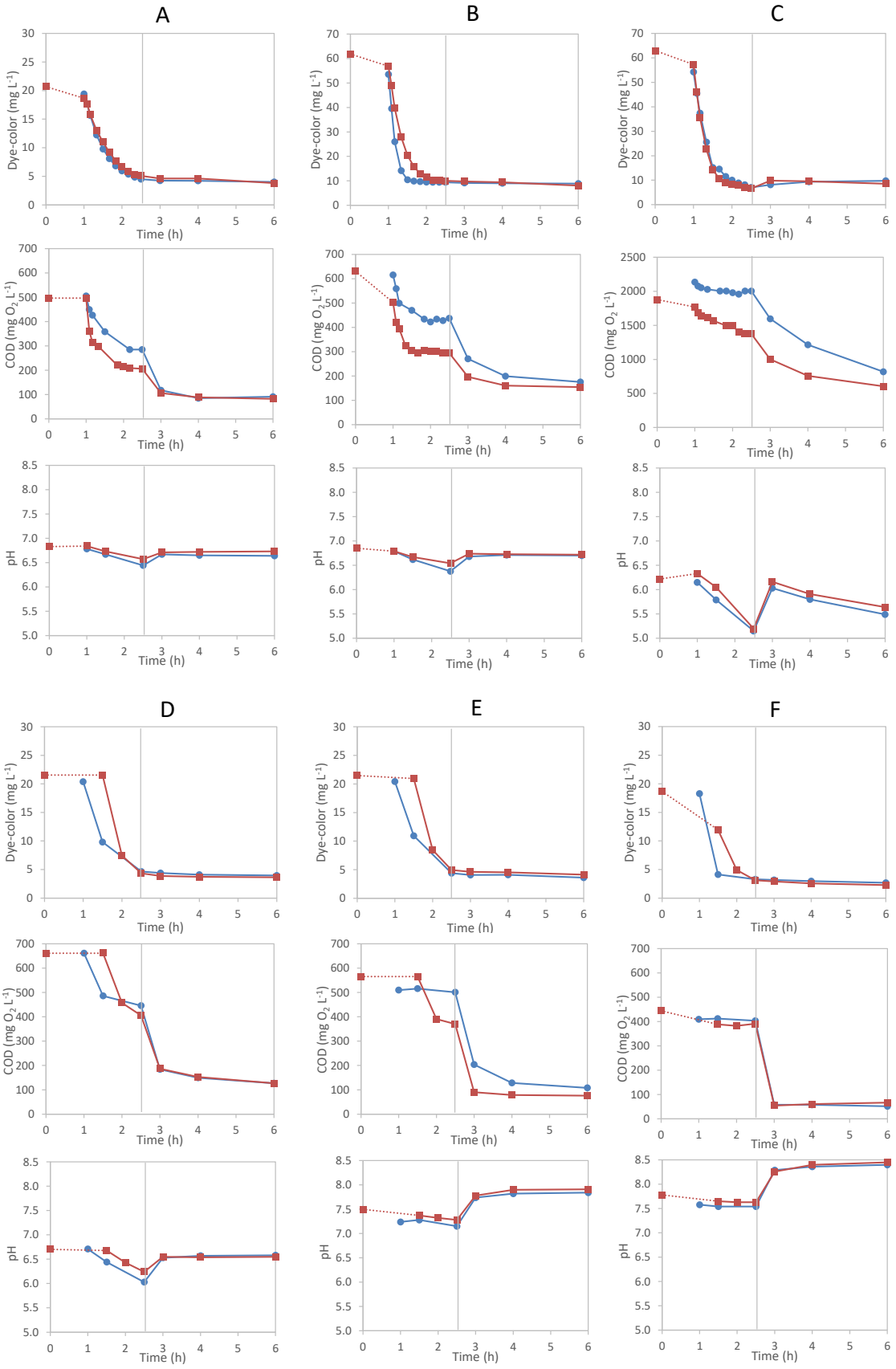


**Figure V.3** - Color, chemical oxygen demand (COD) and pH profiles along the reaction phase in SBR1 (●) and SBR2 (■) cycles representative of periods A-F (Table V.1). The dotted line depicts the plug-flow feeding period in SBR2, the first value point being estimated from values measured in the feed solution (50% of total volume) and in the treated effluent left over from the previous cycle. Vertical lines represent the end of the anaerobic phase, upon the aeration onset..

The change to 50% acetate in the feed did not affect decolorization, and even improved overall COD removal, mostly aerobically (Figure V.3-E). Upon complete replacement of Emsize with acetate, color removal dropped to 16% in SBR1 (days 299-307), being subsequently restored to regular levels from day 309 on. In contrast, color removal in SBR2 responded positively to acetate, namely during the plug-flow feeding period, reaching an overall yield of 91% (Figure V.3-F). In fact, the color profile representative of period F suggests that the anaerobic plug-flow feeding through the sludge bed can be advantageous in terms of decolorization performance when acetate is present in the wastewater as the main carbon source. In addition, the introduction of acetate caused a pH shift to higher values (Figure V.3-E,F). In fact, the pH level was stable throughout the anaerobic phase, denoting the presence of a non-fermentable substrate, the latter being rapidly consumed upon the start of aeration, causing an equally fast pH increase.

The combination of substrate diffusion and microbial consumption rates is known to determine the substrate gradient inside a biofilm and, consequently, its stability (de Kreuk *et al*., 2010). Specifically, a plug-flow hydrodynamic regimen rising through the settled bed, with high substrate concentration allows soluble, easily biodegradable substrates to penetrate the entire AG depth and be converted to storage polymers (Pronk *et al*., 2015a). Consequently, easily biodegradable COD will not be available in the subsequent SBR aerobic phase and slow microbial growth can occur down to the core of the AG, ensuring a stable AG structure. In contrast, in an anaerobic fast feeding-stirred strategy the biomass contacts with a lower substrate concentration, as a result of its dilution with the remaining supernatant from the previous SBR cycle. Thus, in this situation substrate gradients are likely to occur in the AG, which may lead to AG instability (de Kreuk *et al*., 2010).

In addition to the feeding regimen, the reactor geometric configuration should be taken into account. In fact, Rocktäschel *et al*. (2013) noted that in reactors with a small H/D, the plug-flow feeding may develop heterogeneous flow patterns through the granular bed, leading to short contact times between the substrate and the biomass and thus to incomplete anaerobic carbon uptake during this stage. Accordingly, low COD removal occurred during the plug-flow anaerobic feeding of SBR2, with most of the anaerobic COD removal being achieved during the subsequent stirred anaerobic phase, where better mass transfer conditions were provided. Owing to a lower microbial growth rate in the aerobic phase, complete COD removal under anaerobic conditions has been shown to increase AG density and structural stability (Pronk *et al*., 2015a). In fact, despite the negligible COD removal during the plug-flow feeding phase of SBR2, the subsequent stirred anaerobic phase led to faster anaerobic COD removal than in SBR1. This might explain the lower average SVI values in SBR2, from period D on (Table V.2). Yet, complete anaerobic COD removal was never achieved in the SBRs, and this situation worsened when the carbon source was changed from hydrolyzed hydroxypropyl starch (fermentable substrate) to acetate (VFA).

In spite of the limited acetate uptake during the anaerobic phase (Figure V.3-F), results from Nile Blue staining of biomass samples taken along one treatment cycle, during period F, suggest that AGS in both SBRs accumulated intracellular lipid aggregates during the anaerobic phase (Figure V.4). These storage compounds were apparently partly consumed during the aerobic period in SBR1 (Figure V.4). Therefore, AGS in SBR1 was possibly under carbon starvation at the end of the reaction phase, since the biodegradable COD was exhausted from the mixed liquor 30 minutes after the start of aeration (Figure V.3-F). This was not observed in SBR2.

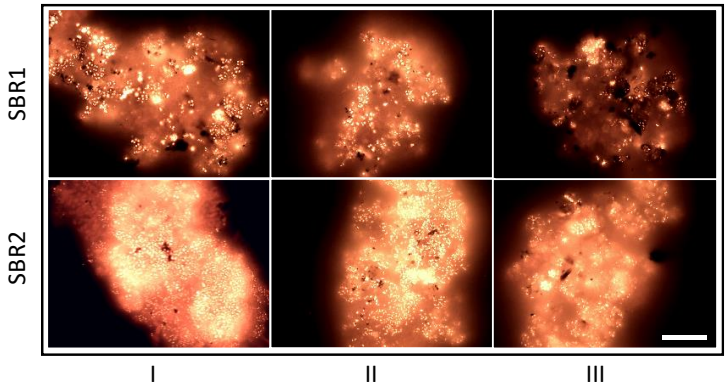


**Figure V.4** - Fluorescence micrographs (magnification 1000, excitation wavelength 540 nm) of Nile Blue-stained biomass samples harvested from the sequencing batch reactors SBR1 and SBR2 on day 313 (period F; 100% acetate) at the end of the anaerobic phase (I), 30 min after the aeration onset (II) and at the end of the aerobic stage (III). Scale bar = 20 μm.

## V.4.3. Azo dye biodegradation and metabolite formation

HPLC analysis confirmed that the azo dye AR14 was anaerobically reduced (Figure V.5-A). Two aromatic amines result: 4A1NS and 1N2A4S. Only the former was detected by HPLC, as 1N2A4S probably undergoes autoxidation reactions (Kudlich *et al.*, 1999). The 4A1NS profiles show that this amine was not aerobically biodegraded (Figure V.5), which might be a consequence of the low SRT (Table V.2). Accordingly, no major differences were observed in the UV-visible spectra of samples harvested along the aerobic phase from both SBRs throughout the whole experimental run (Figure V.S2, in Appendix C). In fact, 4A1NS has been noted as recalcitrant and the few studies reporting its biodegradation (Koupaie *et al.*, 2013; Franca *et al.*, 2015) used strong biomass retention strategies, *i.e.*, biofilms and AGS SBRs under high SRT values, producing more diverse microbial communities.

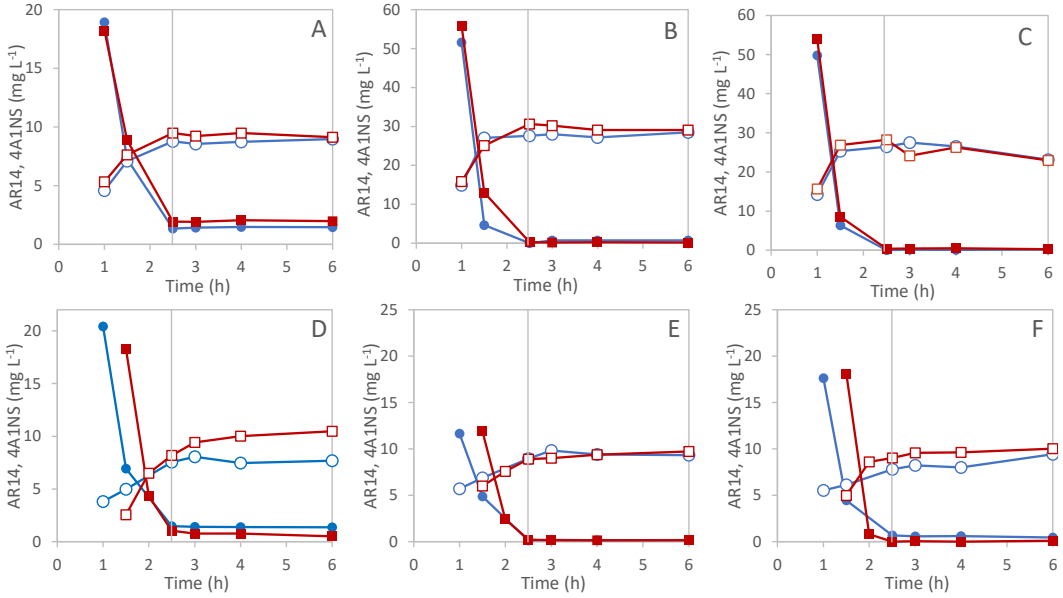


**Figure V.5** - Concentration profiles of the azo dye Acid Red 14 (AR14; filled markers) and the aromatic amine 4-amino-naphthalene-1-sulfonic acid (4A1NS; open markers) along the reaction phases in SBR1 (● and ○) and in SBR2 (■ and □), registered in periods A-F (Table V.1). Vertical lines represent the end of the anaerobic phase, upon the aeration onset.

## V.4.4. Microbial community dynamics

As a preliminary assessment of the differences in the microbial community between the two SBRs, namely upon the changes imposed in their feed composition, FISH analysis was conducted in biomass samples harvested from SBR1 and SBR2 on days 0, 152, 175, 250, 288 and 307 of this experimental run (Figure V.6). The differences regarding the sample from day 0 reflect the distinct inocula used, as SBR1 and SBR2 were seeded with the stored biomass previously developed in the respective SBRs (Chapter IV). Specifically, in addition to *Alphaproteobacteria* and *Actinobacteria*, which were the most abundant groups in both SBR inocula, *Gammaproteobacteria* was also in significant amounts in SBR1. Yet, the microbial communities converged to a similar pattern, *Alphaproteobacteria* becoming dominant in both SBRs at the end of period A (day 152). In fact, as opposed to the previous operation (Chapter IV), the introduction of a mixed anaerobic phase in SBR2 after the plug-flow fill approximated the operational conditions of SBR2 to those of SBR1, their microbial communities becoming more similar in terms of the relative abundance of major bacterial groups.

After the application of azo dye and COD shock loads (days 175 and 250), *Gammaproteobacteria* restored its position among the dominant groups in SBR1 microbial community (Figure V.6). In contrast, the microbial distribution profile among the major groups here analyzed remained practically unaltered in SBR2 during the same period. However, a drastic change in both SBR microbial communities was observed in periods E and F (days 288 and 307, respectively) due to the switch from a starch-based carbon source to acetate. Specifically, this change in the feed composition promoted the dominance of *Gammaproteobacteria*. The previously described sharp decrease in the decolorization efficiency in SBR1 during period F was possibly related to the selection of specific communities

within the *Gammaproteobacteria* major group in this reactor. In fact, a change in the bacteria morphology was observed in SBR1 on day 307, suggesting the emergence of a new community within the *Gammaproteobacteria* group, as opposed to SBR2, where the decolorization performance was not affected. Nonetheless, both SBRs presented some deterioration in the granule settleability and structural stability at the end of the operation (section V.4.1), concomitantly with an unbalanced culture that largely consisted of *Gammaproteobacteria* populations. In this context, the lack of diversity within the microbial community could be associated with granular structure fragility.

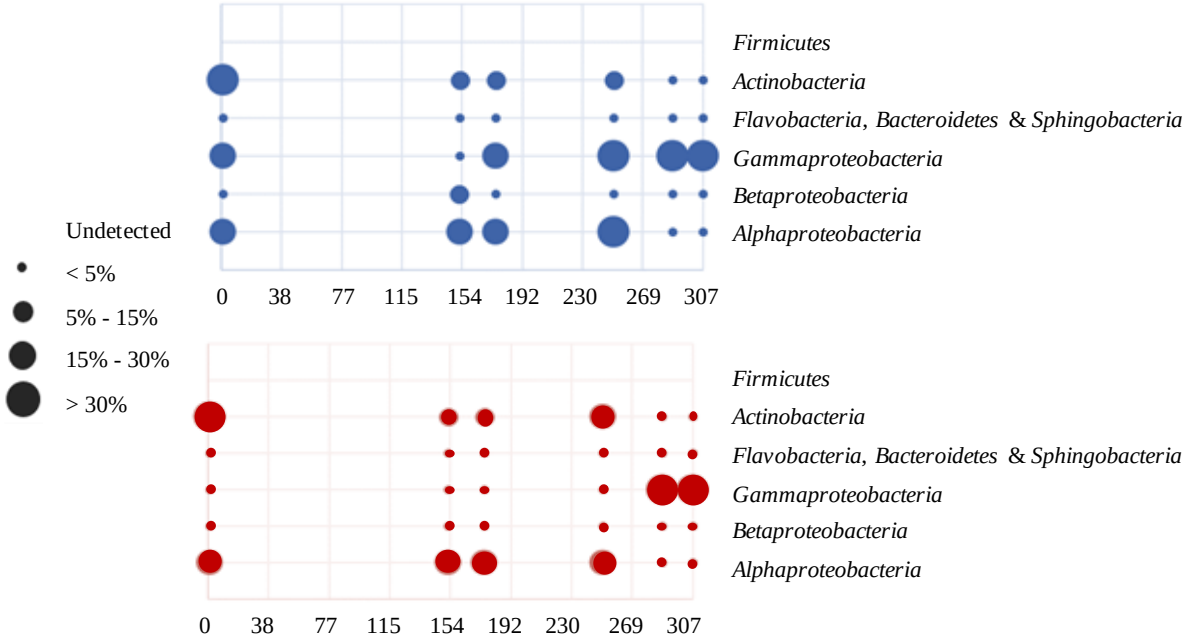


**Figure V.6** - Abundance of the selected *Bacteria* detected by FISH analysis in the mixed microbial culture samples collected on the indicated operational days from the sequencing batch reactors SBR1 (blue circles) and SBR2 (red circles). Adapted from Carvalho (2016).

As noted before, the bacterial community in each SBR on day 1 resulted from a 2.5-month storage period of the biomass previously operated in the respective SBR. Although having in common the same major phyla (*Bacteroidetes*, *Proteobacteria*, *Actinobacteria* and *Saccharibacter*; Figure V.S3, in Appendix C), classes (*Sphingobacteriia*, *Alphaproteobacteria* and *Flavobacteriia*; Figure V.7) and dominant OTUs (belonging to *Niabella* and *Chryseobacterium* genera; Figure V.S4, in Appendix C), the initial microbial communities were significantly different between the two SBRs (Figure V.S4, in Appendix C). Subsequently, operation under different hydrodynamic regimens further differentiated the communities from each SBR after 152 days. Specifically, SBR1 was mostly dominated by members of the *Niabella* (29%) and *Chryseobacterium* (11%) genera (Figure V.S4, in Appendix C), similarly to a previous operation under the same conditions (section IV.4.3). *Chryseobacterium* is reported to be a recurrent genus in AGS systems and hypothesized to contribute to the formation of EPS matrices that support microcolonies of slow-growing bacterial populations, known to benefit the stability of AG (Winkler *et al*., 2018).

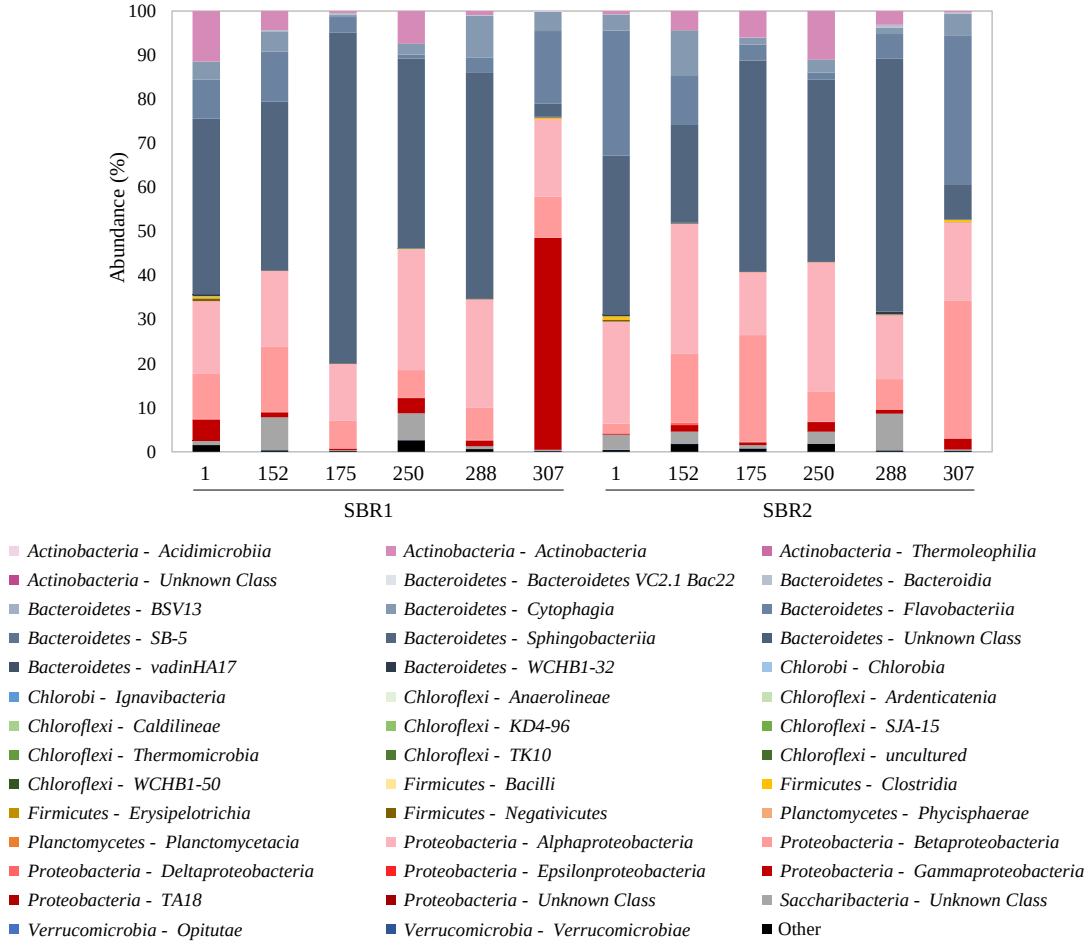


**Figure V.7 -** Composition of bacterial communities at the class level in the sequencing batch reactors SBR1 and SBR2 on the indicated operational days, obtained by 16S rRNA gene sequencing analysis. The most representative "Phylum-Class" are listed below the chart.

On the other hand, SBR2 presented a more homogeneous bacterial distribution, with groups of bacteria belonging to the *Hyphomicrobiaceae* family, *Spirosoma* genus and *Defluviicoccus* representing approximately 12%, 10%, 9% of the bacterial community (Figure V.S4, in Appendix C). In AGS systems, denitrifying PAO and denitrifying GAO, which consume internal storage polymers such as PHA in order to reduce nitrite or nitrate, have generally been reported to belong to six families, among which the *Hyphomicrobiaceae* family (Weissbrodt *et al*., 2013). In addition, *Defluviicoccus vanus*-related GAO were previously registered in an AGS SBR treating the AR14-laden synthetic TWW (Franca *et al*., 2015). The higher abundance of GAO and PAO in the anaerobic plug-flow fed SBR is in accordance with Pronk *et al*. (2015a), who highlighted the importance of the anaerobic feeding through the sludge bed for AG stability. Specifically, in addition to slow-growing bacteria (nitrifying, Anammox), which slowly convert the substrate during the aerobic period, PAO and GAO also promote the formation and stabilization of AGS (de Kreuk and van Loosdrecht, 2004) by anaerobically uptaking easily biodegradable substrates, prior to the aerobic phase (Pronk *et al*., 2015a). Overall, the selection of these microorganisms through the application of an effective feast-

famine regimen decreases the overall microbial maximum growth rate, thus stabilizing AG (de Sousa Rollemberg *et al*., 2018).

The organic and azo dye shock loads led to a major increase in *Bacteroidetes* (specifically, from the *Sphingobacteriia* class) relative abundance, especially in SBR1 (Figure V.7 and Figure V.S3, in Appendix C), where members of the *Niabella* genus constituted 73% of the community on day 175 (Figure V.S4, in Appendix C). *Niabella* was reported to be among the most abundant genera in an AGS SBR system fed with a synthetic municipal wastewater, irrespective of the presence of a specific antibiotic (Kang *et al.*, 2018). In addition, this genus was observed in equivalent relative abundances both in CAS and AGS used to treat *p*-chloroaniline wastewater (Dong *et al.*, 2017). In contrast, despite being also dominant in SBR2, this specific *Niabella* group represented only 24% of the community on day 175, with other bacteria belonging to *Chitinophagaceae* family and to the *Acidovorax* genus being present in 19% and 12% of relative abundance, respectively (Figure V.S4, in Appendix C). Bacterial strains *Acidovorax* sp. and *Sphingobium* sp. were isolated from dibutyl phosphite-degrading AG (Reddy *et al.*, 2014), denoting their potential for removing recalcitrant organic compounds. *Chitinophagaceae* bacteria have also been reported as dominant in AGS systems, being suggested to play an important role in degrading organics at low salinity (Zhang *et al*., 2018b), as well as characterized as a part of the denitrifying consortia (Song *et al*., 2018).

Approximately 1 month after the application of the shock loads, a more diverse bacterial community was re-established in SBR1. Consequently, the microbial community became relatively similar between the SBRs on day 250 (Figure V.7, Figure V.S3 and Figure V.S4, in Appendix C), both being mainly constituted by the bacteria from the *Niabella* genus (32-35% of relative abundance), SBR1 and SBR2 also promoting the development of bacteria from the *Amaricoccus* genus and *Hyphomicrobiaceae* family, respectively (Figure V.S4, in Appendix C), the latter being suggested to be primarily responsible for forming and maintaining the granule structure (Bin *et al.*, 2011; Jiang *et al.*, 2019).

Upon the gradual change in the carbon source type, from a hydrolyzed starch-base to acetate, a drastic shift was observed in both SBR microbial communities, especially on day 307, when 100% acetate was employed. Specifically, this variation in the substrate caused a major decrease in *Sphingobacteriia* relative abundance, the *Flavobacteria* class becoming the dominant one within the *Bacteroidetes* phylum (Figure V.7). Alongside these changes, the *Proteobacteria* phylum also increased its relative abundance, owing to a significant rise in *Gammaproteobacteria* and *Betaproteobacteria* relative abundances in SBR1 and SBR2, respectively (Figure V.7). In addition, *Actinobacteria* and *Saccharibacteria* almost disappeared from the SBRs (Figure V.S3, in Appendix C). Under the new feed conditions, instead of *Niabella*, the main bacteria present in SBR1 and SBR2 belonged to *Plasticicumulans* (48%) and *Acidovorax* (22%) genera, respectively, with bacteria populations from

*Rhizobium* genus, *Flavobacteriaceae* family and *Chryseobacterium* genus also playing a major role (Figure V.S4, in Appendix C). In addition, the presence of bacteria from the *Cloacibacterium* genus in SBR2 in more than 10% of relative abundance was also noticeable on day 307, corresponding to the third most abundant OTU. This genus has been recently observed as a relevant part of the microbial community in an AGS SBR fed with a synthetic wastewater, sodium acetate being the main carbon source (Fan *et al*., 2018b). A previous study reported that *Plasticicumulans acidivorans* was the dominant bacterial species and the main PHA producer in the microbial community in an SBR treating paper mill wastewater, its abundance being largely dependent on the fraction of VFA in the wastewater (Jiang *et al*., 2012). In addition, another study highlighted *Acidovorax* as a dominant genus in mature AG cultivated with a synthetic wastewater comprising glucose and sodium acetate as carbon sources (Wang *et al*., 2018a).

## V.5. Conclusions

The effects of the feeding strategy and feed composition on the stability of AGS in the treatment of TWW were assessed in two non-tubular SBRs, a statically fed, anaerobic-aerobic SBR (SBR1), and an anaerobic plug-flow fed, anaerobic-aerobic SBR **(**SBR2), the latter allowing the biomass to more thoroughly contact with the feed during the fill stage. Overall, high color and COD removal levels were attained in both SBRs. However, dye and COD shock loads had a negative effect on AG integrity and further aerobic bioconversion of the amine metabolite was not observed. COD uptake was minimal in the plug-flow feeding stage of SBR2, but the fraction of COD removed anaerobically was generally higher than in SBR1. Despite being similar, the microbial community in SBR2 was more stable throughout the operational periods when Emsize was used as carbon source, *Alphaproteobacteria* and *Actinobacteria* being the dominant groups. The change from this hydrolyzed starch-based to the acetate-based feed resulted in AGS settleability deterioration in both SBRs and a major shift in their microbial communities as *Gammaproteobacteria* became predominant. After adaptation to the new substrate, lower SVI values were attained in SBR2 and decolorization yields during its plug-flow feeding period improved, revealing a higher capacity of SBR2 to deal with substrate-related variations.

# VI. Comparing hydrodynamic regimens in TWW treatment with AGS: granulation, stability and reactivation

The information included in this chapter was partially published in:

Franca, R.D.G., Sousa, S., Rodrigues, A.M., Pinheiro, H.M., Lourenço, N.D., 2018. Comparing hydrodynamic regimens in textile wastewater treatment with AGS: granulation, stability and reactivation. *IWA Biofilms: Granular Sludge Conference*, 18-21 March, Delft, The Netherlands.

## VI.1. Abstract

Aiming to optimize the AGS SBR performance in the treatment of azo dye-laden TWW, two hydrodynamic regimens (statically fed, anaerobic-aerobic SBR1 *vs* anaerobic plug-flow fed, anaerobic-aerobic SBR2) were compared regarding AGS quality and treatment performance during granulation, long-term operation and reactivation after an idle period. This was assessed in two experimental runs, the first (run I, 404 days) focusing on optimization of cycle conditions during the anaerobic phase, and the second (run II, 434 days) on the system capacity to deal with changes in the feed composition, including the addition of AgNP, an azo dye (AR14) shock load, or supplementation with a nitrate salt. Aerobic granulation was successfully achieved in both reactors along 2 months of operation, the size of the dense, well-settling AG (< 1 mm) being likely limited by the mechanical stirring-associated shear stress. While calcium nitrate supplementation promoted the formation of larger AG containing mineral precipitates, the presence of AgNP did not negatively affect the granulation process or AGS stability in the long-term. Comparing to SBR1, the plug-flow feeding regimen and the 30-min shorter mechanical stirring phase in SBR2 allowed it to maintain stabler AGS and higher biomass concentrations during a longer period of operation, as well as to more efficiently recover from an 18-day biomass storage period (at 4ºC) and from the azo dye shock load. Irrespective of the feeding strategy used, 80% of COD removal yield was reached after 2 weeks of operation and maintained along the experimental runs, with maximal anaerobic COD removal (around 60%) being achieved sooner in SBR1, but sustained for a longer period in SBR2. High color removal levels (80%), via AR14 anaerobic reduction, were reached in SBR1 and SBR2 (when the anaerobic stirred phase was increased to 1h) after one week of operation, and sustained in the long-term operation irrespective of the presence of AgNP, higher dye concentrations or nitrate. The COD and color removal recovery time after a 40-day idle period at room temperature (10 and 17 days in SBR1 and SBR2, respectively) and after the 18-day storage period at 4ºC (0-1 day) was similar in the two SBRs, and the treatment performance was not affected by the presence of AgNP. In addition, although the presence of nitrate did not significantly affect the decolorization performance (simultaneous azo dye reduction and denitrification occurred in both SBRs) in the long-term operation, it initially altered the anaerobic fate of one of the aromatic amines resulting from the azo dye reduction (4A1NS). Overall, complete bioconversion of 4A1NS was registered after 24-56 days of operation in both SBRs and resisted the 18-day biomass storage period. The ability to aerobically transform this aromatic amine was sensitive to drastic operational changes, prolonged lack or excess of aeration leading to the irreversible or reversible interruption of the 4A1NS conversion, respectively. Overall, although SBR2 was able to sustain 4A1NS complete conversion for a longer period than SBR1 (*ca*., 300 *vs* 190 days), namely during the AR14 shock load, SBR1 presented a more effective 4A1NS conversion performance with significant impacts. In fact, interconversion between 4A1NS and an unknown metabolite was

temporarily observed in SBR2, producing less significant effects in the effluent UV spectrum, and suggesting relevant changes at the metabolic or microbial community level.

## VI.2. Introduction

As water resources become scarce, textile industry further stands out as a source of water pollution worldwide. This industry generates large volumes of wastewaters containing high organic loads and recalcitrant dyes, mainly azo dyes which are resistant to conventional wastewater treatment processes and can potentially produce toxic aromatic amines (O'Neill *et al*., 1999). The ability of bacteria to anaerobically decolorize azo dyes and to aerobically mineralize some of the resulting aromatic amines motivated the application of anaerobic-aerobic SBRs to the treatment of TWW (van der Zee and Villaverde, 2005). When compared to CAS processes, the AGS SBR technology (de Kreuk and van Loosdrecht, 2004) presented improvements regarding effluent quality, energy savings and footprint requirements (Pronk *et al*., 2015b). Given the AGS capacity to withstand high organic loads and toxic compounds, recent studies have supported the potential application of this technology to the treatment of dye-laden TWW (Franca *et al*., 2015). Yet, AGS long-term stability is a challenging issue that needs further investigation (Lee *et al*., 2010; Franca *et al*., 2018).

Overall, a key factor to keep biofilm stability is related with microbial selection leading to lower growth rates through the entire granule in the aerobic reaction phase (de Kreuk and van Loosdrecht, 2004). In this sense the use of a plug-flow feeding through the sludge bed has been proposed for allowing the biomass to contact with higher concentrations of substrate, thus enabling soluble, easily biodegradable substrates to penetrate the entire AG depth under anaerobic conditions. As a consequence, this operational strategy promotes the selection of heterotrophic microorganisms able to anaerobically convert easily biodegradable substrates to slowly biodegradable storage polymers (such as PAO and GAO), based on which these microorganisms grow at low rates during the subsequent aerobic phase, thus stabilizing the AG (Bassin *et al*., 2012b; Pronk *et al*., 2015a). Accordingly, Yuan *et al.* (2019) recently showed that while the anaerobic plug-flow feeding mode promoted the formation of compact AGS and high nitrogen removal, the aerobic feeding mode led to a loose AGS structure with a vulnerable anaerobic core and poor nitrogen removal efficiency.

On the other hand, another recent study highlighted the need for developing new operational strategies to maintain AGS long-term stability and to facilitate the retrofitting of existing WWTPs excluding the need for a plug-flow distribution system for the influent wastewater (Sguanci *et al.*, 2019). Furthermore, Rocktäschel *et al*. (2013) highlighted that the use of anaerobic mixed conditions after feeding is particularly relevant in terms of full-scale application, due to the difficulty in achieving conditions approaching plug-flow at this scale, where the reactor H/D is typically low. Accordingly, Sguanci *et al.* (2019) indicated that the presence of a readily biodegradable source of carbon during

the aerobic phase and consequent stimulation of flocculent biomass resulted from the formation of preferential channels during the preceding anaerobic plug-flow feeding and consequent inefficient COD uptake. Moreover, Awang and Shaaban (2016) suggested that the long granulation periods observed in pilot and full-scale reactors (Li *et al*., 2014; Pronk *et al*., 2015b) are due to the low reactor H/D. Yet, although a high H/D is generally a major criteria for ensuring successful granulation, shorter start-up times and more active AGS, low H/D reactors have been preferred in real site applications (*e.g*., AGS full-scale application in Gansbaai WWTP, South Africa; H/D of 0.39; Awang and Shaaban, 2016). In fact, under variable OLR and biomass floating events, reactors with a low H/D have been shown to exhibit a more efficient performance, as well as a lower biomass production compared with high H/D reactors, which is associated with reduced costs (Awang and Shaaban, 2016).

Aiming at long-term AGS stability without the use of a plug-flow feeding, Sguanci *et al.* (2019) adjusted the duration of an anaerobic mixed phase applied after the anaerobic feeding phase in order to maximize the anaerobic biodegradable COD uptake by PAO and/or GAO, thus preventing the competition with aerobic heterotrophic biomass and floc formation. The authors showed that the applied metabolic selective pressure based on the complete biodegradable COD uptake under anaerobic conditions (45-90 min of anaerobic mixing by nitrogen gas recirculation, after 15 min of feeding) was able to minimize flocculent sludge formation (down to 5%), while stimulating the formation of stable and large AG (average size of 1.5 mm) with excellent COD and phosphorus removal efficiencies along 175 days of operation. On the other hand, Kang and Yuan (2019) considered that the use of an anaerobic feeding at high flow-rates should be enough to provide hydrodynamic turbulence and to allow an equal substrate distribution in full-scale reactors, benefiting anaerobic COD uptake and nutrient removal, while being cost-effective as compared to a fast anaerobic feeding followed by mechanical mixing in large-scale SBRs.

Rocktäschel *et al*. (2013) showed that stable aerobic granulation could be achieved with either a fast influent phase followed by anaerobic mixing or an anaerobic plug-flow regimen, the latter's efficiency depending on using a relatively high reactor H/D. Furthermore, these authors indicated that the use of anaerobic mixing was advantageous when compared to the plug-flow regimen because, despite the lower biomass concentrations achieved in the former, AG growth was more stable and nitrogen removal rates were higher (Rocktäschel *et al*., 2013). Overall, while an anaerobic plug-flow feeding followed by aerobic reaction has been linked to improved AGS stability in tubular SBRs (de Kreuk and van Loosdrecht, 2004; Pronk *et al*., 2015a), using an anaerobic stirred phase after feeding might improve anaerobic substrate uptake and, consequently, AGS stability in non-tubular reactors (Rocktäschel *et al*., 2013). Specifically for a TWW feed, plug-flow feeding was associated with a higher AGS capacity to withstand shock loads and changes in wastewater composition, when compared to a control anaerobic-aerobic SBR (Franca *et al*., 2017). Here, the performance of two synthetic TWW-fed AGS SBRs using different hydrodynamic regimens (statically fed, anaerobic-

aerobic SBR1 *vs* anaerobic plug-flow fed, anaerobic-aerobic SBR2) are further compared regarding AG formation and stability during long-term operation, as well as during reactivation after an idle period. These factors were assessed in two experimental runs, the first (run I) focusing on optimization of cycle conditions, namely regarding the anaerobic phase, and the second (run II) on the system capacity to deal with changes in the feed composition, including the addition of AgNP, a dye shock load, or supplementation with nitrate. Specifically, although nitrate is a common compound in TWWs, reports on its effect on the reductive biodecolorization of azo dyes have been contradictory (Carliell *et al.*, 1998; Pearce *et al*., 2006). In addition, the increasing occurrence of AgNP (a finishing additive used in textiles as anti-microbial agent) in TWW has raised some concerns regarding their possible negative impacts during and after biotreatment.

## VI.3. Materials and methods

### VI.3.1. Chemicals

The carbon source (Emsize E1) and the azo dye (AR14) stock solutions were prepared as described in sections III.3.1.1 and IV.3.1., respectively. The synthetic TWW used as feed solution was prepared as described in section III.3.1.2, with the addition of the azo dye to a concentration of 40 mg AR14 $L^{-1}$.

Silver nanopowder (<100 nm particle size; polyvinylpyrrolidone, PVP, as dispersant) was purchased from Sigma-Aldrich. An AgNP suspension of 100 mg $L^{-1}$ was prepared in MiliQ-water and subjected to 30 min of ultrasonication in 5-min ON/1-min OFF pulses (100 W) using an ultrasonic homogenizer (Sonopuls HD 3200, Bandelin).

### VI.3.2. SBR setup and operation

Two non-tubular 1.5-L anaerobic-aerobic SBRs (H/D=2.5; SBR1 and SBR2) were operated in two experimental runs (I - 404 days and II - 434 days) after being inoculated with CAS harvested from a domestic WWTP (Chelas, Portugal). Both SBRs were operated in 6-h cycles, including 30-min static anaerobic feeding (SBR1) or 1.5-h plug-flow feeding (SBR2), followed by 1.5-h (SBR1) or 30-60 min (SBR2; see Table VI.1) stirred anaerobic phase, 3.5-h aeration, 5-60 min of settling (decreased from 60 to 5 min over the first 28 days of operation to promote granulation and maintained at 5 min thereafter; see Table VI.1), 1-min drain and idle. The synthetic TWW was supplied to the SBRs at a 12-h HRT and a 2.0-kg COD $m^{-3}$ $d^{-1}$ OLR, under static and anaerobic conditions using two different feeding strategies: SBR1 was fed at a peripheral site at the bottom, the feed rapidly channeling above the settled biomass with no relevant contact between them, and SBR2 was plug-flow fed from the bottom, allowing the feed to distribute and rise through the sludge bed (Figure VI.1).

Granulation, stability and reactivation performances were accessed in both experimental runs: the first one (run I) focused on cycle conditions and comprised 7 experimental periods (I.A to I.G; Table VI.1);

the second one (run II) focused on the feed composition and was divided in 10 experimental periods (II.A to II.J; Table VI.1). Accordingly, the time length of the SBR2 stirred anaerobic phase was adjusted along experimental run I (increased from 30 min to 40, 45 and 60 min on days 237, 259 and 384, respectively), and some changes in the feed composition of both SBRs were introduced during experimental run II, namely addition of AgNP (up to day 246 the AgNP stock suspension was added at the top of the SBRs for 15 min during the filling period, to a concentration of 20 mg AgNP $L^{-1}$ in the overall feed), three-fold increase in the dye concentration (from 40 to 120 mg AR14 $L^{-1}$ on period II.F), or supplementation with nitrate (60 or 120 mg $NO_3^-$ $L^{-1}$ from $Ca(NO_3)_2$ on periods II.H and II.I, respectively, and 120 mg $NO_3^-$ $L^{-1}$ from $KNO_3$ on period II.J), as described in Table VI.1. Both experimental runs included an idle period (I.E and II.C, Table VI.1), when the biomass was stored at room temperature (period I.E) or at 4ºC (period II.C), after which it was used to re-inoculate the respective SBR to evaluate the reactivation performance.

**Table VI.1** - Overview of the operational conditions imposed in the sequencing batch reactors (SBRs) during experimental runs I and II. Cycle conditions were adjusted regarding the duration of the settling stage in both SBRs (Settling) and the stirred anaerobic phase in SBR2 (Mix SBR2). Along periods I.A and II.A the settling time was reduced from 60 to 5 min in 2-20 min steps (60, 40, 30, 20, 15, 10, 7 and 5 min of settling imposed on the operational days 1, 3, 7, 10, 14, 17, 24 and 28, respectively). Variations to the synthetic textile wastewater composition (Feed composition) were introduced in both reactors regarding the addition of silver nanoparticles (AgNP), variations in the azo dye (AR14) concentration, and supplementation with nitrate ($NO_3^-$) from calcium nitrate or potassium nitrate (Salt). The experimental periods I.E and II.C correspond to periods when the reactors operation was interrupted and the biomass was stored at room temperature and at 4ºC, respectively.

| Run | Period | | | Cycle conditions | | Feed composition | | |
|---|---|---|---|---|---|---|---|---|
| | Name | Operating days | Duration (days) | Settling (min) | Mix SBR2 (min) | AgNP (mg $L^{-1}$) | AR14 (mg $L^{-1}$) | $NO_3^-$ (mg $L^{-1}$) − Salt |
| I | I.A | 1-28 | 28 | 60 to 5 | 30 | - | 40 | - |
| | I.B | 29-236 | 208 | 5 | | | | |
| | I.C | 237-258 | 22 | | 40 | | | |
| | I.D | 259-281 | 23 | | 45 | | | |
| | I.E | 282-321 | 40 | | | | | |
| | I.F | 322-383 | 62 | 5 | 45 | - | 40 | - |
| | I.G | 384-404 | 21 | | 60 | | | |
| II | II.A | 1-28 | 28 | 60 to 5 | 60 | 20 | 40 | - |
| | II.B | 29-192 | 164 | 5 | | | | |
| | II.C | 193-210 | 18 | | | | | |
| | II.D | 211-246 | 36 | 5 | 60 | 20 | 40 | - |
| | II.E | 247-328 | 82 | | | | | |
| | II.F | 329-344 | 16 | | | | 120 | |
| | II.G | 345-356 | 12 | | | - | 40 | |
| | II.H | 357-363 | 7 | | | | | 60 − $Ca(NO_3)_2$ |
| | II.I | 364-415 | 52 | | | | | 120 − $Ca(NO_3)_2$ |
| | II.J | 416-434 | 19 | | | | | 120 − $KNO_3$ |

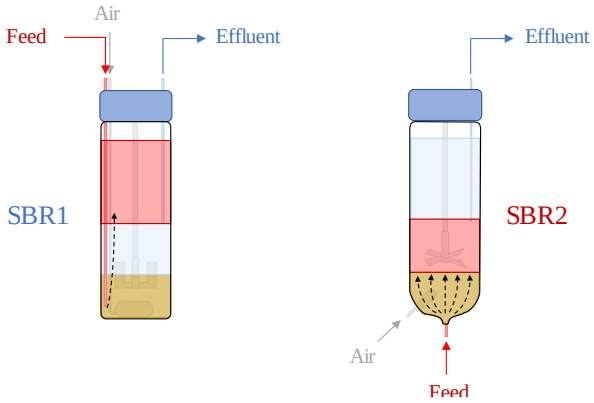


**Figure VI.1 -** Representation of the sequencing batch reactors (SBRs) used to compare different hydrodynamic regimens. SBR1 had a static feeding (30 min) and a mixed anaerobic reaction (1.5 h; anchor-like impeller) followed by aeration (3.5 h), whereas SBR2 had an anaerobic plug-flow feeding stage through the granular sludge bed (1.5 h), followed by a stirred anaerobic reaction (30-60 min, axial impeller with 4 flat, inclined blades) and an aeration stage (3.5 h). The reaction phase was followed by 5-min settling and 1-min drain. The dashed arrows represent the feed flow pattern in each SBR.

## VI.3.3. Analytical methods

TSS, VSS, SVI, biomass morphological analysis, COD, UV-visible absorbance spectra, dye degradation and metabolite formation were determined as described in section III.3.3.1. Color removal was followed as described in section IV.3.3. Nitrate concentration in SBR mixed liquor samples clarified by centrifugation was followed through HPLC (same HPLC conditions as described in section III.3.3.1) using a calibration curve obtained with standard nitrate solutions, as well as colorimetrically determined for specific cycles using a Hach Lange DR3900 VIS spectrophotometer (kits LCK-339 and LCK-34; Hach, Germany). In addition, nitrate and nitrite concentrations were measured along a selected cycle through ion chromatography (Laboratório de Análises do Instituto Superior Técnico, Portugal), according to standard procedures (APHA, 1995).

The proportion of large granules (sizes above 0.65 mm), small granules (sizes within the 0.20-0.65 mm range) and flocs (sizes under 0.20 mm) in the SBRs was estimated by sieving mixed liquor samples through 0.65-mm and 0.20-mm net sieves, and determining the biomass content in each collected fraction using the TSS analysis protocol. AG, selected by 0.65-mm sieving of biomass samples harvested from the bioreactors, were analyzed using a magnifying lens (Stemi 2000-C, Zeiss) fitted with a digital camera and respective software (Moticam 2, Motic). AG were also collected by 0.20-mm sieving of biomass samples harvested from the SBRs and ressuspended in the synthetic TWW medium (without the azo dye) to be analyzed by nuclear microscopy after further sample preparation. Specifically, AG were manually selected under a magnifying lens, imbedded in tissue-freezing medium OCT™ (Tissue-Tek, Sakura Finetech) and immediately frozen in liquid nitrogen. Granules were then sectioned in slices with a thickness of 18-20 μm at -22°C using a microtome (Cryotome 620E, Thermo Shandon, UK). The sliced sections were dehydrated for 24 h in the microtome cryostat and stored at -80ºC for further elemental distribution imaging using the nuclear microscopy endstage (OM2000, Oxford Microbeam, UK) installed at the Van de Graaff accelerator of

the Centro Tecnológico e Nuclear (Instituto Superior Técnico, Portugal), as described by Bento *et al*. (2017). Data acquisition and analysis was carried out by OMDAQ2007, an Oxford Microbeam proprietary software.

Microbial community analysis was assessed by FISH analysis on selected, homogenized biomass samples using oligonucleotide probes for the core community typically detected in WWTPs, as well as by high throughput DNA sequencing as described in sections III.3.3.2.1 and III.3.3.2.2, respectively.

## VI.4. Results

### VI.4.1. AGS morphology and properties

#### VI.4.1.1. Granule size and settling properties

The composition of the sludge in terms of flocs and granules was assessed through biomass size fractionation. The CAS used to inoculate the reactors in the two experimental runs contained approximately 5% of aggregates with sizes above 0.20 mm (Figure VI.2). The sludge size distribution did not significantly vary along the first month of operation, when the settling time was gradually reduced to allow the selective retention of granules in the SBRs (Figure VI.2). Yet, the fraction of granules in the SBRs increased throughout the long-term operation in both experimental runs.

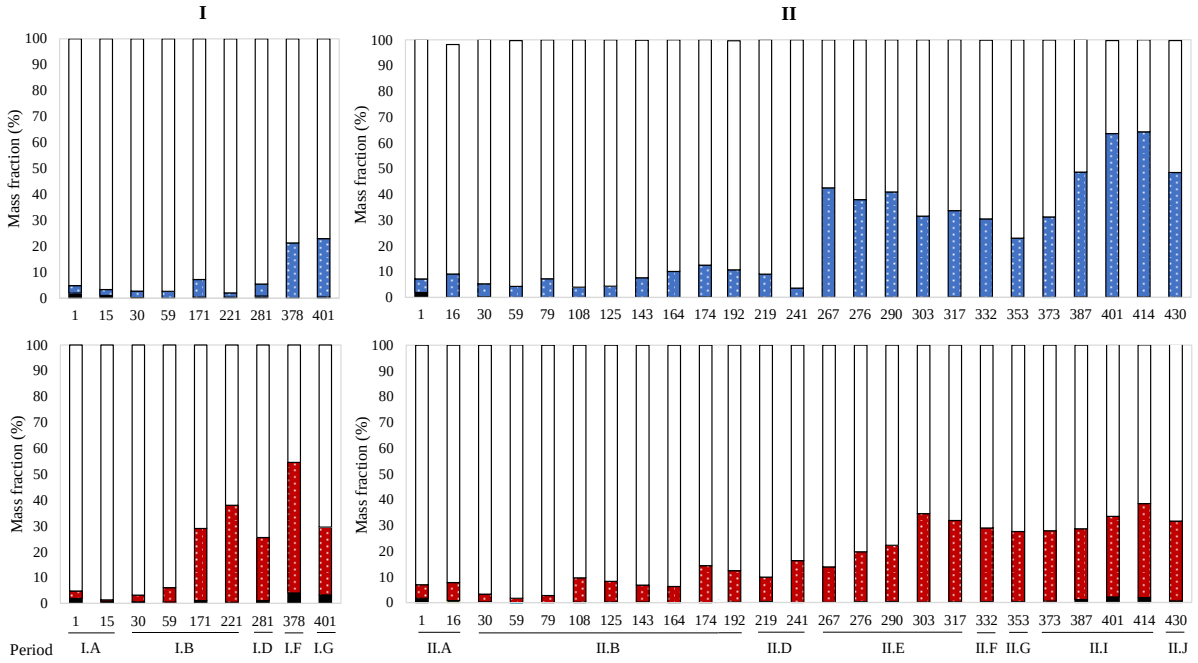


**Figure VI.2** - Distribution of particle sizes in the sequencing batch reactors SBR1 (blue) and SBR2 (red) along the experimental runs I and II. Mass percentage in terms of total suspended solids of flocculent sludge (empty bars; d<0.20 mm), small granules (dotted, colored bars; 0.20<d<0.65 mm) and larger granules (black bars; d>0.65 mm). The operational conditions for each experimental period (I.A-I.G and II.A-II.J) are described in Table VI.1. The analyses correspondent to days 290-430 of experimental run II were performed in duplicate, the respective results presented in this figure corresponding to the calculated average values (relative standard deviations lower than 0.5% for larger granules and lower than 5.7% for small granules and for flocculent sludge).

In the experimental run I, the content of granules in SBR1 was maintained around 5% throughout periods I.A-I.D (Figure VI.2), but increased to 22% upon AGS reactivation after storage. In contrast, SBR2 biomass became enriched in granules (around 30%) at least from day 171 on, representing more than half of the sludge (55% of granules, 4% being larger than 0.65 mm) on day 378 (Figure VI.2), following the storage period (period I.E, days 282-321). The decrease in granular content in SBR2 to approximately 25-30% from day 221 to day 281, as well as from day 378 to 401 can be attributed to the increased shear stress caused by the prolonged SBR2 anaerobic stirred phase imposed on days 237 and 259, as well as on day 384, respectively.

In the experimental run II, when the cycle conditions were equivalent to those applied during the last period of the experimental run I (period I.G, 60-min SBR2 anaerobic stirred phase), SBR1 and SBR2 presented a similar biomass size fractionation profile up to the 18-day idle period (period II.C, days 193-210), maintaining a percentage of granules below 15%. Yet, after biomass reactivation on day 211, while the SBR2 sludge became gradually enriched in granules, stabilizing around 30% from day 303 on, SBR1 presented a sharp increase in the granular content from 4% (day 241) to 43% (day 267) upon interruption of AgNP supplementation. Moreover, this value further increased in SBR1 along the period of high calcium nitrate supplementation (period II.I, days 364-415), leading to a predominance of granules in the sludge (up to 64% registered on days 401 and 414). The subsequent change from calcium nitrate to potassium nitrate supplementation on day 416 (period II.J) led to a decrease in the abundance of granules in both reactors, especially in SBR1. Along this experimental run, the amount of granules with dimensions above 0.65 mm was negligible in SBR1 and represented less than 2% of the sludge in SBR2.

Despite no relevant differences being observed in terms of aggregate size distribution between the inoculum and the SBRs sludge along the first 2 months of operation in both experimental runs (Figure VI.2), the biomass settling properties gradually improved during this period. In fact, the SVI profiles (Figure VI.3) indicated that granulation was achieved in both reactors as the SVI significantly decreased throughout periods I.A and II.A from values above 200 mL $gTSS^{-1}$, typical for CAS, to levels below 80 mL $gTSS^{-1}$, the gap between the $SVI_5$ and $SVI_{30}$ values diminishing alongside these.

Specifically in the experimental run I, even though SBR2 presented higher initial SVI values and a lower SVI decrease rate, $SVI_5$ and $SVI_{30}$ values reached 66 and 42 mL $gTSS^{-1}$ on day 56 (Figure VI.3), respectively, in both reactors. From this point on until the end of period I.B, SBR2 biomass settleability stabilized around 67 and 41 mL $gTSS^{-1}$, as $SVI_5$ and $SVI_{30}$, respectively. Subsequently, these parameters were slightly increased to values just below 100 mL $gTSS^{-1}$ upon the extension of the SBR2 stirred phase in periods I.C and I.D. In contrast, AGS settleability deteriorated in SBR1 after day 140, $SVI_5$ and $SVI_{30}$ increasing to up to 165 and 100 mL $gTSS^{-1}$. The 40-day idle period (period I.E) caused a similar deterioration in terms of biomass settleability in the two reactors. Yet, the SVI

values gradually decreased to levels below 100 mL $gTSS^{-1}$ in both SBRs (Figure VI.3) along the first month of AGS SBR reactivation. Subsequently, the settling properties of the biomass in SBR2 slightly worsened upon the further increase in the anaerobic stirred phase duration from 45 to 60 min, on day 384.

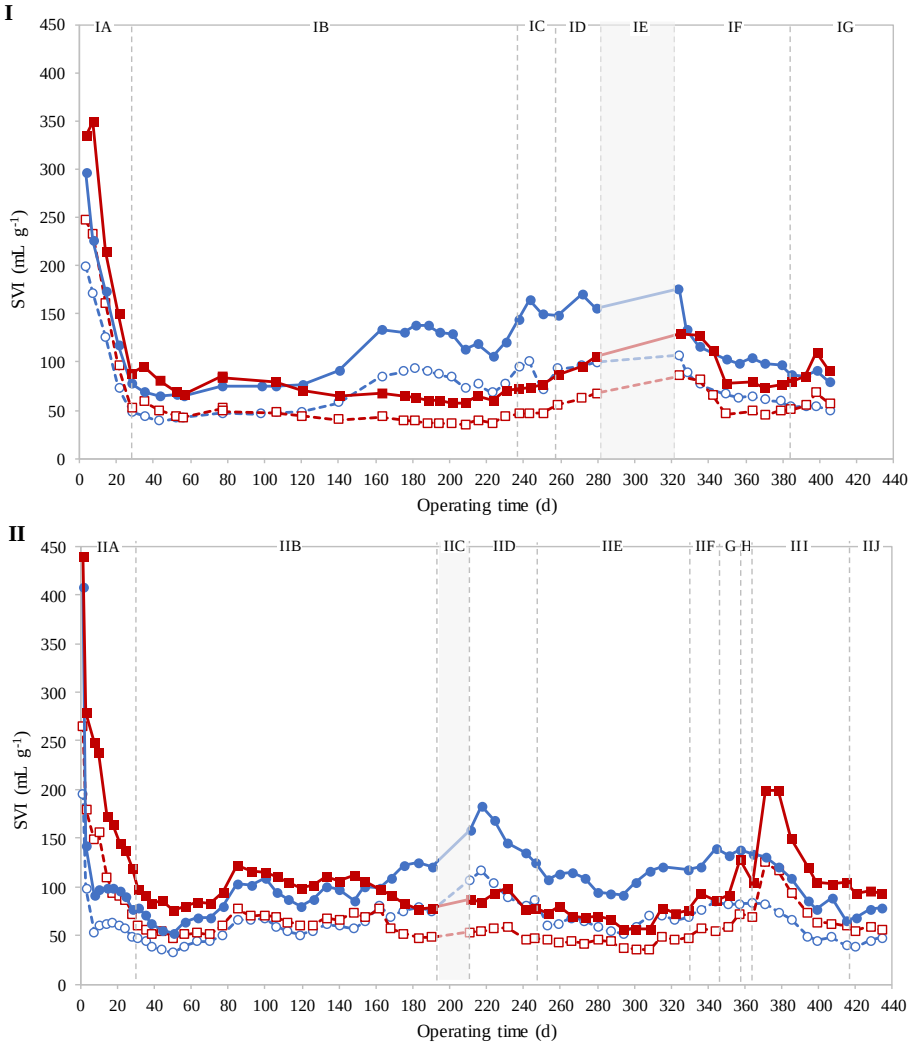


**Figure VI.3** - Sludge volume index (SVI) profile along experimental runs I and II. SVI values measured after 5 min settling ($SVI_5$) in the sequencing batch reactors SBR1 (●) and SBR2 (■), and after 30 min settling ($SVI_{30}$) in SBR1 (○) and SBR2 (□). The operational conditions for each experimental period (I.A-I.G and II.A-II.J) are described in Table VI.1.

Regarding the experimental run II, both reactors reached minimum $SVI_5$ and $SVI_{30}$ values (under 75 and 50 mL $gTSS^{-1}$, respectively; Figure VI.3) around day 50, as a result of the granulation process. Subsequently, alternating periods of settleability deterioration and improvement throughout period II.B ($SVI_5$ and $SVI_{30}$ varied within 33-78 and 53-122 mL $gTSS^{-1}$, respectively) indicated some operational instability in the presence of AgNP. The reactors presented similar behaviors in terms of AGS settleability until day 160, SBR2 evidencing slightly higher values. Yet, significant differences were observed from day 160 on, as SBR1 sludge settling properties further deteriorated and SBR2 recovered low SVI values (Figure VI.3).

In contrast to SBR2, SBR1 suffered sludge settleability deterioration after the 18-day biomass storage at 4ºC in period II.C (Figure VI.3). Similarly to the experimental run I, SVI levels gradually improved in SBR1 upon reactivation (period II.D). Yet, SBR1 did not reach the excellent sludge settling characteristics that SBR2 sustained after reactivation, namely when AgNP addition was stopped (period II.E). Subsequently, the changes introduced in the feed azo dye concentration throughout periods II.F-II.G caused a slight decline in sludge quality. The sharp increase in the SBR2 SVI values from day 364 to 371 was most likely due to an operational problem in the aeration-off control leading to half of the SBR2 biomass being accidentally washed out on day 352. Although this biomass was recovered and transferred back into SBR2, its passage through the drain gear pump apparently irreversibly deteriorated the AGS settleability, therefore affecting the SVI levels and leading to subsequent biomass washout episodes up to day 371. Nevertheless, the biomass settling properties in SBR2 recovered along period II.I, which was mainly attributed to the supplementation of the synthetic TWW with 120 mg $NO_3^-$ $L^{-1}$ from calcium nitrate, as the same SVI trend was observed in SBR1. Finally, switching to potassium nitrate did not cause major changes in the SVI profiles (period II.I).

### VI.4.1.2. AGS morphology

Biomass morphology analysis through light microscopy showed the development of round-shaped, apparently dense AG with a well-defined outline in both SBRs during the first 2 months of experimental runs I and II (Figure VI.4). While Figure VI.4 presents an overview of the largest granules observed in selected samples, Figure VI.S1 and Figure VI.S2 (in Appendix D) depict the complete set of micrographs at magnifications 40 and 100 for experimental runs I and II, respectively. In both experimental runs, filamentous bacteria were not observed after the first week of SBR operation.

The development of granules in SBR2 was similar to that in SBR1 until day 150 of the experimental run I (Figure VI.4, and Figure VI.S1, in Appendix D). Yet, while granules became subsequently smaller in SBR1, new and larger granules continued to form in SBR2 up to the end of period I.D, leading to a higher abundance of small granules and the emergence of larger ones (sizes up to 0.7 mm). After the biomass storage period (period I.E), although SBR1 recovered a higher number of granules, these were not as large as those observed in SBR2, which resisted the storage conditions and further grew to sizes over 0.7 mm. The largest fraction of granules present in SBR2 presented a yellowish color, a clear outline and an irregular shape (Figure VI.5). While most of them looked dense and uniform in terms of structure, few presented a very low density morphology, possibly corresponding to the remaining backbone of a previous “active granule”. In addition, some granules presented crevices, either solely located at the periphery or extending further to the center of the granule, denoting a fragile structure in some of the granules with sizes above 0.65 mm.

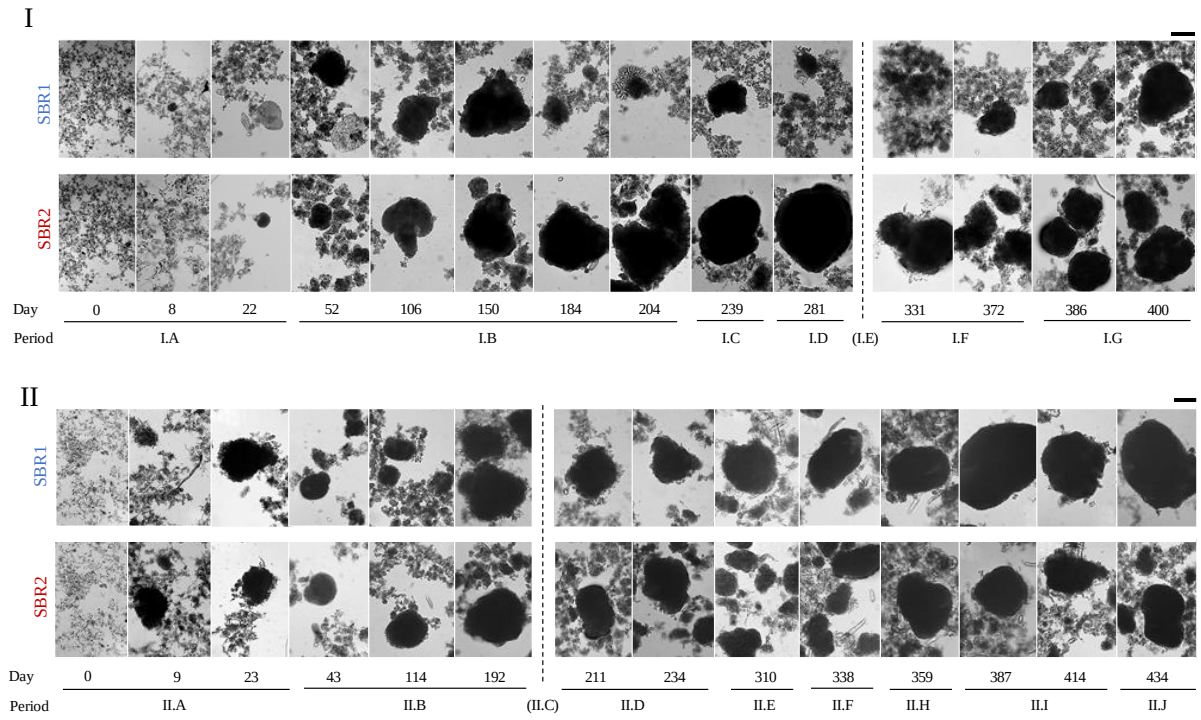


**Figure VI.4** - Morphological development of aerobic granular sludge along the experimental runs I and II. Micrographs, at magnification 100, from biomass samples harvested from the sequencing batch reactors SBR1 and SBR2 on the indicated operational days and periods. The operational conditions for each experimental period (I.A-I.G and II.A-II.J) are described in Table VI.1. Scale bar: 0.2 mm.

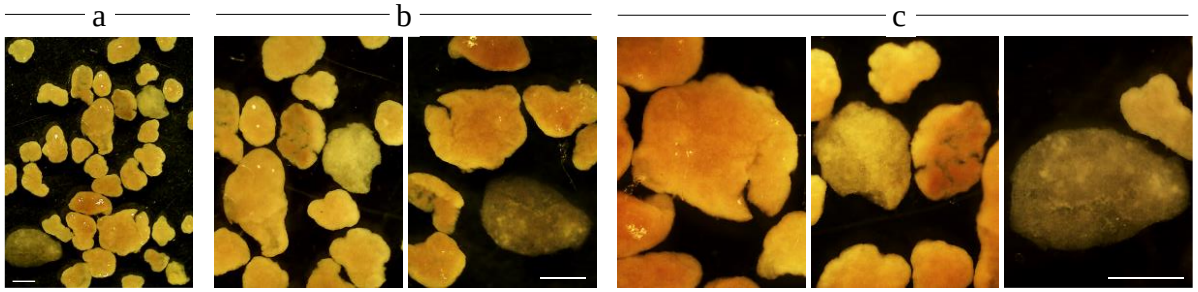


**Figure VI.5** - Morphology of large aerobic granules in the sequencing batch reactor SBR2. Photographs, at magnifying glass using three different amplifications (a, b and c), of aerobic granules harvested and collected by 0.65 mm-sieving from SBR2 at the end of the experimental run I. Scale bar: 1 mm.

Throughout the experimental run II, AG developed at a similar pace in both reactors, presenting comparable morphology changes (Figure VI.4). Not only the presence of AgNP (periods II.A-II.D) did not hinder the AGS formation process, but the subsequent interruption of AgNP addition to the SBRs on day 247 also did not affect AGS morphology (Figure VI.S2, in Appendix D). In fact, dense granules with clear outlines surrounded by clusters of aggregated sludge flocs were generally observed during this experiment, being affected neither by the short idle period (period II.C) nor by the three-fold increase in dye concentration (period II.F). The only exception was during period II.I, when a higher abundance of flocculent sludge was present in SBR2 and granules were rarely observed. This AGS deterioration in SBR2 was likely a consequence of the operational problem registered on day 352, but the reactor was able to recover from this incident with well-defined granules being again

observed after day 410. As a result, SBR1 samples were significantly richer in granules between day 380 and 414 (Figure VI.S2, in Appendix D) than SBR2, the enhanced supplementation with calcium nitrate during period II.I apparently promoting the enlargement of AG in SBR1. The replacement of calcium nitrate with potassium nitrate in the synthetic TWW did not affect AGS morphology in any reactor, as can be seen in Figure VI.4 and Figure VI.S2 (in Appendix D).

### VI.4.1.3. Elemental distribution in AG

AG were harvested through a 0.20-mm sieve from SBR1 and SBR2 on day 408 (period II.I, after 44 days of SBRs feed supplementation with 120 mg $NO_3^-$ $L^{-1}$ from calcium nitrate) and on day 434 (period II.J, after 19 days of SBRs feed supplementation with 120 mg $NO_3^-$ $L^{-1}$ from potassium nitrate) for morphological and elemental distribution analysis through nuclear microscopy. These granules were compared to a control consisting of AG that had not been subjected to any of the nitrate salts (harvested from an SBR equivalent to SBR1 and fed with the synthetic TWW).

Contrarily to the control, granules harvested from SBR1 and SBR2 on day 408 had small mineral inclusions surrounded by biomass, as shown in the respective calcium and phosphorus maps (Figure VI.6-A), these being more consistently observed in SBR1 granules. Subsequently, very large inclusions, with sizes over 20 µm, were observed in most of the granules harvested from SBR1 and SBR2 on day 434 (Figure VI.6-B). These also corresponded to mineral aggregates surrounded by cells, as observed in the respective phosphorus and calcium maps (Figure VI.6-B). Once again, these granular inclusions were not observed in the control granules (Figure VI.6-B). All of the analyzed AG that were harvested from SBR1 on day 434 presented granular inclusions of calcium and phosphorus surrounded by biomass, whereas this phenotype was not so consistently observed in SBR2 granules (Figure VI.6-B). In fact, the SBR2 phosphorus and sulfur maps, which correspond to essential elements of proteins (biological markers), enable the visualization of two AG in the analyzed section, but only the larger one contains the mineral inclusions. In addition, while granules from SBR1 had higher biomass density, SBR2 granules had a jelly-like, less compact appearance on day 434.

Quantitative elemental analysis was performed on the central (core), intermediate and peripheral regions of the AG, as well as on the mineral inclusions, when present, as illustrated in Figure VI.6. Particularly regarding the AG harvested on the last day of experimental run II (day 434), the estimated thickness (mass density) of the lyophilized granule sections varied within the 2-8 µm range, reflecting the differences in the density of granules present in different SBRs. Specifically, SBR1, SBR2 and control granules presented thickness ranges of 3.1-8.0 µm, 2.2-5.7 µm and 2.1-3.0 µm, respectively. The lower values associated with SBR2 granules indicated a relatively more floc-like composition than SBR1's. In addition, the significantly lower thickness of the control granules when compared to those in SBR1 and SBR2 reflects the higher mineral content in the latter.

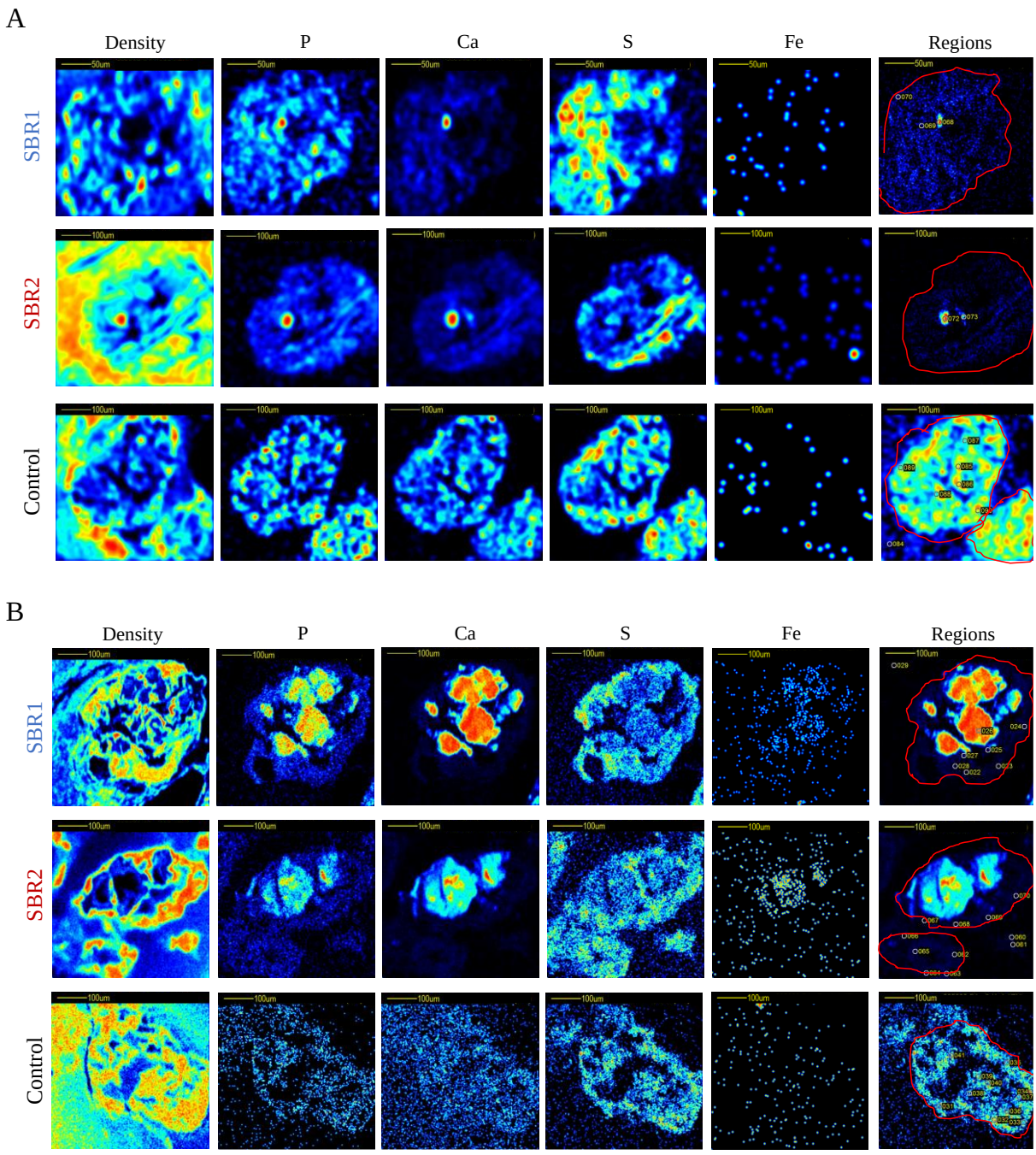


**Figure VI.6 -** Elemental distribution in aerobic granules. Density map and PIXE elemental maps of phosphorus (P), calcium (Ca), sulfur (S) and iron (Fe) of aerobic granules harvested from the sequencing batch reactors SBR1 and SBR2 on days 408 (A) and 434 (B) of experimental run II, as well as from a control SBR not supplemented with nitrate. The respective aerobic granules are delineated and the areas selected for quantitative analysis (central, intermediate and peripheral regions, as well as mineral inclusions) are indicated in the micrograph on the right of each row (Regions).

Results from the quantitative analysis of all elements assessed in areas of the AG outside the observed mineral inclusions are graphically represented in Figure VI.7. The major elements present in these regions of the biomass aggregates were phosphorus, sulfur, potassium, calcium and bromine. The elemental composition of SBR1 granules was similar to that of the control granules, SBR2 generally presenting lower levels of element concentrations, especially on day 408. In addition, the higher

concentration of sulfur in AG from the control in relation to SBR1 and SBR2 (Figure VI.7) indicates the relatively higher amount of organic matter in the former. In fact, as previously mentioned, control granules did not contain the small and large mineral inclusions observed in granules from SBR1 and SBR2 on days 408 and 434, respectively. These inclusions were composed of calcium and phosphorus, as shown in Figure VI.8. In addition, Figure VI.S3 (in Appendix D) reflects the equivalent elemental composition of the mineral inclusions in SBR1 (day 434) and SBR2 (day 408). This elemental distribution is clearly distinct from that of the surrounding regions in the granules, where a similar profile was observed for the center, intermediate and peripheral regions in an SBR2 granule (day 434), being also comparable to that of an SBR1 granule (day 434) in the intermediate zone (Figure VI.S3).

As summarized in Figure VI.9, the concentration of calcium and phosphorus in SBR1 and SBR2 mineral inclusions was significantly higher than in the surrounding regions. As the inclusions became larger from day 408 to day 434, the levels of calcium and phosphorus in SBR1 inclusions increased concomitantly, the calcium-to-phosphorus ratio (Ca/P) remaining constant. In contrast, the concentration of calcium and phosphorus in SBR2 inclusions decreased in the same period. Despite the Ca/P values being slightly higher in SBR2 inclusions than in SBR1's, both presented values close to the Ca/P typical of calcium phosphate, specifically 2.0±0.5 (Ca/P in $Ca_3(PO_4)_2$ = 1.9).

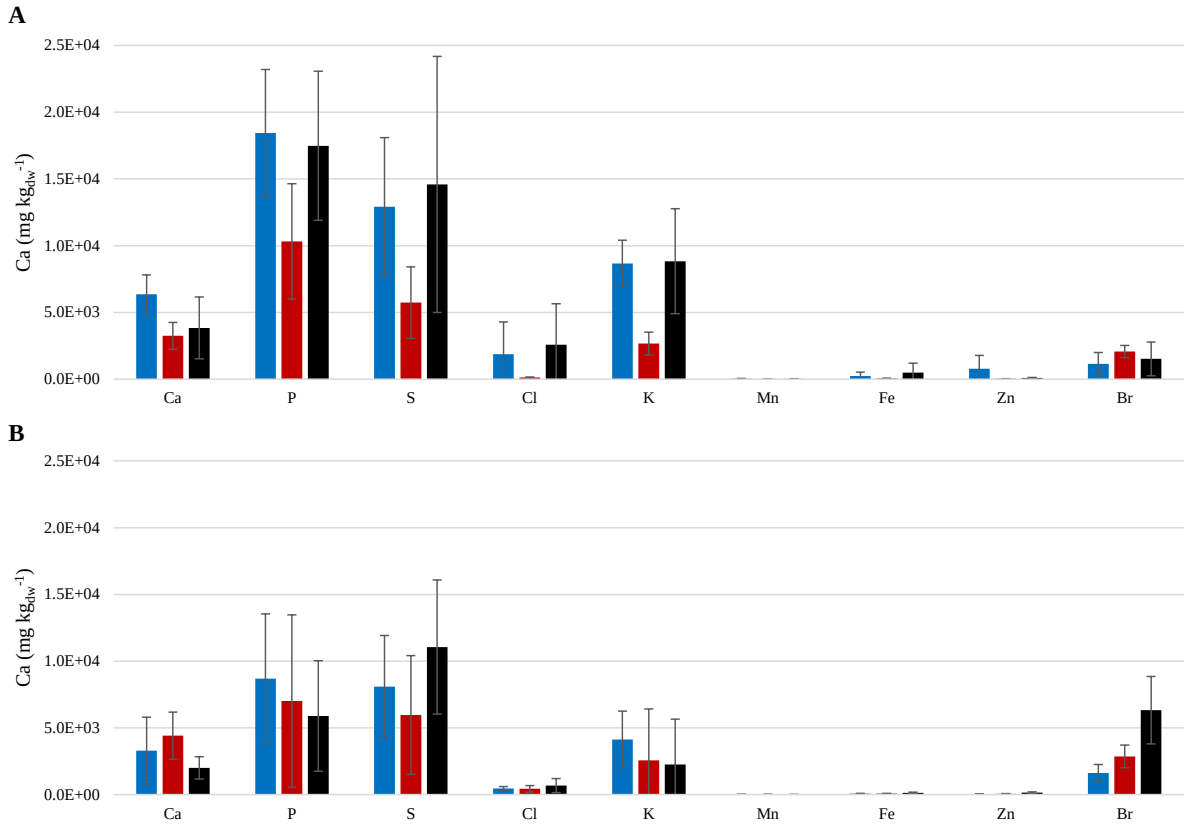


**Figure VI.7** - Quantification of diferent elements in aerobic granules. Concentrations of calcium (Ca), phosphorus (P), sulfur (S), chloride (Cl), potassium (K), manganese (Mn), iron (Fe), zinc (Zn) and bromine (Br) measured in the biomass outside the mineral inclusions, in different regions of the aerobic granules (central, intermediate and peripheral) harvested from the sequencing batch reactors SBR1 (blue), SBR2 (red) and control (black) on days 408 (A) and 434 (B) of experimental run II.

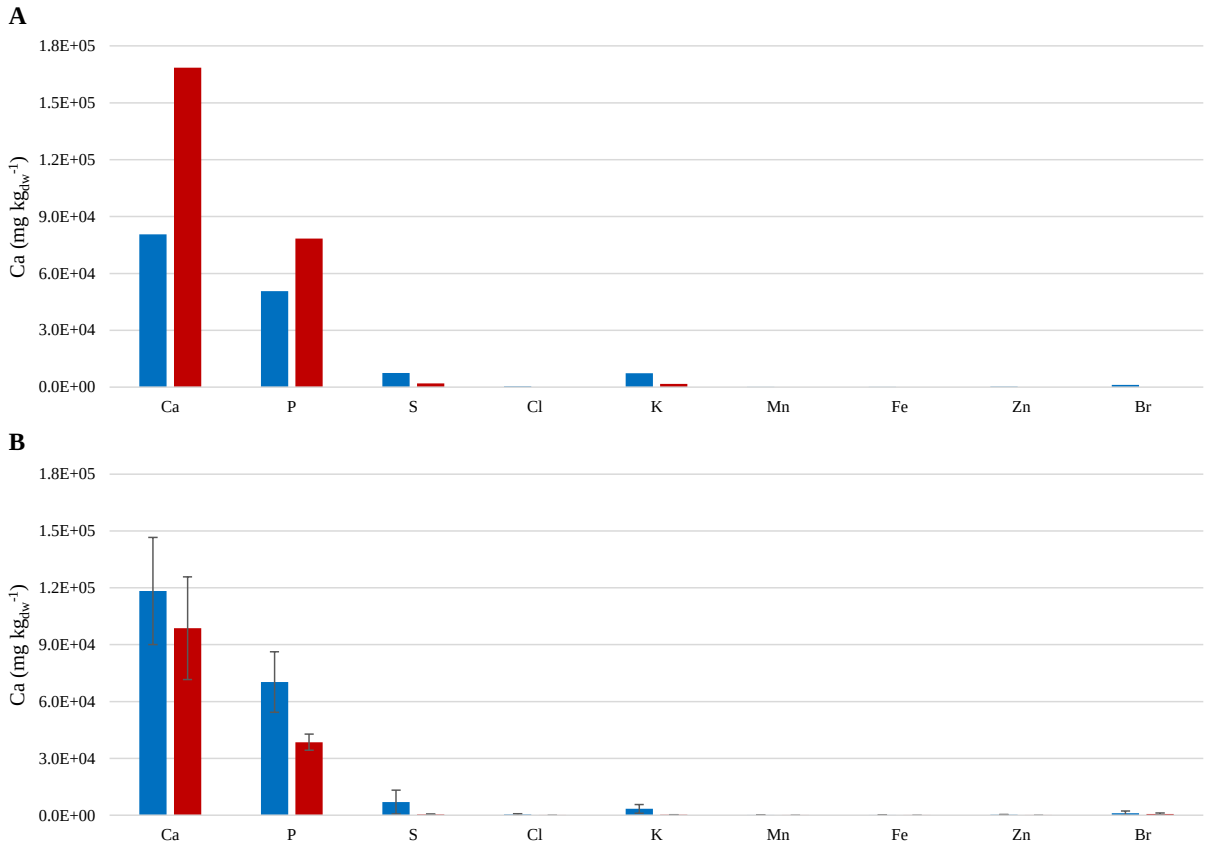


**Figure VI.8** - Quantification of different elements in aerobic granules. Concentrations of calcium (Ca), phosphorus (P), sulfur (S), chloride (Cl), potassium (K), manganese (Mn), iron (Fe), zinc (Zn) and bromine (Br) measured inside the mineral inclusions of aerobic granules harvested from the sequencing batch reactors SBR1 (blue), SBR2 (red) and control (black) on days 408 (A) and 434 (B) of experimental run II.

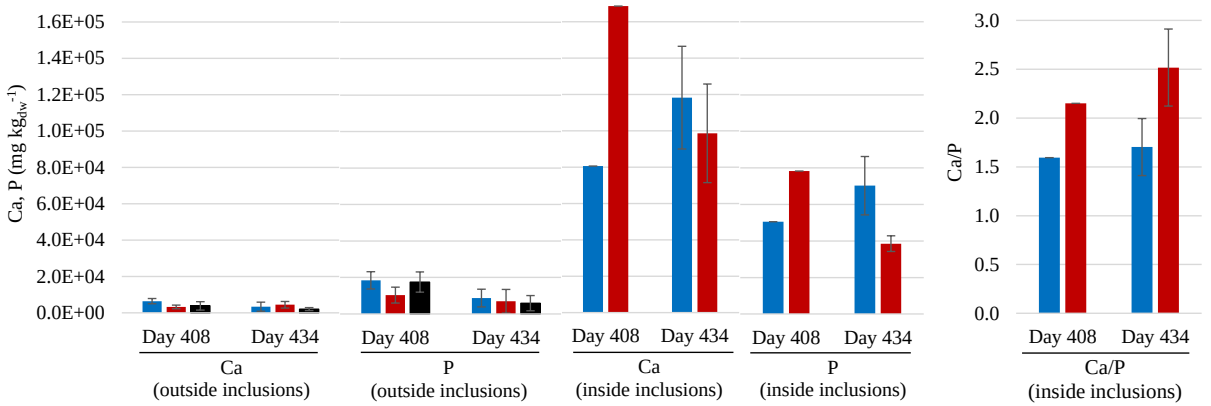


**Figure VI.9** - Quantification of calcium and phosphorus in aerobic granules. Concentrations of calcium (Ca) and phosphorus (P) measured in the biomass outside the mineral inclusions, in different regions of the granules (central, intermediate and peripheral), as well as inside the mineral inclusions in aerobic granules harvested from the sequencing batch reactors SBR1 (blue), SBR2 (red) and control (black) on days 408 and 434 of experimental run II. The right chart indicates the calcium-to-phosphorus (Ca/P) ratio in the mineral inclusions, only observed in granules from SBR1 and SBR2.

## VI.4.2. AGS SBR treatment performance

### VI.4.2.1. Biomass inventory

The biomass concentration profile along experimental runs I and II, based on the TSS analysis in the SBR mixed liquor is represented in Figure VI.10. At the start of the experimental run I, the TSS profile in SBR2 presented a lag phase due to the higher initial SVI (Figure VI.3), in relation to SBR1. Yet, as the biomass settling properties improved along the selective pressure period (period I.A), TSS increased in SBR2, reaching the same levels as in SBR1 at the end of period I.A, 7 gTSS $L^{-1}$. In accordance with the SVI profile (Figure VI.3), SBR2 stabilized around this value until day 43, subsequently increasing up to 9 gTSS $L^{-1}$ on day 52, reaching approximately the same maximum value that SBR1 previously attained on day 38. From day 56 to 98, the biomass concentration varied similarly in both SBRs, being within the range of 6-8 gTSS $L^{-1}$. Nevertheless, after 100 days of operation, significant differences were registered in terms of biomass profile using the two distinct hydrodynamic regimens. Specifically, while SBR2 tended to higher values, reaching a maximum of 11 gTSS $L^{-1}$ on day 215, SBR1 decreased to levels around 4 gTSS $L^{-1}$. Although the biomass concentration registered in SBR2 subsequently decreased, the TSS values in SBR2 were twice as high as those observed in SBR1, specifically 8.1±0.2 gTSS $L^{-1}$ and 4.1±0.4 gTSS $L^{-1}$ (average values for days 230-271), respectively. The decrease in the SBR2 TSS values during periods I.C and I.D reflect the gradual increase in the respective SVI values (Figure VI.3), being possibly related with the extension in the stirred anaerobic phase time imposed during these periods. The drains of the first cycle after the 40-days biomass storage period led to the loss of approximately half of the biomass from SBR1 and SBR2. Nevertheless, the subsequent re-accumulation of biomass allowed the TSS to reach values above 7 gTSS $L^{-1}$ in both SBRs at the end of the experimental run I.

Despite the overall better sludge settling characteristics in SBR2, this reactor also lost considerable amounts of biomass in the treated effluent on some operational days of the experimental run I (up to 1.8 and 1.3 gTSS $L^{-1}$ in SBR1 and SBR2, respectively). As a consequence, the SRT profile presented an irregular character in both reactors, the average SRT values being 12±11 days and 15±11 days in SBR1 and SBR2, respectively.

As shown in Figure VI.11, the inorganic content in the biomass from both SBR1 and SBR2 decreased considerably during the first operational days of the experimental run I, from 22% to stable values around 12%, as the inorganic matter coming from the CAS inoculum was washed out from the reactors. However, from day 42 on, significant differences were encountered between the two SBRs, which are in accordance with the TSS profile (Figure VI.10). Specifically, while SBR1 maintained stable values of approximately 10% of inorganic fraction in AGS until day 208, the biomass in SBR2 became gradually richer in inorganic matter, reaching stable values around 14%. This difference

became smaller in period I.D, as the percentage of inorganic matter gradually increased in SBR1 and decreased in SBR2 to 12%. During the storage period (period I.E), a considerable change occurred in terms of the inorganic content in SBR2 as the levels decreased from around 13% to 10%. During period I.F the inorganic content varied similarly in the two reactors, stabilizing around 10% up to the end of the experimental run I. Only small differences were observed in terms of mixed liquor TSS, respective percentage of inorganic matter, biomass washout and SRT between SBR1 and SBR2 during period I.F, denoting a similar efficiency in biomass reactivation after storage.

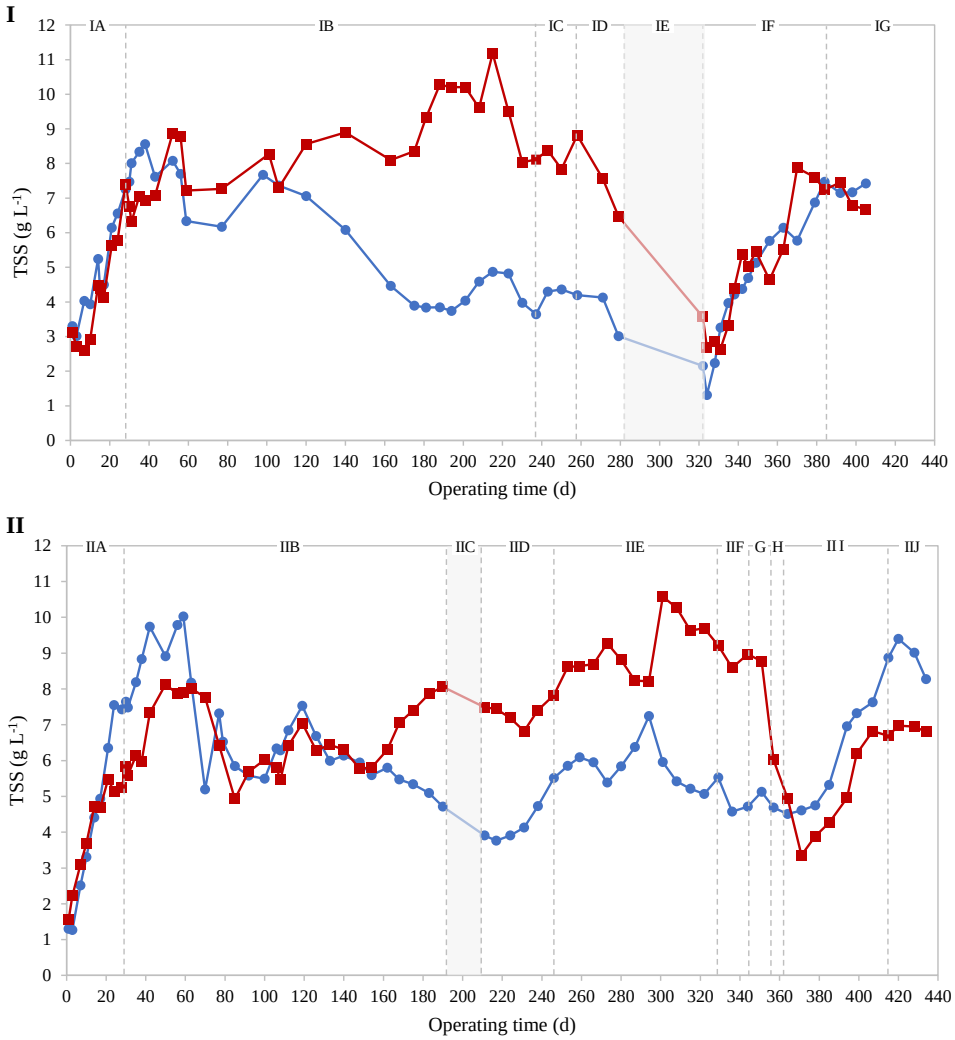


**Figure VI.10** - Profiles of biomass concentration in the mixed liquor. Total suspended solids (TSS) in the mixed liquor registered in sequencing batch reactors SBR1 (●) and SBR2 (■) along experimental runs I and II. The operational conditions for each experimental period (I.A-I.G and II.A-II.J) are described in Table VI.1.

Regarding the experimental run II, after initial AGS formation in the presence of AgNP, with concomitant TSS increase until day 60 (up to 10 and 8 gTSS $L^{-1}$ in SBR1 and SBR2, respectively), both reactors experienced biomass washout episodes leading to similar TSS variations within 5-8 gTSS $L^{-1}$ up to day 154 (Figure VI.10). Yet, similarly to the experimental run I, from this day on the reactors behaved differently, with TSS levels increasing in SBR2 and decreasing in SBR1 until the end of period II.B. Consequently, despite some biomass concentration reduction caused by the 18-day

biomass storage period in both reactors, SBR2 re-started the operation with a higher TSS level than SBR1. After interruption of AgNP supplementation on day 247, SBR1 and SBR2 further increased their biomass content reaching up to 7 and 11 gTSS $L^{-1}$, respectively, around day 300. Overall, SBR2 could sustain higher biomass concentration levels than SBR1, even during the dye shock load (period II.F). The exception observed at the end of this experimental run (periods II.I and II.J) was a consequence of the drastic biomass washout from SBR2 on day 352 probably caused by the previously described operational problem. The TSS levels rapidly increased from around 4-5 to 7-8 gTSS $L^{-1}$ upon supplementation with calcium nitrate in both SBRs (period II.I), the VSS increasing concomitantly from 3-4 to 6-7 gVSS $L^{-1}$. This TSS rise was subsequently hindered when calcium nitrate was replaced with potassium nitrate (period II.J). Similarly to the experimental run I, sporadic episodes of biomass washout occurred throughout the experimental run II, leading to unstable SRT profiles, the average SRT values being 11±8 days and 15±9 days in SBR1 and SBR2, respectively.

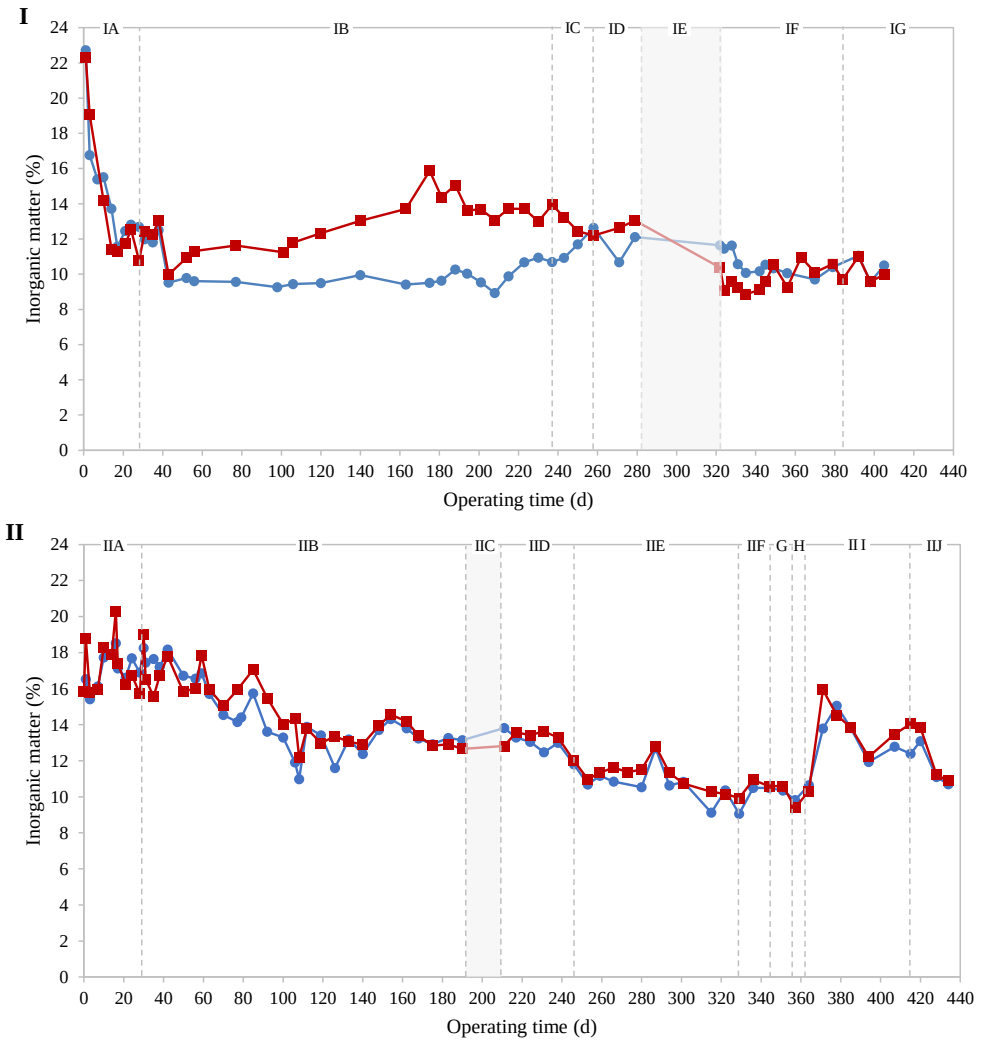


**Figure VI.11** - Profiles of inorganic matter in the mixed liquor suspended solids. Percentage of inorganic matter (calculated from volatile and total suspended solids measurements) in the mixed liquor registered in sequencing batch reactors SBR1 (●) and SBR2 (■) along experimental runs I and II. The operational conditions for each experimental period (I.A-I.G and II.A-II.J) are described in Table VI.1.

Overall, although no major differences were encountered between SBR1 and SBR2, the inorganic matter content in the SBRs suspended solids during the experimental run II was higher than in the experimental run I (Figure VI.11). This could be related with the addition of AgNP during periods II.A-II.D (further discussed in section VII.5). In fact, the inorganic matter in both SBRs gradually decreased to 10% (same stable levels as in period I.G) during period II.E, when AgNP addition was stopped. Subsequently, a sharp increase in the inorganic content was registered upon calcium nitrate supplementation in both bioreactors, the levels being maintained around 14% until the end of period II.I. Finally, both SBRs decreased to 11% of inorganic fraction in their biomass during the period of potassium nitrate supplementation (period II.J). Overall, the percentage of inorganic matter was very similar between the biomass fractions with dimensions 0.20-0.65 mm (granular fraction) and lower than 0.20 mm (flocculent fraction), in both SBRs throughout the two experimental runs. One exception was during the supplementation with calcium nitrate, when the percentage of inorganic matter in the granular fraction increased from 10% to 18%, while that of the flocculent fraction remained constant at 10% until the end of the operation (results not shown).

### VI.4.2.2. Anaerobic and overall COD removal

The overall COD removal yield and the respective percentage removed anaerobically are represented in Figure VI.12. As the biomass adapted to the new substrate, the COD removal performance gradually improved along the first 2 weeks of operation in both reactors reaching 80% of total COD removal, half of which being removed under anaerobic conditions. The overall COD removal yield profiles in SBR1 and SBR2 were comparable throughout the whole experimental run I. Despite the lower COD fraction anaerobically removed in SBR2 during the first 17 days of operation, when compared with SBR1, no other notable differences were encountered between the two reactors in terms of COD removal yield until day 52. From days 57 to 163 SBR1 removed a higher fraction of COD under anaerobic conditions (maximum of 70%) than SBR2 (maximum of 60%), this relation being reversed from day 163 on, as SBR1 values decreased down to 40% while SBR2 sustained levels around 60%. After re-starting the operation of the reactors in period I.F, SBR1 and SBR2 reached stable levels of 80% of overall COD removal yield on days 331 and 338, respectively (Figure VI.12). As for the COD removed under anaerobic conditions, the profiles were comparable between the two reactors, both stabilizing within the 50-60% range after day 341. The COD removal performance in SBR2 slightly improved after the stirred anaerobic period was extended in 15 min on day 384 (period I.G).

Regarding the experimental run II, although 80% of overall COD removal was also achieved during the first period of operation, the anaerobic COD removal levels were much lower, around 15% *vs* 50% at the end of periods II.A and I.A, respectively (Figure VI.12). In fact, despite the relatively steady total COD removal values within 80-90% maintained throughout period II.B, the increase in the

amount of COD removed under anaerobic conditions progressed slowly in both SBRs, only reaching 50-60% levels after 100 days of operation. After the biomass short storage period (period II.C), SBR1 and SBR2 were able to achieve overall COD removal yields of 89% and 87%, respectively, on the first day of SBR reactivation. In addition, despite some initial variation in the anaerobic COD removal performance, both reactors were able to gradually resume the maximal levels previously observed. Specifically, after the azo dye shock load period (period II.F), which brought the COD removal to slightly lower levels, the COD removal performance subsequently improved throughout period II.I, during calcium nitrate supplementation, especially in terms of anaerobic COD removal, both reactors attaining 60% on day 415 (total COD removal yield of 90%).

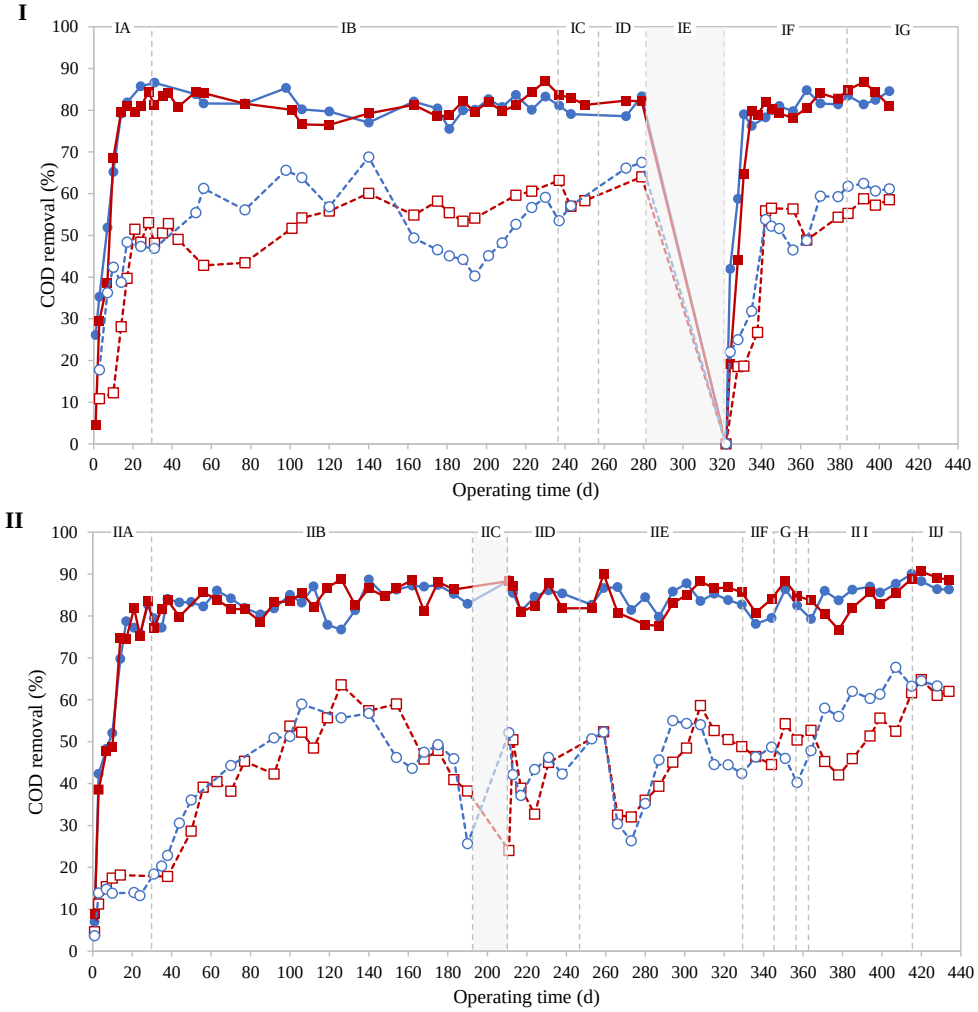


**Figure VI.12** - Organic load removal performance, as chemical oxygen demand (COD), along experimental runs I and II. Total COD removal yield (full line) and percentage of COD removed during the anaerobic phase (dashed line) in sequencing batch reactors SBR1 (●) and SBR2 (■) along experimental runs I and II. The operational conditions for each experimental period (I.A-I.G and II.A-II.J) are described in Table VI.1.

Figure VI.13 shows SBR1 and SBR2 COD-time profiles representative of the majority of the treatment cycles studied during the experimental runs I and II. Despite the use of a different hydrodynamic regimen, the same COD residual level was frequently reached by both SBRs at the end of the anaerobic phase, as similar COD removal rates were observed during the stirred anaerobic

phase. In addition, equivalent aerobic COD profiles were observed throughout both experimental runs, the residual COD being approximately 100 mg $O_2$ $L^{-1}$ (Figure VI.13 and Figure VI.S4, in Appendix D). Moreover, no more than 30% of total COD removal was achieved during the plug-flow feeding stage.

Similarly to the COD profiles, similar pH variations were observed between both SBRs (Figure VI.13), pH values being normally registered within the 6.5-6.8 range, except during the periods of nitrate supplementation, when the pH profile shifted to higher values (pH variation within 6.7-6.9 during periods II.I-II.J). Overall, the pH values decreased along the anaerobic reaction, likely as a result of VFA production during fermentation of the hydrolyzed starch-based substrate. Conversely, the pH subsequently increased during the first 30 min of aeration, concomitantly with the final phase of biodegradable COD removal (Figure VI.13), probably associated with oxidation of the previously released VFA.

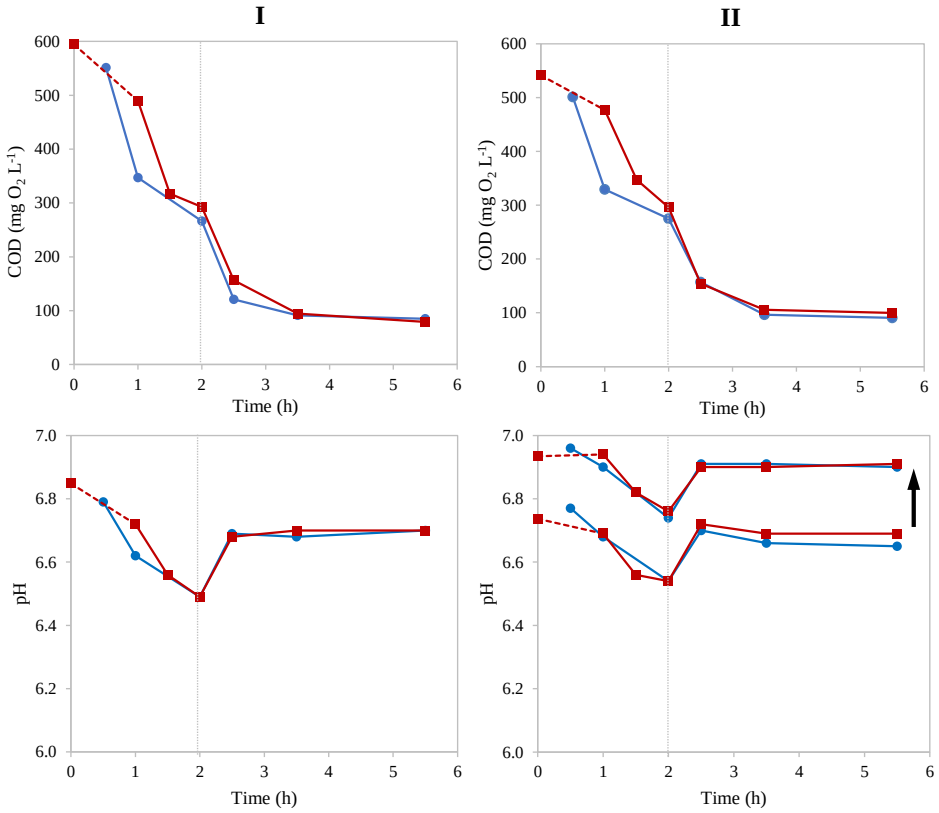


**Figure VI.13** - Comparison between chemical oxygen demand (COD) removal profiles and pH profiles representative of SBR1 (●) and SBR2 (■) treatment cycles studied along experimental runs I and II. Upper charts: COD-time profiles on day 405 of the experimental run I, and on day 77 of the experimental run II. Lower charts: pH-time profiles on day 405 of the experimental run I, and on days 140 (pH 6.5-6.8) and 420 (pH 6.7-6.9) of the experimental run II. The black arrow indicates the shift from the pH profiles registered on day 140 to day 420. The dashed lines represent the plug-flow filling stage in SBR2, the first point being estimated based on values measured in the feed solution (50%) and in the previous cycle treated effluent (50%). Vertical lines represent the end of the anaerobic phase, upon the aeration onset.

### VI.4.2.3. Azo dye biodegradation

#### VI.4.2.3.1. Color removal

During the experimental run I, color removal yields around 80% were reached in SBR1 on operational day 3 and maintained throughout most of the operation (Figure VI.14). One exception occurred after several biomass washout episodes upon settling time reduction to 15-20 min. Specifically, SBR1 color removal yield decreased from 78% (day 14) to 47% (day 17), the residual dye concentration in the reactor being significantly higher on days 17-21 (Figure VI.S5, in Appendix D). From days 17 to 35, SBR1 decolorization capacity improved back to 80% of color removal yield. The other exception occurred during the first 10 days of operation after the biomass storage period (period I.F), while SBR1 gradually recovered 80% of color removal yield.

Overall, the lower color removal yield values reached in SBR2 during period I.A, approximately 60% (Figure VI.14), probably owe to the shorter mixed anaerobic phase (30 min, as opposed to 90 min in SBR1), the plug-flow stage being responsible for a maximum of 45% of decolorization. In fact, SBR2 sustained color removal yields within 55-60% from days 3 to 77, subsequently increasing to stable levels around 70% during the period of days 140-237 (Figure VI.14). Maximum color removal yields of 80% were achieved after the anaerobic stirred phase was increased from 30 min to 40-45 min (periods I.C-I.D). Accordingly, the residual AR14 concentration, as color-equivalents, gradually decreased along the experimental run I in SBR2, although not reaching levels below 5 mg $L^{-1}$, as registered in SBR1 (Figure VI.S5, in Appendix D). Following the 40-day biomass storage period, although SBR2 was operated with 45 min of mixed anaerobic phase, the color removal yields stabilized at lower levels, within 65-70% from day 331 to 370 (Figure VI.14). In fact, higher levels of color removal (75-83%) were only sustained after the anaerobic stirred phase duration was extended to 60 min in SBR2 (period I.G). Accordingly, after adapting to the new cycle conditions, SBR2 reached the same residual dye concentration as SBR1 from day 90 on (Figure VI.S5, in Appendix D), SBR2's stirred anaerobic phase being 30 min shorter than SBR1's.

Regarding the experimental run II, both reactors achieved 80% of color removal yield one week after inoculation and sustained a higher decolorization performance until the end of the operation, the yields varying within 75-90% (Figure VI.14). In fact, even after 18 days of storage, the biomass rapidly resumed its color removal activity, SBR1 and SBR2 reaching decolorization yields of 79% and 78% on the second day of AGS reactivation, respectively (period II.D). In addition, the decolorization yield was not affected by the three-fold increase in dye concentration in the synthetic TWW (period II.F). However, during period II.H and in the first days of period II.I, when calcium nitrate was supplemented to the reactors, a slight deterioration in the decolorization performance was registered in both SBRs, as the residual dye concentration, as color-equivalents, increased from 2-4 to 3-5 mg $L^{-1}$

(Figure VI.S5, in Appendix D), and the color removal yields decreased to 70% (more consistently observed in SBR2; Figure VI.14). Nevertheless, both SBRs were able to overcome this change in the feed composition and resumed high decolorization performance with yields within 80-90% until the end of period II.I and during supplementation with potassium nitrate (period II.J; Figure VI.14).

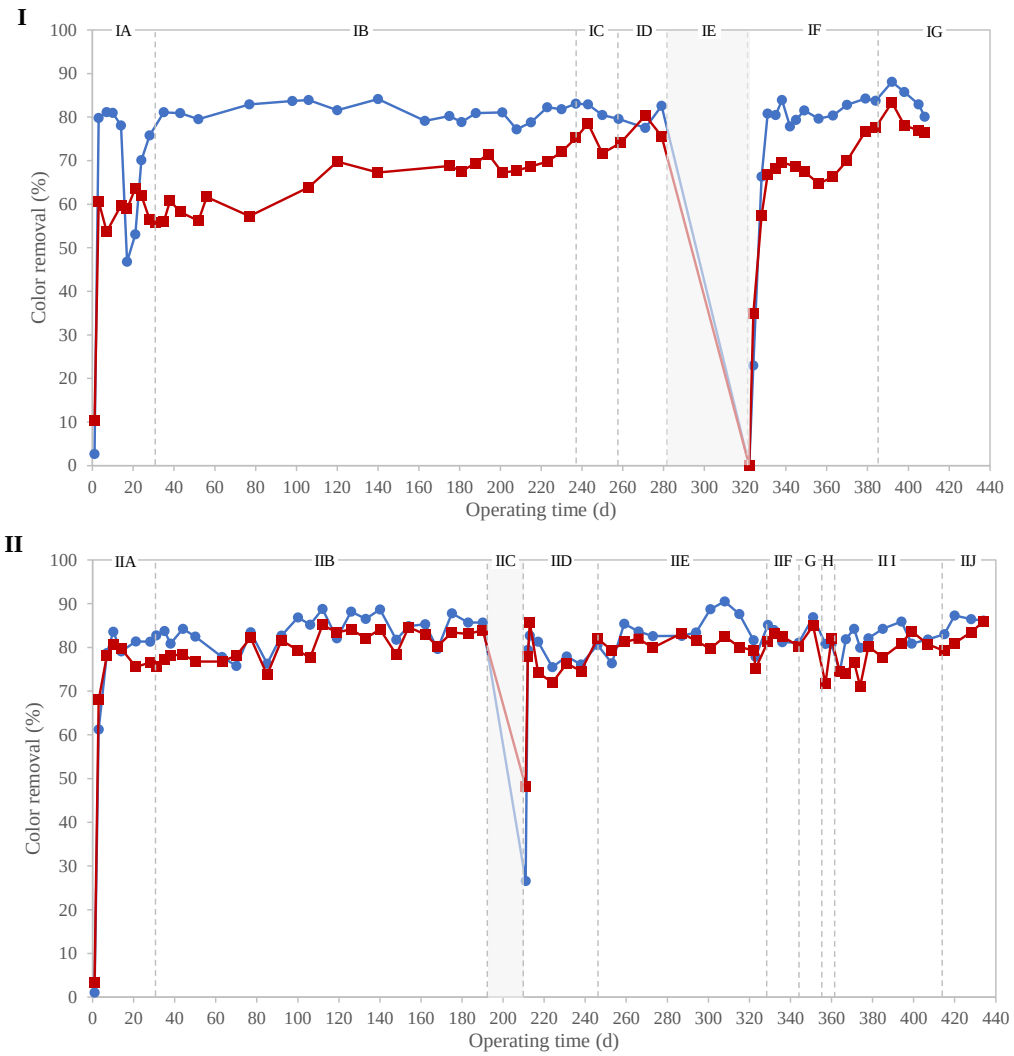


**Figure VI.14** - Color removal performance along the experimental runs I and II. Profiles of color removal yield in the sequencing batch reactors SBR1 (●) and SBR2 (■) along the experimental runs I and II. The operational conditions for each experimental period (I.A-I.G and II.A-II.J) are described in Table VI.1.

Representative color removal profiles of each SBR during the experimental runs I and II are shown in Figure VI.15. As expected from the previously proposed biodecolorization mechanism via azo dye reduction, color decreased during the anaerobic phase, presenting stable values throughout the subsequent aerobic phase. While the same SBR1 color-time profiles were consistently observed throughout the experimental runs (Figure VI.15), SBR2's varied according to the duration of the anaerobic stirred phase (Figure VI.15, I-a to I-c), the final residual AR14 concentration (as color-equivalents) ranging from 9 to 4 mg $L^{-1}$. In fact, the color removal rate during the SBR2 plug-flow feeding was minimal, the lengthening of the anaerobic stirred phase being critical for SBR2 to reach the same final residual color levels as SBR1. Specifically, SBR2 achieved the lowest color residual

levels when the anaerobic reaction phase was extended to 60 min in period I.G (Figure VI.15, I-c). Overall, after a rapid adaptation to the presence of a nitrate salt in the feed composition (periods II.H-II.J), which were associated with minor changes in the decolorization profile, both reactors recovered the typical color-time profile shown in Figure VI.15, II-a. This indicated that neither the presence of a calcium nitrate nor potassium nitrate had any notable impact on the decolorization ability of AGS.

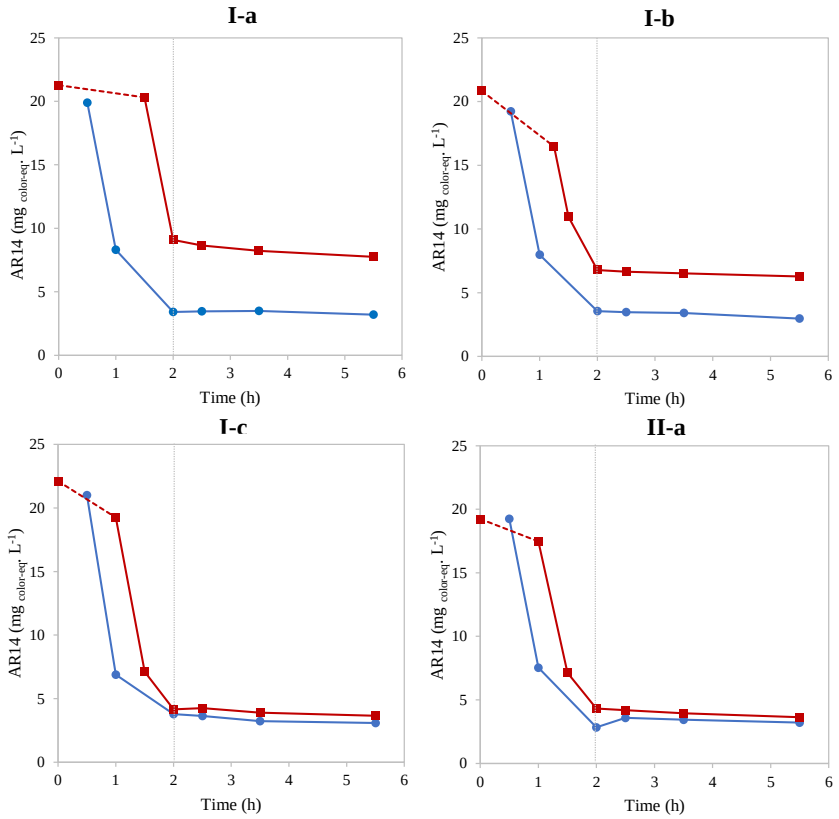


**Figure VI.15** - Comparison between color removal profiles of representative treatment cycles in sequencing batch reactors SBR1 and SBR2 along experimental runs I (I, a-c) and II (II-a). Acid Red 14 (AR14, as color-equivalents)-time profiles observed along the reaction phases of treatment cycles in SBR1 (●) and SBR2 (■) on days 77 (I-a; period I.B), 349 (I-b; period I.F) and 404 (I-c; period I.G) of experimental run I, and on day 106 (II-a; period II.B) of experimental run II. The dashed lines represent the plug-flow filling stage in SBR2, the first point being estimated based on values measured in the feed solution (50%) and in the previous cycle treated effluent (50%). Vertical lines represent the end of the anaerobic phase, upon the aeration onset.

### VI.4.2.3.2. Fate of aromatic amines

HPLC analysis confirmed that the observed color removal in the reactors was a result of the azo dye being anaerobically reduced, thus generating two sulfonated aromatic amines: 4A1NS and 1N2A4S. While AR14 and 4A1NS concentrations could be quantified by HPLC analysis, this was not possible for 1N2A4S due to the unavailability of the correspondent standard and to the unstable character of this amine. Regarding the aromatic amine 4A1NS, although its concentration consistently increased along the anaerobic phase, relevant differences were observed in 4A1NS concentration profiles throughout the subsequent aerobic phase on different cycles from the experimental run I, representative profiles being shown for each SBR on Figure VI.16.

Regarding SBR1, three distinct 4A1NS concentration-time profiles were encountered during the experimental run I (Figure VI.16). Specifically, until day 21, 4A1NS was present in SBR1 at the start of the anaerobic phase (as a residue from the previous cycle) and its concentration increased up to 9.3 mg $L^{-1}$ (Figure VI.16, I-1a). The fate of the aromatic amine in the subsequent aerobic phase was variable, its concentration decreasing and subsequently increasing in several cycles. The aromatic amine was thus still present in the mixed liquor at the end of the aerobic phase. However, from days 24 to 38 a profile typical of complete and irreversible conversion of 4A1NS was observed in SBR1. Specifically, 4A1NS concentration increased from 0 mg $L^{-1}$ to values within 4-5 mg $L^{-1}$, subsequently decreasing along the aerobic phase at a mostly constant rate (Figure VI.16, I-1b). Although the same type of profile was also observed on day 43, 4A1NS concentrations increased up to 6.2 mg $L^{-1}$ during the anaerobic phase, subsequently decreasing to 0.8 mg $L^{-1}$. Finally, after day 52 until the end of the experimental run I, 4A1NS was no longer transformed during the aerobic phase, its concentration remaining within 8-10 mg $L^{-1}$ along the aerobic stage (Figure VI.16, I-1c). This loss of the potential 4A1NS bioconversion capacity between days 38 and 52 may be attributed to the lack of aeration during several cycles in SBR1, resulting from the operational problem in the air diffuser registered on day 41.

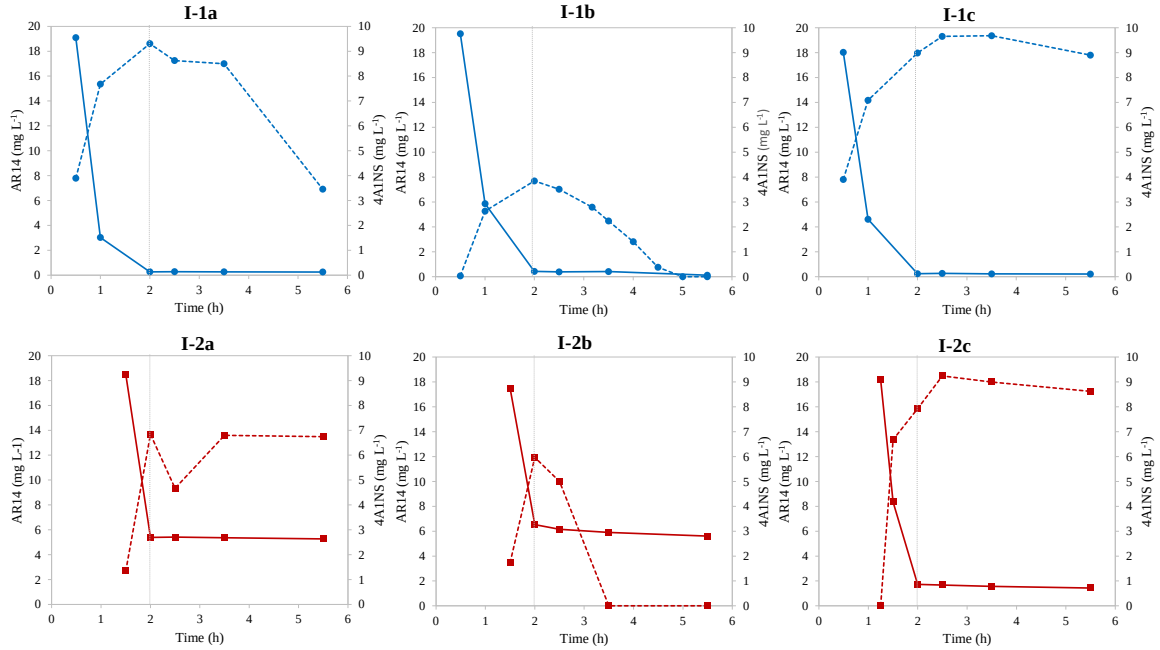


**Figure VI.16** - Concentration-time profiles of the azo dye Acid Red 14 (AR14; full line) and of its cleavage product 4-amino-naphthalene-1-sulfonic acid (4A1NS; dashed line) in SBR1 (●; 1a – day 10, 1b – day 35, 1c – day 163) and SBR2 (■; 2a – day 24, 2b – day 56, 2c – day 279) on selected treatment cycles along experimental run I. Area-time profiles of HPLC peaks for the respective SBR/cycle are represented in Figure VI.S6, in Appendix D. Vertical lines represent the end of the anaerobic phase, upon the aeration onset.

Azo dye reduction occurred to a lesser extent in SBR2, due to the shorter stirred anaerobic phase, as previously described (Figure VI.16). However, after extending the length of the latter stage to 60 min (on day 384 of the experimental run I, period I.G), the residual AR14 concentrations during the aerobic phase in SBR2 became close to zero. Similarly to SBR1, the 4A1NS profiles in SBR2 also

significantly changed throughout the course of the experimental run I (Figure VI.16). In fact, while 4A1NS was initially observed at high levels at the end of the aerobic reaction period (Figure VI.16, I-2a), from day 31 to 56 the concentration of 4A1NS consistently decreased along the first 1.5 h of aeration, being absent at the end of the reaction (Figure VI.16, I-2b). Although this profile could indicate that 4A1NS was removed during the aerobic phase, the maximum 4A1NS concentration achieved at the end of the anaerobic phase (5.1-7.3 mg $L^{-1}$) was slightly higher than that expected if complete, irreversible 4A1NS conversion was occurring (4.4 mg $L^{-1}$, calculated for the cycle represented in Figure VI.16, I-1b). Subsequently, from day 77 on, the disappearance of the 4A1NS along the aerobic phase was no longer observed, as high concentrations were consistently observed (Figure VI.16, I-2c). Upon the extension in the SBR2 anaerobic stirred phase (from day 237 on), higher amounts of 4A1NS were produced, as a higher percentage of azo dye molecules were reduced (Figure VI.16, I-2c). This profile was also observed in SBR2 after the biomass storage period, up to the end of the experimental run I, except for the initial 4A1NS concentration value, which was no longer zero as observed in Figure VI.16, I-2c. In fact, despite the high 4A1NS levels registered at the end of the reaction phase, absence of 4A1NS was registered at the start of the anaerobic reaction in some SBR2 cycles (Figure VI.16, I-2c). These observations suggest that 4A1NS was being reversibly converted into another metabolite, which was further supported by examining the variations in other peaks in the HPLC chromatograms obtained for all the samples collected along selected treatment cycles. Area-time profiles of HPLC peaks are represented in Figure VI.S6, in Appendix D, for the same cycles shown in Figure VI.16.

Figure VI.17 depicts the HPLC chromatograms of centrifuged samples taken from the mixed liquor at the onset of the reaction phase, at the end of the anaerobic phase and at the end of the aerobic phase of selected cycles from the experimental run I. Therein are identified the peaks corresponding to the azo dye AR14, the aromatic amine 4A1NS, as well as unknown metabolites (α, α', β, δ, γ). Metabolites β and γ are possibly produced from the conversion pathway of the unstable 1N2A4S, emerging at the end of the anaerobic phase, the variation in their respective peak area along the aerobic phase being inconsistent and relatively minor (Figure VI.S6, in Appendix D). On the other hand, compound δ, characterized by a low RT, presented a relevant peak area at the end of the aerobic phase (Figure VI.17, I-1a). In fact, it was formed along the aerobic phase in all cycles studied until day 38 in both SBRs (Figure VI.S6, in Appendix D), after which it was no longer observed during the remaining operational days of the experimental run I (Figure VI.17). The fact that the concentration of this compound gradually rose during the aerobic stage but was close to zero during the whole anaerobic phase (Figure VI.17, I-1a) suggests that the latter was removed from the system during the non-aerated, settling/drain/idle/feed stages of the treatment cycle. In addition, no direct correlation was found between 4A1NS and the latter. In fact, as discussed in the next section (VI.4.2.3.3), the HPLC peak δ probably corresponds to nitrate, potentially indicating the occurrence of nitrification up to day

38 in both reactors. In contrast, metabolites α/α' may be inversely related to 4A1NS, as α/α' peaks presented significantly higher areas in samples where 4A1NS was suddenly absent (Figure VI.17). In fact, analysis of area-time profiles of HPLC peaks corresponding to AR14, 4AN1S, and relevant unknown metabolites suggests that 4A1NS and metabolites α' and/or α suffered interconversion during SBR2 cycles, namely when 4A1NS concentration decreased to zero along the aerobic phase, registered from day 31 to 56 (Figure VI.S6, in Appendix D). In addition, the unexpected absence of 4A1NS at the start of the reaction phase in some of SBR2 treatment cycles, namely on days 120 and 279 (as represented in Figure VI.16, I-2c), was also likely due to the temporary conversion of 4A1NS into metabolite α occurring during the idle period (Figure VI.S6, in Appendix D).

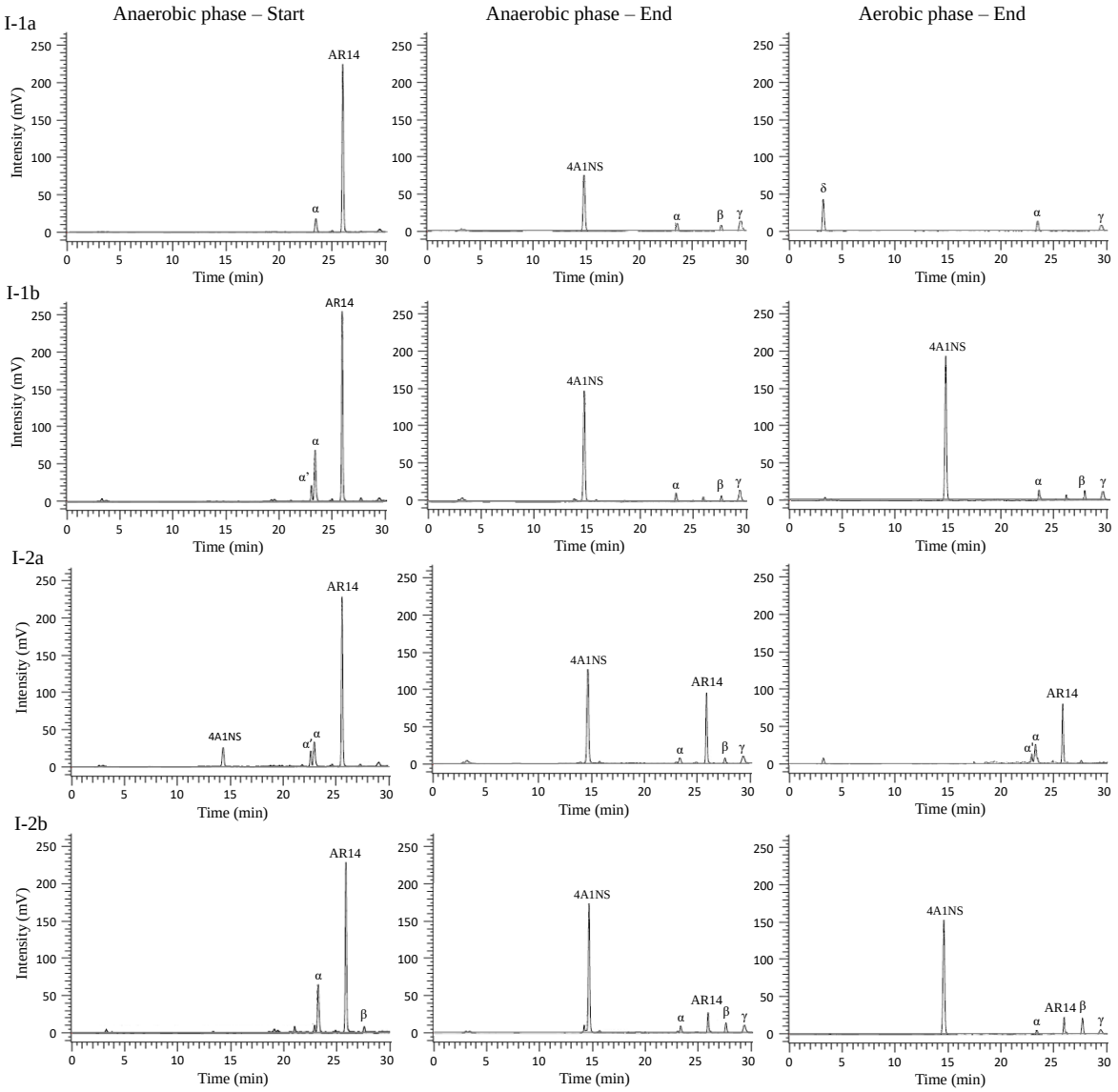


**Figure VI.17 -** HPLC chromatograms of liquid samples from selected cycles representative of experimental run I. Samples were harvested from sequencing batch reactors SBR1 (I-1a – day 38; I-1b – day 163) and SBR2 (I-2a – day 43; I-2b – day 279) at the onset of the reaction phase, at the end of the anaerobic phase and at the end of the aerobic phase of selected cycles. Peaks AR14 and 4A1NS correspond to the azo dye Acid Red 14 and to the aromatic amine 4-amino-naphthalene-1-sulfonic acid resulting from AR14 reduction, respectively; peaks α-γ represent unknown metabolites.

Regarding the experimental run II, Figure VI.18 shows representative profiles of the different 4A1NS fates observed up to day 344 in both reactors. The different 4A1NS profiles specifically observed after day 344 until the end of the experimental run II are discussed in the next section (VI.4.2.3.3), in light of the addition of nitrate to the reactors during periods II.H-II.J (Table VI.1). As represented in Figure VI.18, the evolution in the 4A1NS profile along the experimental run II was initially very similar in both SBRs. In fact, after inoculation and until day 50 no 4A1NS transformation occurred during the aerobic phase (Figure VI.18, II-1a and II-2a), its concentration being maintained close to the expected value when complete azo dye reduction occurs and no 4A1NS is removed on successive treatment cycles, *i.e.*, 9.4 mg $L^{-1}$. Subsequently, from days 56 to 77, both SBRs presented 4A1NS profiles that indicated that further conversion of the aromatic amine was irreversibly occurring along the aerobic phase (Figure VI.18, II-1b and II-2b). In fact, the concentration of 4A1NS at the end of the anaerobic phase was approximately 5 mg $L^{-1}$, corresponding to the expected amount of 4A1NS when complete reduction of 20 mg $L^{-1}$ of AR14 occur and no residual 4A1NS accumulates from the previous cycle, *i.e.*, 4.9 mg $L^{-1}$. Yet, the 4A1NS profile registered on day 85 indicated that 4A1NS was only partially removed during the aerobic phase in both reactors, a residual 4A1NS concentration being accumulated from one cycle to the next, consequently elevating the concentration of 4A1NS registered at the end of the anaerobic phase (Figure VI.18, II-1c to II-2c). This type of profile was repeatedly observed until day 100 in SBR1, but the complete 4A1NS aerobic conversion was recovered in the latter from days 106 to 308 of the experimental run II (Figure VI.18, II-1d and II-1e). On the other hand, the potential 4A1NS degradation was restored sooner in SBR2, on day 92, and was maintained at least until day 344 (Figure VI.18, II-2d, II-2e and II-2f). In fact, the AGS capacity to remove 4A1NS from the mixed liquor along the aerobic phase was maintained in both SBRs even after the 18-day biomass storage period. However, some differences were observed in terms of 4A1NS removal rate after period II.C, specifically in SBR2. In fact, before the biomass storage period, the 4A1NS gradually disappeared along the aerobic phase being absent after 2.5-3.5 h of aeration in both reactors (Figure VI.18, II-2d). The same was observed for SBR1 after the storage period (Figure VI.18, II-1e *vs* II-1d), but not for SBR2, where 4A1NS concentration rapidly decreased to zero after 0.5-1.5 h of aeration (Figure VI.18, II-2e *vs* II-2d). Concomitantly with this change, the peak area of the metabolites α/α' became relevant in SBR2 (Figure VI.S6, in Appendix D), their profiles further supporting the hypothesis of a potentially direct correlation between 4A1NS and the metabolites α/α'. In addition, the gradual formation of the metabolite δ along the aerobic phase was observed in SBR2 in all cycles analyzed on periods II.D-II.G, as opposed to those before the biomass storage.

Only SBR2 was able remove the higher amount of 4A1NS formed upon the increase in the AR14 concentration in the synthetic TWW (Figure VI.18, II-2f). In fact, the SBR1 capacity to remove 4A1NS along the aerobic phase gradually deteriorated after days 98 to 122, prior to the AR14 shock load, resulting in 4A1NS being only partially removed, namely during period II.G (Figure VI.18, II-

1f). In addition to 4A1NS, the peak area of the metabolites α, α', β and γ also increased in the cycles where a higher concentration of AR14 was applied (Figure VI.S6, in Appendix D), confirming that their origin was apparently the azo dye, as opposed to compound δ for which the same was not consistently observed.

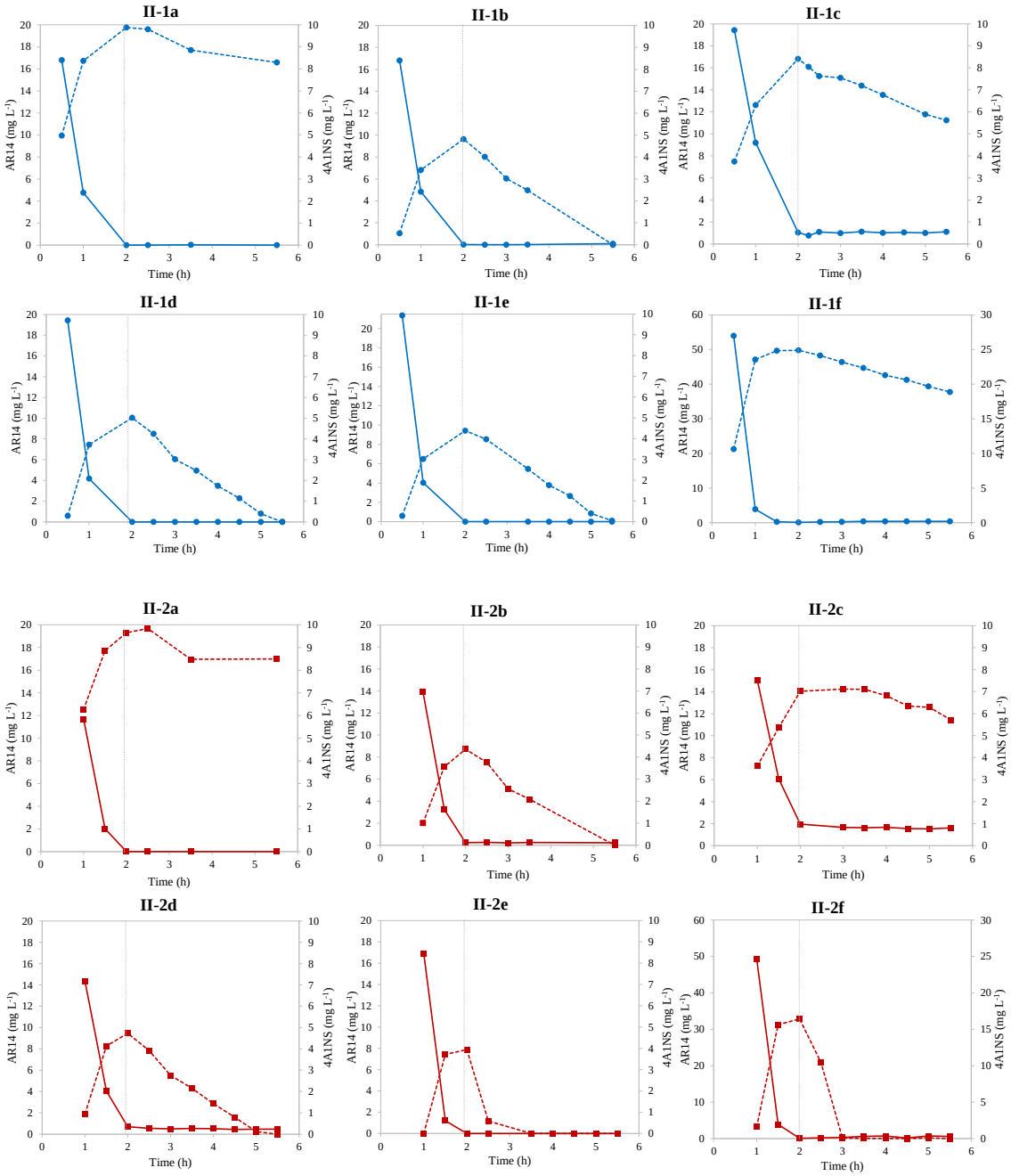


**Figure VI.18** - Concentration-time profiles of the azo dye Acid Red 14 (AR14; full line) and of its cleavage product 4-amino-naphthalene-1-sulfonic acid (4A1NS; dashed line) in sequencing batch reactors SBR1 (●; II.1a – day 50, II.1b – day 77, II.1c – day 85, II.1d – day 112, II.1e – day 308, II.1f – day 344) and SBR2 (■; II.2a – day 50, II.2b – day 77, II.2c – day 85, II.2d – day 126, II.2e – day 308, II.2f – day 344) on selected treatment cycles along experimental run II. Vertical lines represent the end of the anaerobic phase, upon the aeration onset.

Figure VI.19 provides a simplified representation of the different 4A1NS profile types observed along the experimental runs I and II in the two SBRs, differentiating the experimental days when 4A1NS concentration was maintained during the aerobic phase from those when it was completely or partially

removed. In addition to the 4A1NS profiles previously described, a new profile was specifically observed when nitrate was supplemented to the reactors on periods II.H-II.J (Figure VI.19), as presented and discussed in the next section.

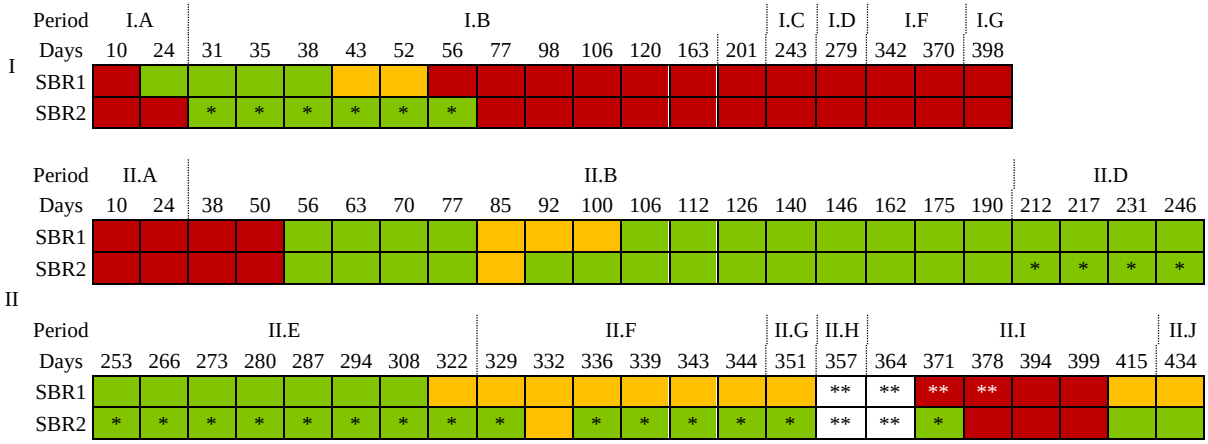


**Figure VI.19** - Schematic representation of the aromatic amine 4-amino-naphthalene-1-sulfonic acid (4A1NS) profile along the aerobic phase of the treatment cycles analyzed on the indicated experimental period, day and sequencing batch reactor (SBR). The different colors represent three main observations along the aerobic phase: 4A1NS concentration was maintained (red), partially reduced (yellow) or reduced to zero (green). * 4A1NS rapidly disappeared within the first 0.5-1.5 h of aeration; **4A1NS was absent during the anaerobic reaction phase, a new peak emerging along this phase instead. Uncolored days correspond to those when 4A1NS was not observed throughout both the anaerobic and the aerobic phases.

The different 4A1NS profiles obtained through HPLC analysis represented in Figure VI.16 and Figure VI.18, respectively referring to the experimental runs I and II, were in accordance with particular changes in the samples' UV-visible spectra along the aerobic stage (Figure VI.S7, in Appendix D). Specifically regarding the experimental run I, UV peaks detected at 220, 240 and 300 nm at the end of the anaerobic phase were significantly reduced along the aerobic phase in SBR1 on cycles from days 21-43 (Figure VI.S7, in Appendix D), though to a lesser extent on day 43. In contrast, no relevant differences were observed in the UV spectra along the cycle's aerobic phase on any of the other days analyzed in SBR1. These UV peaks, typically associated with the presence of aromatic amines, also remained unchanged along the aerobic phase in all SBR2 cycles of the experimental run I (Figure VI.S7, in Appendix D), namely during the period when HPLC results showed the rapid disappearance of 4A1NS (days 31-56), concomitantly with the formation of metabolites α/α' (Figure VI.S6, in Appendix D). These observations further suggest that only SBR1 effectively removed 4A1NS during a short period of the experimental run I (days 21-43). Regarding the experimental run II, the UV peaks remained unchanged in SBR1's aerobic phase until day 50, but significantly decreased from days 56 to 308, although to a lesser extent on days 85-100 (Figure VI.S7, in Appendix D). Subsequently, the decrease in peak intensity became less relevant (days 315-351) until no notable differences were detected along the aerobic phase (days 357-407). However, SBR1 recovered the decreasing UV peaks aerobic profile from day 415 on. Similarly to SBR1, SBR2 initially presented no changes in the UV spectra registered along the aerobic phase up to day 50 (Figure VI.S7, in Appendix D). This tendency was reversed from day 56 to day 213. From this point until day 351, a different UV spectrum profile

was observed at the end of the aerobic phase, as the peak at 220 nm did not decrease as much as before, contrarily to the peaks at 240 and 300 nm (Figure VI.S7, in Appendix). Yet, after day 357 and until day 407 none of the UV peaks decreased in intensity along the aerobic phase in SBR2 cycles. Finally, from day 415 on the initial aerobic profile of UV variation was restored, with the three mentioned peaks decreasing to significantly lower levels (Figure VI.S7, in Appendix).

### VI.4.2.3.3. Nitrate *versus* azo dye reduction

Nitrate has been previously reported as interfering with the decolorization process due to the competition between nitrate and the azo dye for the reducing equivalents, nitrate being described as a preferable electron acceptor (Lourenço *et al*., 2000). In light of the potential delay in the start of color removal in the presence of nitrate, the two hydrodynamic regimens were also compared regarding the azo dye reduction performance when nitrate was added to the feed solution of the SBRs. Several samples were collected during a treatment cycle on day 415 (period II.I) to be analyzed through HPLC to assess the concentrations of azo dye and of 4A1NS, as well as through ion chromatography to follow the nitrate and nitrite concentrations in both SBRs. The results indicated that no nitrite was present and that nitrate and the azo dye AR14 were simultaneously and completely reduced in both SBRs, with no lag stage being observed in the AR14 concentration-time profile in any of the reactors, after an adaptation period (Figure VI.20). In addition, the quantification of nitrate through ion chromatography confirmed that nitrate concentrations could be estimated through the HPLC method used to analyze the azo dye and respective metabolites (nitrate absorbs light at 220 nm, appearing as a peak at 3.3 min of RT in the HPLC chromatograms, previously referred to as compound δ), as evidenced by the overlaying concentration values obtained through the two analytical methods (Figure VI.20). In this sense, and owing to relevant changes in the AR14 metabolites' profiles, Figure VI.21 presents the evolution of concentration-time profiles of AR14, 4A1NS and nitrate (measured through HPLC analysis) during treatment cycles along the experimental periods II.H-II.J, further completing the aromatic amine fate analysis of the experimental run II (Figure VI.18 and Figure VI.19).

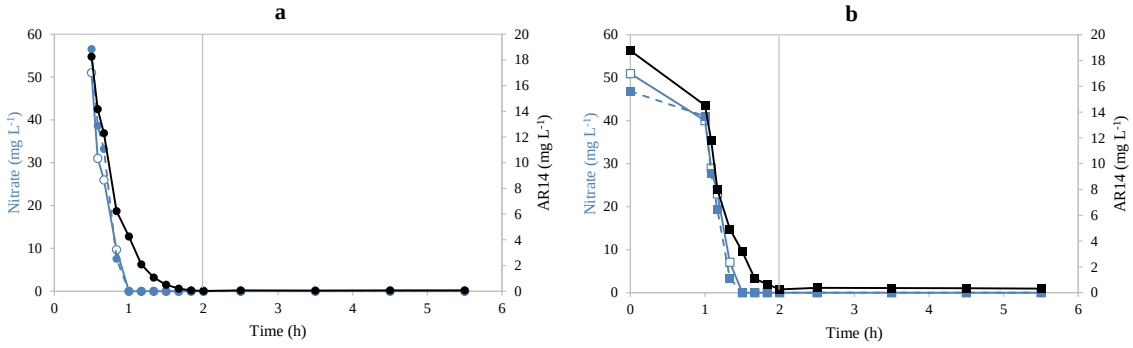


**Figure VI.20** - Nitrate and azo dye Acid Red 14 (AR14) profiles from sequencing batch reactors SBR1 and SBR2 in a treatment cycle of period II.I. Concentration-time profiles of nitrate measured through ion chromatography (blue, full line; blue markers) or by HPLC (blue, dashed line; white markers), and of the azo dye AR14 (black line) in SBR1 (a) and SBR2 (b) on day 415. The first point in chart b was estimated based on values measured in the feed solution (50%) and in the previous cycle treated effluent (50%). Vertical lines represent the end of the anaerobic phase, upon the aeration onset.

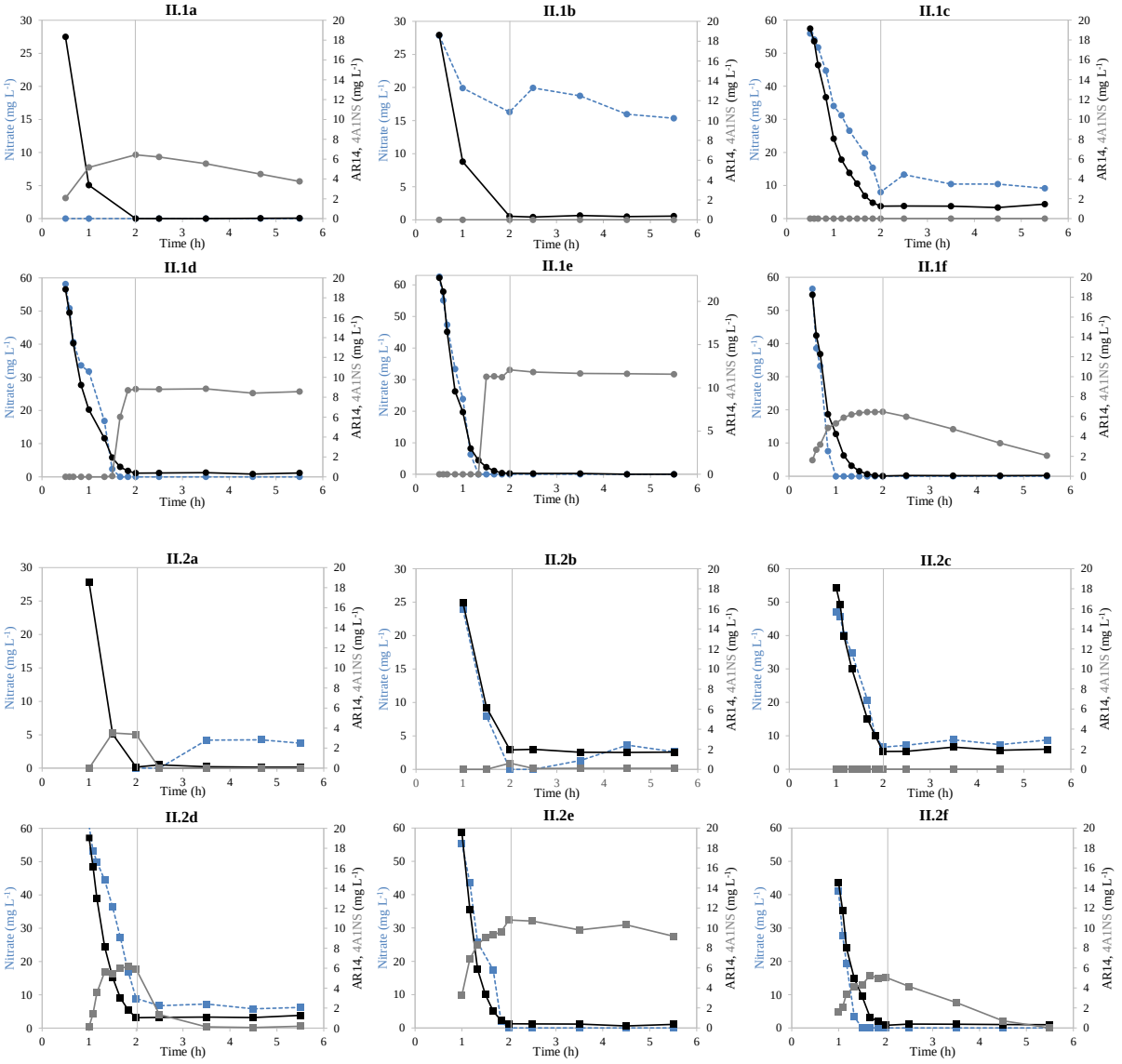


**Figure VI.21** - Nitrate, azo dye Acid Red 14 (AR14) and aromatic amine 4-amino-naphthalene-1-sulfonic acid (4A1NS) profiles during periods II.H-II.J of experimental run II. Concentration-time profiles of nitrate ($NO_3^-$; blue, dashed line), AR14 (black line) and its cleavage product 4A1NS (grey line) in sequencing batch reactors SBR1 (●) and SBR2 (■) on days 351 (II.1a and II.2a), 357 (II.1b and II.2b), 364 (II.1c and II.2c), 371 (II.1d and II.2d), 378 (II.1e and II.2e) and 415 (II.1f and II.2f, respectively for SBR1 and SBR2). Vertical lines represent the end of the anaerobic phase, upon the aeration onset.

After the biomass storage period and before the reactors were supplemented with nitrate (from period II.A to II.G), HPLC results suggest that nitrification consistently occurred in SBR2 cycles, nitrate being formed in the aerobic phase and subsequently denitrified during the non-aerated, idle phase (Figure VI.21, II.2a). In contrast, nitrate was not observed in SBR1 in any of the corresponding cycles (Figure VI.21, II.1a). This was confirmed by measuring the nitrate concentration (through a spectrophotometric method) in samples harvested at the start and end of the anaerobic phase, as well as at the end of the aerobic phase of selected cycles. On the first cycle where calcium nitrate was added to the SBRs to a nitrate concentration of 30 mg $L^{-1}$, nitrate was partially or completely removed along the anaerobic phase in SBR1 or SBR2 (Figure VI.21, II.1b and II.2b), respectively. Conversely,

AR14 concentrations decreased to zero in SBR1 (Figure VI.21, II.1b), but a residual concentration of 2 mg AR14 $L^{-1}$ remained in SBR2 (Figure VI.21, II.2b), the AR14 removal rate being lower when compared to that of cycles when nitrate was not added (Figure VI.21, II.2a). Contrarily to all cycles previously studied, the aromatic amine 4A1NS was not present in the SBRs along the reaction phase, despite the clear AR14 removal registered through the anaerobic phase (Figure VI.21, II.1b and II.2b). Instead of 4A1NS, the concentration of the metabolite α' was high right at the start of the anaerobic mixed phase and further increased during the anaerobic phase, subsequently decreasing under aerobic conditions (Figure VI.S8, II-1a and II-2a, in Appendix D). This occurred in both reactors and a similar observation was registered on the first cycle when calcium nitrate concentration was doubled (Figure VI.S8, II-1b and II-2b, in Appendix D). On this cycle (day 364), none of the SBRs achieved complete azo dye or nitrate removal in the anaerobic phase, and aerobic nitrate formation in SBR2 was no longer evident (Figure VI.21, II.1c and II.2c). Nevertheless, after adaptation to the new nitrate concentration for one week, the azo dye reduction rate was higher in both SBRs (day 371; Figure VI.21, II.1d and II.2d), SBR2 still presenting a residual azo dye concentration (1 mg AR14 $L^{-1}$) until day 415. On this cycle (day 371), both metabolites α and α' were initially present in significant amounts in SBR1, but decreased to zero after 1 h of anaerobic mixed phase, concomitantly with the emergence of 4A1NS in a symmetric, increasing profile, at the moment when nitrate was completely removed (Figure VI.S8, II-1c, in Appendix D). The same types of metabolite α, 4A1NS and nitrate profiles were registered one week later in SBR1, on day 378 (Figure VI.S8, II-1d, in Appendix D). In contrast, on day 371, SBR2 presented its typical 4A1NS profile, the amine concentration increasing simultaneously with the azo dye reduction (Figure VI.21, II.2d). While the 4A1NS concentration was maintained around 9 mg $L^{-1}$ along the aerobic phase in SBR1, it rapidly decreased to zero in SBR2 (Figure VI.21, II.2d), apparently giving rise to metabolite α' that, in turn, was transformed into metabolite α (Figure VI.S8, II-2c, in Appendix D). This profile was not maintained in SBR2, as 4A1NS was no longer removed during the aerobic phase on the subsequent week (cycle analyzed on day 378), similarly to SBR1 (Figure VI.21, II.1e and II.2e). However, from day 415 on, including the period of potassium nitrate supplementation, gradual formation and removal of 4A1NS along the anaerobic and aerobic phases, respectively, were registered in both reactors (Figure VI.21, II.1f and II.2f), with metabolite α being absent and α' remaining at basal levels (Figure VI.S8, II-1e,f and II-2e,f, in Appendix D).

### VI.4.3. Microbial community dynamics

#### VI.4.3.1. FISH analysis

FISH analysis was performed on biomass samples harvested from SBR1 and SBR2 on days 1, 36 and 106 of the experimental run I in order to assess the impact of the different hydrodynamic regimens in the development of the microbial community after inoculation. In addition to analyzing the bacterial

distribution in both SBRs through six major groups, two additional bacterial groups and three extra days were analyzed in SBR1 in light of specific changes in its azo dye degradation performance (Figure VI.22). *Gammaproteobacteria* and *Betaproteobacteria*, dominant groups in the inoculum, became relatively less abundant after 36 days of operation in both SBRs, SBR1 microbial community being predominantly composed of *Alphaproteobacteria*, *Gammaproteobacteria* and *Actinobacteria*, while SBR2 became enriched in *Betaproteobacteria* and *Actinobacteria*. Yet, the microbial communities in the two SBRs further evolved in different ways until day 106, as *Betaproteobacteria* and *Gammaproteobacteria* increased their relative abundance within SBR1 community, as opposed to *Alphaproteobacteria*, while *Gammaproteobacteria* became a minor group in SBR2.

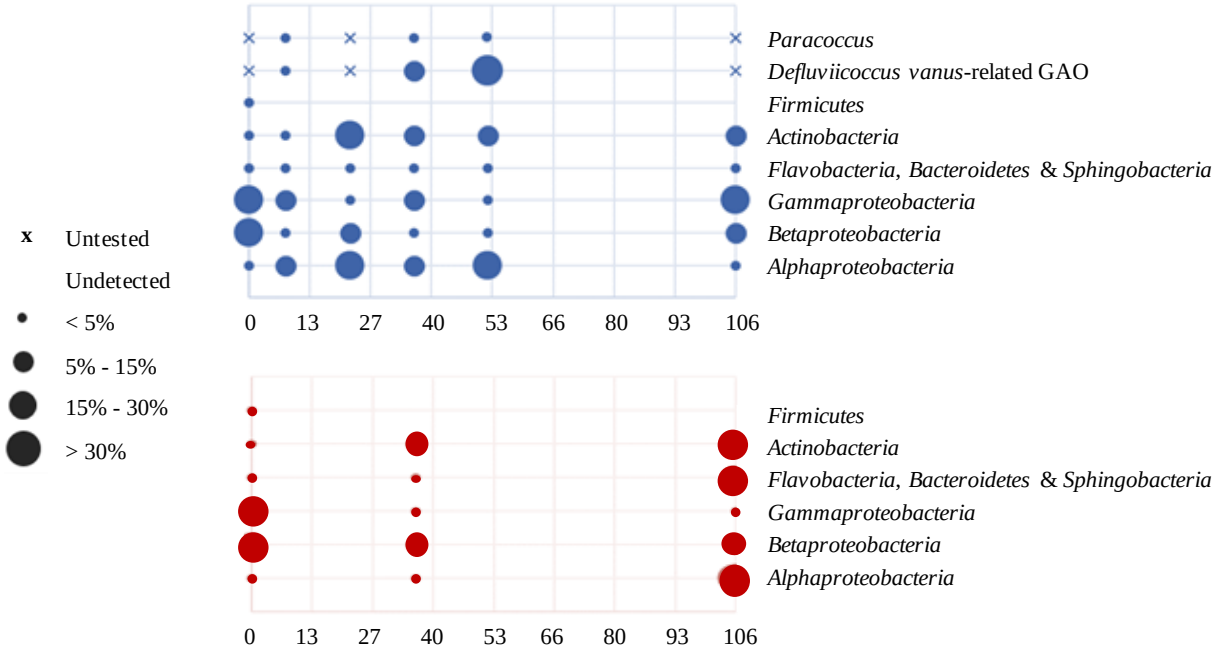


**Figure VI.22 -** Abundance of the selected *Bacteria* detected by FISH analysis in the mixed microbial culture samples from sequencing batch reactors SBR1 (blue circles) and SBR2 (red circles). FISH probes for *Paracoccus* and *Defluviicoccus vanus*-related GAO (glycogen-accumulating organisms) were only applied to SBR1 samples. Additional biomass samples were analyzed in SBR1 (operational days 8, 22 and 52), in light of relevant changes observed in its azo dye biodegradation performance. Adapted from Carvalho (2016).

The previously described decrease in SBR1 decolorization performance (from 80% on day 8 to 45% on day 22; section VI.4.2.3.1) occurred simultaneously with an increase in the relative abundance of *Alphaproteobacteria*, *Betaproteobacteria* and *Actinobacteria*, as opposed to *Gammaproteobacteria* populations that almost disappeared on day 22 (Figure VI.22). In addition, the subsequent increase in the decolorization yield to 80% on day 36, with concomitant removal of 4A1NS in SBR1 (registered from day 24 to 38; section VI.4.2.3.2), was associated with the increase in the abundance of *Defluviicoccus vanus*-related GAO within the *Alphaproteobacteria* group from day 8 to 36 (Figure VI.22). The aromatic amine removal capacity gradually deteriorated from day 38 to 52 (section VI.4.2.3.2), *Defluviicoccus vanus*-related GAO being still present in SBR1 (Figure VI.22), and was subsequently loss up to the end of the experimental run I.

### VI.4.3.2. Microbial community analysis

The high bacterial diversity in the seed sludge was markedly reduced after being inoculated in both SBRs. In fact, after 22 days of operation, the bacterial community in the SBRs was mainly constituted by four phyla: *Proteobacteria*, *Bacteroidetes*, *Actinobacteria* and *Saccharibacteria*, with *Acidobacteria*, *Firmicutes*, *Chloroflexi* and *Chlorobi* phyla becoming irrelevant (Figure VI.S9, in Appendix D). On day 22, the main difference between the SBRs communities at the class level was that SBR2 had a 10% higher and 10% lower relative abundance of *Alphaproteobacteria* and *Sphingobacteriia*, respectively, than SBR1 (Figure VI.23). Regarding the 20 most abundant bacteria among all of the analyzed samples, the same bacterial populations were present in both SBRs in relatively similar abundances, except for specific ones belonging to the *Microbacterium* and *Devosia* genera that were only observed in SBR2, as well as for a bacterial group from the *Saprospiraceae* family, exclusively observed in SBR1 (Figure VI.S10, in Appendix D).

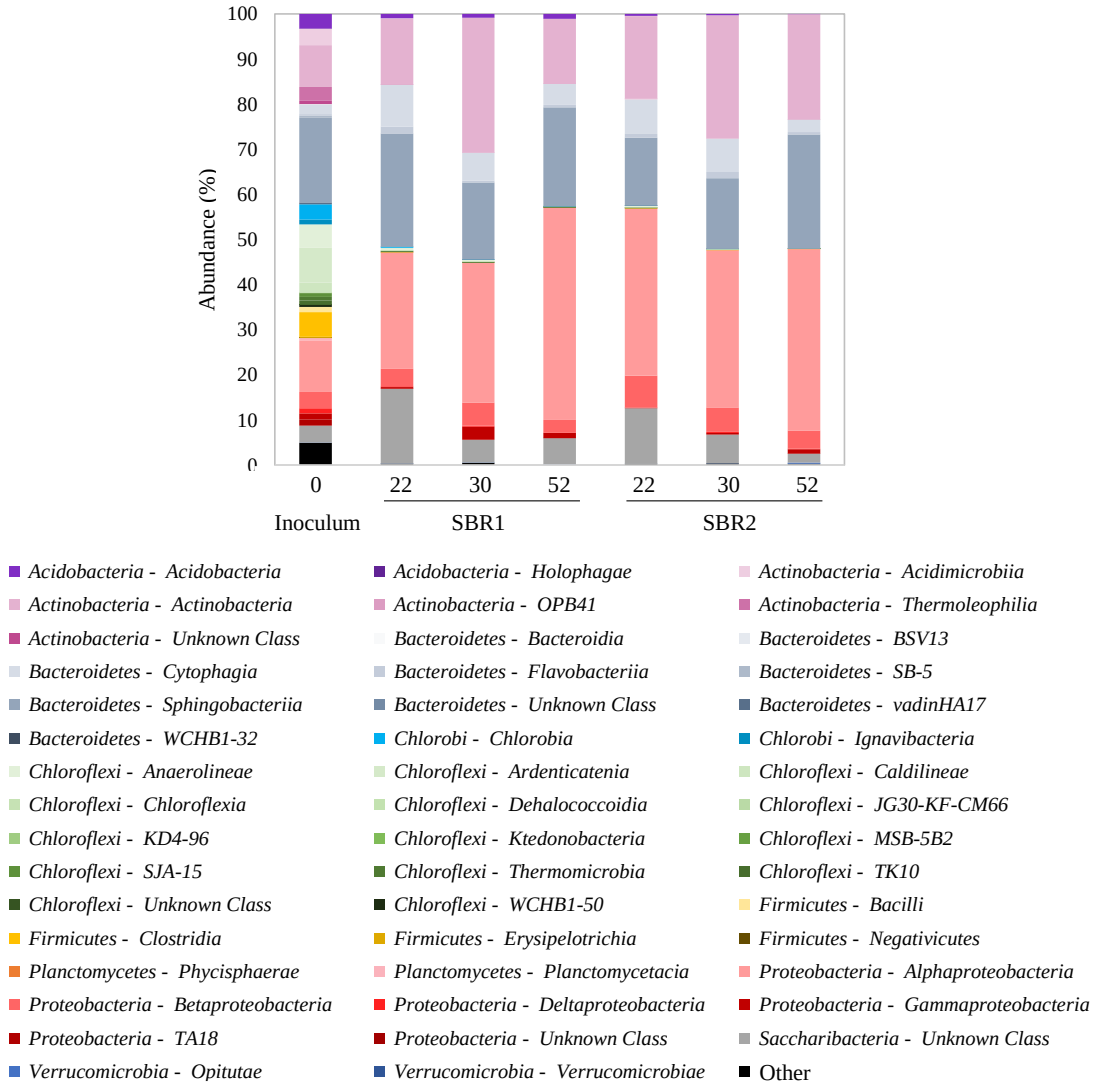


**Figure VI.23** - Composition of bacterial communities at the class level in the inoculum, as well as in sequencing batch reactors SBR1 and SBR2 on the indicated operational days, obtained by 16S rRNA gene sequencing analysis. The most representative "Phylum-Class" are represented below the chart.

Despite slight changes in the relative abundance of the bacterial groups and the emergence of a bacterial population from the *Micropruina* genus in both SBRs, the microbial community did not significantly change from day 22 to day 30 of operation within each SBR in terms of the 20 most abundant bacteria (Figure VI.S10, in Appendix D). Yet, at the class level, both SBRs exhibited an increase in the relative abundance of *Actinobacteria*, mostly in detriment of *Saccharibacteria* phylum, on day 30, when compared with day 22 (Figure VI.23). In addition, and contrarily to SBR2, a higher relative abundance in *Alpha-* and *Gammaproteobacteria* was registered in SBR1.

Subsequently, on day 52, the presence of *Actinobacteria* in SBR1 decreased back to the same relative abundance levels observed on day 22, the distribution of the bacterial community through the different taxonomic phyla and classes being similar in the two reactors (Figure VI.23 and Figure VI.S9, in Appendix D). The same was verified regarding the 20 most abundant bacteria, present in comparable relative amounts in both SBRs, except for a bacterial population from the *Microbacterium* genus, only observed in SBR2 (Figure VI.S10, in Appendix D). Particularly regarding the changes in the microbial community from day 30 to 52, bacterial populations belonging to the *Saprospiraceae* family and *Tetrasphera* genus practically disappeared from SBR1, as well as *Candidatus Promineofilum* from SBR2, giving rise to higher relative abundances of bacteria from the *Hyphomicrobiaceae* and *Niabella* genera in both reactors (Figure VI.S10, in Appendix D). As for the fungal community dynamics in SBR1, a major change occurred from day 30 to 52, as the relatively balanced distribution among the different fungal populations present on day 30 was mostly replaced by two dominant, unknown types of fungi (Figure VI.S12, in Appendix D). This loss of variability within the fungal community was also reflected at the phylum and class levels, as *Ascomycota* and *Basidiomycota*, which constituted approximately 60% of the fungal community on day 30, were reduced to less than 2%, owing to the increased presence of taxonomically unclassified fungi (Figure VI.24 and Figure VI.S11, in Appendix D).

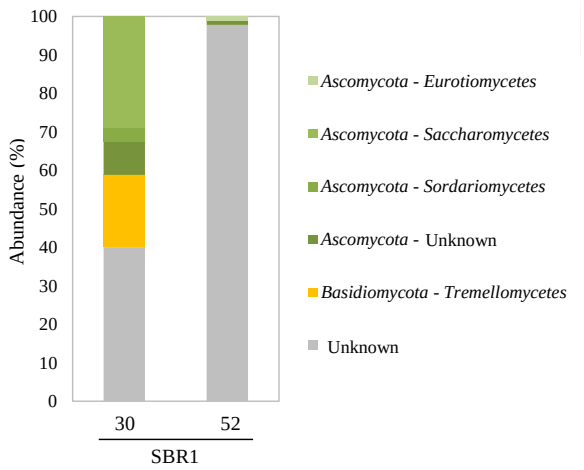


**Figure VI.24** - Composition of fungal communities at the class level in sequencing batch reactor SBR1 on the indicated days, obtained by rRNA gene and internal transcribed spacer (ITS) sequencing analysis. The most representative "Phylum-Class" are represented on the right.

## VI.5. Discussion

### VI.5.1. AGS morphology and properties

#### VI.5.1.1. Granulation and AG size

Aerobic granulation was successfully achieved in both reactors, based on a feast-famine regimen under high hydrodynamic shear forces and short settling times. By comparing an anaerobic plug-flow fed, aerobic SBR with a fully aerobic SBR, Carrera *et al*. (2019) showed that the granulation process was faster in the former (34 days *vs* 90 days). Regarding the present study, analysis of the AGS morphology and properties revealed that AG developed at a similar pace in both reactors (Figure VI.4), the biomass settling properties gradually improving along the first 2 months of operation in both experimental runs (Figure VI.3). In fact, granulation successfully occurred, with small, dense and fast-settling granules dominating the sludge, irrespective of the hydrodynamic regimen. Similarly, Rocktäschel *et al*. (2013) compared two different anaerobic feeding strategies in terms of granulation performance. The authors indicated that stable AG were developed both in an anaerobically-fed plug-flow regimen (H/D of 9), where substrate gradients occurred along the reactor's axis, and in an anaerobically-fed mixed system (fast influent step followed by an anaerobic mixing phase; H/D of 2), where substrate was distributed evenly within the reactor (Rocktäschel *et al*., 2013). On the other hand, when the anaerobically-fed plug-flow regimen was used in an SBR with a H/D of 2, granulation became unstable due to lower storage of organic carbon, a consequence of channeling effects and short contact times of the substrate with the biomass during feeding (Rocktäschel *et al*., 2013; Sguanci *et al.*, 2019). In this sense, owing to the low H/D used in the present study (H/D of 2.5), channeling effects likely occurred in SBR2 during the plug-flow feeding. In fact, the contribution of the anaerobic plug-flow feeding stage to color and COD removal was variable along the experimental runs, suggesting a non-uniform and inconsistent distribution of the feed through the sludge in the non-tubular reactor. Yet, the subsequent anaerobic mixed phase allowed an efficient anaerobic COD removal and stable granulation. Specifically, although anaerobic mixed conditions provided lower substrate gradients, as compared to the plug-flow regimen, this was compensated by higher convective mass transfer coefficients that likely benefited the anaerobic COD uptake. In this sense, achieving efficient anaerobic COD uptake is less dependent on reactor geometry (namely, H/D) if a mixed, instead of a plug-flow, regimen is applied in the feeding step (Rocktäschel *et al*., 2013). Overall, the present results support the study of Rocktäschel *et al*. (2013), who concluded that a steep substrate gradient between the bulk phase and the biomass is not essential to develop stable AGS, SBR1 and SBR2 regimens representing viable alternatives to the anaerobic plug-flow regimen that was first described by de Kreuk and van Loosdrecht (2004).

Along the two experimental runs, the amount of granules with dimensions above 0.65 mm was very low (less than 5%) in both SBRs (Figure VI.2), where most of the AG presented sizes within the 0.20-0.65 mm range. Mata *et al.* (2015), who were the first to report the use of a stirred anaerobic-aerobic, non-tubular SBR for the development and operation of AGS in the treatment of a synthetic TWW, observed that although the granulation period was similar to that of most of the literature studies employing tubular SBRs, the produced AG were smaller (sizes up to 0.5 mm). This was attributed to the higher shear stress caused by the employed mechanical stirring, in addition to the lower selective pressure associated with the use of a lower H/D (2.5). Nevertheless, a study focused on the effects of the H/D on aerobic granulation (Kong *et al.*, 2009) indicated that this parameter (within the 2-24 range) did not affect AG formation, physical characteristics, stability and microbial community structure, highlighting the flexibility of the H/D parameter in the application of the AGS technology. Moreover, a study on the hydrodynamic behavior and aerobic granulation in a stirred tank with a low H/D (Fan *et al.*, 2018) showed that mechanical stirring (impeller rotation speed) had a more significant contribution to the shear rate than aeration (superficial gas velocity). Therefore, the mechanical stirring-associated shear stress was likely the main contributor to the relatively small AG dimensions observed in the present study in both SBRs. This hypothesis was supported by the decrease in the SBR2 granular content (and increase in SVI values) observed after the extension in the SBR2 anaerobic stirred phase (Figure VI.2 and Figure VI.3), slightly disturbing AGS stability. In fact, as compared with a plug-flow feeding regimen, smaller granules have been reported in reactors operated with a mechanically mixed anaerobic phase after fast feeding (0.9 mm *vs* 2.0 mm; Rocktäschel *et al.*, 2013), or even in reactors operated with anaerobic liquid recirculation after a plug-flow anaerobic feeding (<0.6 mm *vs* 0.7 mm; Kang and Yuan, 2019). Accordingly, an increase in the mechanical stirring rate has been shown to significantly reduce the mean particle size (Wan and Sperandio, 2009; Wan *et al.*, 2011).

Overall, although formation of more compact, dense and stable AG has been associated with a relatively high hydrodynamic shear force (Liu and Tay, 2002), excess shear can negatively affect AG structure, eventually causing their disintegration (Kang and Yuan, 2019; Rocktäschel *et al.*, 2013), if the stress applied to the surface overcomes the bonding strength in the core (Nor-Anuar *et al.*, 2012; Wan *et al.*, 2011). Specifically, when AG are small enough in size to minimize substrate internal mass transfer resistance problems, active growth in the AG core further strengthens the aggregate, potentially preventing its disintegration. In fact, some of the largest granules (sizes over 0.65 mm) observed in SBR2 presented a fragile structure (Figure VI.5), possibly being prone to breakage under high shear stress conditions. Accordingly, stability of AG has been defined as the ability of microbial granules to resist hydrodynamic and mechanical shear force (Sheng *et al.*, 2010). On the other hand, densification of the AG core by promoting cellular growth was suggested to be essential to increase the strength of the whole granule. Namely, AG with denitrifying activity (preferably occurring in the

core of AG) have been shown to resist shear forces imposed by mechanical stirring and to maintain their stability during 50 days under these conditions (Zhong *et al*., 2014). In this sense, Kang and Yuan (2019) recently suggested that the feeding system in SBRs should be designed so as to optimize substrate distribution for maximal anaerobic carbon uptake, avoiding the need for further mechanical mixing and associated high shear force that could cause AG disintegration.

### VI.5.1.2. AGS stability

Although the development of granules in SBR2 was similar to that of SBR1 until day 150 of the experimental run I (Figure VI.4), granules subsequently became smaller and AGS settleability deteriorated in SBR1 (Figure VI.3). In fact, AGS stability during long-term operation is a main challenge for broad application of this technology, as highlighted by several studies reporting AG disintegration after prolonged operation (Franca *et al*., 2018; Lee *et al.*, 2010). In contrast with SBR1, granules continued to form and grow in SBR2 up to day 280 (Figure VI.4), leading to a higher abundance of small granules (representing around 30% of the sludge; Figure VI.2) and the emergence of larger ones (sizes up to 0.7 mm; Figure VI.4). Overall, the hydrodynamic regimen in SBR2 allowed the development of more AG than SBR1 (up to 55% *vs* 20% in SBR2 and SBR1, respectively) as well as lower and more stable SVI values (Figure VI.3). Accordingly, although similar biomass profiles were observed during the initial granulation phase, significant differences were registered between the two distinct hydrodynamic regimens after 100 days of operation in the experimental run I, as the biomass concentration in SBR2 increased (maximum of 11 gTSS $L^{-1}$) and remained significantly higher than in SBR1 (4 gTSS $L^{-1}$; Figure VI.10).

An overall superior performance in terms of biomass concentration was achieved using the plug-flow fed reactor, which was more evident over the long-term operation. The higher long-term stability of SBR2 can be attributed to a combination of factors: the use of a shorter mechanical stirring period, associated with a relatively lower shear stress (Fan *et al*., 2018) than in SBR1, and the use of a plug-flow anaerobic feeding regimen, shown to promote stable AG namely by selecting PAO (Carrera *et al*., 2019; de Kreuk and van Loosdrecht, 2004; Pronk *et al*., 2015a). Given the high phosphate concentration in the synthetic TWW and the hydrodynamic regimen used, it is possible that AGS in SBR2 contained more PAO than in SBR1. In fact, the enrichment in the SBR2 suspended solids inorganic content from day 42 on of the experimental run I, in relation to SBR1 (Figure VI.11), may indicate the relevant presence of PAO in SBR2. Specifically, PAO-dominated granules have been associated with a higher ash content, possibly due to the accumulation of polyphosphate (Winkler *et al*., 2011).

Regarding the experimental run II, the presence of AgNP (periods II.A-II.D) did not hinder the AGS formation process (Figure VI.3), and the subsequent interruption of AgNP addition also did not affect

the AGS morphology in the SBRs (Figure VI.S2, in Appendix D). Specifically, during the first part of the experimental run II, in the presence of AgNP, both SBRs maintained a percentage of granules below 15% (Figure VI.2), but alternating periods of settleability deterioration and improvement (Figure VI.3) indicated some operational instability. This could be related to AgNP toxicity, which has previously been shown to impact cyclically on sludge properties through silver accumulation in the biomass (Sheng *et al*., 2018). Subsequently, significant SVI and TSS differences between the SBRs were observed from day 160 on, as SBR1 sludge settling properties deteriorated while SBR2's improved (Figure VI.3 and Figure VI.10). As previously indicated, the anaerobic plug-flow feeding strategy has been shown to favor formation of AG with a compact structure (Yuan *et al*., 2019), being more adequate for obtaining stable AGS using different types of substrates (Pronk *et al*., 2015a). Specifically, the high substrate concentration created by the anaerobic plug-flow feeding regimen allows the substrate to penetrate the entire AG depth and be converted to storage polymers by PAO, which then grow at a low rate on their internally stored carbon source during the subsequent aerobic phase (Pronk *et al*., 2015a), as previously explained. Furthermore, the presence of AgNP apparently prolonged the stability of AGS in SBR1, as deterioration in the SBR1 sludge characteristics (Figure VI.3) occurred approximately 2 months later than in the experimental run I. According to a study on the effect of AgNP in an AGS system during a shorter experimental run (69 days), exposure to AgNP did not significantly affect the AG shape and size (Quan *et al*., 2015).

### VI.5.1.3. AGS reactivation

Regarding the reactivation performance after the 40-day idle period in the experimental run I, the structural integrity of AG was negatively affected due to extended starvation, leading to an initial SVI deterioration after resuming the operation in both SBRs (Figure VI.3). This observation has been previously associated with intracellular protein hydrolysis (Adav *et al*., 2009), cell lysis and disintegration of granules (Lee *et al*., 2010). Yet, the SVI values gradually improved to levels below 100 mL $gTSS^{-1}$ along the first month of AGS SBR reactivation (Figure VI.3), simultaneously with a 20-30% increase in the AG content in both SBRs (Figure VI.2). Similarly, He *et al.* (2017c) reported that AG structure and physical properties could be fully restored after a 58-day extended idle period, highlighting EPS (especially proteins) as major players in AGS resistance to storage (Lee *et al*., 2010). Simultaneously with a selection of EPS-producing bacteria during the idle period, the overall higher percentage of granules observed after the storage period (Figure VI.2) suggests that a significant part of the dispersed and flocculent sludge may have been selectively washed out from the reactors in the first cycles of SBR reactivation as a result of bacterial death during the storage period. In fact, AG have been characterized by their resistance to storage (Gao *et al*., 2012; Wang *et al*., 2008a), as opposed to flocs, which do not have the structural features necessary to keep cell viability under long starvation periods.

Overall, SBR1 and SBR2 presented similar efficiencies in terms of biomass reactivation after storage in the experimental run I, as only small differences were observed in terms of mixed liquor TSS, respective percentage of inorganic matter, biomass washout and SRT along the first 83 days of operation after storage (Figure VI.10 and Figure VI.11). Furthermore, although SBR1 recovered a higher number of granules upon reactivation, these were not as large as those observed in SBR2, which resisted to the storage conditions and further grew to sizes over 0.65 mm (Figure VI.2). However, some of the largest AG presented morphological characteristics indicative of a fragile structure (Figure VI.5). Probably, above a maximum AG size problems associated with diffusion limitation become insurmountable and the AG structural integrity compromised, as reviewed by Franca *et al*. (2018).

Regarding the experimental run II, SBR1 suffered from sludge settleability deterioration after the 18-day storage more than SBR2 (Figure VI.3), denoting the higher resistance of AGS developed in the plug-flow fed reactor, which included a shorter stirred phase than SBR1. Despite the lack of studies regarding the effect of the hydrodynamic regimen in AGS reactivation performance, the anaerobic plug-flow feeding strategy has been generally associated with the formation of stable granules (Pronk *et al*., 2015a). Similarly to the reactivation period in the experimental run I (storage at room temperature), SVI levels improved in SBR1 upon reactivation in the experimental run II (period II.D, after storage at 4ºC), despite the expected more profound deteriorating effect of a higher storage temperature in terms of AG structural integrity (Lee *et al*., 2010). Moreover, while the SBR2 sludge became gradually enriched in granules, stabilizing around 30% after biomass reactivation, SBR1 went through a sharp increase in the granular content to 43% upon interruption of AgNP supplementation (Figure VI.2). Although the effect of AgNP on AGS formation has not yet been described in the literature, contact studies of AgNP with mature AGS did not negatively affect AG dimensions (Gu *et al*., 2014; Quan *et al*., 2015). Nevertheless, SBR1 did not reach the excellent sludge settling characteristics that SBR2 sustained after reactivation (Figure VI.3).

### VI.5.1.4. Dye-shock load and nitrate supplementation

Although the AGS morphology was not significantly affected by the short idle period (period II.C) nor by the three-fold increase in dye concentration (period II.F), the azo dye shock load slightly declined the sludge quality, confirming previous observations (Franca *et al*., 2017). Overall, SBR2 could sustain higher biomass concentration levels than SBR1, even during the dye shock load (Figure VI.10). Accordingly, in a previous study regarding the effect of SBR feeding strategy on AGS stability in the treatment of a simulated TWW (Franca *et al*., 2017), the anaerobic plug-flow fed, anaerobic-aerobic SBR allowed faster AGS recovery from imposed disturbances in the feed composition, when compared with a control anaerobic-aerobic SBR.

Upon supplementation of the synthetic TWW with 120 mg $NO_3^-$ $L^{-1}$ from calcium nitrate (period II.I), the biomass settling properties improved (Figure VI.3) and the TSS levels rapidly increased in both SBRs (Figure VI.10), along with the sludge inorganic matter content (Figure VI.11), indicating the accumulation of minerals in AG. In fact, during calcium nitrate supplementation AG became larger (Figure VI.4), presenting small inclusions composed of calcium and phosphorus (Figure VI.8), apparently corresponding to calcium phosphate precipitates (Figure VI.9). Accordingly, accumulation of minerals inside AG has been associated with higher structural strength and better settling properties (Huang *et al*., 2014; Ren *et al*., 2008), namely AG rich in phosphate salts (Isanta *et al*., 2012). Subsequently, during the period of potassium nitrate supplementation (period II.J), a decrease in the AG abundance (especially in SBR1; Figure VI.2) and in the sludge inorganic matter content (from 14 to 11%; Figure VI.11) were registered in both reactors. Although the presence of nitrate in SBRs has been shown to promote the densification of AG due to enhanced activity of denitrifying bacteria in the AG core (Wan and Sperandio, 2009), the enlargement of granules during period II.I was likely due to the addition of calcium. In fact, Ca precipitation and $Ca^{2+}$ role in enhancing polysaccharide content in AG have been previously associated with an improved granular strength (Lee *et al*., 2010).

## VI.5.2. AGS SBR treatment performance

### VI.5.2.1. Organic load removal

Similarly to other studies on AGS for TWW treatment (Ibrahim *et al*., 2010; Muda *et al*., 2011), the COD removal performance gradually improved along the first 2 weeks of operation in SBR1 and SBR2 reaching 80% of total COD removal in both experimental runs, the overall COD removal yield profiles being stable and comparable between the two SBRs throughout both experimental runs, irrespective of the feeding strategy used (Figure VI.12). A recent study (Carrera *et al*., 2019) indicated that an SBR operated with an anaerobic feeding followed by an aerobic phase presented a slightly more stable COD removal performance (80-90%) than a fully aerobic SBR (75-85%). In fact, regarding the COD removal under anaerobic conditions, SBR1 initially removed a higher fraction (maximum of 70%) than SBR2 (maximum of 60%) during the experimental run I. However, this initial tendency was reversed from day 163 on, as SBR1 values decreased down to 40% when the SBR1 TSS levels were reduced to around 4 gTSS $L^{-1}$, while SBR2, which contained significantly more biomass (up to 11 gTSS $L^{-1}$; Figure VI.10), sustained anaerobic COD removal levels around 60% (Figure VI.12). The reason for SBR2 having taken longer to achieve 50% of anaerobic COD removal is probably related to the need for a longer time to accumulate a minimal amount of biomass in the reactor before the plug-flow feeding stage could contribute for the COD removal, and compensate for the shorter SBR2 anaerobic stirred phase. Similarly, in a previous study treating the same synthetic TWW, the use of a hydrodynamic regimen equivalent to SBR2's generally allowed higher COD removal yields during the anaerobic phase than SBR1's, despite the relatively low contribution of the

plug-flow feeding stage (Franca *et al.*, 2017). In fact, the contribution of the SBR2 plug-flow feeding stage for the total COD removal accounted for less than 30% (Figure VI.13), owing to the low reactor H/D, which likely leads to an heterogeneous flow pattern (channeling effects) and short contact times of the substrate with the settled sludge bed (Rocktäschel *et al*., 2013). Moreover, the COD removal performance in SBR2 slightly improved after the stirred anaerobic period was extended to 1 h (period I.G; Figure VI.12). Accordingly, Kang and Yuan (2019), who compared the performance of two operation strategies (90-min plug-flow anaerobic feeding followed by aeration *vs* 15-min plug-flow anaerobic feeding followed by 75 min anaerobic recirculation of the liquid through the settled biomass and aeration) concluded that the system with anaerobic recirculation enhanced mass transfer and increased anaerobic COD removal (as well as nutrient removal, effluent quality and SRT).

Similarly to a previous study (Franca *et al.*, 2017), complete anaerobic COD removal was never achieved in the SBRs. Despite the longer stirred phase employed in SBR1 (1.5 h), the same residual COD levels were attained at the end of the anaerobic phase in both SBRs, which was subsequently removed during the first 1.5 h of aeration, the remaining 2 h of aerobic phase corresponding to a starvation period (Figure VI.13). Likewise, Carrera *et al*. (2019) reported that because the anaerobic feeding phase was not long enough to guarantee complete organic matter uptake, the remaining COD (as hydrolysis products) was consumed during the initial minutes of the aerobic phase by microorganisms at the surface of the AG. The consequent steep substrate diffusion limitation gradients promoted filamentous growth in AG and instability of the system (Carrera *et al*., 2019; Pronk *et al*., 2015a). In this sense, the correct management of the anaerobic feeding/reaction phase has been pointed out as crucial to assure complete anaerobic storage of the COD and consequent stable AGS (Carrera *et al*., 2019). Despite the fact that the applied COD probably exceeded the anaerobic storage capacity of microorganisms (namely PAO and GAO), filamentous outgrowth was not observed in granules of SBR1 and SBR2, which might have been prevented by the high shear stress (de Kreuk *et al.*, 2010) imposed by the mechanical stirring.

Contrarily to the experimental run I, the anaerobic COD removal levels were much lower in the first period of the experimental run II (around 15%), only reaching 50-60% levels after 100 days of operation (Figure VI.12). The inferior anaerobic COD removal performance in the experimental run II could be attributed to the presence of AgNP or to the different microbial community in the inocula. However, the first hypothesis is less likely owing to the high, stable COD removal yields (>98%) reported by Quan *et al*. (2015) in an AGS SBR exposed to AgNP during 69 days. In fact, heterotrophic bacteria responsible for organic matter removal are generally more resistant to AgNP when compared to autotrophic bacteria (Choi *et al*., 2008).

Regarding AGS reactivation in the experimental run I, SBR1 and SBR2 recovered the 80% overall COD removal yield 10 days and 17 days after the 40-day idle period at room temperature, respectively

(Figure VI.12), both SBRs reaching 50-60% of anaerobic COD removal after 20 days. Accordingly, Wang *et al.* (2008a) demonstrated that the COD removal performance of AG stored at low temperatures for 7 months could be recovered after 2 weeks of operation. In addition, SBR1 and SBR2 were able to achieve overall COD removal yields of 87-89% on the first cycle of SBR reactivation after the 18-day storage period (at 4ºC) applied in the experimental run II (period II.C; Figure VI.12), denoting the AGS ability to preserve the organic matter degradation potential through short periods of storage at low temperatures, irrespective of the hydrodynamic regimen used. Similarly, Zhu and Wilderer (2003) reported that AGS restored microbial activity within a week after 7 weeks of storage at room temperature.

The COD removal performance was slightly deteriorated after the azo dye shock load period, but subsequently improved during nitrate supplementation, especially in terms of anaerobic COD removal, with 90% of overall COD removal at the end of the operation, 60% of which being removed anaerobically in both SBRs (Figure VI.12). The improved anaerobic COD removal in the presence of nitrate was possibly a result of denitrification, further contributing to oxidation of the organic matter (Beun *et al*., 2001). In fact, the pH profiles in both SBRs shifted to higher values (6.7-6.9) during the periods of nitrate supplementation (periods II.H-II.J; Figure VI.13), presumably due to denitrification which is a pH-increasing process (Pereira *et al*., 2011).

### VI.5.2.2. Azo dye biodegradation

#### VI.5.2.2.1. Color removal

During the experimental run I, color removal yields around 80% were reached in SBR1 on the operational day 3 and were maintained throughout most of the operation (Figure VI.14), denoting the capacity of CAS to remove color under anaerobic conditions after a short adaptation period. This color removal performance is consistent with previous studies (Franca *et al*., 2015; Mata *et al*., 2015), the color removal yields being generally higher than those reported in other AGS studies (55-62%; Kee *et al*., 2014; Muda *et al*., 2010; Muda *et al*., 2012). In fact, Moghaddam and Moghaddam (2016), who employed cycle conditions similar to those of the present work (6-h cycles, comprising 1.3 h of stirred anaerobic phase followed by 4.3 h of aeration) to treat a synthetic TWW containing the azo dye Acid Red 18 could only achieve 54% of color removal. In addition, Muda *et al.* (2011) and Ibrahim *et al*. (2010) could only reach yields above 90% when using higher HRT values (24 h) and a longer anaerobic phase (12-18 h).

The temporary deterioration in SBR1 color removal performance (47% on day 17; 80% recovered on day 35) registered after several biomass washout episodes due to settling time reduction, was similar to that reported by Franca *et al.* (2015) during a period of daily biomass purge for SRT control. This could suggest that microbial populations relevant for the decolorization process were washed out from

the system due to the shortening of the settling time. However, this hypothesis is not likely owing to the functional redundancy of the microbial community regarding color removal (van der Zee and Villaverde, 2005). On the other hand, these low color removal events could be related with the lower biomass concentrations, which can lead to higher oxygen diffusion from the headspace to the liquid and the consequent increase in the ORP during the anaerobic phase, previously associated with lower decolorization performances (Lourenço *et al*., 2001).

Regarding SBR2, only 60% of color removal yield were achieved when the reactor was operated with a 30-min stirred anaerobic phase in the experimental run I (Figure VI.14), the plug-flow stage accounting for a maximum of 45% of total decolorization. Yet, maximal color removal yields of 80% were reached and sustained in SBR2 when the anaerobic stirred phase was increased to 1 h (period I.G). Therefore, SBR2 achieved the same color removal performance than SBR1 despite having a stirred anaerobic phase 30 min shorter (Figure VI.15), which comes as an advantage in terms of energy costs. In fact, these cycle conditions allowed both SBRs to achieve the same high color removal yields one week after inoculation in the experimental run II, 75-90% being sustained along the operation, irrespective of the presence of AgNP, higher dye concentrations or nitrate (Figure VI.14). In contrast, other studies focused on AGS SBRs for TWW treatment reported the deterioration in AG stability and in dye removal efficiency (Moghaddam and Moghaddam, 2016), as well as in the COD removal yield (Kolekar *et al*., 2012) upon increase of the initial azo dye concentration.

In terms of AGS reactivation after storage, while SBR1 and SBR2 reached 80% and 70% of color removal yield, respectively, 10 days after the 40-days biomass storage period at room temperature (experimental run I), 80% of decolorization was restored in both SBRs on the second day of operation after the 18-day idle period at 4ºC (experimental run II). The AGS resistance to extended idle periods is especially important in TWW treatment systems, since wastewater production often faces interruptions for several days or weeks, according to the manufacturing schedules (Mata *et al*., 2015). Despite the lack of studies on color removal performance by reactivated AGS, these results are in accordance with previous studies on AGS reactivation (Lee *et al*., 2010), namely a recent work reporting the full recovery of the AGS SBR performance 16 days after a 58-day idle period with no temperature control (He *et al*., 2017c).

#### VI.5.2.2.2. Nitrate *versus* azo dye reduction

Nitrate is a common compound in TWWs, reports on its effect on the reductive decolorization of azo dyes being contradictory (Carliell *et al.*, 1998; Pearce *et al*., 2006). Some previous studies reported significant nitrate interference in the azo dye decolorization process, namely the appearance of a lag-phase, due to the competition for reducing equivalents, nitrate being indicated as a preferable electron acceptor (Carliell *et al.*, 1998; Lourenço *et al*., 2000; Panswad and Luangdilok, 2000). In contrast,

complete and simultaneous azo dye reduction and denitrification occurred in both AGS SBRs (Figure VI.20), which is in agreement with the findings reported by Pearce *et al*. (2006) regarding Remazol Black B decolorization. Accordingly, in light of the absence of an effect of nitrate on the Reactive Red 2 reduction efficiency, dos Santos *et al*. (2008) indicated that the presence of nitrate in TWWs will not likely decrease the capacity of bioreactors to anaerobically biodecolorize azo dyes. In fact, despite the initial slight reduction in the color removal yield to 70% (especially in SBR2) during the first cycles of nitrate addition in the feed composition (Figure VI.21), the presence of calcium nitrate or potassium nitrate had no long-term effect in the decolorization performance, as both reactors rapidly recovered their typical color-time profile (Figure VI.15). The relatively more relevant susceptibility of SBR2 to nitrate interference in the decolorization performance, when compared to SBR1, is probably due to the occurrence of higher rates of denitrification in SBR2, where the anaerobic plug-flow feeding regimen allows the biomass to contact with a higher nitrate concentration and has been shown to favor the presence of denitrifiers (Pronk *et al*., 2015a). In fact, HPLC results suggested the occurrence of nitrification and denitrification in SBR2 (but not in SBR1), before the nitrate supplementation periods (periods II.D-II.G; Figure VI.21).

### VI.5.2.2.3. Fate of aromatic amines

The 4A1NS profiles significantly changed throughout the course of the experimental run I in both SBRs (Figure VI.16). Complete bioconversion of 4A1NS was registered in SBR1 from day 24 to 38, after recovering from an unstable color removal period, similarly to a previous study (Franca *et al.*, 2015). On the other hand, interconversion between 4A1NS and an unknown metabolite (α' and/or α) was apparently observed in SBR2 from day 31 to 56, equivalent observations being described by Franca *et al*. (2015) under a hydrodynamic regimen equivalent to SBR1's. In fact, analysis of the UV spectra of the reaction liquid along the aerobic phase suggested that only SBR1 effectively removed 4A1NS during a 3-week period of the experimental run I. Overall, while some SBR studies were unsuccessful in further converting 4A1NS under aerobic conditions (Mata *et al*., 2015; Moghaddam and Moghaddam, 2016), others report the transformation of the aromatic amine after at least 3 weeks of operation of biofilm or AGS reactors (Franca *et al*., 2015; Koupaie *et al*., 2013), denoting the need for microbial adaptation to this recalcitrant compound and for relatively high SRT values. The 4A1NS removal profile in SBR1 was subsequently lost after day 38, likely due to a prolonged period with poor aeration, reinforcing the need for aerobic conditions for further degradation of these azo dye breakdown products (Pinheiro *et al*., 2004). Similarly, the 4A1NS transformation in SBR2 was no longer observed after day 77 (Figure VI.16), probably because of ineffective stirring in the anaerobic phase during 4-5 days (due to problems in the stirring system), consequently leading to low 4A1NS production and eventually inhibition of the bacteria and/or metabolic pathways responsible for the previously observed conversions. These results reflect the need for stable, fine-tuned operational

conditions in order to maintain the activity of microorganisms responsible for further biodegrading this sulfonated aromatic amine, as well as for better control of the competition between biodegradation and autoxidation (Stolz, 2001).

While association between the presence of *Defluviicoccus vanus*-related GAO and 4A1NS transformation was here proposed, this group of bacteria capable of anaerobic carbon storage was still present after the prolonged period with poor aeration in the experimental run I despite the absence of 4A1NS conversion. In this sense, the expression of enzymes hypothetically implicated in the amine transformation pathway might have been turned off by the prolonged anaerobic period. In addition to *Defluviicoccus vanus*-related GAO, the transformation of 4A1NS during the aerobic phase in SBR1 was associated with changes in the bacterial community, namely an increase in the relative abundance of *Alphaproteobacteria*, *Betaproteobacteria* and *Actinobacteria*, as opposed to a decrease in *Gammaproteobacteria*, *Saccharibacteria* phylum, *Saprospiraceae* family and *Tetrasphera* genus (Figure VI.22; Figure VI.23; Figure VI.S10, in Appendix D). According to a recent study (Sun *et al*., 2019), *Alphaproteobacteria* are involved in aromatic compound degradation. Furthermore, diverse genes encoding enzymes for aromatics degradation were mainly carried by species in *Alphaproteobacteria* (*Rhodobacter*), *Betaproteobacteria* (*Bordetella*, *Acidovorax*, *Ramlibacter* and *Pusillimonas*), and *Bacteroidetes* (*Flavobacteriaceae* and *Sphingobacteriales*), present in enriched nitrifying sludge (Sun *et al*., 2019). In addition, the loss of 4A1NS conversion capacity in SBR1 was associated with a significant decrease in the fungal diversity (Figure VI.S12, in Appendix D), indicating a potential role of fungi in aromatic amine transformations. In fact, although most of the studies reporting aromatic amine removal do not reveal the underlying mechanism, several works revealed the potential of fungal laccases, oxidative enzymes characterized by a high non-specific oxidation capacity, to remove aromatic amines produced during anaerobic cleavage of azo dyes via oxidative coupling reactions (Franciscon *et al*., 2010; Zille *et al*., 2005). Moreover, studies suggest that laccases may also be widespread in bacteria, including autotrophs such as nitrifying bacteria (Ausec *et al*., 2011). In addition, bacterial laccases have been implied in the oxidation of aromatic amines arising from textile azo dyes (Mendes *et al*., 2011; Molina-Guijarro *et al*., 2009; Sousa *et al*., 2014).

Regarding the experimental run II, the presence of AgNP did not prevent 4A1NS transformation, as conversion of 4A1NS was registered from day 56 to 77 in both SBRs (Figure VI.19). The delay in the transformation of 4A1NS in comparison with the experimental run I (day 56 *vs* 31) could be attributed to the use of a different inoculum, or to the presence of AgNP. Despite the absence of studies on the effect of AgNP in the azo dye biodegradation in AGS SBR systems, the potential application of these nanoparticles in the treatment of TWW has been recently described. Specifically, AgNP were described as efficient catalysts in the reductive degradation of textile dyes Methyl Red (Husain *et al*., 2019), Methyl Orange and Congo red (Edison *et al*., 2016; Saravanan *et al*., 2017). In addition to these

studies, which focus primarily on decolorization, the fate of the resulting aromatic amines not being specifically addressed, complete mineralization of the latter dyes has been suggested using $Ag/TiO_2$ nanocomposite as photocatalyst (Rostami-Vartooni *et al.*, 2016). Similarly, the photocatalytic degradation of Acid Red 27 (Amaranth) by AgNP has also been described (Haritha *et al.*, 2017).

The subsequent temporary deterioration in the 4A1NS removal in SBR1 and SBR2 (on days 85-100 and on day 85, respectively; Figure VI.19) was associated with an operational control accident, which led to a prolonged aeration period (15.5 h, on days 84-85) in both reactors. The sudden change in the operating conditions likely induced changes in the microbial metabolism in response to stress conditions, namely to a prolonged starvation period. Yet, contrarily to the consequences of lack of aeration that led to loss of 4A1NS in the experimental run I, prolonged aeration only caused the temporary worsening of 4A1NS removal. Similarly to a previous work (Franca *et al.*, 2017), the plug-flow fed SBR recovered more rapidly from this disturbance, as SBR1 and SBR2 achieved the previous complete conversion of 4A1NS on days 106 and 92, respectively. In addition, SBR2 was able to sustain 4A1NS removal for a longer period than SBR1 (*ca.*, 300 *vs* 190 days) and was the only one to completely remove 4A1NS during the AR14 shock load (Figure VI.18 and Figure VI.19).

Although both SBRs maintained the capacity to transform the aromatic amine after the 18-day idle period, SBR2 presented a less effective 4A1NS removal than before the idle period, as observed by HPLC and UV spectra analysis (Figure VI.S6 and Figure VI.S7, in Appendix D), reflecting a relevant change at the metabolic or microbial community level during the idle period. Finally, after a 50-day period of no 4A1NS removal in any of the reactors, concomitantly with the high calcium nitrate supplementation, 4A1NS conversion resumed in both SBRs up to the end of the experimental run II, the amine only being completely converted in SBR2 (Figure VI.19). The differences between the 4A1NS fates observed in the two SBRs indicate the presence of different microbial communities. In fact, in addition to de Kreuk and van Loosdrecht (2004), recent studies further demonstrated the impact of the feeding regimen on the SRT and in the selection of key functional groups, such as GAO, PAO, nitrifying and denitrifying organisms (Carrera *et al.*, 2019; Yuan *et al.*, 2019). Nevertheless, after 52 days of operation in the experimental run I, the bacterial community was similar in the two reactors (Figure VI.23 and Figure VI.S9, in Appendix D), except for a bacterial population from the *Microbacterium* genus, only observed in SBR2 (Figure VI.S10, in Appendix D). Accordingly, AG developed in a column SBR operated with 1 h of anaerobic phase (including 30 min of feeding from the bottom of the reactor) and 3 h of aerobic phase were dominated by *Microbacteriaceae* members *Microbacterium* and *Leucobacter*, which were strongly correlated to biomass settling velocity and bioreactor performance (Gonzalez-Martinez *et al.*, 2017).

Finally, despite the generally low biodegradation potential of sulfonated aromatic amines under anaerobic conditions (Pandey *et al.*, 2007), the absence of 4A1NS formation during the first weeks of

SBR1 (3 weeks) and SBR2 (1 week) supplementation with calcium nitrate in the experimental run II (Figure VI.21) was correlated with the production of an unknown metabolite along the anaerobic phase (Figure VI.S6, in Appendix D). Yet, after adaptation to the new feed conditions, normal anaerobic 4A1NS formation and its subsequent conversion during the aerobic phase were resumed in both SBRs. This indicated that although the presence of nitrate did not significantly affect the decolorization performance, it initially interfered with the anaerobic fate of azo dye reduction products. According to Pereira *et al*. (2011), who investigated the fate of aromatic amines under denitrifying conditions, the presence of nitrate does not lead to autoxidation of aromatic amines. Specifically, aniline biodegradation under anaerobic conditions has been associated with nitrate reduction by several authors, as reviewed by Pereira *et al*. (2011). In addition, Seymor *et al.* (2002) showed that nitrite, produced from nitrate in the first step of denitrification, can react with aromatic amines, resulting in deamination, thus potentially yielding aromatics with a higher biodegradation potential. Furthermore, Pereira *et al*. (2011) observed that nitrite caused a chemical reaction that led to immediate disappearance of aniline and/or sulfanilic acid, concomitantly with the formation of an intense yellow colored solution, probably associated with the formation of azo compounds via electrophilic aromatic substitution (nitration), diazotization and coupling reactions.

## VI.6. Conclusions

Aerobic granulation was successfully achieved both in the statically fed, anaerobic-aerobic SBR1 and in the plug-flow fed, anaerobic-aerobic SBR2, with small, dense and fast-settling granules being formed along 2 months of operation. The size of the granules (< 1 mm) was likely limited by the shear stress associated to mechanical stirring. When supplemented with calcium nitrate the reactors achieved higher TSS levels and further produced fast-settling, larger AG, containing inclusions likely composed of calcium phosphate. The presence of AgNP did not negatively affect the granulation process and AGS stability in the long-term, despite some variations in the settleability. Overall, SBR1 and SBR2 similarly improved their sludge properties upon reactivation after a 40-day idle period at room temperature, but AGS in SBR2 resisted better than SBR1's to the 18-day storage at 4ºC, as well as to the azo dye shock load. When compared to SBR1, the plug-flow feeding regimen and the shorter mechanical stirring phase in SBR2 allowed it to maintain stable AGS and higher biomass concentrations during a longer period of operation. Particularly in the experimental run I, the significantly higher inorganic matter content in SBR2 biomass, as well as the higher abundance of larger AG and better sludge settling properties, suggested the presence of PAO.

Irrespective of the feeding strategy used, 80% of COD removal yield was reached after 2 weeks of operation and maintained along the experimental runs, up to 60% of which being removed during the anaerobic phase. Although SBR1 reached higher levels of anaerobic COD removal sooner than SBR2, the latter was able to sustain higher removal efficiencies during long-term operation. When the

anaerobic stirred phase of SBR2 was increased to 1h, both reactors reached a stable 80% color removal yield in the experimental run I, decolorization occurring through anaerobic reduction of the azo bond of AR14, as confirmed by HPLC. Furthermore, the SBRs reached high color removal yields one week after inoculation in the experimental run II, 75-90% being sustained along the operation, irrespective of the presence of AgNP, higher dye concentrations or nitrate. In fact, despite the non-uniform feed distribution during the plug-flow feeding, the subsequent anaerobic mixed phase allowed SBR2 to reach the same anaerobic COD and color removal levels than SBR1 even though employing a 30-min shorter stirred phase. Maximal anaerobic COD uptake during the plug-flow feeding could be further optimized to minimize the length, associated shear stress and cost of the subsequent stirred anaerobic phase. Regarding the reactivation performance, although SBR1 and SBR2 took more than 10 days to restore high COD and color removal yields after the 40-day idle period, their treatment performance was not significantly affected by the 18-day biomass storage period, further supporting the application of AGS in the treatment of the typically irregular TWW discharges.

Despite an initial, slight reduction in the color removal yield to 70% (especially in SBR2) during the first cycles of nitrate supplementation, the latter had no long-term effects in the decolorization performance, as complete and simultaneous azo dye reduction and denitrification occurred in both SBRs. Although the presence of nitrate did not significantly affect the decolorization performance, it initially interfered with the anaerobic fate of one azo dye reduction product, as a new, unknown metabolite was formed along the anaerobic phase instead of the aromatic amine 4A1NS, potentially supporting previous studies reporting its rapid deamination by reaction with nitrite. Yet, after adaptation to the new feed conditions, normal anaerobic 4A1NS formation and, subsequently, its conversion during the aerobic phase were resumed in both SBRs. In contrast, the azo dye biodegradation performance of both reactors was not affected by the presence of AgNP.

Approximately after 1 month of operation in the experimental run I, complete bioconversion of 4A1NS was registered in SBR1 producing significant changes in the liquid effluent's UV spectrum, and interconversions between 4A1NS and an unknown metabolite were observed in SBR2. Yet, the reactors lost the capacity to aerobically transform 4A1NS due to operational problems (namely, prolonged periods of poor aeration or ineffective stirring), being possibly associated with a significant decrease in the fungal diversity. On the other hand, complete 4A1NS conversion was only temporarily deteriorated in both SBRs upon an accidental, prolonged period of aeration during the experimental run II. In addition, SBR2 was able to sustain 4A1NS complete conversion for a longer period than SBR1 (*ca*., 300 *vs* 190 days), namely during the AR14 shock load. Although both SBRs maintained the capacity to transform the aromatic amine after the 18-day biomass storage period, SBR2 presented a different and less effective 4A1NS conversion performance, reflecting a relevant change at the metabolic or microbial community level caused by the idle period.

# VII. Impact of AgNP on long-term operation of an AGS SBR for TWW treatment

The information included in this chapter was partially published in:

Franca, R.D.G., Rodrigues, A.M., Pinheiro, H.M., Lourenço, N.D., 2018. Impact of silver nanoparticles on long-term operation of AGS SBR for textile wastewater treatment. *IWA Biofilms: Granular Sludge Conference*, 18-21 March, Delft, The Netherlands.

## VII.1. Abstract

In addition to high organic loads and recalcitrant azo dyes that characterize the highly polluting textile industry wastewater, the increasing use of AgNP in textiles represents a new environmental problem. In light of the potential application of AGS technology for TWW treatment, this study investigated for the first time the impact of AgNP on TWW treatment performance by anaerobic-aerobic AGS SBRs during long-term operation, including aerobic granulation and AGS reactivation after an idle period. In this sense, SBR1 was fed with a synthetic TWW containing 10 or 20 mg $L^{-1}$ of AgNP in the experimental runs I and II, respectively, and run in parallel with a AgNP-free control (SBR2) for 404 and 434 days (run I and II, respectively). The response of the SBRs towards an azo dye shock load and the presence of nitrate salts in the feed solution was also compared after interrupting AgNP addition in SBR1. Successful granulation was achieved after 40-50 days of operation, irrespective of the presence of AgNP, the latter slightly enhancing AGS settling properties and biomass accumulation in the long-term operation, including during reactivation after prolonged idle periods. Despite the cumulative adsorption of AgNP to the biomass, the treatment performance was not affected, with 80% of color and organic load removal being reached after 1 and 2 weeks of operation, respectively, and maintained along the two experimental runs in both SBRs. Furthermore, although the COD and color removal were not significantly affected by the 18-day idle period (at 4ºC) in the experimental run II, the longer biomass storage period and higher storage temperature (40-day idle period, at room temperature) in the experimental run I led to a 10-day recovery period to reach again 80% of color and of total COD removal, 60% of the latter being removed under anaerobic conditions, irrespective of the AgNP presence. Furthermore, while only the AgNP-free SBR effectively converted one of the aromatic amines (4A1NS) deriving from the azo dye reduction process during a short period of time in the experimental run I, the AgNP-fed SBR sustained 4A1NS transformation for longer periods of time during the experimental run II, namely throughout the azo dye-shock load period and beyond. Despite the observed toxic effect of AgNP on protozoa, the lack of a negative impact in the SBR treatment performance highlights the protecting effect of the AG structure to bacteria potentially susceptible to the AgNP-associated antimicrobial action. Nevertheless, exposure to AgNP induced specific changes in the SBR microbial community at least after 1 month of operation, supporting the functional redundancy of bacteria. Finally, denitrification and decolorization occurred simultaneously, the color removal yield not being affected by the presence of nitrate in the long-term operation. This study provided relevant further support for the application of AGS in TWW treatment, in light of the typically irregular wastewater discharges from the wet processing textile industry, predictably containing increasing AgNP concentrations.

## VII.2. Introduction

In response to the growing demand for textile diversity, ENP have been widely used by the textile industry, namely AgNP for their antimicrobial properties (Rezić, 2011). As a result of the increasing use of AgNP and inefficient fixation processes, the occurrence of AgNP in textile industry wastewater is expected, adding to the high organic loads and recalcitrant dyes that characterize these highly polluting effluents (O'Neill *et al*., 1999). The potential toxicity of AgNP and their unknown fate in WWTPs classify them as an emergent environmental concern. Moreover, the AgNP antimicrobial properties suggest a potential negative impact on biological treatment processes (Yang *et al*., 2014), the effects being partially dependent on the type of sludge used (Gu *et al*., 2014). Specifically, despite the AGS (Beun *et al*., 2002) robustness towards high organic loads and toxic compounds, the long-term impacts of AgNP on AGS stability and microbial community have not been thoroughly investigated yet (Quan *et al*., 2015; Sheng and Liu, 2017).

Owing to the lower investment, footprint and operational energy requirements of AGS SBR when compared to CAS processes (Pronk *et al*., 2015b), AGS technology has been designated as the new generation in wastewater biological treatment. Its potential application in TWW treatment has been supported by recent studies focused on COD removal and biodegradation of azo dyes (main type of textile dyes used) in anaerobic-aerobic AGS SBR (Franca *et al*., 2015). Specifically, in addition to the successful color removal via azo dye anaerobic reduction, AGS has been shown to potentially perform further aerobic bioconversion of the possibly toxic, resulting aromatic amines (Franca *et al*., 2015). Moreover, the AGS capacity for maintaining appropriate physicochemical characteristics and to efficiently recover high treatment performances after prolonged idle periods are particularly relevant for the practical application of AGS (He *et al*., 2017c), namely in the treatment of irregular wastewater discharges from the wet processing textile industry, typically characterized by a discontinuous production regimen. In this context, the present study investigated the impact of AgNP on TWW treatment performance by AGS SBR during long-term operation, assessing AGS formation, stability and reactivation after an idle period. In this sense, two SBRs (one AgNP-fed and one AgNP-free control) were operated during two experimental runs, the AgNP concentration being doubled in the second experimental run (20 mg $L^{-1}$ in the synthetic TWW). After interruption of the AgNP addition in a final stage of the operation, the SBRs were further compared regarding the AGS properties and treatment performance upon the introduction of a three-fold increase in the azo dye concentration. Finally, the effect of nitrate salts in the treatment performance was also assessed.

## VII.3. Materials and methods

### VII.3.1. Chemicals

The carbon source (Emsize E1) and the azo dye (AR14) stock solutions were prepared as described in sections III.3.1.1 and IV.3.1., respectively. The synthetic TWW used as feed solution was prepared as described in section III.3.1.2, with the addition of the azo dye to a concentration of 40 mg AR14 $L^{-1}$.

An AgNP suspension of 100 mg $L^{-1}$ was prepared as described in section VI.3.1 and used as is as stock suspension during the experimental run II. During the experimental run I, this suspension was subsequently diluted in MiliQ-water to a final stock suspension concentration of 50 mg $L^{-1}$. The average particle size of AgNP in the stock suspension and at the reactor inlet was 228±8 nm and 190±15 nm, respectively.

### VII.3.2. SBR setup and operation

Two 1.5-L bubble-column SBRs were inoculated with CAS from a domestic WWTP (Chelas, Portugal), fed with the azo dye-laden synthetic TWW and operated during two distinct experimental runs. Both SBRs were operated with 6-h cycles, comprising 1.5 h of stirred anaerobic phase (mechanical mixing, 70 rpm), followed by 3.5-h aeration, 5-min settling (settling time decreased from 1 h to 5 min along the first 28 days of each experimental run) and 1-min discharge. The feed solution was supplied to the SBRs with a volumetric OLR of 2.0 kg COD $L^{-1}$ $d^{-1}$, the HRT being 12 h. SBR1 was supplied with AgNP during the filling stage (AgNP concentration in the feed solution: 10 and 20 mg $L^{-1}$ during the experimental runs I and II, respectively) and SBR2 was used as AgNP-free control. The experimental run I lasted 404 days and comprised 6 experimental periods (Table VII.1), including the initial settling time reduction to 5 min (period I.A), an AgNP clean-up period, where AgNP supply to SBR1 was temporarily interrupted (period I.C), followed by reintroduction of AgNP (period I.D). In addition, after a 40-day idle period (period E; biomass reserved in the SBRs at room temperature, static, no feeding and no aeration), AGS was reactivated in both SBRs and operated for another 83 days (period I.F). Similarly, the experimental run II (434 days; 10 experimental periods, Table VII.1) was initiated with the reduction in the settling time (period II.A) to induce aerobic granulation in the absence (SBR2) or presence of AgNP (SBR1), 5 min of settling being established from day 29 on (period II.B). After an 18-day idle period (period II.C; biomass stored at 4ºC, in dark, static conditions with no feeding or aeration), the reactors were reinoculated with the stored biomass and operated under the same conditions as before the idle period (period II.D). Subsequently, different changes were introduced in their wastewater composition. Specifically, the AgNP supply to SBR2 was interrupted from day 247 on (period II.E), and a three-fold increase in AR14 concentration to 120 mg $L^{-1}$ was imposed in both reactors (period II.F), after which it was reset at 40 mg $L^{-1}$ (period II.G). In addition, nitrate was introduced in the feed of SBR1 (SBR2 used as a nitrate-free control) at 60 mg

$NO_3^-$ $L^{-1}$ from calcium nitrate (period II.H), and subsequently at 120 mg $NO_3^-$ $L^{-1}$, either from calcium nitrate (period II.I) or potassium nitrate (period II.J).

As mentioned in section I.3, this study was run in parallel with that reported in chapter VI, with three SBRs in operation simultaneously. Therefore, for experimental run I, the results for SBR2 correspond to those presented in chapter VI for the reactor there identified as SBR1. For experimental run II, the results for SBR1 correspond to those presented in chapter VI for the reactor there identified as SBR1. The results for SBR1 in run I and SBR2 in run II are newly presented in the present chapter.

**Table VII.1** - Overview of the operational conditions imposed to the sequencing batch reactors (SBRs) during experimental runs I and II. Cycle conditions were adjusted regarding the duration of the settling stage in both SBRs (Settling). Along periods I.A and II.A the settling time was reduced from 60 to 5 min in 2-20 min steps (60, 40, 30, 20, 15, 10, 7 and 5 min of settling imposed on operational days 1, 3, 7, 10, 14, 17, 24 and 28, respectively). Variations to the synthetic TWW composition were introduced in both reactors regarding variations in the azo dye (AR14) concentration, but only in SBR1 regarding the addition of silver nanoparticles (AgNP) and supplementation with nitrate ($NO_3^-$) from calcium nitrate or potassium nitrate (Salt). The indicated values refer to the concentration of the respective component in the SBR feed solution. The experimental periods I.E and II.C correspond to periods when the reactors' operation was interrupted and the biomass was stored at room temperature (period I.E) or at 4ºC (period II.C).

| Run | Period | | | SBR1 and SBR2 | | SBR1 | |
|---|---|---|---|---|---|---|---|
| | Name | Operating days | Duration (days) | Settling (min) | AR14 (mg $L^{-1}$) | AgNP (mg $L^{-1}$) | $NO_3^-$ (mg $L^{-1}$) ─ Salt |
| I | I.A | 1-28 | 28 | 60 to 5 | 40 | 10 | - |
| | I.B | 29-177 | 149 | 5 | | | |
| | I.C | 178-236 | 59 | | | - | |
| | I.D | 237-281 | 45 | | | 10 | |
| | I.E | 282-321 | 40 | | | | |
| | I.F | 322-404 | 83 | 5 | 40 | 10 | - |
| II | II.A | 1-28 | 28 | 60 to 5 | 40 | 20 | - |
| | II.B | 29-192 | 164 | 5 | | | |
| | II.C | 193-210 | 18 | | | | |
| | II.D | 211-246 | 36 | 5 | 40 | 20 | - |
| | II.E | 247-328 | 82 | | | - | |
| | II.F | 329-344 | 16 | | 120 | | |
| | II.G | 345-356 | 12 | | 40 | | |
| | II.H | 357-363 | 7 | | | | 60 ─ $Ca(NO_3)_2$ |
| | II.I | 364-415 | 52 | | | | 120 ─ $Ca(NO_3)_2$ |
| | II.J | 416-434 | 19 | | | | 120 ─ $KNO_3$ |

## VII.3.3. Analytical methods

TSS, VSS, SVI, biomass morphological analysis, COD, UV-visible absorbance spectra, dye degradation and metabolite formation were determined as described in section III.3.3.1. In addition, color removal was followed as described in section IV.3.3. Biomass size distribution was analyzed by sieving, according to section VI.3.3. Dynamic light scattering was employed to measure the average

particle size in AgNP stock suspensions and at the reactor inlet, using a Malvern Zetasizer Nano ZS (Malvern Instruments, UK).

Microbial community analysis was assessed by FISH analysis on selected, homogenized biomass samples using oligonucleotide probes for the core community typically detected in WWTPs, as well as by high throughput DNA sequencing as described in sections III.3.3.2.1 and III.3.3.2.2, respectively.

## VII.4. Results

### VII.4.1. AGS morphology and properties

#### VII.4.1.1. Granule size and settling properties

The AGS was composed by flocs and granules, *i.e.*, aggregates with sizes over 0.2 mm. Yet, the fraction of granules greater than 0.65 mm was very small in both SBRs throughout the two experimental runs. Overall, the biomass size fractionation profile in SBR1 and SBR2 was approximately the same throughout the experimental periods I.A-I-D, the fraction of granules larger than 0.2 mm not representing more than 7% of the sludge (Figure VII.1). After the storage period, this number increased in both reactors, SBR2 sustaining a higher percentage of granules (22%) than SBR1 (14%) during period I.F.

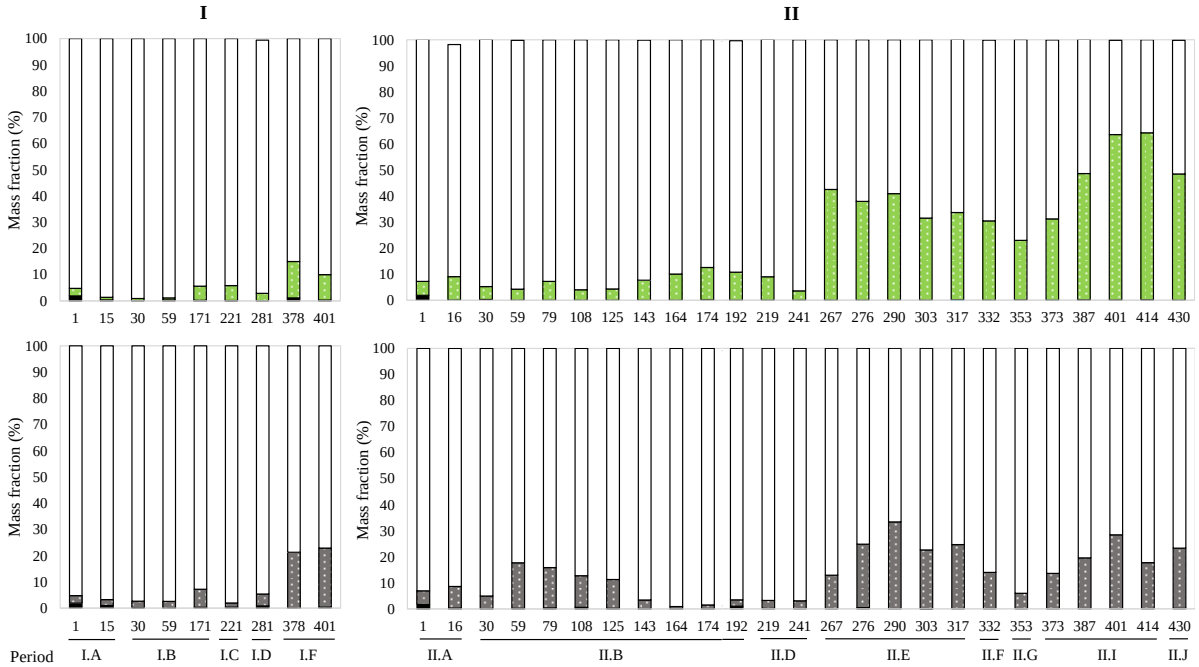


**Figure VII.1** - Distribution of particle sizes in SBR1 (blue) and SBR2 (red) along experimental runs I and II. Mass percentage in terms of total suspended solids of flocculent sludge (empty bars; d<0.20 mm), small granules (dotted, colored bars; 0.20<d<0.65 mm) and larger granules (black bars; d>0.65 mm). The operational conditions for each experimental period (I.A-I.F and II.A-II.J) are described in Table VII.1. The analyses corresponding to days 290-430 of experimental run II were performed in duplicate, the respective results presented in this figure corresponding to the calculated average values (relative standard deviation values lower than 0.2% for larger granules and lower than 7.2% for small granules and for flocculent sludge).

This granular prevalence in SBR2 over SBR1 was also observed after the granulation period in the experimental run II (from day 59 to 125), but the granular fraction became subsequently more relevant in SBR1 than in SBR2, as the latter presented no more than 3% of granules from day 143 to 241. In fact, from day 143 on, SBR1 presented a larger granule fraction than SBR2, namely after the AgNP were removed from the former's feed solution on day 247. Specifically, the percentage of granules increased in both reactors on day 267, especially in SBR1 (from 4% on day 241 to 43% on day 267 in SBR1, and from 3 to 13% in SBR2; Figure VII.1). In fact, after AgNP feeding was interrupted, SBR1 was able to recover and thrive until the end of the operation, with a granular fraction within 23-64%, much higher than in SBR2 (6-33%). In addition, although a slight increase in the granule abundance was also noted in the calcium nitrate-free control, SBR2 (from 6% on day 353 to 28% on day 401), the more intense increase in the granular fraction along period II.I in SBR1 (from 23% to 64%) suggests that calcium nitrate promoted the development of AG.

Despite not being evident from the biomass size distribution analysis, the application of a feast-famine regimen with high hydrodynamic shear force and gradually shorter settling times allowed successful aerobic granulation to be achieved irrespective of the presence of AgNP, as denoted by the equivalent initial SVI profiles and the low $SVI_5$ and $SVI_{30}$ reached on day 35 of the experimental run I (66 and 44 mL $gTSS^{-1}$, respectively) in both SBRs (Figure VII.2). Subsequently, while the control SBR2 maintained low $SVI_5$ and $SVI_{30}$ (76 and 48 mL $gTSS^{-1}$, respectively) during the experimental days 77-120, the values increased in SBR1 reaching 116 and 78 mL $gTSS^{-1}$, respectively, on day 140. Nevertheless, from this point until day 201, the trend was inverted, as SBR2 biomass settleability deteriorated, the $SVI_5$ and $SVI_{30}$ increasing to average levels of 133 and 88 mL $gTSS^{-1}$, respectively, values notably higher than those registered in SBR1 (stable values around 99 and 65 mL $gTSS^{-1}$, respectively). Subsequently, SVI values in SBR2 gradually decreased meeting those registered in SBR1 at 107 and 67 mL $gTSS^{-1}$ ($SVI_5$ and $SVI_{30}$, respectively) on day 223. Upon the re-start of AgNP addition to SBR1 (period I.D), SVI values rapidly decreased until day 258, but then increased again reaching the same values as SBR2 at the end of this period. Along periods I.B-I.D, the average $SVI_5$ and $SVI_{30}$ values registered from day 35 on were 102±24 and 65±15 mL $gTSS^{-1}$ in SBR1 and 114±34 and 72±21 mL $gTSS^{-1}$ in SBR2, respectively. After the 40-day idle stage (period I.E), the settling capacity improved, as $SVI_5$ and $SVI_{30}$ decreased from the initial 170 and 100 mL $gTSS^{-1}$, respectively, to levels below 100 mL $gTSS^{-1}$ along period I.F in both SBRs, indicating a fast AGS settleability recovery irrespective of the presence of AgNP. The sudden $SVI_5$ and $SVI_{30}$ increase to 135 and 92 mL $gTSS^{-1}$, respectively, registered on day 379 in SBR1 was a consequence of a problem in the automatic control of the SBR1 air compressor that resulted in deterioration of the biomass, as half of the SBR1 biomass was washed off though a gear drain pump, and was subsequently recovered and transferred back into the reactor.

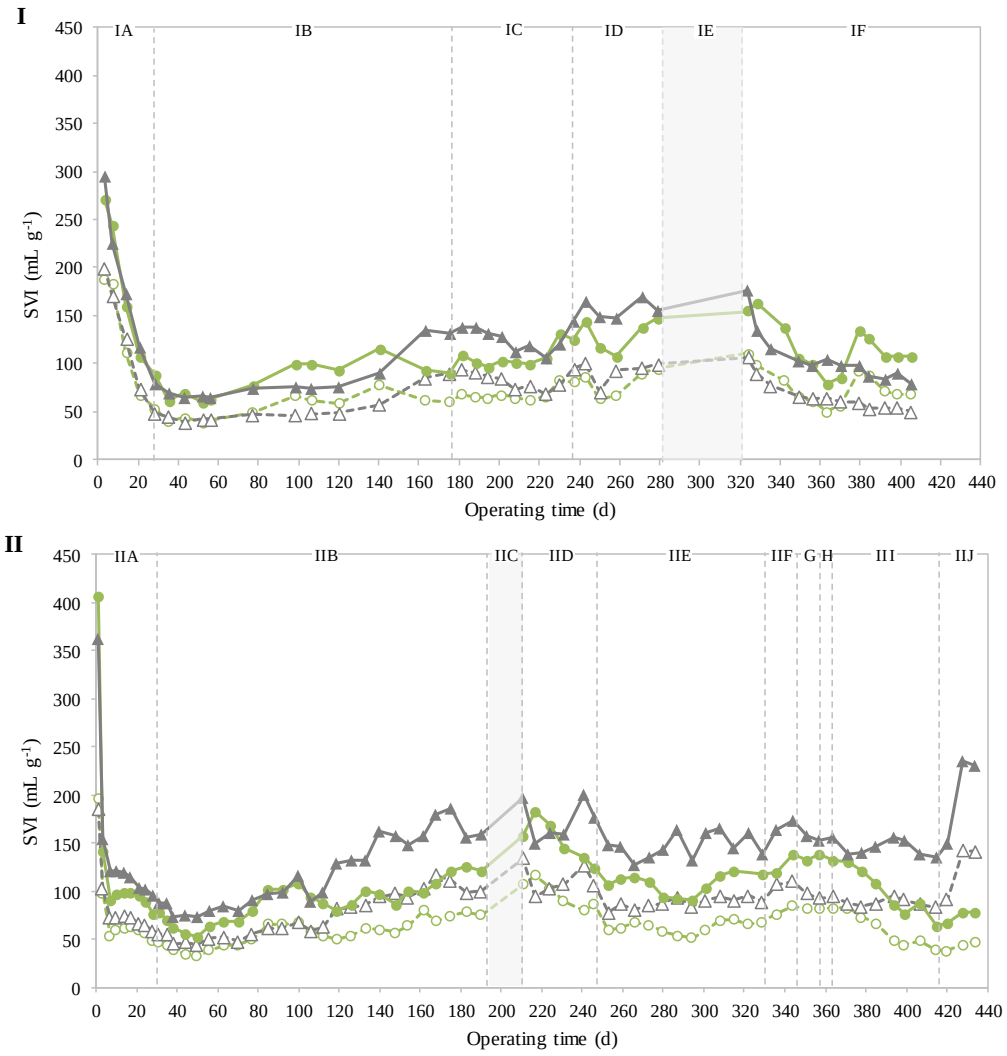


**Figure VII.2** - Sludge volume index (SVI) profile along experimental runs I and II. SVI values measured after 5 min settling ($SVI_5$) for sequencing batch reactors SBR1 (●) and SBR2 (▲), and after 30 min settling ($SVI_{30}$) for SBR1 (○) and SBR2 (△). The operational conditions for each experimental period (I.A-I.F and II.A-II.J) are described in Table VII.1.

Similarly to the experimental run I, SVI values decreased in both SBRs along period II.A of the experimental run II, indicating that aerobic granulation was attained, even in the presence of a higher AgNP concentration in SBR1 (Figure VII.2). Specifically, after a sharp initial SVI drop (values above 400 mL $gTSS^{-1}$ in the inoculum), $SVI_5$ and $SVI_{30}$ gradually decreased until day 50 in both SBRs reaching minimum values of 53 and 33 mL $gTSS^{-1}$ in SBR1, and 73 and 45 mL $gTSS^{-1}$ in SBR2, respectively. Subsequently, the settling properties of the biomass gradually worsened along period II.B, more markedly in SBR2 (Figure VII.2). The 18-day idle period similarly affected the biomass in both SBRs in terms of SVI increase. Yet, while the SVI values continuously decreased in SBR1 upon AGS reactivation on period II.D, further reaching lower values after the interruption of AgNP addition on period II.E ($SVI_5$ and $SVI_{30}$ of 91 and 52 mL $gTSS^{-1}$, respectively, on day 294), SBR2 SVI stabilized at higher values ($SVI_5$ and $SVI_{30}$ around 165 and 95 mL $gTSS^{-1}$, respectively). Moreover, after a slight sludge settleability deterioration upon the azo dye shock load (period II.F), equally observed in both SBRs, the SBR1 $SVI_5$ and $SVI_{30}$ values recovered the previous low values and further

decreased to 68 and 38 mL $gTSS^{-1}$, respectively, when its feed was supplied with 120 mg $L^{-1}$ of calcium nitrate (period II.I). This was not observed in the control SBR2, which maintained stable, higher $SVI_5$ and $SVI_{30}$ values of 147 and 87 mL $gTSS^{-1}$, respectively) during period II.I. Finally, the replacement of calcium nitrate with potassium nitrate suspended the SVI decreasing trend in SBR1, the values slightly increasing until the end of the operation. As for SBR2, despite no changes being introduced in its operational conditions, the SVI values sharply increased on day 428 to $SVI_5$ and $SVI_{30}$ values of 235 and 143 mL $gTSS^{-1}$, respectively.

### VII.4.1.2. AGS morphology

Comparing SBR1 and SBR2, the morphology of the sludge was similar until day 94 of the experimental run I (Figure VII.3 and Figure VII.S1, in Appendix E). Subsequently, until day 150, the control SBR2 presented less flocculent sludge and a higher abundance of granules than SBR1. Nonetheless, this situation changed from day 164 on, as rare, small granules were observed and more flocculent sludge emerged in SBR2. On the other hand, sludge in SBR1 maintained approximately the same morphology until the end of period I.D, the largest granules observed displaying dimensions below 0.5 mm in both reactors. After the 40-day idle period (period I.E), the sludge in both SBRs was characterized by dispersed, irregular aggregates, EPS-like structures, and small aggregates. However, within 1 month of operation AGS recovered in both SBRs, as granules with rounded shapes and irregular outlines were formed and further enlarged and became more compact over the course of period I.F (dimensions up to 0.5 and 0.6 mm in SBR1 and SBR2, respectively). In addition to the larger granules, an increasing number of small, spherical and dense nuclei were formed within the flocculent fraction in both reactors during period I.F, potentially constituting granule precursors. This AGS morphology contrasted with the considerable fraction of flocculent sludge observed prior to period I.E, indicating that a new granulation process occurred when the SBRs operation was resumed.

In the experimental run II, the loose and dispersed sludge, including filamentous bacteria, that was inoculated in the SBRs developed into AGS, as denser and more compact structures were observed in both reactors along period II.A, with no visible filamentous bacteria (Figure VII.3 and Figure VII.S2, in Appendix E). Along period II.B, AG became larger, denser, more rounded and with clearer outlines. However, in contrast with SBR1, a deterioration in terms of granule morphology was observed in SBR2 after day 129, indicating that disintegration of larger granules took place, as small aggregates with dimensions around 0.2 mm were still observed until the end of this period. In addition, after the 18-day biomass storage (period II.C), although AG were visible in both SBRs, those in SBR1 were not only in greater number than in SBR2, but also presented larger dimensions and clearer outlines, being surrounded by dense sludge flocs aggregates. In fact, contrarily to SBR1, the morphology of SBR2 sludge was variable throughout periods II.D-II.G, the number and size of granules becoming minimal upon the dye shock load (period II.F), but subsequently recovering during periods II.H-II.J. The

addition of calcium nitrate to SBR1 promoted the enlargement of AG along period II.I, the same maximal sizes being maintained during the subsequent period of potassium nitrate supplementation (period II.J), though with a higher amount of surrounding flocculent sludge.

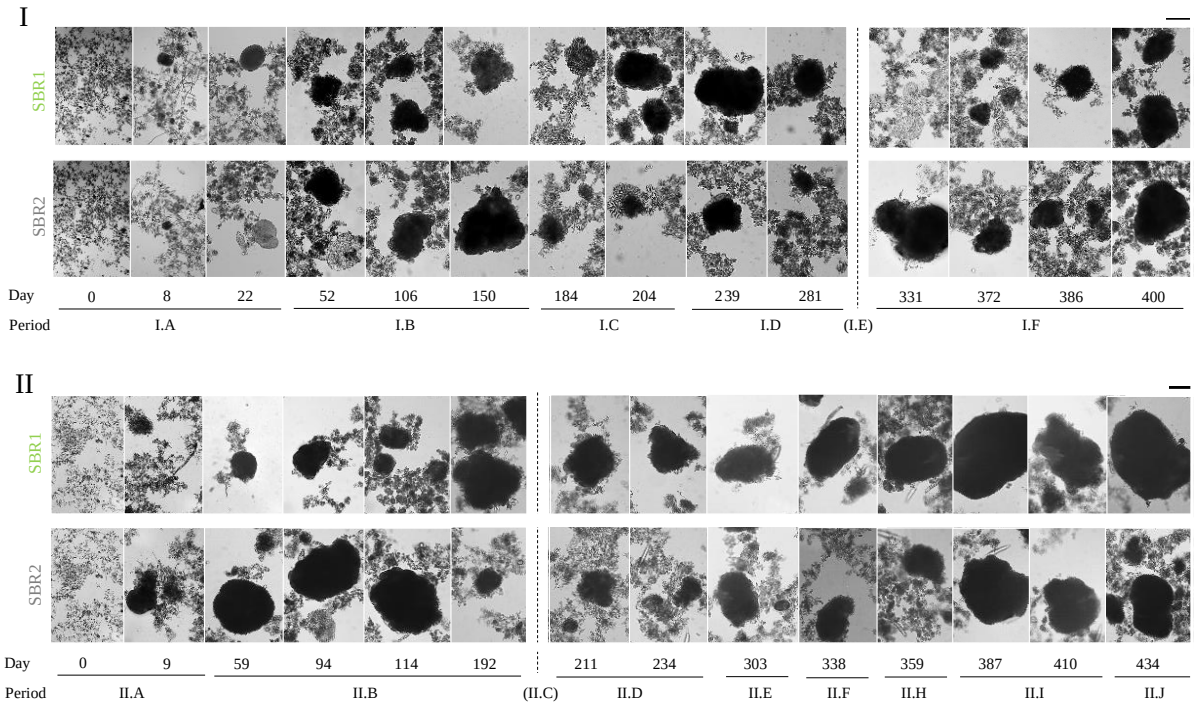


**Figure VII.3** - Morphological development of aerobic granular sludge along experimental runs I and II. Micrographs, at magnification 100, of biomass samples harvested from SBR1 and SBR2 on the indicated operational days and periods. The operational conditions for each experimental period (I.A-I.F and II.A-II.J) are described in Table VII.1. Scale bar: 0.2 mm.

Overall, AG were formed and grew in size and number over time, becoming denser, the maximal dimensions and morphology (spherical shapes and irregular outlines) being comparable in the two SBRs (Figure VII.S1 and Figure VII.S2, in Appendix E). However, the AgNP-fed SBR sustained a granule-rich sludge for longer operational periods. In addition, a marked decrease in the protozoa (namely, rotifers and nematodes) abundance was registered in the AgNP-fed SBR, suggesting a toxic effect of the latter. In fact, small, opaque and dark aggregates were observed only within SBR1 biomass during the periods of AgNP supplementation to this reactor.

## VII.4.2. AGS SBR treatment performance

### VII.4.2.1. Biomass inventory

After inoculation, the TSS profile in SBR1 perfectly overlapped with that in SBR2 along the first 2 weeks of the experimental run I (Figure VII.4). Moreover, although biomass progressively accumulated in SBR1 and SBR2 at comparable rates, reaching maximal values of approximately 9 gTSS $L^{-1}$ on day 38, the AgNP-fed reactor presented slightly higher TSS values, probably due to the accumulation of AgNP. After the settling time reduction period (period I.A), SBR1 and SBR2 stabilized within 8-9 gTSS $L^{-1}$, but a marked decrease in TSS to 6-7 gTSS $L^{-1}$ was registered from day

56 to 59. However, while the TSS content in SBR1 further decreased, SBR2 recovered 8 gTSS $L^{-1}$ on day 98. Nevertheless, as a result of the deterioration in the sludge settling properties (Figure VII.2), the biomass concentration gradually decreased in SBR2 along period I.B, reaching 4 gTSS $L^{-1}$ on day 175 (Figure VII.4). The subsequent variations in SBR1 and SBR2 TSS profiles follow the respective SVI profiles, the average TSS values for periods I.C-I.D being 5.1±0.5 gTSS $L^{-1}$ and 4.1±0.5 gTSS $L^{-1}$, respectively. After the 40-day idle stage, the biomass concentration increased from 2 gTSS $L^{-1}$ to levels above 6 gTSS $L^{-1}$ in both SBRs until day 379 (Figure VII.4). Subsequently, while the biomass concentration continued to increase in SBR2 (up to 8 gTSS $L^{-1}$), SBR1 registered a sharp decrease to 4 gTSS $L^{-1}$ on day 384 due to an operational problem that deteriorated the sludge settleability, but subsequently resumed the TSS increase, reaching 7 gTSS $L^{-1}$ at the end of the experimental run I (Figure VII.4). As a result of the irregular TSS levels in the effluent of both reactors, the respective SRT profiles varied in an unstable way throughout the operation, the average SRT values in SBR1 and SBR2 being 8±4 days and 9±8 days along periods I.A-I.D, and 18±11 days and 17±16 days along period I.F, respectively.

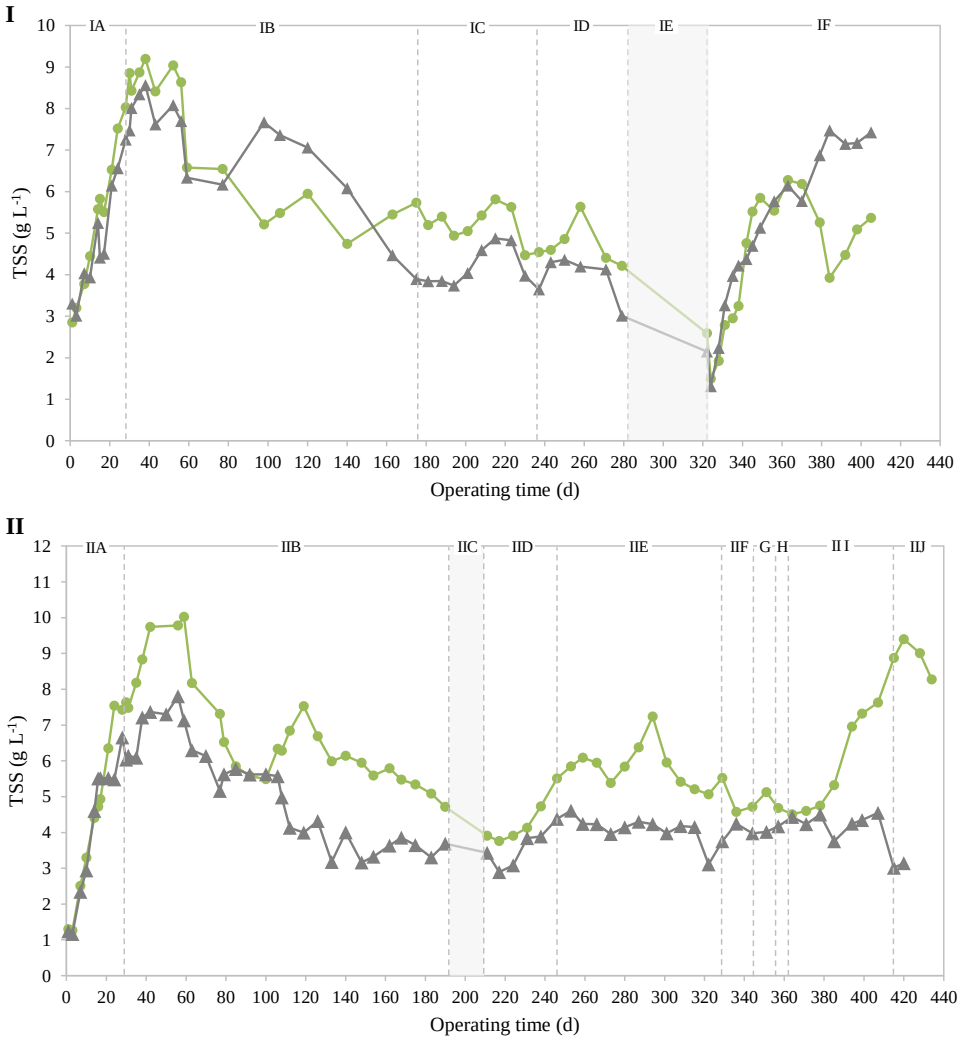


**Figure VII.4** - Profiles of biomass concentration in the mixed liquor. Total suspended solids (TSS) in the mixed liquor registered in sequencing batch reactors SBR1 (●) and SBR2 (▲) along experimental runs I and II. The operational conditions for each experimental period (I.A-I.F and II.A-II.J) are described in Table VII.1.

In the experimental run I, from day 14 on, the percentage of inorganic matter in the suspended solids of SBR1 became significantly higher than in SBR2, suggesting the accumulation of AgNP in SBR1 (Figure VII.5), either as suspended AgNP agglomerates larger than 1.2 μm (pore size of the filter used in TSS analysis) in the mixed liquor or through adsorption onto the biomass. During the period when AgNP addition to SBR1 was interrupted (period I.C), the percentage of inorganic matter in this reactor decreased to the same levels registered in the control SBR2 (Figure VII.5). Specifically, the latter values became equivalent 10 days after the holdup of the AgNP addition, indicating that AgNP were cleared out from the reactor. Conversely, once the AgNP feeding to SBR1 was resumed (period I.D), it was only after 22 days of operation that the percentage of inorganic matter in SBR1 increased, relatively to SBR2.

The difference between the percentage of inorganic matter in the two reactors reached an apparent steady state of approximately 2% on days 43-163 (period I.B; Figure VII.5), suggesting that AgNP potentially accumulating in the sludge reached a maximal level, as the biomass became saturated with AgNP. These results indicate that it takes more than 2 weeks of operation with an initial 5 g $L^{-1}$ of AgNP in the mixed liquor to produce a noticeable difference in the VSS values. In fact, the presence of AgNP within the biomass in SBR1 was macroscopically observed as the color of the sludge gradually acquired a dark grey hue (similar to that of the AgNP suspension), as opposed to the yellowish color of the control SBR sludge (Figure VII.S3, in Appendix E). Accordingly, after the addition of AgNP to SBR1 was interrupted, the grey color of the sludge in the latter reactor gradually vanished, revealing a color similar to that of the biomass in the control SBR, the dark grey sludge subsequently reappearing once AgNP were reintroduced in SBR1 (Figure VII.S3, in Appendix E). The high inorganic matter content registered in SBR1 immediately after period I.E reflect the loss of organic matter due to cell lysis during the biomass storage period (Figure VII.5). The rapid decrease to values equivalent to those registered in the control during the first month after reactivation suggest that the AgNP were washed out from the reactor along with the sludge to which they were adsorbed, the settling properties of which were negatively affected during the idle period. The subsequent deviation of the inorganic mass content in SBR1 to levels 1% above SBR2's (period I.F) indicates the reaccumulation of AgNP in the former reactor (Figure VII.5).

Regarding the experimental run II, the TSS values in the mixed liquor increased similarly in both reactors during the first 2 weeks of operation, after which the biomass further accumulated at a higher rate in SBR1 than in SBR2 until day 60 (10 and 8 gTSS $L^{-1}$ in SBR1 and SBR2, respectively), as a more significant amount of sludge was washed out of SBR2 along period II.A (Figure VII.4). Overall, the biomass concentration, in terms of TSS, decreased in both SBRs along period II.B (to 5 and 4 gTSS $L^{-1}$ in SBR1 and SBR2, respectively), SBR1 being able to sustain higher levels along the whole experimental run (Figure VII.4). Similarly to the experimental run I, biomass resumed its accumulation in the SBRs when the stored biomass was reinoculated in the reactors (period II.D),

stabilizing around 4 gTSS $L^{-1}$ in SBR1 and varying within 5-7 gTSS $L^{-1}$ in SBR2 through period II.E. The dye shock load period (period II.F) brought SBR1 TSS levels slightly down, closer to SBR2 stable TSS levels. Finally, the calcium nitrate supplementation in SBR1 (periods II.H-II.I) induced a rapid increase in the TSS levels (from 4.5 to 9.4 gTSS $L^{-1}$), as well as in the VSS values (from 4.0 to 8.2 gVSS $L^{-1}$, data not shown), revealing a high sludge accumulation throughout period II.I. This trend was reversed once calcium nitrate was replaced with potassium nitrate in SBR1 (period II.J). Although no operational conditions were changed in the control, a significant TSS decrease was also registered in SBR2 in period II.J, potentially due to partial loss of granule stability due to the extended time of operation. Overall, SBR1 and SBR2 presented similar SRT values, the averages being 11±10 days and 10±8 days, respectively.

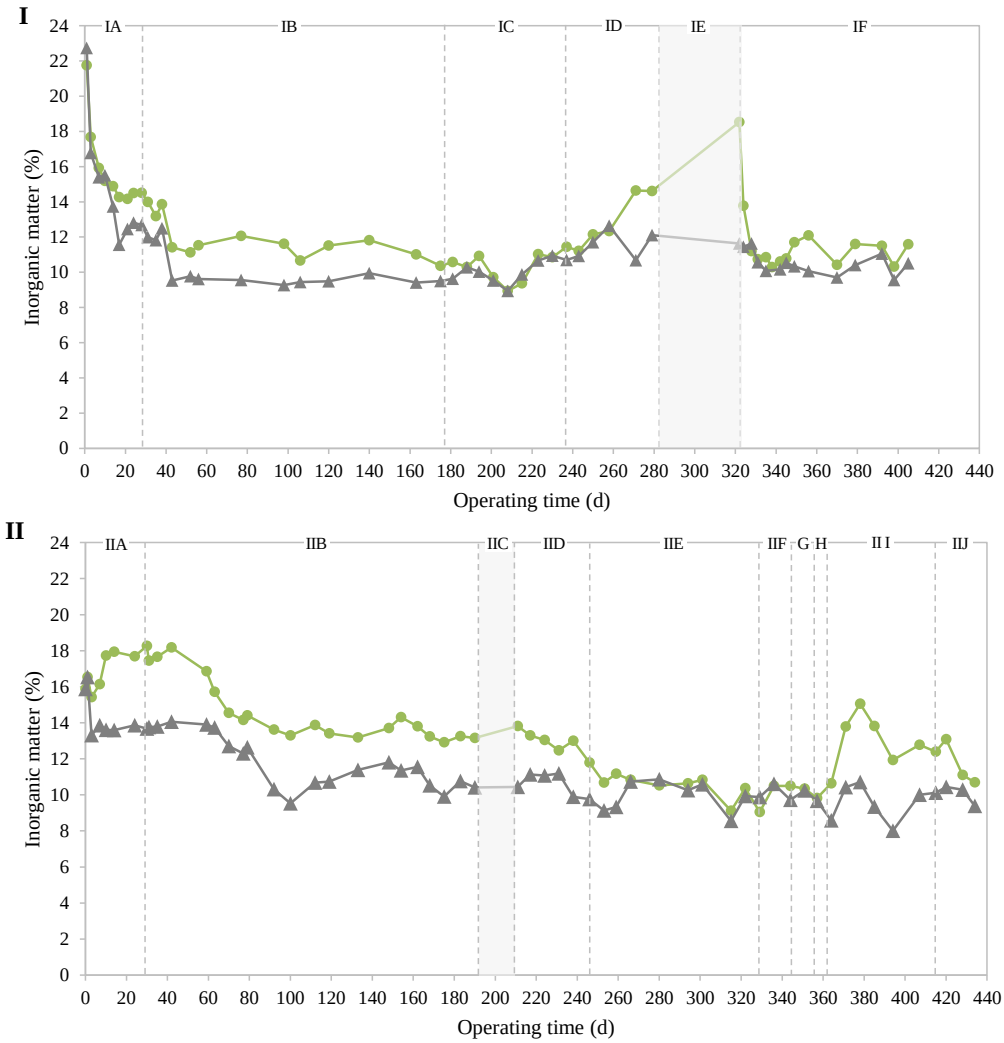


**Figure VII.5** - Profiles of inorganic matter in the mixed liquor suspended solids. Percentage of inorganic matter (based on volatile and total suspended solids measurements) in sequencing batch reactors SBR1 (●) and SBR2 (▲) along experimental runs I and II. The operational conditions for each experimental period (I.A-I.F and II.A-II.J) are described in Table VII.1.

In the experimental run II, the difference in the inorganic mass content between the suspended solids in the AgNP-fed SBR and the control reached 4% after 10 days of operation, and was maintained within 2-4% along the periods when SBR1 was supplemented with AgNP (periods II.A-II-D; Figure

VII.5). Specifically, SBR1 and SBR2 inorganic content stabilized around 14% (higher than in the experimental run I, 12%) and 11% (similarly to the experimental run I, 10%), respectively. Subsequently, the ceasing of AgNP supply to SBR1 on day 247 led to a decrease in the SBR1 inorganic content, meeting the control SBR values at 11% after 20 days of AgNP clean-up (period II.E). Nevertheless, SBR1 maintained higher TSS levels afterwards (Figure VII.4). As opposed to the control SBR, the percentage of inorganic mass in SBR1 increased to 15% and then stabilized around 13% when supplemented with calcium nitrate (period II.I; Figure VII.5). Finally, upon SBR1 supplementation with potassium nitrate in period II.J, the inorganic content in SBR1 decreased to 11%, reaching values closer to those of the control. The SRT profile was irregular along the experimental run II, reflecting the varying TSS levels in the analyzed treated effluents.

### VII.4.2.2. Anaerobic and overall COD removal

Regarding the treatment performance in terms of organic load removal, the biomass adapted to the new carbon source, as the overall COD removal yield gradually improved to 80% along the first 2 weeks of both experimental runs, at an equivalent rate in SBR1 and SBR2 (Figure VII.6). In fact, regarding the effect of AgNP in the overall COD removal yield, no notable differences were observed since, on the whole, both SBRs presented stable values within the 75-85% range along the experimental runs. The exception on day 77 of the experimental run I (67% of COD removal yield in SBR1; Figure VII.6) was a consequence of an unintended absence of aeration during one or more cycles on the previous three days, leading to an adaptive lower aerobic metabolic activity. Specifically comparing the anaerobic COD removal performance of the two reactors in the experimental run I (Figure VII.6), while SBR1 maintained values within the 50-60% range during period I.B-I.C, the measured values in SBR2 oscillated more, between a maximum of 70% (day 140) and a minimum of 40% (day 194). Some of these variations could be attributed to the small differences in the initial COD values, such as the high values registered at the end of period I.D (Figure VII.S4, in Appendix E). After the biomass storage period (period I.E), SBR2 reached approximately 80% of total COD removal after 10 days of reactivation, with small oscillations around this value throughout period I.F, 60% of which being removed under anaerobic conditions (Figure VII.6). SBR1 presented a similar performance, the slightly lower overall and anaerobic COD removal yields after day 363 being a result of lower initial COD values in the respective feed solution (Figure VII.S4, in Appendix E), and possibly being also associated with the accidental biomass deterioration episode and consequent reduction in the biomass concentration levels in this reactor (Figure VII.4). Nonetheless, SBR1 restored 80% and 60% of overall and anaerobic COD removal yields, respectively, at the end of the experimental run I (Figure VII.6).

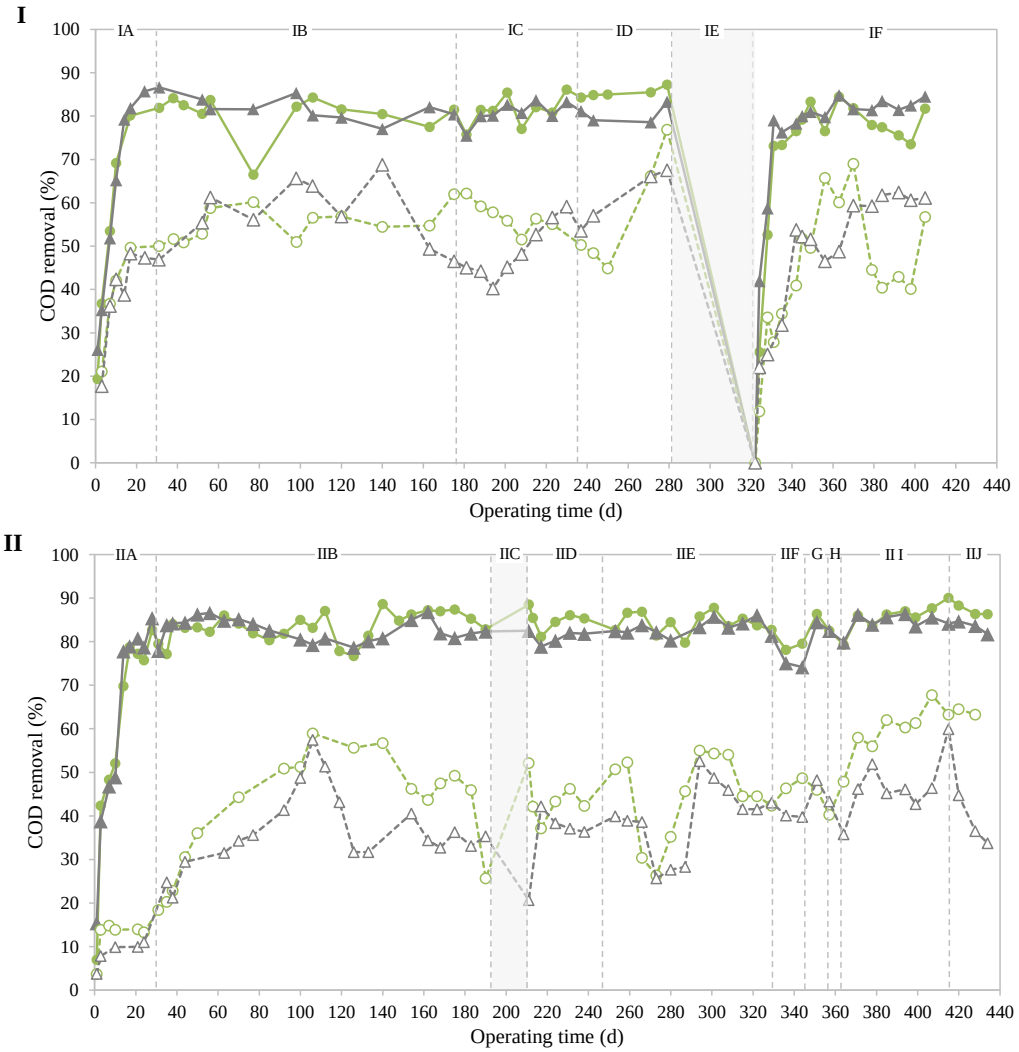


**Figure VII.6** - Organic load removal performance, as chemical oxygen demand (COD), along experimental runs I and II. Total COD removal yield (full line) and percentage of COD removed during the anaerobic phase (dashed line) in sequencing batch reactors SBR1 (●) and SBR2 (▲) along experimental runs I and II. The operational conditions for each experimental period (I.A-I.F and II.A-II.J) are described in Table VII.1.

The total COD removal yield was also maintained at approximately 80% throughout the experimental run II, irrespective of the presence of a higher AgNP concentration (Figure VII.6). This level of treatment performance includes the days immediately after AGS reactivation during period II.D, no deterioration in the organic load removal capacity being noticed after 18 days of biomass storage at 4ºC (89% and 83% of COD removal yields reached on the first day of reactivation in SBR1 and SBR2, respectively). Slightly lower values, down to 75%, were registered during the period when a three-fold increase in the azo dye concentration was applied in both SBRs (period II.F), the final residual COD increasing from 90 to 170 mg $O_2$ $L^{-1}$ (Figure VII.S4, in Appendix E). When compared to the experimental run I, despite the equivalent values in terms of overall COD removal, the amount of organic matter removed under anaerobic conditions was, in general, lower during the experimental run II, namely for the control SBR (Figure VII.6). In fact, 60% of anaerobic COD removal yield were only reached on day 106 of the experimental run II (as opposed to day 56 on the experimental run I). From this day on, values varied similarly in both SBRs, within the 25-55% range, until period II.H.

However, the supplementation of SBR1 with calcium nitrate was correlated with an increase in the fraction of COD removed under anaerobic conditions (from 40 to 65% over period II.I). This, in turn, led to a slight increase in overall COD removal, SBR1 reaching 90% at the end of period II.I. In contrast to SBR1, where the addition of potassium nitrate did not significantly affect the treatment performance (period II.J), a decrease in the anaerobic COD removal yield occurred in SBR2 throughout the last period of the experimental run II, possibly due to AGS deterioration related with the long operational time.

Figure VII.7 compares some of the representative COD profiles in SBR1 and SBR2. Up to approximately 200 mg $O_2$ $L^{-1}$ were rapidly removed from the mixed liquid during the first 30 min of anaerobic phase. The residual amount of COD in the medium was either maintained constant or further removed at a lower rate during the subsequent 1 h of anaerobic conditions. Afterwards, upon the onset of aeration, microorganisms rapidly oxidized the remaining biodegradable COD during the first 30 min of the aerobic phase. Despite differences in the residual COD level reached at the end of the anaerobic phase registered on distinct cycles, this value was not lower than 250 mg $O_2$ $L^{-1}$, and consistently dropped to approximately 100 mg $O_2$ $L^{-1}$ throughout the treatment cycle, irrespective of the presence of AgNP, indicating that about 100 mg $O_2$ $L^{-1}$ of the substrate is probably not biodegradable.

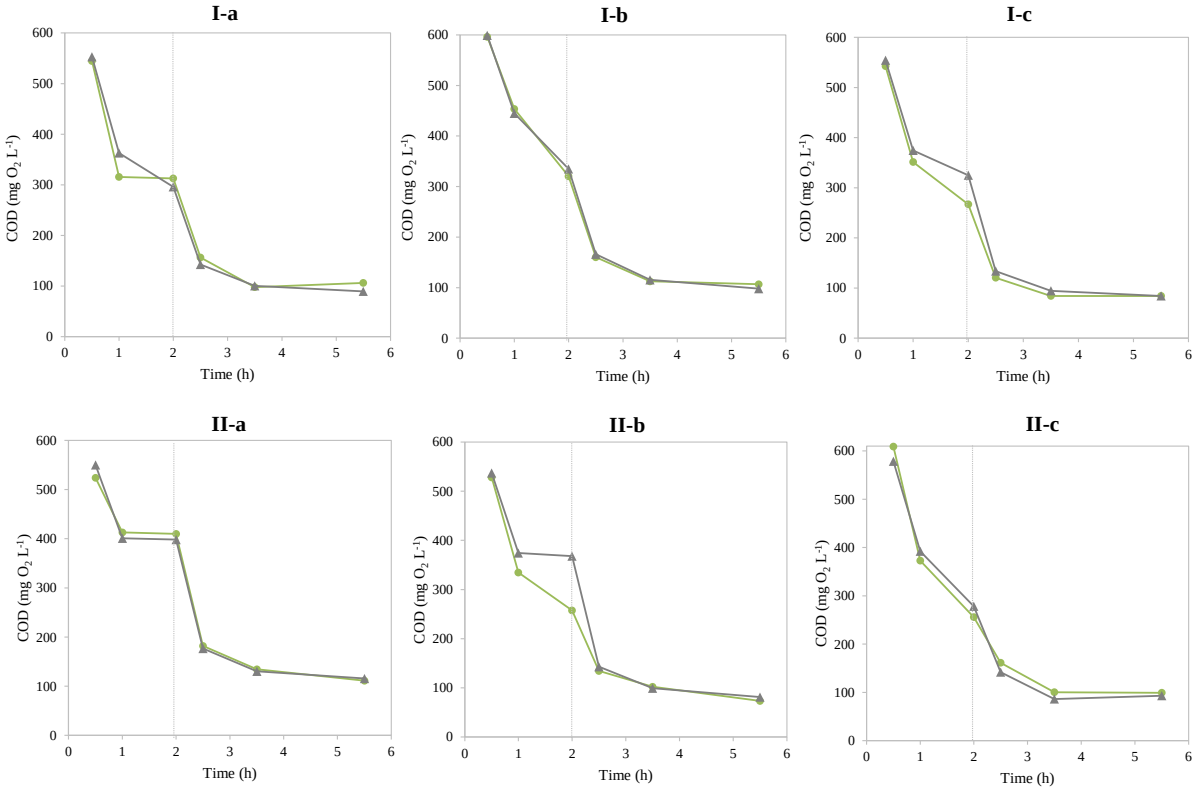


**Figure VII.7** - Comparison between chemical oxygen demand (COD) removal profiles of SBR1 and SBR2 during representative treatment cycles along experimental runs I and II. Comparison between the COD-time profiles observed along the reaction phase of treatment cycles in sequencing batch reactors SBR1 (●) and SBR2 (▲) on days 52 (I-a; period I.B), 215 (I-b; period I.C) and 364 (I-c; period I.F) of experimental run I, and on days 17 (II-a; period II.A), 63 (II-b; period II.B) and 378 (II-c; period II.I) of experimental run II. Vertical lines represent the end of the anaerobic phase, upon the aeration onset.

The representative cycles of both experimental runs show equivalent COD removal profiles in the AgNP-fed and the control SBRs (Figure VII.7). Therefore, the addition of AgNP to an initial concentration up to 10 mg $L^{-1}$ neither affected the overall COD removal performance of the AGS SBR, nor produced large or consistent changes in the COD removal profile, as compared to the AgNP-free control SBR, namely during long experimental runs and following a biomass storage period. Similarly, no relevant differences in the pH-time profiles were observed between the AgNP-fed SBR and the AgNP-free control SBR along both experimental runs, except during periods II.H-II.J when the addition of nitrate to SBR1 brought the respective pH profile to higher values (Figure VII.S5, in Appendix E).

### VII.4.2.3. Azo dye biodegradation

#### VII.4.2.3.1. Color removal

Regarding the color removal performance, the biomass rapidly adapted to the synthetic TWW containing the azo dye AR14 since color removal levels reached 80% three and seven days after inoculation in the experimental runs I and II, respectively, irrespective of the presence of AgNP (Figure VII.8). This good decolorization performance was maintained in SBR1 throughout periods I.A-I.D. The same was observed in the control SBR, except for a short period of days during period I.A, when the color removal yield decreased to around 50%, concomitantly with strong biomass washout episodes registered upon the settling time reduction to 15-20 min. Accordingly, the residual dye concentration in SBR2 was significantly higher on days 17-21 (Figure VII.S6, in Appendix E). Although less pronouncedly, the control SBR also presented some deterioration in the color removal capacity on days 17-24 of the experimental run II (Figure VII.8). The maximum color removal performance was subsequently restored to 80% at the end of period I.A and II.A, when 5 min of settling were finally imposed in the system.

After the biomass storage periods I.E and II.C, AGS reactivation in terms of color removal performance was rapidly achieved, irrespective of the presence of AgNP in the reactor. Specifically, SBR1 and SBR2 restored high, stable color removal yield levels, after rising from 0% on the first day of reactivation to 80% within 7 and 10 days of operation, respectively, in the experimental run I (Figure VII.8). On the other hand, the shorter time and lower temperature applied during the storage period in the experimental run II allowed the biomass to resume its metabolic activity in the first cycle of operation, the decolorization yields being 27% and 42% in SBR1 and SBR2, respectively, rising to 75-80% on the following day. Subsequently, the color removal yield profile was comparable in the two SBRs until the end of the experimental runs.

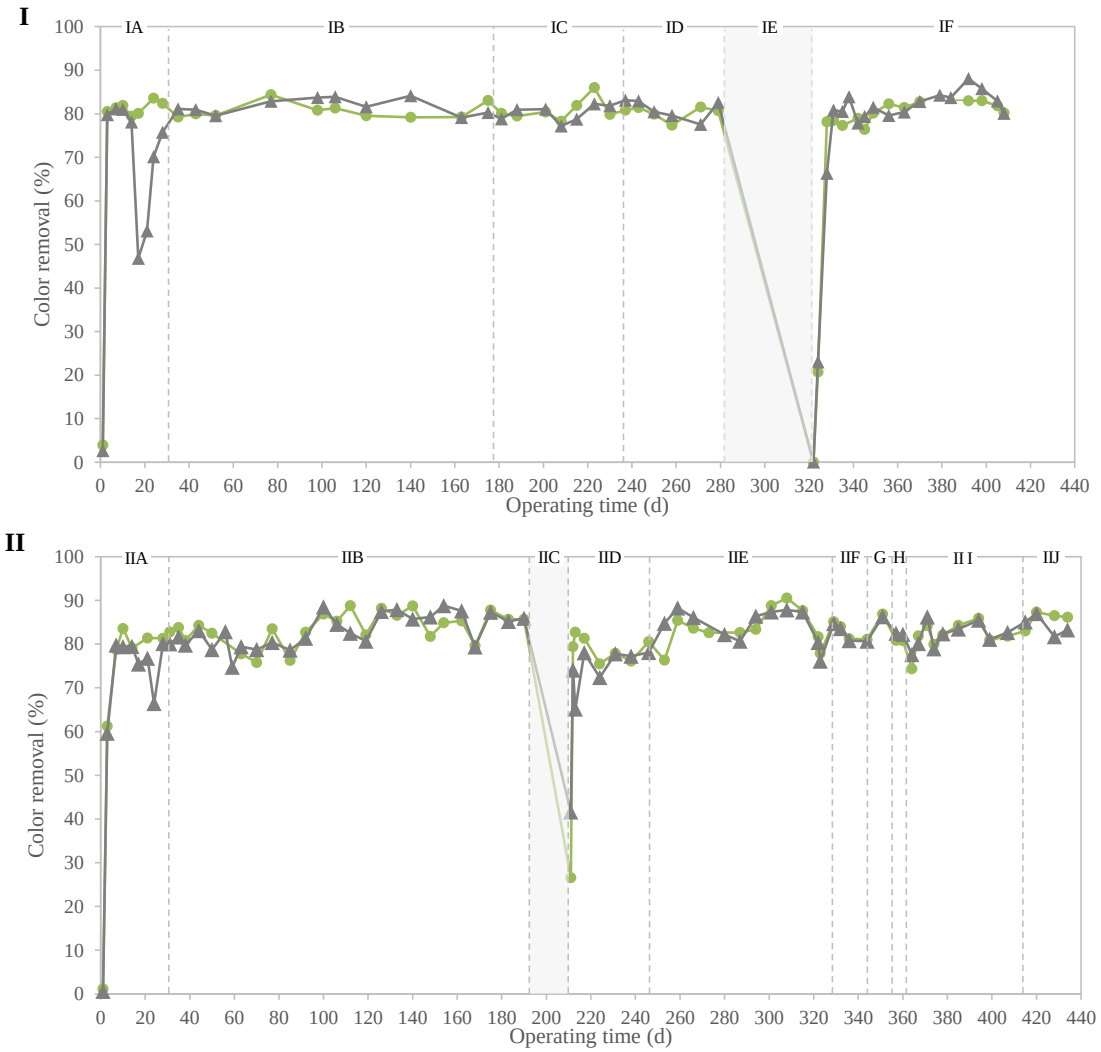


**Figure VII.8** - Color removal performance along experimental runs I and II. Profiles of color removal yield in sequencing batch reactors SBR1 (●) and SBR2 (▲) along experimental runs I and II. The operational conditions for each experimental period (I.A-I.F and II.A-II.J) are described in Table VII.1.

Overlapping color-time profiles were registered in the reactors along different experimental periods, except during the initial SBR2 color removal deteriorating period (Figure VII.9), showing that the presence of at least 10 mg AgNP $L^{-1}$ did not affect the color removal performance. In fact, as evident by the representative color-time profiles, decolorization occurred along the anaerobic phase at an equivalent rate in the two SBRs, the residual azo dye concentration of 3 mg color-equivalents $L^{-1}$ (10 mg color-equivalents $L^{-1}$ during three-fold increase in AR14 concentration, period II.F) being maintained until the end of the aerobic phase. As further demonstrated by HPLC (section VII.4.2.3.2), the residual color results from products of AR14 reduction and not from AR14 itself, which was completely reduced in both SBRs.

In addition to AgNP, also calcium nitrate and potassium nitrate did not affect the color removal performance in the long-term. In fact, although AR14 reduction presented a slight delay and consequent higher residual color on the first cycle in which nitrate was applied at 120 mg $L^{-1}$ in the feed (residual 5 mg color-equivalents $L^{-1}$ in SBR1, *vs* 4 mg color-equivalents $L^{-1}$ in SBR2, on day 364;

Figure VII.S6, in Appendix E), the SBR1 was able to rapidly adapt and restore the same decolorization profile as the nirate-free control (Figure VII.9).

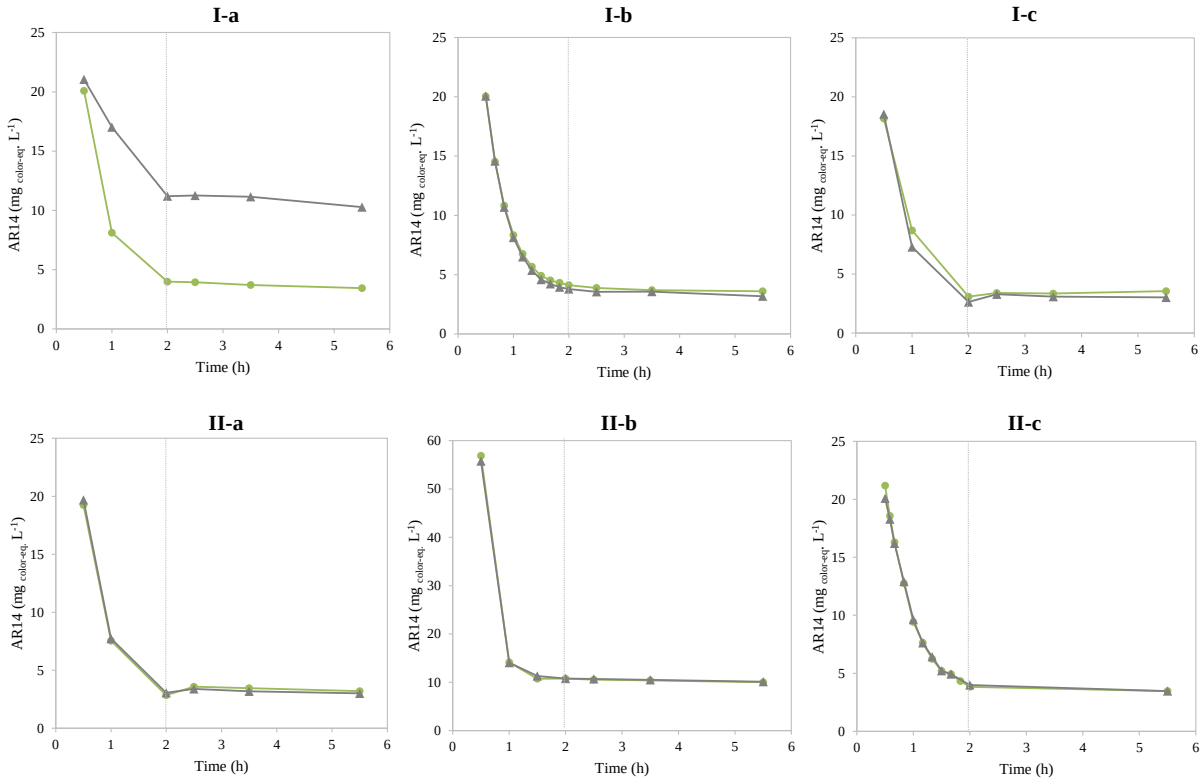


**Figure VII.9** - Comparison between color removal profiles representative of SBR1 and SBR2 treatment cycles along experimental runs I (I, a-c) and II (II, a-c). Comparison between the Acid Red 14 (AR14, as color-equivalents)-time profiles observed along the reaction phase of treatment cycles in sequencing batch reactors SBR1 (●) and SBR2 (▲) on days 17 (I-a; period I.A), 120 (I-b; period I.B) and 399 (I-c; period I.F) of experimental run I, and on days 106 (II-a; period II.B), 344 (II-b; period II.F) and 367 (II-c; period II.I) of experimental run II. Vertical lines represent the end of the anaerobic phase, upon the aeration onset.

## VII.4.2.3.2. Fate of aromatic amines

Decolorization was confirmed to occur through anaerobic azo dye reduction, as the aromatic amine 4A1NS was detected through HPLC, its concentration gradually increasing along the anaerobic phase, concomitantly with AR14 removal from the mixed liquor. Regarding the fate of this aromatic amine during the subsequent aerobic phase, different profiles were observed along the experimental runs (Figure VII.10 and Figure VII.11).

Specifically in SBR1 during the experimental run I, at least until day 24, the 4A1NS concentrations were maintained at high values along the aerobic phase, around 8.0-9.2 mg $L^{-1}$ (Figure VII.10, I-1a), 9.8 mg $L^{-1}$ corresponding to the expected 4A1NS residual concentration after 8 successive cycles with no removal and, consequent accumulation, of 4A1NS. On days 35-38 the aromatic amine profile in SBR1 changed, as the 4A1NS concentration sharply decreased in the first 30 min of aeration, but subsequently increased along the remaining 3 h of aerobic phase (data not shown). Despite not being degraded during the aerobic phase, the unexpected absence of 4A1NS at the start of the anaerobic

stage suggests that a transformation of 4A1NS was occurring during the SBR1 settle/idle/fill phases. In fact, the HPLC analyses revealed the presence of two metabolites, α and α', at the start of the treatment cycle (Figure VII.S7, I-1a, in Appendix E). Afterwards, on days 43-56, the concentration of 4A1NS dropped to zero during the first 1.5 h of aeration (Figure VII.10, I-1b), concomitantly with the rise in the concentration of metabolite α', which was subsequently transformed (Figure VII.S7, I-1b, in Appendix E). Moreover, the maximum 4A1NS concentration value registered was within 6.5-7.8 mg $L^{-1}$ (higher than the expected value when complete and irreversible removal of 4A1NS occurs, 4.9 mg $L^{-1}$), suggesting that partial 4A1NS removal may have occurred during this period. Yet, from day 98 until the end of the experimental run I, no effective removal of 4A1NS occurred, as 4A1NS concentrations were maintained at high values along the aerobic phase (up to 10 mg $L^{-1}$) and its concentration at the start of the anaerobic phase was approximately 4 mg $L^{-1}$ (Figure VII.10, I-1c), the peak areas of metabolites α and α' being maintained close to zero (Figure VII.S7, I-1c, in Appendix E).

Regarding the control SBR, the apparent, reversible conversion between 4A1NS and metabolites α and α' was also observed in some of the studied cycles during the experimental run I, namely on day 3 (Figure VII.10, I-2a, and Figure VII.S7, I-2a, in Appendix E), further indicating that these metabolites established a chemical equilibrium with 4A1NS and that no further degradation of the latter was occurring. In contrast, on the operational days 24-43 the AR14 concentration decreased and the 4A1NS concentration increased at corresponding rates and in stoichiometric amounts along the SBR2 anaerobic phase, giving rise to the expected 4A1NS concentration when there was no accumulation of residual 4A1NS from the previous cycles, 4.9 mg $L^{-1}$ (Figure VII.10, I-2b). Furthermore, the 4A1NS concentration gradually decreased along the 3.5-h aerated stage at a relatively constant rate, being absent at the end of the reaction phase, with no other metabolites being observed in notable amounts (Figure VII.S7, I-2b, in Appendix E). Hence, these results suggest that 4A1NS was completely and irreversibly bioconverted under aerobic conditions during the operational days 24-38. Subsequently, this 4A1NS profile was no longer observed in the experimental run I, as the potential aromatic amine degradation capacity was lost after SBR2 was accidentally subjected to some cycles without aeration during the period of days 41-50 (Figure VII.10, I-2c). In fact, the analysis of the UV-visible spectra of centrifuged samples harvested along the aerobic phase (Figure VII.S8, in Appendix E) showed that the only period of the experimental run I when a relevant decrease in the UV absorbance occurred in SBR2 was during the operational days 22-43 (to a lesser extent on day 43). On the other hand, despite the changes in the HPLC profiles in SBR1 on period I.B (Figure VII.10, I-1b), the typical UV spectral peaks observed at the end the anaerobic phase maintained their absorbance levels throughout the aerobic phase, for every SBR1 analyzed cycle of the experimental run I (Figure VII.S8, in Appendix E).

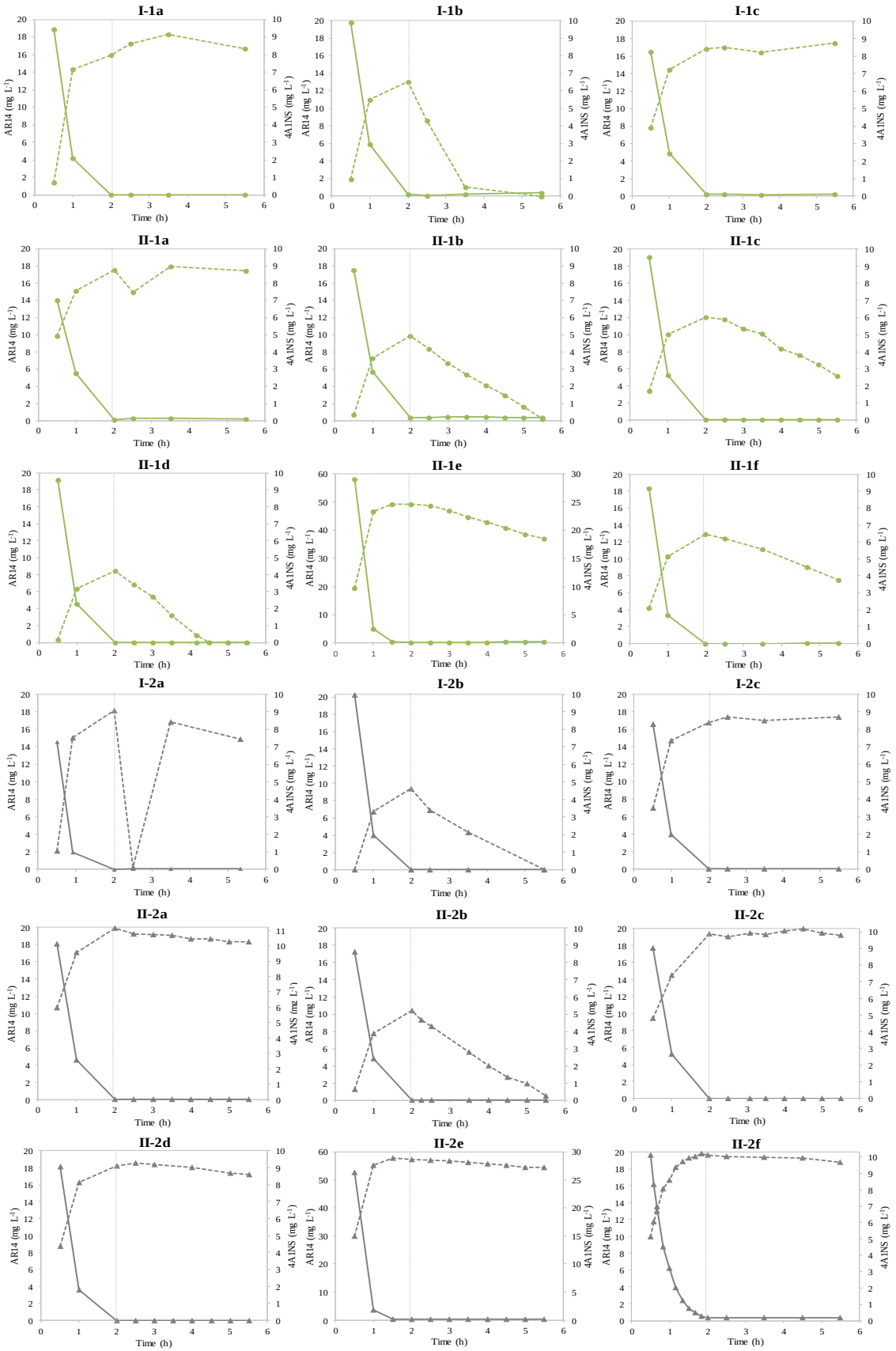


**Figure VII.10** - Concentration-time profiles of the azo dye Acid Red 14 (AR14; full line) and of its cleavage product 4-amino-naphthalene-1-sulfonic acid (4A1NS; dashed line) on selected treatment cycles in sequencing batch reactors SBR1 (●) and SBR2 (▲) from experimental runs I – days 24 (I.1a), 52 (I.1b), 398 (I.1c), 3 (I.2a), 38 (I.2b), 398 (I.2c) – and II – days 24 (II.1a), 63 (II.1b), 100 (II.1c), 175 (II.1d), 336 (II.1e), 350 (II.1f), 63 (II.2a), 92 (II.2b), 190 (II.2c), 323 (II.2d), 344 (II.2e), 415 (II.2f). The vertical lines represent the end of the anaerobic phase.

During the experimental run II, after an initial period when 4A1NS profiles remained unchanged with no aerobic conversion (Figure VII.10, II-1a and II-2a), both SBRs were able to irreversibly convert 4A1NS along the aerobic phase (Figure VII.10, II-1b, II-1d and II-2b), this profile being observed for a longer period of time in SBR1 (from day 56 to 308, with incomplete 4A1NS removal on days 85-100; Figure VII.10, II-1c) than in SBR2 (from day 287 to 322). Upon the increase in the azo dye concentration on day 329, none of the SBRs was able to completely, aerobically transform the resulting higher amount 4A1NS formed during the anaerobic phase, a residual amount of the aromatic amine being still present at the end of the treatment cycle (Figure VII.10, II-1e and II-2e). Yet, while SBR1 was able to sustain partial 4A1NS transformation throughout the azo dye shock load period and beyond (until day 351; Figure VII.10, II-1f), SBR2 lost its capacity to further transform the aromatic amine from day 336 on (Figure VII.10, II-2f). In addition, despite the deterioration in the 4A1NS conversion capacity and specific changes in the 4A1NS-time profile during the period of nitrate supplementation to SBR1 (extensively described in section VI.4.2.3.3), this reactor was able to partially recover its previous 4A1NS removal potential on the last stage of the experimental run II, from day 415 on (Figure VII.11).

In accordance with the HPLC results, significant variations occurred in the UV-visible spectra of liquid samples harvested along the aerobic phase of selected treatment cycles along the experimental run II. Specifically, sample absorbance in the UV range (namely, relevant peaks at 220, 240 and 300 nm) decreased along the aerobic phase of SBR1 cycles on days 211-351 (less intensely on days 315-351) and on days 415-434, as well as on days 287-323 (also slightly on day 280) in SBR2 (Figure VII.S8, in Appendix E).

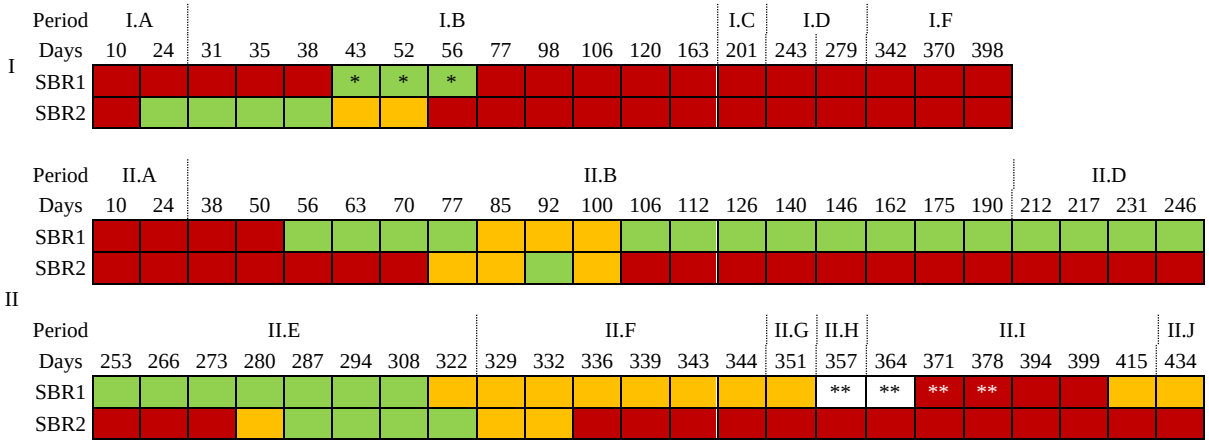


**Figure VII.11** - Schematic representation of the aromatic amine 4-amino-naphthalene-1-sulfonic acid (4A1NS) profile along the aerobic phase of the treatment cycles analyzed on the indicated experimental period, day and sequencing batch reactor (SBR). The different colors represent three main observations along the aerobic phase: 4A1NS concentration was maintained (red), partially reduced (yellow) or reduced to zero (green). * 4A1NS rapidly disappeared within the first 0.5-1.5 h of aeration; **4A1NS was absent during the anaerobic reaction phase, a new peak emerging along this phase instead. Uncolored days correspond to those when 4A1NS was not observed throughout both the anaerobic and the aerobic phases.

### VII.4.3. Microbial community dynamics

#### VII.4.3.1. FISH analysis

In order to assess the impact of AgNP on the microbial community, FISH analysis was conducted in biomass samples taken from SBR1 and SBR2 on specific days of the experimental periods I.A-I.B. As represented in Figure VII.12, the proteobacterial major groups *Betaproteobacteria* and *Gammaproteobacteria* were in high abundance in the inoculum used in the experimental run I. The relative abundance of *Gammaproteobacteria* decreased, while *Alphaproteobacteria* and *Actinobacteria* became more relevant in both SBRs after 36 days of operation. SBR1 also presented a relevant presence of *Citophaga-Flavobacteria* on day 36, contrarily to the control. The differences observed between the SBRs indicate that the presence of AgNP affected the microbial community at least after 1 month of operation under continuous supplementation with 10 mg AgNP $L^{-1}$ in the feed solution. Furthermore, despite a slight decrease in the relative abundance of *Betaproteobacteria* from day 36 to 106 in SBR1, the community remained quite stable, as opposed to the control, where the microbial community further evolved during this period of time, *Gammaproteobacteria* becoming predominant and *Alphaproteobacteria* in minority on day 106.

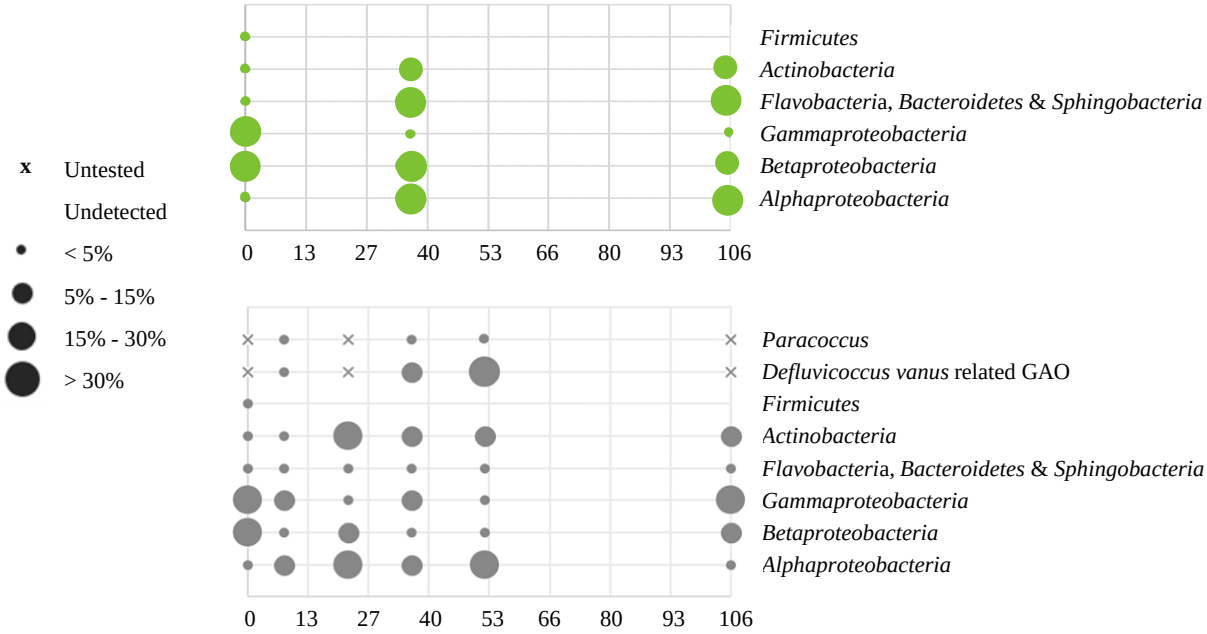


**Figure VII.12 -** Abundance of the selected *Bacteria* detected by FISH analysis in the mixed microbial culture samples from sequencing batch reactors SBR1 (green circles) and SBR2 (grey circles). FISH probes for *Paracoccus* and *Defluviicoccus vanus*-related GAO (glycogen-accumulating organisms) were only applied to SBR2 samples. Additional biomass samples were analyzed in SBR2 (operational days 8, 22 and 52), in light of relevant changes observed in its azo dye biodegradation performance. Adapted from Carvalho (2016).

In light of the specific changes in the azo dye biodegradation performance registered in SBR2, additional biomass samples were analyzed for this reactor. Specifically, the decrease in the color removal performance (from 80% on day 8 to 45% on day 22) with subsequent recovery (80% of color removal yield on day 36, including the complete aerobic removal of the aromatic amine 4A1NS)

occurred along with changes in the microbial community (Figure VII.12). In fact, while the relative abundance of *Alphaproteobacteria* and *Betaproteobacteria* increased in SBR2 from day 8 to 22, *Gammaproteobacteria* decreased. Subsequently, *Defluviicoccus vanus*-related GAO emerged within the *Alphaproteobacteria* group on day 36 (Figure VII.12), being potentially correlated with the aromatic amine transformation profile registered during the operational days 24-43 (Figure VII.11). However, *Defluviicoccus vanus*-related GAO further increased its relative abundance on day 52, when the 4A1NS irreversible conversion was no longer observed.

### VII.4.3.2. Microbial community analysis

The microbial community was analyzed in both SBRs on the experimental days 22, 30 and 52 in order to evaluate the impact of AgNP on bacterial diversity. The initial, very diverse microbial community present in the inoculum, containing *Acidobacteria*, *Chlorobi*, *Chloroflexi* and *Firmicutes* populations in relevant amounts, was markedly reduced after 22 days of SBR operation (Figure VII.S9, in Appendix E). Irrespective of the presence of AgNP, the SBRs bacterial communities were mainly composed of *Proteobacteria* (mostly corresponding to the *Alphaproteobacteria* class), *Bacteroidetes* (mostly, from the *Sphingobacteriia* class), *Actinobacteria* and *Saccharibacteria* (Figure VII.13 and Figure VII.S9, in Appendix E). Differences between the SBRs were more evident when analyzing the 20 most abundant OTUs. Specifically, on day 22, the AgNP-fed SBR presented a notably higher relative abundance of a group of bacteria belonging to *Niabella* (22%), when compared to SBR2, in addition to exclusively containing a bacterial population from the *Microbacterium* genus (Figure VII.S10, in Appendix E). In contrast, specific bacteria from the *Leadbetterela* genus, *Saccharibacteria* phylum and *Saprospiraceae* family were almost absent in SBR1, contrarily to that observed in the AgNP-free SBR (Figure VII.S10, in Appendix E).

The evolution of the microbial community in SBR1 from day 22 to 52 was characterized by a decrease in the *Sphingobacteriia* and an increase in *Actinobacteria* (in majority on day 52, representing 37% of the bacterial community) and *Alphaproteobacteria* classes (Figure VII.13). At the genus level, the relative abundance of a *Caldilineae* bacterial population gradually increased to 18%, becoming the dominant one on day 52, in addition to a slight increase in other bacterial groups belonging to *Hyphomicrobiaceae*, *Amaricoccus* and *Microbacterium* genera (Figure VII.S10, in Appendix E). On the other hand, bacteria from the *Niabella* genus decreased to 10% in terms of relative abundance, though being the second most abundant OTU in SBR1 on day 52 (Figure VII.S10, in Appendix E). Regarding the AgNP-free SBR, despite a temporary increase in the relative abundance of *Actinobacteria* on day 30, the main difference from day 22 to 52 at the class level was the greater dominance of *Alphaproteobacteria* (from 25% to 47% of the bacterial community), mainly at the expense of *Saccharibacteria* (from 17% to 1%; Figure VII.13). Contrarily to SBR1, the bacteria population belonging to the *Niabella* genus increased from day 22 to 52 in SBR2 (Figure VII.S10, in

Appendix E). Similarly to the AgNP-fed SBR, bacteria from the *Hyphomicrobiaceae*, *Amaricoccus* and *Microbacterium* genera also increased their relative abundance in SBR2, but the presence of a *Saccharibacteria* bacteria population, which represented 8% of SBR2 community on day 22, became irrelevant on day 52 (Figure VII.S10, in Appendix E).

Overall, the main differences between the bacterial community in the two SBRs after 52 days of operation were the prevalence of *Salana*, *Microbacterium* and *Micropruina* bacteria in SBR1, *vs* the major relative abundance of *Hyphomicrobiaceae*, *Leadbetterella* and of a specific *Saccharibacteria* population in SBR2 (Figure VII.S10, in Appendix E). At the class level, these differences correspond to a higher predominance of *Actinobacteria* (37%) and *Alphaproteobacteria* (47%) in SBR1 and SBR2, respectively (Figure VII.13), the relative amount of *Bacteroidetes* and *Saccharibacteria* phyla being comparable in both SBRs (Figure VII.S9, in Appendix E).

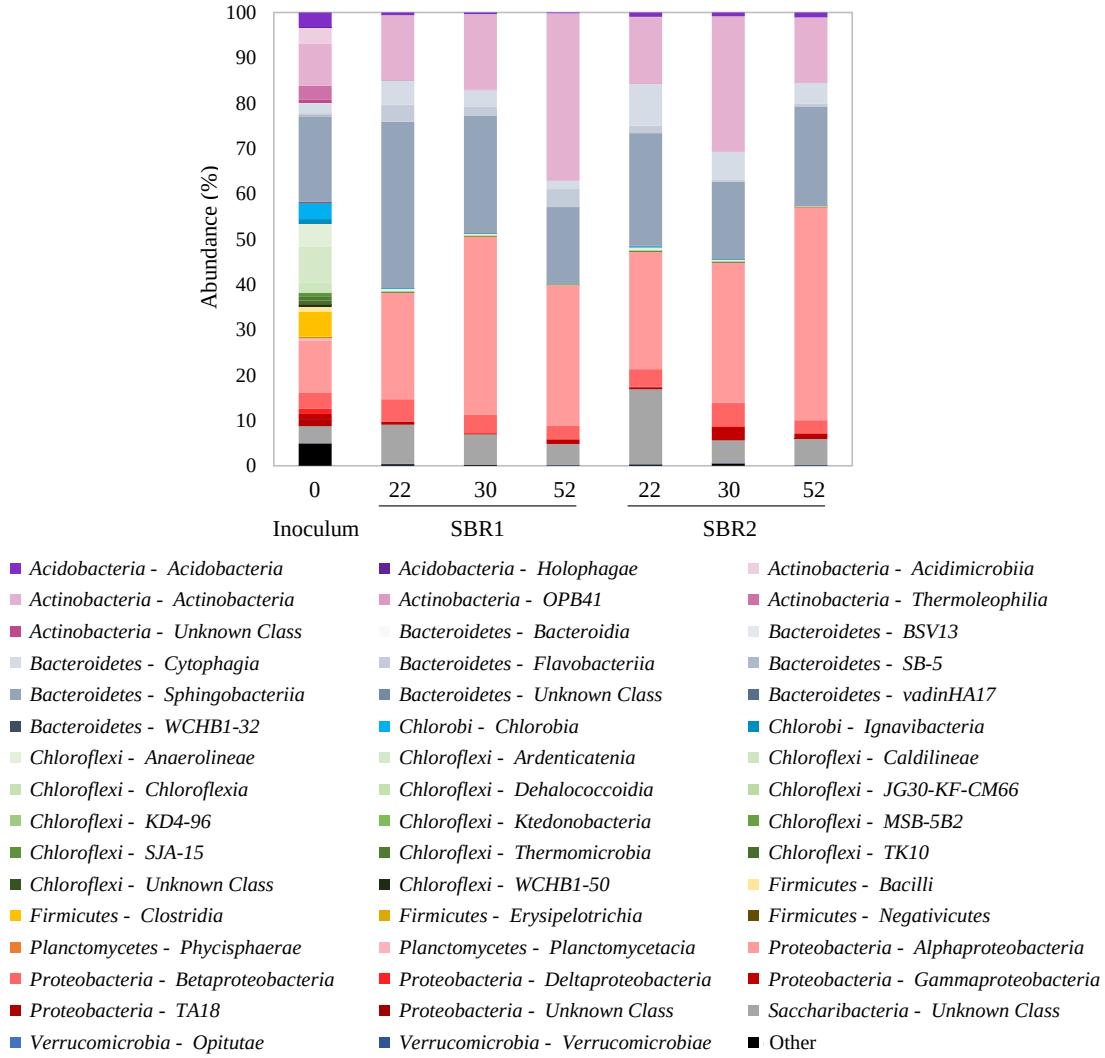


**Figure VII.13** - Composition of bacterial communities at the class level in the inoculum, as well as in sequencing batch reactors SBR1 and SBR2 on the indicated operational days, obtained by 16S rRNA gene sequencing analysis. The most representative "Phylum-Class" are represented below the chart.

## VII.5. Discussion

### VII.5.1. AGS morphology and properties

The role of AgNP in the inhibition of biofilm formation has been extensively described, the application of a sufficiently high AgNP concentration being a key factor to achieve effective inhibition (Sheng and Liu, 2017). Moreover, the few studies addressing the effects of AgNP on AGS systems have not assessed the impact of these nanoparticles in the formation of AG from CAS (Gu *et al*., 2014; Quan *et al*., 2015). On the other hand, the presence of $TiO_2$-NP (10-50 mg $L^{-1}$) was shown to enhance granulation (Li *et al*., 2015). The present study showed that successful aerobic granulation was achieved approximately after 40-50 days of operation, irrespective of the presence of AgNP, even when a higher concentration (20 mg $L^{-1}$) was applied in the experimental run II (Figure VII.2; Figure VII.3). These results indicated that inhibition of AGS formation by AgNP in a real scenario is not expected, since the influent AgNP concentration tested was much higher than the estimated maximum influent silver concentration from industrial discharges, 0.1 mg $L^{-1}$ (Shafer *et al*., 2009; Sheng and Liu, 2017). Furthermore, while the biomass concentration progressively increased in both SBRs at similar rates during the experimental run I's granulation phase (up to 9 gTSS $L^{-1}$), increasing the concentration of AgNP in the experimental run II allowed SBR1 to reach higher TSS levels (10 gTSS $L^{-1}$ in SBR1 *vs* 8 gTSS $L^{-1}$ in SBR2; Figure VII.4). Accordingly, Sheng *et al.* (2018) indicated that the presence of AgNP led to an increased floc size and density, with consequent better settleability and more intense biomass accumulation in the reactor. On the other hand, Quan *et al.* (2015) showed that AGS SBRs fed with 5 and 50 mg AgNP $L^{-1}$ presented lower biomass concentration levels (6 and 4 gVSS $L^{-1}$, respectively) than the AgNP-free control (7 gVSS $L^{-1}$) after 69 days of operation, despite their biomass concentration profiles (increasing from 3 to 6 gVSS $L^{-1}$) being initially similar to the control, until day 45 of operation.

The sudden decrease in the TSS values upon reactivation was a result of the biomass being stored at room temperature for 40 days during the summer period, without feed sources (Figure VII.4). In fact, a high storage temperature combined with the absence of external substrate supply may lead to endogenous respiration and AG disintegration (Liu and Tay, 2004). Subsequently, as the sludge settling capacity improved and the biomass concentration recovered up to 6 gTSS $L^{-1}$ (Figure VII.4), the fraction of granules larger than 0.2 mm, which was initially lower than 10%, markedly increased in both SBRs after the 40-day biomass storage period (Figure VII.1), as new AG were formed (Figure VII.3). In fact, previous studies have shown that both AG structure and physical properties could be fully restored after long-term extended idle conditions (58 days), owing to the role of EPS (especially PN) in the resistance to storage and in reactivation of the AGS system (He *et al*., 2017c). Specifically, Wang *et al.* (2008a) indicated that the accumulation of EPS was an effective strategy for maintaining the AG structural integrity during long-term storage (7 months), and that the decrease in EPS during

reactivation improved mass transfer within granules, contributing to their recovery within the first month of operation. The results from the present study indicated that AgNP, namely the fraction adsorbed in EPS (Bento *et al*., 2017), did not significantly interfere with the latter's role. In fact, the resistance of AGS to long starvation periods and its capacity to recover good physical properties, as well as the formation of new granules during reactivation after storage, were not affected by the presence of AgNP. Moreover, although the effect of AgNP on AGS reactivation after storage has not been reported in the literature, AgNP has been shown to accumulate in AGS along the exposure period, stimulating the preferential production of PN over PS in EPS (Quan *et al*., 2015), and eventually supporting AGS resistance to storage and its reactivation capacity.

Overall, the granular fraction of the sludge was slightly lower in SBR1 during the first 125 days of the experimental run II (Figure VII.1), similarly to a 69-day study where AGS in an AgNP-fed SBR presented worse settleability and lower TSS levels during the first month of exposure to AgNP, as compared with an AgNP-free control (Quan *et al*., 2015). However, this relation was inverted during the subsequent 121 days, due to disintegration of AG larger than 0.2 mm in the AgNP-free SBR2, AG becoming more abundant in SBR1 (Figure VII.1; Figure VII.3). This suggested that the cumulative adsorption of AgNP onto AG (Bento *et al*., 2017) may have increased their density and promoted a more stable AGS by preventing the long-term deterioration of the sludge settling capacity. Moreover, after the idle period in the experimental run II (period II.C), the AG in SBR1 not only were in greater number than in SBR2, but also presented larger dimensions and clearer outlines, being surrounded by dense sludge aggregates (Figure VII.3 and Figure VII.S2, in Appendix E). These observations further supported the hypothesis that AgNP contributed to the stability of AG, probably by stimulating EPS production in bacteria as a stress response. In fact, AgNP were shown to accumulate in AGS along the exposure period, stimulating the preferential production of PN over PS in EPS as a response to the toxic stress (Zhang *et al*., 2018c). Accordingly, He *et al.* (2017a) reported that the presence of ZnO-NP stimulated the increase in EPS levels and PN/PS, AGS settleability not being affected. Furthermore, following the successful formation and maintenance of stable algal-bacterial granules during 100 days in the presence of $TiO_2$-NP, Li *et al*. (2015) suggested the role of these nanoparticles in preventing AG disintegration and enhancing the long-term AG stability, possibly through stimulation of EPS excretion and inhibition of filamentous growth.

Upon the interruption of AgNP addition to SBR1 in the experimental run II, the AG properties were further enhanced in SBR1, the number of granules (>0.2 mm) rapidly increasing up to 43%, as opposed to the gradual increase to 33% registered in the control (Figure VII.1). This could indicate that, although the presence of AgNP apparently contributed to stabilize AG, their accumulation in the biomass seems to have limited the full potential of AGS, in terms of formation of new AG. Hypothetically, the interaction of AgNP with the EPS (Bento *et al*., 2017) may have interfered with the cell adhesion process necessary for further granule formation. On the other hand, it is possible that

the toxicity associated with the previous presence of AgNP induced long-term cellular stress and the associated EPS production, which, in turn, further enhanced cell adhesion and granule enlargement even after AgNP addition was stopped. This long-lasting effect in AGS physical properties is supported by the inorganic fraction results, which indicated that AgNP were still present in the biomass at least after 20 days of AgNP clean-up from SBR1 (Figure VII.5). According to a review exploring the impacts of AgNP in bacteria, the increased stability after long-term exposure and the recovery capacity represent stimulatory responses to AgNP (Sheng and Liu, 2017). The microbial community in AG developed during the long period of AgNP supplementation possibly retained an enhanced capacity to produce EPS, leading to long-term stability of the formed AG, independently of the continued addition of AgNP. Furthermore, AG in SBR1 were maintained at significantly higher numbers until the end of the operation, when compared to the control, including during the azo dye shock load (Figure VII.1). This indicated that the formation of AG in the presence of AgNP and the previous contact with AgNP during 228 days had subsequent, long-lasting beneficial effects in terms of sludge properties.

Overall, although SBR1 and SBR2 presented essentially equivalent SVI results during the first 100 days of operation in both experimental runs, the subsequent gradual deterioration in the sludge settleability noted in both SBRs up to the idle period was more marked in the AgNP-free SBR2 (Figure VII.2). Accordingly, not only did AgNP not hinder the aggregation ability of the sludge, but also possibly promoted granulation and contributed for a prolonged preservation of the granular structure over long operational periods, namely when subjected to a dye shock load. In fact, although the morphology of the sludge was similar between the reactors (Figure VII.3), SBR1 sustained a granule-rich sludge (Figure VII.1), better SVI values (Figure VII.2) and higher TSS (Figure VII.4) for longer operational periods, both during and after AgNP supplementation, before and after the idle period. In addition, contrarily to SBR1, the control SBR presented a sharp increase in SVI values on day 428 of the experimental run II (Figure VII.2). This AGS instability probably reflects the weakening of the AGS core due to mass transfer limitations across the granule structure. The consequent limitation of oxygen and substrate availability in the AG inner region can cause cell death and the appearance of cavities in the core of AG, their weaker physical structure becoming more prone to break under shear stress (Franca *et al*., 2018; Toh *et al*., 2003). Nevertheless, the cause was not associated with outgrowth of filamentous organisms, which were not observed. In fact, the anaerobic feed mode and the high shear stress imposed in the system probably contributed to restrain the proliferation of filamentous bacteria.

Microscopic analysis (small, opaque and dark aggregates associated with flocs and AG surfaces; Figure VII.3), macroscopic observation (change of biomass color from yellowish to dark grey when supplemented with AgNP; Figure VII.S3, in Appendix E) and sludge inorganic fraction measurements (Figure VII.5) indicated that AgNP accumulated in SBR1, either adsorbed onto the biomass or as

AgNP agglomerates suspended in the mixed liquor. In fact, Bento *et al.* (2017) confirmed that AgNP clustered in agglomerates (<10 μm), being distributed throughout AG, but preferentially associated with external EPS. Accordingly, previous studies (Gu *et al*., 2014; Quan *et al*., 2015) also highlighted the role of EPS in the capture and physical retention of AgNP, 500-nm clusters of silver being observed on the surface of AG (Gu *et al*., 2014). Furthermore, according to the sludge inorganic fraction analysis, it took 22 days to reach an apparent steady state in terms of AgNP accumulation in SBR1 biomass (the sludge becoming saturated at 2% of AgNP), and 10 days to clear out most of the AgNP from the reactor in the experimental run I (Figure VII.5). Moreover, when a higher AgNP concentration was used, the biomass became saturated with AgNP sooner (*i.e*., after 10 days of operation with cyclic addition of AgNP; AgNP accounting for approximately 4% of the TSS in SBR1), and a longer clean-up period was necessary (*i.e*., approximately 20 days; Figure VII.5). The marked decrease in the protozoa abundance in SBR1 indicated that AgNP have a toxic effect on protozoa. In fact, although the antimicrobial potential of AgNP has been more often reported in bacteria and fungi, studies have shown similar results, namely the size-dependent effect, against protozoa (Silva *et al*., 2017).

After interrupting AgNP feeding to SBR1, addition of calcium nitrate in SBR1 contributed to the increase in VSS levels, namely through the enlargement of AG and development of new granules (reaching 64% of AG larger than 0.2 mm) with good settling characteristics (Figure VII.1; Figure VII.2; Figure VII.3; Figure VII.4). Furthermore, addition of calcium nitrate caused a 2% increase in terms of sludge inorganic content in SBR1, in relation to the control SBR2 (Figure VII.5), indicating the accumulation of calcium in the granules, probably through precipitation with phosphates (see section VI.4.1.3), dosed at high concentrations for buffering of mixed liquor pH. Changing from calcium nitrate to potassium nitrate caused a decrease in the inorganic content of the sludge (to levels equivalent to the control; Figure VII.5) and an increase in the amount of flocculent sludge in SBR1 (Figure VII.3). In fact, the role of calcium precipitation and calcium ions in enhancing EPS content in AG has been previously associated with an improved granular strength and stability (Lee *et al*., 2010; Zhang *et al*., 2019). Specifically, calcium ion has been shown to promote EPS cross-linkage, further enhancing the structural integrity of AG (Ren *et al*., 2008). In addition, calcium and/or iron precipitates have been reported to substantially enhance the structural stability of AG, as stable granules containing high amounts of calcium and iron precipitates (namely, phosphate salts of calcium) were maintained in continuous-flow reactors for 216 days (Juang *et al*., 2010). Moreover, calcium and iron precipitation inside granules was favored by the enriched presence of denitrifiers, which produced alkalinity as a result of denitrification reactions occurring inside AG (Juang *et al*., 2010). Similarly, in addition to an improvement in the anaerobic COD removal registered in SBR1 during the period of calcium nitrate supplementation (Figure VII.6), denitrification of the added nitrate

was registered in SBR1 (see section VI.4.2.3.3), likely promoting the precipitation of calcium inside the AG.

### VII.5.2. AGS SBR treatment performance

#### VII.5.2.1. Anaerobic and overall COD removal

Usually, AgNP have been associated with stronger adverse effects on nitrification than on COD removal in wastewater treatment systems (Liang *et al*., 2010; Zhang *et al*., 2016a). In fact, the presence of AgNP did not observably affect the overall COD removal yield, stable values within the 75-85% range being reached after 2 weeks of operation and maintained along the two experimental runs in both SBRs (Figure VII.6). Although COD removal was not affected by the 18-day idle period in the experimental run II, the longer biomass storage period (and higher storage temperature) in the experimental run I led to a 10-day recovery period to reach again 80% of total COD removal, 60% of which being removed under anaerobic conditions irrespective of the presence of AgNP (Figure VII.6). Similarly, high COD and $NH_4$-N removal yields (>98%) were maintained in an AGS SBR fed with AgNP along 69 days (Quan *et al*., 2015). However, the AGS microbial activity was negatively affected by the presence of AgNP from the operational day 36 on, namely in terms of ammonia oxidizing rate (33%), respiration rate (18-46%) and denitrification rate (7%; Quan *et al*., 2015). In this sense, in spite of the overall AGS tolerance to AgNP and absence of acute toxicity, Quan *et al*. (2015) warned of a possible chronic, toxic long-term effect resulting from the cumulative adsorption of AgNP in AGS. Yet, addition of AgNP to an initial concentration up to 10 mg $L^{-1}$ did not affect the overall COD removal performance of the AGS SBR (Figure VII.6), neither did it produce marked or consistent changes in the COD removal profile in relation to the AgNP-free control SBR (Figure VII.7) throughout the long experimental runs (305 and 228 days of AgNP addition to SBR1 in the experimental runs I and II, respectively), including reactivation after idle periods.

The absence of a negative effect by the antimicrobial AgNP on the COD treatment performance could be explained by the binding of the AgNP or the released $Ag^+$ to dissolved organic carbon and inorganic ions (namely sulfide and chloride), which has been shown to lower their bactericidal effects (Levard *et al*., 2012; Kaegi *et al*., 2013). Moreover, mixed cultures have been associated with a higher resistance to the adverse effects of AgNP than pure cultures due to microbial functional redundancy maintaining process stability in a wastewater treatment system, namely COD degradation (Zhang *et al*., 2016a). In addition, the physical structure of the sludge also plays a critical role, microorganisms in attached-growth bioreactors (biofilm/granular sludge) being less susceptible to AgNP exposure than in suspended-growth bioreactors (flocculent sludge; Gu *et al*., 2014; Sheng and Liu, 2011).

### VII.5.2.2. Azo dye biodegradation

Maximal color removal performance (80%) was reached within one week after inoculation and after biomass storage, irrespective of the presence of AgNP (Figure VII.8). These results showed that the presence of AgNP did not affect the azo dye biodecolorization capacity of AGS. Moreover, despite the suggested use of AgNP as a catalyst for azo dye reductive degradation (Ahmed *et al*., 2018; Edison *et al*., 2016; Saravanan *et al*., 2017; Varadavenkatesan *et al*., 2016), the decolorization rate was equivalent in both SBRs (Figure VII.9). This high decolorization performance was maintained in the reactors, except for a temporary deterioration in the SBR2 color removal yield registered when the settling time was reduced to 15-20 min in both experimental runs, leading to some biomass washout. This could indicate that microbial populations playing a key role in the decolorization process were washed out from the system. For instance, when the biomediated chemical reduction of azo dyes through biological sulfate reduction occurs (sulphide acting as an electron donor to the azo dye), inhibition of sulfate reducing bacteria has been shown to negatively affect the decolorization of azo dyes (Albuquerque *et al*., 2005). On the other hand, a significant decrease in the biomass concentration could lead to an at least small reduction in the abundance of relevant redox mediators in the mixed liquor, which in turn would significantly impact the decolorization rate (van der Zee and Cervantes, 2009). For instance, some aromatic amines or their aerobic transformation products have been suggested to act as redox mediators able to anaerobically shuttle reduction equivalents from the cells to extracellular azo dyes (Keck *et al*., 1997; Liu *et al*., 2009). Specifically, 1N2A4S, which is one of the azo bond reduction products of AR14, may function as redox mediator to speed up azo dye biodecolorization (Liu *et al*., 2009).

According to previous studies, nitrate could be reduced preferentially to AR14, eventually leading to a delay and a less efficient color removal process (Carliell *et al.*, 1998; Lourenço *et al*., 2000). Despite a slight delay in AR14 reduction on the first cycle of calcium nitrate supplementation at 120 mg $L^{-1}$ in SBR1, relatively to SBR2, this delay was not repeated in the subsequent analyzed cycles, nor observed during any of the cycles when SBR1 was supplemented with a lower nitrate concentration (60 mg $L^{-1}$ in the feed; Figure VII.9). These observations support dos Santos *et al*. (2008), who indicated that the presence of nitrate in TWWs will not likely decrease the capacity of bioreactors to anaerobically biodecolorize azo dyes.

The shorter time and lower temperature applied during the storage period in the experimental run II allowed the biomass to resume its metabolic activity in the first cycle of operation, well sooner than in the experimental run I (7-10 days; Figure VII.8). Similarly, Adav *et al*. (2008a) indicated that phenol-fed AG stored at -20ºC for up to 6 months could recover 80-99% of the initial activity after 48 h reactivation, concluding that low or even freezing temperatures and the presence of a toxic substance inhibit intra-granular bioactivity, hence assisting in preserving granule stability and cell viability for recovery. Conversely, another study reported that AG stored at room temperature for 8 months

presented the worst restoration performance (when compared to storage at 4ºC and -25ºC), full recovery of the SBR treatment performance being attained after approximately 2 weeks of operation (Gao *et al.*, 2012). In general, granule activity upon reactivation increases as storage temperature decreases, and declines as storage time increases (Adav *et al.*, 2007).

Regarding the experimental run I, effective transformation of 4A1NS apparently only occurred in SBR2 on days 22-43, when color removal was recovered after a temporary deterioration (Figure VII.11). On the other hand, in the experimental run II, SBR1 sustained 4A1NS transformation for longer periods of time than SBR2, namely throughout the azo dye shock load period and beyond (Figure VII.11). Although the effect of AgNP on the biodegradation of aromatic amines has not been specifically addressed in the literature, the presence of AgNP may have hypothetically promoted a higher biodegradation potential by inducing the presence of a more diverse microbial community within the denser AG. In fact, results from a recent study indicated that AgNP can help to maintain or even increase the diversity of the microbial community in activated sludge, as well as the biomass concentration even under long-term operation (Sheng *et al.*, 2018). In turn, the consequently higher SRT can further promote the presence of slow-growing populations, whose activity may be advantageous for the degradation of recalcitrant compounds (Clara *et al.*, 2005).

### VII.5.3. Microbial community dynamics

As opposed to *Gammaproteobacteria*, *Alphaproteobacteria* and *Actinobacteria* became more relevant in both SBRs after 36 days of operation (Figure VII.12), indicating a better adaptation of the latter to the new operational conditions, namely to the starch-based carbon source and azo dye in the feed. Irrespective of the presence of AgNP, the SBRs bacterial communities were mainly composed of *Proteobacteria* (mostly corresponding to *Alphaproteobacteria* class), *Bacteroidetes* (mostly, from the *Sphingobacteriia* class), *Actinobacteria* and *Saccharibacteria* (Figure VII.13 and Figure VII.S9, in Appendix E). The tolerance of *Sphingobacteriia* towards AgNP has been previously reported in activated sludge (Yang *et al.*, 2014). Similarly, Gwin *et al.* (2018) demonstrated the resilient nature of an SBR microbial community towards AgNP, as its composition resembled that of the AgNP-free SBR after being exposed to silver multiple times. Yet, in the present study, some differences were observed between the SBRs, indicating that the presence of AgNP affected the microbial community at least after 1 month of operation under continuous supplementation with AgNP during the experimental run I. Specifically, on day 22, the AgNP-fed SBR presented a significantly higher relative abundance of a group of bacteria belonging to *Niabella* (22%), when compared to SBR2, in addition to exclusively containing a bacterial population from the *Microbacterium* genus (Figure VII.S10, in Appendix E). In contrast, specific bacteria from the *Leadbetterela* genus, *Saccharibacteria* phylum and *Saprospiraceae* family were almost absent in SBR1, contrarily to that observed in the AgNP-free SBR (Figure VII.S10, in Appendix E). In fact, owing to functional redundancy, the application of high AgNP concentrations (mg $L^{-1}$ levels or higher) can cause major shifts in the

bacteria community structure without significantly affecting the reactor's treatment performance (Zhang *et al*., 2016a). Furthermore, the presence of *Citophaga-Flavobacteria* was also relevant in SBR1 on day 36, contrarily to the control (Figure VII.12). This group belongs to the *Bacteroidetes* phylum, which represented the second most dominant phylum in SBR1 along the first month of operation (Figure VII.S9, in Appendix E), similarly to another study assessing the microbial community response to AgNP (Gwin *et al*., 2018). *Bacteroidetes* have been associated with the capacity to degrade recalcitrant materials (Gwin *et al*., 2018) and described as relatively resistant to AgNP, since their abundance significantly increased in activated sludge exposed to AgNP (Yang *et al*., 2014). In fact, silver-resistant genera have been mainly described in *Acidobacteria* and *Proteobacteria* phyla, but also in *Bacteroidetes* (Yang *et al*., 2014).

Overall, the main differences between the bacterial community in the two SBRs after 52 days of operation were the prevalence of *Salana*, *Microbacterium* and *Micropruina* bacteria in SBR1, *vs* the major relative abundance of *Hyphomicrobiaceae*, *Leadbetterella* and of a specific *Saccharibacteria* population in SBR2 (Figure VII.S10, in Appendix E). At the class level, these differences correspond to a higher predominance of *Actinobacteria* (37%) and *Alphaproteobacteria* (47%) in SBR1 and SBR2, respectively (Figure VII.13), the relative amounts of *Bacteroidetes* and *Saccharibacteria* phyla being comparable in both SBRs (Figure VII.S9, in Appendix E). Furthermore, despite a slight decrease in the relative abundance of *Betaproteobacteria* from day 36 to 106 in SBR1, the culture remained quite stable, as opposed to the control, where the microbial community further evolved during this period of time (Figure VII.12). Similarly to this study, Quan *et al*. (2015) observed that, despite slight changes in the microbial community, the dominant microbial population in AGS remained stable along the 69-day exposure to AgNP. This highlights the protecting effect of the AG structure to bacteria more susceptible to toxic environments. Specifically, the silver distribution in cross sectioned AGS samples from SBR1 demonstrated that the outer layers of the granules greatly hindered the dispersion of AgNP into the central part, which may have protected the microbial communities present in the inner layers against AgNP and $Ag^{+}$ toxicity (Bento, 2016). In general, most AgNP probably cannot reach bacteria cells inside biofilms since they are trapped in the EPS matrix due to aggregation (Sheng and Liu, 2017). According to Fabrega *et al*. (2011), as the AgNP concentration increased to 2 mg $L^{-1}$ in a biofilm reactor, the volume of the biofilm decreased but no significant effects on the dominant community were detected. Overall, the SBR supplemented with AgNP maintained a high microbial diversity along 106 days of operation (Figure VII.12). Furthermore, Sheng and Liu (2017) observed that fresh AgNP induced an increase in microbial community diversity, which was proposed to contribute to a higher resistance to AgNP toxicity.

Regarding the AgNP-free SBR, the temporary deterioration in color removal performance occurred along with the increase in the abundance of the major proteobacterial groups *Alphaproteobacteria* and *Betaproteobacteria* from day 8 to 22, *Gammaproteobacteria* becoming minimal (Figure VII.12). The

subsequent recovery, including the complete aerobic removal of the aromatic amine 4A1NS (days 24-43), was associated with the emergence of *Defluviicoccus vanus*-related GAO on day 36 (Figure VII.12). However, *Defluviicoccus vanus*-related GAO further increased their relative abundance on day 52, when the 4A1NS irreversible conversion was no longer observed. Furthermore, despite a temporary increase in the relative abundance of *Actinobacteria* on day 30, the main difference from day 22 to 52 at the class level was the greater dominance of *Alphaproteobacteria* (from 25% to 47% of the bacterial community), mainly at the expense of *Saccharibacteria* (from 17% to 1%; Figure VII.13). Contrarily to SBR1, the bacteria population belonging to the *Niabella* genus increased their presence from day 22 to 52 in SBR2 (Figure VII.S10, in Appendix E). Similarly to the AgNP-fed SBR, bacteria from the *Hyphomicrobiaceae*, *Amaricoccus* and *Microbacterium* genera also increased their relative abundance in SBR2, but the presence of a *Saccharibacteria* population, representing 8% of SBR2 community on day 22, became irrelevant on day 52 (Figure VII.S10, in Appendix E). Some of these changes could be associated with the loss of the 4A1NS conversion capacity registered in SBR2, gradually occurring from day 43 on (Figure VII.11). *Microbacterium*, which was amongst the most abundant bacteria in SBR2, was reported as being part of a microbial consortium able to degrade 4A1NS in a packed bed continuous reactor, along with strains belonging to the genera *Variovorax*, *Pseudomonas*, *Bacillus*, *Arthrobacter* and *Nocardioides* (Juárez-Ramírez *et al*., 2015).

## VII.6. Conclusions

This study investigated for the first time the impact of AgNP on TWW treatment performance by anaerobic-aerobic AGS SBRs during long-term operation, including aerobic granulation and AGS reactivation after an idle period. Successful aerobic granulation was achieved approximately after 40-50 days of operation, irrespective of the presence of AgNP (up to 20 mg $L^{-1}$ in the feed solution). Similarly, the resistance of AGS to long starvation periods and its capacity to recover good physical properties and the formation of new granules during reactivation after storage were not affected by the presence of AgNP. In fact, not only did AgNP not hinder the aggregation ability of the sludge, but they also possibly promoted granulation and contributed for a preservation of the granular structure over long operational periods, namely when subjected to a dye shock load. In fact, AgNP-fed SBR sustained a granule-rich sludge, with better settleability and higher biomass concentration levels for longer operational periods, both during and after AgNP supplementation, before and after the idle period. This suggested that the formation of AGS in the presence of AgNP and the cumulative adsorption of AgNP onto AG (preferentially associated with external EPS) may have increased their density by stimulating EPS production and promoted the long-term stability of AGS. The higher the AgNP concentration applied, the sooner the AGS became saturated with AgNP (accounting for approximately 4% of the TSS after 10 days of operation with cyclic addition of 20 mg AgNP $L^{-1}$) and the longer the AgNP clean-up period (approximately 20 days).

Regarding the treatment performance, the presence of AgNP did not significantly affect the overall COD removal yield, stable values within the 75-85% range being reached after 2 weeks of operation and maintained along the two experimental runs in both SBRs. Furthermore, although the COD removal was not affected by the 18-day idle period in the experimental run II, the longer biomass storage period and higher storage temperature (40-day idle period, at room temperature) in the experimental run I led to a 10-day recovery period being needed to reach again 80% of total COD removal, 60% of which being removed under anaerobic conditions, irrespective of the AgNP presence. Similarly, the azo dye biodecolorization capacity of AGS was not affected by AgNP. Maximal color removal performance (80%) was reached within one week after inoculation in both SBRs and restored 7-10 days or 1 day after the idle periods in the experimental runs I and II, respectively. Furthermore, while only the AgNP-free SBR effectively converted one of the aromatic amines (4A1NS) deriving from the azo dye reduction process during a short period of time in the experimental run I, the AgNP-fed SBR sustained 4A1NS transformation for longer periods of time during the experimental run II, namely throughout the azo dye shock load period and beyond. Despite the observed toxic effect of AgNP on protozoa (marked decrease in their abundance in the AgNP-fed SBR), the lack of a negative impact in SBR treatment performance highlights the protecting effect of the AG structure to bacteria potentially susceptible to the AgNP-associated antimicrobial action. Nevertheless, exposure to AgNP induced specific changes in the SBR microbial community at least after 1 month of operation, supporting the functional redundancy of bacteria. As opposed to the control, *Actinobacteria* class, *Salana*, *Microbacterium* and *Micropruina* genera prevailed in the AgNP-fed SBR after 52 days of operation, the relative amount of *Bacteroidetes* and *Saccharibacteria* phyla being comparable in both SBRs. In general, the bacterial communities were mainly composed of *Proteobacteria* (mostly corresponding to *Alphaproteobacteria* class), *Bacteroidetes* (mostly, from the *Sphingobacteriia* class), *Actinobacteria* and *Saccharibacteria* in both SBRs.

After interrupting AgNP feeding, the effect of nitrate in the reactor performance was studied. Addition of calcium nitrate in SBR1 induced an increase in VSS, namely through the enlargement of AG and development of new granules with good settling characteristics, as well as a higher anaerobic COD removal yield. Denitrification, which likely contributed for the precipitation of calcium inside AG, occurred simultaneously with azo dye anaerobic reduction, not significantly affecting the color removal performance.

# VIII. Biodegradation products of a sulfonated azo dye in AGS SBRs treating a simulated TWW

The information included in this chapter was partially published in:

Franca, R.D.G., Oliveira, M.C., Pinheiro, H.M., Lourenço, N.D., 2019. Biodegradation products of a sulfonated azo dye in aerobic granular sludge sequencing batch reactors treating a simulated textile wastewater. *ACS Sustainable Chemistry & Engineering* 7, 17, 14697-14706. DOI: 10.1021/acssuschemeng.9b02635.

Franca, R.D.G., Oliveira, M.C., Pinheiro, H.M., Lourenço, N.D., 2018. Biodegradation of a sulfonated azo dye in anaerobic-aerobic bioreactors treating a simulated textile wastewater investigated by liquid chromatography-tandem mass spectrometry. *ChemPor 2018, 13th International Chemical and Biological Engineering Conference*, 2-4 October, Aveiro, Portugal.

## VIII.1. Abstract

This study focused on the biodegradation of an azo dye (AR14) in two anaerobic-aerobic SBRs treating a synthetic TWW, operated with AGS under different hydrodynamic regimens. The aim was to investigate the fate of the anaerobic AR14 breakdown products (aromatic amines) during the SBRs' aerobic reaction phase. Specifically, liquid chromatography coupled with electrospray ionization tandem mass spectrometry (LC-ESI-MS/MS) was used for structural characterization of AR14 biodegradation metabolites, their molecular formulae being confirmed by accurate mass measurements. Nineteen molecules potentially related to AR14 were detected in the SBRs and their relative abundances were followed along the aerobic stage of treatment cycles. The two SBRs shared most of the identified compounds, but with differences in their metabolite profiles. Biodecolorization through AR14 anaerobic azo bond reduction was confirmed by the identification of the aromatic amine 4A1NS, which was further aerobically biodegraded, involving deamination and hydroxylation of the aromatic ring. The other aromatic amine (1N2A4S) was not detected, being suggested to undergo autoxidation reactions forming dimeric, stable products. A different AR14 biodegradation pathway was observed when nitrate was added to the feed, a new intermediate product being detected (naphthalene-1-sulfonate).

## VIII.2. Introduction

### VIII.2.1. Context and aim of this work

Textile industry wastewater represents one of the main sources of pollution worldwide, carrying high organic loads and recalcitrant dyes, with azo dyes as the main type used (representing 60-70% of all the dye groups; Ghaly *et al*., 2014; O'Neill *et al*., 1999). Acid dyes (including azo, triarylmethane and anthraquinone dyes), used to color protein fibers (wool, silk, angora, mohair, cashmere), nylon and certain modified synthetic fibers, are one of the largest classes of anionic dyes (Khan *et al*., 2016). In 1990, acid dyes were the type of dyes most commonly used, with more than 2000 entries in the color index (O'Neill *et al*., 1999), the global import and export market for acid dyes being more recently estimated as 680,000 tons (Ghaly *et al*., 2014). Together with reactive dyes, acid dyes are considered the most problematic anionic dyes for being recalcitrant to conventional treatment systems (Carmen *et al*., 2010). This represents a critical environmental concern, owing to the high degree of acid dyes' loss to the TWW after dyeing of typical fibers (namely, 5-20% when applied to polyamide; O'Neill *et al*., 1999). The need for efficient and environmentally friendly dye removal processes led to the study of biological wastewater treatment systems. Generally, these involve mixed bacterial cultures and include an anaerobic treatment stage for the reductive cleavage of the dye's azo bond, followed by an aerobic stage for degradation of potentially toxic, colorless aromatic amine products (Pinheiro *et al*., 2004). The use of flocculent activated sludge in anaerobic-aerobic SBR systems has been studied in recent years (van der Zee and Villaverde, 2005), with notable success in the anaerobic decolorization

stage. Yet, the scarce information on the fate of the breakdown aromatic amines during the aerobic stage revealed that most are not degraded, thus constituting a health hazard (Pinheiro e*t al*., 2004; van der Zee and Villaverde, 2005).

Sulfonated aromatic amines are resistant to biodegradation due to the hydrophilic nature of the sulfonate group (Tan *et al*., 2005). Biodegradation has mostly been demonstrated for relatively simple sulfonated amino-benzene/naphthalene compounds (van der Zee and Villaverde, 2005). This limitation has generally been attributed to the lack of an adequate aerobic microbial population capable of metabolizing such compounds. Yet, the operation of SBRs using the innovative AGS technology (de Kreuk and van Loosdrecht, 2004) was recently shown to be advantageous for azo dye degradation, as compared to CAS (Lourenço *et al*., 2015). The excellent biomass retention capacity of AGS systems can favor the establishment of a more diverse microbial population, namely slow-growing bacteria, with the potential ability to biodegrade recalcitrant aromatic amines, such as 4A1NS resulting from AR14 bioreduction (Lourenço *et al*., 2015). Accordingly, 4A1NS biodegradation was also accomplished in biofilm reactors, which allow high biomass retention (Koupaie *et al*., 2013). Moreover, the use of a plug-flow feeding regimen in AGS SBR systems was shown to play an important role in the selection of slow-growing bacteria (de Kreuk and van Loosdrecht, 2004; Pronk *et al*., 2015a).

The aim of this study was to further compare two anaerobic-aerobic AGS SBRs using different feeding regimens (static feed, anaerobic-aerobic reaction *vs* anaerobic plug-flow feed, anaerobic-aerobic reaction) regarding azo dye degradation performance, focusing on the aerobic conversion of sulfonated aromatic amines resulting from azo bond anaerobic reduction. The SBRs were fed with a synthetic TWW containing the azo dye AR14 with changes in the feed solution along the experimental run, including an azo dye shock load and nitrate supplementation (corresponds to the experimental run II described in section VI.3.2). Based on preliminary HPLC analysis, cycles representative of different 4A1NS profiles were further analyzed by LC-ESI-MS/MS for the structural characterization of AR14 reduction metabolites and subsequent degradation products produced in the SBRs under different operational conditions. This allowed the study of the fate of AR14 breakdown products regarding the effect of the hydrodynamic regimen and also that of increasing the azo dye concentration and of the nitrate feed.

### VIII.2.2. Liquid chromatography-mass spectrometry (LC-MS) application to TWW samples

This section presents a brief review of the literature regarding mass spectrometry (MS) application to TWW sample analysis, which served as a basis to select the analytical method and sample pre-treatment procedures most suited to the objective of this work.

Azo dye degradation is one of the main parameters investigated during TWW treatment. During the process of dye degradation, potentially toxic aromatic amines are formed and require identification by using a proper analytical technique. Methods for the analysis of aromatic sulfonates in aqueous media, namely amino- and hydroxy-substituted benzene and naphthalene sulfonates, have been reviewed (Reemtsma, 1996). This review focused on extraction of these compounds from water (solid-phase extraction, SPE), clean-up from co-extracted substances, chromatographic separation (HPLC; capillary electrophoresis, CE; gas chromatography, GC) and detection methods (GC-MS or LC-MS), and concluded that further method development was required to allow the analysis of polar sulfonates in difficult matrices such as industrial wastewater. Since then, many efforts have been done towards the development of accurate, reproducible and low detection limit methods for the detection and quantification of aromatic amines.

The increased method sophistication and sensitivity attained in the analysis of aromatic amines arising from the reduction of azo dyes was highlighted in a subsequent review (Pinheiro *et al*., 2004). In this context, several reports on applications of GC-MS and LC-MS to aromatic amine analysis have been published (Pinheiro *et al*., 2004). Yet, separation of aromatic amines in water samples has been most commonly performed by HPLC, avoiding the need for pre-derivatization and the problem of thermal degradation of these polar compounds in GC protocols. Moreover, reversed-phase HPLC has been developed with optimization of the mobile phase composition and gradient.

A review on LC-MS using atmospheric pressure ionization to detect polar pollutants in water (Reemtsma, 2003) indicated that sulfonated azo dyes were among the first compounds used to demonstrate the benefits of LC-ESI-MS (Reemtsma, 2003). Accordingly, the same technique has received preference in separation, monitoring and identification of azo dye degradation products and by-products, namely sulfonated aromatic amines, with lower molecular mass and a more polar character than the parent compounds (Hisaindee *et al*., 2013). Furthermore, the detection of strongly acidic sulfonates is generally performed by ESI-MS in the negative mode (Reemtsma, 2003).

The identification of sulfonated metabolic degradation products arising from degradation of a textile dye (Remazol Brilliant Blue R) by a fungal strain was successfully achieved through application of an HPLC-ESI-MS/MS method, operated in the negative mode (Perlatti *et al*., 2012). In addition, reversed phase HPLC was used with a mobile phase composed of a mixture of water and acetonitrile, and MS analysis was carried out in a triple-quadrupole mass spectrometer (Perlatti *et al*., 2012). Similarly, another study using LC-ESI-MS/MS identified several aromatic intermediates and metabolites resulting from biodegradation of an azo dye (Amaranth) by a bacterial consortium (Chan *et al*., 2012). In this case, MS analyses were carried out using an ESI source and a triple-quadrupole-linear ion trap of tandem mass spectrometer. The LC system was equipped with a C18 reversed phase column and a

mobile phase of binary solvent system consisting of 0.1% formic acid and acetonitrile (Chan *et al*., 2012).

A recent study used an LC-MS/MS method for the determination of 21 molecules of carcinogenic aromatic amines released from azo dyes in food wrappers (Yang *et al*., 2016). A C18 column was used together with a mobile phase that consisted of 0.1% acetic acid and methanol. The mass spectrometer was a triple-quadrupole and the ESI-MS interface was operated in positive mode. The fact that the negative mode was not employed is explained by the absence of acidic sulfonate groups in the analyzed aromatic amines. Therefore, the positive mode was preferred owing to the presence of amino groups in the investigated compounds (Yang *et al*., 2016).

Overall, it is consensual that valuable information regarding the formation of intermediates and degradation products resulting from azo dye degradation processes can be obtained by using LC-MS as an analytical technique, ESI being most commonly reported in of the published studies (Table VIII.1). To achieve higher levels of separation and lower detection limits for azo dye metabolites in complex matrices such as wastewater, several sample pre-treatment methods have been proposed, aiming both at removing interfering substances (sample clean-up) and pre-concentration (Pinheiro *et al*., 2004). These pre-treatments include basic liquid-liquid extraction (LLE) and SPE, although some studies do not report any specific pre-treatment (Table VIII.1).

In the particular case of amines arising from the reductive cleavage of azo dyes, several standard methods have been established in Europe for the detection of the 22 amines restricted by European regulations (Pinheiro *et al*., 2004). These methods usually involve LLE with methyl tert-butyl ether, MTBE (Nadigera, 2001; Sutthivaiyakit *et al*., 2005; Yang *et al*., 2016; Zhu *et al*., 2002). In other studies ethyl acetate has been indicated as suitable for aromatic amine extraction (Sánchez *et al*., 2014; Yazdi and Es'haghi, 2005). In general, organic solvents with higher polarity are more adequate for aromatic amine extraction (Zhu *et al*., 2002). Furthermore, different parameters can be optimized in LLE, such as the volume ratio between the aqueous and organic phases and *salting-out* effects (Sánchez *et al*., 2014), as well as the number of successive extractions and the mixing of the two phases (Yang *et al*., 2016).

Alternatively to LLE, SPE has also been used for aromatic amine extraction. Studies comparing the extraction performance using different cartridges indicate Oasis HLB cartridges as one of the best options (Li *et al*., 2010b). In fact, a recent review about the analysis of sulfonamides and their by-products in environmental samples using MS techniques, highlighted Oasis HLB cartridges as being the most used for this type of application (Hoff *et al*., 2016).

**Table VIII.1** - Summary of a literature review of studies employing high-performance liquid chromatography coupled with electrospray ionization mass spectrometry (HPLC-ESI-MS) to analyze textile dye degradation metabolites, focused on the sample preparation method. The major components of the medium used, and the main steps of the sample preparation protocol are indicated. LLE: liquid-liquid extraction; SPE: solid-phase extraction; YE: yeast extract. *Exception: this study aimed to extract and concentrate aromatic amines in water samples only for HPLC analysis (not for HPLC-MS).

| Study | Medium composition | Sample preparation | Method |
|---|---|---|---|
| Forss *et al*., 2011 | Dyes, YE. | Filtered (0.45 µm). | none |
| Franciscon *et al*., 2012 | Dye, mineral salts medium, glucose, sodium pyruvate and/or YE. | Centrifuged and filtered (0.25 µm). | none |
| Pereira *et al*., 2011 | Aromatic amines, $NH_4Cl$, $KH_2PO_4$, $CaCO_3$, $MgSO_4$, $FeCl_2$, $H_3BO_3$, $ZnCl_2$, $CuCl_2$. | Filtered (0.20 µm). | none |
| Wang *et al*., 2008b | Dye, sodium lactate, $NH_4Cl$, $NaHCO_3$, $K_2HPO_4$, NaCl, $MgSO_4$, $FeSO_4$, YE. | Filtered (0.45 µm). | none |
| Yu *et al*., 2015 | Dye, glucose, $NaHCO_3$, $NH_4Cl$, $CaCl_2$, K2HPO4, $MgSO_4$, YE. | Centrifuged and filtered (0.45 µm). | none |
| Cui *et al*., 2014 | Dye, sodium acetate, potassium phosphate, KCl, $NH_4Cl$. | Filtered (0.22 µm). | none |
| Wang *et al*., 2011 | Dye, sodium lactate, $NH_4Cl$, $K_2HPO_4$, NaCl, $MgSO_4$, $FeSO_4$, $NaHCO_3$, YE. | Filtered (0.45 µm). | none |
| Forss *et al*., 2013 | Dyes, YE. | Filtered (0.45 µm). | none |
| Prased *et al*., 2013 | Dye, LB broth medium. | 1) Centrifuged and filtered (0.45 µm);<br>2) metabolites extracted from the supernatant using equal volume of ethyl acetate;<br>3) extracts evaporated to dryness in a rotary evaporator and dissolved in methanol. | LLE |
| Chan *et al*., 2012 | Dye, glucose, nutrient broth, $K_2HPO_4$, $KH_2PO_4$, $NH_4Cl$. | 1) Centrifuged;<br>2) extracted with an equal volume of ethyl acetate in a separating funnel;<br>3) top layer concentrated in a rotary evaporator;<br>4) filtered (0.2 µm). | LLE |
| Zhang *et al*., 2012 | Dyes, phosphate buffer, chloroperoxidase, $H_2O_2$. | 1) Centrifuged;<br>2) extracted 3 times with ethyl acetate and organic extracts were combined;<br>3) recovered by rotary evaporation of the solvent and re-dissolved in methanol. | LLE |
| Franciscon *et al*., 2015 | Dye, mineral salts medium, glucose, potassium phosphate buffer. | 1) Centrifuged;<br>2) extracted using solid-phase cartridges (Strata X): conditioning with methanol, equilibration with water, sample loading, elution with 50:50 methanol:water containing 0.1% (v/v) formic acid. | SPE |
| Li *et al*., 2010b * | Real influent and effluent from WWTP containing aromatic amines. | 1) Double filtered (2.5 µm and 0.45 µm).<br>2) pH adjusted to 7.0 with NaOH or HCl;<br>3) extracted using solid-phase cartridges (Oasis HLB or Cleanert PEP): conditioning with methanol, equilibration with distilled water, sample loading, washing with 2% methanol, elution with methanol;<br>4) extracts evaporated to dryness under nitrogen and reconstituted in a HPLC mobile phase. | SPE |

## VIII.3. Materials and methods

### VIII.3.1. SBR setup and operation

AGS, previously used in SBRs and subsequently stored at 4ºC for 18 days, was reactivated by inoculating two 1.5-L SBRs (H/D=2.5). The SBRs were operated for 205 days using different feeding regimens: statically fed (from top), anaerobic-aerobic SBR1 *vs* anaerobic plug-flow fed (from bottom), anaerobic-aerobic SBR2 (as described in section VI.3.2 regarding the experimental run II). They were operated in 6-h cycles: 30-min or 1-h feeding, followed by a 1.5-h or 1-h stirred anaerobic phase in SBR1 or SBR2, respectively, 3.5-h aeration, 5-min settling, 1-min drain and idle. A synthetic TWW containing a hydrolyzed starch-based sizing agent (Emsize E1), nutrients, pH buffering phosphates and 40 mg $L^{-1}$ AR14 (Chromotrope FB, Sigma-Aldrich, 50% dye content), was supplied to the SBRs at a 12-h HRT and an OLR, as COD, of 2.0 kg $O_2$ $m^{-3}$ $d^{-1}$. Along the experimental run (corresponds to the experimental run II described in section VI.3.2), changes were introduced in the feed composition of both SBRs: supplementation with 20 mg $L^{-1}$ of AgNP (days 0-35); dye-shock load, with a three-fold increase in AR14 concentration to 120 mg $L^{-1}$ (days 119-134); or supplementation with calcium nitrate to 60 and 120 mg $NO_3^-$ $L^{-1}$ (days 147-153 and 154-205, respectively).

### VIII.3.2. Sample selection

Samples were taken from the SBRs mixed liquor along selected treatment cycles, centrifuged and the supernatant was stored at -20ºC for subsequent examination. HPLC analysis (as described in section III.3.3.1) was performed to assess the concentration-time profile of AR14 and of one of its reduction products (4A1NS). Based on this preliminary analysis (described in detail in section VI.4.2.3.2, and schematically represented in Figure VI.19), three specific treatment cycles (I, II and III) representative of different experimental periods and correspondent 4A1NS aerobic profiles (Figure VIII.1) were selected for further examination by MS. Specifically, cycle I on day 98 of AGS reactivation (corresponding to day 308 and period II.E in section VI.3.2) represents an operational period when the SBRs were under the base operational conditions and 4A1NS was consistently converted in both reactors (Figure VIII.1-I), although with different metabolite profiles being registered between the two reactors (Figure VI.S6, in Appendix D); cycle II on day 134 of AGS reactivation (corresponding to day 344 and period II.F in section VI.3.2) represents the dye shock load period, when SBR1 consistently presented incomplete 4A1NS conversion, while SBR2 sustained complete 4A1NS conversion (Figure VIII.1-II); cycle III on day 154 of AGS reactivation (corresponding to day 364 and period II.I in section VI.3.2) represents the period when the SBRs were supplemented with nitrate and 4A1NS formation was not observed (Figure VIII.1-III). For each selected cycle and SBR, samples taken at the end of the anaerobic and aerobic phases (samples A and B, respectively) were analyzed by MS, in addition to a sample taken after 1 h of aeration (sample AB) in the case of cycle II (Figure

VIII.1). Corresponding A and B samples from a dye-free control SBR (corresponding to the SBR1 described in section III.3.2) were also analyzed for comparison.

| **Cycle** | **I** | **II** | **III** |
|---|---|---|---|
| Feed composition | Regular conditions | Dye shock load | Nitrate supplementation |
| Dye (mg AR14 $L^{-1}$) | 40 | 120 | 40 |
| Nitrate (mg $NO_3$ $L^{-1}$) | 0 | 0 | 120 |

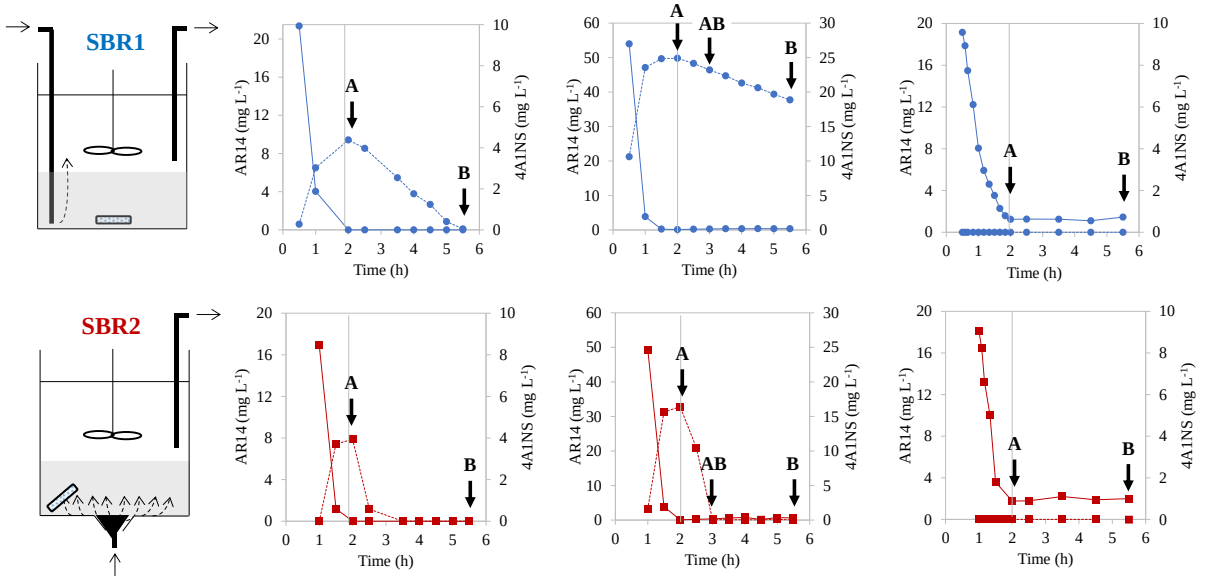


**Figure VIII.1** - Concentration-time profiles of the azo dye Acid Red 14 (AR14; full line) and of its cleavage product 4-amino-naphthalene-1-sulfonic acid (4A1NS; dashed line) obtained through HPLC analysis of samples harvested along the selected treatment cycles I (day 98), II (day 134) and III (day 154) from the sequencing batch reactors SBR1 (●) and SBR2 (■). Cycle I corresponds to the base operational conditions in feed composition (40 mg AR14 $L^{-1}$), cycle II represents the dye shock load period (120 mg AR14 $L^{-1}$), and cycle III represents the period of nitrate supplementation (120 mg $NO_3^-$ $L^{-1}$). The selected cycles cover the different 4A1NS aerobic fates observed: complete conversion (cycle I of both SBRs and cycle II of SBR2), partial conversion (cycle II of SBR1) and not formed (cycle III of both SBRs). The vertical lines in the charts represent the end of the anaerobic phase, aeration onset. The arrows in the charts indicate the sampling times of the samples that were further analyzed by mass spectrometry: A, AB and B correspond to the end of the anaerobic phase, 1 h of aeration and end of the aerobic phase, respectively.

## VIII.3.3. Sample pre-treatment

To achieve higher levels of separation and lower detection limits in LC-MS targeting azo dye metabolites in complex matrices such as wastewater, several sample pre-treatment methods have been proposed (reviewed in section VIII.2.2). The detailed procedure and optimization of the sample pre-treatment, including several LLE and SPE tests, are provided in section F.VIII.1, in Appendix F. LLE, which was based on the method described by Chan *et al.* (2012), was discarded because no satisfactory results were obtained, as opposed to SPE. After optimization, sample clean-up was performed by SPE, using the generic Oasis HLB (Waters) method without the wash step. Briefly, the SPE cartridge was initially conditioned with 1 mL methanol followed by 1 mL of MilliQ water. Subsequently, 1 mL of the sample solution was loaded onto the cartridge at room temperature, followed by elution with 1 mL of methanol, the eluted fraction being collected for further analysis.

### VIII.3.4. Liquid chromatography-sequential mass spectrometry (LC-$MS^2$)

LC-MS analyses were conducted on a Dionex Ultimate 3000 HPLC system coupled inline to an LCQ Fleet ion trap mass spectrometer equipped with an ESI source (Thermo Scientific). Chromatographic separation was performed on a C18 reversed-phase Cortecs column (150 mm x 2.1 mm, 2.7 μm particle size; Waters) at a constant temperature of 30ºC, using a gradient elution of 0.1% formic acid in water (mobile phase A) and acetonitrile (mobile phase B) at a flow rate of 250 μL $min^{-1}$. After optimization (as described in section F.VIII.2, in Appendix F), the gradient conditions were as follows: 0-18 min, linear gradient from 0 to 50% B; 18-20 min, linear gradient to 90% B; 20-23 min, isocratic 90% B; 23-24 min, linear gradient to 0% B; 11 min re-equilibration, isocratic 0% B). The mass spectrometer was operated in the ESI positive and negative modes, with the following optimized parameters: ion spray voltage, ±4.5 kV; capillary voltage, 16/-18 V; tube lens offset, -70/58 V, sheath gas ($N_2$), 80 arbitrary units; auxiliary gas ($N_2$), 10 arbitrary units; capillary temperature, 270ºC. Spectra typically corresponded to the average of 20-35 scans, and were recorded in the 100-1000 Da range. Sequential mass spectra ($MS^n$, n=2) were obtained with an isolation window of 1 or 2 mass-to-charge ratio (*m/z*) units; 25-27% relative collision energy; and with an excitation time of 30 ms. Data acquisition and processing were performed using the Xcalibur 2.2 software.

### VIII.3.5. Liquid chromatography-tandem high resolution mass spectrometry (LC-HRMS/MS)

Samples were analyzed by liquid chromatography (UHPLC Elute) interfaced with a QqTOF Impact II mass spectrometer equipped with an ESI source (Bruker Daltonics). Chromatographic separation was carried out on a C18 reversed-phase Cortecs column (150 mm x 2.1 mm, 2.7 μm particle size; Waters). The mobile phase and elution conditions were equivalent to those described for LC-$MS^2$ analysis, but with a flow rate of 200 μL $min^{-1}$. The column and the autosampler were maintained at 40ºC and 8ºC, respectively. The high resolution mass spectra were acquired in both ESI positive and negative modes. The optimized parameters were set as follows: ion spray voltage, +4.5/-2.5 kV; end plate offset, 500 V, nebulizer gas ($N_2$), 2.8 bars; dry gas ($N_2$), 8 L $min^{-1}$; dry heater, 200ºC. Internal calibration was performed on the high-precision calibration mode (HPC) with a solution of sodium formate 10 mM introduced to the ion source via a 20 μL loop at the beginning of each analysis using a six-port valve. Acquisition was performed in full scan mode in the *m/z* 50-800 range, and in a data-depending MS/MS mode, with an acquisition of 3 Hz using a fixed cycle time of 3 s, and a dynamic exclusion duration of 0.4 min. A list of precursors was also included and an *m/z*-dependent isolation window of 0.03 Da was used. The acquired data were processed by DataAnalysis 4.1 software (Bruker Daltoniks). Data acquisition and processing were performed using the Data Analysis 4.2 software.

## VIII.4. Results and discussion

### VIII.4.1. LC-MS analysis

Each SBR1 and SBR2 sample was analyzed by LC-MS in parallel with the correspondent time sample from the dye-free control SBR in order to select the most significant ions that were present in SBR1 or SBR2 samples but absent in the dye-free SBR. The aim was to select uniquely the metabolites deriving from the azo dye AR14, as opposed to other molecules resulting from the carbon source metabolism. In addition, an AR14 solution was also analyzed by LC-MS in order to identify the impurities present in the AR14 commercial product (as described in section F.VIII.3, in Appendix F). Analysis of the samples together with the controls resulted in the selection of 19 ions (Table VIII.2) possibly related to degradation products from AR14.

Most of the selected ions were shared by different samples and SBRs. In addition, some metabolites typically observed in cycles I and II were absent in cycle III (deprotonated molecules *m/z* 189, 222, 391, 393 and 394), and *vice versa* (deprotonated molecules *m/z* 228, 268, 379, 457, 592), suggesting that a change in the azo dye metabolism occurred upon nitrate supplementation of the SBRs. The deprotonated molecules *m/z* 222 and 457 (as well as 228, $[M-2H]^{2-}$) detected in the ESI negative mode correspond to the deprotonated aromatic amine 4A1NS and AR14, respectively, as confirmed by analysis of the respective standards. The other aromatic amine resulting from AR14 azo bond reduction, 1N2A4S, was not detected through LC-MS (expected *m/z* 238, as deprotonated molecule), as expected from its unstable character. The abundance of each selected ion (Table VIII.2) in the analyzed samples is graphically represented in Figure VIII.2 and Figure VIII.3. Assuming that no significant variations occurred during the analysis of all the samples in the low resolution MS (performed in a single run to minimize variations), the results presented in Figure VIII.2 and Figure VIII.3 can give an indication of the changes in each ion abundance. Despite the relevant information that can be extracted by analyzing each ion profile, it is important to note that relative abundance comparison between different ions is not appropriate owing to the fact that ESI favors ionization of the most polar compounds.

According to Figure VIII.2 and Figure VIII.3, the deprotonated molecules whose abundance was typically observed to decrease along the aerobic phase in both SBRs include *m/z* 207, 222, 377, 393 and 592. In contrast, deprotonated molecules corresponding to *m/z* 239, 252, 268, 379, 394 and 689 generally increased in abundance along the aerobic phase in both SBRs, representing good candidates for transformation products of the former ions. Specifically, taking into account their relatively symmetrical abundance variation along the aerobic phase (Figure VIII.2), a correlation might exist between the ions *m/z* 207 and 252. In contrast, none of the ions whose abundance increased in the aerobic phase could be directly correlated with the disappearance of *m/z* 222, supporting the hypothesis of complete mineralization of 4A1NS in cycle I in both SBRs and cycle II in SBR2.

**Table VIII.2** - Most significant ions detected in electrospray ionization (ESI) negative (metabolites 1-16) and positive (metabolites 17-19) modes in each sequencing batch reactor (SBR) sample from cycles I, II and III analyzed by LC-MS. RT: retention time; *m/z*: mass-to-charge ratio.

| | | | I | | | | II | | | | | | III | | | |
|---|---|---|---|---|---|---|---|---|---|---|---|---|---|---|---|---|
| | | | SBR1 | | SBR2 | | SBR1 | | | SBR2 | | | SBR1 | | SBR2 | |
| Metabolite | RT (min) | ***m/z*** | A | B | A | B | A | AB | B | A | AB | B | A | B | A | B |
| 1 | 15.9 | **189** | x | x | x | x | x | x | x | x | x | x | | | | |
| 2 | 10.0 | **207** | | | x | x | x | x | x | x | x | x | x | x | x | x |
| 3 | 3.7 | **222** | x | x | x | | x | x | x | x | | | | | | |
| 4 | 12.7 | **228** | | | | | | | | | | | x | x | x | x |
| 5 | 6.7 | **239** | x | x | x | x | x | x | x | x | x | x | x | x | x | x |
| 6 | 12.3 | **252** | | | | | | | | | x | x | x | x | x | x |
| 7 | 11.9 | **268** | | | | | | | | | | | x | x | x | x |
| 8 | 12.8 | **377** | x | x | x | x | x | x | x | x | x | x | x | x | x | x |
| 9 | 13.7 | **379** | | | | | | | | | x | | x | x | x | x |
| 10 | 15.6 | **391** | x | x | x | x | x | x | x | x | x | x | | | | |
| 11 | 10.1 | **393** | x | x | x | x | x | x | x | x | x | x | | | | |
| 12 | 10.7 | **394** | x | x | x | x | x | x | x | x | x | x | | | | |
| 13 | 17.3 | **419** | x | x | x | x | x | x | x | x | x | x | x | x | x | x |
| 14 | 12.7 | **457** | | | | | | | | | | | x | x | x | x |
| 15 | 14.7 | **592** | | | | | | | | | | | x | x | x | x |
| 16 | 19.5 | **689** | | | | x | | | | | x | x | x | x | x | x |
| 17 | 7.3 | **173** | x | x | x | x | x | x | x | x | x | x | x | x | x | x |
| 18 | 12.6 | **174** | x | x | x | x | x | x | x | x | x | x | x | x | x | x |
| 19 | 13.7 | **189** | x | x | x | x | x | x | x | x | x | x | x | x | | |

Although both SBRs shared most of the identified compounds in each experimental period, specific differences were observed in their metabolites' aerobic profiles. For instance, some deprotonated molecules presented opposite variation trends in the two SBRs (Figure VIII.2 and Figure VIII.3). Specifically, the abundance of ions with *m/z* 189, 391 and 419 increased along the aerobic phase in SBR1, while decreasing in SBR2. Regarding protonated molecules, while the abundance of the majority was maintained along the aerobic phase in SBR1, the number of ions with *m/z* 174 and 189 decreased in SBR2, as opposed to *m/z* 173 and 346, the abundance of which increased in the latter. Overall, a decrease in metabolite abundance along the aerobic phase was more often observed in SBR2 than in SBR1, indicating a potential advantage in using a plug-flow feeding regimen.

Comparing the abundance of the same ion between samples harvested in cycles I and II, it was possible to observe that the number of deprotonated molecules with *m/z* 189, 239 and 391 (as well as 4A1NS, *m/z* 222) significantly increased in both SBRs upon the three-fold increase in AR14 concentration (Figure VIII.2). This result further supports a possible direct (or indirect) relation of the respective compounds to AR14 or its reduction products, 4A1NS and 1N2A4S. Furthermore, a comparison between cycles III and I (same AR14 concentration in the SBRs feed), allowed the identification of compounds whose presence possibly resulted from the supplementation of the SBRs

with nitrate. Specifically, deprotonated molecules with *m/z* 207, 252, 268, 379 and 592 (besides AR14, *m/z* 228 and 457) were only significantly observed in samples from cycle III. In contrast, deprotonated molecules with *m/z* 189, 391, 393 and 394 (besides 4A1NS, *m/z* 222), as well as protonated molecules with *m/z* 189 were absent in cycle III (Figure VIII.2 and Figure VIII.3). Additionally, the ion abundance profiles obtained in the LC-MS analysis were compared with the corresponding HPLC peak area profiles as an attempt to establish a correlation between the metabolites detected in LC-MS and HPLC (as described in section F.VIII.4, in Appendix F).

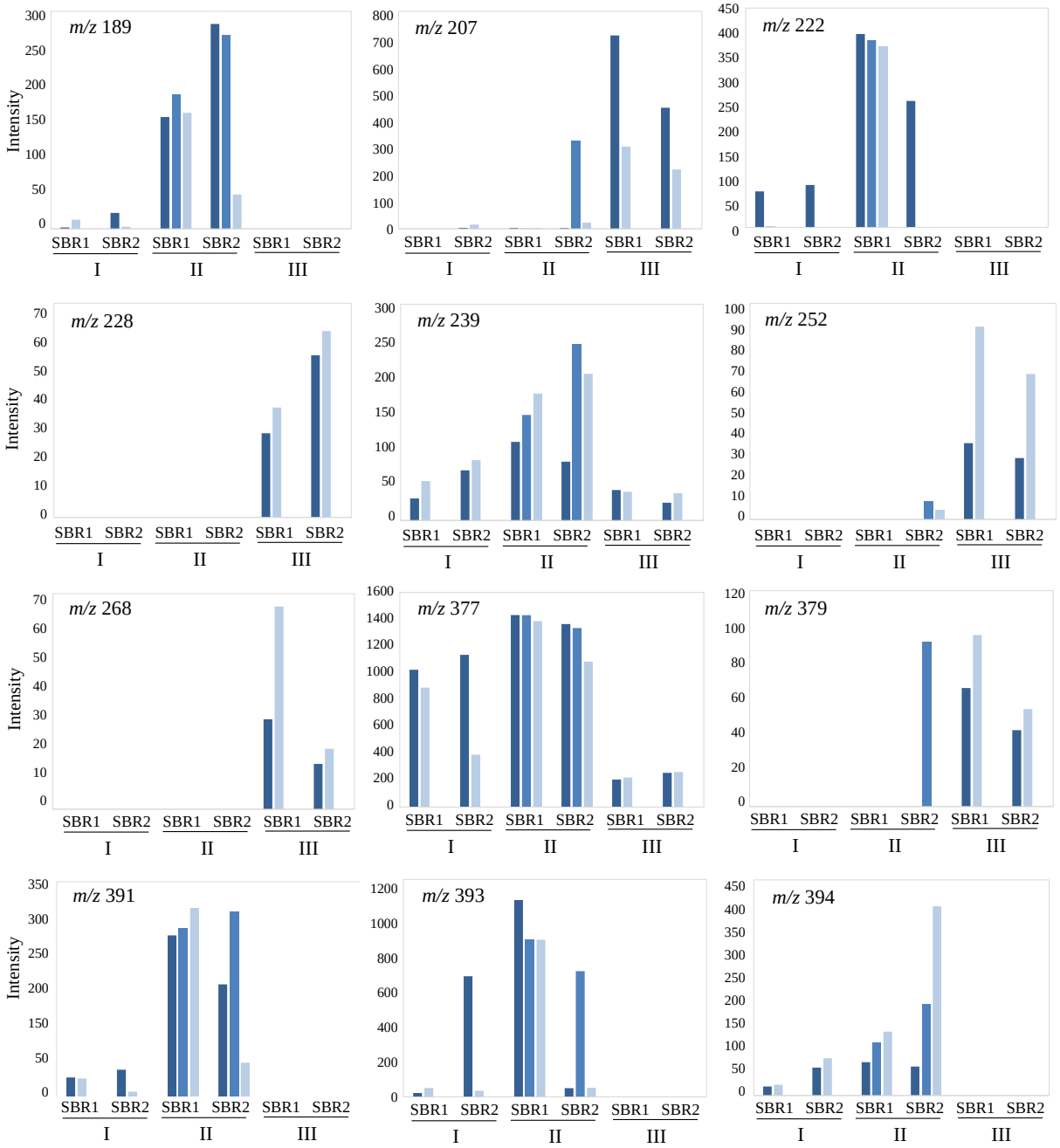


**Figure VIII.2** - Abundance (intensity) of ions *m/z* 174 to 394 (ESI negative mode) in samples harvested in cycles I, II and III from the sequencing batch reactors SBR1 and SBR2 at the end of the anaerobic phase (darkest blue bars; sample A), after 1 h of aeration (middle blue bars; sample AB; only analyzed in cycle II), and at the end of the aerobic phase (lightest blue bars; sample B).

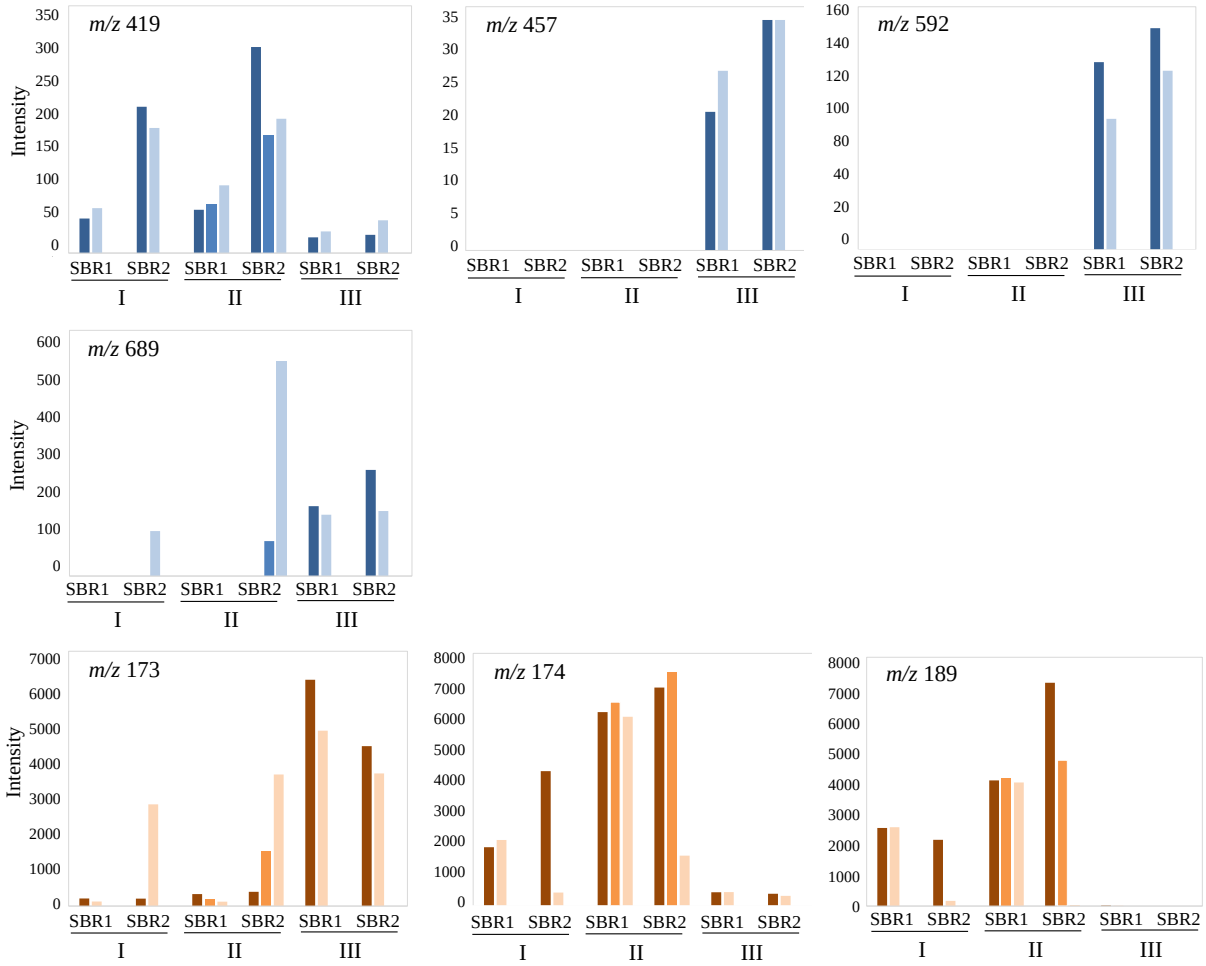


**Figure VIII.3** - Abundance (intensity) of ions in the ESI negative mode (blue charts; *m/z* 419 to 689) and ESI positive mode (orange charts; *m/z* 173 to 189) in samples harvested in cycles I, II and III from the sequencing batch reactors SBR1 and SBR2 at the end of the anaerobic phase (dark blue or orange bars; sample A), after 1 h of aeration (middle blue or orange bars; sample AB; only analyzed in cycle II), and at the end of the aerobic phase (light blue or orange bars; sample B).

## VIII.4.2. LC-HRMS/MS analysis

For each SBR1 and SBR2 sample, precursor ions were selected (Table VIII.2) and collision-induced dissociation was performed to obtain the respective product ions spectra. After analyzing all LC-MS$^2$ data, the fragmentation pattern found for each of the 19 selected ions was summarized in Table F.VIII.5, in Appendix F. In addition, LC-HRMS/MS was conducted in ESI negative and positive modes for some of the samples, covering the 19 precursor ions previously selected, the results being summarized in Table VIII.3. Tandem MS experiments performed on a QqTOF mass spectrometer allowed to propose fragmentation pathways for selected precursor ions with higher accuracy than in an ion trap, which was particularly relevant to distinguish ions with very similar *m/z* values, as well as to confirm some of the neutral losses through their accurate mass values (Table VIII.3).

**Table VIII.3** - LC-HRMS/MS results. Measured accurate mass of precursor ions, respective product ions (most relevant ones highlighted in bold) and neutral loss are indicated, along with attributable species. *Precursor ion absent in respective MS/MS spectra (total fragmentation); RT: retention time. $[M-H]^-$: deprotonated molecule; $[M+H]^+$; protonated molecule.

| Metabolite | MS | | | MS/MS | | |
|---|---|---|---|---|---|---|
| | ***m/z*** | **Precursor ion** | **RT (min)** | ***m/z*** | **Product ions** | **Neutral loss (u)** |
| 1 | 189.0585 * | $[M-H]^-$ | 12.3 | 173.0280 | $[(M-H)-CH_4]^-$ | 16.0305 |
| | | | | 145.0329 | $[(M-H)-CH_4-CO]^-$ | 44.0256 |
| 2 | 207.0143 | $[M-H]^-$ | 8.1 | **143.0529** | $[(M-H)-SO_2]^-$ | 63.9614 |
| | | | | 115.0606 | $[(M-H)-C_2H_4]^-$ | 91.9537 |
| 3 | 222.0280 | $[M-H]^-$ | 1.7 | **158.0644** | $[(M-H)-SO_2]^-$ | 63.9636 |
| | | | | 128.0555 | $[(M-H)-SO_2-CH_2O]^-$ | 93.9725 |
| 4 | 228.0112 | $[M-2H]^{2-}$ | 10.8 | 221.0203 | $[(M-H)-C_{10}H_6NO_4S^{\bullet}]^{\bullet-}$ | 236.0099 |
| | | | | **170.0291** | $[(M-H)-C_{10}H_7O_3S^{\bullet}-SO_3]^{\bullet-}$ | 287.0011 |
| 5 | 239.0072 | $[M-H]^-$ | 4.7 | **220.9974** | $[(M-H)-H_2O]^-$ | 18.0098 |
| | | | | **174.0352** | $[(M-H)-SO_2H^{\bullet}]^{-\bullet}$ | 64.9720 |
| | | | | 159.0468 | $[(M-H)-SO_3]^-$ | 79.9605 |
| | | | | **145.0323** | $[(M-H)-SO_2-CH_2O]^-$ | 93.9749 |
| | | | | **129.0378** | $[(M-H)-SO_3-CH_2O]^-$ | 109.9694 |
| 6 | 252.0030 | $[M-H]^-$ | 10.3 | 222.0039 | $[(M-H)-CH_2O]^-$ | 29.9991 |
| | | | | **206.0095** | $[(M-H)-CH_2O_2]^-$ | 45.9935 |
| | | | | **188.0397** | $[(M-H)-SO_2]^-$ | 63.9633 |
| 7 | 267.9923 | $[M-H]^-$ | 9.9 | **250.9898** | $[(M-H)-NH_3]^-$ | 17.0025 |
| | | | | **220.9915** | $[(M-H)-NH_3-CH_2O]^-$ | 47.0008 |
| | | | | 192.9973 | $[(M-H)-NH_3-CH_2O-CO]^-$ | 74.9950 |
| | | | | 188.0364 | $[(M-H)-SO_3]^-$ | 79.9559 |
| | | | | 170.0253 | $[(M-H)-SO_3-H_2O]^-$ | 97.967 |
| 8 | 377.0599 | $[M-H]^-$ | 10.9 | 361.0407 | $[(M-H)-CH_4]^-$ | 16.0192 |
| | | | | **313.0982** | $[(M-H)-SO_2]^-$ | 63.9617 |
| | | | | **297.1035** | $[(M-H)-SO_3]^-$ | 79.9564 |
| | | | | 281.0850 | $[(M-H)-SO_3-CH_4]^-$ | 95.9749 |
| | | | | 270.0927 | $[(M-H)-SO_3-CHN]^-$ | 106.9672 |
| 9 | 379.0362 | $[M-H]^-$ | 12.0 | 313.1053 | $[(M-H)-SO_2H_2]^-$ | 65.9309 |
| | | | | **299.0787** | $[(M-H)-SO_3]^-$ | 79.9575 |
| | | | | **271.0834** | $[(M-H)-SO_3-CO]^-$ | 107.9528 |
| 10 | 391.0483 | $[M-H]^-$ | 13.5 | 327.0847 | $[(M-H)-SO_2]^-$ | 63.9636 |
| | | | | 310.0823 | $[(M-H)-SO_3H^{\bullet}]^{-\bullet}$ | 80.9660 |
| | | | | 299.0894 | $[(M-H)-SO_2-CO]^-$ | 91.9589 |
| 11 | 393.0636 | $[M-H]^-$ | 10.0 | **329.0918** | $[(M-H)-SO_2]^-$ | 63.9633 |
| | | | | **313.0989** | $[(M-H)-SO_3]^-$ | 79.9562 |
| 12 | 394.0470 | $[M-H]^-$ | 8.9 | **314.0890** | $[(M-H)-SO_3]^-$ | 79.9580 |
| | | | | 296.0779 | $[(M-H)-SO_3-H_2O]^-$ | 97.9691 |
| | | | | **286.0939** | $[(M-H)-SO_3-CO]^-$ | 107.9531 |
| 13 | 419.0705 | $[M-H]^-$ | 15 | **377.0604** | $[(M-H)-C_2H_2O]^-$ | 42.0101 |
| | | | | **355.1088** | $[(M-H)-SO_2]^-$ | 63.9617 |
| | | | | **339.1143** | $[(M-H)-SO_3]^-$ | 79.9562 |
| | | | | **324.0905** | $[(M-H)-SO_2H^{\bullet}-CH_2O]^-$ | 94.9800 |
| | | | | **313.0986** | $[(M-H)-C_2H_2O-SO_2]^-$ | 105.9719 |
| | | | | 297.1029 | $[(M-H)-C_2H_2O-SO_3]^-$ | 121.9676 |
| 14 | 457.0251 | $[M-H]^-$ | 10.7 | **377.0649** | $[(M-H)-SO_3]^-$ | 79.9602 |
| | | | | **297.1066** | $[(M-H)-SO_3-SO_3]^-$ | 159.9185 |
| | | | | 236.0060 | $[(M-H)-C_{10}H_7NO_3S^{\bullet\bullet}]^{\bullet\bullet-}$ | 221.0191 |
| | | | | **221.0180** | $[(M-H)-C_{10}H_6NO_4S^{\bullet}]^{\bullet-}$ | 236.0071 |
| | | | | 170.0280 | $[(M-H)-SO_3-SO_3]^-$ | 286.9971 |
| 15 | 592.0349 | $[M-H]^-$ | 12.7 | **528.0725** | $[(M-H)-SO_2]^-$ | 63.9624 |
| | | | | **464.1096** | $[(M-H)-SO_2-SO_2]^-$ | 127.9253 |
| 16 | 689.1617 | $[M-H]^-$ | 15.8 | 672.1355 | $[(M-H)-NH_3]^-$ | 17.0262 |
| | | | | 609.2059 | $[(M-H)-SO_3]^-$ | 79.9558 |
| 17 | 173.0739 | $[M+H]^+$ | 5 | **146.0621** | $[(M+H)-CHN]^+$ | 27.0118 |
| | | | | **128.0547** | $[(M+H)-CHN-H_2O]^+$ | 45.0192 |
| 18 | 174.0571 | $[M+H]^+$ | 11.1 | **146.0629** | $[(M+H)-CO]^+$ | 27.9942 |
| | | | | **129.0457** | $[(M+H)-CHN-H_2O]^+$ | 45.0114 |
| 19 | 189.0572 | $[M+H]^+$ | 12.3 | **161.0619** | $[(M+H)-CO]^+$ | 27.9953 |
| | | | | **146.0391** | $[(M+H)-CO-CH_3^{\bullet}]^{+\bullet}$ | 43.0181 |
| | | | | 143.0521 | $[(M+H)-CO-H_2O]^+$ | 46.0051 |

Fragmentation patterns characteristic of compounds containing the sulfonate group were repeatedly observed in the ESI negative mode, as neutral losses of 64 u and 80 u typically correspond to the loss of $SO_2$ and $SO_3$, respectively (Table VIII.3). This specific fragmentation pattern further indicates that most of the selected ions originated from the azo dye AR14, since this was the only compound in the SBR feed that contained sulfonate groups. In addition, other fragments possibly involved the loss of $NH_3$ (17 u), $CH_4$ (16 u), CHN (27 u), and CO (28 u), among others (Table VIII.3).

Based on the RT, *m/z* and fragmentation pattern of each precursor ion (Table VIII.3), it was possible to suggest some correlations between the metabolites. Specifically, metabolites 6 (*m/z* 252) and 7 (*m/z* 268) probably correspond to a similar molecule, metabolite 7 containing one extra oxygen atom. Owing to the similarities between their fragmentation patterns, metabolite 8 (*m/z* 377) probably corresponds to the AR14 molecule (metabolite 14, *m/z* 457) without one sulfonic acid group. In addition, metabolite 13 (*m/z* 419) is possibly an adduct of metabolite 8 (*m/z* 377) with $C_2H_2O$. Also, metabolites 8 (*m/z* 377) and 9 (*m/z* 379) likely have a similar structure, with the difference of the latter containing two extra protons. The same can be hypothesized for metabolites 10 (*m/z* 391) and 11 (*m/z* 393). Furthermore, metabolite 12 (*m/z* 394) possibly corresponds to metabolite 11 (*m/z* 393) but containing a nitrogen atom instead of an oxygen atom. The same can be inferred regarding metabolites 17 (*m/z* 173) and 18 (*m/z* 174). Based on the fragmentation patterns detailed in Table VIII.3 and on these assumptions, the tentative attribution of some of the ions previously selected as relevant in the AR14-fed SBRs was performed, the proposed chemical structures being summarized in Figure VIII.4 (see sections F.VIII.6 and F.VIII.7, in Appendix F, for the respective fragmentation pattern, MS and MS/MS spectra). Although it is not possible to precisely determine the molecular structure of the metabolites with the available information, Figure VIII.4 gives an indication of the general structure. Confirmation of the proposed structures would require further study, namely comparison with commercial standards, when available (confirmed for metabolites 3, 4 and 14), nuclear magnetic resonance (NMR) and further MS/MS analysis.

The molecular formula of each proposed chemical structure (Figure VIII.4) was assessed on accurate mass measurements of the corresponding precursor taking into account the accuracy and precision of the measurement parameters, such as error (ppm) and mSigma (Table VIII.4). The molecular formulas were validated through the fragmentation patterns, supporting the respective proposed chemical structure (Figure VIII.4). Although future work is needed to confirm their chemical structure, correlations between the identified metabolites are suggested (Figure VIII.5), in light of the predicted degradation pathway for AR14 (Figure VIII.S44, in Appendix F) and the associations previously established based on the LC-MS analysis.

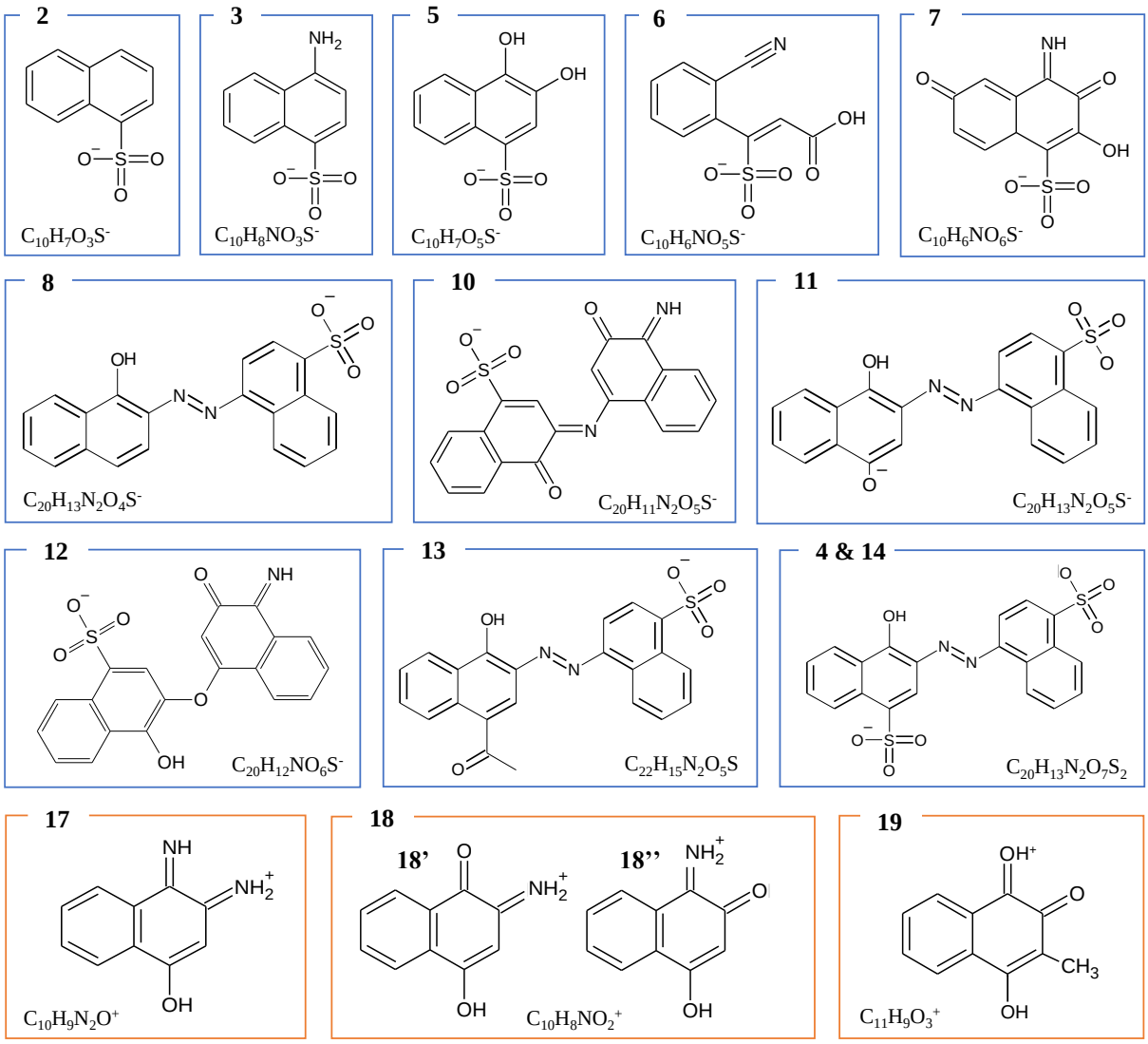


**Figure VIII.4 -** Summary of some of the plausible molecular formulas and chemical structures proposed for metabolites detected in the electrospray ionization (ESI) negative and positive modes (blue and orange squares, respectively).

Identification of the sulfonated aromatic amine 4A1NS in both SBRs confirmed the occurrence of AR14 reduction in the anaerobic stage. Accordingly, the first step of AR14 biodegradation (Figure VIII.5) apparently corresponded to the anaerobic AR14 azo bond reduction, at least in cycles I and II, when 4A1NS was detected. However, it is possible that AR14 (corresponding to compounds 4 and 14) suffered other transformations before the cleavage of its azo bond. Specifically, desulfonation of AR14 may have occurred resulting in metabolite 11 and, subsequently, metabolite 8, in addition to the incomplete cleavage of the AR14 azo bond (Figure VIII.5). Since these metabolites were observed at the end of the anaerobic phase (Figure VIII.2), the hypothetical desulfonation of the aromatic ring occurred under anaerobic conditions.

**Table VIII.4** - Classification of the correspondence between the measured accurate *m/z* value in LC-HRMS analysis, and the proposed ion chemical formula (Score = 100%). n.a.: not attributed. $[M-H]^-$: deprotonated molecule; $[M+H]^+$; protonated molecule.

| Metabolite | Measured *m/z* | Attribution | Ion Formula | Calculated *m/z* | Δ (ppm) | mSigma |
|---|---|---|---|---|---|---|
| 2 | 207.0139 | $[M-H]^-$ | $C_{10}H_7O_3S$ | 207.0121 | -8.5 | 10.1 |
| 3 | 222.0280 | $[M-H]^-$ | $C_{10}H_8NO_3S$ | 222.0230 | -22.6 | 32.5 |
| 4 | 228.0112 | $[M-2H]^{2-}$ | $C_{20}H_{12}N_2O_7S_2$ | 228.0048 | -28.1 | 17.9 |
| 5 | 239.0072 | $[M-H]^-$ | $C_{10}H_7O_5S$ | 239.0020 | -22 | 16.6 |
| 6 | 251.9979 | $[M-H]^-$ | $C_{10}H_6NO_5S$ | 251.9972 | -2.6 | 31.3 |
| 7 | 267.9956 | $[M-H]^-$ | $C_{10}H_6NO_6S$ | 267.9921 | -12.8 | n.a. |
| 8 | 377.0602 | $[M-H]^-$ | $C_{20}H_{13}N_2O_4S$ | 377.0602 | -0.2 | 19.1 |
| 10 | 391.0483 | $[M-H]^-$ | $C_{20}H_{11}N_2O_5S$ | 391.0394 | -22.7 | 9.9 |
| 11 | 393.0625 | $[M-H]^-$ | $C_{20}H_{13}N_2O_5S$ | 393.0551 | -18.9 | 8.2 |
| 12 | 394.0449 | $[M-H]^-$ | $C_{20}H_{12}NO_6S$ | 394.0391 | -14.7 | 48.3 |
| 13 | 419.0785 | $[M-H]^-$ | $C_{22}H_{15}N_2O_5S$ | 419.0707 | -18.7 | 36.8 |
| 14 | 457.0251 | $[M-H]^-$ | $C_{20}H_{13}N_2O_7S_2$ | 457.017 | -17.8 | 24.0 |
| 17 | 173.0739 | $[M+H]^+$ | $C_{10}H_9N_2O$ | 173.0709 | -16.9 | n.a. |
| 18 | 174.0566 | $[M+H]^+$ | $C_{10}H_8NO_2$ | 174.0550 | -9.4 | 5.8 |
| 19 | 189.0561 | $[M+H]^+$ | $C_{11}H_9O_3$ | 189.0546 | -7.8 | n.a. |

On the other hand, when the original AR14 molecule was completely reduced, two aromatic amines were formed, as confirmed by the presence of 4A1NS (metabolite 3). The complete disappearance of the recalcitrant 4A1NS from the SBR samples indicated that it was further transformed during the aerobic stage (Figure VIII.1 and Figure VIII.2), representing a progress relative to previous work (Mata *et al*., 2015). In accordance with the predicted AR14 degradation pathway (Figure VIII.S44, in Appendix F), 4A1NS probably underwent deamination and aromatic ring hydroxylation forming metabolite 5, as previously suggested (Chan *et al*., 2012). Subsequently, metabolite 5 is expected to suffer aromatic ring cleavage (Figure VIII.5), with further oxidation eventually leading to the production of aliphatic carboxylic acids and ultimately mineralization (Chan *et al.*, 2012; Roşu *et al*., 2016). Based on the putative structures proposed for metabolites 18'' and 6, another aromatic ring opening pathway was suggested (Figure VIII.5), although the probability of these transformations must be further addressed.

Upon SBRs supplementation with nitrate (cycle III), 4A1NS was no longer detected in SBR1 and SBR2 (Figure VIII.1 and Figure VIII.2). Instead, new metabolites emerged (Table VIII.2), suggesting that a different AR14 biodegradation pathway took place in the presence of nitrate. In fact, in light of the proposed structure for metabolite 2, direct deamination of 4A1NS was suggested to occur upon AR14 reduction under anaerobic conditions. This observation is in accordance with a previous study reporting the degradation of some aromatic amines under denitrifying conditions (Pereira *et al*., 2011). Specifically, this finding is supported by Seymour *et al*. (2002) who showed that nitrite, which is produced during the first step of denitrification, reacts with aromatic amines, resulting in deamination, thus improving their biodegradation potential.

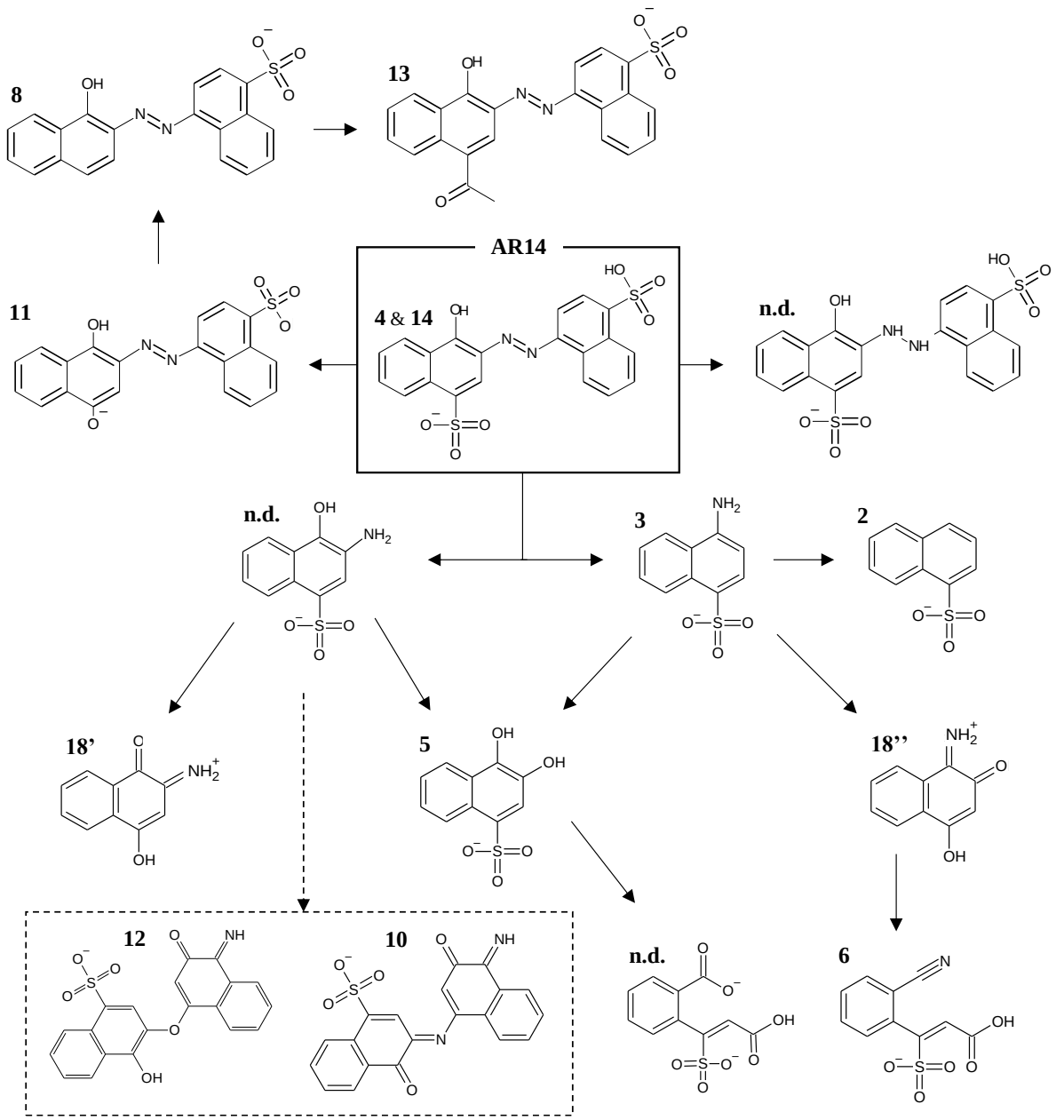


**Figure VIII.5** - Proposed conversion relations between the putative structures proposed for the different metabolites detected through LC-MS/MS, with a focus on the biodegradation of Acid Red 14 (AR14) and the aromatic amines resulting from its reduction, namely 4-amino-naphthalene-1-sulfonic acid (4A1NS; metabolite 3), according to the EAWAGBBD Pathway Prediction System. n.d.: not detected in LC-MS analysis.

In contrast to 4A1NS, the other aromatic amine derived from AR14 azo bond reduction (1N2A4S) was not detected. In this sense, some transformations of 1N2A4S are proposed, involving metabolite 18' (Figure VIII.5). In addition, similarly to 4A1NS, deamination of 1N2A4S and aromatic ring hydroxylation can be proposed to generate metabolite 5 (Figure VIII.5). However, the presence of a hydroxyl group in the *ortho*-position relatively to the amino group in 1N2A4S provides an unstable character to this molecule (Kudlich *et al*., 1999), which explains why it was not detected by LC-MS. Consequently, 1N2A4S is likely to undergo spontaneous autoxidation reactions forming dimeric, stable products, which might be at the origin of complex aromatic structures containing sulfonate groups, such as metabolites 10 and 12 (Figure VIII.5).

## VIII.5. Conclusions

Aiming to elucidate the biodegradation pathways of the azo dye AR14, LC-ESI-MS/MS was used for structural characterization of AR14 biodegradation metabolites in samples from two AGS SBRs treating a synthetic TWW and operated under different hydrodynamic regimens. After optimization of the sample pre-treatment and LC conditions, 19 molecules potentially related to AR14 were detected in the analyzed SBR samples and their relative abundances were followed along the aerobic stage of the treatment cycles. Although both SBRs shared most of the identified compounds in each experimental period, specific differences were observed in the aerobic profiles of their metabolites. Overall, a decrease in ion abundance along the aerobic stage was more often observed in the plug-flow fed SBR2 than in SBR1, indicating a potential advantage in using a plug-flow feeding regimen.

Identification of the sulfonated aromatic amine 4A1NS confirmed the occurrence of AR14 reduction through azo bond cleavage in the anaerobic stage. Moreover, complete disappearance of the recalcitrant 4A1NS from the SBR samples indicated that it was further transformed during the aerobic stage. Based on the identified metabolites, 4A1NS aerobic biodegradation was proposed to follow deamination and aromatic ring hydroxylation. On the contrary, the other aromatic amine derived from AR14 azo bond reduction (1N2A4S) was not detected, probably due to autoxidation reactions forming some of the complex aromatic structures containing sulfonate groups which were identified in the samples. The presence of nitrate was associated with a different AR14 biodegradation pathway, possibly involving deamination of 4A1NS under anaerobic conditions. Further investigation is needed to understand the underlying mechanism, as well as to confirm some of the proposed chemical structures. Overall, these results represent a relevant contribution towards the elucidation of AR14 biodegradation pathways, involving mechanisms the understanding of which may be crucial for efficient TWW biotreatment.

# IX. *Oerskovia paurometabola* isolated from a laboratory mixed culture treating a simulated TWW efficiently decolorizes azo dye Acid Red 14 with further aerobic aromatic amine conversion

The information included in this chapter was partially published in:

Franca, R.D.G., Vieira, A., Carvalho, G., Pinheiro, H.M., Barreto Crespo, M.T., Lourenço, N.D., 2016. Biodegradation of a sulfonated azo dye in a synthetic textile wastewater by a newly isolated *Oerskovia* strain. *IWA World Water Congress & Exhibition*, 9-14 October, Brisbane, Australia.

## IX.1. Abstract

Among the 18 bacterial strains isolated from a lab-scale anaerobic-aerobic SBR fed with azo dye-laden synthetic TWW, *Oerskovia paurometabola* presented the highest decolorization capacity (91% after 24 h in static anaerobic culture). Growth assays supported that this is a facultative bacterium, and decolorization batch tests with 20-100 mg $L^{-1}$ of the azo dye AR14 in a synthetic TWW supplemented with yeast extract (YE) indicated that *O. paurometabola* has a high color removal capacity for a significant range of AR14 concentrations. In addition, a model typically used to describe biodegradation of xenobiotic compounds was adjusted to the results, to predict AR14 biodegradation time profiles at different initial concentrations. HPLC analysis confirmed that decolorization occurred through azo bond reduction under anaerobic conditions, the azo dye being completely reduced after 24 h of anaerobic incubation for the range of concentrations tested. Interestingly, partial (up to 63%) removal of one of the resulting aromatic amines (4A1NS) was observed when subsequent incubation in aerobic conditions was applied. Overall, this work showed the azo dye biodegradation potential of specific bacterial strains isolated from mixed culture bioreactors, newly reporting the decolorization capacity of an *Oerskovia* sp. with further biodegradation of a recalcitrant sulfonated aromatic amine metabolite.

## IX.2. Introduction

The increased demand for textile products and the incomplete fixation process of dyes to fabrics during their manufacture both contribute for the classification of textile industry wastewater as one of the most relevant sources of worldwide pollution, namely due to the release of recalcitrant textile dyes into natural water bodies. Around 280,000 tons of textile dyes are annually discharged in TWW (Solís *et al.*, 2012), azo dyes being the most widely used class, accounting for over 80% of the total amount used (O'Neill *et al*., 1999). The complex aromatic structure of these compounds confers them high stability against physical, chemical and biological agents, making them resistant to degradation, namely in conventional aerobic wastewater treatment bioprocesses. The release of untreated, azo dye containing, colored effluents in aquatic systems is a major concern due to their interference in photosynthesis and consequent depletion of DO, thus negatively affecting the whole ecosystem. In addition, some azo dyes and their potential breakdown products may be toxic and/or mutagenic to aquatic life forms and humans (Pinheiro *et al*., 2004; van der Zee and Villaverde, 2005). In this context, several physical and chemical processes have been developed to promote color removal from TWWs. However, these approaches are often associated with high costs and limited versatility, and create relevant secondary pollution problems, such as the generation of hazardous waste products that must be handled (dos Santos *et al*., 2007). In addition, as regulations become stricter, companies are faced with increasing waste management costs (Solís *et al*., 2012).

The urgent need for effective, accessible, economically attractive and environmentally friendly azo dye removal processes led to the study of microbial alternatives (Solís *et al*., 2012). In fact, many microorganisms have been noted for their ability to decolorize azo dyes. They belong to different taxonomic groups of algae, fungi, yeasts and bacteria (Solís *et al*. 2012), the latter having several advantages associated with their high flexibility in what regards cultivation conditions (Pearce *et al*., 2003). Scientific literature extensively reports on the use of pure bacterial cultures able to decolorize azo dyes, the most promising microorganisms being those isolated from textile industry effluent contaminated environments (Solís *et al*., 2012). Decolorization of azo dyes by bacteria can occur through adsorption, enzymatic degradation (reductase or oxidase activity) or a combination of both (Solís *et al*, 2012). Anaerobic azo dye reduction by bacteria has been extensively investigated and most studies indicate that it is a non-specific and presumably extracellular process, where the dye receives reducing equivalents from either biological or chemical sources (van der Zee and Villaverde, 2005; dos Santos *et al*., 2007).

Overall, the combination of anaerobic and aerobic processes has been highlighted as the most promising concept for the removal of azo dyes in biological wastewater treatment systems using mixed bacterial cultures (van der Zee and Villaverde, 2005). Specifically, these include an anaerobic treatment stage for the reductive cleavage of the azo bond (Pearce *et al*., 2003), followed by an aerobic stage for the degradation of the resulting, potentially toxic, colorless aromatic amines (Pinheiro *et al*., 2004). An example is the use of flocculent activated sludge anaerobic-aerobic SBR systems (Lourenço *et al*., 2000). However, in spite of the successful decolorization results, investigations on the fate of the aromatic amines revealed that most of these compounds, namely sulfonated aromatic amines, are not aerobically degraded (van der Zee and Villaverde, 2005). In general, difficulties in achieving complete mineralization of azo dyes has been attributed to the absence of an adequate aerobic microbial population able to metabolize such aromatic amines. In some cases, this could be achieved only after bioaugmentation with a properly selected bacterial culture (Tan *et al*., 2000). In fact, van der Zee and Villaverde (2005) highlighted the need to obtain better insights into the aerobic fate of aromatic amines and, years later, Solís *et al.* (2012) further reinforced the necessity to achieve dye mineralization in addition to decolorization, suggesting the use of new combinations of strains and consortia isolated from dye-contaminated sites.

In this sense, it is still an essential effort to investigate the azo dye biodegradation performance of specific bacterial strains present in the mixed culture bioreactors, both to devise ways of enhancing their activity within the consortia, and to understand the inherent decolorization and mineralization mechanisms. The present study aimed to isolate bacterial strains with the ability to decolorize a model textile azo dye (AR14), from an anaerobic-aerobic laboratory SBR which had been fed for a prolonged period with a dye-laden synthetic wastewater, and consistently exhibited high dye removal capacity.

New isolates from this source could potentially be employed to improve the reliability and consistency of TWW treatment facilities with regard to the removal of color and also of the intermediate aromatic amines thus formed.

## IX.3. Materials and methods

### IX.3.1. Chemicals and synthetic TWW

The carbon source used in the synthetic feed was a starch-based sizing agent commonly employed in the textile industry, Emsize E1 (Emsland-Stärke GmbH, Germany). The hydrolyzed Emsize E1 and the azo dye AR14 stock solutions were prepared as described in section III.3.1.1.

The synthetic TWW (pH 6.9-7.0) was prepared with a COD of 1000 mg $O_2$ $L^{-1}$, through the dilution of the Emsize E1 stock solution in distilled water, and the addition of pH buffering phosphates and nutrients, as described in section III.3.1.2.

### IX.3.2. Isolation and identification of bacterial strains with decolorization capacity

Bacterial strains were isolated from a laboratory scale anaerobic-aerobic SBR, previously inoculated with activated sludge from a full-scale municipal WWTP (Chelas, Portugal) and operated on 8-h cycles. The reactors were fed with the synthetic TWW described above, supplemented with the azo dye AR14 to a concentration of 20 mg $L^{-1}$ (Lourenço *et al.*, 2015). Biomass samples collected from the SBR after 150 days of operation on the synthetic TWW feed were cultured at 30ºC on solid medium composed of the same synthetic wastewater supplemented with 20 mg $L^{-1}$ AR14 and agar. Colonies with different morphologies were further isolated onto nutrient agar medium. Each isolate exhibiting a decolorized zone surrounding its colonies in wastewater agar plates was further cultured in nutrient broth for 24 h, under aerobic, shake-flask conditions (150 rpm) at 30ºC, and subsequently stored in 20% glycerol, at -20ºC.

Total genomic DNA was extracted from the isolates using the Ultraclean™ Microbial DNA Isolation Kit (MO BIO Laboratories, CA, USA) according to the manufacturer's instructions. Following the spectrometric quantification of the extracted DNA (NanoDrop 1000, ThermoScientific, Rockford, IL, USA), PCR amplification of bacterial DNA was performed using 16S rRNA universal primers, 27f and 968rBac (Lane, 1991). The reaction mixture (50 µl) contained 2 ng $\mu L^{-1}$ of template DNA, 1× PCR buffer (Invitrogen), 3 mM $MgCl_2$ (Invitrogen), 0.2 mM dNTP mix (Bioline), 1 U of Taq DNA polymerase (Invitrogen) and 0.3 µM of each primer. The PCR conditions consisted of an initial denaturing step of 5 min at 95ºC followed by 30 cycles of 95ºC, for 30 s, 55ºC for 60 s and 72ºC for 60 s. The reaction was completed with a final extension at 72ºC for 5 min. The PCR products were subsequently purified (MinElute PCR purification Kit, Qiagen) and sequenced (Stabvida, Oeiras, Portugal). Sequences were analyzed using the public nucleotide databases and the NCBI Mega

BLAST algorithm, and deposited in GenBank (KX034798, KM579615 to KM579621, KM576924 to KM579634). Phylogenetic analysis of the isolates was performed using the MEGA version 5.0 software (Tamura *et al*., 2011), after multiple alignments of experimental and reference sequences using the ClustalW algorithm. A phylogenetic tree was constructed by the neighbor-joining method, and the statistical significance was evaluated by bootstrap analysis with 1000 repeats.

### IX.3.3. Screening of azo dye decolorizing bacteria

The isolated strains were screened for their decolorization capacity in a screening medium containing 10 g $L^{-1}$ YE, 5 g $L^{-1}$ NaCl and 20 mg $L^{-1}$ AR14. Anaerobic cultures were grown under static conditions in rubber stopper glass bottles containing the screening medium, previously sparged with nitrogen gas. All the experiments were performed at 30ºC with an initial cell density of 0.1, as $OD_{600nm}$ (optical density, at 600 nm). Samples were collected after 24 and 48 h of incubation, and the supernatant was recovered through centrifugation (10000 x g, 5 min) for measurement of its absorbance at 515 nm (maximum absorbance wavelength of AR14 in the visible range) against distilled water. Decolorization efficiency values were determined through equation IX.1, where $Abs_0$ refers to the absorbance at the start of the incubation time, and $Abs_t$ to the absorbance at the end of the incubation time.

$$Decolorization\ efficiency\ (\%) = \frac{(Abs_0 - Abs_t)}{Abs_0} \times 100 \qquad \text{(IX.1)}$$

### IX.3.4. Growth assays of a selected bacterial isolate

The isolated bacterial strain with the highest decolorization efficiency was characterized in terms of growth in anaerobic (rubber stopper glass bottles; medium previously sparged with nitrogen gas; static conditions) and aerobic (shake flasks at 150 rpm) conditions, on the synthetic TWW (section IX.3.1) supplemented with 1 g $L^{-1}$ YE. Cultures were inoculated with an initial cell density of 0.1 as $OD_{600nm}$, using an aerobic pre-culture on the same medium. Each culture was performed in duplicate, at 30ºC. Samples were collected along the incubation time and biomass concentration was determined through $OD_{600nm}$ measurements and subsequent conversion to VSS values, using a calibration curve previously established between $OD_{600nm}$ and VSS, the latter being measured through a standard procedure (APHA, 1995). Maximum specific growth rate values were calculated through linear regression of the plots of $\ln(OD_{600nm})$ *versus* time during the exponential growth phase.

### IX.3.5. Decolorization assays with a selected bacterial isolate

The most efficient strain selected from the screening assay was studied for its decolorization efficiency. Decolorization time course profiles were obtained using the same medium as in the growth assays (section IX.3.4), supplemented with different AR14 concentrations (20, 50, 75 or 100 mg $L^{-1}$).

From aerobic pre-cultures grown in the same medium, cultures were inoculated with an initial cell density of 0.1 as $OD_{600nm}$. Media, in rubber stopper glass bottles, were previously sparged with nitrogen gas and static incubation was carried out at 30ºC for a period of 27 h.

After complete color removal under the described static anaerobic conditions, the cultures were subsequently supplemented with allylthiourea (ATU) to a concentration of 0.01 g $L^{-1}$ to prevent the eventual occurrence of nitrification, and incubated under aerobic conditions, in shake flasks, at 150 rpm and 30ºC, for a further period of 27 h, to assess the capacity of the strain to further metabolize the products of AR14 anaerobic reduction.

Uninoculated controls were included to check for abiotic dye conversion, and each culture was performed in duplicate. Culture samples were collected along the anaerobic and aerobic incubation periods, cells were removed by centrifugation (10000 x g, 5 min) and the clear supernatants were used for further analysis.

Dye concentration was spectrophotometrically assessed by measuring the absorbance of the culture supernatants at 515 nm against distilled water, these values being converted to the equivalent dye concentration through a calibration curve for AR14, and subsequently referred as color-eq. Supernatant samples stored at -20ºC were subsequently used to follow dye degradation and metabolite formation by reversed-phase HPLC as described in section III.3.3.1.

### IX.3.6. Abiotic assay with a selected bacterial isolate

The decolorization assays described in section IX.3.5 were complemented with an abiotic test to assess the extent of aerobic removal of one product of AR14 anaerobic reduction, the aromatic amine 4A1NS, attributable to adsorption onto the biomass. Using the synthetic TWW (section IX.3.1), duplicate cultures were inoculated with an initial cell density of 0.9 as $OD_{600nm}$, representative of the values registered during the aerobic stage of the decolorization assays ($OD_{600nm}$=0.6-1.0). Cells were then inactivated by autoclaving at 120ºC during 60 min. Subsequently, 4A1NS was added to a concentration of 18 mg $L^{-1}$, correspondent to the value expected after complete reduction of 75 mg $L^{-1}$ AR14. The cultures were incubated under the same conditions of the aerobic stage of the decolorization assays, and samples were collected over time to measure $OD_{600nm}$ values and to analyze the centrifuged supernatants through HPLC as described in section III.3.3.1.

### IX.3.7. Modelling of Acid Red 14 (AR14) decolorization by a selected bacterial isolate

The decolorization profile of the bacterial strain with the highest decolorization capacity was modelled through equation IX.2, adapted from previous studies modelling the biodegradation of xenobiotics by pure and mixed microbial cultures (Chong, 2009; Almeida *et al*., 2013).

$$\frac{dS}{dt} \cdot \frac{1}{X} = \frac{S}{X} \cdot \frac{ab}{1+e^{-b(t-c)}} \left(1 - \frac{1}{1+e^{-b(t-c)}}\right) \quad \text{(IX.2)}$$

In equation IX.2, $S$ is the AR14 concentration measured by HPLC (mg $L^{-1}$), $X$ is the biomass concentration (mg VSS $L^{-1}$) and $a$ (unitless), $b$ ($h^{-1}$), and $c$ (h) are constants. These constants were estimated using non-linear regression fitting to the experimental data using Aquasim (Reichert, 1995). Parameter estimation for the three constants was performed using data from the experiments fed with 50, 75 and 100 mg $L^{-1}$ AR14.

## IX.4. Results and discussion

### IX.4.1. Decolorization capacity screening of bacterial isolates

Eighteen morphologically distinct bacterial colonies exhibiting decolorized halos in wastewater agar plates were picked and re-cultured on nutrient agar medium. The phylogenetic tree in Figure IX.1 shows the strains isolated in this work alongside organisms closely related to them. The isolates represented diverse genera, including *Acinetobacter*, *Pseudomonas* and *Oerskovia*. Each isolate was matched with NCBI database accessions to the species or genera levels with 97 to 100% similarities (Table IX.1).

All isolated bacterial strains successfully decolorized AR14, most of which achieving color removal yields over 90% after 48 h of static incubation (Table IX.1). The bacterial strain 2a SBR, with the best performance (91% and 96% decolorization yields after 24 and 48 h, respectively), presented high similarity (99%) to *Oerskovia paurometabola* (Table IX.1). In a similar study, out of 76 strains isolated from textile industry wastewater, 45 strains were able to decolorize the azo dye Reactive Black 5 (100 mg $L^{-1}$) in 48 h of static incubation, with varying yields (14.4-98.5%), the most efficient decolorizing bacterium being *Pseudomonas* sp. RA20 (Hussain *et al*., 2013). In the present study, the *Pseudomonas* strain with the highest AR14 decolorization capacity presented a decolorization efficiency of 85% after 48 h, the performance of *Oerskovia* sp. being significantly better.

Different taxonomic groups of bacteria have been extensively reported for their ability to decolorize azo dyes, including aerobic, obligate anaerobic and facultative anaerobic bacteria (dos Santos *et al*., 2007). Solís *et al*. (2012) reviewed a number of studies revealing the azo dye decolorization capacity of pure bacterial cultures under static/anaerobic conditions, including *Pseudomonas*, *Acinetobacter*, *Bacillus*, *Shewanella*, *Staphyloccus*, *Aeromonas*, *Shingobacterium*, *Halomonas*, *Lactobacillus* among others. However, to this date, the azo dye decolorization ability of *Oerskovia* sp., which are non-spore-forming, Gram-positive bacteria widespread in nature (Prauser *et al*. 1970), has not been reported.

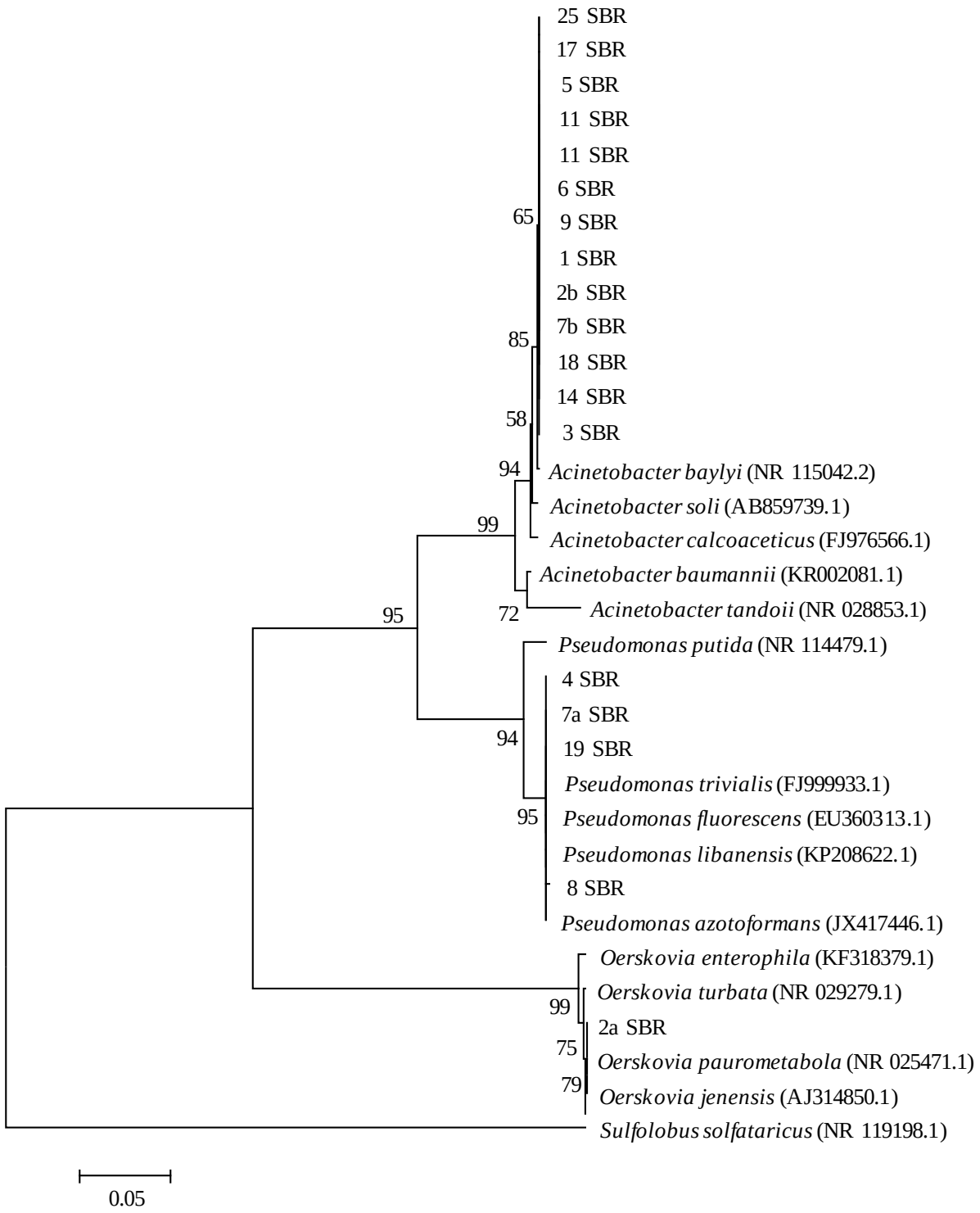


**Figure IX.1** - Neighbor-joining tree showing the phylogenetic relationship of the 16S rRNA gene sequences obtained from GenBank at NCBI and from this work. *Sulfolobus solfataricus* was used as an outgroup in this analysis. The scale bar represents 5% sequence dissimilarity.

**Table IX.1** - Phylogenetic affiliation of isolates and their decolorization efficiency values, observed 24 and 48 h after the addition of Acid Red 14, on synthetic medium.

| Isolate | Accession number | Closest relative | % Sequence identity | Decolorization efficiency (%) | |
|---|---|---|---|---|---|
| | | | | 24 h | 48 h |
| 1_SBR | KM579629 | *Acinetobacter baylyi* | 99 | 52 | 91 |
| 2a_SBR | KX034798 | *Oerskovia paurometabola* | 99 | 91 | 96 |
| 2b_SBR | KM579628 | *Acinetobacter baylyi* | 99 | 47 | 83 |
| 3_SBR | KM579615 | *Acinetobacter* sp. | 99 | 57 | 91 |
| 4_SBR | KM579616 | *Pseudomonas fluorescens* | 99 | 55 | 84 |
| 5_SBR | KM579627 | *Acinetobacter* sp. | 100 | 35 | 75 |
| 6_SBR | KM579617 | *Acinetobacter* sp. | 99 | 59 | 92 |
| 7a_SBR | KM579618 | *Pseudomonas* sp. | 100 | 54 | 85 |
| 7b_SBR | KM579626 | *Acinetobacter baylyi* | 99 | 57 | 91 |
| 8_SBR | KM579619 | *Pseudomonas libanensis* | 99 | 33 | 69 |
| 9_SBR | KM579632 | *Acinetobacter baylyi* | 99 | 61 | 95 |
| 10_SBR | KM579620 | *Acinetobacter* sp. | 97 | 70 | 96 |
| 11_SBR | KM579625 | *Acinetobacter baylyi* | 99 | 55 | 91 |
| 13_SBR | KM579621 | *Acinetobacter* sp. | 97 | 63 | 95 |
| 17_SBR | KM579631 | *Acinetobacter* sp. | 99 | 51 | 87 |
| 19_SBR | KM579624 | *Pseudomonas libanensis* | 99 | 19 | 59 |
| 20_SBR | KM579630 | *Acinetobacter* sp. | 100 | 52 | 89 |
| 25_SBR | KM579634 | *Acinetobacter* sp. | 98 | 27 | 78 |

Among the studies reviewed by Solís *et al*., (2012), most of the strains that were isolated from dye contaminated sites presented decolorization efficiencies over 90% after 24 h of static incubation. In more recent studies, a number of bacterial strains have been isolated from areas contaminated with textile industry wastewater, and their decolorization capacity was characterized: *Pseudomonas* sp. RA20 (Hussain *et al.*, 2013) and *Bacillus* sp. YZU1 (Wang *et al*., 2013) removed 95% and 60% of Reactive Black 5 (100 mg $L^{-1}$) in 24 h, respectively; *Klebsiella pneumonial* (Cui *et al*., 2012) and *Bacillus* sp. YZU1 (Wang *et al*., 2013) reduced Methyl Red (100 mg $L^{-1}$) by 78% after 12 h and by 99% after 10 h, respectively; *Lysinibacillus* sp. AK2 completely decolorized Metanil Yellow (200 mg $L^{-1}$) in 12 h and Amaranth (200 mg $L^{-1}$) in 24 h (Anjaneya *et al*., 2011); *Lysinibacillus* sp. RG removed total color from Remazol Red (50 mg $L^{-1}$) in 6 h (Saratale *et al*., 2013). Despite the excellent performance of the latter under optimized conditions, only 84% of decolorization could be achieved in 24 h when YE was used as nitrogen source (Saratale *et al*., 2013). On the other hand, the addition of

YE enhanced the decolorization of Methyl Orange (100 mg $L^{-1}$) by *Aeromonas* sp. from approximately 80 to 100% in 24 h (Du *et al*. 2015). However, performance comparisons between these reports are difficult because of their varying conditions potentially affecting the biodecolorization process, such as azo dye structure and concentration (van der Zee and Villaverde, 2005; Anjaneya *et al*., 2011; Wang *et al*., 2013), carbon and nitrogen sources (Saratale *et al*., 2013), salinity, pH and temperature (Solís *et al*., 2012; Hussain *et al*., 2013; Liu *et al*., 2017).

In addition to the absence of other decolorization studies using *Oerskovia* sp., AR14 has rarely been used as a model dye in pure culture studies, which impairs a more direct comparison of *O. paurometabola* performance with other reports in the literature. Nevertheless, this bacterial strain showed a significantly higher AR14 decolorizing ability when compared with the other bacteria that were isolated in the present study, the latter belonging to genera that have previously been associated with high decolorization potential, namely *Pseudomonas* and *Acinetobacter* (Solís *et al*., 2012; Hussain *et al*., 2013). For these reasons, *O. paurometabola* was selected for further characterization.

## IX.4.2. Aerobic and anaerobic growth profiles of *Oerskovia paurometabola*

As referred in section IX.4.1, the isolate corresponding to *Oerskovia paurometabola* was selected for further growth profile characterization. Supplementation of the medium with YE was used due to the observed slow growth of this strain in the synthetic TWW. Growth assays confirmed that *O. paurometabola* is a facultative bacterium. Although its growth rate is approximately ten-fold higher under aerobic conditions, it is also able to grow in the absence of oxygen (Figure IX.2). The maximum specific growth rates attained under aerobic and anaerobic conditions were 0.29 $h^{-1}$ and 0.03 $h^{-1}$, respectively.

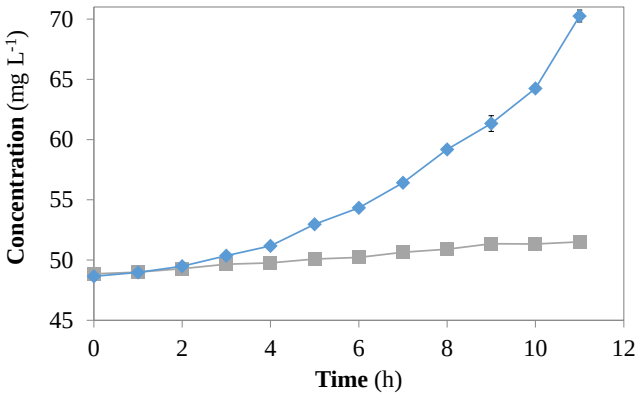


**Figure IX.2** - Growth profile of *Oerskovia paurometabola*, in terms of volatile suspended solids concentration, in anaerobic (■) and aerobic (♦) cultures, at 30ºC, in a synthetic textile wastewater supplemented with yeast extract. Symbols and error bars represent the mean and standard deviation values, n = 2.

## IX.4.3. Azo dye biodegradation by *Oerskovia paurometabola*

### IX.4.3.1. Decolorization performance

Similarly to the growth assays (section IX.4.2), supplementation of the medium with YE was used in the decolorization assays due to the observed slow growth of this strain in the synthetic TWW with concomitant low color removal yields (only 22% of decolorization after 27 h; results not shown). This observation is in accordance with decolorization studies using pure bacterial cultures that tested different nitrogen sources and indicated that YE significantly enhanced the azo dye decolorization rate (Elisangela *et al*., 2009; Solís *et al*., 2012; Hussain *et al*., 2013). Other studies also revealed that YE is often the best nitrogen source for efficient azo dye decolorization, additionally ensuring the regeneration of NADH, which has been shown to act as electron donor for azo bond reduction in several microorganisms (Joshi *et al.*, 2008; Rajeswari *et al.*, 2011).

Decolorization profile of AR14 by *Oerskovia paurometabola* using different AR14 concentrations (25, 50, 75 and 100 mg $L^{-1}$) showed that the color removal rate consistently increased with the increase in the initial AR14 concentration for the tested range, complete decolorization being attained after 24 h of static, anaerobic conditions (Figure IX.3). Other decolorization studies reported lower color removal efficiencies at higher initial dye concentrations (Anjaneya *et al*., 2011; Saratale *et al*., 2013; Wang *et al*., 2013). Namely, Wang *et al.* (2009) reported that the maximum decolorization yield of 25, 100 and 500 mg $L^{-1}$ of Reactive Black 5 was reached after 72, 108 and 120 h, respectively, a result attributable to toxicity effects of the dyes and/or accumulated dye metabolites. Such a negative effect of high dye concentrations on the decolorization rate was not observed in the case of *O. paurometabola* within the tested range of AR14 concentrations (20-100 mg $L^{-1}$), which is comparable to the values reported for dyes in dyehouse effluents, 10-250 mg $L^{-1}$ (O'Neill *et al*., 1999).

The lag phase in color removal, observed during the first 3 h of incubation (Figure IX.3), can be attributed to the presence of a residual amount of oxygen in the test bottles, given earlier reports that this process is sensitive to oxygen (dos Santos *et al*., 2007), as the latter is a more effective electron acceptor than azo dyes. In accordance, decolorization of AR14 was not observed in a 24-h aerobic incubation test with *O. paurometabola* (results not shown). Additionally, in an attempt to promote the aerobic biodegradation of the primary azo bond cleavage products, *i.e.*, sulfonated aromatic amines, the 27-h anaerobic cultures were submitted to a further 27-h incubation period in aerobic conditions. Color removal was not reversed during the subsequent aerobic stage (Figure IX.3), suggesting that decolorization resulted from irreversible azo bond bioreduction. This was further confirmed by HPLC analysis (see section IX.4.3.2).

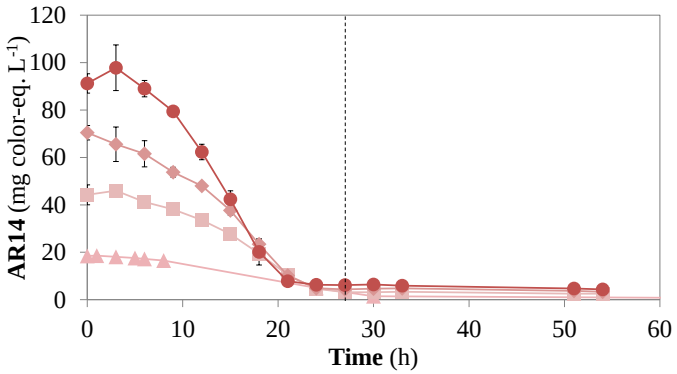


**Figure IX.3** - Azo dye (AR14) concentration profiles (expressed as color-eq.) along time for added AR14 concentrations of 20 mg $L^{-1}$ (▲), 50 mg $L^{-1}$ (■), 75 mg $L^{-1}$ (♦) and 100 mg $L^{-1}$ (●), in anaerobic-aerobic cultures of *Oerskovia paurometabola*. The vertical dashed line indicates the switch to aerobic conditions. Symbols and error bars represent the mean and standard deviation values, n = 2-4.

## IX.4.3.2. Azo dye metabolite fate

In general, pure culture studies on the biodegradation of azo dyes demonstrate efficient decolorization under anaerobic conditions, but do not report on further azo dye degradation, namely through quantification of the metabolites formed from dye reduction and their follow-up during subsequent aerobic incubation (Chang *et al.*, 2001; Asad *et al*., 2007; Anjaneya *et al*., 2011; Hussain *et al*., 2013). This is a very relevant issue since the anaerobic biodegradation of aromatic amines has been reported as very unlikely (van der Zee and Villaverde, 2005) and these azo dye breakdown products may be more toxic than the parent compound. Elisangela *et al.* (2009) indicated that studies on the sequential anaerobic/microaerophilic-aerobic azo dye biodegradation using a single strain were scarce and that the development of bacterial strains with good performance under such conditions was necessary. In the present study, the *Oerskovia paurometabola* culture was subjected to a 27-h aerobic incubation period, after 27 h of anaerobic conditions, and samples were analyzed by HPLC to assess the evolution of the profile of metabolites, namely primary aromatic amines.

HPLC analysis on clarified samples from the decolorization assays with *O. paurometabola* confirmed that the azo dye AR14 was anaerobically reduced, which would result in two sulfonated aromatic amines (Franca *et al*., 2015): 4A1NS and 1N2A4S. Through peak RT comparison with standards, the peaks corresponding to AR14 (RT: 26 min) and to 4A1NS (RT: 14 min) were identified and their areas converted to concentration units using calibration curves. The aromatic amine 1N2A4S could not be identified due to unavailability of the correspondent standard. Moreover, in the presence of oxygen 1N2A4S potentially undergoes autoxidation reactions due to the *ortho*-position of the hydroxyl group in relation to the amino group (Kudlich *et al*., 1999).

HPLC chromatograms registered at the start, end of the anaerobic stage, and end of the aerobic stage in the decolorization assay using 75 mg $L^{-1}$ of AR14 are shown in Figure IX.4a, Figure IX.4b and Figure IX.4c, respectively. Though with different peak areas, equivalent chromatograms were

obtained for the other AR14 concentrations tested. The small non-identified peaks, mostly unchanged along the assay (Figure IX.4), were found to correspond to components present in YE. The azo dye peak I completely disappeared during the anaerobic phase (Figure IX.4a and Figure IX.4b), and was not further registered in the subsequent aerobic stage (Figure IX.4c). Conversely, the aromatic amine 4A1NS peak II appeared during the anaerobic stage (Figure IX.4a and Figure IX.4b) and was significantly reduced after the aerobic stage (Figure IX.4c). This represents a relevant observation since 4A1NS has been shown to be resistant to aerobic biodegradation (Kudlich *et al*., 1999; Mata *et al.*, 2015). Sulfonated aromatic amines, as is the case of the present AR14 metabolites, are particularly difficult to biodegrade due to the hydrophilic nature of the sulfonate group. In fact, biodegradation of sulfonated aromatic amines has mainly been demonstrated for relatively simple sulfonated aminobenzene and aminonaphthalene compounds (Pinheiro *et al*., 2004) and generally requires culture enrichment with specialized aerobes (van der Zee and Villaverde, 2005).

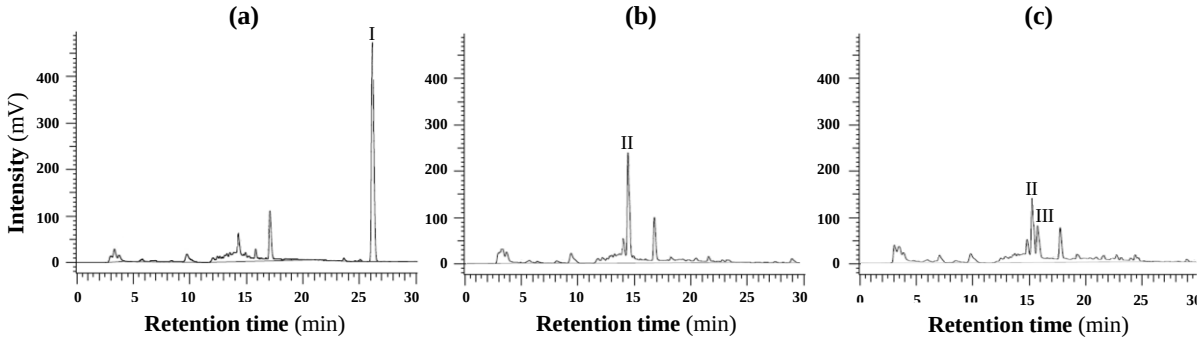


**Figure IX.4** - HPLC chromatograms of samples from the decolorization assay at 75 mg $L^{-1}$ of Acid Red 14 (AR14) with *Oerskovia paurometabola* at the start of the assay – 0 h (a), at the end of the anaerobic phase – 27 h (b), and at the end of the aerobic phase – 54 h (c). Peak I corresponds to AR14, peak II corresponds to the aromatic amine 4-amino-naphthalene-1-sulfonic acid (4A1NS) resulting from AR14 reduction, and peak III is from allylthiourea (ATU), added at the start of the aerobic stage.

AR14 and 4A1NS concentration-time profiles from HPLC analyses, following a similar trend, are depicted in Figure IX.5a, Figure IX.5b and Figure IX.5c, for the assays with 50, 75 and 100 mg AR14 $L^{-1}$, respectively. In general, the 4A1NS concentration values measured at the end of the anaerobic stage were in accordance with the expected values, based on the measured initial azo dye concentration and the stoichiometry of the reductive cleavage reaction, *i.e.*, 1 mol of 4A1NS recovered per 1 mol of reduced AR14. The slight deviations of the measured 4A1NS concentration values relative to the expected values, in some of the anaerobic phase time-points, could be attributed to reversible chemical conversion of the aromatic amine into another intermediate metabolite upon exposure to oxygen during sampling and analysis (Franca *et al*., 2015). The AR14 and 4A1NS concentration-time profiles during the anaerobic stage thus supported that AR14 biodecolorization by *O. paurometabola* resulted from reduction of the azo dye, rather than adsorption to the bacterial biomass.

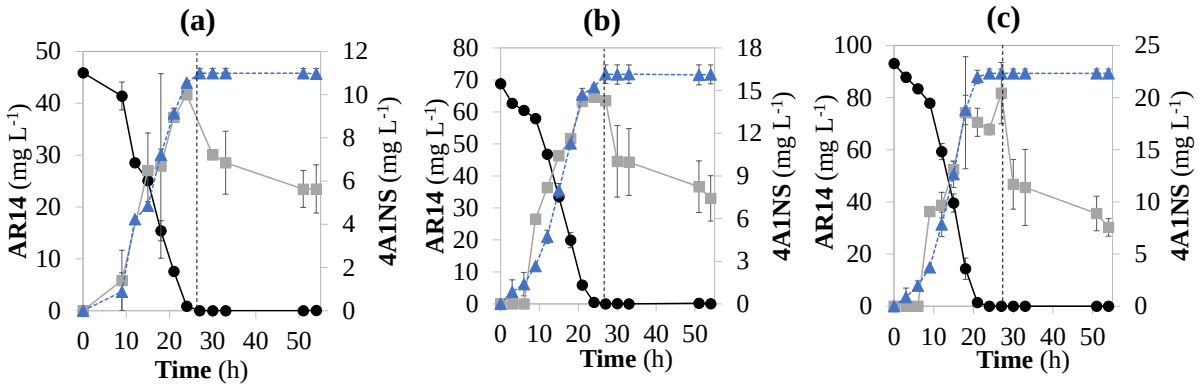


**Figure IX.5** - Concentration profiles of the azo dye Acid Red 14 (AR14; ●) and of its reduction product 4-amino-naphthalene-1-sulfonic acid (4A1NS) – measured (■) and stoichiometry-calculated values (▲) considering no 4A1NS degradation, for added AR14 concentrations of 50 mg $L^{-1}$ (a), 75 mg $L^{-1}$ (b) and 100 mg $L^{-1}$ (c). The dashed vertical line indicates the start of aerobic conditions. Symbols and error bars represent the mean and standard deviation values, n = 2.

During the subsequent aerobic stage, 4A1NS concentration values were significantly reduced along the first 3 h of aeration, further decreasing at a much lower rate up to the end of the incubation period (Figure IX.5a, Figure IX.5b and Figure IX.5c). The removal efficiencies of 4A1NS during the 27-h aerobic stage corresponded to approximately 44, 56 and 63% when 50, 75 and 100 mg $L^{-1}$ of AR14 were used as initial azo dye concentrations, respectively. The rapid removal of 4A1NS at the onset of aeration could indicate chemical oxidation. However, new HPLC peaks were not observed in the chromatograms obtained during this period. On the other hand, adsorption onto the biomass was not expected to be the main mechanism of 4A1NS removal due to the high water solubility of this sulfonated aromatic amine. This effect did not occur during the anaerobic incubation stage, in the presence of high concentrations of 4A1NS. In addition, an abiotic assay with inactivated *O. paurometabola* cells in the presence of 18 mg 4A1NS $L^{-1}$ was performed to assess the potential absorption of 4A1NS onto the biomass during the 27-h aerobic stage of the decolorization assays. The HPLC results presented in Figure IX.6 showed that 4A1NS did not adsorb onto the inactivated *O. paurometabola* biomass under aerobic conditions, when present at a concentration within the range of those registered in the aerobic stage of the decolorization assays. Contrarily to that observed in the aerobic stage of the decolorization assay with 75 mg AR14 $L^{-1}$ (Figure IX.4b and Figure IX.4c), the 4A1NS peak did not decrease in the abiotic assay (Figure IX.6), 4A1NS concentration being maintained at 17.8±0.6 mg $L^{-1}$ throughout the 27-h aerobic incubation period. These results suggest that *O. paurometabola* has the capacity to biodegrade this sulfonated aromatic amine, which has been previously described as recalcitrant (Kudlich *et al.*, 1999). The fact that the putative 4A1NS degradation occurred mainly during the first 3 h of the aerobic stage suggests a case of co-metabolism with the carbon source substrate.

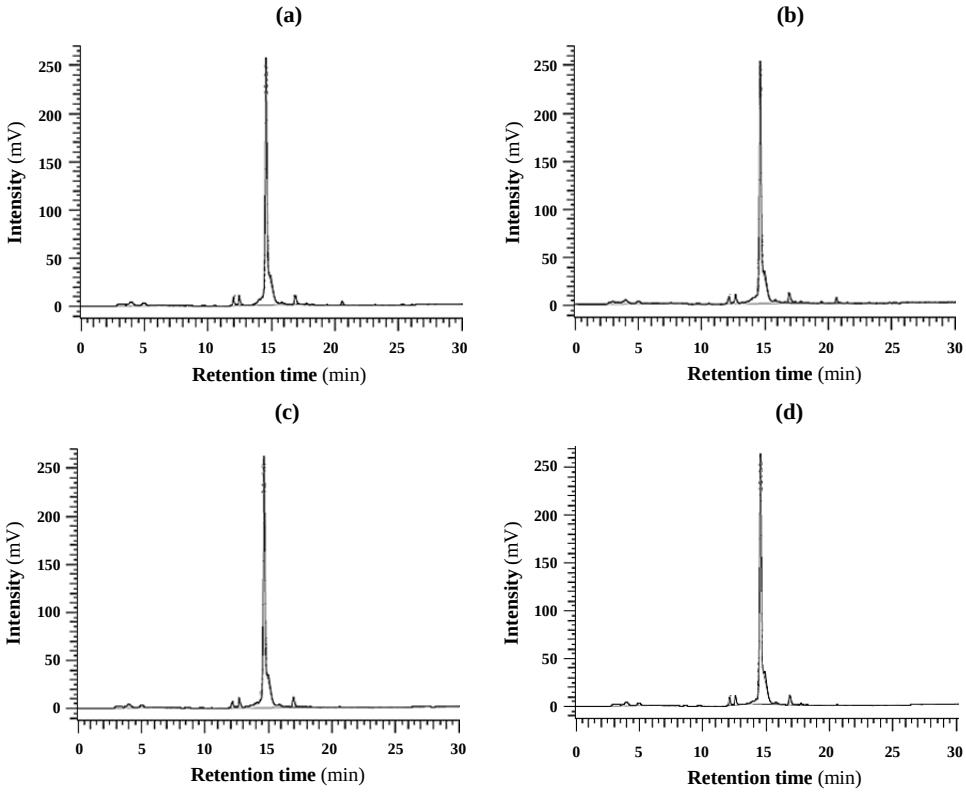


**Figure IX.6 -** HPLC chromatograms of samples from the abiotic assay with inactivated *Oerskovia paurometabola* at 0 h (a), 3 h (b), 15 h (c) and 27 h (d).

Many individual bacterial strains are able to decolorize azo dyes, but further removal of the aromatic amines is rarely demonstrated. On the other hand, the use of microbial consortia has a higher potential to achieve the mineralization of azo dyes due to synergistic metabolic activities within the microbial community (Chan *et al*., 2012; Solís *et al*, 2012). Specifically, a bacterial consortium composed of three strains (genera *Citrobacter* and *Enterococcus*) was able to mineralize the azo dye Amaranth and its degradation intermediates, including 4A1NS, under sequential microaerophilic-aerobic conditions (Chan *et al*., 2012). The biodegradation mechanism was predicted to follow the steps of azo reduction, deamination, desulfonation and aromatic ring cleavage. Chan *et al*., (2012) observed that the bacterial consortium presented a better potential in accomplishing these consecutive steps when compared to individual bacterial strains. Accordingly, given the 4A1NS removal performance of *O. paurometabola* in a pure culture, this strain will potentially provide a relevant contribution to achieve the complete mineralization of 4A1NS, and eventually of other sulfonated aromatic amines, when conjugated with other bacteria in a microbial consortium.

### IX.4.4. Modelling of AR14 decolorization by *Oerskovia paurometabola*

In this study, the kinetics of AR14 decolorization with *Oerskovia paurometabola* was modelled using an equation originally proposed by Chong (2009), equation IX.2 (section IX.3.7). This was done to enable comparison with future studies on the kinetics of dye bioreduction, a trait often neglected in

pure culture studies. The time course of anaerobic AR14 degradation by *O. paurometabola* was well described by equation IX.2, a comparison between the model predictions and experimental data being shown in Figure IX.7. The model equation employs a modified logistical function, with a sigmoidal shape, and successfully described the experimental data for three different initial dye concentrations. A similar model equation has previously been used to describe the biodegradation of other xenobiotic compounds (Chong, 2009; Almeida *et al*., 2013). Through the parameter estimation tool of Aquasim, the values of the three model parameters were estimated as $a$= 33.4±1.3 (unitless), $b$= 0.21±0.04 $h^{-1}$ and $c$= 32.3±0.2 h. The model is thus a useful means of predicting AR14 degradation kinetics by *O. paurometabola*, and can be used in subsequent studies, including process scale-up in the treatment of azo dye containing TWWs.

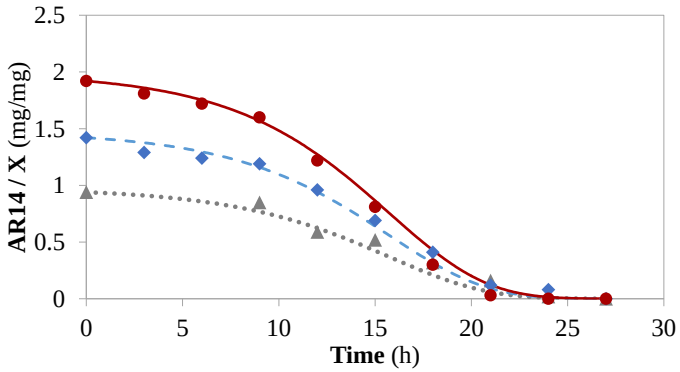


**Figure IX.7 -** Predicted and measured specific concentration profiles of azo dye Acid Red 14 (AR14) per biomass concentration (X) at initial AR14 concentrations of 50 mg $L^{-1}$ (dotted line and ▲), 75 mg $L^{-1}$ (dashed line and ♦) and 100 mg $L^{-1}$ (full line and ●), respectively.

## IX.5. Conclusions

Eighteen AR14-decolorizing bacterial strains were isolated from an anaerobic-aerobic laboratory SBR under long-term operation with a synthetic TWW feed, belonging to *Acinetobacter*, *Pseudomonas* and *Oerskovia* genera. The high color removal capacity of *Oerskovia paurometabola* was newly demonstrated, reaching 100% AR14 (up to 100 mg AR14 $L^{-1}$) removal in 24 h under anaerobic conditions. A model that effectively described the kinetics of this process within the tested AR14 concentration range was presented and can be used for future studies. Decolorization occurred through anaerobic azo bond reduction with aromatic amine formation, including the highly recalcitrant 4A1NS. Contributing to overcome the lack of pure culture studies demonstrating the biodegradation of azo dyes and that of their aromatic amine metabolites, this study showed that 4A1NS was further removed by *O. paurometabola* under aerobic conditions. Abiotic tests with inactivated cells supported the assumption that this aromatic amine was not removed by adsorption onto the biomass, thus confirming the potential of *O. paurometabola* to biodegrade 4A1NS, in addition to its high azo dye decolorization capacity.

# X. Conclusions and Perspectives

## X.1. Conclusions

The present thesis aimed to contribute for the development of an effective TWW treatment bioprocess using the novel AGS technology. Four specific objectives were established, focusing on the main environmental problems raised by TWW: 1) assess the applicability of AGS in the treatment of dye-containing TWW in an anaerobic-aerobic SBR; 2) optimize the SBR hydrodynamic regimen, with emphasis on granulation and decolorization; 3) assess the potential aerobic biodegradation of aromatic amines and 4) evaluate the fate of AgNP in the AGS system, including their effects on aerobic granulation and treatment performance. In this context, the application of AGS to treat a simulated TWW containing a model azo dye (AR14) was evaluated under different scenarios using non-tubular, 1.5-L SBRs (H/D=2.5) operated with 6-h anaerobic-aerobic cycles.

The first study used a dye-free control AGS SBR to analyze the effect of an azo dye on the performance of an anaerobic-aerobic AGS SBR system in the treatment of a synthetic TWW. AR14 did not negatively affect the treatment performance, as organic load removal yields higher than 80% were attained in both reactors, up to 77% occurring within the anaerobic phase. Stable dye removal yields above 90% were attained during the anaerobic reaction phase through azo bond reduction. Yet, frequent biomass wastage episodes triggered a temporary, 30% reduction in the biodecolorization yield. After recovery of maximal color removal yields and operation at high SRT values (>25 days), complete bioconversion of the identified aromatic amine metabolite (4A1NS) was registered during the aerobic reaction phase. The capacity of the system to deal with shocks of high dye concentration and organic load in the feed was successfully demonstrated. In addition, the presence of dye potentially promoted the densification of the AG cores, preventing their disintegration after 90 days of operation, as observed in the dye-free SBR.

Aiming to optimize the treatment of a colored synthetic TWW in AGS SBRs, the second study compared two hydrodynamic regimens in terms of post-storage AGS reactivation performance, with a focus on azo dye biodegradation and organic load removal efficiencies. A 6.5-month stored AGS (resulting from the dye-fed SBR in the first study) recovered its organic load removal capacity to the previous 80% level 9 days after inoculation in both an anaerobic (1.5-h) - aerobic (3.5-h) SBR and an anaerobic plug-flow fed (2-h) - aerobic (3.5-h) SBR. Yet, maximal color removal yields (80%) were not reached in the latter probably because of unfavorable mass transfer conditions. Aerobic bioconversion of the aromatic amine 4A1NS resulting from azo dye reduction was not recovered after storage, likely due to the significant decrease in the microbial community diversity during the storage period. In terms of AGS stability, the anaerobic plug-flow fed - aerobic SBR presented better AGS settling properties and reached a higher biomass concentration.

Following a 2.5-month AGS storage period after the second experimental run, a third study proceeded by comparing two feeding strategies in stirred anaerobic-aerobic AGS SBRs regarding their capacity

to deal with disturbances in the composition of the simulated TWW feed. Both a statically fed, anaerobic-aerobic SBR and an anaerobic plug-flow fed, anaerobic-aerobic SBR could cope with shocks of high azo dye concentration and organic load, the overall COD and color removal yields being rapidly restored to 80%. Similarly to the second study, azo dye metabolite bioconversion was never observed, along the 315-day run. Moreover, switching from a starch-based substrate to acetate in the feed composition deteriorated AGS stability. Overall, the plug-flow fed SBR recovered more rapidly from the imposed disturbances.

These hydrodynamic regimens (0.5-h statically fed, 1.5-h anaerobic - 3.5-h aerobic SBR1 *vs* 1.5-h anaerobic plug-flow fed, 1-h anaerobic - 3.5-h aerobic SBR2) were further compared in a fourth study, regarding AGS quality and treatment performance during aerobic granulation, long-term operation and reactivation after an idle period. Aerobic granulation was successfully achieved in both SBRs, with small, dense and fast-settling granules being formed along 2 months of operation. When supplemented with calcium nitrate the reactors achieved higher TSS levels and further produced faster-settling, larger AG, containing inclusions likely composed of calcium phosphate. When compared to SBR1, the plug-flow feeding regimen and the shorter mechanical stirring phase in SBR2 allowed it to maintain stable AGS and higher biomass concentrations during a longer period of operation, as well as to more efficiently recover from an 18-day idle period and an azo dye shock load. Both reactors reached 80% color and COD removal yields after 1 and 2 weeks of operation, respectively, and maintained these levels along the experimental runs, irrespective of the presence of AgNP, higher dye concentrations or nitrate. Specifically, nitrate and azo dye reduction occurred simultaneously during the anaerobic phase in both SBRs. Although SBR1 reached higher levels of anaerobic COD removal sooner than SBR2 (up to 60%), the latter was able to sustain higher removal efficiencies during long-term operation. Regarding the reactivation performance, although SBR1 and SBR2 took more than 10 days to restore high COD and color removal yields after the 40-day idle period (at room temperature), their color and COD treatment performance was not significantly affected by the 18-day biomass storage period (at 4ºC), further supporting the application of AGS in the treatment of the typically irregular TWW discharges. SBR2 was able to sustain complete conversion of the 4A1NS metabolite for a longer period than SBR1 (*ca.*, 300 *vs* 190 days), namely during the AR14 shock load. Although both SBRs maintained the capacity to transform this aromatic amine after the 18-day biomass storage period, SBR2 presented a different and less effective 4A1NS conversion performance, reflecting a relevant change at the metabolic or microbial community levels caused by the idle period.

The fifth study investigated the impact of AgNP on TWW treatment performance by anaerobic-aerobic AGS SBRs during long-term operation, including aerobic granulation and AGS reactivation after an idle period. Irrespective of the presence of AgNP (up to 20 mg $L^{-1}$ in the feed solution), successful aerobic granulation was achieved approximately after 40-50 days of operation, and AGS recovered good physical properties and the formation of new granules during reactivation after

storage. The better settleability and higher biomass concentration levels generally observed in the AgNP-fed reactor suggested that the formation of AGS in the presence of AgNP and the cumulative adsorption of AgNP onto AG (preferentially associated with external EPS) may have promoted the long-term stability of AGS. The treatment performance was not affected by the presence of AgNP, with 80% of color and organic load removal (60% of the COD removal occurred anaerobically) being attained 1 and 2 weeks after inoculation, respectively, and sustained in both SBRs, namely upon biomass reactivation (maximal yields were recovered 1 and 10 days after the 18-day and 40-day idle periods, respectively). The AgNP-fed SBR sustained 4A1NS transformation for longer periods of time, namely throughout the azo dye shock load period and beyond. Despite the observed toxic effect of AgNP on protozoa (marked decrease in their abundance in the AgNP-fed SBR), the lack of a negative impact on the SBR treatment performance highlights the protecting effect of the AG structure to bacteria potentially susceptible to the AgNP-associated antimicrobial action. Nevertheless, exposure to AgNP induced specific changes in the SBR microbial community at least after 1 month of operation, supporting the functional redundancy of bacteria. After interrupting AgNP feeding, the effect of nitrate in the reactor performance was studied. Addition of calcium nitrate in SBR1 induced an increase in VSS, namely through the enlargement of AG and development of new granules with good settling characteristics, as well as a higher anaerobic COD removal. Denitrification, which likely contributed for the precipitation of calcium inside AG, occurred simultaneously with azo dye anaerobic reduction, not significantly affecting the color removal performance.

Aiming to further investigate the fate of the anaerobic AR14 breakdown products during the subsequent aerobic phase, specific treatment cycles from the fourth study were further examined by LC-ESI-MS/MS. After optimization of the sample pre-treatment and LC conditions, 19 molecules potentially related to AR14 were detected in the SBRs and their relative abundances were followed along the aerobic stage of selected treatment cycles. The two SBRs shared most of the identified compounds, but with differences in their metabolite profiles. Biodecolorization through AR14 anaerobic azo bond reduction was confirmed by the identification of the aromatic amine 4A1NS, which was further aerobically biodegraded, involving deamination and hydroxylation of the aromatic ring. The other aromatic amine (1N2A4S) was not detected, being suggested to undergo autoxidation reactions forming dimeric, stable products. A different AR14 biodegradation pathway was observed when nitrate was added to the feed, a new intermediate product being detected (naphthalene-1-sulfonate), potentially supporting previous studies reporting rapid deamination of aromatic amines by reaction with nitrite.

Among the 18 bacterial strains isolated from an anaerobic-aerobic SBR fed with the AR14-laden synthetic wastewater, *Oerskovia paurometabola* presented the highest decolorization capacity (91% after 24 h in static anaerobic culture). Growth assays supported that this is a facultative bacterium, and decolorization batch tests indicated that *O. paurometabola* has a high color removal capacity for a

significant range of AR14 concentrations (20-100 mg $L^{-1}$), decolorization occurring through anaerobic azo bond reduction. Partial removal (up to 63%) of the aromatic amine 4A1NS was observed when subsequent incubation in aerobic conditions was applied. Overall, this work showed the azo dye biodegradation potential of specific bacterial strains isolated from mixed culture bioreactors, being the first to report the decolorization capacity of *Oerskovia* sp. with further biodegradation of a recalcitrant sulfonated aromatic amine metabolite.

Overall, the results from this thesis provided relevant support for the application of AGS SBRs in TWW treatment as a potential sustainable alternative to avoid the pollution of natural water bodies with synthetic dyes.

## X.2. Final remarks and perspectives

In general, textile companies typically discharge their wastewaters into municipal WWTPs without proper pre-treatment, because sophisticated wastewater treatment technologies are unaffordable for small to medium-sized textile companies. As environmental protection becomes a global concern, textile industries are looking for efficient, environmentally friendly and economically attractive TWW treatment solutions capable of diminishing their environmental impact. In this context, a biological treatment process such as the AGS technology, which allows efficient municipal wastewater treatment with a reduced footprint, lower investment and operational costs, stands out as a potential solution.

The results from this thesis showed that the anaerobic-aerobic AGS SBR can be an appropriate system for the stable organic load removal and decolorization of azo dye-laden textile effluents, including the ability to further biodegrade some of the recalcitrant aromatic amines originated from the azo dye reduction. Nevertheless, complete mineralization of the tested sulfonated azo dye was not achieved, namely due to the formation of an unstable aromatic amine and complex autoxidation products with low biodegradation potential. In this sense, it would be very valuable to confirm the proposed structures in the AR14 biodegradation pathway, namely through comparison with commercial standards, when available, through NMR and further MS/MS analysis. Previous results of toxicity yeast-based assays revealed that the aromatic amines arising from AR14 reduction can have a higher cyto- and genotoxicity potential than the original azo dye. From an environmental risk perspective, in order to conduct an ecologically relevant assessment of the treatment efficiency, the risk associated with the persistent metabolites should be further quantified by evaluating the degree of wastewater detoxification along the treatment process. Accordingly, the operational conditions could be adjusted to minimize the associated environmental risk, and the need for a post-treatment step (*e.g.*, AOP) would be eventually considered.

Variations in the AGS SBR microbial community diversity and their correlation with specific changes in the SBR treatment performance, namely regarding the fate of aromatic amines, should be further analyzed. In this sense, if specific microbial consortia essential for aromatic amine biodegradation

were identified, elucidation of the azo dye biodegradation pathway and involved mechanisms could be more accurately studied, contributing for the development of efficient TWW treatments.

AGS SBR proved to be a robust system able to deal with organic and dye shock loads and prolonged idle periods, efficiently reactivating its former treatment performance after 1-2 weeks. Complete color removal through azo dye bioreduction was shown to depend on a mixed anaerobic phase. Despite the similar treatment performance obtained using two different hydrodynamic regimens, the use of a 1.5-h plug-flow feeding, followed by 1-h stirred anaerobic phase and 3.5-h aerobic phase was generally more advantageous in light of the higher AGS stability during long-term operation. Future research should focus on reactor geometry, feeding system design and type of impellers to achieve the most effective feed distribution and mixing conditions, aiming for optimal AGS stability and cost-efficient treatment performance.

The conclusions drawn from this thesis regarding the performance and efficiency of AGS SBR systems in terms of COD and color removal from TWW constitute a valuable starting point for further studies with simulated TWW focused on different variables relevant for the textile industry and ultimately with real TWW. In fact, once the AGS SBR operational conditions are fully optimized for the treatment of the AR14-laden synthetic TWW, the complexity of the wastewater should be gradually increased by introducing other typical TWW components (*e.g.*, other dyes, surfactants, soaps, waxes, salinity) in order to adjust the treatment process, before eventually testing the system in the treatment of real TWW, and proceeding to scale-up.

Besides the onsite TWW treatment in textile industries, considering the co-treatment of these wastewaters with domestic sewage after a pre-treatment is also essential in view of the practical application of AGS technology for the treatment of dye-laden TWW. In this context, simultaneous biodegradation of residual textile dyes and nutrient removal (*i.e.*, total nitrogen and total phosphorus removal) should be further studied. Although one major advantage of the AGS technology is the possibility to remove COD, nitrogen and phosphorus in a single system, the impact of azo dyes and resulting aromatic amines on nutrient removal efficiency deserves more investigation owing to their possible toxicity to key microbial groups (*e.g.*, nitrifying bacteria), consequently compromising the nutrient removal efficiency. In addition, the potential competition between the azo dye and nutrients for reducing equivalents during the anaerobic phase could eventually decrease the decolorization or phosphorus release performances. In this context, results from this thesis showed that efficient denitrification and color removal occurred simultaneously during the anaerobic phase, but a different aromatic amine fate was also revealed in the presence of nitrate. In order to study the total nitrogen and phosphorus removal in the tested AGS system, it would be necessary to increase the amount of ammonia and to reduce the amount of phosphorus (present in high concentrations due to the use of pH buffering phosphates) supplied to the simulated wastewater.

The presence of AgNP (10-20 mg $L^{-1}$ in the feed) did not affect granulation or the treatment performance on the synthetic TWW, namely during AGS reactivation after storage, and possibly enhanced the long-term stability of AG. Although adsorption of AgNP onto AG (preferentially associated with external EPS) was demonstrated, the fate of AgNP in the AGS system (*e.g.*, aggregation, adsorption, dissolution, precipitation, and sulfidation) requires further investigation, namely through the qualitative and quantitative analysis of silver in the biomass and treated effluent along the operation. In parallel, it would be interesting to study the total EPS content along the SBR operation, in order to correlate the AGS exposure to AgNP with the PN/PS ratio in EPS, as well as with specific changes in the microbial community diversity during granulation and long-term SBR operation. In this sense, suitable methods for isolating, quantifying and characterizing structural EPS from AGS need to be further developed and standardized in order to better control EPS production, essential for aerobic granulation and long-term stability of AG. Furthermore, the use of AGS as a source of structural gel forming polymers can be a way to integrate wastewater treatment in a future more circular economy. Similarly, viable strategies to recover silver from AgNP adsorbed to AGS could be worth developing, in the context of resource recovery from wastewater. Finally, owing to the increasing application of diverse ENP in the textile industry, with their inevitable release into industrial WWTPs, studying the impact and fate of other relevant ENP (*e.g.*, $TiO_2$-NP) in the developed AGS SBR system is of utmost interest.

# References

Adav, S.S., Lee, D.-J., Lai, J.-Y. 2009. Proteolytic activity in stored aerobic granular sludge and structural integrity. Bioresour. Technol. 100, 68-73.

Adav, S.S., Lee, D.-J., Lai, J.-Y., 2010. Potential cause of aerobic granular sludge breakdown at high organic loading rates. Appl. Microbiol. Biotechnol. 85, 1601-1610.

Adav, S.S., Lee, D.-J., Show, K.-Y., Tay, J.-H., 2008a. Aerobic granular sludge: recent advances. Biotechnol. Adv. 26, 411-423.

Adav, S.S., Lee, D-J., Tay, J.H., 2007. Activity and Structure of Stored Aerobic Granules, Environ. Technol. 28, 1227-1235.

Adav, S.S., Lee, D.-J., Tay, J.-H., 2008b. Extracellular polymeric substances and structural stability of aerobic granule. Water Res. 42, 1644-1650.

Ahmed, F., Qayyum, S., Husain, Q., 2018. Benign nano-assemblages of silver induced by β galactosidase with augmented antimicrobial and industrial dye degeneration potential. Mater. Sci. Eng. C. 91, 570-578.

Albertsen, M., Karst, S.M., Ziegler, A.S., Kirkegaard, R.H., Nielsen, P.H., 2015. Back to Basics - The Influence of DNA Extraction and Primer Choice on Phylogenetic Analysis of Activated Sludge Communities. PLOS ONE 10: e0132783.

Albuquerque, M.G.E., Lopes, A.T., Serralheiro, M.L., Novais, J.M., Pinheiro, H.M., 2005. Biological sulphate reduction and redox mediator effects on azo dye decolouration in anaerobic-aerobic sequencing batch reactors. Enzyme Microb. Technol. 36, 790-799.

Almeida, B., Oehmen, A., Marques, R., Brito, D., Carvalho, G., Barreto Crespo, M.T., 2013. Modelling the biodegradation of non-steroidal anti-inflammatory drugs (NSAIDs) by activated sludge and a pure culture. Bioresour. Technol. 133, 31-37.

Amann, R.I., 1995. *In situ* identification of microorganisms by whole cell hybridization with rRNA-targeted nucleic acid probes. In: Akkermans, A.D.L., van Elsas, J.D., de Bruijn, F.J. (eds), Molecular Microbial Ecology Manual, vol. 3.3.6. Dordrecht, Holland: Kluwer Academic Publications, 1-15.

Amann, R.I., Binder, B.J., Olson, R.J., Chisholm, S.W., Devereux, R., Stahl, D.A., 1990. Combination of 16S ribosomal-RNA-targeted oligonucleotide probes with flow-cytometry for analyzing mixed microbial-populations. J. Appl. Environ. Microbiol. 56, 1919-1925.

Amorim, C.L., Maia, A.S., Mesquita, R.B.R., Rangel, A.O.S.S., van Loosdrecht, M.C.M., Tiritan, M.E., Castro, P.M.L., 2014. Performance of aerobic granular sludge in a sequencing batch bioreactor exposed to ofloxacin, norfloxacin and ciprofloxacin. Water Res. 50, 101-13.

Anjaneya, O., Souche, S.Y., Santoshkumar, M., Karegoudar, T.B., 2011. Decolorization of sulfonated azo dye Metanil Yellow by newly isolated bacterial strains: *Bacillus* sp. strain AK1 and *Lysinibacillus* sp. strain AK2. J. Hazard. Mater. 190, 351-358.

APHA - American Public Health Association, 1995 Standard methods for the examination of water and wastewater. In: Eaton A.D., Clesceri L.S. and Greenberg A.E. (Ed.), 19th edn., American Public Health Association, American Water Works, Water Environment Federation, Washington DC.

Asad, S., Amoozegar, M.A., Pourbabaee, A.A., Sarbolouki, M.N., Dastgheib, S.M.M., 2007. Decolorization of textile azo dyes by newly isolated halophilic and halotolerant bacteria. Bioresour. Technol. 98, 2082-2088.

Ausec, L., Zakrzewski, M., Goesmann, A., Schlüter, A., Mandic-Mulec, I., 2011. Bioinformatic analysis reveals high diversity of bacterial genes for laccase-like enzymes. PLoS ONE 6(10), e25724.

Awang, N.A., Shaaban, M.G., 2016. Effect of reactor height/diameter ratio and organic loading rate on formation of aerobic granular sludge in sewage treatment. Int. Biodeterior. Biodegrad. 112, 1-11.

Balapure, K., Bhatt, N., Madamwar, D., 2015. Mineralization of reactive azo dyes present in simulated textile waste water using down flow microaerophilic fixed film bioreactor. Bioresour. Technol. 175, 1-7.

Barsing, P., Tiwari, A., Joshi, T., Garg, S., 2011. Application of a novel bacterial consortium for mineralization of sulphonated aromatic amines. Bioresour. Technol. 102, 765-771.

Bassin, J.P., Kleerebezem, R., Dezotti, M., van Loosdrecht, M.C.M., 2012a. Measuring biomass specific ammonium, nitrite and phosphate uptake rates in aerobic granular sludge. Chemosphere 89, 1161-1168.

Bassin, J.P., Winkler, M.-K.H., Kleerebezem, R., Dezotti, M., van Loosdrecht, M.C.M., 2012b. Improved phosphate removal by selective sludge discharge in aerobic granular sludge reactors. Biotechnol. Bioeng. 109, 1919-1928.

Bento, J.B., 2016. Interaction of silver nanoparticles with aerobic granular sludge in textile wastewater treatment bioreactors (MSc). Instituto Superior Técnico, Universidade de Lisboa.

Bento, J.B., Franca, R.D.G., Pinheiro, T., Alves, L.C., Pinheiro, H.M., Lourenço, N.D., 2017. Using nuclear microscopy to characterize the interaction of textile-used silver nanoparticles with a biological wastewater treatment system. Nucl. Instrum. Methods Phys. Res. B. 404, 150-154.

Beun, J.J., Heijnen, J.J., van Loosdrecht, M.C.M., 2001. N-removal in a granular sludge sequencing batch airlift reactor. Biotechnol. Bioeng. 75, 82-92.

Beun, J.J., Hendriks, A., van Loosdrecht, M.C.M., Morgenroth, E., Wilderer, P.A., Heijnen, J.J., 1999. Aerobic granulation in a sequencing batch reactor. Water Res. 33, 2283-2290.

Beun, J.J., van Loosdrecht, M.C.M., Heijnen, J.J., 2000. Aerobic granulation. Water Sci. Technol. 41, 41-48.

Beun, J.J., van Loosdrecht, M.C.M., Heijnen, J.J., 2002. Aerobic granulation in a sequencing batch airlift reactor. Water Res. 36, 702-712.

Blaser, S.A., Scheringer, M., MacLeod, M., Hungerbühler, K., 2008. Estimation of cumulative aquatic exposure and risk due to silver: Contribution of nano-functionalized plastics and textiles. Sci. Total Environ. 390, 396-409.

Bolger, A.M., Lohse, M., Usadel, B., 2014. Trimmomatic: A flexible trimmer for Illumina sequence data. Bioinformatics 30, 2114-2120.

Brar, S.K., Verma, M., Tyagi, R.D., Surampalli, R.Y., 2010. Engineered nanoparticles in wastewater and wastewater sludge - Evidence and impacts. Waste Manag. 30, 504-520.

Bridgham, S.D., Ye, R., 2013. Organic Matter Mineralization and Decomposition. In: DeLaune, R.D., Reddy, K.R., Richardson, C.J., Megonigal, J.P. (eds), Methods in Biogeochemistry of Wetlands, vol. 10, 385-406. Soil Science Society of America Book Series.

Brigé, A., Motte, B., Borloo, J., Buysschaert, G., Devreese, B., Van Beeumen, J.J., 2008. Bacterial decolorization of textile dyes is an extracellular process requiring a multicomponent electron transfer pathway. Microb. Biotechnol. 1, 40-52.

Cao, X., Zhang, S., Wang, H., Li, X., 2019. Azo dye as part of co-substrate in a biofilm electrode reactor-microbial fuel cell coupled system and an analysis of the relevant microorganisms. Chemosphere 216, 742-748.

Caporaso, J.G., Kuczynski, J., Stombaugh, J., Bittinger, K., Bushman, F.D., Costello, E.K., *et al*., 2010. QIIME allows analysis of high-throughput community sequencing data. Nat. Methods 7, 335-336.

Caporaso, J.G., Lauber, C.L., Walters, W.A., Berg-Lyons, D., Huntley, J., Fierer, N., *et al.* (2012) Ultra-highthroughput microbial community analysis on the Illumina HiSeq and MiSeq platforms. ISME J. 6, 1621-4.

Carliell, C.M., Barclay, S.J., Shaw, C., Wheatley, A.D., Buckley, C.A., 1998. The effect of salts used in textile dyeing on microbial decolourisation of a reactive azo dye. Environ. Technol. 19, 1133-1137.

Carmen, Z., Daniela, S., 2010. Textile Organic dyes – characteristics, polluting effects and separation/elimination procedures from industrial effluents – a critical overview, Organic Pollutants Ten Years After the Stockholm Convention – Environmental and Analytical Update, 55-86.

Carrera, P., Campo, R., Méndez, R., Di Bella, G., Campos, J.L., Mosquera-Corral, A., Val del Rio, A., 2019. Does the feeding strategy enhance the aerobic granular sludge stability treating saline effluents? Chemosphere 226, 865-873.

Carvalho, C., 2016. Microbial ecology of a sequencing batch reactor system with aerobic granular sludge for textile wastewater treatment (MSc). Instituto Superior Técnico, Universidade de Lisboa.

Castillo-Michel, H.A., Larue, C., del Real, A.E.P., Cotte, M., Sarret, G., 2017. Practical review on the use of synchrotron based micro-and nano-X-ray fluorescence mapping and X-ray absorption spectroscopy to investigate the interactions between plants and engineered nanomaterials. Plant Physiol. Biochem. 110, 13-32.

Chan, G.F., Rashid, N.A.A., Chua, L.S., Ab.llah, N., Nasiri R., Ikubar, M.R.M., 2012. Communal microaerophilic-aerobic biodegradation of Amaranth by novel NAR-2 bacterial consortium. Bioresour. Technol. 105, 48-59.

Chang, J.S., Chou, C., Lin, Y.C., Lin, P.J., Ho, J.Y., Lee Hu, T., 2001. Kinetic characteristics of bacterial azo-dye decolorization by *Pseudomonas luteola*. Water Res. 35, 2841-2850.

Chaudhari, A.U., Paul, D., Dhotre, D., Kodam, K.M., 2017. Effective biotransformation and detoxification of anthraquinone dye reactive blue 4 by using aerobic bacterial granules. Water Res. 122, 603-613.

Chen, H., Zhou, S., Li, T., 2010. Impact of extracellular polymeric substances on the settlement ability of aerobic granular sludge. Environ. Technol. 31, 1601-1612.

Chen, Y.-Y., Ju, S.-P., Lee, D.-J., 2016. Aerobic granulation of protein-rich granules from nitrogen-lean wastewaters. Bioresour. Technol. 218, 469-475.

Chin, K.J., Liesack, W., Janssen, P.H.., 2001. *Opitutus terrae* gen. nov., sp. nov., to accommodate novel strains of the division 'Verrucomicrobia' isolated from rice paddy soil. Int. J. Syst. Evol. Microbiol. 51, 1965-1968.

Choi, O., Deng, K.K., Kim, N.-J., Ross Jr.L., Surampalli, R.Y., Hua, Z., 2008. The inhibitory effects of silver nanoparticles, silver ions, and silver chloride colloids on microbial growth. Water Res. 42, 3066-3074.

Chong, N.M., 2009. Modeling the acclimation of activated sludge to a xenobiotic. Bioresour. Technol. 100, 5750-5756.

Çinar, Ö., Demiröz, K., 2010. Biodegradation of Azo Dyes in Anaerobic–Aerobic Sequencing Batch Reactors. In: Atacag Erkurt H. (eds) Biodegradation of Azo Dyes. The Handbook of Environmental Chemistry, vol 9. Springer, Berlin, Heidelberg.

Çinar, Ö., Yaşar, S., Kertmen, M., Demiröz, K., Yigit, N.Ö., Kitis, M., 2008. Effect of cycle time on biodegradation of azo dye in sequencing batch reactor. Process Saf. Environ. Prot. 86, 455-460.

Citeve, 2012. Estudo das dificuldades das empresas do setor têxtil e vestuário no cumprimento de legislação ambiental 52.

Clara, M., Kreuzinger, N., Strenn, B., Gans, O., Kroiss, H., 2005. The solids retention time - A suitable design parameter to evaluate the capacity of wastewater treatment plants to remove micropollutants. Water Res. 39, 97-106.

Coelho, M.S., 2018. Comparing the operation of aerobic granular sludge under different hydrodynamic regimes during the treatment of textile wastewater containing engineered silver nanoparticles (MSc). Instituto Superior Técnico, Universidade de Lisboa.

Collivignarelli, M.C., Abbà, A., Miino, M.C., Damiania, S., 2019. Treatments for color removal from wastewater: State of the art. J. Environ. Manage. 236, 727-745.

Crocetti, G.R., Banfield, J.F., Keller, J., Bond, P.L., Blackall, L.L., 2002. Glycogen-accumulating organisms in laboratory-scale and full-scale wastewater treatment processes. Microbiology 148, 3353-3364.

Crocetti, G.R., Hugenholtz, P., Bond, P.L., Schuler, A., Keller, J., Jenkins, D., Blackall, L.L., 2000. Identification of polyphosphate-accumulating organisms and design of 16S rRNA-directed probes for their detection and quantitation. Appl. Environ. Microbiol. 66, 1175-1182.

Cui, D., Guo, Y.-Q., Lee, H.-S., Cheng, H.-Y., Liang, B., Kong, F.-Y., Wang, Y.-Z., Huang, L.-P., Xu, M.-Y., Wang, A.-J., 2014. Efficient azo dye removal in bioelectrochemical system and post-aerobic bioreactor: optimization and characterization. Chem. Eng. J. 243, 355-363.

Cui, D., Li, G., Zhao, D., Gu, X., Wang, C., Zhao, M., 2012. Microbial community structures in mixed bacterial consortia for azo dye treatment under aerobic and anaerobic conditions. J. Hazard. Mater. 221-222, 185-192.

Dafale, N., Wate, S., Meshram, S., Nandy, T., 2008. Kinetic study approach of remazol black-B use for the development of two-stage anoxic-oxic reactor for decolorization/biodegradation of azo dyes by activated bacterial consortium. J. Hazard. Mater. 159, 319-328.

Dai, Y., Jiang, Y., Su, H., 2015. Influence of an aniline supplement on the stability of aerobic granularsludge. J. Environ. Manage. 162, 115-122.

Daims, H., Bruhl, A., Amann, R., Schleifer, K.H., Wagner, M., 1999. The domain-specific probe EUB338 is insufficient for the detection of all Bacteria: development and evaluation of a more comprehensive probe set. Syst. Appl. Microbiol. 22, 434-44.

Daims, H., Lucker, S., Wagner, M., 2006. Daime, a novel image analysis program for microbial ecology and biofilm research. Environ. Microbiol. 8, 200-213.

Dasgupta, Sikder, J., Chakraborty, S., Curcio, S., Drioli, E., 2015. Remediation of textile effluents by membrane based treatment techniques: a state of the art review. J. Environ. Manage. 147, 55-72.

de Bruin, L.M.M., de Kreuk, M.K., van der Roest, H.F.R., Uijterlinde, C., van Loosdrecht, M.C.M., 2004. Aerobic granular sludge technology: an alternative to activated sludge? Water Sci. Technol. 49, 1-7.

de Kreuk, M.K., Heijnen, J.J., van Loosdrecht, M.C.M., 2005a. Simultaneous COD, nitrogen, and phosphate removal by aerobic granular sludge. Biotechnol. Bioeng. 90, 761-769.

de Kreuk, M.K., Kishida, N., Tsuneda, S., van Loosdrecht, M.C.M., 2010. Behavior of polymeric substrates in an aerobic granular sludge system. Water Res. 44, 5929-5938.

de Kreuk, M.K., Kishida, N., van Loosdrecht, M.C.M., 2007. Aerobic granular sludge - state of the art. Water Sci. Technol. 55, 75-81.

de Kreuk, M.K., Pronk, M., van Loosdrecht, M.C.M., 2005b. Formation of aerobic granules and conversion processes in an aerobic granular sludge reactor at moderate and low temperatures. Water Res. 39, 4476-4484.

de Kreuk, M.K., van Loosdrecht, M.C., 2006. Formation of Aerobic Granules with Domestic Sewage. J. Environ. Eng. 132, 694-697.

de Kreuk, M.K., van Loosdrecht, M.C.M., 2004. Selection of slow growing organisms as a means for improving aerobic granular sludge stability. Water Sci. Technol. 49, 9-17.

de Lima, D.P., dos Santos, E. dos A., Marques, M.R., Giannesi, G.C., Beatriz, A., Yonekawa, M.K.A., Montanholi, A. dos S., 2018. Fungal bioremediation of pollutant aromatic amines. Curr. Opin. Green Sustain. Chem. 11, 34-44.

de Sousa Rollemberg, S.L., Mendes Barros, A.R., Milen Firmino, P.I., Bezerra dos Santos, A., 2018. Aerobic granular sludge: Cultivation parameters and removal mechanisms. Bioresour. Technol. 270, 678-688.

Delée, W., O'Neill, C., Hawkes, F.R., Pinheiro, H.M., 1998. Anaerobic treatment of textile effluents: A review. J. Chem. Technol. Biotechnol. 73, 323-335.

Demirel, B., 2016. The impacts of engineered nanomaterials (ENMs) on anaerobic digestion processes. Process Biochem. 51, 308-313.

Dong, J., Zhang, Z., Yu, Z., Dai, X., Xu, X., Alvarez, P.J.J., Zhu, L., 2017. Evolution and functional analysis of extracellular polymeric substances during the granulation of aerobic sludge used to treat p-chloroaniline wastewater. Chem. Eng. J. 330, 596-604.

dos Santos, A.B., Cervantes, F.J., Van Lier, J.B., 2007. Review paper on current technologies for decoloration of textile wastewaters: Perspectives for anaerobic biotechnology. Bioresour. Technol. 98, 2369-2385.

dos Santos, A.B., Braúna, C.H., Mota, S., Cervantes, F.J., 2008. Effect of nitrate on the reduction of Reactive Red 2 by mesophilic anaerobic sludge. Water Sci. Technol. 57, 1067-71.

Du, L.N., Li, G., Zhao, Y.H., Xu, H.K., Wang, Y., Zhou, Y., Wang, L., 2015. Efficient metabolism of the azo dye methyl orange by *Aeromonas* sp. strain DH-6: Characteristics and partial mechanism. Int. Biodeterior. Biodegrad. 105, 66-72.

Edgar, R.C., 2013. UPARSE: highly accurate OTU sequences from microbial amplicon reads. Nat. Methods 10, 996-8.

Edison, T.N.J.I., Atchudan, R., Sethuraman, M.G., Lee, Y.R., 2016. Reductive-degradation of carcinogenic azo dyes using Anacardium occidentale testa derived silver nanoparticles. J. Photochem. Photobiol. B Biol. 162, 604-610.

Elisangela, F., Andrea, Z., Fabio, D.G., de Menezes Cristiano, R., Regina, D.L., Artur, C.P., 2009. Biodegradation of textile azo dyes by a facultative Staphylococcus arlettae strain VN-11 using a sequential microaerophilic/aerobic process. Int. Biodeterior. Biodegrad. 63, 280-288.

Erşan, Y.Ç., Erguder, T.H., 2013. The effects of aerobic/anoxic period sequence on aerobic granulation and COD/N treatment efficiency. Bioresour. Technol. 148, 149-156.

European Commission, 2017. Textiles and clothing in the EU. Retrieved 28 February 2019, from https://ec.europa.eu/growth/sectors/fashion/textiles-clothing/eu_en.

EWA, 2005. Efficient use of water in the textile finishing industry, E-WAter, Official Publication of the European Water Association.

Fabrega, J., Fawcett, S.R., Renshaw, J.C., Lead, J.R., 2009. Silver nanoparticle impact on bacterial growth: effect of pH, concentration, and organic matter. Environ. Sci. Technol. 43, 7285-7290.

Fabrega, J., Zhang, R., Renshaw, J.C., Liu, W.T., Lead, J.R., 2011. Impact of silver nanoparticles on natural marine biofilm bacteria. Chemosphere, 85, 961-966.

Fan, W., Yuan, L., Qu, X., 2018a. CFD simulation of hydrodynamic behaviors and aerobic sludge granulation in a stirred tank with lower ratio of height to diameter. Biochem. Eng. J. 137, 78-94.

Fan, X., Gao, J., Pan, K., Li, D., Zhang, L., Wang, S., 2018b. Shifts in bacterial community composition and abundance of nitrifiers during aerobic granulation in two nitrifying sequencing batch reactors. Bioresour. Technol. 251, 99-107.

Fatima, M., Farooq, R., Lindström, R.W., Saeed, M., 2017. A review on biocatalytic decomposition of azo dyes and electrons recovery. J. Mol. Liq. 246, 275-281.

Field, J.A., Stams, A.J.M., Kato, M., Schraa, G., 1995. Enhanced biodegradation of aromatic pollutants in cocultures of anaerobic and aerobic bacterial consortia. Antoine van Leeuwenhoek 67, 47-77.

Filali, A., Mañas, A., Mercade, M., Bessière, Y., Biscans, B., Spérandio, M., 2012. Stability and performance of two GSBR operated in alternating anoxic/aerobic or anaerobic/aerobic conditions for nutrient removal. Biochem. Eng. J. 67, 10-19.

Figueroa, M., Val Del Río, A., Campos, J.L., Méndez, R., Mosquera-Corral, A., 2015. Filamentous bacteria existence in aerobic granular reactors. Bioprocess. Biosyst. Eng. 38, 841-851.

Fitzgerald, S.W., Bishop, P.L., 1995. Two stage anaerobic/aerobic treatment of sulfonated azo dyes. J. Environ. Sci. Health A30, 1251-1276.

Forgacs, E., Cserháti, T., Oros, G., 2004. Removal of synthetic dyes from wastewaters: a review. Environ. Int. 30, 953-971.

Forss, J., Pinhassi, J., Lindh, M., Welander, U., 2013. Microbial diversity in a continuous system based on rice husks for biodegradation of the azo dyes Reactive Red 2 and Reactive Black 5. Bioresour. Technol. 130., 681-688.

Forss, J., Welander, U., 2011. Biodegradation of azo and anthraquinone dyes in continuous systems. Int. Biodeterior. Biodegrad. 65, 227-237.

Franca, R.D.G., Ortigueira, J., Pinheiro, H.M., Lourenço, N.D., 2017. Effect of SBR feeding strategy and feed composition on the stability of aerobic granular sludge in the treatment of a simulated textile wastewater. Water Sci. Technol. 76, 1188-1195.

Franca, R.D.G., Pinheiro, H.M., van Loosdrecht, M.C.M., Lourenço, N.D., 2018. Stability of aerobic granules during long-term bioreactor operation. Biotechnol Adv. 36, 228-246.

Franca, R.D.G., Vieira, A., Mata, A.M.T., Carvalho, G.S., Pinheiro, H.M., Lourenço, N.D., 2015. Effect of an azo dye on the performance of an aerobic granular sludge sequencing batch reactor treating a simulated textile wastewater. Water Res. 85, 327-336.

Franciscon, E., Mendonca, D., Seber, S., 2015. Potential of a bacterial consortium to degrade azo dye Disperse Red 1 in a pilot scale anaerobic-aerobic reactor. Process Biochem. 50, 816-825.

Franciscon, E., Grossman, M.J., Paschoal, J.A.R., Reyes, F.G.R., Durrant, L.R., 2012. Decolorization and biodegradation of reactive sulfonated azo dyes by a newly isolated *Brevibacterium* sp. strain VN-15. SpringerPlus 1, 37-47.

Franciscon, E., Piubeli, F., Fantinatti-Garboggini, F., Ragagnin, C. de M., Silva, I.S., Cavaco-Paulo, A., Grossman, M.J., Durrant, L.R., 2010. Polymerization study of the aromatic amines generated by the biodegradation of azo dyes using the laccase enzyme. Enzyme Microb. Technol. 46, 360-365.

Gao, D., Liu, L., Liang, H., Wu, W.M., 2011. Comparison of four enhancement strategies for aerobic granulation in sequencing batch reactors. J. Hazard. Mater. 186, 320-327.

Gao, D., Yuan, X., Liang, H., 2012. Reactivation performance of aerobic granules under different storage strategies. Water Res. 46, 3315-3322.

Gao, J., Zhang, Q., Su, K., Chen, R., Peng, Y., 2010a. Biosorption of Acid Yellow 17 from aqueous solution by non-living aerobic granular sludge. J. Hazard. Mater. 174, 215-225.

Gao, J.F., Zhang, Q., Su, K., Wang, J.H., 2010b. Competitive biosorption of Yellow 2G and Reactive Brilliant Red K-2G onto inactive aerobic granules: simultaneous determination of two dyes by first-order derivative spectrophotometry and isotherm studies. Bioresour. Technol. 101, 5793-5801.

Geyik, A.G., Çeçen, F., 2016. Exposure of activated sludge to nanosilver and silver ion: Inhibitory effects and binding to the fractions of extracellular polymeric substances. Bioresour. Technol. 211, 691-697.

Ghannoum, M.A., Jurevic, R.J., Mukherjee, P.K., Cui, F., Sikaroodi, M., Naqvi, A., and Gillevet, P.M., 2010. Characterization of the oral fungal microbiome (mycobiome) in healthy individuals. PLoS Pathogens 6, e1000713.

Ghaly, A.E, Ananthashankar, R., Alhattab, M., Ramakrishnan, V.V., 2014. Production, characterization and treatment of textile effluents: a critical review. J. Chem. Eng. Process Technol. 5, 1-18.

Giesen, A., De Bruin, L.M.M., Niermans, R.P., Van der Roest, H.F., 2013. Advancements in the application of aerobic granular biomass technology for sustainable treatment of wastewater. Water Pract. Tech. 8, 47-54.

Gobi, K., Mashitah, M.D., Vadivelu, V.M., 2011. Development and utilization of aerobic granules for the palm oil mill (POM) wastewater treatment. Chem. Eng. J. 174, 213-220.

Gonzalez-Martinez, A., Muñoz-Palazon, B., Rodriguez-Sanchez, A., Maza-Márquez, P., Mikola, A., Gonzalez-Lopez, J., Vahala, R., 2017. Start-up and operation of an aerobic granular sludge system under low working temperature inoculated with cold-adapted activated sludge from Finland. Bioresour. Technol. 239, 180-189.

Gottschalk, F., Nowack, B., 2011. The release of engineered nanomaterials to the environment. J. Environ. Monit. 13, 1145-1155.

Gu, L., Li, Q., Quan, X., Cen, Y., Jiang, X., 2014. Comparison of nanosilver removal by flocculent and granular sludge and short- and long-term inhibition impacts. Water Res. 58, 62-70.

Gwin, C.A., Lefevre, E., Alito, C.L., Gunsch, C.K., 2018. Microbial community response to silver nanoparticles and $Ag^{+}$ in nitrifying activated sludge revealed by ion semiconductor sequencing. Sci. Total Environ. 616-617, 1014-1021.

Hailei, W., Ping, L., Guosheng, L., Xin, L., Jianming, Y., 2010. Rapid biodecolourization of eriochrome black T wastewater by bioaugmented aerobic granules cultivated through a specific method. Enzyme Microb. Technol. 47, 37-43.

Haritha, E., Mohana, S., Madhavi, G., Elango, G., Arunachalam, P., 2017. Catunaregum spinosa capped Ag NPs and its photocatalytic application against amaranth toxic azo dye. J. Mol. Liq. 225, 531-535.

Haug, W., Schmidt, A., Nörtemann, B., Hempel, D.C., Stolz, A., Knackmuss, H.J., 1991. Mineralization of sulfonated azo dye Mordant Yellow 3 by a 6-aminonaphthalene-2-sulfonate-degrading bacterial consortium. Appl. Environ. Microbiol. 57, 3144-3149.

He, Q., Gao, S., Zhang, S., Zhang, W., Wang, H., 2017a. Chronic responses of aerobic granules to zinc oxide nanoparticles in a sequencing batch reactor performing simultaneous nitrification, denitrification and phosphorus removal. Bioresour. Technol. 238, 95-101.

He, Q., Yuan, Z., Zhang, J., Zhang, S., Zhang, W., Zou, Z., Wang, H., 2017b. Insight into the impact of ZnO nanoparticles on aerobic granular sludge under shock loading. Chemosphere 173, 411-416.

He, Q., Zhang, W., Zhang, S., Zou, Z., Wang, H., 2017c. Performance and microbial population dynamics during stable operation and reactivation after extended idle conditions in an aerobic granular sequencing batch reactor. Bioresour. Technol. 238, 116-121.

Henriet, O., Meunier, C., Henry, P., Mahillon, J., 2016. Improving phosphorus removal in aerobic granular sludge processes through selective microbial management. Bioresour. Technol. 211, 298-306.

Henze, M., Harremoes, P., Jansen, J.C., Arvin E., 2002. Anaerobic Wastewater Treatment. In: Wastewater Treatment: Biological and Chemical Processes, 300-305.

Hisaindee, S., Meetani, M.A., Rauf, M.A., 2013. Application of LC-MS to the analysis of advanced oxidation process (AOP) degradation of dye products and reaction mechanisms. TrAC - Trends Anal. Chem. 49, 31-44.

Hoff, R., Pizzolato, T.M., Diaz-Cruz, M.S., 2016. Trends in sulfonamides and their by-products analysis in environmental samples using mass spectrometry techniques. Trends Environ. Anal. Chem. 9, 24-36.

Holkar, C.R., Jadhav, A.J., Pinjari, D.V., Mahamuni, N.M., Pandit, A.B., 2016. A critical review on textile wastewater treatments: Possible approaches. J. Environ. Manage. 182, 351-366.

Hong, Y., Guo, J., Xu, Z., Mo, C., Xu, M., Sun, G., 2007. Reduction and partial degradation mechanisms of naphthylaminesulfonic azo dye amaranth by *Shewanella* decolorationis S12. Appl. Microbiol. Biotechnol. 75, 647-54.

Hoque, M.E., Khosravi, K., Newman, K., Metcalfe, C.D., 2012. Detection and characterization of silver nanoparticles in aqueous matrices using asymmetric-flow field flow fractionation with inductively coupled plasma mass spectrometry. J. Chromatogr. A. 1233, 109-115.

Hou, L., Li, K., Ding, Y., Li, Y., Chen, J., Wu, X., Li, X., 2012. Removal of silver nanoparticles in simulated wastewater treatment processes and its impact on COD and $NH_4$ reduction. Chemosphere 87, 248-252.

Huang, W., Wang, W., Shi, W., Lei, Z., Zhang, Z., Chen, R., Zhou, B., 2014. Use low direct current electric field to augment nitrification and structural stability of aerobic granular sludge when treating low COD/$NH_4$-N wastewater. Bioresour. Technol. 171, 139-144.

Huang, X., Wei, D., Yan, L., Du, B., Wei, Q., 2018. High-efficient biosorption of dye wastewater onto aerobic granular sludge and photocatalytic regeneration of biosorbent by acid $TiO_2$ hydrosol. Environ. Sci. Pollut. Res. 25, 27606–27613.

Huangfu, X., Xu, Y., Liu, C., He, Q., Ma, J., Ma, C., 2019. A review on the interactions between engineered nanoparticles with extracellular and intracellular polymeric substances from wastewater treatment aggregates. Chemosphere 219, 766-783.

Husain, S., Afreen, S., Yasin, D., Afzal, B., Fatma, T., 2019. Cyanobacteria as a bioreactor for synthesis of silver nanoparticles-an effect of different reaction conditions on the size of nanoparticles and their dye decolorization ability. J. Microbiol. Methods 162, 77-82.

Hussain, S., Maqbool, Z., Ali, S., Yasmeen, T., Imran, M., Mahmood, F., Abbas, F., 2013. Biodecolorization of reactive black-5 by a metal and salt tolerant bacterial strain *Pseudomonas* sp. RA20 isolated from Paharang drain effluents in Pakistan. Ecotox. Environ. Safe. 98, 331-338.

Ibrahim, Z., Amin, M.F.M., Yahya, A., Aris, A., Muda, K., 2010. Characteristics of developed granules containing selected decolourising bacteria for the degradation of textile wastewater. Water Sci. Technol. 61, 1279-1288.

Illumina, I., 2015. 16S Metagenomic Sequencing Library Preparation, Part #15044223 Rev. B.

Impellitteri, C.A., Harmon, S., Silva, R.G., Miller, B.W., Scheckel, K.G., Luxton, T.P., Schupp, D., Panguluri, S., 2013. Transformation of silver nanoparticles in fresh, aged, and incinerated biosolids. Water Res. 47, 3878-3886.

Inocêncio, P., Coelho, F., van Loosdrecht, M.C.M., Giesen, A., 2013. The future of sewage treatment: Nereda technology exceeds high expectations. Water 21, 28-30.

International Organization for Standardization (ISO), ISO TS 27687, Nanotechnologies – Terminology and definitions for nano-objects – Nanoparticle, nanofibre and nanoplate, ISO, Geneva, Switzerland, 2008.

Isanta, E., Suárez-Ojeda, M.E., Val del Río, Á., Morales, N., Pérez, J., Carrera, J., 2012. Long-term operation of a granular sequencing batch reactor at pilot scale treating a low-strength wastewater. Chem. Eng. J. 198-199, 163-170.

Işik, M., Sponza, D.T., 2003. Aromatic amine degradation in a UASB/CSTR sequential system treating Congo Red dye. J. Environ. Sci. Health. A. Tox. Hazard. Subst. Environ. Eng. 38, 2301-2315.

Işık, M., Sponza, D.T., 2008. Anaerobic/aerobic treatment of a simulated textile wastewater. Sep. Purif. Technol. 60, 64-72.

Işık, M., Sponza, D.T., 2004a. Anaerobic/aerobic sequential treatment of a cotton textile mill wastewater. J. Chem. Technol. Biotechnol. 79, 1268-1274.

Işik, M., Sponza, D.T., 2004b. Monitoring of toxicity and intermediates of C.I. Direct Black 38 azo dye through decolorization in an anaerobic/aerobic sequential reactor system. J. Hazard. Mater. 114, 29-39.

Jacob, H.-E. (1970). Redox Potential. In: Methods in Microbiology, J. R. Norris and D. W. Ribbons (eds.), Academic Press London and New York, pp. 91-123.

Jeong, E., Im, W., Kim, D., Kim, M., Kang, S., Shin, H., Chae, S., 2014. Different susceptibilities of bacterial community to silver nanoparticles in wastewater treatment systems. J. Environ. Sci. Heal A. 49, 685-693.

Jiang, B., Liu, Y., 2013. Dependence of structure stability and integrity of aerobic granules on ATP and cell communication. Appl. Microbiol. Biotechnol. 97, 5105-5112.

Jiang, Y., Marang, L., Tamis, J., van Loosdrecht, M.C.M., Dijkman, H., Kleerebezem, R., 2012. Waste to resource: Converting paper mill wastewater to bioplastic. Water Res. 46, 5517-5530.

Jonstrup, M., Kumar, N., Murto, M., Mattiasson, B., 2011. Sequential anaerobic-aerobic treatment of azo dyes: Decolourisation and amine degradability. Desalination 280, 339-346.

Joshi, T., Iyengar, L., Singh, K., Garg, S., 2008. Isolation, identification and application of novel bacterial consortium TJ-1 for the decolourization of structurally different azo dyes. Bioresour. Technol. 15, 7115-7121.

Juang, Y.C., Adav, S.S., Lee, D.J., Tay, J.H., 2010. Stable aerobic granules for continuous-flow reactors: Precipitating calcium and iron salts in granular interiors. Bioresour. Technol. 101, 8051-8057.

Juárez-Ramírez, C., Velázquez-García, R., Ruiz-Ordaz, N., Galíndez-Mayer, J., Ramos Monroy, O., 2012. Degradation kinetics of 4-amino naphthalene-1-sulfonic acid by a biofilm-forming bacterial consortium under carbon and nitrogen limitations. J. Industrial Microbiol. Biotechnol. 39, 1169-1177.

Juárez-Ramírez, C., Galíndez-Mayer, J., Ruiz-Ordaz, N., Ramos-Monroy, O., Santoyo-Tepole, F., Poggi-Varaldo, H., 2015. Steady-state inhibition model for the biodegradation of sulfonated amines in a packed bed reactor. New Biotechnol. 32, 379-386.

Kaegi, R., Voegelin, A., Ort, C., Sinnet, B., Thalmann, B., Krismer, J., Hagendorfer, H., Elumelu, M., Mueller, E., 2013. Fate and transformation of silver nanoparticles in urban wastewater systems. Water Res. 47, 3866-3877.

Kalyuzhnyi, S., Sklyar, V., Mosolova, T., Kucherenko, I., Russkova, J.A., Degtyaryova, N., 2000. Methanogenic biodegradation of aromatic amines. Water Sci. Technol. 42, 363-370.

Kang, A.J., Brown, A.K., Wong, C.S., Huang, Z., Yuan, Q., 2018. Variation in bacterial community structure of aerobic granular and suspended activated sludge in the presence of the antibiotic sulfamethoxazole. Bioresour. Technol. 261, 322-328.

Kang, A.J., Yuan, Q.Y., 2019. Effect of anaerobic COD utilization on characteristics and treatment performance of aerobic granular sludge in anaerobic/anoxic/oxic SBRs. J. Water Process Eng. 28, 100-106.

Kee, T.C., Bay, H.H., Lim, C.K., Muda, K., Ibrahim, Z., 2014. Development of bio-granules using selected mixed culture of decolorizing bacteria for the treatment of textile wastewater. Desalin. Water Treat. 54, 132-139.

Keck, A., Klein, J., Kudlich, M., Stolz, A., Knackmuss, H.J., Mattes, R., 1997. Reduction of azo dyes by redox mediators originating in the naphthalenesulfonic acid degradation pathway of Sphingomonas sp. strain BN6. Appl. Environ. Microbiol. 63, 3684-3690.

Keller, A.A., McFerran, S., Lazareva, A., Suh, S., 2013. Global life cycle releases of engineered nanomaterials. J. Nanopart. Res. 15, 1692-1709.

Khan, M., Lo, I.M.C., 2016. Removal of ionizable aromatic pollutants from contaminated water using nano γ-Fe2O3 based magnetic cationic hydrogel: sorptive performance, magnetic separation and reusability. J. Hazard. Mater. 322, 195-204.

Khandarea, R.V., Govindwar, S.P., 2015. Phytoremediation of textile dyes and effluents: current scenario and future prospects. Biotechnol. Adv. 33, 1697-1714.

Khehra, M.S., Saini, H.S., Sharma, D.K., Chadha, B.S., Chimni, S.S., 2006. Biodegradation of azo dye C.I. Acid Red 88 by an anoxic - Aerobic sequential bioreactor. Dye. Pigment. 70, 1-7.

King, S.M., Jarvie, H., Bowes, M., Gozzard, E., Lawlor, A., Lawrence, M.J., 2015. Exploring controls on the fate of PVP-capped silver nanoparticles in primary wastewater treatment. Environ. Sci. Nano. 2, 177-190.

Kocaturk, I., Erguder, T.H., 2016. Influent COD/TAN ratio affects the carbon and nitrogen removal efficiency and stability of aerobic granules. Ecol. Eng. 90, 12-24.

Kodam, K.M., Kolekar, Y.M., 2014. Bacterial Degradation of Textile Dyes. Springer International Publishing Switzerland 2015 S.N. Singh (ed.), Microbial Degradation of Synthetic Dyes in Wastewaters, Environmental Science and Engineering, 243-266.

Kolekar, Y.M., Nemade, H.N., Markad, V.L., Adav, S.S., Patole, M.S., Kodam, K.M., 2012. Decolorization and biodegradation of azo dye, reactive blue 59 by aerobic granules. Bioresour. Technol. 104, 818-822.

Kong, Y., Ong, S.L., Ng, W.J., Liu, W.-T., 2002. Diversity and distribution of a deeply branched novel proteobacterial group found in anaerobic-aerobic activated sludge processes. Environ. Microbiol. 4, 753-757.

Kong, Y., Liu, Y.Q., Tay, J.H., Wong, F.S., Zhu, J., 2009. Aerobic granulation in sequencing batch reactors with different reactor height/diameter ratios. Enzym. Microb. Technol. 45, 379-383.

Koupaie, E.H., Moghaddam, M.R.A., Hashemi, S.H., 2011. Post-treatment of anaerobically degraded azo dye Acid Red 18 using aerobic moving bed biofilm process: Enhanced removal of aromatic amines. J. Hazard. Mater. 195, 147-154.

Koupaie, E.H., Moghaddam, M.R.A., Hashemi, S.H., 2013. Evaluation of integrated anaerobic/aerobic fixed-bed sequencing batch biofilm reactor for decolorization and biodegradation of azo dye Acid Red 18: Comparison of using two types of packing media. Bioresour. Technol. 127, 415-421.

Kudlich, M., Bishop, P., Knackmuss, HJ., Stolz, A., 1996. Simultaneous anaerobic and aerobic degradation of the sulfonated azo dye Mordant Yellow 3 by immobilized cells from a naphthalenesulfonate-degrading mixed culture. Appl. Microbiol. Biotechnol. 46, 597.

Kudlich, M., Hetheridge, M.J., Knackmuss, H.J., Stolz, A., 1999. Autoxidation reactions of different aromatic o-aminohydroxynaphthalenes that are formed during the anaerobic reduction of sulfonated azo dyes. Environ. Sci. Technol. 33, 896-901.

Langford, K.H., Scrimshawa, M.D., Birkettb J.W., Lestera, J.N., 2005. Degradation of nonylphenolic surfactants in activated sludge batch tests. Water Res. 39, 870-876.

Le, C., Kunacheva, C., Stuckey, D.C., 2016. "Protein" Measurement in Biological Wastewater Treatment Systems: A Critical Evaluation. Environ. Sci. Technol. 50, 3074-3081.

Le, C., Stuckey, D.C., 2016. Colorimetric measurement of carbohydrates in biological wastewater treatment systems: A critical evaluation. Water Res. 94, 280-287.

Lee, D.-J., Chen, Y.-Y., 2015. Magnesium carbonate precipitate strengthened aerobic granules. Bioresour. Technol. 183, 136-140.

Lee, D.-J., Chen, Y.-Y., Show, K.-Y., Whiteley, C.G., Tay, J.-H., 2010. Advances in aerobic granule formation and granule stability in the course of storage and reactor operation. Biotechnol. Adv. 28, 919-934.

Lemaire, R., Webb, R.I., Yuan, Z., 2008. Micro-scale observations of the structure of aerobic microbial granules used for the treatment of nutrient-rich industrial wastewater. ISME J. 2, 528-541.

Levard, C., Hotze, E.M., Lowry, G.V., Brown, Jr.G.E., 2012. Environmental transformations of silver nanoparticles: impact on stability and toxicity. Environ. Sci. Technol. 46, 6900-6914.

Li, A.-J., Li, X.-Y., Yu, H.-Q., 2011. Effect of the food-to-microorganism (F/M) ratio on the formation and size of aerobic sludge granules. Process Biochem. 46, 2269-2276.

Li, A.-J., Yang, S.-F., Li, X.-Y., Gu, J.-D., 2008. Microbial population dynamics during aerobic sludge granulation at different organic loading rates. Water Res. 42, 3552-3560.

Li, A.J., Zhang, T., Li, X.Y., 2010a. Fate of aerobic bacterial granules with fungal contamination under different organic loading conditions. Chemosphere 78, 500-509.

Li, B., Huang, W., Zhang, C., Feng, S., Zhang, Z., Lei, Z., Sugiura, N., 2015. Effect of TiO2 nanoparticles on aerobic granulation of algal–bacterial symbiosis system and nutrients removal from synthetic wastewater. Bioresour. Technol. 187, 214-220.

Li, J., Ding, L.B., Cai, A., Huang, G.X., Horn, H., 2014. Aerobic sludge granulation in a full-scale sequencing batch reactor. BioMed Res. Int. 2014. Article ID 268789, 12 pages.

Li, L., Hartmann, G., Döblinger, M., Schuster, M., 2013. Quantification of nanoscale silver particles removal and release from municipal wastewater treatment plants in Germany. Environ. Sci. Technol. 47, 7317-7323.

Li, R., Zhang, Y., Lee, C.C., Lu, R., Huang, Y., 2010b. Development and validation of a hydrophilic interaction liquid chromatographic method for determination of aromatic amines in environmental water. J. Chromatogr. A 1217, 1799-1805.

Li, Y., Liu, Y., 2005. Diffusion of substrate and oxygen in aerobic granule. Biochem. Eng. J. 27, 45-52.

Li, Z.H., Kuba, T., Kusuda, T., 2006. Selective force and mature phase affect the stability of aerobic granule: An experimental study by applying different removal methods of sludge. Enzyme Microb. Technol. 39, 976-981.

Liang, Z., Atreyee, D., Zhiqiang H., 2010. Bacterial response to a shock load of nanosilver in an activated sludge treatment system. Water Res. 44, 5432-5438.

Libra, J.A., Borchert, M., Vigelahn, L., Storm, T., 2004. Two stage biological treatment of a diazo reactive textile dye and the fate of the dye metabolites. Chemosphere 56, 167-180.

Lin, Y.M., Nierop, K.G.J, Girbal-Neuhauser, E., Adriaanse, M., van Loosdrecht, M.C.M., 2015. Sustainable polysaccharide-based biomaterial recovered from waste aerobic granular sludge as a surface coating material. Sustainable Mater. Technol. 4, 24-29.

Liu, G., Wang, J., Lu, H., Jin, R., Zhou, J., Zhang, L., 2009. Effects of reduction products of *ortho*-hydroxyl substituted azo dyes on biodecolorization of azo dyes. J. Hazard Mater. 171, 222-229.

Liu, H., Li, Y., Yang, C., Pu, W., He, L., Bo, F., 2012. Stable aerobic granules in continuous-flow bioreactor with self-forming dynamic membrane. Bioresour. Technol. 121, 111-118.

Liu, J., Li, J., Tao, Y., Sellamuthu, B., Walsh, R., 2017a. Analysis of bacterial, fungal and archaeal populations from a municipal wastewater treatment plant developing an innovative aerobic granular sludge process. World J. Microbiol. Biotechnol. 33, 14-22.

Liu, J., Li, J., Wang, X., Zhang, Q., Littleton, H., 2017b. Rapid aerobic granulation in an SBR treating piggery wastewater by seeding sludge from a municipal WWTP. J. Environ. Sci., 51, 332-341.

Liu, J., Zhang, H., Zhang, P., Wu, Y., Gou, X., Song, Y., Tian, Z., Zeng, G., 2017c. Two-stage anoxic/oxic combined membrane bioreactor system for landfill leachate treatment: Pollutant removal performances and microbial community. Bioresour. Technol. 243, 738-746.

Liu, L., Li, W.W., Sheng, G.P., Liu, Z.F., Zeng, R.J., Liu, J.X., Yu, H.Q., Lee, D.J., 2010. Microscale hydrodynamic analysis of aerobic granules in the mass transfer process. Environ. Sci. Technol. 44, 7555-7560.

Liu, Y.-Q., Tay, J.-H., 2006. Variable aeration in sequencing batch reactor with aerobic granular sludge. J. Biotechnol. 124, 338-346.

Liu, Y.-Q., Tay, J.-H., 2007a. Influence of cycle time on kinetic behaviors of steady-state aerobic granules in sequencing batch reactors. Enzyme Microb. Technol. 41, 516-522.

Liu, Y.-Q., Tay, J.-H., 2007b. Cultivation of aerobic granules in a bubble column and an airlift reactor with divided draft tubes at low aeration rate. Biochem. Eng. J. 34, 1-7.

Liu, Y., Liu, Q.-S., 2006. Causes and control of filamentous growth in aerobic granular sludge sequencing batch reactors. Biotechnol. Adv. 24, 115-127.

Liu, Y., Tay, J.-H., 2004. State of the art of biogranulation technology for wastewater treatment. Biotechnol. Adv. 22, 533-563.

Liu, Y., Tay, J.H., 2002. The essential role of hydrodynamic shear force in the formation of biofilm and granular sludge. Water Res. 36, 1653-1665.

Liu, Y., Wang, Z.-W., Qin, L., Liu, Y.-Q., Tay, J.-H., 2005. Selection pressure-driven aerobic granulation in a sequencing batch reactor. Appl. Microbiol. Biotechnol. 67, 26-32.

Liu, Y., Yang, S.F., Tay, J.H., 2004. Improved stability of aerobic granules by selecting slow-growing nitrifying bacteria. J. Biotechnol. 108, 161-169.

Liu, Y.Q., Liu, Y., Tay, J.H., 2005. Relationship between size and mass transfer resistance in aerobic granules. Lett. Appl. Microbiol. 40, 312-315.

Liu, Y.Q., Moy, B., Kong, Y.H., Tay, J.H., 2010. Formation, physical characteristics and microbial community structure of aerobic granules in a pilot-scale sequencing batch reactor for real wastewater treatment. Enzyme Microb. Technol. 46, 520-525.

Liu, Y.Q., Tay, J.H., 2008. Influence of starvation time on formation and stability of aerobic granules in sequencing batch reactors. Bioresour. Technol. 99, 980-985.

Liu, Y.Q., Tay, J.H., 2015. Fast formation of aerobic granules by combining strong hydraulic selection pressure with overstressed organic loading rate. Water Res. 80, 256-266.

Long, B., Yang, C.-Z., Pu, W.-H., Yang, J.-K., Liu, F.-B., Zhang, L., Zhang, J., Cheng, K., 2015. Tolerance to organic loading rate by aerobic granular sludge in a cyclic aerobic granular reactor. Bioresour. Technol. 182, 314-322.

López-Palau, S., Pinto, A., Basset, N., Dosta, J., Mata-Álvarez, J., 2012. ORP slope and feast-famine strategy as the basis of the control of a granular sequencing batch reactor treating winery wastewater. Biochem. Eng. J. 68, 190-198.

Lotito, A.M., Di Iaconi, C., Lotito, V., 2012a. Physical characterisation of the sludge produced in a sequencing batch biofilter granular reactor. Water Res. 46, 5316-5326.

Lotito, A.M., Fration, U., Mancini, A., Bergna, G.,Di Iaconi, C., 2012b. Effective aerobic granular sludge treatment of a real dyeing textile wastewater. Int. Biodeterior. Biodegradation 69, 62-68.

Lotito, A.M., Sanctis, M.D., Di Iaconi, C., Bergna, G., 2014. Textile wastewater treatment: aerobic granular sludge *vs* activated sludge systems. Water Res. 54, 337-346.

Lourenço, N.D., Franca, R.D.G., Moreira, M.A., Gil, F.N., Viegas, C.A., Pinheiro, H.M., 2015. Comparing aerobic granular sludge and flocculent sequencing batch reactor technologies for textile wastewater treatment. Biochem. Eng. J. 104, 57-63.

Lourenço, N.D., Novais, J.M., Pinheiro, H.M., 2000. Reactive textile dye color removal in a sequencing batch reactor. Water Sci. Technol. 42, 321-328.

Lourenço, N.D., Novais, J.M., Pinheiro, H.M., 2001. Effect of some operational parameters on textile dye biodegradation in a sequential batch reactor. J. Biotechnol. 89, 163-174.

Lourenço, N.D., Novais, J.M., Pinheiro, H.M., 2003. Analysis of secondary metabolite fate during anaerobic-aerobic azo dye biodegradation in a sequential batch reactor. Environ. Technol. 24, 679-686.

Lourenço, N.D., Novais, J.M., Pinheiro, H.M., 2009. Treatment of colored textile wastewater in SBR with emphasis on the biodegradation of sulfonated aromatic amines. Water Pract. Tech. 4, 1-8.

Loza, K., Diendorf, J., Sengstock, C., Ruiz-Gonzalez, L., Gonzalez-Calbet, J. M., Vallet-Regi, M., Köller, M., Epple, M., 2014. The dissolution and biological effects of silver nanoparticles in biological media. J. Mater. Chem. B. 2, 1634-1643.

Luo, J., Hao, T., Wei, L., Mackey, H.R., Lin, Z., Chen, G.H., 2014. Impact of influent COD/N ratio on disintegration of aerobic granular sludge. Water Res. 62, 127-135.

Ma, D.-Y, Wang, X.-H., Song, C., Wang, S.-G., Fan, M.-H., Li, X.-M., 2011. Aerobic granulation for methylene blue biodegradation in a sequencing batch reactor. Desalination 276, 233-238.

Magoc, T., Salzberg, S.L., 2011. FLASH: fast length adjustment of short reads to improve genome assemblies. Bioinformatics 27, 2957-63.

Manavi, N., Kazemi, A.S., Bonakdarpour, B., 2017. The development of aerobic granules from conventional activated sludge under anaerobic-aerobic cycles and their adaptation for treatment of dyeing wastewater. Chem. Eng. J. 312, 375-384.

Manz, W., Amann, R., Ludwig, W., Wagner, M., 1992. Phylogenetic oligodeoxynucleotide probes for the major subclasses of *Proteobacteria*: problems and solutions. Syst. Appl. Microbiol. 15, 593-600.

Manz, W., Amann, R., Ludwig, W., Vancanneyt, M., Schleiferl, K., 1996. Application of a suite of 16s rRNA-specific oligonucleotide probes designed to investigate bacteria of the phylum cytophaga-flavobacteria-bacteroides in the natural environment. Microbiology 142, 1097-1106.

Martins, A.M.P., Heijnen, J.J., Van Loosdrecht, M.C.M., 2003. Effect of feeding pattern and storage on the sludge settleability under aerobic conditions. Water Res. 37, 2555-2570.

Maszenan, A.M., Liu, Y., Ng, W.J., 2011. Bioremediation of wastewaters with recalcitrant organic compounds and metals by aerobic granules. Biotechnol. Adv. 29, 111-123.

Mata, A.M.T., Pinheiro, H.M., Lourenço, N.D., 2015. Effect of sequencing batch cycle strategy on the treatment of a simulated textile wastewater with aerobic granular sludge. Biochem. Eng. J. 104, 106-114.

McIlroy, S., Seviour, R.J., 2009. Elucidating further phylogenetic diversity among the *Defluviicoccus*-related glycogen-accumulating organisms in activated sludge. Environ. Microbiol. Rep. 1, 563-568.

McIlroy, S.J., Saunders, A.M., Albertsen, M., Nierychlo, M., McIlroy, B., Hansen, A.A., Karst, S.M., Nielsen, J.L., Nielsen, P.H., 2015. MiDAS: the field guide to the microbes of activated sludge. Database (Oxford), bav062.

Meerbergen, K., Crauwels, S., Willems, K.A., Dewil, R., van Impe, J., Appels, L., Lievens, B., 2017. Decolorization of reactive azo dyes using a sequential chemical and activated sludge treatment. 124, 668-673.

Meier, H., Amann, R., Ludwig, W., Schleifer, K.H., 1999. Specific oligonucleotide probes for *in situ* detection of a major group of Gram-positive bacteria with low DNA G+C Content. Syst. Appl. Microbiol. 22, 186-196.

Mendes, S., Farinha, A., Ramos, C.G., Leitão, J.H., Viegas, C.A., Martins, L.O., 2011. Synergistic action of azoreductase and laccase leads to maximal decolourization and detoxification of model dye-containing wastewaters. Bioresour. Technol. 102, 9852-9859.

Meyer, R.L., Saunders, A.M., Blackall, L.L., 2006. Putative glycogen-accumulating organisms belonging to the Alphaproteobacteria identified through rRNA-based stable isotope probing. Microbiology 152, 419-429.

Mobarry, B.K., Wagner, M., Urbain, V., Rittman, B.E., Stahl, D.A., 1996. Phylogenetic probes for analyzing abundance and spatial organization of nitrifying bacteria. Appl. Environ. Microbiol. 62, 2156-2162.

Moghaddam, S.S., Moghaddam, M.R.A., 2015. Cultivation of aerobic granules under different pre-anaerobic reaction times in sequencing batch reactors. Sep. Purif. Technol. 142, 149-154.

Moghaddam, S.S., Moghaddam, M.R.A., 2016. Aerobic granular sludge for dye biodegradation in a sequencing batch reactor with anaerobic/aerobic cycles. CLEAN Soil Air Water 44, 438-443.

Molina-Guijarro, J.M., Pérez, J., Muñoz-Dorado, J., Guillén, F., Moya, R., Herńndez, M., Arias, M.E., 2009. Detoxification of azo dyes by a novel pH-versatile, salt-resistant laccase from Streptomyces ipomoea. Int. Microbiol. 12, 13-21.

Morgenroth, E., Sherden, T., van Loosdrecht, M.C.M., Heijnen, J.J., Wilderer, P.A., 1997. Aerobic granular sludge in a sequencing batch reactor. Water Res. 31, 3191-3194.

Morones, J.R., Elechiguerra, J.L., Camacho, A., Holt, K., Kouri, J.B., Ramirez, J.T., Yacaman, M.J., 2005. The bactericidal effect of silver nanoparticles. Nanotechnology 16, 2346-2353.

Mosquera-Corral, A., De Kreuk, M.K., Heijnen, J.J., Van Loosdrecht, M.C.M., 2005. Effects of oxygen concentration on N-removal in an aerobic granular sludge reactor. Water Res. 39, 2676-2686.

Mosquera-Corral, A., Montràs, A., Heijnen, J.J., Van Loosdrecht, M.C.M., 2003. Degradation of polymers in a biofilm airlift suspension reactor. Water Res. 37, 485-492.

Moy, B.Y.-P., Tay, J.-H., Toh, S.-K., Liu, Y., Tay, S.T.-L., 2002. High organic loading influences the physical characteristics of aerobic sludge granules. Lett. Appl. Microbiol. 34, 407-412.

Muda, K., Aris, A., Salim, M.R., Ibrahim, Z., Yahya, A., Van Loosdrecht, M.C., Ahmad, A., Nawahwi, M.Z., 2010. Development of granular sludge for textile wastewater treatment, Water Res. 44, 4341-4350.

Muda, K., Aris, A., Salim, M.R., Ibrahim, Z., van Loosdrecht, M.C.M., Ahmad, A., Nawahwi, M.Z., 2011. The effect of hydraulic retention time on granular sludge biomass in treating textile wastewater. Water Res. 45, 4711-4721.

Muda, K., Aris, A., Salim, M.R., Ibrahim, Z., Yahya, A., 2012. Textile Wastewater Treatment Using Biogranules Under Intermittent Anaerobic/Aerobic Reaction Phase. JWET 10, 303-315.

Muñoz-Palazon, B., Pesciaroli, C., Rodriguez-Sanchez, A., Gonzalez-Lopez, J., Gonzalez-Martinez, A., 2018. Pollutants degradation performance and microbial community structure of aerobic granular sludge systems using inoculums adapted at mild and low temperature. Chemosphere 204, 431-441.

Nadigera, G.S., 2001. Azo ban, eco-norms and testing. IJFTR 26, 55-60.

Nancharaiah, Y.V., Reddy, G.K.K., 2018. Aerobic granular sludge technology: mechanisms of granulation and biotechnological applications. Bioresour. Technol. 247, 1128-1143.

Neef, A., Zaglauer, A., Meier, H., Amann, R., Lemmer, H., Schleifer, K.H., 1996. Population Analysis in a Denitrifying Sand Filter: Conventional and In Situ Identification of Paracoccus spp. in Methanol-Fed Biofilms. Appl. Environ. Microbiol. 62, 4329-4339.

Nel, A.E., Mädler, L., Velegol, D., Xia, T., Hoek, E.M., Somasundaran, P., Klaessig, F., Castranova, V., Thompson, M., 2009. Understanding biophysicochemical interactions at the nano-bio interface. Nat. Mater. 8, 543-557.

Nguyen, H.T.T., Le, V.Q., Hansen, A.A., Nielsen, J.L., Nielsen, P.H., 2011. High diversity and abundance of putative polyphosphate-accumulating *Tetrasphaera*-related bacteria in activated sludge systems. FEMS Microbiol. Ecol. 76, 256-267.

Nimkar, U., 2018. Sustainable chemistry: A solution to the textile industry in a developing world. Curr. Opin. Green Sustainable Chem. 9, 13-17.

Nittami, T., McIlroy, S., Seviour, E.M., Schroeder, S., Seviour, R.J., 2009. Candidatus *Monilibacter* spp., common bulking filaments in activated sludge, are members of Cluster III *Defluviicoccus*. Syst. Appl. Microbiol. 32, 480-489.

Nemergut, D.R., Martin, A.P., Schmidt, S.K., 2004. Integron diversity in heavy-metal-contaminated mine tailings and inferences about integron evolution. Appl. Environ. Microbiol. 70, 1160-1168.

Nor-Anuar, A., Ujang, Z., Van Loosdrecht, M.C.M., De Kreuk, M.K., Olsson, G., 2012. Strength characteristics of aerobic granular sludge. Water Sci. Technol. 65, 309-316.

Nortemann, B., Baumgarten, J., Rast, H.G., Knackmuss, H.J., 1986. Bacterial communities degrading amino- and hydroxynaphthalene-2-sulfonates. Appl. Environ. Microbiol. 52, 1195-1202.

Nörtemann, B., Kuhm, A.E., Knackmuss, H.-J., Stolz, A., 1994. Conversion of substituted naphthalenesulfonates by *Pseudomonas* sp. BN6. Arch. Microbiol. 161, 320-327.

O'Neill, C., Hawkes, F.R., Hawkes, D.L., Lourenço, N.D., Pinheiro, H.M., Delée, W., 1999. Colour in textile effluents - sources, measurement, discharge consents and simulation: a review. J. Chem. Technol. Biotechnol. 74, 1009-1018.

O'Neill, C., Lopez, A., Esteves, S., Hawkes, F.R., Hawkes, D.L., Wilcox, S., 2000. Azo-dye degradation in an anaerobic-aerobic treatment system operating on simulated textile effluent. Appl. Microbiol. Biotechnol. 53, 249-254.

Oehmen, A., Lemos, P.C., Carvalho, G., Yuan, Z., Keller, J., Blackall, L.L., Reis, M.A., 2007. Advances in enhanced biological phosphorus removal: from micro to macro scale. Water Res. 41, 2271-2300.

Oliveira, C.S., Silva, C.E., Carvalho, G., Reis, M.A., 2017. Strategies for efficiently selecting PHA producing mixed microbial cultures using complex feedstocks: Feast and famine regime and uncoupled carbon and nitrogen availabilities. N. Biotechnol. 37, 69-79.

Ostle, A.G., Holt, J.G., 1982. Nile Blue A as a fluorescent stain for poly-beta-hydroxybutyrate. Appl. Environ. Microbiol. 44, 238.

Pandey, A., Singh, P., Iyengar, L., 2007. Bacterial decolorization and degradation of azo dyes. Int. Biodeterior. Biodegrad. 59, 73-84.

Panswad, T., Luangdilok, W., 2000. Decolorization of reactive dyes with different molecular structures under different environmental conditions. Water Res. 34, 4177-4184.

Paździor, K., Klepacz-smółka, A., Ledakowicz, S., Sójka-ledakowicz, J., Zyłła, R., 2009. Integration of nanofiltration and biological degradation of textile wastewater containing azo dye. Chemosphere 75, 250-255.

Pearce, C.I., Lloyd, J.R., Guthrie, J.T., 2003. The removal of colour from textile wastewater using whole bacterial cells: a review. Dyes Pigm. 58, 179-196.

Pearce, C.I., Christie, R., Boothman, C., Von Canstein, H., Guthrie, J.T., Lloyd, J.R., 2006. Reactive azo dye reduction by Shewanella Strain J18 143. Biotechnol. Bioeng. 95, 692-703.

Pereira, L., Mondal, P.K., Alves, M., 2015. Aromatic Amines Sources, Environmental Impact and Remediation. In: Lichtfouse, E., Schwarzbauer, J., Robert, D. (eds) Pollutants in Buildings, Water and Living Organisms. Environmental Chemistry for a Sustainable World, vol 7. Springer, Cham.

Pereira, R., Pereira, L., van der Zee, F.P., Alves, M.M., 2011. Fate of aniline and sulfanilic acid in UASB bioreactors under denitrifying conditions. Water Res. 45, 191-200.

Peretyazhko, T.S., Zhang, Q., Colvin, V.L., 2014. Size-Controlled dissolution of silver nanoparticles at neutral and acidic pH conditions: kinetics and size changes. Environ. Sci. Technol. 48, 11954-11961.

Perlatti, B., Fátima, M., Fernandes, J.B., Forim, M.R., 2012. Validation and application of HPLC – ESI-MS / MS method for the quantification of RBBR decolorization , a model for highly toxic molecules , using several fungi strains. Bioresour. Technol. 124, 37-44.

Peyong, Y.N., Zhou, Y., Abdullah, A.Z., Vadivelu, V., 2012. The effect of organic loading rates and nitrogenous compounds on the aerobic granules developed using low strength wastewater. Biochem. Eng. J. 67, 52-59.

Pijuan, M., Werner, U., Yuan, Z., 2009. Effect of long-term anaerobic and intermittent anaerobic/aerobic starvation on aerobic granules. Water Res. 43, 3622-3632.

Pinheiro, H.M., Touraud, E., Thomas, O., 2004. Aromatic amines from azo dye reduction: status review with emphasis on direct UV spectrophotometric detection in textile industry wastewaters. Dye. Pigment. 61, 121-139.

Prasad, A.S.A., Satyanarayana, V.S.V., Rao, K.V.B., 2013. Biotransformation of Direct Blue 1 by a moderately halophilic bacterium Marinobacter sp. Strain HBRA and toxicity assessment of degraded metabolites. J. Hazard. Mater., 262, 674-684.

Prauser, H., Lechevalier, M.P., Lechevalier, H., 1970. Description of *Oerskovia* gen. n. to harbor ørskov's motile Nocardia. Appl. Microbiol. 19, 534.

Pronk, M., Abbas, B., Al-zuhairy, S.H.K., Kraan, R., Kleerebezem, R., van Loosdrecht, M.C.M., 2015a. Effect and behavior of different substrates in relation to the formation of aerobic granular sludge. Appl. Microbiol. Biotechnol. 99, 5257-5268.

Pronk, M., de Kreuk, M.K., de Bruin, B., Kamminga, P., Kleerebezem, R., van Loosdrecht, M.C.M., 2015b. Full-scale performance of the aerobic granular sludge process for sewage treatment. Water Res. 84, 207-217.

Quan, X., Cen, Y., Lu, F., Gu, L., Ma, J., 2015. Response of aerobic granular sludge to the long-term presence to nanosilver in sequencing batch reactors: Reactor performance, sludge property, microbial activity and community. Sci. Total Environ. 506-507, 226-233.

R Core Team, 2015. R: A language and environment for statistical computing.

Radetić, M., 2013. Functionalization of textile materials with silver nanoparticles. J. Mater. Sci. 48, 95-107.

Rajeswari, K., Subashkumar, R., Vijayaraman, K., 2011. Biodegradation of mixed textile dyes by bacterial strains isolated from dyewaste effluent. RJET 5, 97-107.

Raman, C.D., Kanmani, S., 2016. Textile dye degradation using nano zero valent iron: A review. J. Environ. Manage. 177, 341-355.

Ramos, C., Suárez-Ojeda, M.E., Carrera, J., 2016. Long-term performance and stability of a continuous granular airlift reactor treating a high-strength wastewater containing a mixture of aromatic compounds. J. Hazard. Mater. 303, 154-161.

Rangabhashiyam, S., Anu, N., Selvaraju, N., 2013. Sequestration of dye from textile industry wastewater using agricultural waste products as adsorbents. J. Environ. Chem. Eng. 1, 629-641.

Rasool, K., Shahzad, A., Lee, D.S., 2016. Exploring the potential of anaerobic sulfate reduction process in treating sulfonated diazo dye: Microbial community analysis using bar-coded pyrosequencing. J. Hazard. Mater. 318, 641-649.

Razo-Flores, E., Luijten, M., Donlon, B., Lettinga, G., Field, J., 1997. Biodegradation of selected azo dyes under methanogenic conditions. Water Sci. Technol. 36, 65-72.

Rawat, D., Mishra, V., Sharma, R.S., 2016. Detoxification of azo dyes in the context of environmental processes. Chemosphere 155, 591-605.

Reemtsma, T., 1996. Methods of analysis of polar aromatic sulfonates from aquatic environments. J. Chromatogr. A 733, 473-489.

Reemtsma, T., 2003. Liquid chromatography-mass spectrometry and strategies for trace-level analysis of polar organic pollutants. J. Chromatogr. 1000, 477-501.

Reddy, G.K.K., Nancharaiah, Y.V., Venugopalan, V.P., 2014. Biodegradation of dibutyl phosphite by Sphingobium sp. AMGD5 isolated from aerobic granular biomass. Int. Biodeterior. Biodegrad. 91, 60-65.

Reichert, P., 1995. AQUASIM - A tool for simulation and data analysis of aquatic systems. Water Sci. Technol. 30, 21-30.

Ren, T.T., Liu, L., Sheng, G.P., Liu, X.W., Yu, H.Q., Zhang, M.C., Zhu, J.R., 2008. Calcium spatial distribution in aerobic granules and its effects on granule structure, strength and bioactivity. Water Res. 42, 3343-3352.

Rezić, I., 2011. Determination of engineered nanoparticles on textiles and in textile wastewaters. Trends Anal. Chem. 30, 1159-1167.

Rocktäschel, T., Klarmann, C., Helmreich, B., Ochoa, J., Boisson, P., Sørensen, K.H., Horn, H., 2013. Comparison of two different anaerobic feeding strategies to establish a stable aerobic granulated sludge bed. Water Res. 47, 6423-6431.

Rollemberg, S.L.S., Barros, A.R.M., Milen Firmino, P.I., dos Santos, A.B. 2018. Aerobic granular sludge: cultivation parameters and removal mechanisms. Bioresour. Technol. 270, 678-688.

Roller, C., Wagner, M., Amann R., Ludwig, W., 1994. *In situ* probing of Gram-positive bacteria with high DNA G+C content using 23S r-RNA-targeted oligonucleotides. Microbiology 140, 2849-2858.

Rostami-Vartooni, A., Nasrollahzadeh, M., Salavati-Niasari, M., Atarod, M., 2016. Photocatalytic degradation of azo dyes by titanium dioxide supported silver nanoparticles prepared by a green method using Carpobrotus acinaciformis extract. J. Alloy. Comp. 689, 15-20.

Roşu, M., Socaci, C., Floare-Avram, V., Borodi, G., Pogăcean, F., Coroş, M., Măgeruşan, L., Pruneanu, S., 2016. Photocatalytic performance of graphene/TiO2-Ag composites on amaranth dye degradation. Mater. Chem. Phys. 179, 232-241.

Sánchez, M.D.N., Santos, P.M., Sappó, C.P., Pavón, J.L.P., Cordero, B.M., 2014. Microextraction by packed sorbent and salting-out-assisted liquid-liquid extraction for the determination of aromatic amines formed from azo dyes in textiles. Talanta 119, 375-384.

Saratale, R.G., Gandhi, S.S., Purankar, M.V., Kurade, M.B., Govindwar, S.P., Oh, S.E., Saratale, G.D., 2013. Decolorization and detoxification of sulfonated azo dye C.I. Remazol Red and textile effluent by isolated *Lysinibacillus* sp. RGS. J. Biosci. Bioeng. 115, 658-667.

Saratale, R.G., Saratale, G.D., Chang, J.S., Govindwar, S.P., 2011. Bacterial decolorization and degradation of azo dyes: A review. J. Taiwan Inst. Chem. Eng. 42, 138-157.

Saravanan, C., Rajesh, R., Kaviarasan, T., 2017. Synthesis of silver nanoparticles using bacterial exopolysaccharide and its application for degradation of azo-dyes. Biotechnol. Rep., 15, 33-40.

Sarayu, K., Sandhya, S., 2012. Current technologies for biological treatment of textile wastewater - a review, Appl Biochem Biotechnol. 167, 645-661.

Sarvajith, M., Reddy, G.K.K., Nancharaiah Y., 2018. Textile dye biodecolourization and ammonium removal over nitrite in aerobic granular sludge sequencing batch reactors. J. Hazard Mater. 342, 536-543.

Saunders, A.M., Albertsen, M., Vollertsen, J., Nielsen, P.H., 2015. The activated sludge ecosystem contains a core community of abundant organisms. ISME J. 10, 11-20.

Schwarzenbeck, N., Borges, J.M., Wilderer, P.A., 2005. Treatment of dairy effluents in an aerobic granular sludge sequencing batch reactor. Appl. Microbiol. Biotechnol. 66, 711-718.

Sen, S.K., Raut, S.,Bandyopadhyaya, P., Raut, S., 2016. Fungal decolouration and degradation of azo dyes: A review. Fungal Biol. Rev. 30, 112-133.

Seviour, T., Yuan, Z., van Loosdrecht, M.C.M., Lin, Y., 2012. Aerobic sludge granulation: A tale of two polysaccharides? Water Res. 46, 4803-4813.

Seymour, E.H., Lawrence, N.S., Pandurangappa, M., Compton, R.G., 2002. Indirect electrochemical detection of nitrite via diazotization of aromatic amines. Microchim. Acta 140, 211-217.

Sguanci, S., Lubello, C., Caffaz, S., Lotti, T., 2019. Long-term stability of aerobic granular sludge for the treatment of very low-strength real domestic wastewater. J. Clean Prod. 222, 882-890.

Shaw, C.B., Carliell, C.M., Wheatley, A.D., 2002. Anaerobic/aerobic treatment of coloured textile effluents using sequencing batch reactors. Water Res. 36, 1993-2001.

Shafer, M.M., Overdier, J.T., Armstong, D.E., 2009. Removal, partitioning, and fate of silver and other metals in wastewater treatment plants and effluent-receiving streams. Environ. Toxicol. Chem. 17, 630-641.

Sheng, G.-P., Yu, H.-Q., Li, X.-Y., 2010. Extracellular polymeric substances (EPS) of microbial aggregates in biological wastewater treatment systems: A review. Biotechnol. Adv. 28, 882-894.

Sheng, Z., Liu, Y., 2011. Effects of silver nanoparticles on wastewater biofilms. Water Res. 45, 6039-6050.

Sheng, Z., Van Nostrand, J.D., Zhou, J., Liu, Y., 2015. The effects of silver nanoparticles on intact wastewater biofilms. Front. Microbiol. 6, article 680.

Sheng, Z.Y., Liu, Y., 2017. Potential impacts of silver nanoparticles on bacteria in the aquatic environment. J. Environ. Manage. 191, 290-296.

Sheng, Z.W., Nostrand, J.D.V., Zhou, J.Z., Liu, Y., 2018. Contradictory effects of silver nanoparticles on activated sludge wastewater treatment. J. Hazard. Mater. 341, 448-456.

Show, K.Y., Lee, D.J., Tay, J.H., 2012. Aerobic granulation: Advances and challenges. Appl. Biochem. Biotechnol. 167, 1622-1640.

Silva, L.P., Silveira, A.P., Bonatto, C.C., Reis, I.G., Milreu, P.V., 2017. Silver Nanoparticles as Antimicrobial Agents: Past, Present, and Future. Nanostructures for Antimicrobial Therapy, 577-596.

Singh, R.L., Singh, P.K., Singh, R.P., 2015. Enzymatic decolorization and degradation of azo dyes – A review. Int. Biodeterior. Biodegradation 104, 21-31.

Solís, M., Solís, A., Pérez, H.I., Manjarrez, N., Flores, M., 2012. Microbial decolouration of azo dyes: a review. Process Biochem. 47, 1723-1748.

Somasiri, W., Li, X.-F., Ruan, W.-Q., Jian, C., 2008. Evaluation of the efficacy of upflow anaerobic sludge blanket reactor in removal of colour and reduction of COD in real textile wastewater. Bioresour Technol. 99, 3692-3699.

Song, D., Zhang, W., Liu, C., Wang, P., Sun, Z., Zhao, L., Zhai, X., Qi, J., Ma, J., 2018. Development of a novel anoxic/oxic fed-batch membrane bioreactor (AFMBR) based on gravity-driven and partial aeration modes: A pilot scale study. Bioresour. Technol. 270, 255-262.

Sousa, A.C., Oliveira, M.C., Martins, L.O., Robalo, M.P., 2014. Towards the rational biosynthesis of substituted phenazines and phenoxazinones by laccases. Green Chem. 16, 4127-4136.

Spagni, A., Grilli, S., Casu, S., Mattioli, D., 2010. Treatment of a simulated textile wastewater containing the azo-dye reactive orange 16 in an anaerobic-biofilm anoxic-aerobic membrane bioreactor. Int. Biodeterior. Biodegrad. 64, 676-681.

Sponza, D.T., Işık, M., 2002. Decolorization and azo dye degradation by anaerobic/aerobic sequential process. Enzyme Microb. Technol. 31, 102-110.

Sponza, D.T., Işık, M., 2005a. Reactor performances and fate of aromatic amines through decolorization of Direct Black 38 dye under anaerobic/aerobic sequentials. Process Biochem. 40, 35-44.

Sponza, D.T., Işik, M., 2005b. Toxicity and intermediates of C.I. Direct Red 28 dye through sequential anaerobic/aerobic treatment. Process Biochem. 40, 2735-2744.

Stahl, D.A., Amann, R., 1991. Development and application of nucleic acid probes in bacterial systematics, 205-248. In: Stackebrandt, E. and Goodfellow, M. (Ed.), Nucleic acid techniques in bacterial systematics, John Wiley & Sons Ltd., Chichester.

Stolz, A. 2001. Basic and applied aspects in the microbial degradation of azo dyes. Appl. Microbiol. Biotechnol. 56, 69-80.

Stolz, A., Knackmuss, H.J., 1993. Bacterial metabolism of 5-aminosalicylic acid enzymic conversion to L-malate, pyruvate and ammonia. J. Gen. Microbiol. 139, 1019-1025.

Sturm, B.S.M., Irvine, R.L., 2008. Dissolved oxygen as a key parameter to aerobic granule formation. Water Sci. Technol. 58, 781-787.

Suja, E., Nancharaiah, Y.V., Venugopalan, V.P., 2014. Biogenic nanopalladium production by self-immobilized granular biomass: application for contaminant remediation. Water Res. 65, 395-401.

Sun, H., Narihiro, T., Ma, X., Zhang, X.X., Ren, H., Ye, L., 2019. Diverse aromatic-degrading bacteria present in a highly enriched autotrophic nitrifying sludge. Sci. Total Environ. 666, 245-251.

Sun, T.Y., Gottschalk, F., Hungerbuhler, K., Nowack, B., 2014. Probabilistic modelling of engineered nanomaterial emissions to the environment: a spatio-temporal approach. Environ. Poll. 185, 69-76.

Sutthivaiyakit, P., Achatz, S., Lintelmann, J., Aungpradit, T., Chanwirat, R., Chumanee, S., Kettrup, A., 2005. LC-MS/MS method for the confirmatory determination of aromatic amines and its application in textile analysis. Anal. Bioanal. Chem. 381, 268-276.

Tamura, D., Peterson, N., Peterson, G., Stecher, M., Kumar, N.S., 2011. MEGA5: molecular evolutionary genetics analysis using maximum likelihood, evolutionary distance, and maximum parsimony methods. Mol. Biol. Evol. 28, 2731-2739.

Tan, N.C.G., Lettinga, G., Field, J.A., 1999a. Reduction of the azo dye Mordant Orange 1 by methanogenic granular sludge exposed to oxygen. Bioresour. Technol. 67, 35-42.

Tan, N.C.G., Prenafeta-Boldú, F.X., Opsteeg, J.L., Lettinga, G., Field, J.A., 1999b. Biodegradation of azo dyes in cocultures of anaerobic granular sludge with aerobic aromatic amine degrading enrichment cultures. Appl. Microbiol. Biotechnol. 51, 865-871.

Tan, N.C.G., Slenders, P., Svitelskaya, A., Lettinga, G., Field, J.A., 2000. Degradation of azo dye Mordant Yellow 10 in a sequential anaerobic and bioaugmented aerobic bioreactor. Water Sci. Technol. 42, 337-344.

Tan, N.C.G., Van Leeuwen, A., Van Voorthuizen, E.M., Slenders, P., Prenafeta-Boldú, F.X., Temmink, H., Lettinga, G., Field, J.A., 2005. Fate and biodegradability of sulfonated aromatic amines. Biodegradation 16, 527-537.

Tay, J.-H., Ivanov, V., Pan, S., Tay, S.T.L., 2002. Specific layers in aerobically grown microbial granules. Lett. Appl. Microbiol. 34, 254-257.

Tay, J.-H., Liu, Q.-S., Liu, Y., 2001a. Microscopic observation of aerobic granulation in sequential aerobic sludge blanket reactor. J. Appl. Microbiol. 91, 168-175.

Tay, J.-H., Liu, Q.-S., Liu, Y., 2001b. The effects of shear force on the formation, structure and metabolism of aerobic granules. Appl. Microbiol. Biotechnol. 57, 227-233.

Tay, J.-H., Liu, Q.-S., Liu, Y., 2001c. The role of cellular polysaccharides in the formation and stability of aerobic granules. Lett. Appl. Microbiol. 33, 222-226.

Tay, S.T.-L., Moy, B.Y.-P., Jiang, H.-L., Tay, J.-H., 2005. Rapid cultivation of stable aerobic phenol-degrading granules using acetate-fed granules as microbial seed. J. Biotechnol. 115, 387-395.

Toh, S.K., Tay, J.H., Moy, B.Y.P., Ivanov, V., Tay, S.T.L., 2003. Size-effect on the physical characteristics of the aerobic granule in a SBR. Appl. Microbiol. Biotechnol. 60, 687-95.

Val del Río, A., Figueroa, M., Mosquera-Corral, A., Campos, J.L., Méndez, R., 2013. Stability of Aerobic Granular Biomass Treating the Effluent from A Seafood Industry. Environ. Res. 7, 265-276.

Vajnhandl, S., Valh, J.V., 2014. The status of water reuse in European textile sector. J. Environ. Manage. 141, 29-35.

van der Zee, F.P., Cervantes, F.J., 2009. Impact and application of electron shuttles on the redox (bio)transformation of contaminants: a review. Biotechnol. Adv. 27, 256-277.

van der Zee, F.P., Villaverde, S., 2005. Combined anaerobic-aerobic treatment of azo dyes - a short review of bioreactor studies. Water Res. 39, 1425-1440.

van Loosdrecht, M.C.M., Pot, M.A., Heijnen, J.J., 1997. Importance of bacterial storage polymers in bioprocesses. Water Sci. Technol. 35, 41-47.

Varadavenkatesan, T., Selvaraj, R., Vinayagam, R., 2016. Phyto-synthesis of silver nanoparticles from Mussaendaerythrophylla leaf extract and their application in catalytic degradation of methyl orange dye. J. Mol. Liq. 221, 1063-1070.

Verma, A.K., Dash, R.R., Bhunia, P., 2012. A review on chemical coagulation/flocculation technologies for removal of colour from textile wastewaters. J. Environ. Manage. 93, 154-168.

Verawaty, M., Tait, S., Pijuan, M., Yuan, Z., Bond, P.L., 2013. Breakage and growth towards a stable aerobic granule size during the treatment of wastewater. Water Res. 47, 5338-5349.

Voelker, D., Schlich, K., Hohndorf, L., Koch, W., Kuehnen, U., Polleichtner, C., Kussatz, C., Hund-Rinke, K., 2015. Approach on environmental risk assessment of nanosilver released from textiles. Environ. Res. 140, 661-672.

Wan, C., Yang, X., Lee, D.J., Wang, X.Y., Yang, Q., Pan, X., 2014. Aerobic granulation of aggregating consortium X9 isolated from aerobic granules and role of cyclic di-GMP. Bioresour. Technol. 152, 557-561.

Wan, C., Zhang, P., Lee, D.J., Yang, X., Liu, X., Sun, S., Pan, X., 2013. Disintegration of aerobic granules: Role of second messenger cyclic di-GMP. Bioresour. Technol. 146, 330-335.

Wan, J., Mozo, I., Filali, A., Liné, A., Bessière, Y., Spérandio, M., 2011. Evolution of bioaggregate strength during aerobic granular sludge formation. Biochem. Eng. J. 58-59, 69-78.

Wan, J., Sperandio, M., 2009. Possible role of denitrification on aerobic granular sludge formation in sequencing batch reactor. Chemosphere 75, 220-227.

Wang, H., Zheng, X.W., Su, J.Q., Tian, Y., Xiong, X.J., Zheng, T.L., 2009. Biological decolorization of the reactive dyes Reactive Black 5 by a novel isolated bacterial strain *Enterobacter* sp. EC3. J. Hazard. Mater. 171, 654-659.

Wang, Q., Garrity, G.M., Tiedje, J.M., Cole, J.R., 2007a. Naive Bayesian classifier for rapid assignment of rRNA sequences into the new bacterial taxonomy. Appl. Environ. Microbiol. 73, 5261-7.

Wang, X., Oehmen, A., Freitas, E.B., Carvalho, G., Reis, M.A., 2017. The link of feast-phase dissolved oxygen (DO) with substrate competition and microbial selection in PHA production. Water Res. 112, 269-278

Wang, X.C., Chen, Z.L., Kang, J., Zhao, X., Shen, J.M., Yang, L., 2018a. The key role of inoculated sludge in fast start-up of sequencing batch reactor for the domestication of aerobic granular sludge. J. Environ. Sci. 78, 127-136.

Wang, X.H., Zhang, H.M., Yang, F.L., Xia, L.P., Gao, M.M., 2007b. Improved stability and performance of aerobic granules under stepwise increased selection pressure. Enzyme Microb. Technol. 41, 205-211.

Wang, X.H., Zhang, H.M., Yang, F.L., Wang, Y.F., Gao, M.M., 2008a. Long-term storage and subsequent reactivation of aerobic granules. Bioresource Technol. 99, 8304-8309.

Wang, X.Z., Cheng, X., Sun, D., Hong, Q., 2008b. Biodecolorization and partial mineralization of reactive black 5 by a strain of Rhodopseudomonas palustris. J. Environ. Sci. 20, 1218-1225

Wang, Y., Pan, Y., Zhu, T., Wang, A., Lu, Y., Lv, L., Zhang, K., Li, Z., 2018b. Enhanced performance and microbial community analysis of bioelectrochemical system integrated with bio-contact oxidation reactor for treatment of wastewater containing azo dye. Sci. Total Environ. 634, 616-627.

Wang, Z.W., Li, Y., Zhou, J.Q., Liu, Y., 2006. The influence of short-term starvation on aerobic granules. Process Biochem. 41, 2373-2378.

Wang, Z.W., Liang, J.S., Liang, Y., 2013. Decolorization of Reactive Black 5 by a newly isolated bacterium *Bacillus* sp. YZU1. Int. Biodeterior. Biodegrad. 76, 41-48.

Ward, D.V., Gevers, D., Giannoukos, G., Earl, A.M., Methé, B.A., Sodergren, E., *et al*., 2012. Evaluation of 16s rDNA-based community profiling for human microbiome research. PLoS ONE 7, e39315.

Weber, S.D., Hofmann, A., Pilhofer, M., Wanner, G., Agerer, R., Ludwig, W., Schleifer, K.H., Fried, J., 2009. The diversity of fungi in aerobic sewage granules assessed by 18S rRNA gene and ITS sequence analyses. FEMS Microbiol. Ecol. 68, 246-254.

Wei, D., Wang, B.F., Ngo, H.H., Guo, W.S., Han, F., Wang, X.D., Du, B., Wei, Q., 2015. Role of extracellular polymeric substances in biosorption of dye wastewater using aerobic granular sludge. Bioresour. Technol. 185, 14-20.

Weissbrodt, D.G., Neu, T.R., Kuhlicke, U., Rappaz, Y., Holliger, C., 2013. Assessment of bacterial and structural dynamics in aerobic granular biofilms. Front. Microbiol. 4, 1-18.

Weon, H.Y., Yoo, S.H., Kim, B.Y., Son, J.A., Kim, Y.J., Kwon, S.W., 2009. Niabella ginsengisoli sp. nov., isolated from soil cultivated with Korean ginseng. Int. J. Syst. Evol. Microbiol. 59, 1282-1285.

Whiteley, C.G., Lee, D.-J., 2015. Bacterial diguanylate cyclases: Structure, function and mechanism in exopolysaccharide biofilm development. Biotechnol. Adv. 33, 124-141.

Windler, L., Height, M., Nowack, B., 2013. Comparative evaluation of antimicrobials for textile applications. Environ. Int. 53, 62-73.

Winkler, M.-K.H., Bassin, J.P., Kleerebezem, R., de Bruin, L.M.M., van den Brand, T.P.H., van Loosdrecht, M.C.M., 2011. Selective sludge removal in a segregated aerobic granular biomass system as a strategy to control PAO-GAO competition at high temperatures. Water Res. 45, 3291-3299.

Winkler, M.-K.H., Kleerebezem, R., de Bruin, L.M.M., Verheijen, P.J.T., Abbas, B., Habermacher, J., van Loosdrecht, M.C.M., 2013. Microbial diversity differences within aerobic granular sludge and activated sludge flocs. Appl. Microbiol. Biotechnol. 97, 7447-7458.

Winkler, M.-K.H., Kleerebezem, R., Khunjar, W.O., de Bruin, B., van Loosdrecht, M.C.M., 2012. Evaluating the solid retention time of bacteria in flocculent and granular sludge. Water Res. 46, 4973-4980.

Winkler, M.-K.H., Meunier, C., Henriet, O., Mahillon, J., Suárez-Ojeda, M.E., Del Moro, G., De Sanctis, M., Di Iaconi, C., Weissbrodt, D.G., 2018. An integrative review of granular sludge for the biological removal of nutrients and recalcitrant organic matter from wastewater. Chem. Eng. J. 336, 489-502.

Wintzingerode, F. Von, Go, U.B., Siddiqui, R.A., Schumann, P., Fru, A., Rohde, M., 2001. *Salana multivorans* gen . nov ., sp . nov ., a novel actinobacterium isolated from an anaerobic bioreactor and capable of selenate reduction. Int. J. Syst. Evol. Microbiol. 51, 1653-1661.

Wong, M.-T., Tan, F.M., Ng, W.J., Liu, W.-T., 2004. Identification and occurrence of tetrad-forming *Alphaproteobacteria* in anaerobic-aerobic activated sludge processes. Microbiology 150, 3741-3748.

Wu, D., Zhang, Z., Yu, Z., Zhu, L., 2018a. Optimization of F/M ratio for stability of aerobic granular process via quantitative sludge discharge. Bioresour Technol. 252, 150-156.

Wu, J., Zhu, G., Yu, R., 2018b. Fates and Impacts of Nanomaterial Contaminants in Biological Wastewater Treatment System: a Review. Water Air Soil Pollut. 229, 1-21.

Xiao, Y., Wiesner, M.R., 2013. Transport and retention of selected engineered nanoparticles by porous media in the presence of a biofilm. Environ. Sci. Technol. 47, 2246-2253.

Xiong, Y., Liu, Y., 2013. Importance of extracellular proteins in maintaining structural integrity of aerobic granules. Colloids Surf B Biointerfaces 112, 435-440.

Yang, F., Bian, Z., Li, Z., Fan, Z., Wang, Y., Liu, S.S., Deng, H., Tang, G., 2016. Determination of aromatic amines released from azo dyes in paper packaging by liquid chromatography-tandem mass spectrometry. J. AOAC Int. 99, 1370-1376.

Yang, Q., Wang, J., Wang, H., Chen, X., Ren, S., Li, X., Xu, Y., Zhang, H., Li, X., 2012. Evolution of the microbial community in a full-scale printing and dyeing wastewater treatment system. Bioresour. Technol. 117, 155-163.

Yang, Y., Quensen, J., Mathieu, J., Wang, Q., Wang, J., Li, M.Y., Tiedje, J.M., Alvarez, P.J.J., 2014. Pyrosequencing reveals higher impact of silver nanoparticles than Ag+ on the microbial community structure of activated sludge. Water Res. 48, 317-325.

Yazdi, A.S., Es'haghi, Z., 2005. Two-step hollow fiber-based, liquid-phase microextraction combined with high-performance liquid chromatography: A new approach to determination of aromatic amines in water. J. Chromatogr. A 1082, 136-142.

You, S.J., Teng, J.Y., 2009. Performance and dye-degrading bacteria isolation of a hybrid membrane process. J. Hazard. Mater. 172, 172-179.

Yu, L., Zhang, X.Y., Wang, S., Tang, Q.W., Xie, T., Lei, N.Y., Chen, Y.L., Qiao, W.C., Li, W.W., Lam, M.H.W., 2015. Microbial community structure associated with treatment of azo dye in a start-up anaerobic sequenced batch reactor. J. Taiwan Inst. Chem. Eng. 54, 118-124.

Yu, S., Yin, Y., Zhou, X., Dong, L., Liu, J., 2016. Transformation kinetics of silver nanoparticles and silver ions in aquatic environments revealed by double stable isotope labeling. Environ. Sci. Nano. 3, 883-893.

Yuan, Q., Gong, H., Xi, H., Xu, H., Jin, Z., Ali, N., Wang, K., 2019. Strategies to improve aerobic granular sludge stability and nitrogen removal based on feeding mode and substrate. J. Environ. Sci. 84, 144-154.

Yuan, Z., Yang, X., Hu, A., Yu, C., 2015. Long-term impacts of silver nanoparticles in an anaerobic-anoxic-oxic membrane bioreactor system. Chem. Eng. J., 276, 83-90.

Yurtsever, A., Calimlioglu, B., Sahinkaya, E., 2017. Impact of SRT on the efficiency and microbial community of sequential anaerobic and aerobic membrane bioreactors for the treatment of textile industry wastewater. Chem. Eng. J. 314, 378-387.

Zero Discharge of Hazardous Chemicals Programme (ZDHC), 2015. Textile Industry Wastewater Discharge Quality Standards, 80-84.

Zhang, C., Hu, Z., Li, P., Gajaraj, S., 2016a. Governing factors affecting the impacts of silver nanoparticles on wastewater treatment. Sci. Total Environ. 572, 852-873.

Zhang, C., Liang, Z., Hu, Z., 2014. Bacterial response to a continuous long-term exposure of silver nanoparticles at sub-ppm silver concentrations in a membrane bioreactor activated sludge system. Water Res. 50, 350-358.

Zhang, C., Zhang, H., Yang, F., 2015. Diameter control and stability maintenance of aerobic granular sludge in an A/O/A SBR. Sep. Purif. Technol. 149, 362-369.

Zhang, H., Dong, F., Jiang, T., Wei, Y., Wang, T., Yang, F., 2011. Aerobic granulation with low strength wastewater at low aeration rate in A/O/A SBR reactor. Enzyme Microb. Technol. 49, 215-222.

Zhang, J., Feng, M., Jiang, Y., Hu, M., Li, S., Zhai, Q., 2012. Efficient decolorization/degradation of aqueous Azo Dyes using buffered H2O2 oxidation catalyzed by a dosage below ppm level of chloroperoxidase. Chem. Eng. J. 191, 236-242.

Zhang, L., Feng, X., Zhu, N., Chen, J., 2007. Role of extracellular protein in the formation and stability of aerobic granules. Enzyme Microb. Technol. 41, 551-557.

Zhang, Q., Hu, J., Lee, D.-J., 2016b. Aerobic granular processes: Current research trends. Bioresour. Technol. 210, 1-7.

Zhang, W., Xiao, B., Fang, T., 2018a. Chemical transformation of silver nanoparticles in aquatic environments: mechanism, morphology and toxicity. Chemosphere 191, 324-334.

Zhang, X., Chen, A., Zhang, D., Kou, S., Lu, P., 2018b. The treatment of flowback water in a sequencing batch reactor with aerobic granular sludge: Performance and microbial community structure. Chemosphere 211, 1065-1072.

Zhang, Y., Li, J., Li, W., Chen, G., 2016c. Utilization of inactivated aerobic granular sludge as a potential adsorbent for the removal of sunset yellow FCF. Desalin. Water Treat. 57, 7334-7344.

Zhang, Z.Z., Cheng, Y.F., Xu, L.Z.J., Bai, Y.H., Jin, R.C., 2018c. Anammox granules show strong resistance to engineered silver nanoparticles during long-term exposure. Bioresour. Technol. 259, 10-17.

Zhang, Z., Ji, Y., Cao, R., Yu, Z., Xu, X., Zhu, L., 2019. A novel mode of air recycling favored stable operation of the aerobic granular sludge process via calcium accumulation. Chem. Eng. J. 371, 600-608.

Zheng, Y.M., Yu, H.Q., 2007. Determination of the pore size distribution and porosity of aerobic granules using size-exclusion chromatography. Water Res. 41, 39-46.

Zheng, Y.M., Yu, H.Q., Liu, S.J., Liu, X.Z., 2006. Formation and instability of aerobic granules under high organic loading conditions. Chemosphere 63, 1791-1800.

Zheng, Y.M., Yu, H.Q., Sheng G.P., 2005. Physical and chemical characteristics of granular activated sludge from a sequencing batch airlift reactor. Process Biochem. 40, 645-650.

Zhong, C., Wang, Y., Li, Y., Lv, J., Hao, W., Zhu, J., 2014. The characteristic and comparison of denitrification potential in granular sequence batch reactor under different mixing conditions. Chem. Eng. J. 240, 589-594.

Zhou, H., Xu, G., 2019. Effect of silver nanoparticles on an integrated fixed-film activated sludge–sequencing batch reactor: Performance and community structure. J. Environ. Sci. 80, 229-239.

Zhou, J.H., Zhang, Z.M., Zhao, H., Yu, H.T., Alvarez, P.J.J., Xu, X.Y., Zhu, L., 2016. Optimizing granules size distribution for aerobic granular sludge stability: Effect of a novel funnel-shaped internals on hydraulic shear stress. Bioresour. Technol. 216, 562-570.

Zhu, J., Wilderer, P.A., 2003. Effect of extended idle conditions on structure and activity of granular activated sludge. Water Res. 37, 2013-2018.

Zhu, L., Lv, M.L., Dai, X., Yu, Y.W., Qi, H.Y., Xu, X.Y., 2012. Role and significance of extracellular polymeric substances on the property of aerobic granule. Bioresour. Technol. 107, 46-54.

Zhu, L., Lv, M.L., Dai, X., Zhou, J.H., Xu, X.Y., 2013a. The stability of aerobic granular sludge under 4-chloroaniline shock in a sequential air-lift bioreactor (SABR). Bioresour. Technol. 140, 126-130.

Zhu, L., Tay, C.B., Lee, H.K., 2002. Liquid-liquid-liquid microextraction of aromatic amines from water samples combined with high-performance liquid chromatography. J. Chromatogr. A 963, 231-237.

Zhu, L., Xu, X., Luo., W., Cao, D., Yang, Y., 2008. Formation and microbial community analysis of chloroanilines-degrading aerobic granules in the sequencing airlift bioreactor. J. Appl. Microb. 104, 152-160.

Zhu, L., Yu, Y., Dai, X., Xu, X., Qi, H., 2013b. Optimization of selective sludge discharge mode for enhancing the stability of aerobic granular sludge process. Chem. Eng. J. 217, 442-446.

Zhu, L., Zhou, J., Lv, M., Yu, H., Zhao, H., Xu, X., 2015. Specific component comparison of extracellular polymeric substances (EPS) in flocs and granular sludge using EEM and SDS-PAGE. Chemosphere 121, 26-32.

Zhu, Y., Xu, J., Cao, X., Cheng, Y., Zhu, T., 2018. Characterization of functional microbial communities involved in diazo dyes decolorization and mineralization stages. Int Biodeterior Biodegradation 132, 166-177.

Zille, A., Munteanu, F.D., Gübitz, G.M., Cavaco-Paulo, A., 2005. Laccase kinetics of degradation and coupling reactions. J. Mol. Catal. B Enzym. 33, 23-28.

# Appendices

## Appendix A – Supporting Information for Chapter III

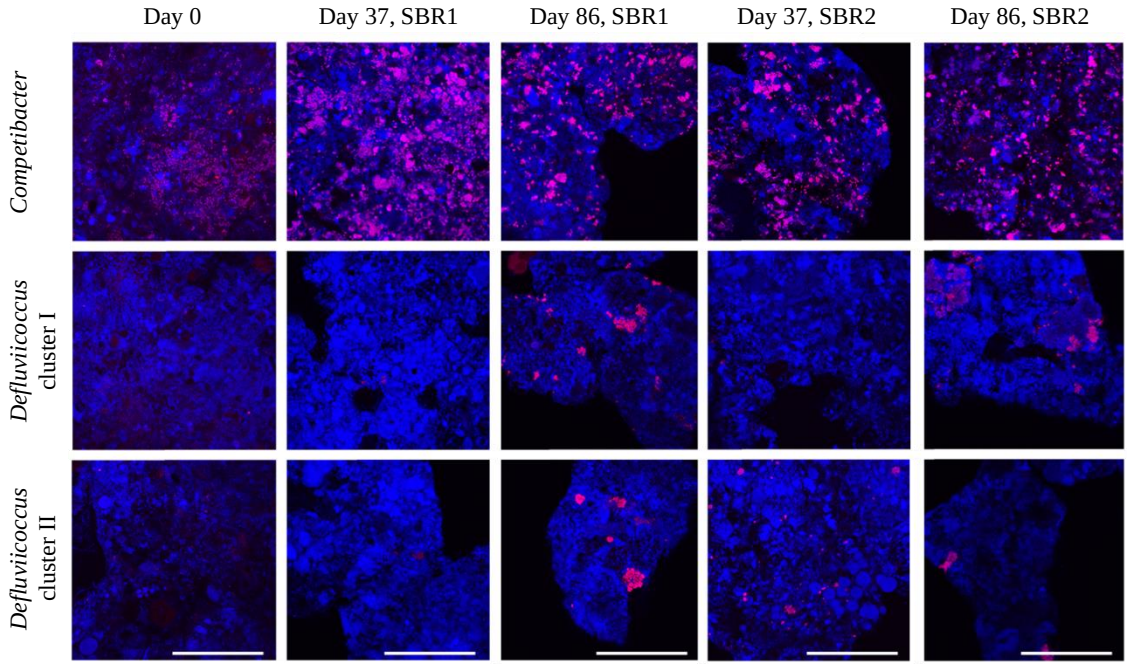


**Figure III.S1** - FISH micrographs of granules from the inoculum (day 0), and from samples taken after 37 and 86 days of operation from the dye-free control SBR1 and the dye-fed SBR2, hybridized with probes for all bacteria (EUBmix, cells in blue) and for glycogen-accumulating organisms (GAOmix, TFOmix and DFmix, cells in magenta). Scale bar = 100 μm.

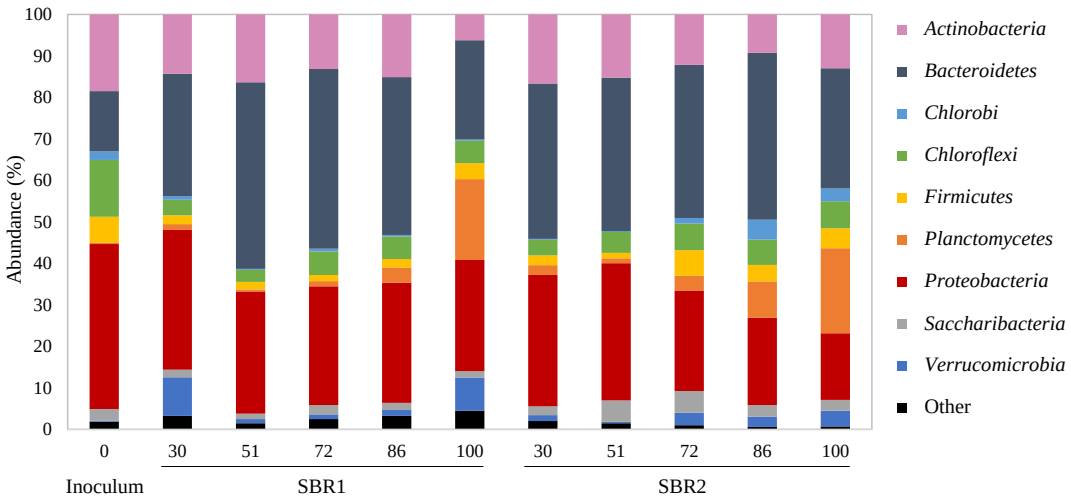


**Figure III.S2** - Composition of bacterial communities at the phylum level in the inoculum, as well as in sequencing batch reactors SBR1 and SBR2 on the indicated operational days, obtained by 16S rRNA gene sequencing analysis. The most representative phyla are indicated on the right.

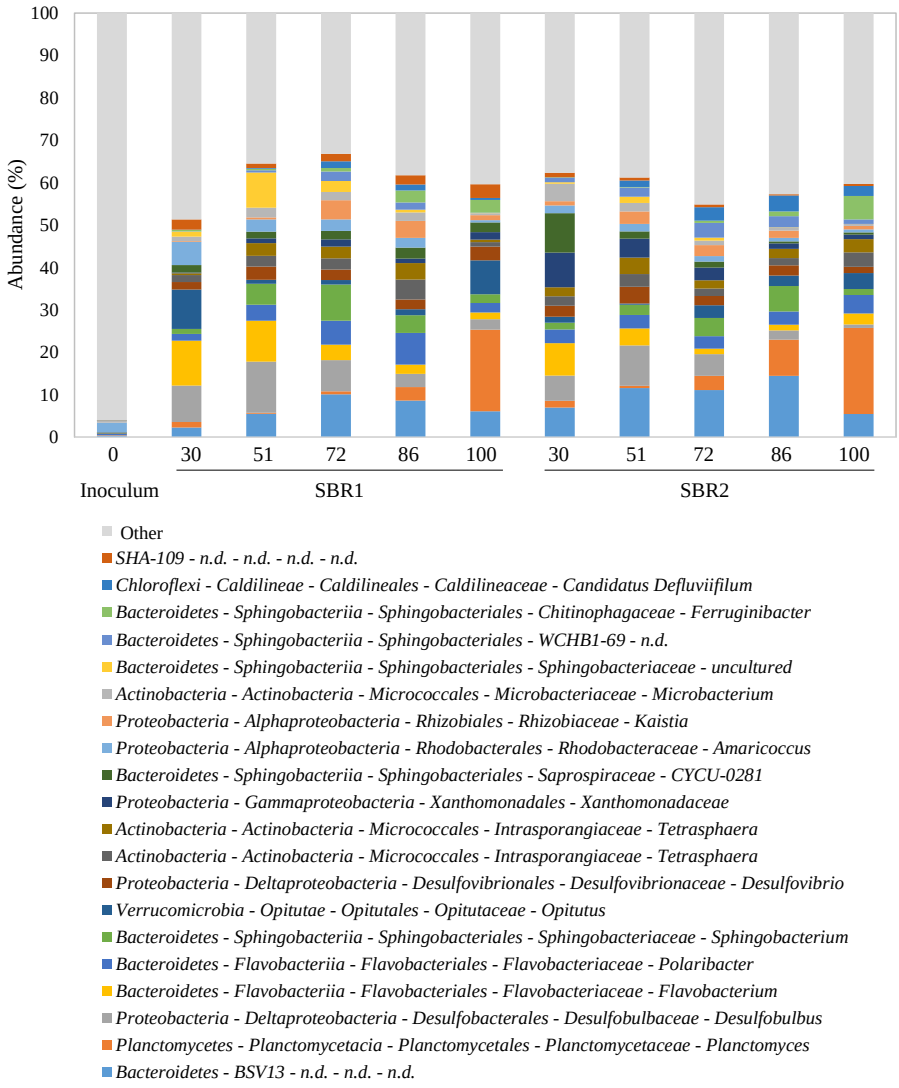


**Figure III.S3** - Composition of bacterial communities at the genus level in the inoculum, as well as in sequencing batch reactors SBR1 and SBR2 on the indicated operational days obtained by 16S rRNA gene sequencing analysis. Below the chart is indicated the "Phylum-Class-Order-Family-Genus" for the 20 most abundant bacteria among all of the analyzed samples. n.d. – not defined.

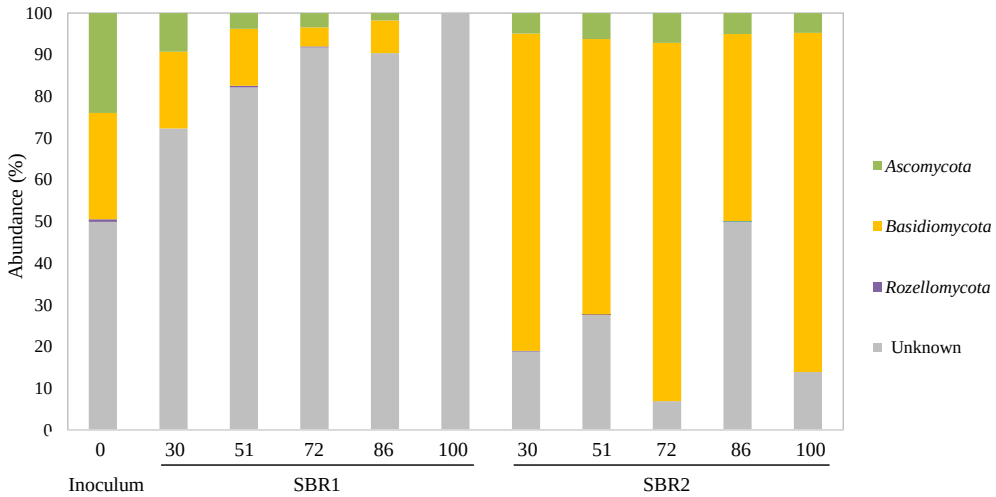


**Figure III.S4** - Composition of fungal communities at the phylum level in the inoculum, as well as in sequencing batch reactors SBR1 and SBR2 on the indicated operational days, obtained by rRNA gene and internal transcribed spacer (ITS) sequencing analysis. The most representative phyla are indicated on the right.

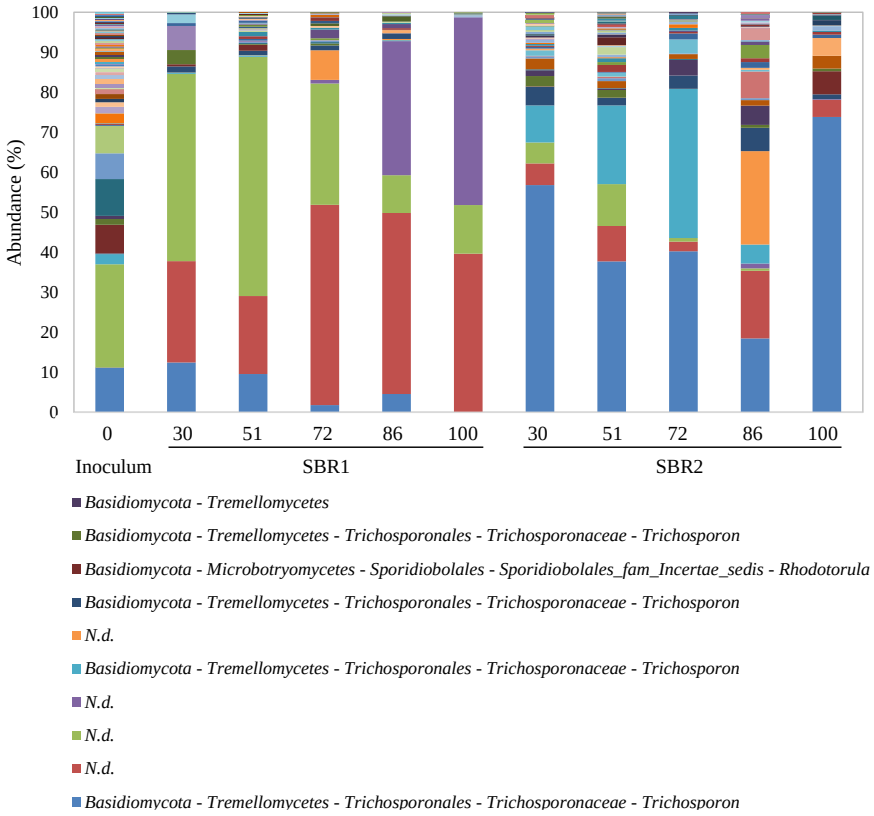


**Figure III.S5** - Composition of fungal communities at the genus level in the inoculum, as well as in sequencing batch reactors SBR1 and SBR2 on the indicated operational days, obtained by rRNA gene and internal transcribed spacer (ITS) sequencing analysis. Below the chart is indicated the "Phylum-Class-Order-Family-Genus" for the 10 most abundant fungi among all of the analyzed samples. n.d. – not defined.

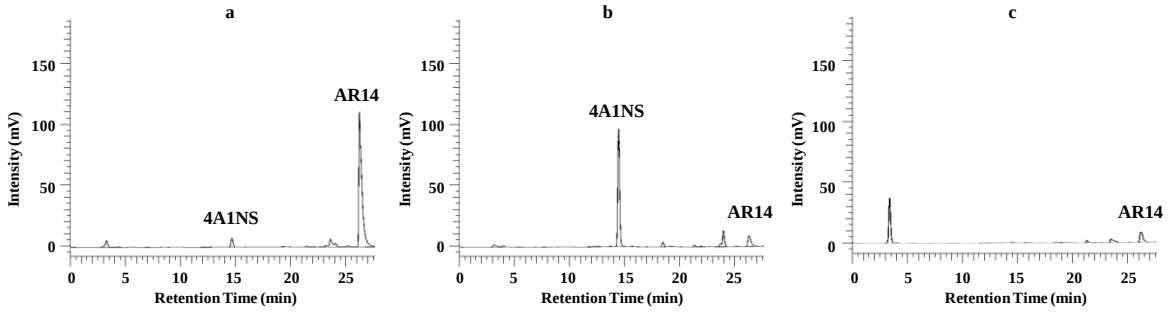


**Figure III.S6** - HPLC chromatograms of a selected cycle (day 71) from sequencing batch reactor SBR2 obtained at the onset of the anaerobic reaction phase (a), at the end of the anaerobic phase (b) and at the end of the aerobic phase (c). Peaks corresponding to Acid Red 14 and to the aromatic amine 4-amino-naphthalene-1-sulfonic acid are indicated as AR14 and 4A1NS, respectively.

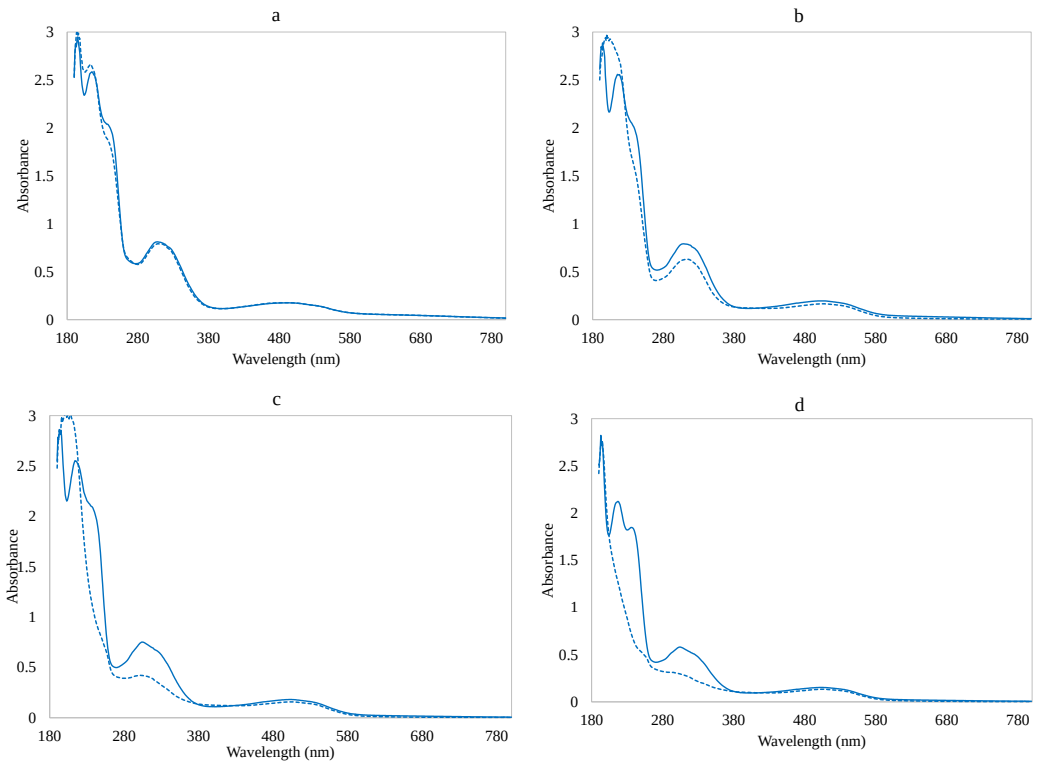


**Figure III.S7 -** UV-visible spectra of centrifuged samples taken from the mixed liquor of sequencing batch reactor SBR2 at the end of the anaerobic phase (full line) and at the end of the aerobic phase (dashed line) of selected treatment cycles on days 15 (a), 32 (b), 39 (c) and 85 (d).

## Appendix B – Supporting Information for Chapter IV

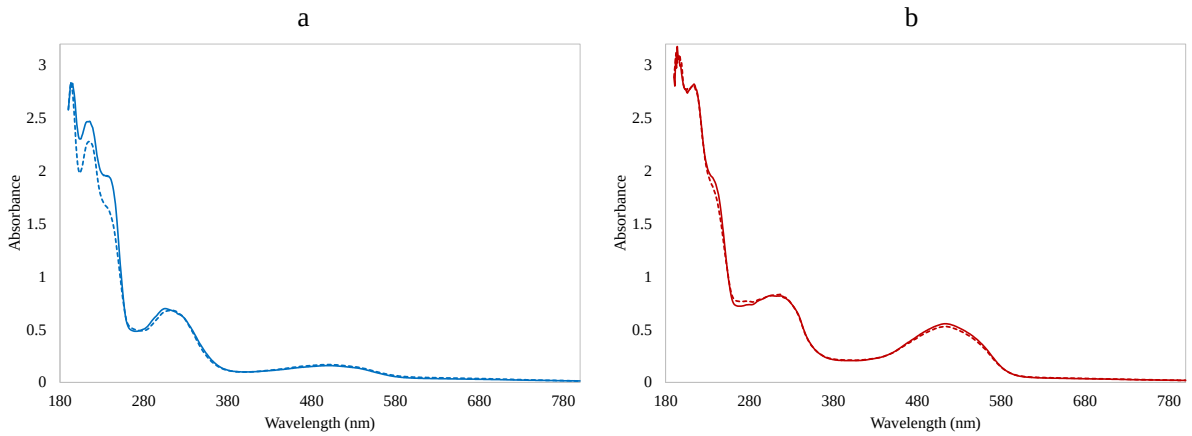


**Figure IV.S1** - UV-visible spectra of centrifuged samples taken from the mixed liquor of sequencing batch reactors SBR1 (a) and SBR2 (b) at the end of the anaerobic phase (full line) and at the end of the aerobic phase (dashed line) of a representative treatment cycle (day 44).

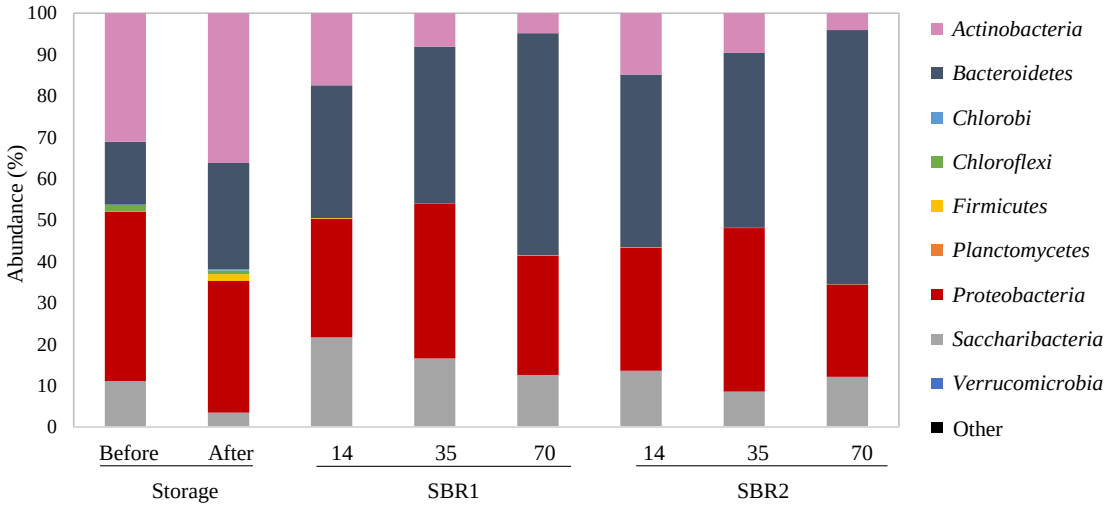


**Figure IV.S2** - Composition of bacterial communities at the phylum level before and after the 6.5-month storage period, as well as in sequencing batch reactors SBR1 and SBR2 on the indicated operational days obtained by 16S rRNA gene sequencing analysis. The most representative phyla are indicated on the right.

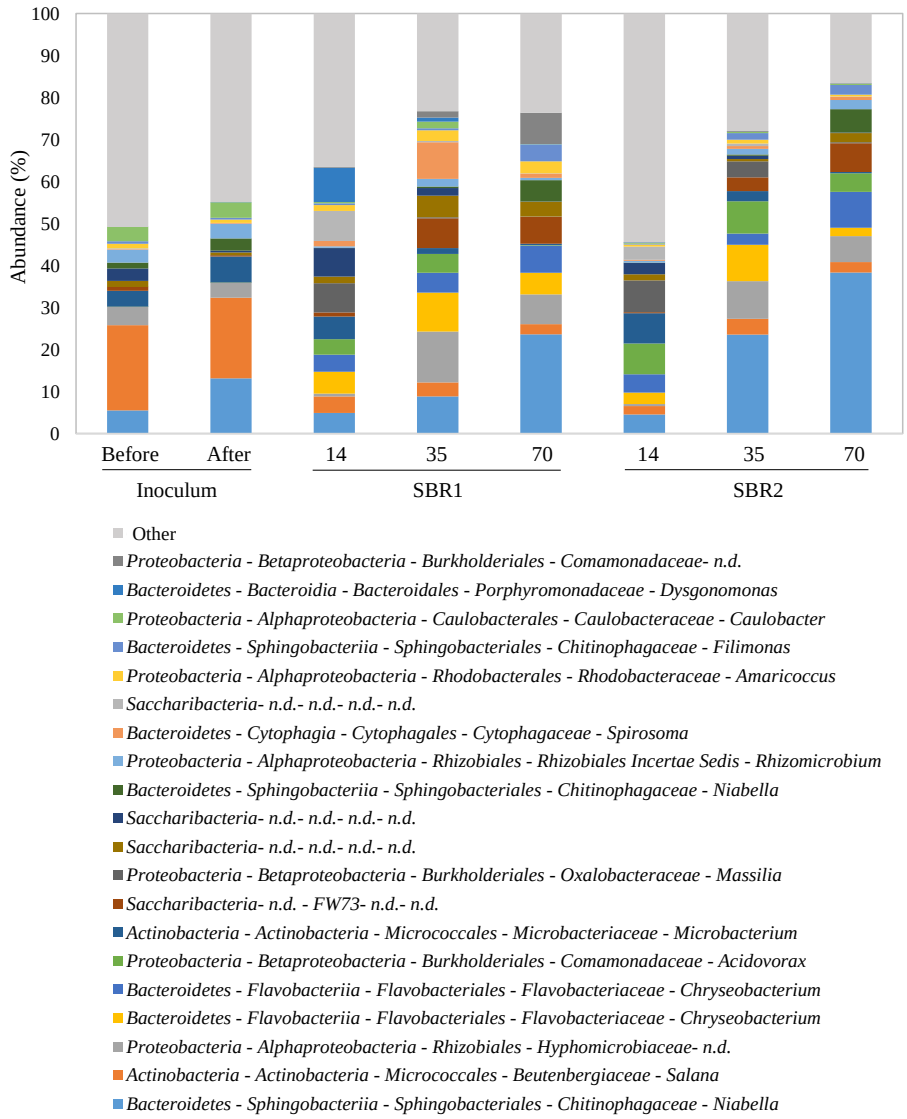


**Figure IV.S3** - Composition of bacterial communities at the genus level in the inoculum, as well as in sequencing batch reactors SBR1 and SBR2 on the indicated operational days, obtained by 16S rRNA gene sequencing analysis. Below the chart is indicated the "Phylum-Class-Order-Family-Genus" for the 20 most abundant bacteria among all of the analyzed samples. n.d. – not defined.

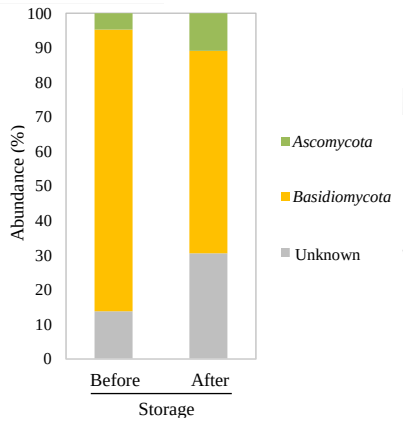


**Figure IV.S4 -** Composition of fungal communities at the phylum level before and after the 6.5-month storage of the aerobic granular sludge used as inoculum in this study, obtained by rRNA gene and internal transcribed spacer (ITS) sequencing analysis. The most representative phyla are represented on the right.


**Figure IV.S5** - Composition of fungal communities at the genus level before and after the 6.5-month storage of the aerobic granular sludge used as inoculum in this study, obtained by rRNA gene and internal transcribed spacer (ITS) sequencing analysis . To the right of the chart is indicated the "Phylum-Class-Order-Family-Genus" for the 10 most abundant fungi. n.d. – not defined.

# Appendix C – Supporting Information for Chapter V

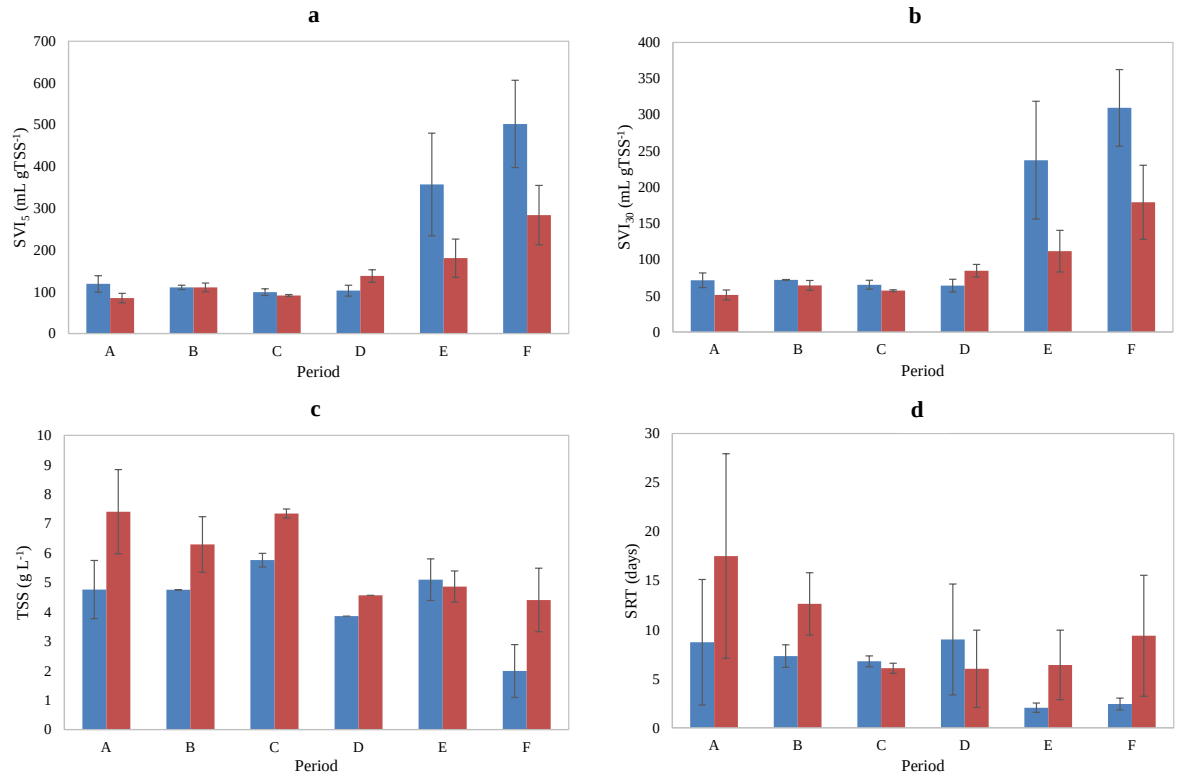


**Figure V.S1** - Average and standard deviation values registered for the sludge volume index after 5 and 30 min settling ($SVI_5$ and $SVI_{30}$; a and b, respectively), total suspended solids (TSS; c) and sludge retention time (SRT; d) in each experimental period (A-F), for SBR1 (blue bars) and SBR2 (red bars).

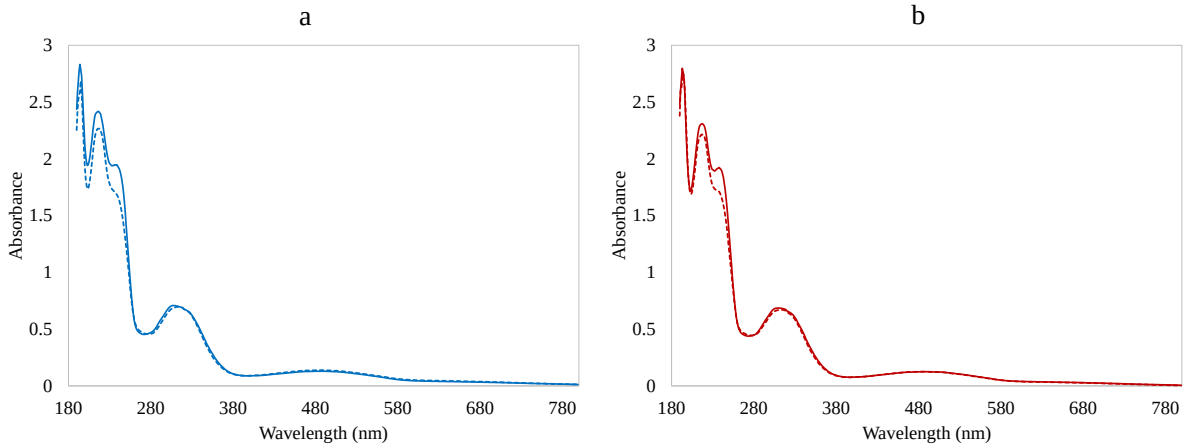


**Figure V.S2** - UV-visible spectra of centrifuged samples harvested from sequencing batch reactors SBR1 (a) and SBR2 (b) at the end of the anaerobic phase (full line) and at the end of the aerobic phase (dashed line) of a representative treatment cycle (day 152).

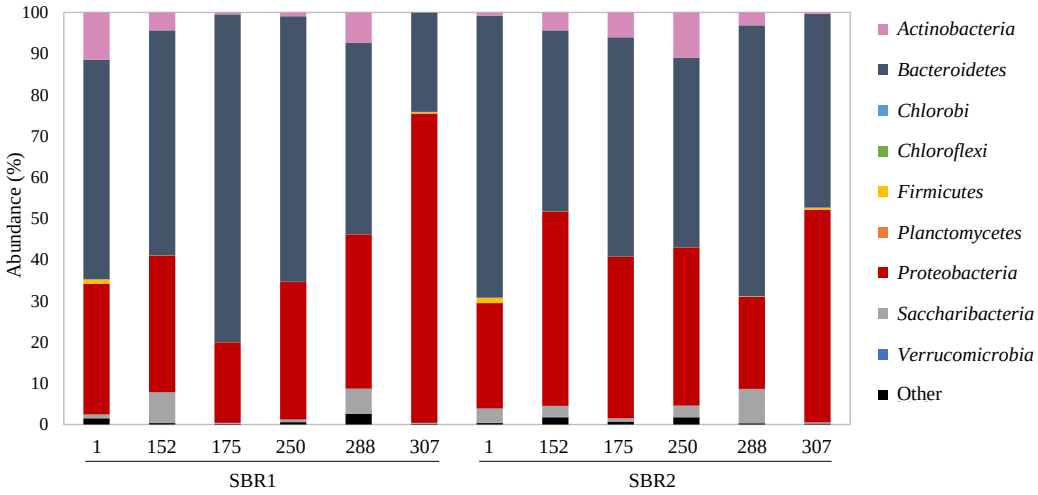


**Figure V.S3** - Composition of bacterial communities at the phylum level in sequencing batch reactors SBR1 and SBR2 on the indicated operational days, obtained by 16S rRNA gene sequencing analysis. The most representative phyla are represented on the right.

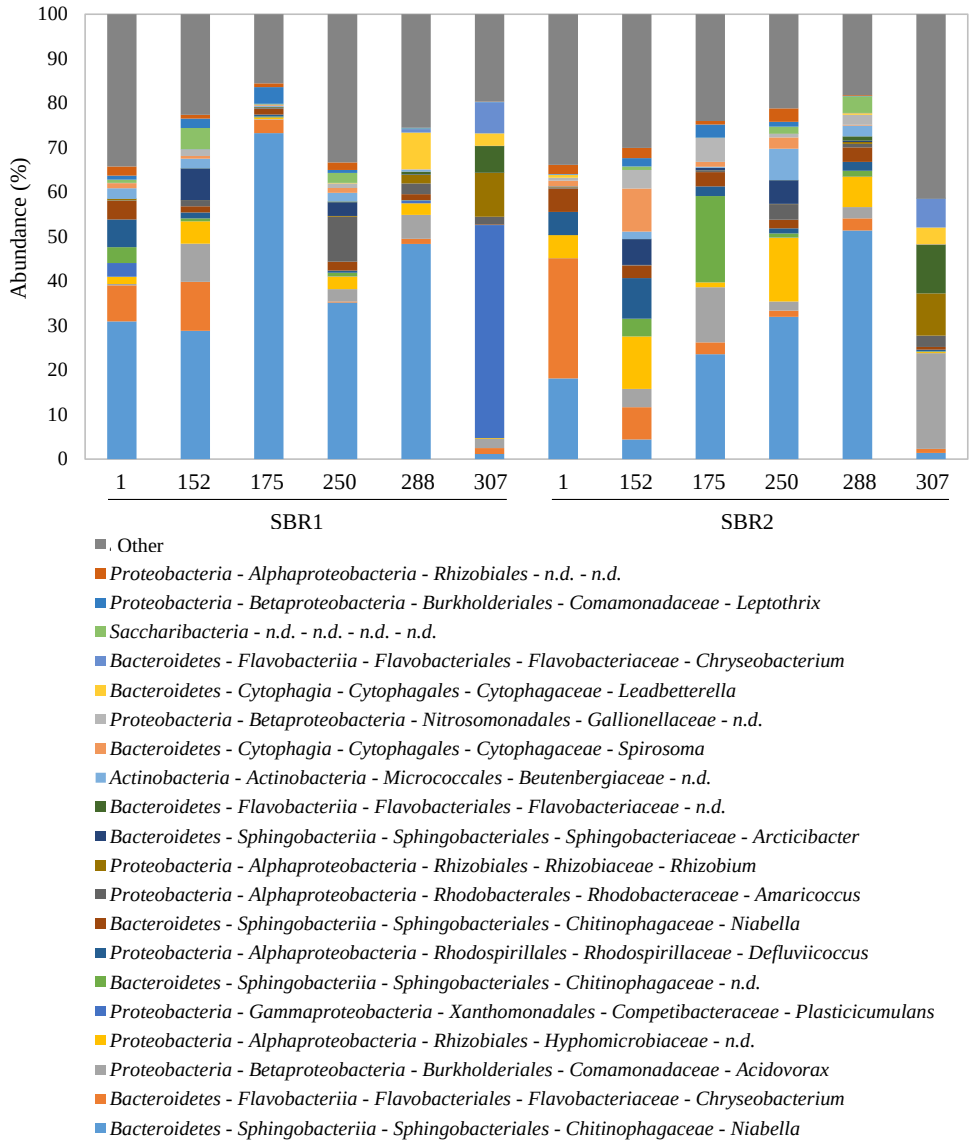


**Figure V.S4** - Composition of bacterial communities at the genus level in sequencing batch reactors SBR1 and SBR2 on the indicated operational days, obtained by 16S rRNA gene sequencing analysis. Below the chart is indicated the "Phylum-Class-Order-Family-Genus" for the 20 most abundant bacteria among all of the analyzed samples. n.d. – not defined.

## Appendix D – Supporting Information for Chapter VI

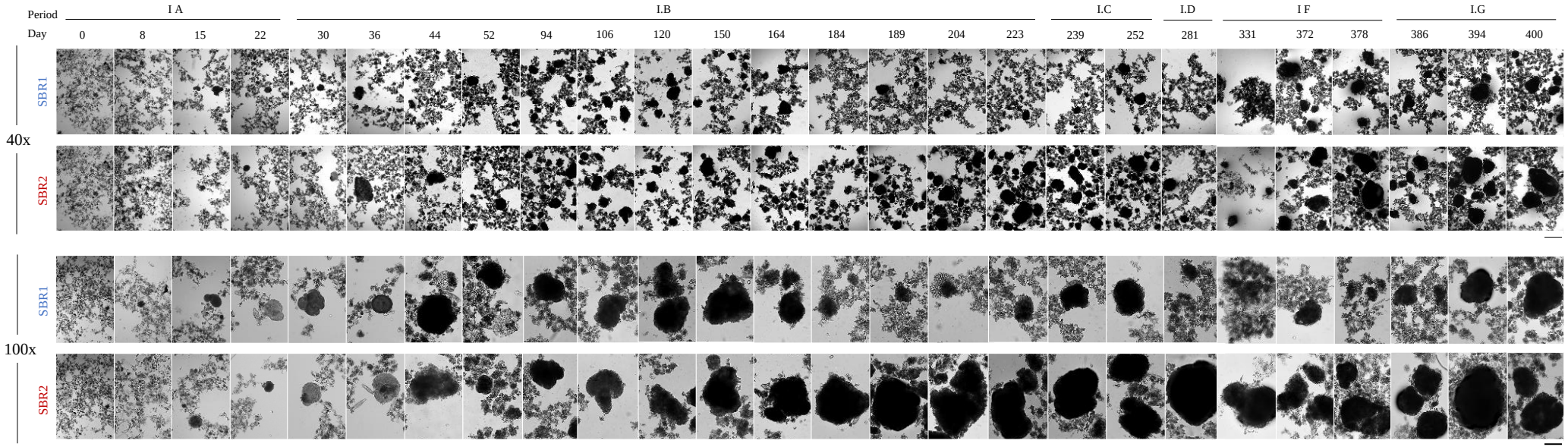


**Figure VI.S1** - Morphological development of aerobic granular sludge along experimental run I. Micrographs, at magnifications 40 and 100, from biomass samples harvested from sequencing batch reactors SBR1 and SBR2 on the operational days and periods indicated on top. Scale bars: 40x – 0.5 mm; 100x – 0.2 mm.

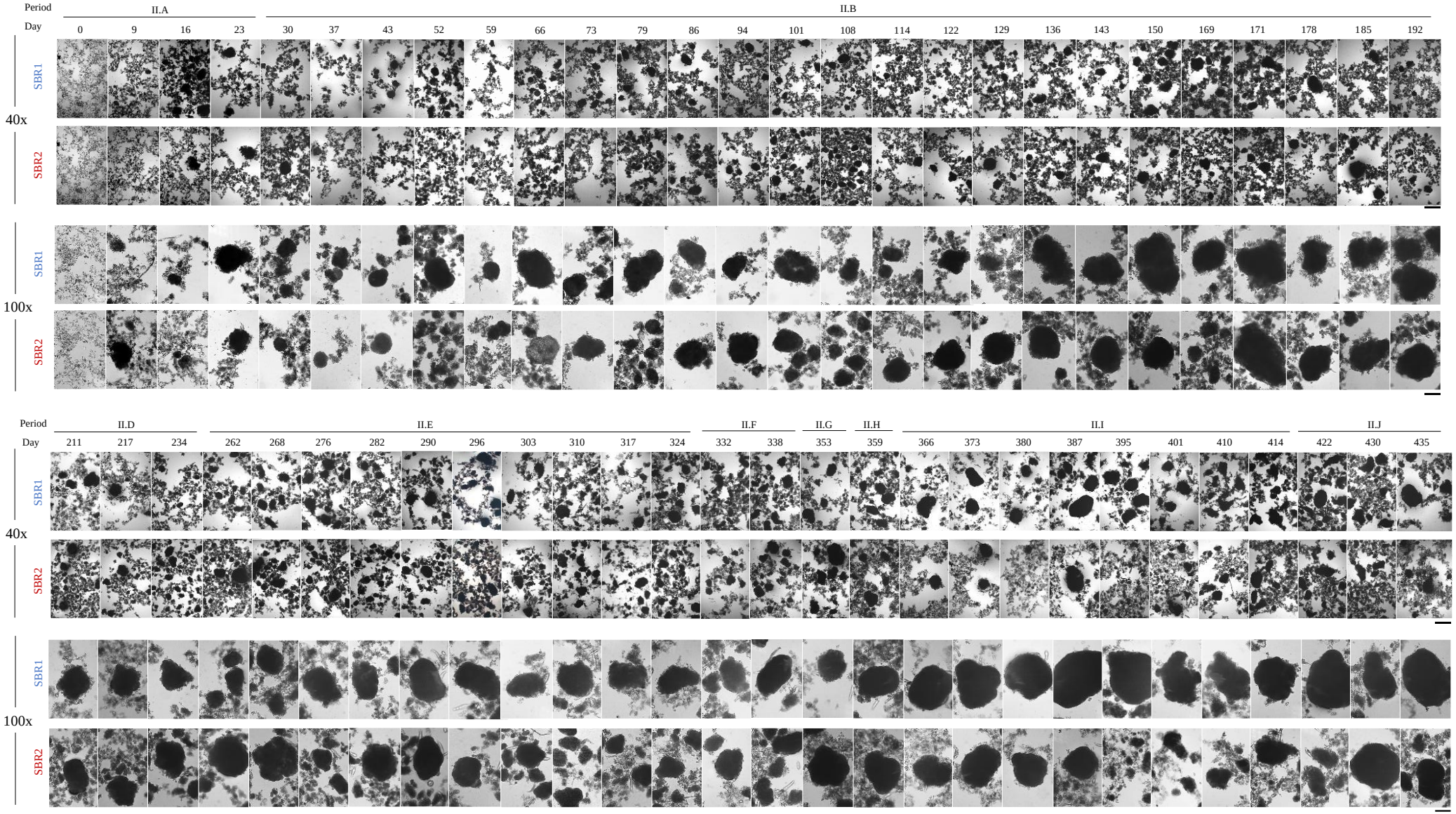


**Figure VI.S2** - Morphological development of aerobic granular sludge along experimental run II. Micrographs, at magnifications 40 and 100, from biomass samples harvested from sequencing batch reactors SBR1 and SBR2 on the operational days and periods indicated on top. Scale bars: 40x – 0.5 mm; 100x – 0.2 mm.

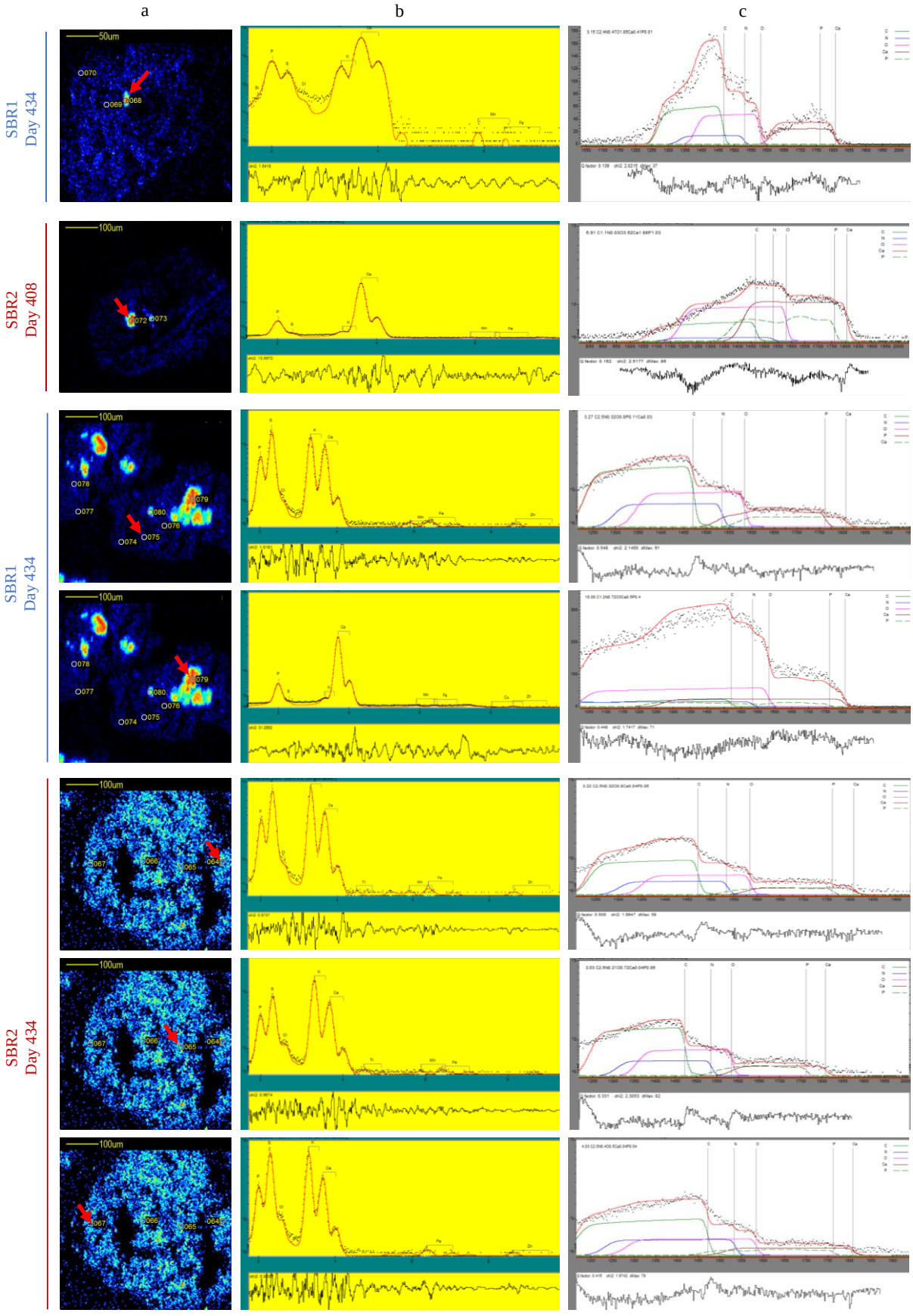


**Figure VI.S3** - Elemental analysis of aerobic granules. Elemental spectra obtained by Rutherford Backscattering (RBS; b) and Particle Induced X-ray Emission (PIXE; c) techniques regarding the area highlighted by a red arrow in the respective calcium map (a): in mineral inclusions or at the center, intermediate or peripheral regions of aerobic granules harvested from sequencing batch reactors SBR1 and SBR2 on days 408 and 434 of experimental run II.

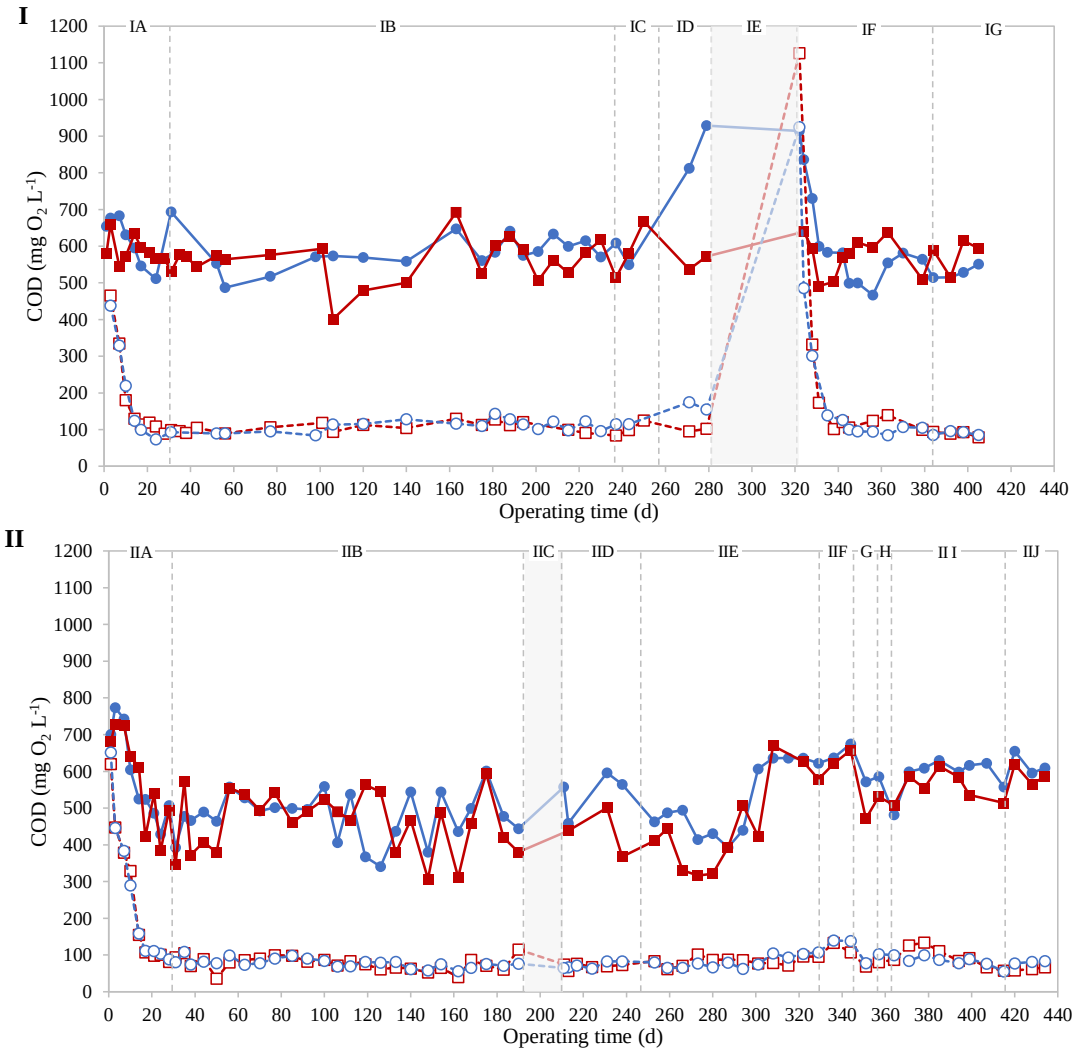


**Figure VI.S4** - Organic load removal performance along experimental runs I and II. Soluble chemical oxygen demand (COD) levels at the end of the fill phase* (full line) and at the end of the aerobic stage (dashed line), in sequencing batch reactors SBR1 (●) and SBR2 (■). The operational conditions for each experimental period (I.A-I.G and II.A-II.J) are described in Table VI.1. *In case of SBR2 this value corresponds to an estimate based on values measured in the feed solution (50%) and in the treated effluent from the previous cycle (50%).

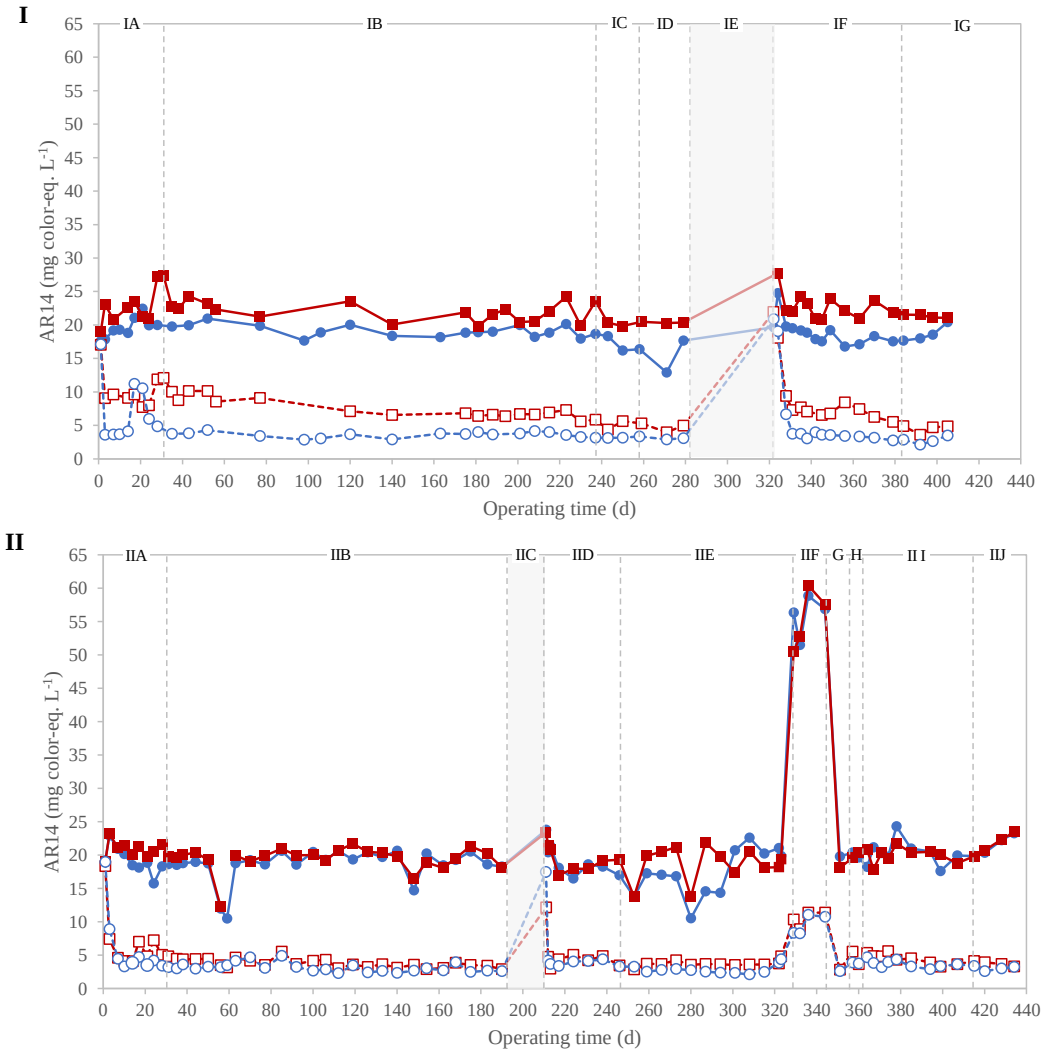


**Figure VI.S5** - Color removal performance along experimental runs I and II. Acid red 14 (AR14) concentrations, as color-equivalents, at the end of the fill phase* (full line) and at the end of the anaerobic stage (dashed line), in sequencing batch reactors SBR1 (●) and SBR2 (■). The operational conditions for each experimental period (I.A-I.G and II.A-II.J) are described in Table VI.1. * In case of SBR2 this value corresponds to an estimate based on values measured in the feed solution (50%) and in the treated effluent from the previous cycle (50%).

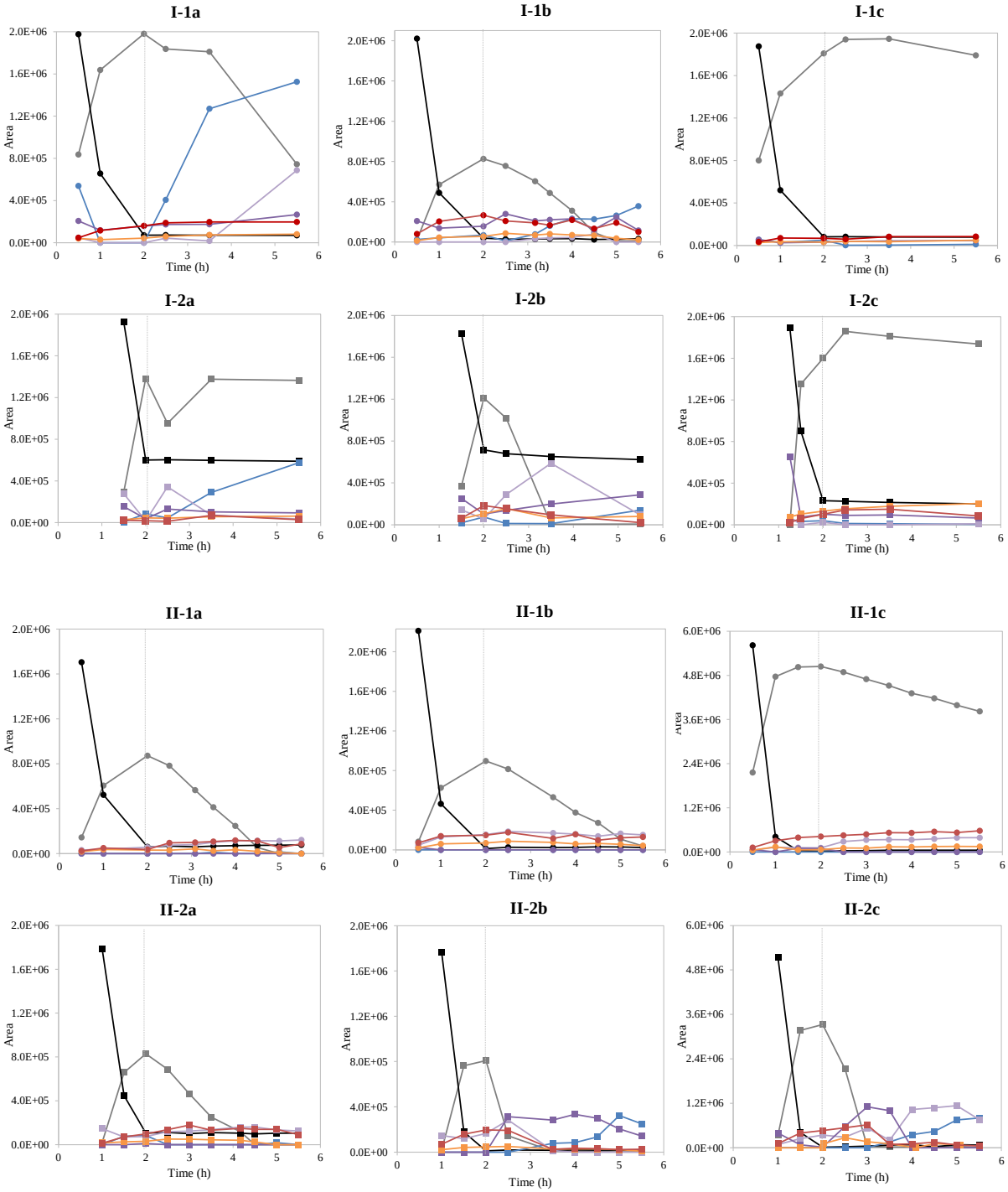


**Figure VI.S6 -** Acid Red 14 (AR14) and its breakdown metabolites profiles representative of experimental runs I and II. Area-time profiles of HPLC peaks corresponding to AR14 (black line), its cleavage product 4-amino-naphthalene-1-sulfonic acid (4A1NS; grey line), and unknown metabolites α (dark purple line), α' (light purple line), β (orange line), γ (red line) and δ (blue line), according to Figure VI.17, on selected treatment cycles of sequencing batch reactors SBR1 (●; experimental run I – I-1a: day 10, I-1b: day 35, I-1c: day 163; experimental run II – II-1a: day 190, II-1b: day 308, II-1c: day 344) and SBR2 (■; experimental run I – I-2a: day 24, I-2b: day 56, I-2c: day 279; experimental run II – II-2a: day 175, II-2b: day 308, II-2c: day 344). Vertical lines represent the end of the anaerobic phase, upon the aeration onset.

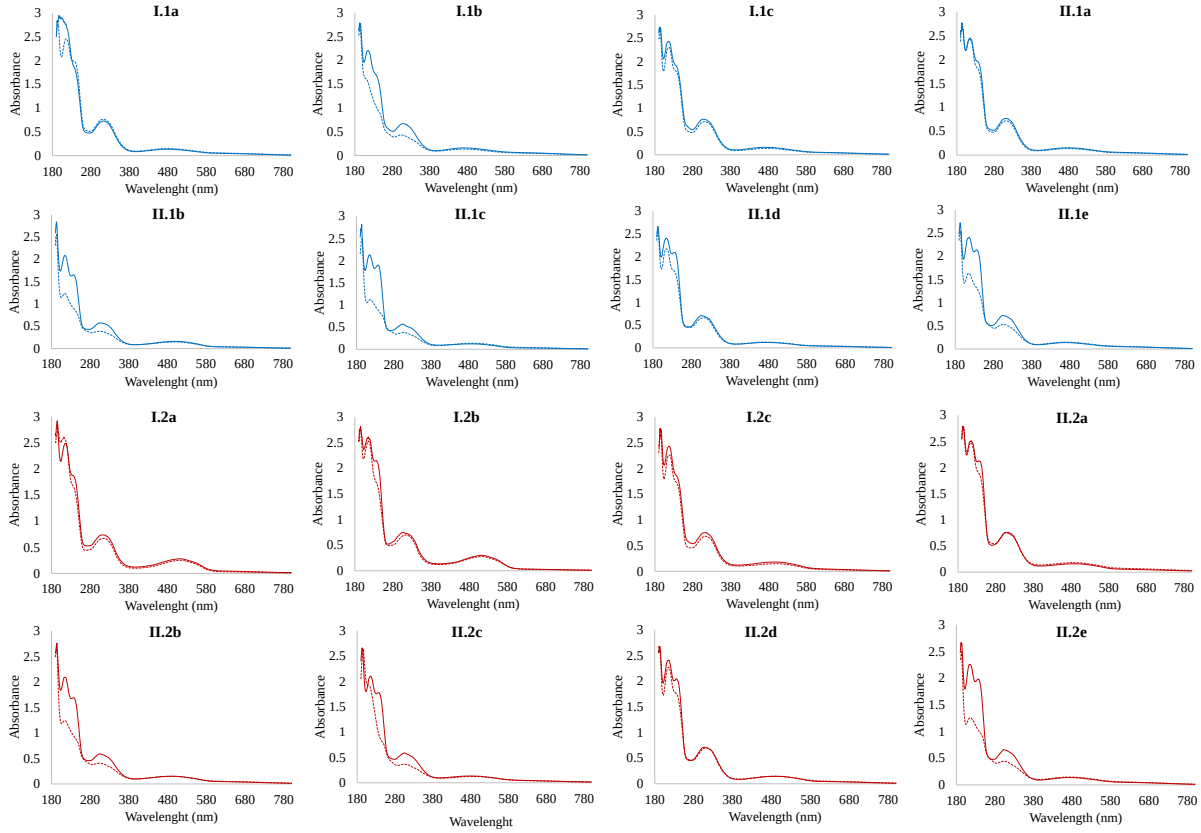


**Figure VI.S7** - UV-visible spectra of centrifuged samples harvested from sequencing batch reactors SBR1 (blue lines) and SBR2 (red lines) at the end of the anaerobic phase (full line) and at the end of the aerobic phase (dashed line) of selected treatment cycles from experimental runs I and II. SBR1: experimental run I – days 10 (I.1a), 35 (I.1b), 163 (I.1c); experimental run II – days 24 (II.1a), 70 (II.1b), 246 (II.1c), 394 (II.1d), 434 (II.1e). SBR2: experimental run I – days 24 (I.2a), 56 (I.2b), 279 (I.2c); experimental run II – days 35 (II.2a), 70 (II.2b), 246 (II.2c), 394 (II.1d), 434 (II.2e).

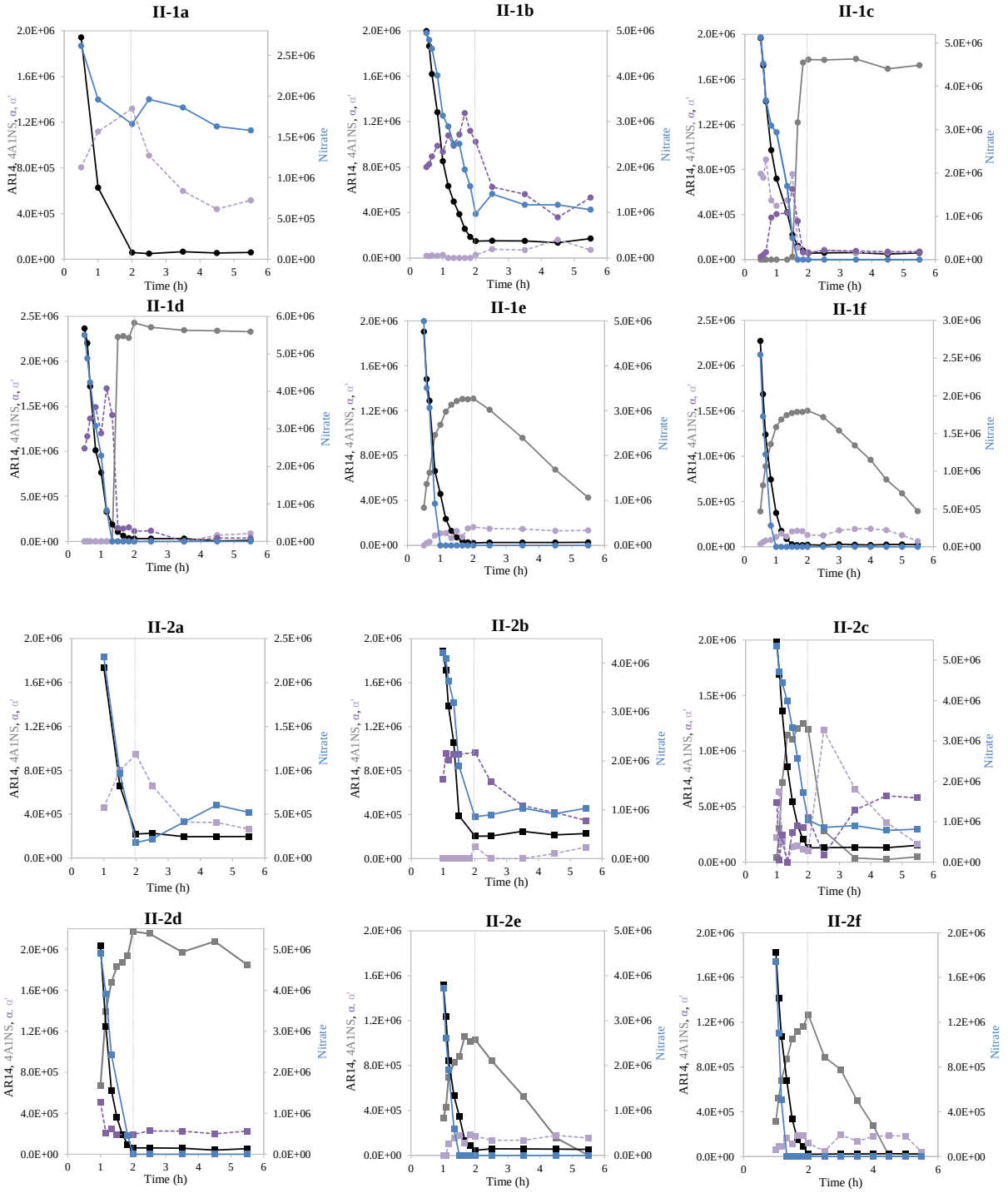


**Figure VI.S8** - Nitrate, Acid Red 14 (AR14), aromatic amine 4-amino-naphthalene-1-sulfonic acid (4A1NS) and other dye breakdown metabolites profiles during periods II.H-II.J of experimental run II. Area-time profiles of HPLC peaks corresponding to nitrate (blue line), AR14 (black line), its cleavage product 4A1NS (grey line), and unknown metabolites α (dark purple line) and α' (light purple line) on selected treatment cycles of sequencing batch reactors SBR1 (●) and SBR2 (■) on days 357 (II.1a and II.2a), 364 (II.1b and II.2b), 371 (II.1c and II.2c), 378 (II.1d and II.2d), 415 (II.1e and II.2e) and 434 (II.1f and II.2f, respectively for SBR1 and SBR2). Vertical lines represent the end of the anaerobic phase, upon the aeration onset.

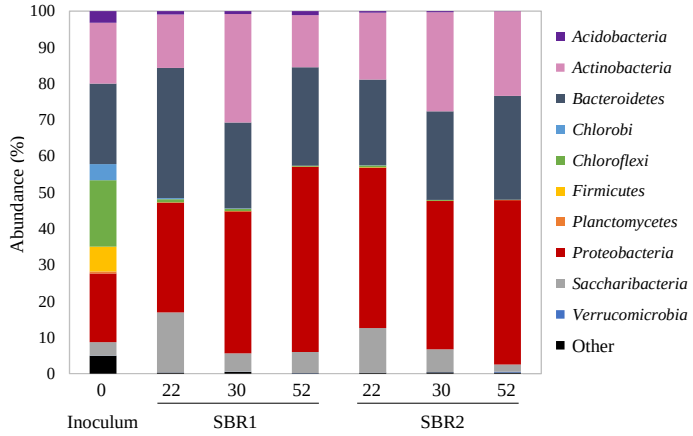


**Figure VI.S9** - Composition of bacterial communities at the phylum level in the inoculum, as well as in sequencing batch reactors SBR1 and SBR2 on the indicated operational days, obtained by 16S rRNA gene sequencing analysis. The most representative phyla are represented on the right.

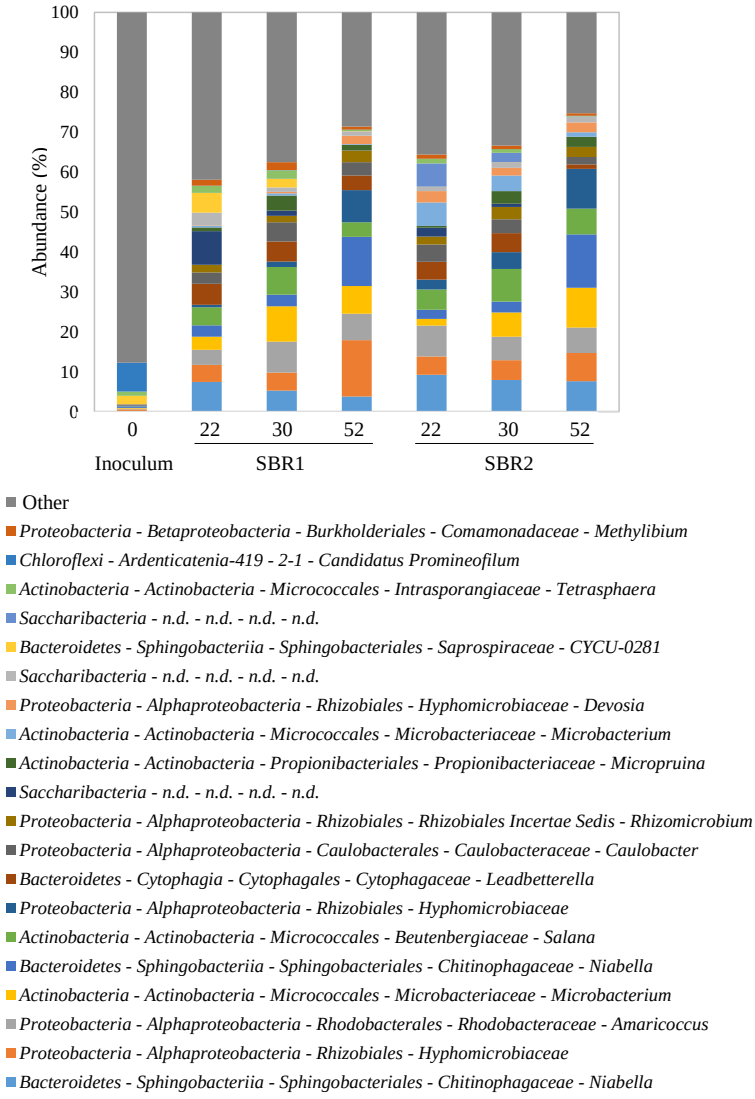


**Figure VI.S10** - Composition of bacterial communities at the genus level in the inoculum, as well as in sequencing batch reactors SBR1 and SBR2 on the indicated operational days obtained by 16S rRNA gene sequencing analysis. Below the chart is indicated the "Phylum-Class-Order-Family-Genus" for the 20 most abundant bacteria among all of the analyzed samples. n.d. – not defined.

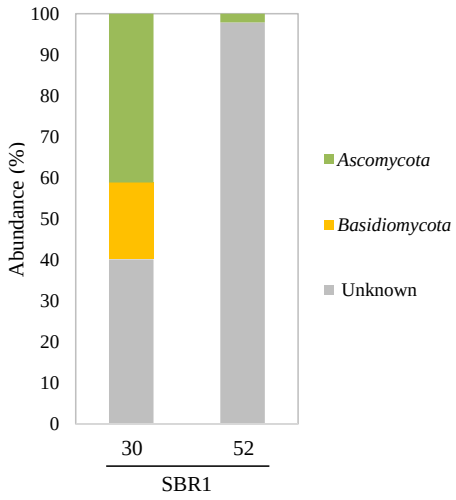


**Figure VI.S11** - Composition of fungal communities at the phylum level in sequencing batch reactor SBR1 on the indicated days, obtained by rRNA gene and internal transcribed spacer (ITS) sequencing analysis. The most representative phyla are represented on the right.

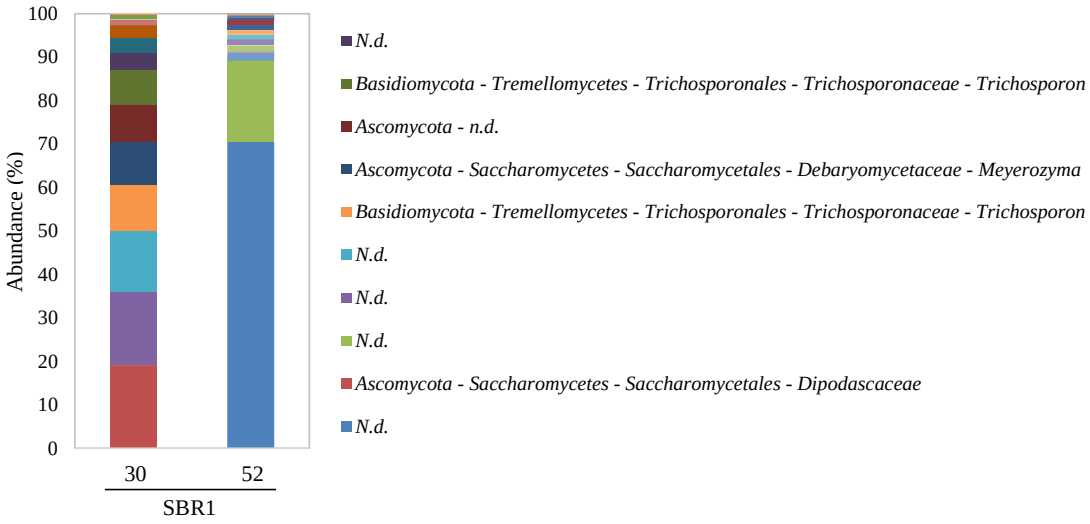


**Figure VI.S12** - Composition of fungal communities at the genus level in sequencing batch reactor SBR1 on the indicated days, obtained by rRNA gene and internal transcribed spacer (ITS) sequencing analysis. Below the chart is indicated the "Phylum-Class-Order-Family-Genus" for the 10 most abundant fungi. n.d. – not defined.

## Appendix E – Supporting Information for Chapter VII

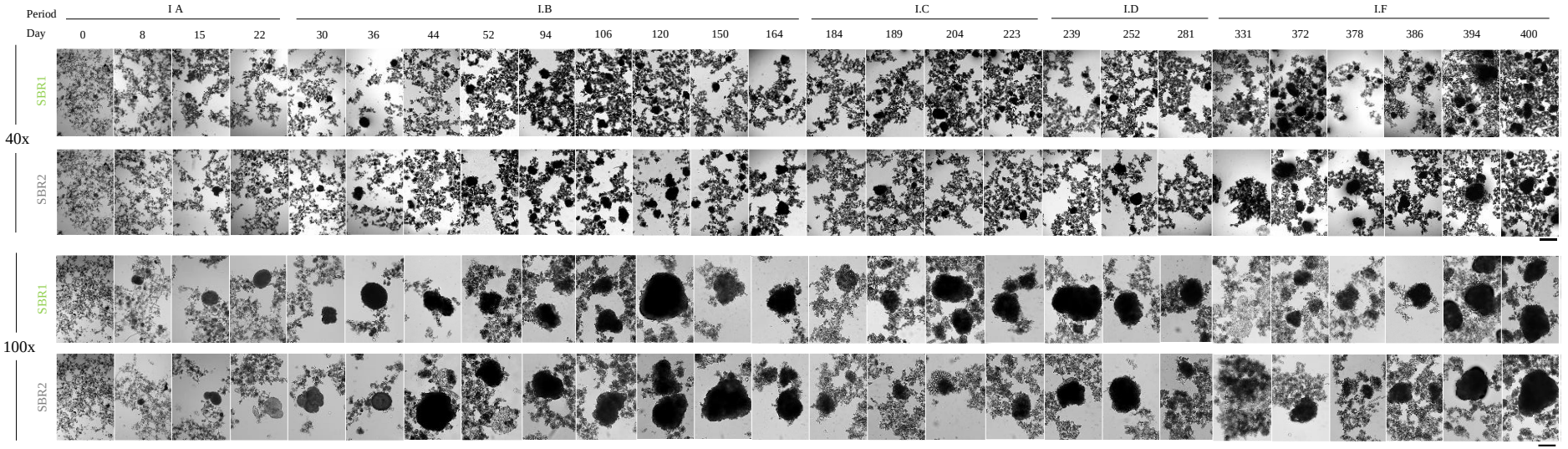


**Figure VII.S1** - Morphological development of aerobic granular sludge along experimental run I. Micrographs, at magnifications 40 and 100, from biomass samples harvested from sequencing batch reactors SBR1 and SBR2 on the operational days and periods indicated on top. Scale bars: 40x – 0.5 mm; 100x – 0.2 mm.

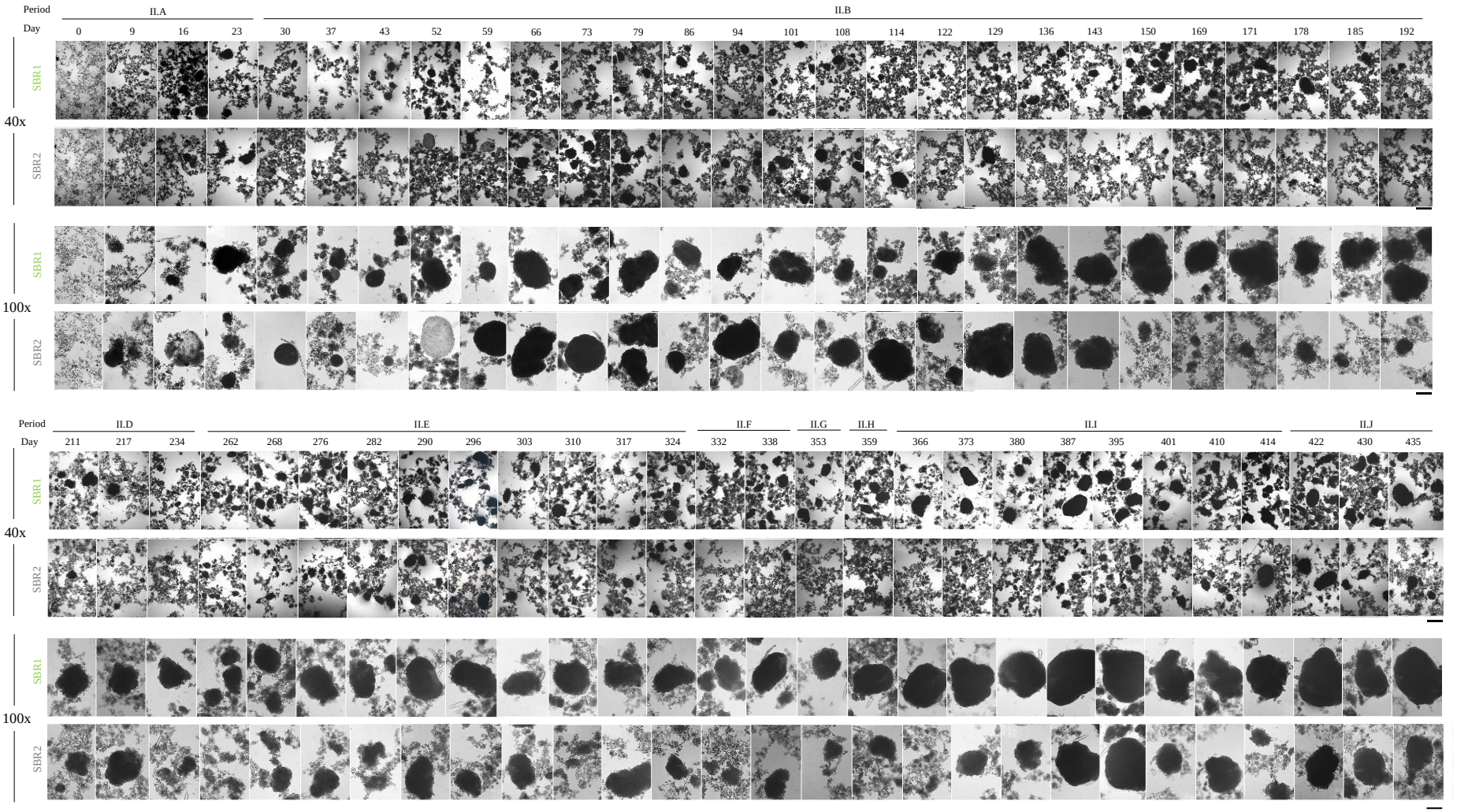


**Figure VII.S2** - Morphological development of aerobic granular sludge along experimental run II. Micrographs, at magnifications 40 and 100, from biomass samples harvested from sequencing batch reactos SBR1 and SBR2 on the operational days and periods indicated on top. Scale bars: 40x – 0.5 mm; 100x – 0.2 mm.

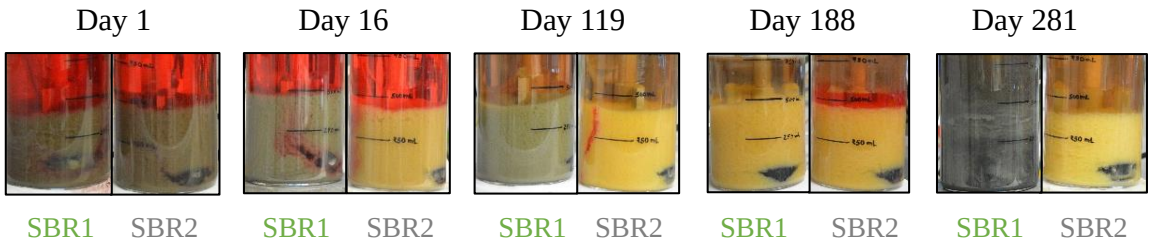


**Figure VII.S3** - Photographs of the settled biomass in sequencing batch reactors SBR1 and SBR2 on the indicated days along experimental run I.

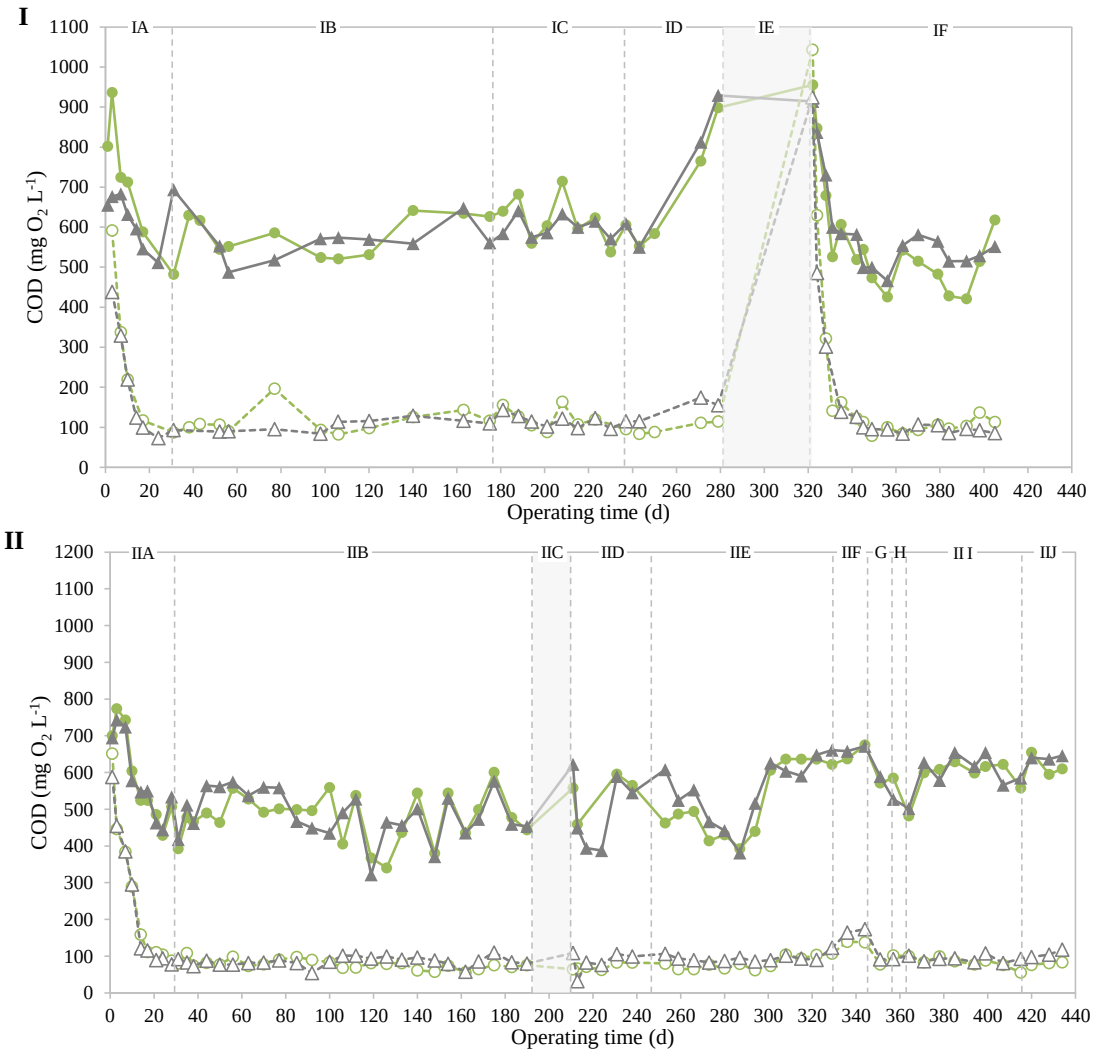


**Figure VII.S4** - Organic load removal performance along experimental runs I and II. Soluble chemical oxygen demand (COD) levels at the end of the fill phase* (full line) and at the end of the aerobic stage (dashed line), in sequencing batch reactors SBR1 (●) and SBR2 (▲). The operational conditions for each experimental period (I.A-I.F and II.A-II.J) are described in Table VII.1.

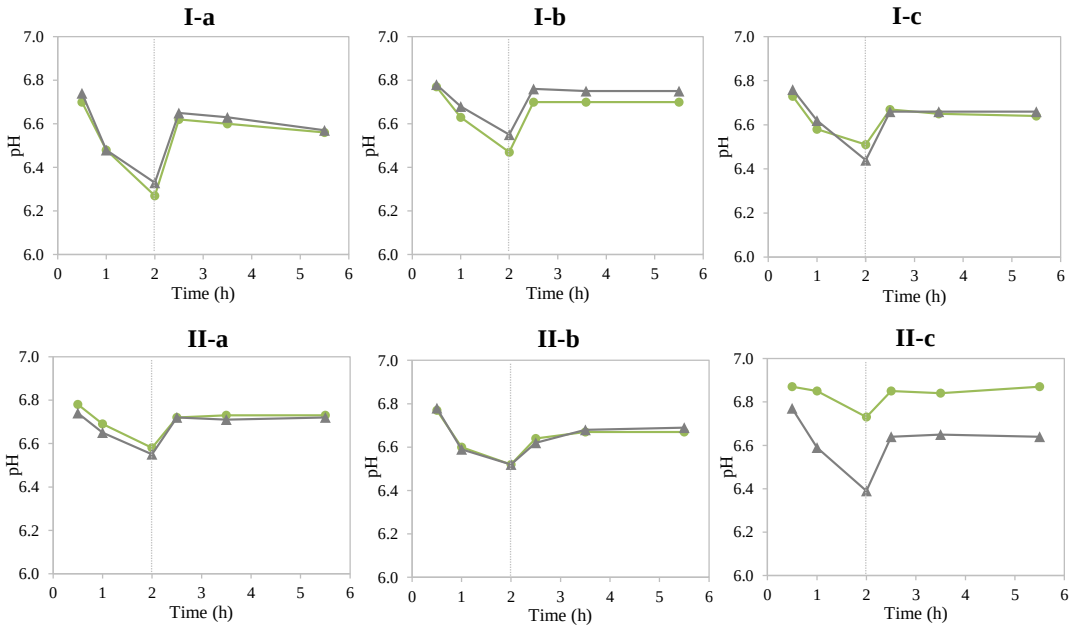


**Figure VII.S5** - Comparison between pH profiles of sequencing batch reactors SBR1 and SBR2 treatment cycles studied along experimental runs I and II. Comparison between the pH-time profiles observed along the reaction phase of treatment cycles in SBR1 (●) and SBR2 (▲) on days 24 (I-a; period I.A), 98 (I-b; period I.B) and 379 (I-c; period I.F) of experimental run I, and on days 92 (II-a; period II.B), 316 (II-b; period II.E) and 399 (II-c; period II.I) of experimental run II. Vertical lines represent the end of the anaerobic phase, upon the aeration onset.

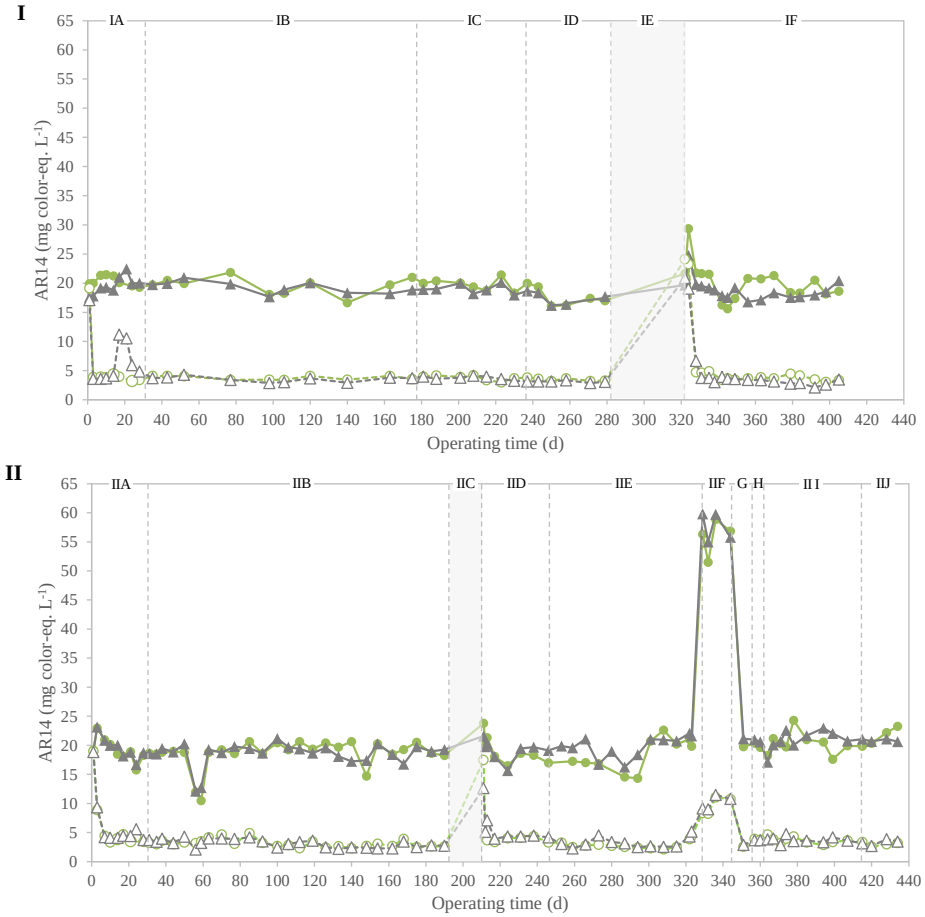


**Figure VII.S6** - Color removal performance along experimental runs I and II. Acid red 14 (AR14) concentrations, as color-equivalents, at the start (full line) and at the end of the anaerobic stage (dashed line), in sequencing batch reactors SBR1 (●) and SBR2 (▲). The operational conditions for each experimental period (I.A-I.F and II.A-II.J) are described in Table VII.1.

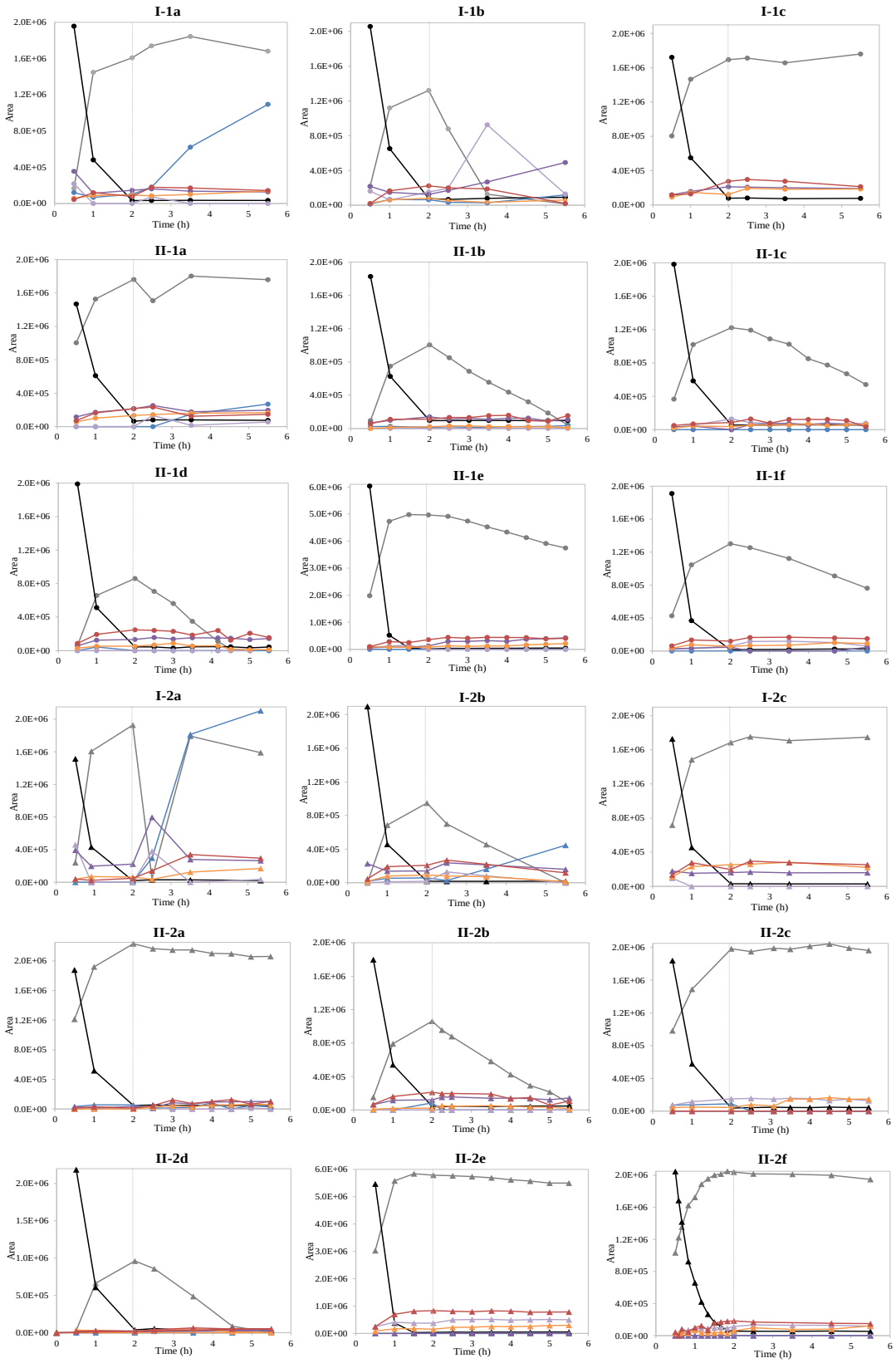


**Figure VII.S7** - Acid Red 14 (AR14) and its breakdown metabolites profiles representative of experimental run I and II. Area-time profiles of HPLC peaks corresponding to AR14 (black line), its cleavage product 4-amino-naphthalene-1-sulfonic acid (4A1NS; grey line), and unknown metabolites α (dark purple line), α' (light purple line), β (orange line), γ (red line) and δ (blue line), according to Figure VI.17, on selected treatment cycles in sequencing batch reactors SBR1 (●) and SBR2 (▲) from experimental runs I ─ days 24 (I.1a), 52 (I.1b), 398 (I.1c), 3 (I.2a), 38 (I.2b), 398 (I.2c) ─ and II ─ days 24 (II.1a), 63 (II.1b), 100 (II.1c), 175 (II.1d), 336 (II.1e), 350 (II.1f), 63 (II.2a), 92 (II.2b), 190 (II.2c), 323 (II.2d), 344 (II.2e), 415 (II.2f). Vertical lines represent the end of the anaerobic phase, upon the aeration onset.

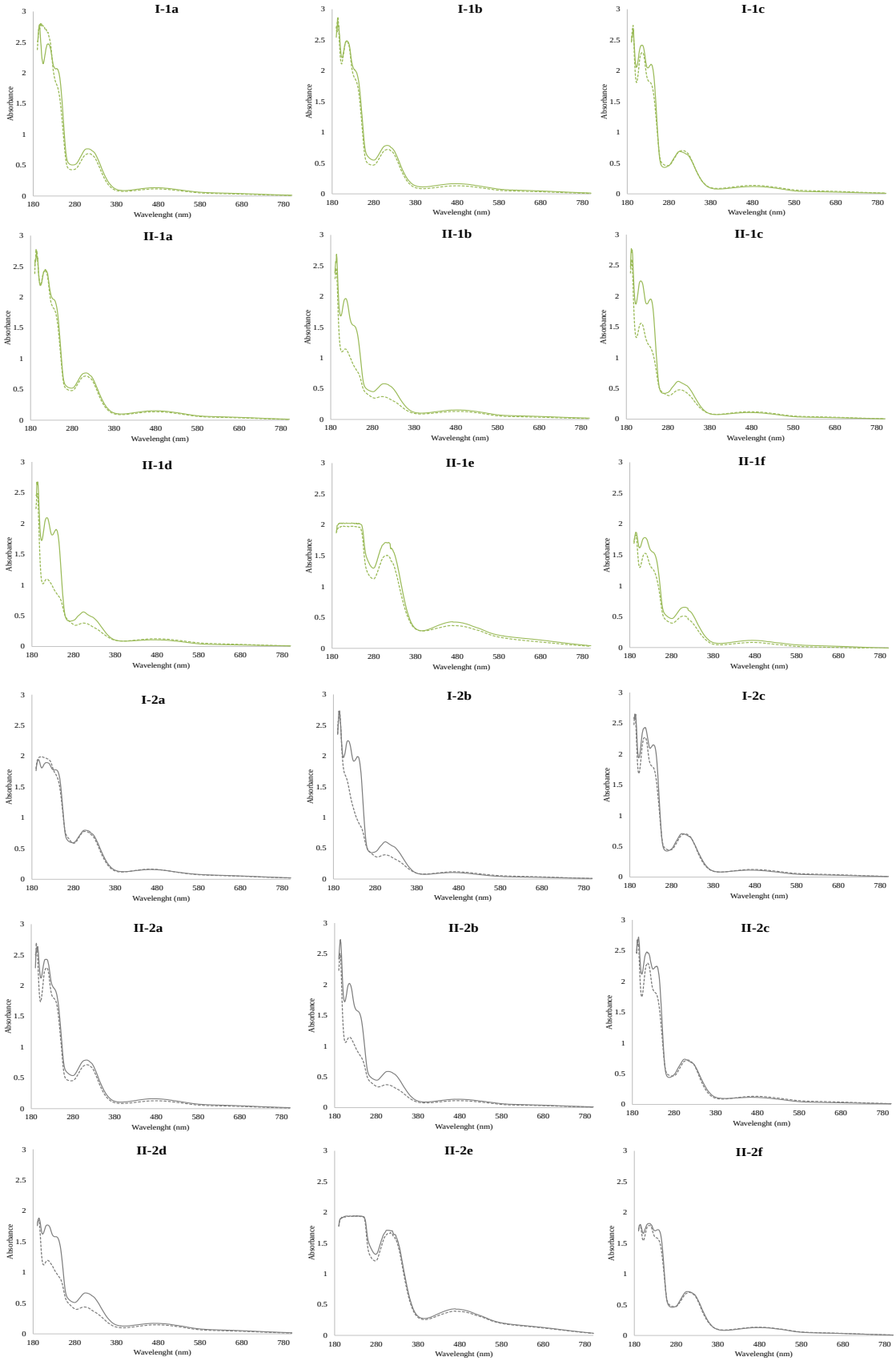


**Figure VII.S8** - UV-visible spectra of centrifuged samples harvested from sequencing batch reactors SBR1 (green lines) and SBR2 (grey lines) at the end of the anaerobic phase (full line) and at the end of the aerobic phase (dashed line) of selected treatment cycles from experimental runs I ─ days 24 (I.1a), 52 (I.1b), 398 (I.1c), 3 (I.2a), 38 (I.2b), 398 (I.2c) ─ and II ─ days 24 (II.1a), 63 (II.1b), 100 (II.1c), 175 (II.1d), 336 (II.1e), 350 (II.1f), 63 (II.2a), 92 (II.2b), 190 (II.2c), 323 (II.2d), 344 (II.2e), 415 (II.2f).

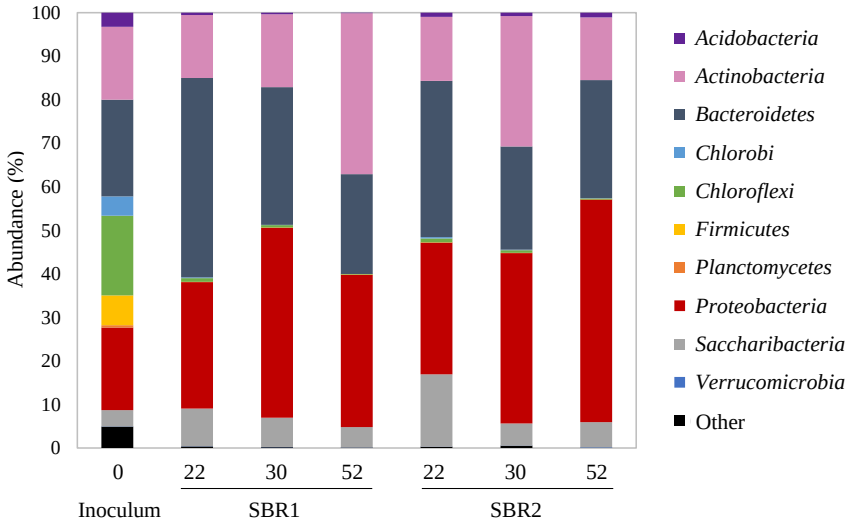


**Figure VII.S9** - Composition of bacterial communities at the phylum level in the inoculum, as well as in sequencing batch reactors SBR1 and SBR2 on the indicated operational days, obtained by 16S rRNA gene sequencing analysis. The most representative phyla are represented on the right.

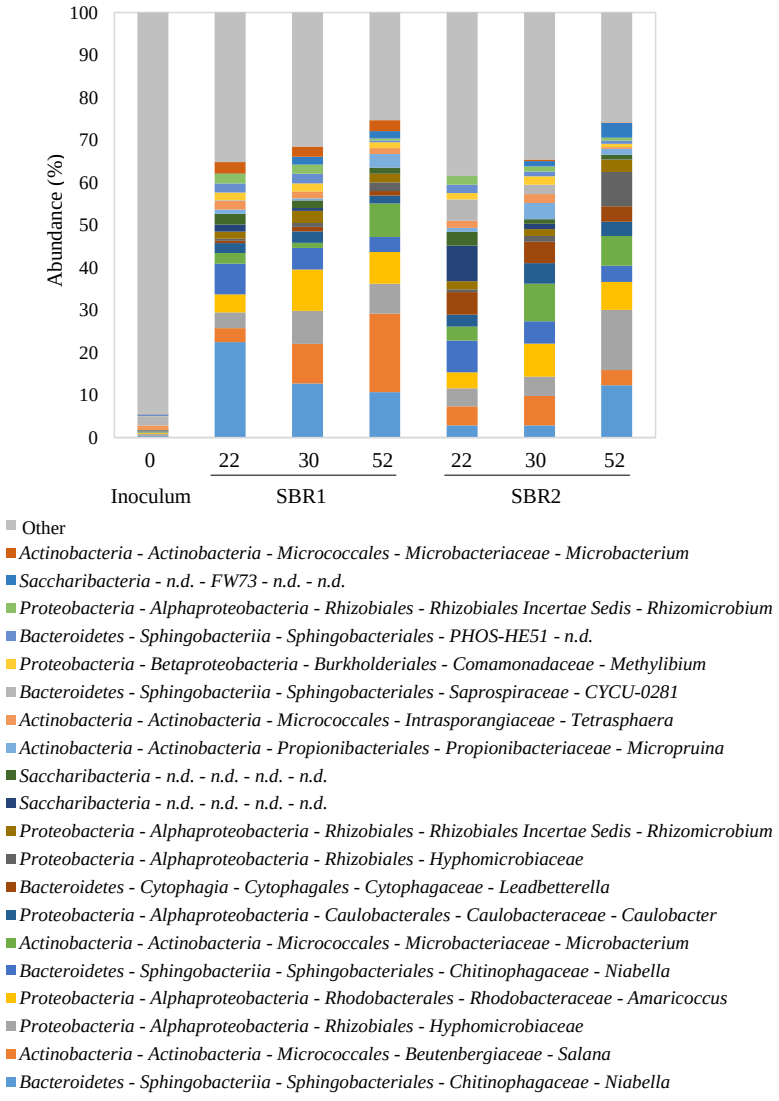


**Figure VII.S10** - Composition of bacterial communities at the genus level in the inoculum, as well as in sequencing batch reactors SBR1 and SBR2 on the indicated operational days, obtained by 16S rRNA gene sequencing analysis. Below the chart is indicated the "Phylum-Class-Order-Family-Genus" for the 20 most abundant bacteria among all of the analyzed samples. n.d. – not defined.

# Appendix F – Supporting Information for Chapter VIII

## F.VIII.1. Sample pre-treatment optimization

Owing to the complex composition of the reactor medium, the samples selected for mass spectrometry analysis required a clean-up pre-treatment in order to remove salts and other compounds that could not only interfere with and reduce the accuracy of the MS analysis, but also damage the ESI source over time. In order to optimize the recovery of azo dye metabolites during this preliminary clean-up step, two general extraction methods were tested, namely, LLE and SPE.

### LLE methodology

LLE was adapted from the extraction method used by Chan *et al*. (2012), who successfully analyzed by LC-ESI-MS metabolites resulting from Amaranth biotransformation in successive anaerobic-aerobic conditions. The fact that, similarly to AR14, the reductive cleavage of Amaranth also produced the aromatic amine 4A1NS was the main reason for selecting this study as a reference. Specifically, in order to optimize the recovery of the AR14 breakdown metabolites generally observed in the SBR treatment cycles, a sample representative of the end of the SBR anaerobic phase was used to perform several LLE tests (Figure VIII.S1). The extraction conditions for each LLE test are shown in Table VIII.S1.

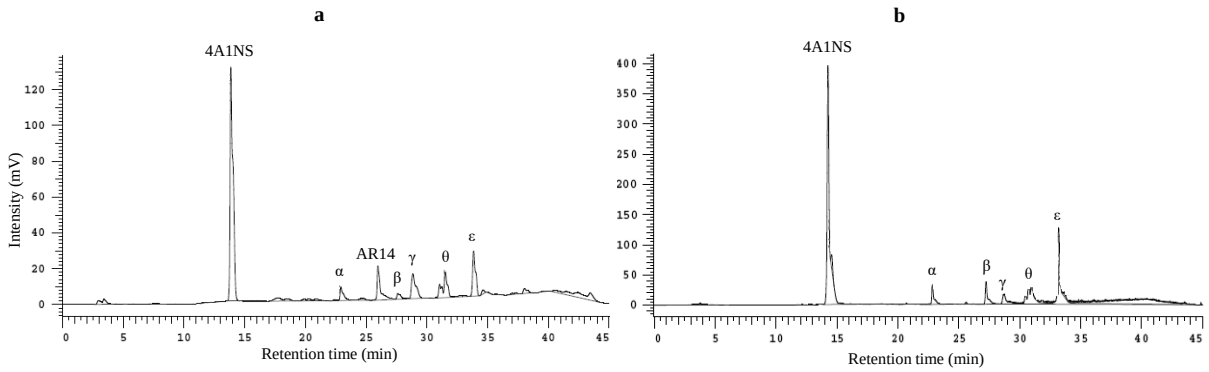


**Figure VIII.S1** - HPLC chromatogram of the test sample harvested at the end of the anaerobic phase of a representative treatment cycle, used to optimize a) liquid-liquid extraction and b) solid-phase extraction conditions. Peaks corresponding to Acid red 14 (AR14), 4-amino-naphthalene-1-sulfonic acid (4A1NS) and unknown metabolites α, β, γ, θ and ε are highlighted in the chromatograms.

As presented in Table VIII.S1, test A was performed by mixing (vortex for 1 min) the test sample with an equal volume of ethyl acetate (1 mL of each added into a 10-ml test tube), followed by centrifugation (4000 rpm for 5 min, at 21ºC) to separate the organic phase from the aqueous phase (corresponding to the top and bottom layers, respectively). Both phases were separately collected and analyzed by HPLC to evaluate the extraction performance. Test B evaluated the effect of increasing the mixing time on the metabolites recovery yields, by using the vortex for 5 min. Similarly, test C assessed the effect of increasing the number of extractions by subjecting the first collected aqueous

phase to a second step of mixing with 1 mL ethyl acetate and centrifugation, leading to the collection of two organic fractions. Test D was conducted to assess the effect of the volumetric proportion of liquid and organic phase (dilution ratio in ethyl acetate). In addition, test E was performed to analyze the impact of the sample pH in the extraction yield. For this purpose, the sample pH was adjusted to acid (test E1) or alkaline (test E2) values with HCl (12 M) or NaOH (2 M) solutions, respectively, and the same extraction conditions used for test A were employed. Finally, the *salting-out* effect was studied by adding salt ($Na_2SO_4$) to the mixture of sample and ethyl acetate, to a concentration in the aqueous phase below or above saturation (F1 and F2, respectively; Table VIII.S1).

**Table VIII.S1** - Summary of the conditions tested for liquid-liquid extraction (LLE) of a test sample. In order to optimize the LLE method, tests B, C, D, E and F were performed to assess the effect of the mixing time (vortex), number of successive extractions, volumetric proportion of liquid and organic phase (dilution ratio in ethyl acetate, EtAc), sample pH and *salting-out* using $Na_2SO_4$, respectively. *Sample pH adjusted with HCl (12 M) and NaOH (2M) solutions.

| Test | | Sample : EtAc | Mixing | # Extractions | Sample pH | $Na_2SO_4$ |
|---|---|---|---|---|---|---|
| **A** | | 1 : 1 | 1 min | 1 | 6.5 | - |
| **B** | | 1 : 1 | 5 min | 1 | 6.5 | - |
| **C** | | 1 : 1 | 1 min | 2 | 6.5 | - |
| **D** | | 1 : 2 | 1 min | 1 | 6.5 | - |
| **E** | E1 | 1 : 1 | 1 min | 1 | 1.5* | - |
| | E2 | | | | 11.6* | |
| **F** | F1 | 1 : 1 | 1 min | 1 | 6.5 | 0.18 g $mL^{-1}$ |
| | F2 | | | | | 0.54 g $mL^{-1}$ |

The LLE extraction performance was evaluated by HPLC, specifically by analyzing the aqueous phase collected after extraction, since the high absorption of ethyl acetate at the absorbance wavelength used (220 nm) interfered with the detection of the metabolites with the HPLC method employed (described in section III.3.3.1). Therefore, the decrease in the dye and metabolite peaks areas in the extracted aqueous phase relative to the original sample was quantified to provide an indication of the extraction yield.

### LLE results

A first LLE with ethyl acetate (test A, Table VIII.S1) of a representative SBR sample containing the usually observed metabolites (Figure VIII.S1) resulted in very poor extraction, with only 1% and 14% of 4A1NS and AR14, respectively, being extracted from the aqueous phase. In order to optimize the LLE method, tests B, C, D, E and F (Table VIII.S1) were performed. Except for the *salting-out* experiments (Table VIII.S1), none of the other tested conditions contributed for a substantial improvement in metabolite extraction yields. Regarding the *salting-out* effect, $Na_2SO_4$ was selected for the tests based on a previous optimization study (Yang *et al*., 2016). In the present study, the best conditions were obtained by adding $Na_2SO_4$ to the sample/ethyl acetate mixture (1:1) to a concentration above the saturation level (test F2, Table VIII.S1). These LLE conditions allowed the

extraction of 16% and 70% of 4A1NS and AR14 from the aqueous phase, a major portion of 4A1NS still being present in the aqueous phase (Figure VIII.S2). In fact, the addition of salts can not only facilitate the separation of the aqueous and organic phases after mixing (Yang *et al*., 2016), but also decrease the metabolites' solubility in water due to the *salting-out* effect (where fewer water molecules are available for dissolving the analyte molecules, preferably forming hydration spheres around the salt ions), thus promoting their extraction to the organic phase.

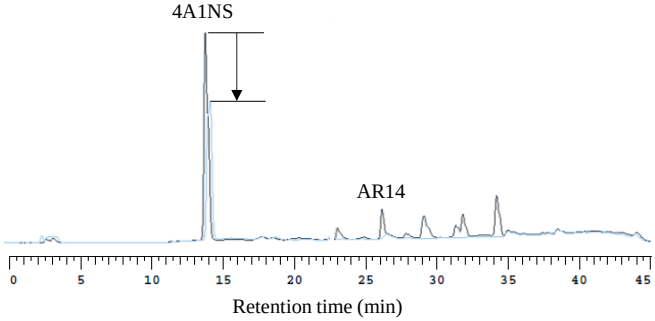


**Figure VIII.S2** - Comparison between the HPLC chromatograms of the original test sample (dark blue) and of the aqueous phase collected after extraction with ethyl acetate (light blue) according to the test F2 (Table VIII.S1). HPLC peaks correspondent to 4-amino-naphthalene-1-sulfonic acid (4A1NS) and Acid Red 14 (AR14) are highlighted. The arrow indicates the difference in the 4A1NS peak area from the original sample to the extracted fraction.

## SPE methodology

SPE was performed using Oasis HLB cartridges (1cc/30mg, Waters) on a vacuum manifold (Waters) only for sample clean-up (*i.e*., no analyte concentration). SPE conditions were optimized by performing different tests with an SBR test sample containing the metabolites usually observed at the end of the anaerobic phase of a treatment cycle during the period of azo dye-shock load (Figure VIII.S1). According to Table VIII.S2, a first test was done by following the generic Oasis HLB SPE method (provided by the manufacturer), to which some changes were subsequently added in order to optimize the method. Prior to extraction, the SPE cartridge was conditioned with 1 mL methanol followed by 1 mL of MilliQ water. Subsequently, 1 mL of the sample solution (or 2 mL in the cases when 1 mL of sample was diluted 1:1) was loaded onto the cartridge at room temperature. When performed, the subsequent wash step involved the addition of 1 mL of wash solution (5% methanol in MilliQ water, as standard procedure) to the cartridge. The washing solution was subsequently changed as described in Table VIII.S2. The cartridge was subjected to 0.5-1.0 min vacuum to eliminate residual wash solvent and eluted with 1 mL of methanol. Afterwards, 0.5-1.0 min vacuum was applied to guarantee that all elution solvent was collected. In addition to the eluate fraction, the load and wash fractions were also collected for HPLC analysis during the optimization tests. The vacuum varied within the 3-10''Hg range along the extraction procedure, being adjusted to control the load and eluate flow rates at values below 1 mL $min^{-1}$.

**Table VIII.S2** - Summary of the conditions tested for solid-phase extraction (SPE) of a test sample. In order to optimize the SPE method, specific tests were performed to assess the effect of sample dilution and sample pH adjustment (by diluting the sample with the indicated acid or base solution), while testing different wash solutions. MeOH: methanol; AcOH: acetic acid.

| **Wash solution** | **Sample dilution** | | | |
|---|---|---|---|---|
| | No dilution | 1:1 ($H_2O$) | 1:1 ($H_3PO_4$ 4%) | 1:1 ($NH_4OH$ 2%) |
| No Wash | x | | | |
| $H_2O$ | x | | x | x |
| MeOH 2% | x | | | |
| MeOH 5% | x | x | x | x |
| AcOH 2% | | | x | |
| AcOH 2% in MeOH 5% | | | x | |
| $NH_4OH$ 2% | x | | | x |
| $NH_4OH$ 2% in MeOH 5% | | | | x |
| $NH_4OH$ 5% | x | | | |
| $NH_4OH$ 10% | x | | | |
| $NH_4OH$ 10% in MeOH 2% | x | | | |

## SPE results

The low 4A1NS extraction performance achieved with LLE, even after optimization of the extraction conditions, led to the use of an SPE method as alternative. Owing to their successful application in the extraction of biotransformation products from textile azo dyes, Oasis HLB cartridges (Waters) were selected for SPE experiments (Hoff *et al.*, 2016; Li *et al.*, 2010b). Similarly to LLE, a test sample containing the aromatic amine 4A1NS and other unknown metabolites deriving from AR14 transformation was used for several tests (Figure VIII.S1).

The generic Oasis HLB SPE method, which included a wash step with 5% methanol in water followed by elution with methanol, was initially tested. In addition, in order to confirm the efficacy of using a single elution step, a second elution was performed immediately after the first (1 mL methanol applied in both cases), the elution fractions being separately collected for analysis. This generic method resulted in no extraction of 4A1NS into any of the elution fractions (Figure VIII.S3-A). In fact, the HPLC analysis of each fraction collected along the extraction process (load, wash and elution fractions) indicated that 4A1NS interacted with the Oasis HLB sorbent during the loading stage, but was subsequently washed off from the cartridge during the wash step, leading to no recovery in the eluted fractions (Figure VIII.S3-A). The same results were obtained in a parallel test when the sample was diluted with water and loaded in higher volume. In contrast to 4A1NS, the unknown metabolites were not washed off from the cartridge and could be eluted using a single elution step (Figure VIII.S3-A). Although 4A1NS was already identified by HPLC (through the use of the respective standard), optimizing the extraction conditions for 4A1NS recovery along with the other unidentified HPLC peaks could increase the probability of recovering most of the metabolites related with AR14

biotransformation, including some that were not detected through the HPLC method used (detection at 220 nm, as described in section III.3.3.1).

According to the manufacturer suggestions for optimizing the SPE procedure when the analyte is lost in the wash step, the recovery of very polar analytes can be increased by using water (instead of 5% methanol) as wash solution. Given the loss of 4A1NS in the wash step using the generic Oasis HLB SPE method (washing step with 5% methanol), the SPE procedure was repeated using different washing conditions, namely, 2% methanol or water, or leaving out the washing step (Table VIII.S2). The HPLC chromatograms of the eluted fraction from each SPE test are represented in Figure VIII.S3-B, along with the original sample. Results indicated that, similarly to washing with 5% methanol, washing with a lower concentration of methanol or water also led to 4A1NS wash off from the cartridge (confirmed by HPLC analysis of the respective wash fractions; results not shown). Accordingly, 4A1NS was only recovered in the eluted fraction when no wash step was performed; Figure VIII.S3-B).

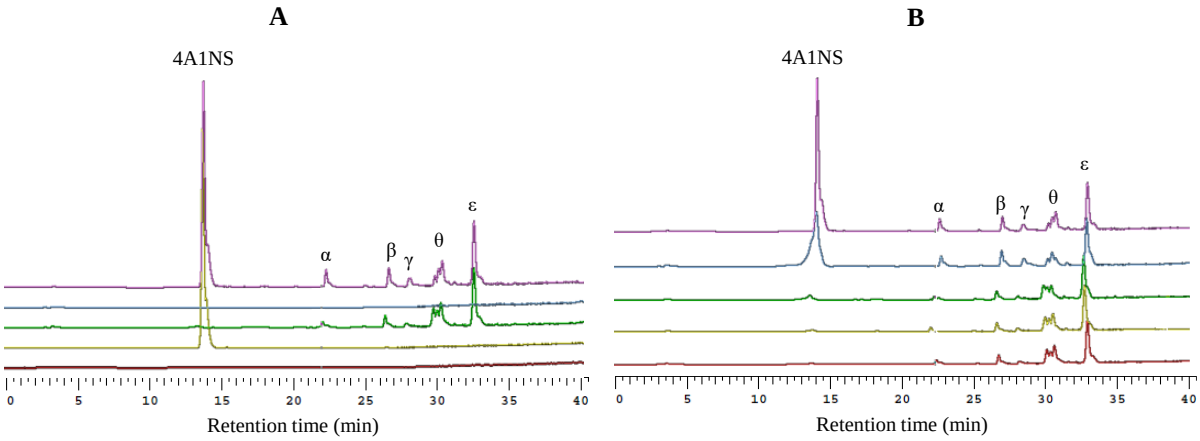


**Figure VIII.S3** - Comparison between the HPLC chromatograms of the original test sample (purple) and the sequentially collected solid-phase extraction (SPE) fractions from: A) the load (red), wash (yellow), first elution (green) and second elution (blue) steps. Washing was performed with a solution of 5% methanol in water; B) the eluted fractions from SPE tests using different washing conditions, namely, washing with 5% methanol (red), 2% methanol (yellow) or water (green) and with no wash step (blue). Peaks corresponding to 4-amino-naphthalene-1-sulfonic acid (4A1NS) and unknown metabolites α, β, γ, θ and ε are highlighted in the original sample chromatograms.

Despite solving the problem of 4A1NS recovery, skipping the wash step is not an ideal solution, as it is recommended for ensuring the removal of salts and proteins. According to the manufacturer, recoveries may be enhanced when analyte ionization is suppressed. In fact, when the analyte is in its charged state it can be eluted with weak mobile phases (low organic solvent concentrations), which might explain why 4A1NS was removed during the wash step. In contrast, when converted to a neutral form, the analyte is retained in the cartridge primarily by the strength of its hydrophobic interaction with the sorbent surface, stronger mobile phases being required for successful elution. Specifically, the manufacturer advises to adjust the sample pH to at least two pH units below the pKa for acidic analytes, or to at least two pH units above the pKa of the conjugate acid in case of basic analytes.

As the sulfonated aromatic amine 4A1NS contains one basic amine group ($–NH_2$) and one sulfonic acid group ($–SO_3H$), it is an amphoteric substance with weakly basic and strong acidic characteristics. As a reference, the pKa of benzenesulfonic acid is -2.8 and the pKa of the aniline conjugate acid is 4.6. Therefore, the 4A1NS molecule is expected to be negatively charged at pH values above 4.6 ($–SO_3^-$ and $–NH_2$) and both negatively and positively charged in acidic conditions up to pH 4.6 ($–SO_3^-$ and $–NH_3^+$). Due to its strong acid character, it was not possible to suppress 4A1NS ionization by adjusting the pH. Nevertheless, several SPE experiments were conducted by adjusting the test sample pH from 6.6 to 2.7 or 11.2 (1:1 dilution with 4% $H_3PO_4$ or 2% $NH_4OH$, respectively) and changing the wash solution, as described in Table VIII.S2. Specifically, 5% methanol, water and acid or alkaline solutions were employed as wash solutions for the acidified or alkalinized sample, respectively. The acidification of the sample led to the disappearance of two metabolite peaks from the HPLC chromatogram, discouraging the use of acidic conditions in the SPE process (Figure VIII.S4). Furthermore, alkaline washes with varying strength (10% $NH_4OH$ with 0 or 2% methanol; Table VIII.S2) were also tested for the original sample (without pH adjustment of the sample). The results in terms of 4A1NS recovery yield from all the tests performed for SPE optimization are summarized in Table VIII.S3.

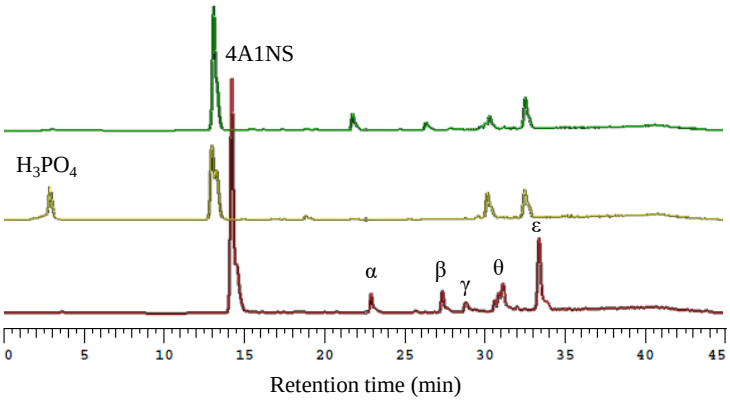


**Figure VIII.S4** - HPLC chromatograms of the test sample used in the optimization of the solid-phase extraction method: original sample (red), sample diluted 1:1 with 4% $H_3PO_4$ (yellow) and sample diluted 1:1 with 2% $NH_4OH$ (green). Peaks corresponding to 4-amino-naphthalene-1-sulfonic acid (4A1NS), unknown metabolites α, β, γ, θ, ε and $H_3PO_4$ are highlighted in the chromatograms of the original and acidified sample, respectively

Overall, the best recovery of 4A1NS (94%) was reached when no wash step was applied during SPE, the yields being below 50% in all other tested conditions (Table VIII.S3). Given this scenario, the SPE method without the wash step was chosen as the optimal method in terms of metabolites' recovery, namely 4A1NS, despite generating a less clean extract.

In order to assess the impact of skipping the SPE wash step in the subsequent MS results, the same sample was run through the protocol including either a wash with 5% methanol or water or no wash, and subsequently analyzed by LC-MS. Despite the slightly higher background noise observed in the lower *m/z* range when the wash step was not performed, the overall accuracy of the results was not

compromised (results not shown). Therefore, all SBR supernatant samples selected for MS analysis were cleaned-up by SPE, using the generic Oasis HLB (Waters) method without the wash step.

Finally, in order to verify whether the selected SPE procedure introduced any contamination, a sample of MilliQ water was subjected to the same SPE conditions as those applied to the SBR samples. Comparison between the total ion chromatogram (TIC) from the original water sample and from the eluted organic fraction (corresponding to methanol), indicated that new chromatographic peaks did not emerge after subjecting a sample to the SPE procedure, both TICs being equivalent to that of pure methanol (results not shown).

**Table VIII.S3** - Summary of the recovery results obtained for each condition tested during the optimization of 4-amino-naphthalene-1-sulfonic acid (4A1NS) extraction through solid-phase extraction. Sample pH was adjusted by diluting the sample (1:1) with the indicated acid or base solution and different wash solutions were tested. 4A1NS recovery results were calculated based on the 4A1NS peak in HPLC chromatograms. MeOH: methanol; AcOH: acetic acid.

| Sample | | Wash solution | 4A1NS extraction yield (%) |
|---|---|---|---|
| Dilution | pH | | |
| - | 6.6 | 5% MeOH | 2 |
| | | 2% MeOH | 3 |
| | | $H_2O$ | 6 |
| | | No wash | **94** |
| | | 2% $NH_4OH$ | 27 |
| | | 5% $NH_4OH$ | 37 |
| | | 10% $NH_4OH$ | 33 |
| | | 10% $NH_4OH$ in 2% MeOH | 18 |
| $H_2O$ | 6.3 | 5% MeOH | 1 |
| $NH_4OH$ 2% | 10.7 | 5% MeOH | 0 |
| | | $H_2O$ | 5 |
| | | 2% $NH_4OH$ | 14 |
| | | 2% $NH_4OH$ in 5% MeOH | 8 |
| $H_3PO_4$ 4% | 2.7 | 5% MeOH | 31 |
| | | $H_2O$ | 45 |
| | | 2% AcOH | 10 |
| | | 2% AcOH in 5% MeOH | 8 |

## F.VIII.2. LC conditions optimization

Regarding LC-MS analysis, the LC conditions initially used were similar to those employed in a study where 4A1NS degradation was followed (Chan *et al*., 2012). In order to assess the suitability of these conditions for identifying AR14, and 4A1NS and derivative compounds, an AR14 and 4A1NS standard solution was tested in both ESI positive and negative modes. The LC-MS results from this standard (Figure VIII.S5) showed that AR14 and 4A1NS could be detected using these chromatographic conditions. Specifically, both compounds could be detected in the negative mode, 4A1NS also presenting a significant peak in the ESI positive mode. Acidic characteristics of 4A1NS arise from the hydroxyl in the sulfonic acid group which is able to release a proton during the ESI step of MS (*m/z* 222, $[M-H]^-$), whereas weakly basic characteristics arise from the nitrogen of the amino substituent, which is able to receive a proton under specific pH conditions (*m/z* 224, $[M+H]^+$). In

addition, AR14 contains two sulfonic acid groups, which explains the detection of AR14 ion with a double negative charge (*m/z* 228, $[M-2H]^{2-}$) in addition to the monocharged negative ion (*m/z* 457, $[M-H]^{-}$) in the ESI negative mode.

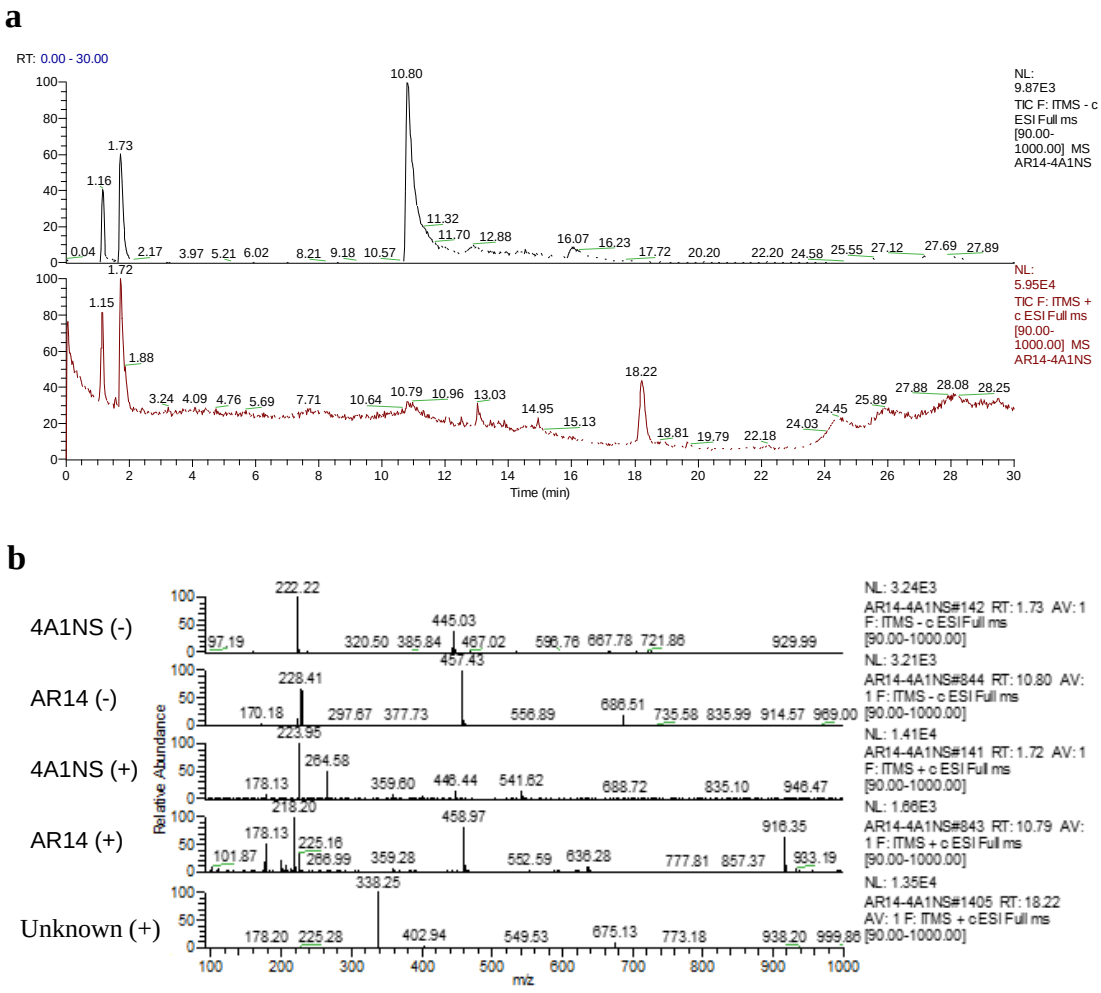


**Figure VIII.S5** - LC-MS analysis of a solution containing Acid Red 14 (AR14; 30 mg $L^{-1}$) and 4-amino-naphthalene-1-sulfonic acid (4A1NS; 15 mg 4A1NS $L^{-1}$). a) Total ion chromatograms in electrospray ionization negative (ESI-) and positive (ESI+) ion modes (black and red chromatograms, respectively). The peaks at 1.16 min (ESI-) and 1.15 min (ESI+) originate from the solvent. b) Mass spectra (MS) of the ions corresponding to 4A1NS and AR14, the retention times (RT) being respectively indicated on the right side of each MS. The lower MS (ESI+; RT = 18.22 min) probably corresponds to an impurity from the AR14 reagent (50% AR14 content). The ion *m/z* 445 in 4A1NS (-) MS probably corresponds to a 4A1NS dimer formed in the gas-phase. The liquid chromatography conditions employed in this analysis used the same gradient as Chan *et al.*, 2012.

Although both AR14 and 4A1NS could be detected using the same chromatographic gradient as Chan *et al.* (2012), 4A1NS eluted at 1.7 min (Figure VIII.S5), during the initial isocratic phase (0-5 min, 10% acetonitrile; Figure VIII.S6). This resulted in a poor separation of 4A1NS from other compounds present in the reactor samples. For this reason, the chromatographic conditions were changed to include a gradient starting immediately after injection of the samples (Figure VIII.S6), similarly to the gradient used in the HPLC method (described in section III.3.3.1). This allowed a slightly better separation of the sample compounds eluting during the initial period of the chromatographic run (Figure VIII.S7).

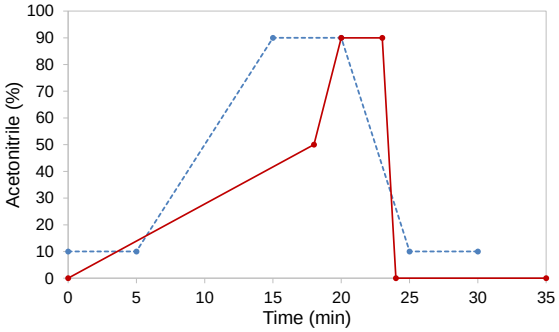


**Figure VIII.S6** - Graphical representation of the two gradients tested in LC-MS using a mixture of 0.1% formic acid and acetonitrile (ACN) as mobile phase. First gradient tested (dashed, blue line): 0-5 min, isocratic 10% ACN; 5-15 min, linear gradient to 90% ACN; 15-20 min, isocratic 90% ACN; 20-25 min, linear gradient to 10% ACN. Optimized gradient (full, red line): 0-18 min, linear gradient to 50% ACN; 18-20 min, linear gradient to 90% ACN; 20-23 min, isocratic 90% ACN; and 23-24 min, linear gradient to 0% ACN.

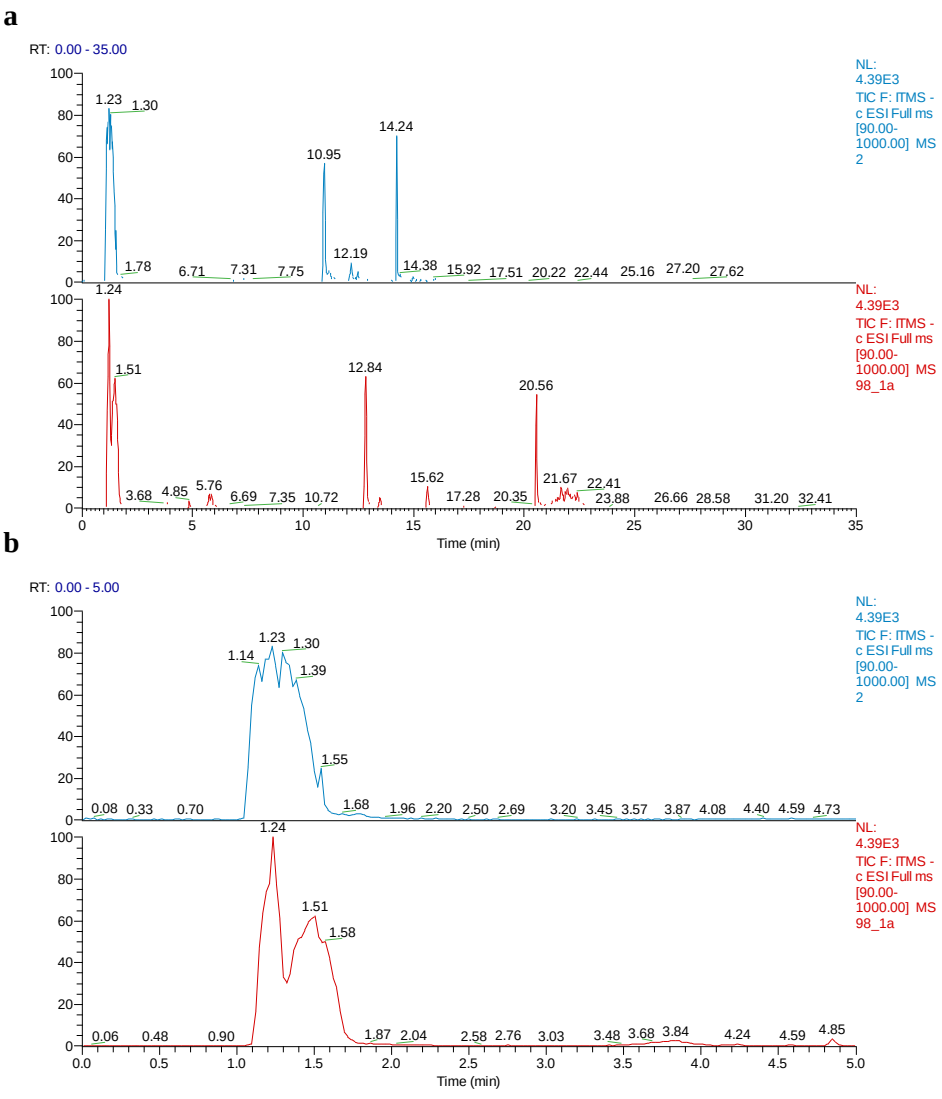


**Figure VIII.S7 -** Comparison between the total ion chromatograms (TIC) in negative mode resulting from LC-MS analysis of a test sample using two different gradients of 0.1% formic acid/acetonitrile (ACN). First gradient tested (blue line): 0-5 min, isocratic 10% ACN; 5-15 min, linear gradient to 90% ACN; 15-20 min, isocratic 90% ACN; 20-25 min, linear gradient to 10% ACN. Optimized gradient (red line): 0-18 min, linear gradient to 50% ACN; 18-20 min, linear gradient to 90% ACN; 20-23 min, isocratic 90% ACN; and 23-24 min, linear gradient to 0% ACN. b) Detail (RT=0-5 min) of the full TIC represented in a).

Therefore, the LC gradient conditions selected for further analysis of SPE-treated SBR samples correspond to the following gradient elution of 0.1% formic acid in water and acetonitrile (ACN): 0-18 min, linear gradient to 50% ACN; 18-20 min, linear gradient to 90% ACN; 20-23 min, isocratic 90% ACN; and 23-24 min, linear gradient to 0% ACN. The application of these optimized chromatographic conditions in the LC-MS of SPE-treated standard solutions of 4A1NS and AR14 revealed that 4A1NS (*m/z* 222, $[M\text{-}H^-]$) and AR14 (*m/z* 457, $[M\text{-}H]^-$; *m/z* 228, $[M\text{-}2H]^{2-}$) eluted at around 3.7 min and 12.6 min, respectively.

## F.VIII.3. LC-MS analysis of AR14 commercial product

The purity of the AR14 used in this study was 50% (Chromotrope FB, Sigma-Aldrich, 50% dye content). In order to identify the masses of the impurities present in the AR14 commercial product, a solution of AR14 (7.5 mg $L^{-1}$ of the commercial product) was analyzed by LC-MS, after being subjected to the same pre-treatment applied to the samples, SPE (solid-phase extraction to methanol). The resulting TICs and respective MS spectra obtained in ESI negative and positive modes are represented in Figure VIII.S8 and Figure VIII.S9, respectively. Accordingly, the *m/z* of the main impurities in the AR14 commercial product are as follows, for each RT:

ESI negative mode: RT 1.16 min - *m/z* 317, 385, 453, 521, 589, 656, 724.

ESI positive mode: RT 1.17 min - *m/z* 159, 227, 295, 363, 431, 499, 567, 635, 703, 770, 839, 906; RT 1.33 min - *m/z* 153, 183, 239; RT 15.7 min - *m/z* 246; RT 16.58 min - *m/z* 244; RT 18.45 min - *m/z* 274; RT 18.65 min - *m/z* 318.

These results were taken into account during the selection of the molecules potentially corresponding to degradation products of AR14. As a result, none of the 19 metabolites selected in the study correspond to the *m/z* of impurities contained in the AR14 commercial product.

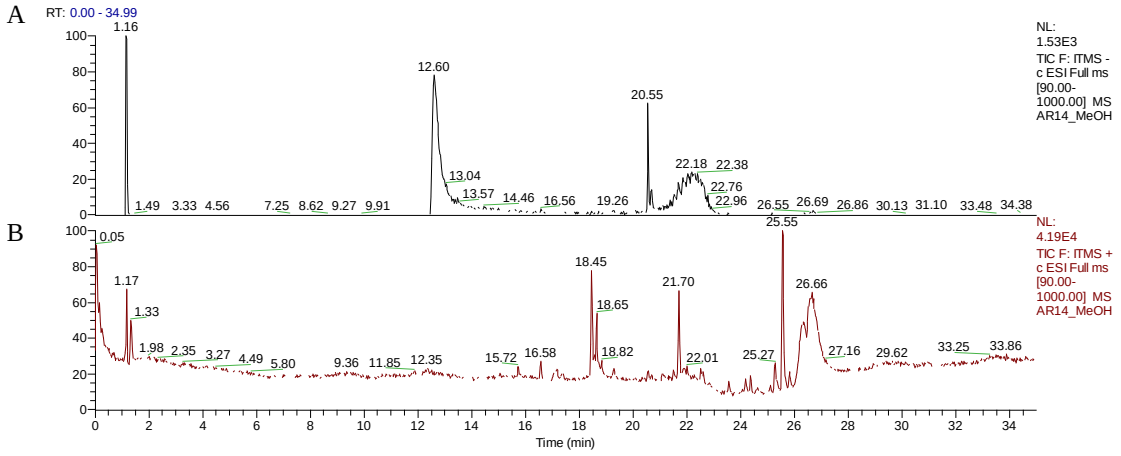


**Figure VIII.S8** - Liquid chromatography-mass spectrometry analysis of an Acid Red 14 (AR14, Chromotrope FB, Sigma-Aldrich, 50% dye content) solution (7.5 mg $L^{-1}$) after being subjected to solid-phase extraction to methanol: A and B correspond to the total ion chromatograms (TICs) obtained in the ESI negative and positive modes, respectively.

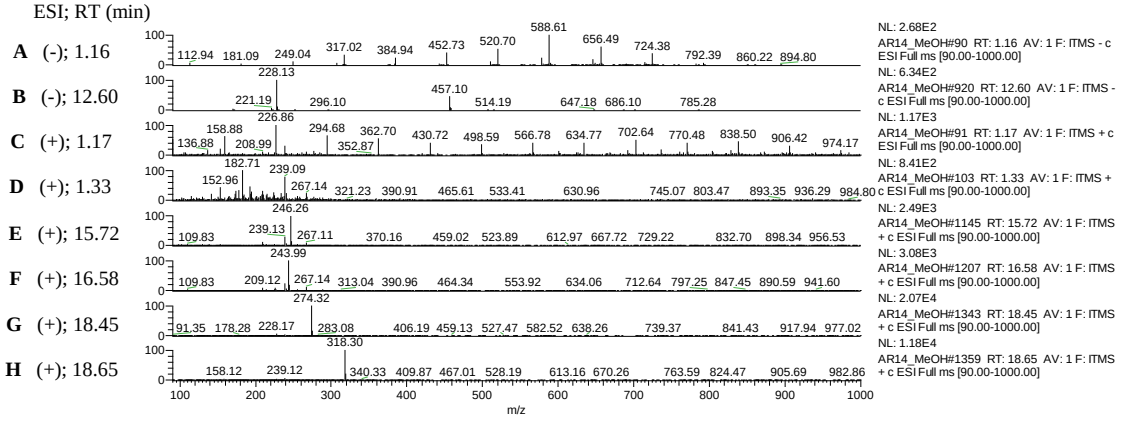


**Figure VIII.S9** - Liquid chromatography-mass spectrometry analysis of an Acid Red 14 (AR14, Chromotrope FB, Sigma-Aldrich, 50% dye content) solution (7.5 mg $L^{-1}$) after being subjected to solid phase extraction to methanol: mass spectra obtained at different retention times (RTs) in the ESI negative (A-B) and positive (C-H) modes. Mass spectrum B shows a signal at *m/z* 228 attributed to the deprotonated molecule of the AR14 molecule, $[M-2H]^{2-}$; the remaining mass spectra display as main peaks the (de)protonated molecules assigned to impurities in the commercial product.

## F.VIII.4. Correlation between metabolites detected by LC-MS and HPLC

The ion abundance profiles along the different analyzed cycles (Figure VIII.2 and Figure VIII.3, in section VIII.4.1) were compared with the HPLC peak area profiles of AR14, 4A1NS and metabolites α and α' in the same cycles (Figure VIII.S10 and Figure VIII.S11). As expected, it was possible to correlate AR14 with *m/z* 457 and 228, as well as 4A1NS with *m/z* 222. Similarly to the LC-MS results a drastic change was also observed in HPLC chromatograms from samples analyzed on cycle III, when compared with those from cycles I and II (Figure VIII.S10). Specifically, instead of 4A1NS, the unknown metabolite α' was formed during the anaerobic phase in SBR1 and SBR2 on cycle III, its concentration partially decreasing along the subsequent aerobic stage (Figure VIII.S10). The similar results obtained for the ion *m/z* 207 (Figure VIII.2, in section VIII.4.1) suggests that this compound might correspond to metabolite α' (Figure VIII.S11).

Another significant difference between the HPLC chromatograms of samples analyzed on cycles III when compared to those from cycles I and II was the absence of metabolites θ and ε on cycle III (Figure VIII.S10). In addition, while the concentration of these unknown metabolites was maintained along the aerobic phase in SBR1 on cycles I and II, their HPLC peak intensities decreased in SBR2, most significantly on cycle II (Figure VIII.S10). The abundance of the deprotonated molecules *m/z* 189 and 391 presents a similar behavior (Figure VIII.2, in section VIII.4.1). In addition, these ions eluted close to one another, at RT=15.6 min (*m/z* 391) and 15.9 min (*m/z* 189), during the final stage of the gradient (mobile phase: acetonitrile/0.1% formic acid; acetonitrile at approximately 44%), similarly to the unknown metabolites detected at RT=30-35 min in HPLC (mobile phase: acetonitrile/phosphate buffer 25 mM; acetonitrile at 50-70%; Figure VIII.S10). For these reasons, the compounds corresponding to the ions *m/z* 189 and 391 represent possible candidates for the metabolites θ and ε detected in HPLC analysis.

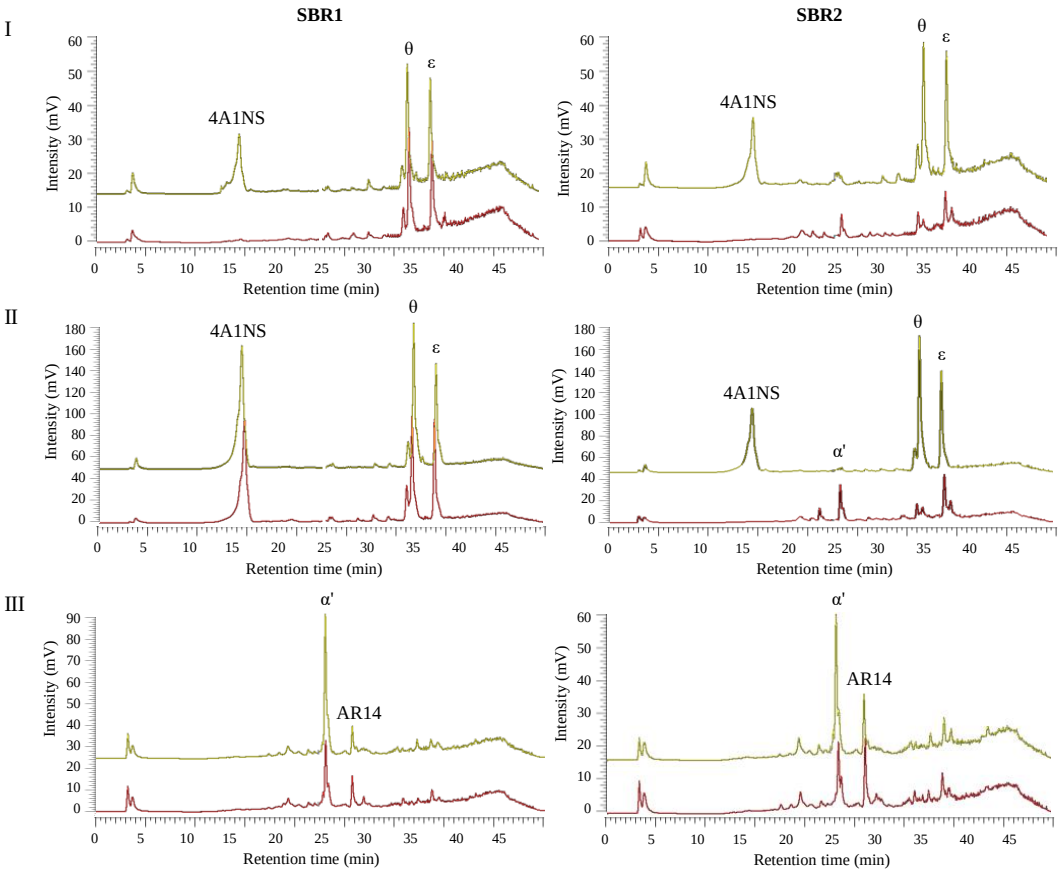


**Figure VIII.S10** - HPLC chromatograms of solid-phase extracted samples that were harvested at the end of the anaerobic phase (yellow line) and at the end of the aerobic phase (red line) from sequencing batch reactors SBR1 and SBR2 on treatment cycles I, II and III. Peaks corresponding to Acid Red 14 (AR14), 4-amino-naphthalene-1-sulfonic acid (4A1NS), and other relevant unknown metabolites (α',θ, ε) are indicated.

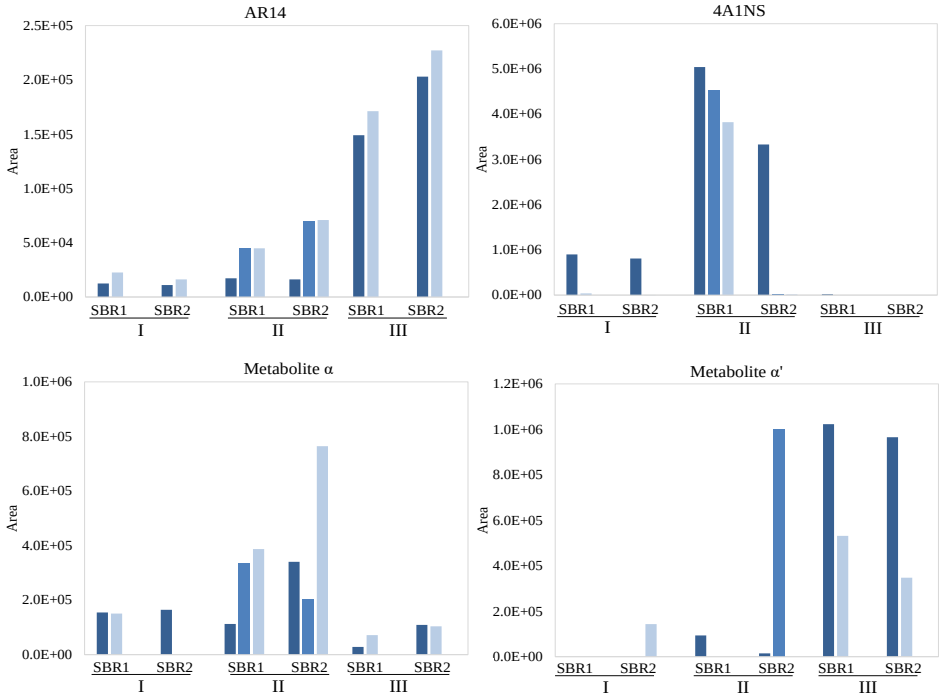


**Figure VIII.S11** - Area of HPLC peaks corresponding to the azo dye Acid Red 14 (AR14), the aromatic amine 4-amino-naphthalene-1-sulfonic acid (4A1NS) and two unknown metabolites, α and α', present in solid-phase extracted samples that were harvested on cycles I, II and III from the sequencing batch reactors at the end of the anaerobic phase (dark blue), after 1 h of aeration (middle blue; only analyzed on cycle II), and at the end of the aerobic phase (light blue).

## F.VIII.5. Summary of results obtained in LC-MS$^2$ analysis

The results from the LC-MS$^2$ analysis are summarized in Table VIII.S4 for each of the 19 selected ions.

**Table VIII.S4** - Relevant metabolites observed in the LC-MS analysis and typical product ions resulting from the fragmentation of each precursor ion in LC-MS$^2$ analysis, with indication of the proposed fragment ions and respective neutral loss. $[M-H]^-$: deprotonated molecule; $[M+H]^+$; protonated molecule; n.f.: not fragmented; RT: retention time. * Precursor ion absent in respective MS$^2$ spectra due to excess of collision-induced dissociation energy leading to complete fragmentation.

| Metabolite | MS | | | MS$^2$ | | |
|---|---|---|---|---|---|---|
| | *m/z* | Precursor ion | RT (min) | *m/z* | Product ions | Neutral loss (u) |
| 1 | **189** | $[M-H]^-$ | 15.9 | 173 | $[(M-H)-CH_4]^-$ | 16 |
| 2 | **207** | $[M-H]^-$ | 10 | 143 | $[(M-H)-SO_2]^-$ | 64 |
| 3 | **222** | $[M-H]^-$ | 3.7 | 158 | $[(M-H)-SO_2]^-$ | 64 |
| 4 | **228 *** | $[M-2H]^{2-}$ | 12.7 | 221 | $[(M-H)-C_{10}H_6NO_4S^{\bullet}]^{\bullet-}$ | 236 |
| | | | | 170 | $[(M-H)-C_{10}H_7O_3S^{\bullet}-SO_3]^{\bullet-}$ | 287 |
| 5 | **239** | $[M-H]^-$ | 6.7 | 159 | $[(M-H)-SO_3]^-$ | 80 |
| 6 | **252** | $[M-H]^-$ | 12.3 | 188 | $[(M-H)-SO_2]^-$ | 64 |
| 7 | **268** | $[M-H]^-$ | 11.9 | 188 | $[(M-H)-SO_3]^-$ | 80 |
| 8 | **377** | $[M-H]^-$ | 12.8 | 313 | $[(M-H)-SO_2]^-$ | 64 |
| | | | | 297 | $[(M-H)-SO_3]^-$ | 80 |
| 9 | **379** | $[M-H]^-$ | 13.7 | 315 | $[(M-H)-SO_2]^-$ | 64 |
| | | | | 299 | $[(M-H)-SO_3]^-$ | 80 |
| 10 | **391** | $[M-H]^-$ | 15.6 | 327 | $[(M-H)-SO_2]^-$ | 64 |
| | | | | 311 | $[(M-H)-SO_3]^-$ | 80 |
| 11 | **393** | $[M-H]^-$ | 10.1 | n.f. | n.f. | |
| 12 | **394** | $[M-H]^-$ | 10.7 | 314 | $[(M-H)-SO_3]^-$ | 80 |
| 13 | **419 *** | $[M-H]^-$ | 17.3 | 377 | $[(M-H)-C_2H_2O]^-$ | 42 |
| | | | | 355 | $[(M-H)-SO_2]^-$ | 64 |
| | | | | 339 | $[(M-H)-SO_3]^-$ | 80 |
| | | | | 313 | $[(M-H)-C_2H_2O-SO_2]^-$ | 106 |
| | | | | 297 | $[(M-H)-C_2H_2O-SO_3]^-$ | 122 |
| 14 | **457 *** | $[M-H]^-$ | 12.5 | 377 | $[(M-H)-SO_3]^-$ | 80 |
| | | | | 297 | $[(M-H)-SO_3-SO_3]^-$ | 160 |
| 15 | **592 *** | $[M-H]^-$ | 14.7 | 528 | $[(M-H)-SO_2]^-$ | 64 |
| 16 | **689 *** | $[M-H]^-$ | 19.5 | 672 | $[(M-H)-NH_3]^-$ | 17 |
| | | | | 609 | $[(M-H)-SO_3]^-$ | 80 |
| 17 | **173** | $[M+H]^+$ | 7.3 | 146 | $[(M+H)-CHN]^+$ | 27 |
| 18 | **174** | $[M+H]^+$ | 12.6 | 146 | $[(M+H)-CO]^+$ | 28 |
| 19 | **189** | $[M+H]^+$ | 13.9 | 161 | $[(M+H)-CO]^+$ | 28 |

## F.VIII.6. Fragmentation patterns according to LC-HRMS/MS analysis

Based on the information regarding the HRMS/MS fragments (Table VIII.3, in section VIII.4.2), the fragmentation pattern of some of the compounds to which a chemical formula was attributed (Table VIII.4, in section VIII.4.2) is represented in Figure VIII.S12 to Figure VIII.S24.

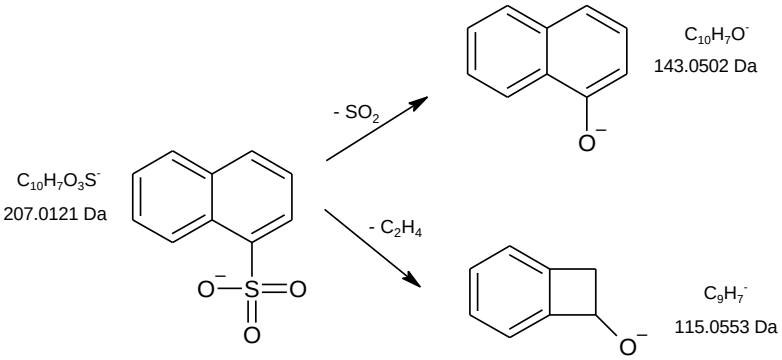


**Figure VIII.S12** - Proposed fragmentation pattern for metabolite 2.

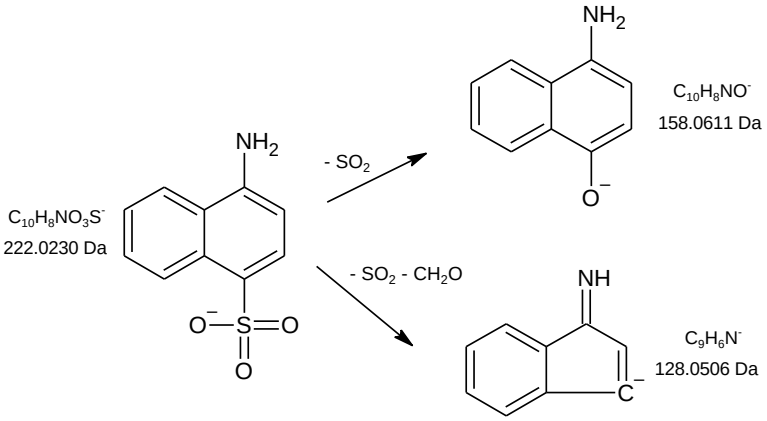


**Figure VIII.S13** - Proposed fragmentation pattern for metabolite 3.

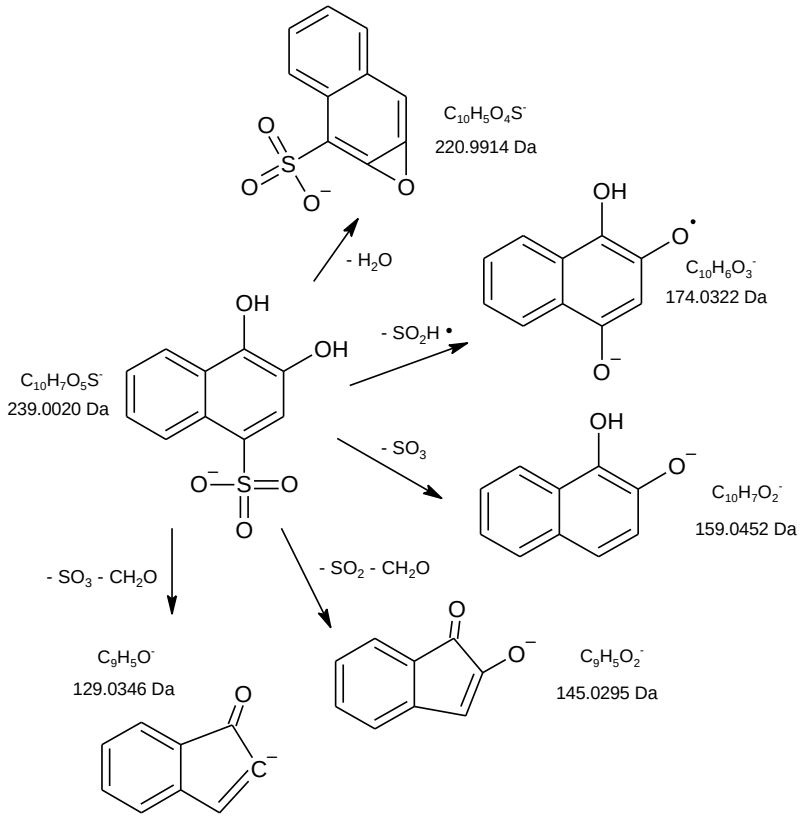


**Figure VIII.S14** - Proposed fragmentation pattern for metabolite 5.

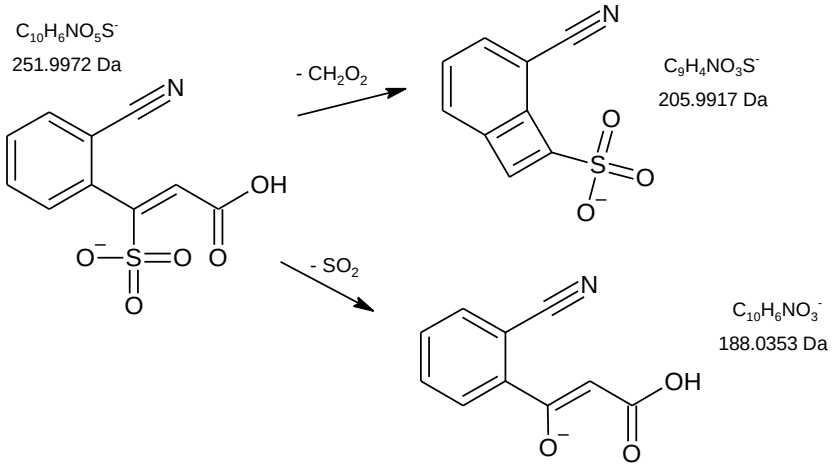


**Figure VIII.S15** - Proposed fragmentation pattern for metabolite 6.

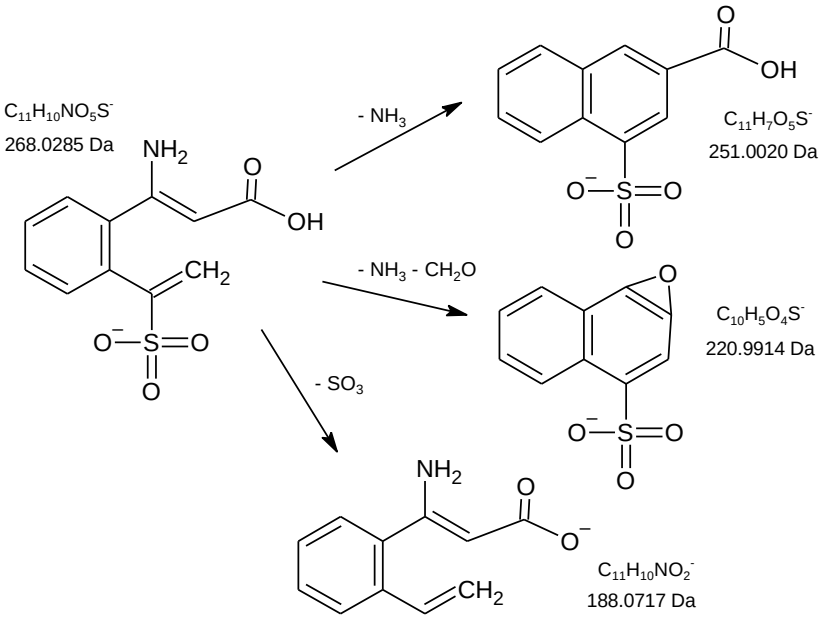


**Figure VIII.S16** - Proposed fragmentation pattern for metabolite 7.

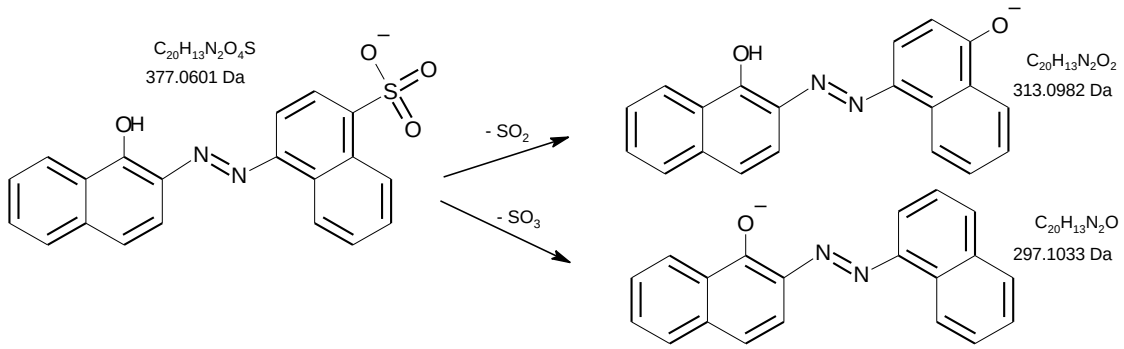


**Figure VIII.S17** - Proposed fragmentation pattern for metabolite 8.

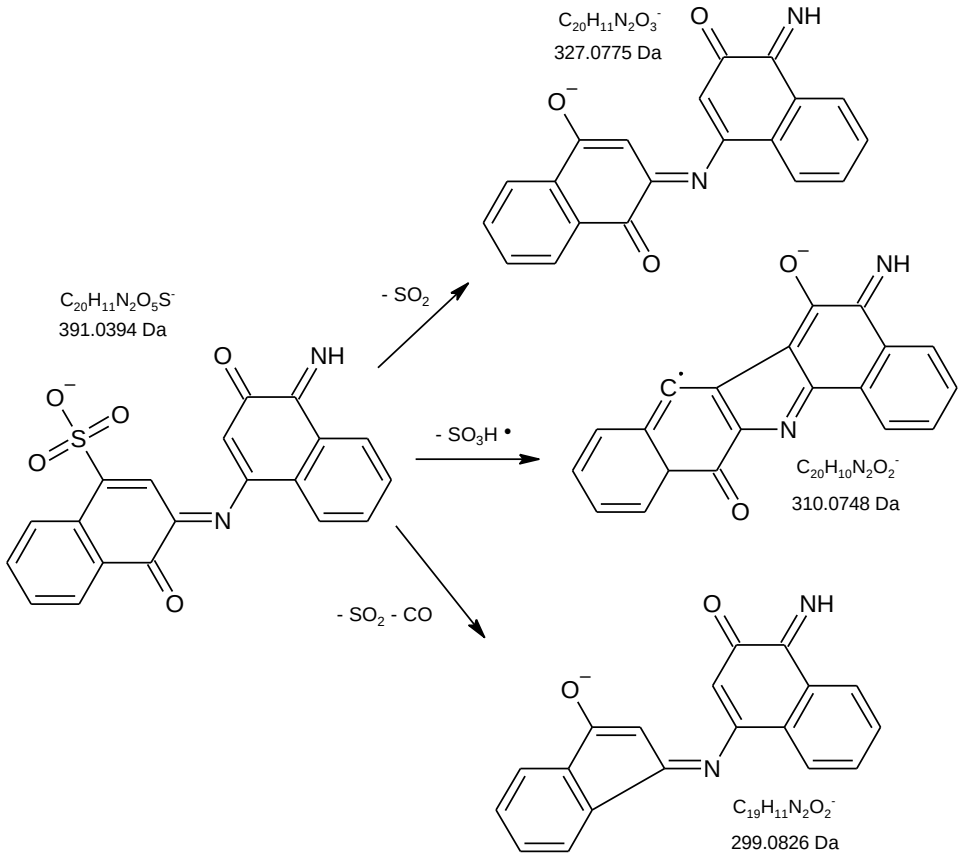


**Figure VIII.S18** - Proposed fragmentation pattern for metabolite 10.

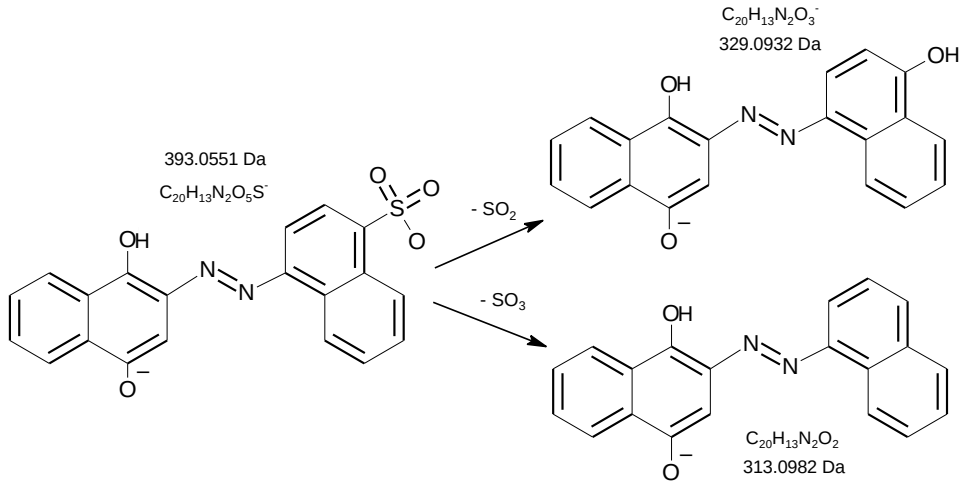


**Figure VIII.S19** - Proposed fragmentation pattern for metabolite 11.

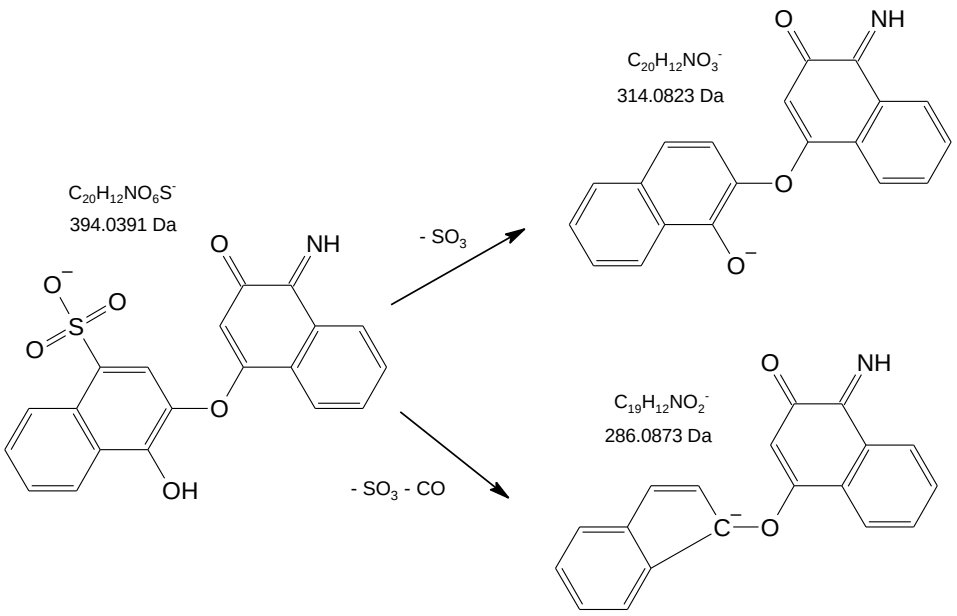


**Figure VIII.S20** - Proposed fragmentation pattern for metabolite 12.

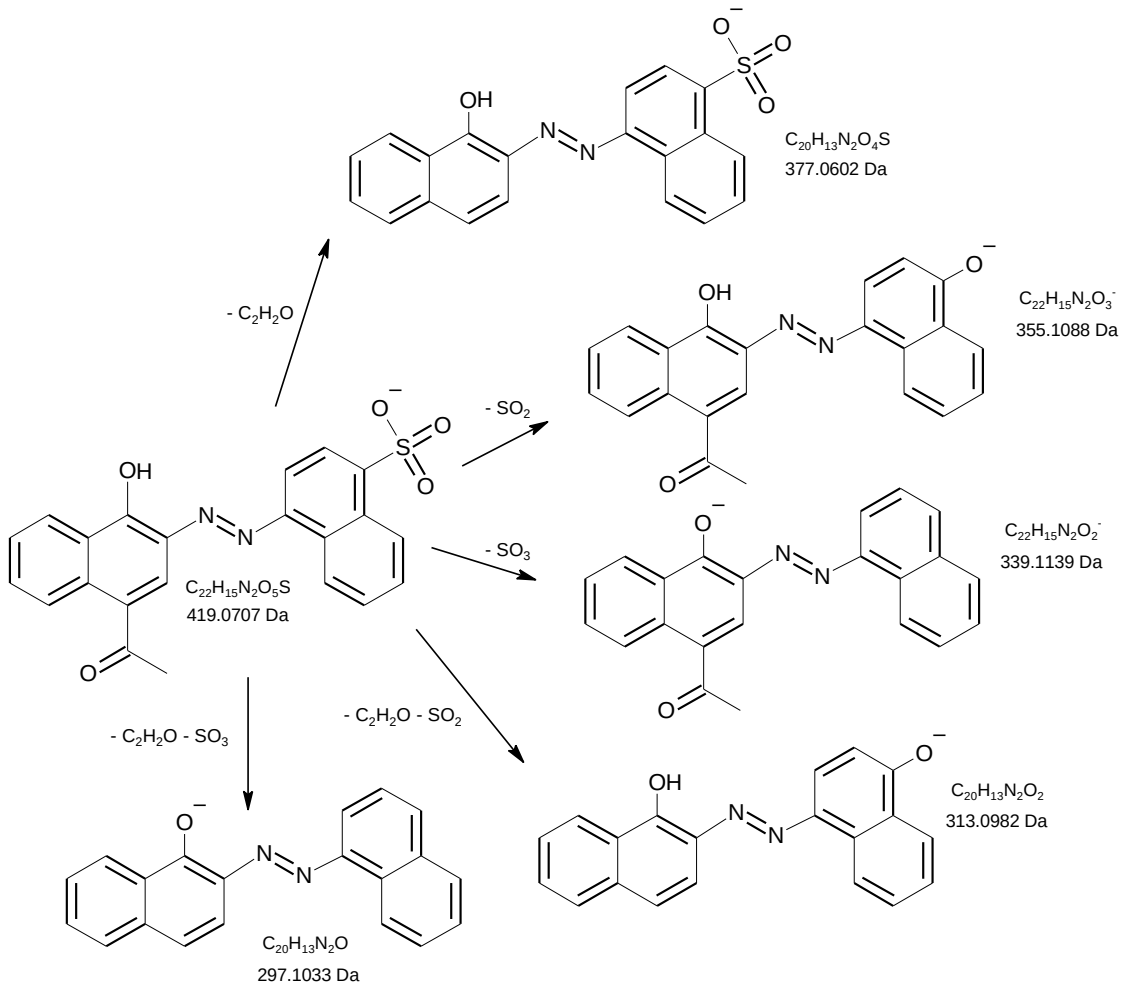


**Figure VIII.S21** - Proposed fragmentation pattern for metabolite 13.

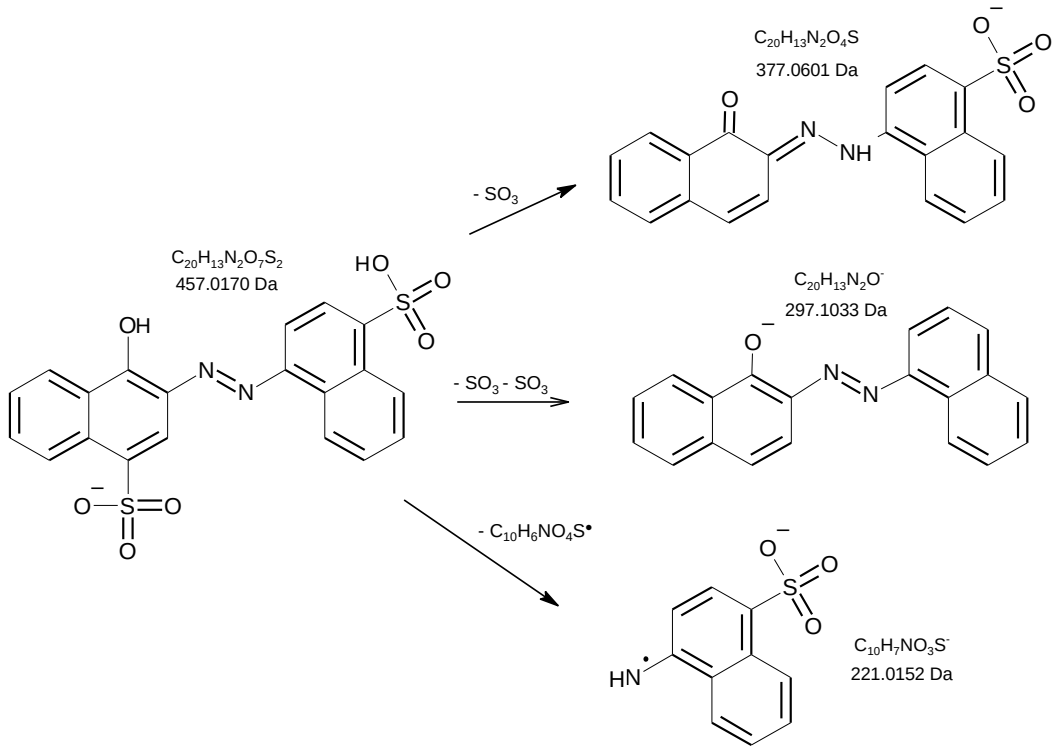


**Figure VIII.S22** - Proposed fragmentation pattern for metabolite 14.

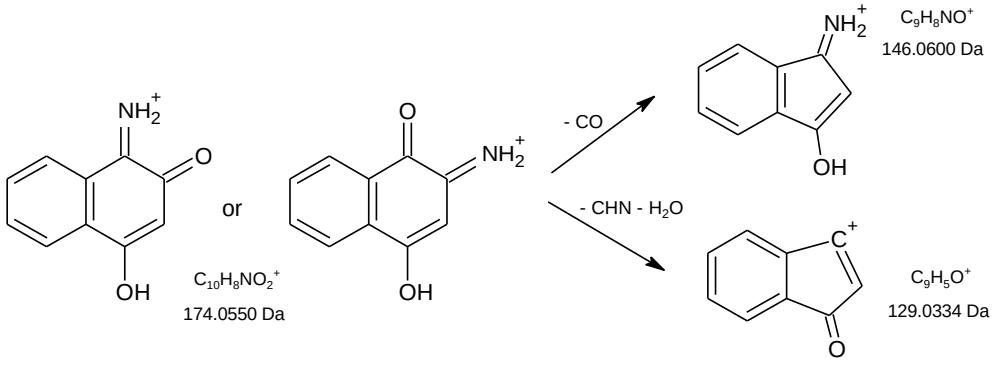


**Figure VIII.S23** - Proposed fragmentation pattern for metabolite 18.

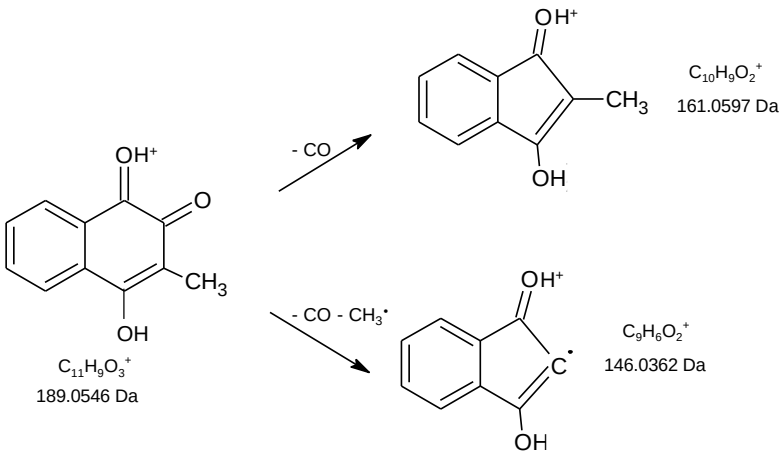


**Figure VIII.S24** - Proposed fragmentation pattern for metabolite 19.

## F.VIII.7. LC-HRMS/MS results: ion chromatograms, MS and MS/MS spectra

Based on the LC-HRMS/MS analysis, the ion chromatograms of SBR1 and SBR2 samples collected at the end of the anaerobic reaction phase (sample A) and at the end of the subsequent aerobic reaction phase (sample B) in cycles II and III (Figure VIII.1, in section VIII.3.2) are presented in Figure VIII.S25 to Figure VIII.S43, together with the respective MS spectra and MS/MS spectra, covering all of the degradation products referred in the manuscripts (19 metabolites).

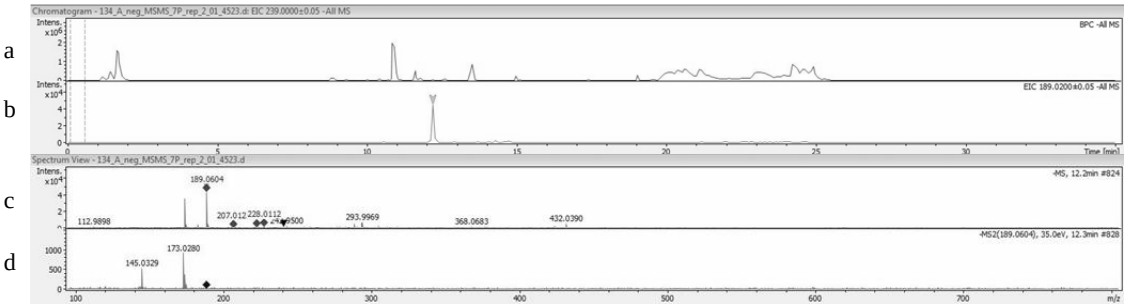


**Figure VIII.S25 -** Metabolite 1: base peak chromatogram (ESI negative mode) of sample A from SBR1 on cycle II (a), extracted ion chromatogram for *m/z* 189 (b) and corresponding mass spectrum (c) and tandem mass spectrum (d).

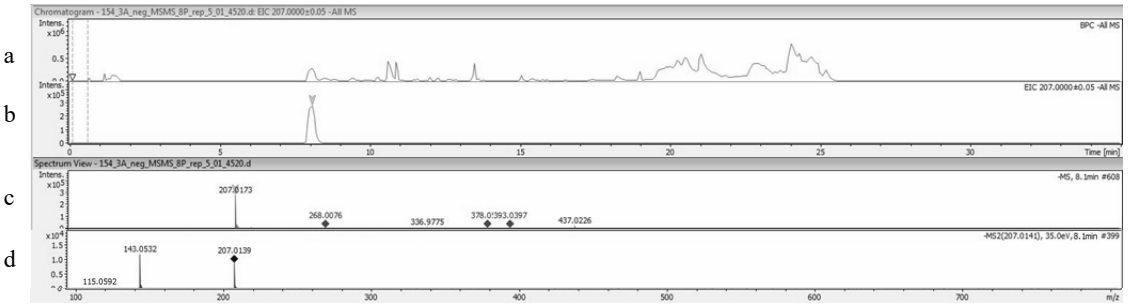


**Figure VIII.S26 -** Metabolite 2: base peak chromatogram (ESI negative mode) of sample B from SBR2 on cycle III (a), extracted ion chromatogram for *m/z* 207 (b) and corresponding mass spectrum (c) and tandem mass spectrum (d).

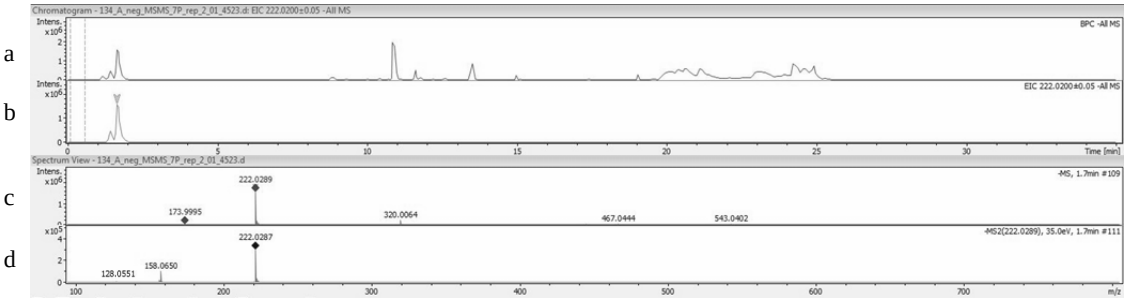


**Figure VIII.S27 -** Metabolite 3: base peak chromatogram (ESI negative mode) of sample A from SBR1 on cycle II (a), extracted ion chromatogram for *m/z* 222 (b) and corresponding mass spectrum (c) and tandem mass spectrum (d).

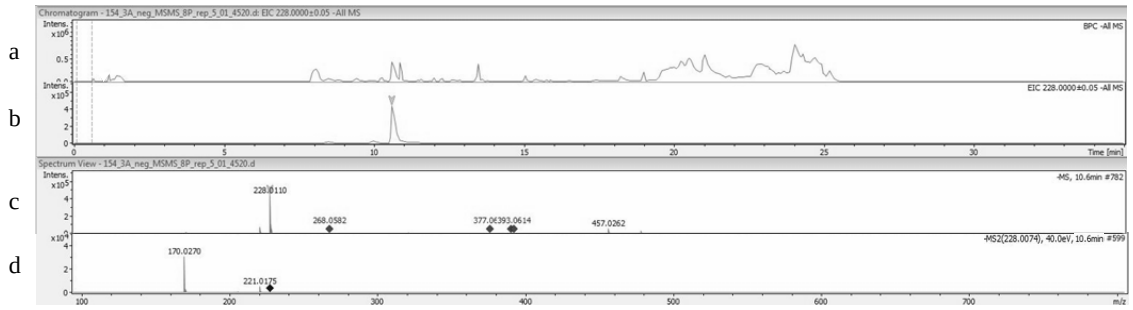


**Figure VIII.S28 -** Metabolite 4: base peak chromatogram (ESI negative mode) of sample B from SBR2 on cycle III (a), extracted ion chromatogram for *m/z* 228 (b) and corresponding mass spectrum (c) and tandem mass spectrum (d).

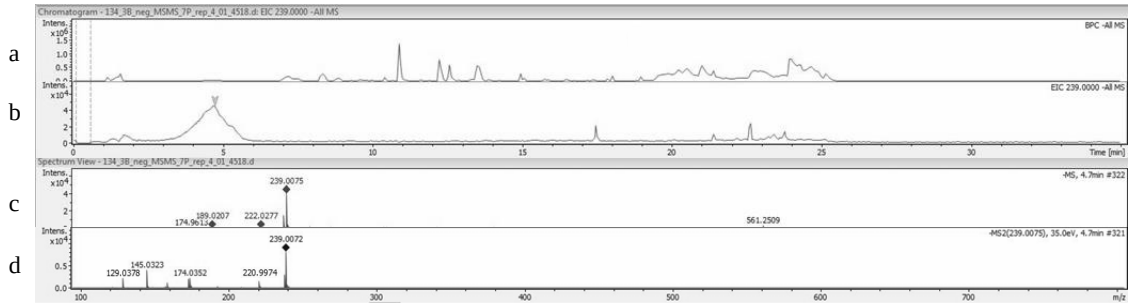


**Figure VIII.S29 -** Metabolite 5: base peak chromatogram (ESI negative mode) of sample B from SBR2 on cycle II (a), extracted ion chromatogram for *m/z* 239 (b) and corresponding mass spectrum (c) and tandem mass spectrum (d).

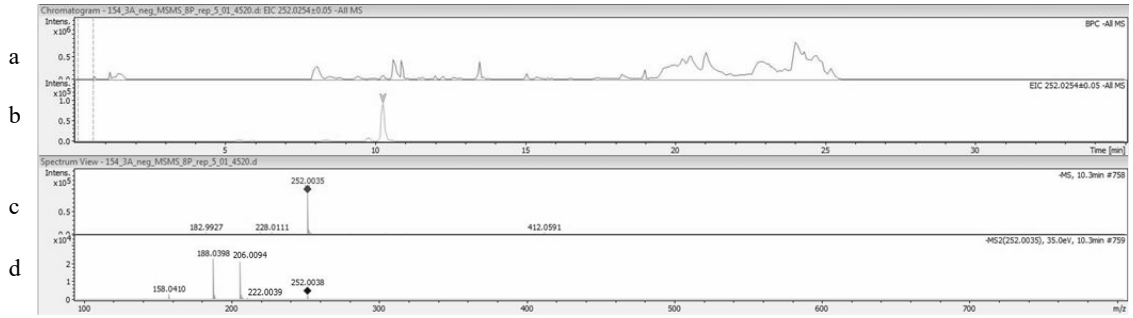


**Figure VIII.S30 -** Metabolite 6: base peak chromatogram (ESI negative mode) of sample A from SBR2 on cycle III (a), extracted ion chromatogram for *m/z* 252 (b) and corresponding mass spectrum (c) and tandem mass spectrum (d).

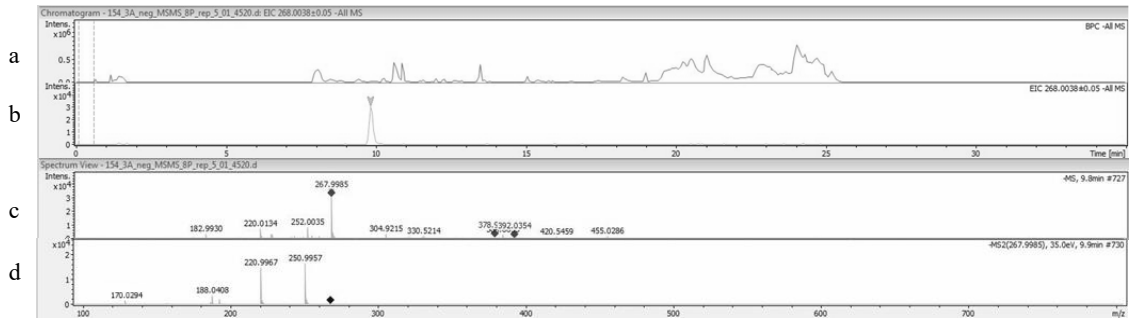


**Figure VIII.S31 -** Metabolite 7: base peak chromatogram (ESI negative mode) of sample B from SBR2 on cycle III (a), extracted ion chromatogram for *m/z* 268 (b) and corresponding mass spectrum (c) and tandem mass spectrum (d).

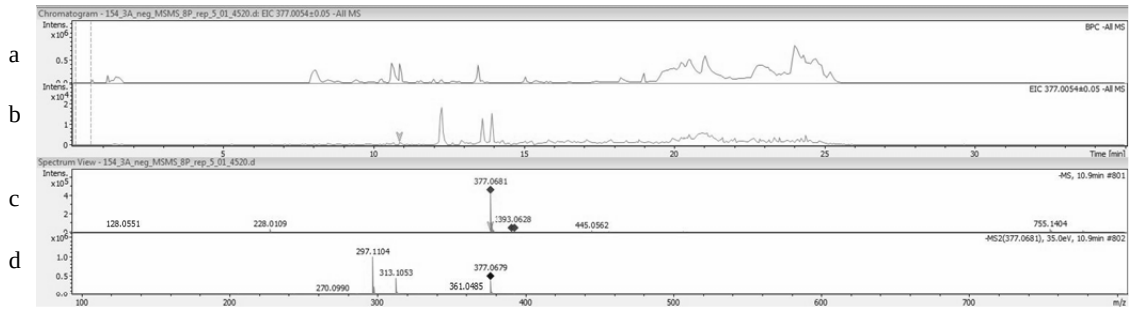


**Figure VIII.S32 -** Metabolite 8: base peak chromatogram (ESI negative mode) of sample A from SBR2 on cycle III (a), extracted ion chromatogram for *m/z* 377 (b) and corresponding mass spectrum (c) and tandem mass spectrum (d).

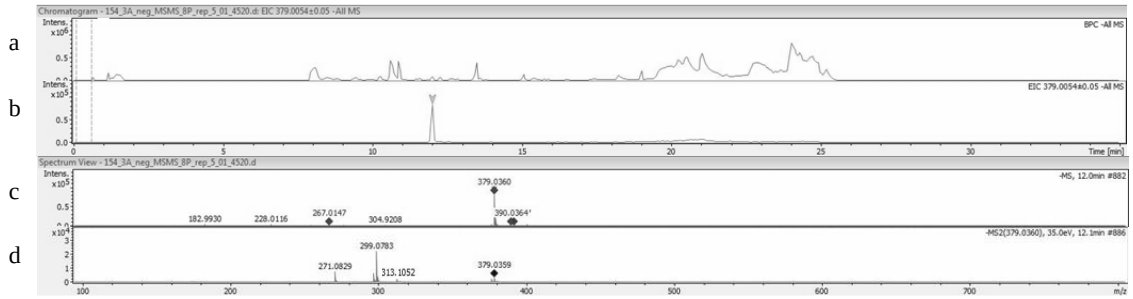


**Figure VIII.S33 -** Metabolite 9: base peak chromatogram (ESI negative mode) of sample A from SBR2 on cycle III (a), extracted ion chromatogram for *m/z* 379 (b) and corresponding mass spectrum (c) and tandem mass spectrum (d).

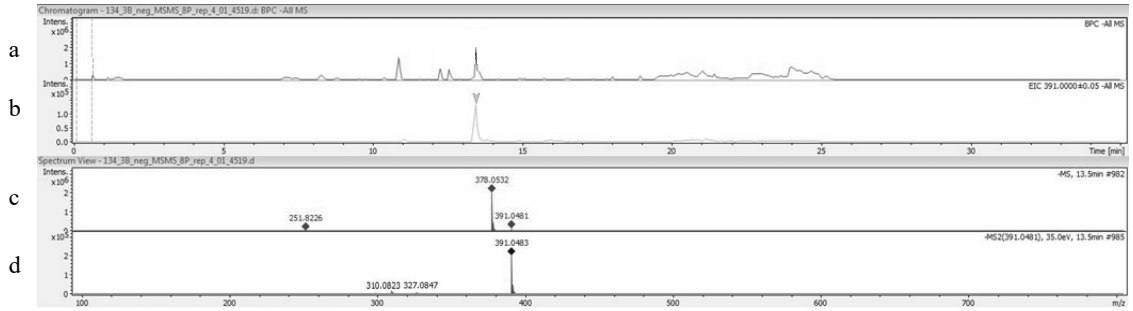


**Figure VIII.S34 -** Metabolite 10: base peak chromatogram (ESI negative mode) of sample B from SBR2 on cycle II (a), extracted ion chromatogram for *m/z* 391 (b) and corresponding mass spectrum (c) and tandem mass spectrum (d).

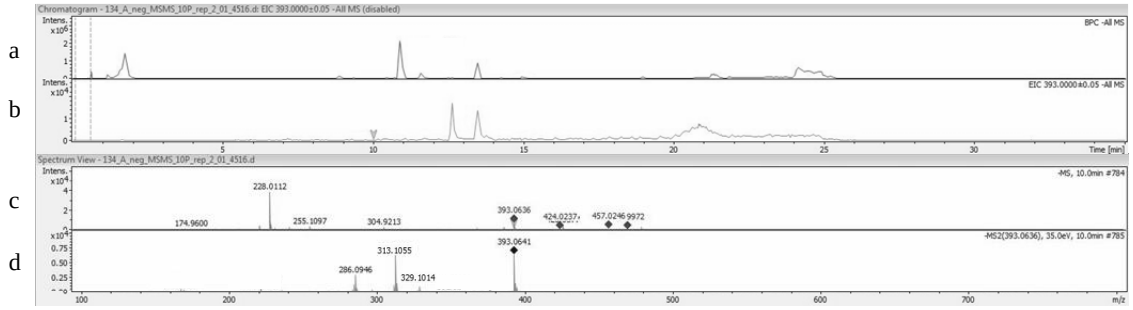


**Figure VIII.S35 -** Metabolite 11: base peak chromatogram (ESI negative mode) of sample A from SBR1 on cycle II (a), extracted ion chromatogram for *m/z* 393 (b) and corresponding mass spectrum (c) and tandem mass spectrum (d).

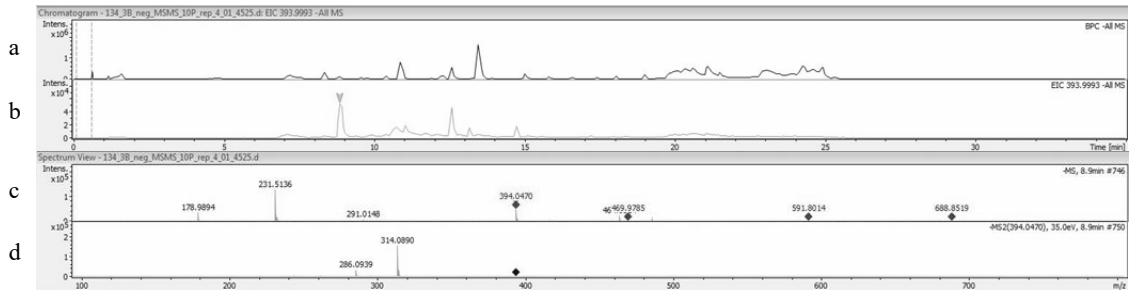


**Figure VIII.S36 -** Metabolite 12: base peak chromatogram (ESI negative mode) of sample B from SBR2 on cycle III (a), extracted ion chromatogram for *m/z* 394 (b) and corresponding mass spectrum (c) and tandem mass spectrum (d).

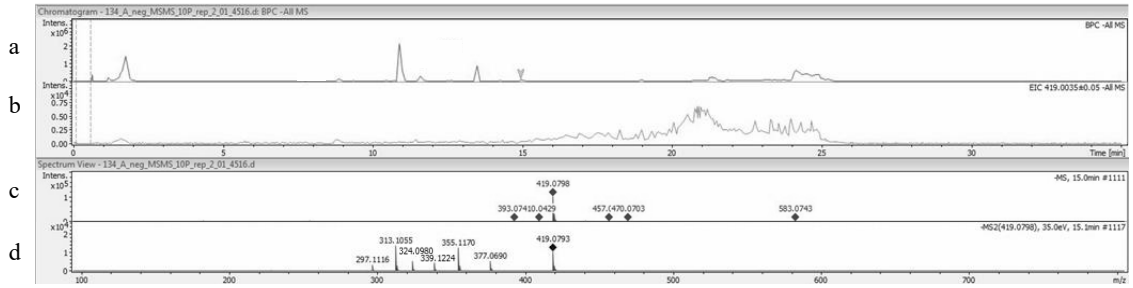


**Figure VIII.S37 -** Metabolite 13: base peak chromatogram (ESI negative mode) of sample A from SBR1 on cycle II (a), extracted ion chromatogram for *m/z* 419 (b) and corresponding mass spectrum (c) and tandem mass spectrum (d).

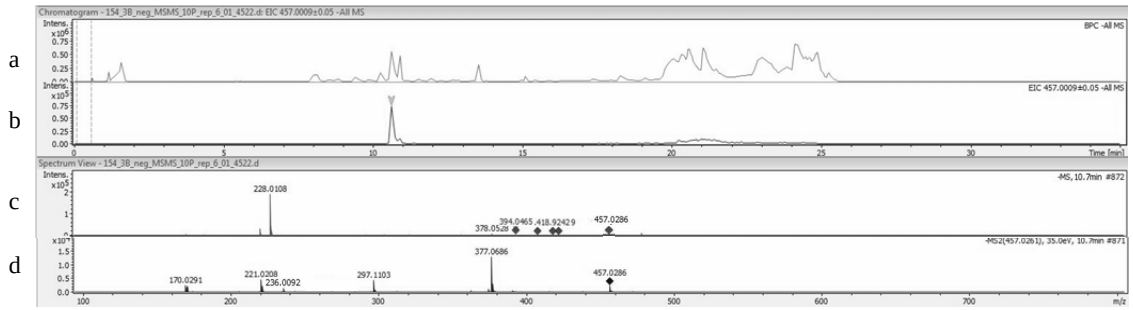


**Figure VIII.S38 -** Metabolite 14: base peak chromatogram (ESI negative mode) of sample B from SBR2 on cycle III (a), extracted ion chromatogram for *m/z* 457 (b) and corresponding mass spectrum (c) and tandem mass spectrum (d).

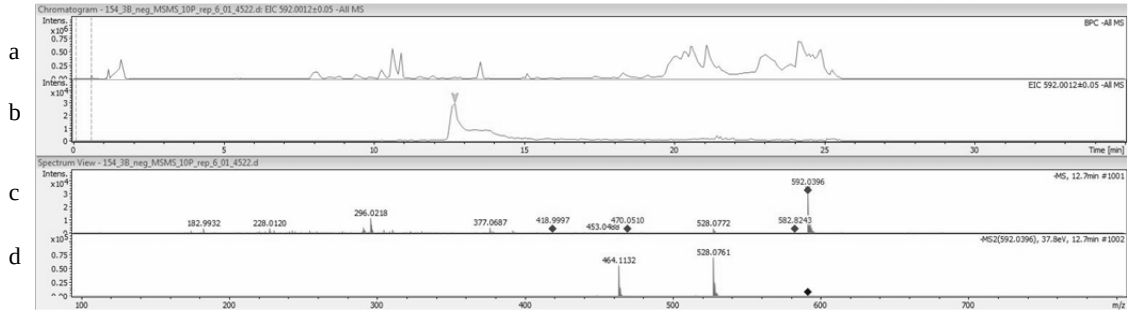


**Figure VIII.S39 -** Metabolite 15: base peak chromatogram (ESI negative mode) of sample B from SBR2 on cycle III (a), extracted ion chromatogram for *m/z* 592 (b) and corresponding mass spectrum (c) and tandem mass spectrum (d).

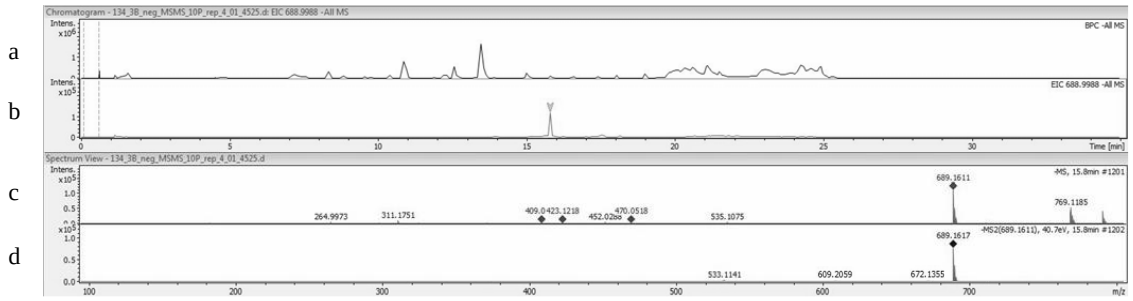


**Figure VIII.S40** - Metabolite 16: base peak chromatogram (ESI negative mode) of sample B from SBR2 on cycle II (a), extracted ion chromatogram for *m/z* 689 (b) and corresponding mass spectrum (c) and tandem mass spectrum (d).

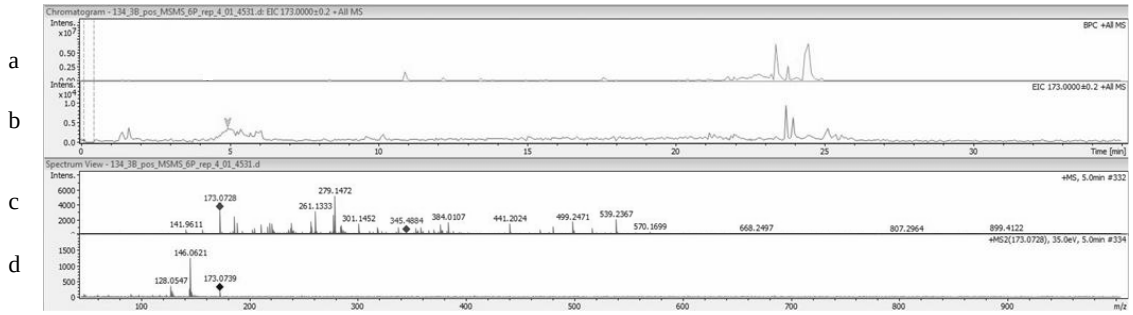


**Figure VIII.S41** - Metabolite 17: base peak chromatogram (ESI positive mode) of sample B from SBR2 on cycle II (a), extracted ion chromatogram for *m/z* 173 (b) and corresponding mass spectrum (c) and tandem mass spectrum (d).

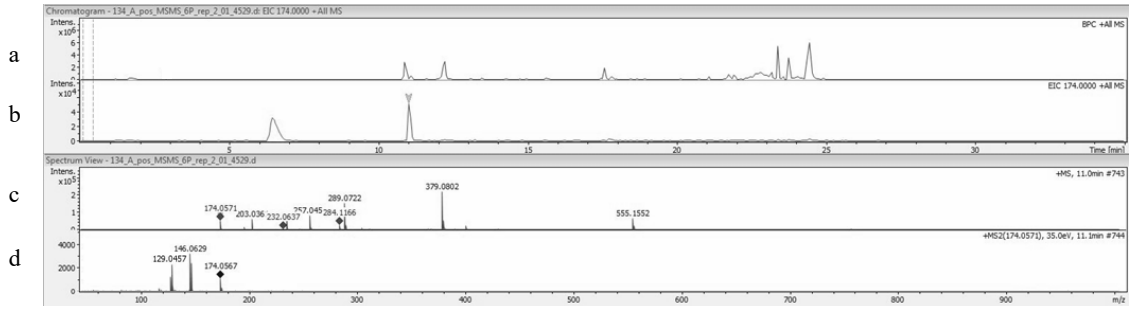


**Figure VIII.S42** - Metabolite 18: base peak chromatogram (ESI positive mode) of sample A from SBR1 on cycle II (a), extracted ion chromatogram for *m/z* 174 (b) and corresponding mass spectrum (c) and tandem mass spectrum (d).

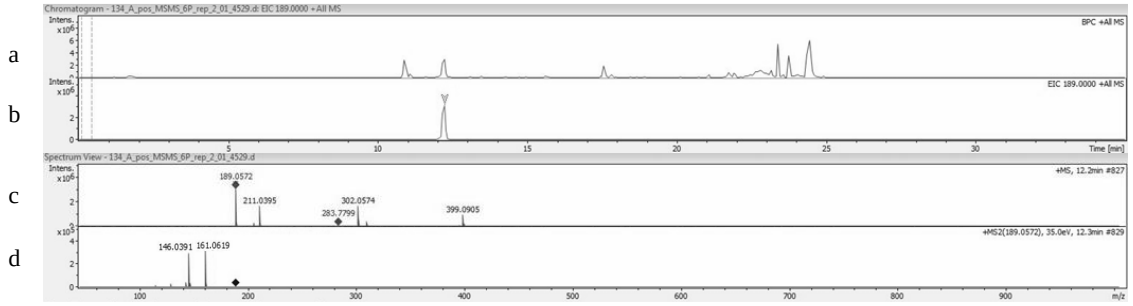


**Figure VIII.S43** - Metabolite 19: base peak chromatogram (ESI positive mode) of sample A from SBR1 on cycle II (a), extracted ion chromatogram for *m/z* 189 (b) and corresponding mass spectrum (c) and tandem mass spectrum (d).

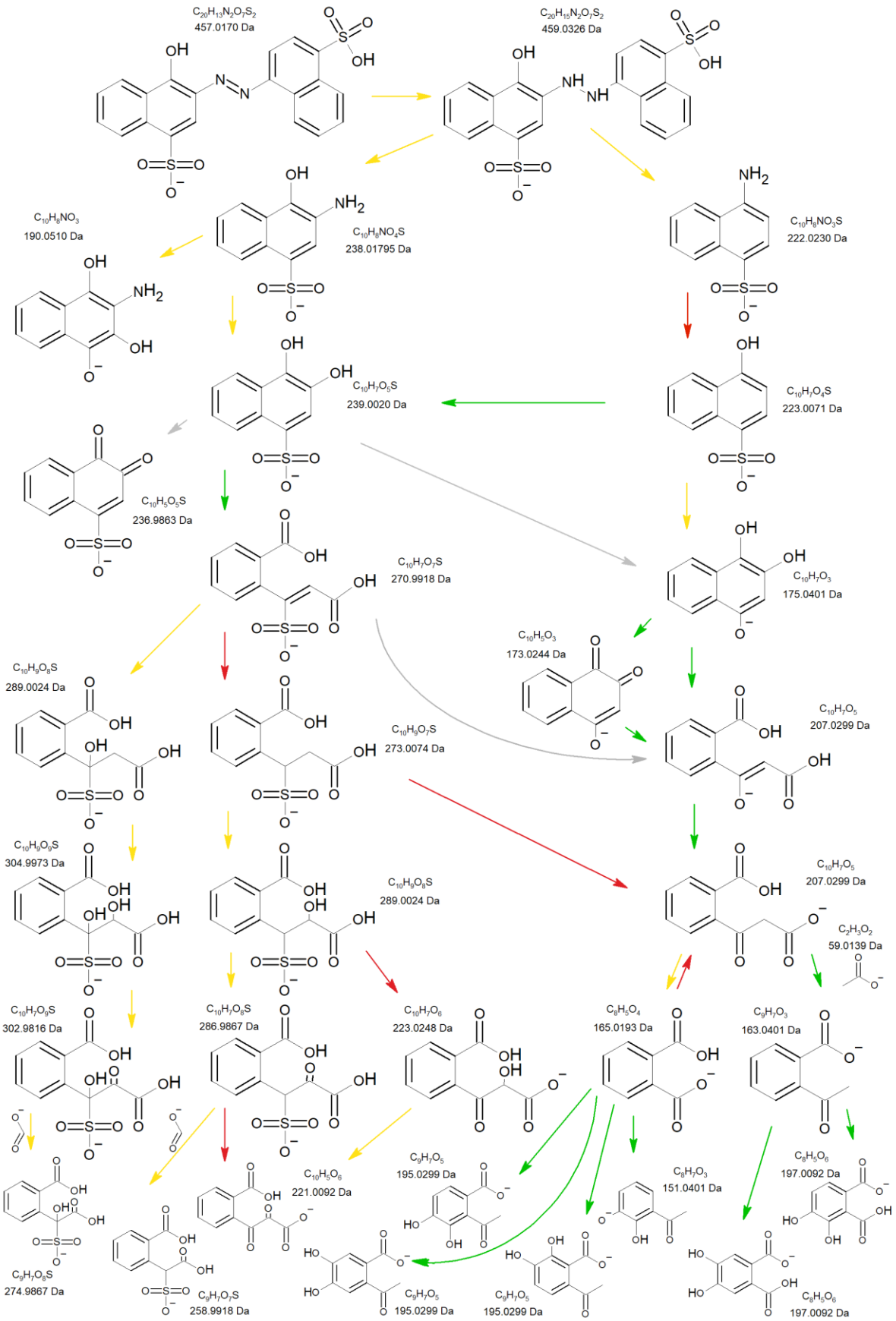


**Figure VIII.S44 -** Predicted Acid Red 14 biodegradation pathways as described in EAWAGBBD Pathway Prediction System (http://umbbd.ethz.ch/predict/). Green, yellow and red arrows represent bioreactions that are likely, neutral and unlikely to occur. The values indicated next to each structure correspond to the respective monoisotopic mass.

## Appendix G – Scientific publications and communications

### List of publications

Franca, R.D.G., Pinheiro, H.M., Lourenço, N.D., 2019. Aerobic granular sludge application to textile wastewater treatment: A review with emphasis on dye bioconversion and the fate and effects of engineered nanoparticles. *Hazardous Materials*. (submitted)

Franca, R.D.G., Vieira, A., Carvalho, G., Oehmen, A., Pinheiro, H.M., Crespo, M.T.B., Lourenço, N.D., 2019. Oerskovia paurometabola isolated from a laboratory mixed culture treating a simulated textile wastewater efficiently decolorizes azo dye Acid Red 14 with further aerobic aromatic amine conversion. *Ecotoxicology and Environmental Safety*. (under review)

Franca, R.D.G., Oliveira, M.C., Pinheiro, H.M., Lourenço, N.D., 2019. Biodegradation products of a sulfonated azo dye in aerobic granular sludge sequencing batch reactors treating a simulated textile wastewater. *ACS Sustainable Chemistry & Engineering* 7, 17, 14697-14706. DOI: 10.1021/acssuschemeng.9b02635.

Franca, R.D.G., Pinheiro, H.M., van Loosdrecht, M.C.M., Lourenço, N.D., 2018. Stability of aerobic granules during long-term bioreactor operation. *Biotechnology Advances* 36, 228-246. DOI: 10.1016/j.biotechadv.2017.11.005.

Franca, R.D.G., Ortigueira, J., Pinheiro, H.M., Lourenço, N.D., 2017. Effect of SBR strategy and feed composition on the stability of aerobic granular sludge in the treatment of a simulated textile wastewater. *Water Science and Technology* 76.5, 1188-1195. DOI: 10.2166/wst.2017.300.

Bento, J.B., Franca, R.D.G., Pinheiro, T., Alves, L.C., Pinheiro, H.M., Lourenço, N.D., 2017. Using nuclear microscopy to characterize the interaction of textile-used silver nanoparticles with a biological wastewater treatment system. *Nuclear Instruments and Methods in Physics Research Section B*. 404, 150-154. DOI: 10.1016/j.nimb.2017.01.016.

Franca, R.D.G., Vieira, A., Mata, A.M.T., Carvalho, G.S., Pinheiro, H.M., Lourenço, N.D., 2015. Effect of an azo dye on the characteristics of an aerobic granular sludge sequencing batch reactor treating a simulated textile wastewater. *Water Research* 85, 327-336. DOI: 10.1016/j.watres.2015.08.043.

Lourenço, N.D., Franca, R.D.G., Moreira, M.A., Gil, F.N., Viegas, C.A., Pinheiro, H.M., 2015. Comparing aerobic granular sludge and flocculent sequencing batch reactor technologies for textile wastewater treatment. *Biochemical Engineering Journal* 104, 57-63. DOI: 10.1016/j.bej.2015.04.025.

## List of oral communications

Sousa, S., Coelho, M.S., Rodrigues, A.M., Franca, R.D.G., Viegas, C.A., Pinheiro, H.M., Lourenço, N.D., 2019. Aerobic granular sludge bioreactor performance under different hydrodynamic regimens with or without silver nanoparticles regarding abatement of textile wastewater toxicity. *BioRemid 2019, 2nd International Meeting on New Strategies in Bioremediation Processes*, 24-25 October, Porto, Portugal.

Coelho, M.S., Sousa, S., Rodrigues, A.M., Franca, R.D.G., Viegas, C.A., Pinheiro, H.M., Lourenço, N.D., 2018. Comparing the operation of aerobic granular sludge bioreactors under different hydrodynamic regimens during the treatment of textile wastewater containing silver nanoparticles. *ChemPor 2018, 13th International Chemical and Biological Engineering Conference*, 2-4 October, Aveiro, Portugal.

Franca, R.D.G., Carvalho, C.I.S., Carvalho, G., Pinheiro, H.M., Lourenço, N.D., 2017. Aerobic granular sludge reactivation under different hydrodynamic regimens: microbial ecology and bioreactor performance. *MICROBIOTEC'17*, 7-9 December, Porto, Portugal.

Franca, R.D.G., Ortigueira, J., Pinheiro, H.M., Lourenço, N.D., 2016. Effect of SBR feeding strategy and feed composition on the stability of aerobic granular sludge in the treatment of a simulated textile wastewater. *IWA World Water Congress & Exhibition*, 9-14 October, Brisbane, Australia.

Lourenço, N.D., Franca, R.D.G., Moreira, M.A., Pinheiro, H.M., 2014. Comparing aerobic granular sludge and flocculent sequencing batch reactor technologies for textile wastewater treatment. *ChemPor 2014, 12th International Chemical and Biological Engineering Conference*, 10-12 September, Porto, Portugal.

Franca, R.D.G., Mata, A.M.T., Pinheiro, H.M., Lourenço, N.D., 2014. Effect of sludge retention time on azo dye biodegradation in an aerobic granular sludge SBR system. *IWA World Water Congress & Exhibition*, 21-26 September, Lisbon, Portugal.

## List of poster communications

Franca, R.D.G., Oliveira, M.C., Pinheiro, H.M., Lourenço, N.D., 2018. Biodegradation of a sulfonated azo dye in anaerobic-aerobic bioreactors treating a simulated textile wastewater investigated by liquid chromatography-tandem mass spectrometry. *ChemPor 2018, 13th International Chemical and Biological Engineering Conference*, 2-4 October, Aveiro, Portugal.

Sousa, S., Coelho, M.S., Franca, R.D.G., Viegas, C.A., Pinheiro, H.M., Lourenço, N.D., 2018. Effect of engineered silver nanoparticles on the performance of aerobic granular sludge regarding the potential for abatement of textile wastewater toxicity. *ChemPor 2018, 13th International Chemical and Biological Engineering Conference*, 2-4 October, Aveiro, Portugal.

Rodrigues, A.M., Rosa, R., Franca, R.D.G., Pinheiro, H.M., Lourenço, N.D., 2018. Impact of textile wastewater composition on the performance and properties of an aerobic granular sludge sequencing batch reactor system during operation after granule storage. *ChemPor 2018, 13th International Chemical and Biological Engineering Conference*, 2-4 October, Aveiro, Portugal.

Franca, R.D.G., Rodrigues, A.M., Pinheiro, H.M., Lourenço, N.D., 2018. Impact of silver nanoparticles on long-term operation of AGS SBR for textile wastewater treatment. *IWA Biofilms: Granular Sludge Conference*, 18-21 March, Delft, The Netherlands.

Franca, R.D.G., Sousa, S., Rodrigues, A.M., Pinheiro, H.M., Lourenço, N.D., 2018. Comparing hydrodynamic regimens in textile wastewater treatment with AGS: granulation, stability and reactivation. *IWA Biofilms: Granular Sludge Conference*, 18-21 March, Delft, The Netherlands.

Rodrigues, A.M., Franca, R.D.G., Pinheiro, H.M., Lourenço, N.D., 2017. Impact of silver nanoparticles on quorum sensing during aerobic granulation. *MICROBIOTEC'17*, 7-9 December, Porto, Portugal.

Franca, R.D.G., Vieira, A., Carvalho, G., Pinheiro, H.M., Barreto Crespo, M.T., Lourenço, N.D., 2016. Biodegradation of a sulfonated azo dye in a synthetic textile wastewater by a newly isolated *Oerskovia* strain. *IWA World Water Congress & Exhibition*, 9-14 October, Brisbane, Australia.

Franca, R.D.G., Pinheiro, H.M., Lourenço, N.D., 2016. Comparing AGS reactivation and operation performance in two SBR hydrodynamic regimes treating a synthetic textile wastewater. *IWA World Water Congress & Exhibition*, 9-14 October, Brisbane, Australia.

Bento, J.B., Franca, R.D.G., Pinheiro, T., Alves, L.C., Pinheiro, H.M., Lourenço, N.D., 2016. Using nuclear microscopy to characterize the interaction of textile-used silver nanoparticles with a biological wastewater treatment system. *15th International Conference on Nuclear Microprobe Technology and Applications*, 31 July - 5 August, Lanzhou, China.

Franca, R.D.G., Pinheiro, H.M., Lourenço, N.D., 2014. Aerobic granular sludge reactivation performance in an anaerobic-aerobic sequencing batch reactor after long-term storage. *ChemPor 2014, 12th International Chemical and Biological Engineering Conference*, 10-12 September, Porto, Portugal.